MEKONG RIVER COMMISSION

THE COUNCIL STUDY

WUP-FIN IWRM Scenario Modelling Report

Council Study Modelling Team in Collaboration with the University of Nice and M2 Euroaquae

22 January 2018

Disclaimer:

These Council Study reports are considered final drafts prepared by the technical experts and specialists of the Mekong River Commission, through a process of consultation with representatives of member countries. The contents or findings of the reports are not necessarily the views of the MRC member countries but will serve as knowledge base and reference in the work of the MRC and its member countries in their ongoing technical and policy dialogues in ensuring the sustainable development of the Mekong river basin.

The MRC is funded by contribution from its member countries and development partners of Australia, Belgium, European Union, Finland, France, Germany, Japan, Luxembourg, the Netherlands, Sweden, Switzerland, the United States and the World Bank

CONTENTS AMENDMENT RECORD

This report has been issued and amended as follows:

Version	Revision	Description	Date	Signed
1	0	First version of the Baseline Report	1/03/2016	Jorma Koponen, Hannu Lauri, Arto Inkala (WUP-FIN International Consultant Team)
1	1	Final version of the Baseline Report taking into account country additional comments	30/10/2016	Jorma Koponen
2	0	First version of the Scenario Modelling Report	18/05/2017	Jorma Koponen, Andrés Muñoz
2	1	Revised and expanded version of the Scenario Modelling Report; updated results based on revised ISIS	15/06/2017	Jorma Koponen, Andrés Muñoz
2	2	Corrected Delta fish production figures	29/06/2017	Jorma Koponen
2	3	Major updates including report re-structuring, further results for main scenarios, figure updates and sub-scenario results	01/08/2017	Jorma Koponen, Andrés Muñoz
3	0	Revision to highlight scenario results and results learned. Added comparison between all scenarios for upstream and downstream Kratie. Total revamp of chapter 5 for more clarity and information.	30/10/2017	Jorma Koponen

4	0	Report revision based on the Member Country questions and suggestions.	22/01/2018	Jorma Koponen

Table of Contents

List of Figures

Tables

Abbreviations and acronyms

AIP	:	Agriculture and Irrigation Programme (of the MRC)
AquaCrop	:	FAO state-of-the-art physiological crop model
BDP	:	Basin Development Plan
BDP2	:	BDP Programme, phase 2 (2006 –10)
BDS	:	(IWRM-based) Basin Development Strategy
BioRA	:	Biological resource assessment team (under Council Study)
CCAI	:	Climate Change and Adaptation Initiative (of the MRC)
CIA	:	Cumulative Impact Assessment
CNMC	:	Cambodia National Mekong Committee
CS	:	Council Study
DMP	:	Drought Management Programme (of the MRC)
DSF	:	MRC Decision Support Framework based on hydrological, water resources and hydrodynamic models
EP	:	Environment Programme (of the MRC)
FAO	:	Food and Agriculture Organisation
FMMP	:	Flood Mitigation and Management Programme (of the MRC)
FP	:	Fisheries Programme (of the MRC)
HH	:	Household
IQQM	:	Integrated Quantity and Quality Model
IBFM	:	Integrated Basin Flow Management (MRC study)
IFAD	:	International Fund for Agricultural Development
IKMP	:	Information and Knowledge Management Programme (of the MRC)
ILO	:	International Labour Organisation
IWRM	:	Integrated Water Resources Management
IWRM-model	:	Modelling framework integrating DSF, SOURCE and WUP-FIN for socio-economic and environmental indicators
ISH	:	Initiative for Sustainable Hydropower (of the MRC)
JC	:	Joint Committee (of the MRC)
LMB	:	Lower Mekong Basin
LNMC	:	Lao National Mekong Committee
M&E	:	Monitoring and evaluation
MRC	:	Mekong River Commission
MRCS	:	Mekong River Commission Secretariat
MRC-SP	:	MRC Strategic Plan
NMC	:	National Mekong Committee
NMCS	:	National Mekong Committee Secretariat
NAP	:	Navigation Programme (of the MRC)
PMFM	:	Procedures for Maintenance of Flow on the Mainstream
PWUM	:	Procedures for Water Use Monitoring
SEDB	:	Socio-economic database (of the MRC)
SIMVA	:	Social impact Monitoring and Vulnerability Assessment (conducted by MRCS)
SoB	:	State of Basin report (of the MRC)
SocEc	:	Social Assessment team (of the Council Study)
SWAT	:	Soil and Water Assessment Tool, hydrological and water quality model
TCU	:	Technical Coordination Unit (of the MRCS)
TNMC	:	Thai National Mekong Committee
UMB	:	Upper Mekong Basin
UN	:	United Nations
UNDP	:	United Nations Development Programme
VNMC	:	Viet Nam National Mekong Committee
WUP-FIN	:	MRC Water Utilization Program Finnish component

1. Executive summary

Development, both local and transboundary, affects Mekong conditions in complex ways as climate, reservoirs, irrigation, land use, flood protection and sea levels change. This report validates, details, quantifies and explains the expected impact of the human impacts on the Mekong system for the Council Study main and sub-scenarios.

Combined DSF/WUP-FIN modelling has been applied to the Council Study impact assessment corridor in order to:

- Integrate DSF, eWater SOURCE and WUP-FIN results and models into a cross-sectoral assessment tool
- Support MRC and MRC Member Country adaptation of the Council Study assessment methodology through user friendly implementation of the tool
- Provide socioeconomic and environmental indicator data for the Council Study discipline teams
- Conduct scenario assessment focusing on Mekong sediments and productivity.

The results of the modeling show largest impacts to the Mekong system from hydropower reservoir sediment and nutrient trapping. The decline of fisheries, in the worst-case scenario up to 70%, has most critical consequences in Cambodia because its population is more dependent on natural fisheries than in the other Mekong countries. The modelling results show that effective reservoir sediment management measures (sediment flushing) can maintain fertile sediment fluxes and fisheries production.

Sediments affect also agricultural production that benefits from flooding and supply of fertile sediments. Yield losses are up to 20% if sediments are not compensated by fertilizers and maintenance of soil structure with organic material.

Another critical factor for the future Mekong development will be climate change. Modelling results show significant decline of soil water in the Tonle Sap watershed and consequent large decline in rainfed agriculture yields for the dry climate scenario C3. Also required irrigation amounts would increase in C2 up to 20%. Consequently planning is required to mitigate possible future critical conditions.

In addition of detailing modeling results, principles, calibration and validation, this report proposes implementation plan for the Integrated Mekong Impact Assessment Tool (IMIAT) implementation as part of the whole MRC information system development. For the Council Study focus should be supporting the MRCS and Country capacity building.

2. Modelling methodology, calibration and verification

The WUP-FIN models have been applied for scenario impact assessment focusing on agriculture, irrigation, fisheries production and BioRA, socio-economic and macro-economic discipline team support. WUP-FIN models have been applied to four areas:

- Upper Kratie (Chiang Saen – Kratie) SIMVA corridor around the Mekong main stream
- Lower Kratie floodplains (Cambodian floodplains & Vietnam Delta)
- Tonle Sap floodplains and Lake
- Mekong coastal areas (focus on coast but includes whole South and East Sea areas).

Three types of models have been utilized:

- IWRM integrated model for hydrology, agriculture, flood indicators, fisheries production etc.; based on the WUP-FIN VMOD hydrological model
- 3D EIA hydrodynamic and water quality model for Tonle Sap and coastal area water quality, fisheries production and other indicators
- 3D EIA specialized water quality model for nutrient cycle modelling. Model utilizes the flow fields computed by the EIA 3D hydrodynamic model.

In order to focus on the scenario impact modelling results, modelling methodology and principles and model calibration and verification are presented in the ANNEX. It consists of:

1. Overview of the IWRM modelling approach
2. Tonle Sap watershed hydrological and water quality modelling
3. Tonle Sap Lake and floodplain hydrodynamic and productivity modelling
4. Tonle Sap Lake and floodplain nutrient cycle modelling
5. Delta impact modelling
6. IWRM/VMOD model description and validation
7. 3D EIA model description and validation
8. Tonle Sap productivity model description and validation
9. Tonle Sap 3D EIA water quality model description and validation.

Nearly all of the IWRM model results are based on the DSF ISIS model results. ISIS model provides water level, sediment, nutrient and salinity values in the river channel points which the IWRM model utilizes as input data for instance for flood computation. Figure 1 compares ISIS and IWRM model computed maximum flooding for the year 2000. As the flood maps are based on the same information they are also close to each other. The main discrepancy is North-East of Prey Veng where the IWRM model over-estimates flooding extent. This can be caused by three factors:

- More ISIS nodes need to be included in the IWRM model for this area
- No dyke information has been available for the area to be implemented in the IWRM model
- DEM differs for this area in the ISIS and IWRM models.

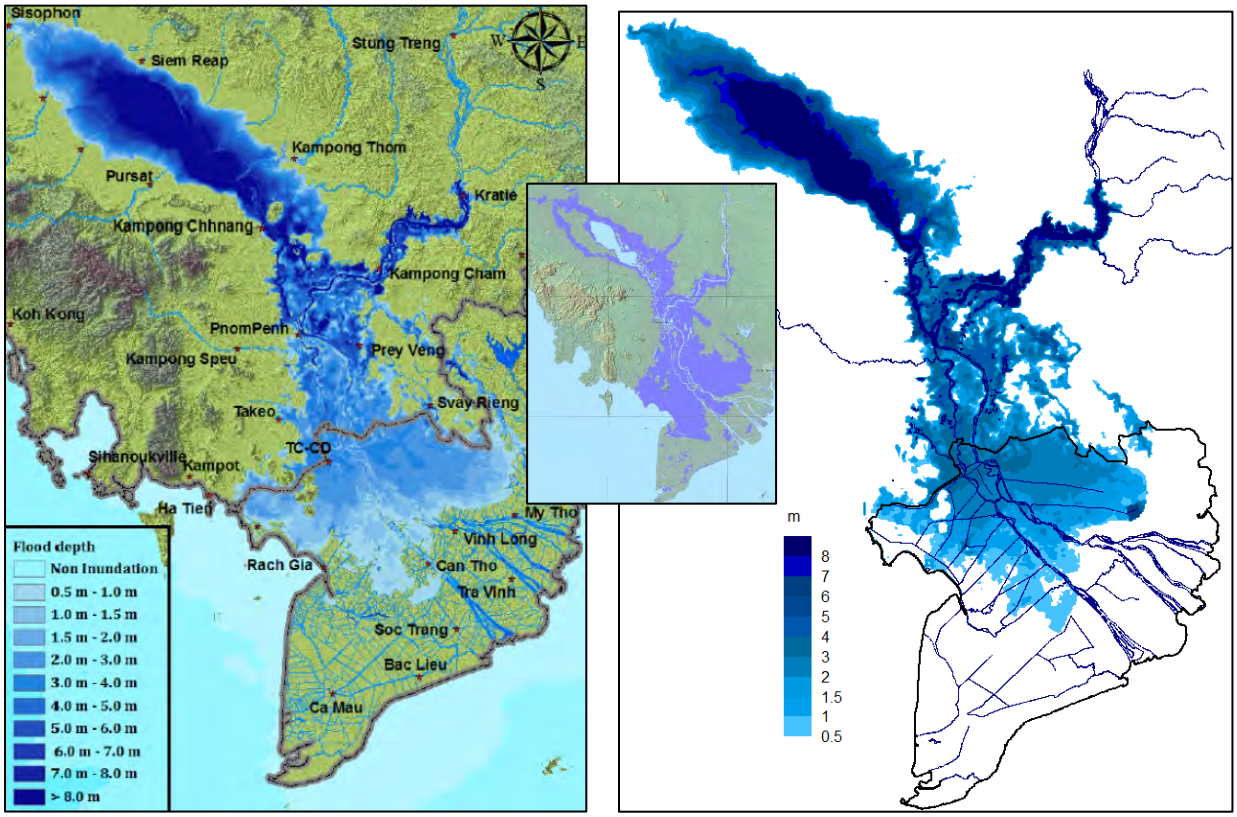

Figure 1. Comparison of ISIS computed year 2000 maximum flood depth (left figure, ref. The ISIS Model in Lower Mekong Area to Support the Council Study, Final Technical Report) computed with the IWRM ISIS based flood mapping (right figure). The middle small figure is remote sensing flood map from Dartmouth Flood Observatory.

3. Modelling limitations and direction for future work

The Council Study has created of a fully integrated assessment framework from bio-geo-physical characteristics of the Mekong Basin reaching up to the policy level. The assessment methodology is *evidence based and quantitative* as the large economic, social and environmental values of the Mekong development require solid information basis. The assessment methodology is fully integrated as data and modelling are directly feeding into social, economic and environmental indicators and assessment and these in turn into the Thematic sectors. Other strong point of the Council Study is its thorough analysis of monitoring data, especially sediments and water quality, that has not been executed before. At the same time there are limitations involved with the study that stem from lacking data and broad scope of the exercise which constraints how far modelling have been implemented.

The main limitations and constraints for the **data** relating both to the overall and WUP-FIN modelling can be summarized as:

- No dyke data has been available for the baseline nor the scenarios;
- Salinity information is constrained to two dry seasons only;
- The irrigation and land use change numbers are based on best available information and estimates at the time of the project implementation but that they need to be updated based on latest national surveys, policies and plans.

- Irrigation area locations are not necessarily up-to-date or non-existent (Vietnam);
- Irrigation storage data needs to be checked and updated;
- There is no information about using hydropower reservoirs for local irrigation;
- Irrigation efficiency is not up-to-date for the latest and future Thai irrigation developments;
- Information on agrochemical (nutrients, pesticides, herbicides) releases is almost non-existent;
- Data on rice paddy fisheries and aquaculture is lacking such as how much fish is produced and how different farming practices affect the fisheries;
- Irrigated area crop calendars need to be checked;
- Information on where, when and how much other crops than rice are cultivated is seriously lacking;
- For detailed nutrient cycle modelling more water quality data is necessary;
- There is no primary production data (this is basic limnological measurement easy to conduct);
- There is no information on industrial and domestic nutrient and harmful substances releases;
- Information on mining releases is non-existent;
- Sand mining information needs to be clarified;
- Impact of land use change on hydrology, sediments and nutrients needs to be verified;
- Coastal data for stratification, water quality, sediments and erosion need to be obtained.

The main limitations and constraints for the **IWRM modelling scope** requiring improvement in the future can be summarized as:

- Upstream Kratie the detailed impact analysis has been conducted only in the narrow corridor around the Mekong mainstream including tributary floodplains affected by the Mekong; for the socio-economic analysis this corridor has been further restricted so that the floodplains are not included. This causes the analysis to be non-representative spatially and overly sensitive for water level changes in the mainstream such as caused by flood fluctuations and construction of the mainstream dams. The main related issue is that more detailed macro-economic analysis is not meaningful using the restricted corridor and the socio-economic analysis covers only communities in the immediate vicinity of the mainstream;
- Although on the national irrigation modelling using the DSF includes secondary and tertiary crops, the more detailed IWRM modelling has been restricted for only one dry season irrigated crop and for some indicators also for one wet season supplementary irrigation. The IWRM farming system modelling can be implemented for any type of crop calendars and crop mixes but the current Council Study scope doesn't include more realistic implementation;
- Other crops than rice have not been modelled;
- Nutrient load modelling from agriculture has not been conducted due to lack of verification data;
- It is possible to model actual return flows with the IWRM model but this has not been implemented yet because of the time required for model verification;
- There should be much more emphasis on drought modelling than what has been implemented so far;
- Salinity intrusion is a complex issue because of many factors (sea level rise, flood control structures, upstream flow, channel morphology, water regulation) affecting it. As salinity intrusion has large impact on irrigation and crop production it should be understood better and the salinity intrusion model should be verified in detail. Also, salinity intrusion has been modelled only for two dry seasons which is too little;
- Tonle Sap and reservoir nutrient dynamics and trapping should be understood much better – more time needs to be dedicated to these;
- Due to resource constraints coastal modelling has been conducted as indicative so far.

The key limitations of the **DSF modelling** impacting on the IWRM impact modelling are:

- Climate scenarios need to be re-analysed and downscaled in order to capture ranges of possible future climates including more seasonal, drier, wetter and more variable climates;
- Hydropower impacts on water quality and nutrient trapping need to be verified;
- Estimated and computed baseline sediment and nutrient loads probably work on annual basis for the mainstream but more detailed analysis required for instance for hydropower regulation require update for the land based SWAT modelling;
- Land use change modelling requires verification and SWAT update;
- In general, number of issues in how SWAT has been constructed and how it is performing have been identified and need to be addressed.

Lastly **policy messages** have following limitations requiring further work:

- Systematic risk-based approach has not been exercised in the irrigation analysis. For instance water availability during dry periods, worst case salinity intrusion and dam operation risks have not been included in the analysis;
- Flood damages to irrigated areas have been analysed in general terms only;
- Drought management has not been part of the study;
- Multi-purpose reservoir potential for irrigation expansion have not been included in the study.
- Mitigation options such as increased fertilizer use to compensate reservoir sediment and nutrient trapping have not analysed quantitatively;
- In general there should be much more emphasis on mitigation measures especially for the hydropower development;
- Groundwater potential for irrigation has not been analysed;
- Options for fisheries management would be extremely important for Cambodia;
- Climate change adaptation has not been in the Council Study scope;
- Linkage between modelling and the triple bottom line analysis (ecological, socioeconomic and macro-economic) should be further expanded and results verified with the countries.

The Member Countries have indicated that the Council Study technology needs to be transferred to the countries for their independent update and iteration of the assessment. For instance, the countries have indicated that there is need to run new scenarios and use different future development policies and assumptions. Because of this the Council Study has been designed to be flexible, transparent, repeatable and open-ended to accommodate improved data and assessment tools in the future. The importance of the Council Study Assessment Framework is not so much that it is definitive, perfect and without information gaps but that it provides consistent scientific evidence based practical methodology and knowledge base to support further studies and processes. It would be important not to lose this knowledge and to continue improving it as indicated above. In the future MRCS and the Member Countries should integrate the Council Study knowledge and methodology in the existing frameworks and activities.

4. Upper Kratie scenario impacts

Most of the results for both upstream and downstream Kratie are presented in zones depicted in . The zones are based on the MRCS Social Impact Monitoring and Vulnerability Assessment (SIMVA) zones. SIMVA has been carried out by the MRCS Environment Program and continued by the Environment Division after the MRCS organizational change in 2015. Zones 2 (upper Lao mainstream), 3A (middle and lower Lao mainstream) and 3B (middle and lower Thailand mainstream) have been selected as representative areas where results are presented.

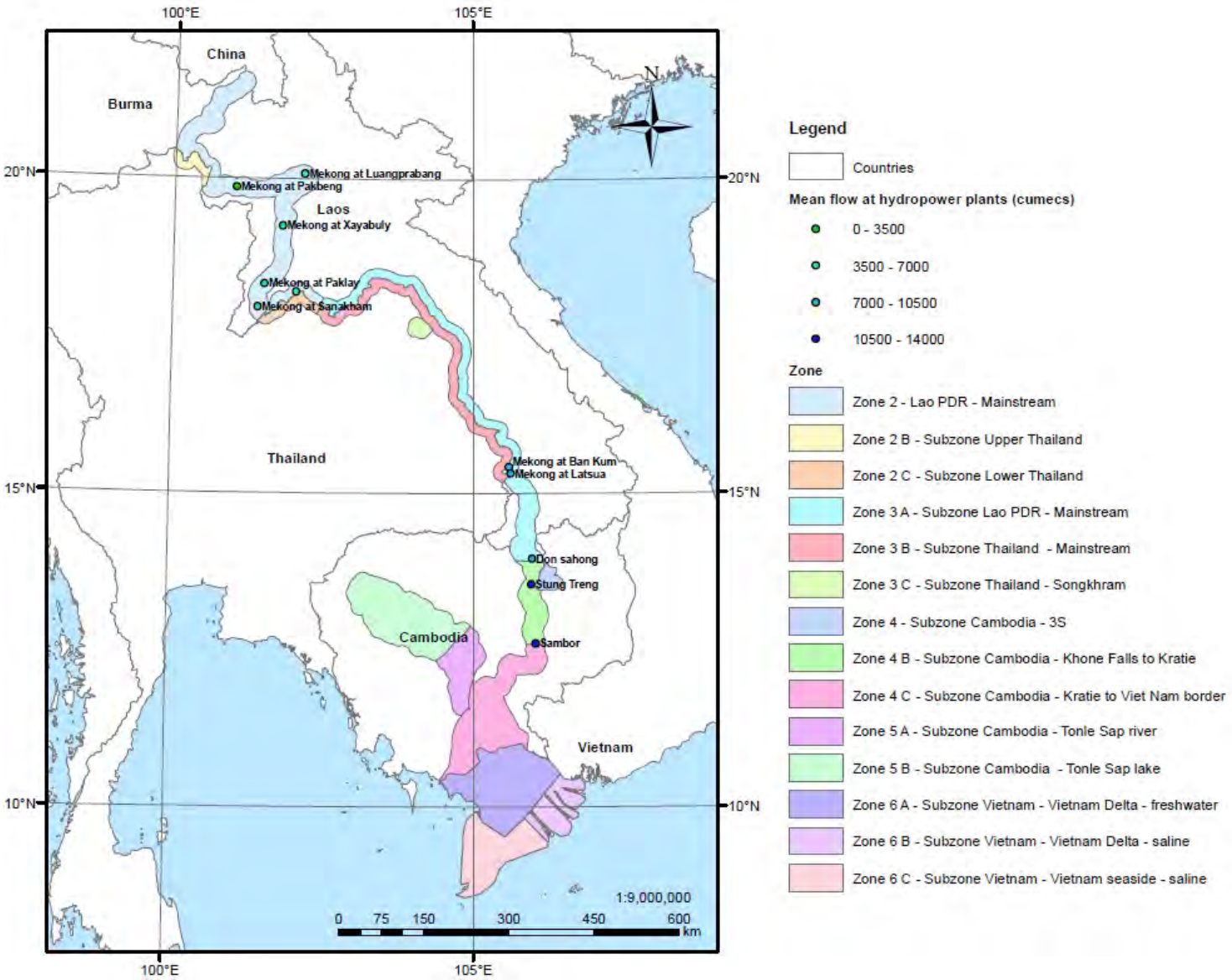

Figure 2. Council Study impact assessment and socio-economic assessment areas

4.1. Flooding characteristics

The WUP-FIN/IWRM modelling results are based on the MRCS DSF model outputs. Specifically ISIS model water levels, discharge and concentrations have been used as an input for the WUP-FIN impact assessment. The methodology is presented in the ANNEX

Flooding derived from the ISIS results are relevant for a wide range of purposes, including flood protection and preparedness but for the impact assessment they have been used mostly for fisheries and agricultural impact assessment. For flooding only the main outputs utilized are flood probability, duration and depth. Examples for the upstream Kratie area for the main scenarios are shown in the Figure 3, Figure 4 and Figure 5.

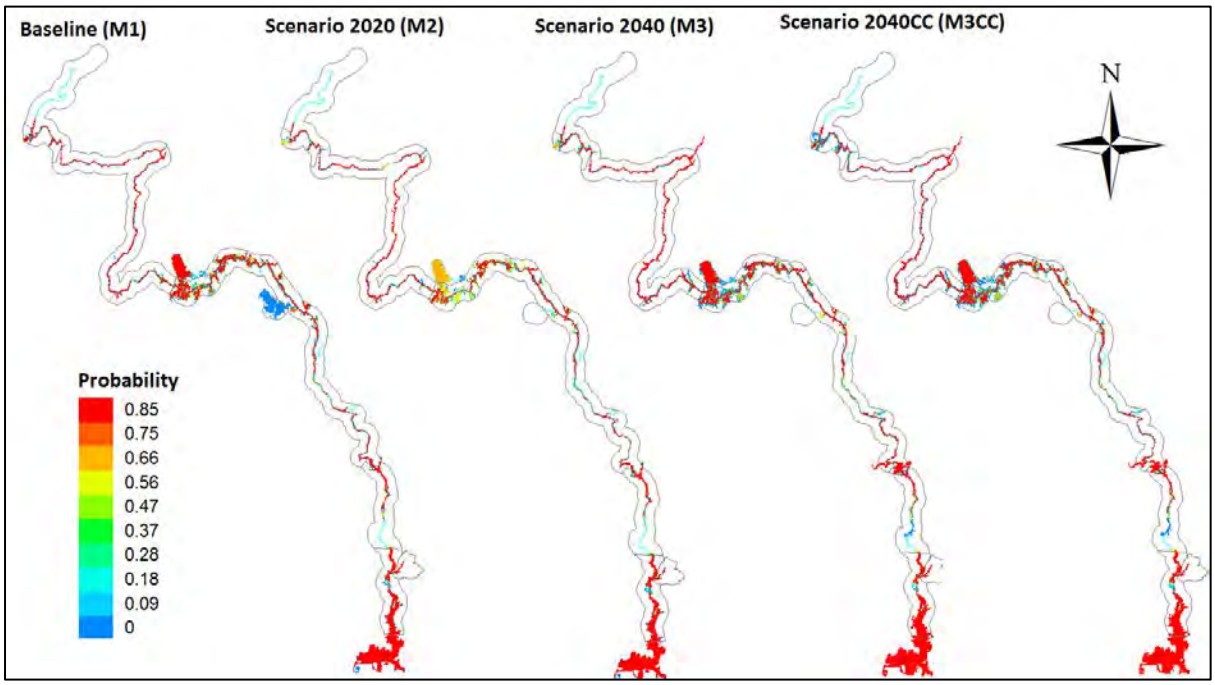

Figure 3. Map of probability of floods for the three scenarios (Baseline, 2020 and 2040)

Figure 3 shows the flood probability. River channels are flooded permanently and many of the floodplains nearly each year. These are shown with red color in Figure 3. Flooding decreases in 2020 and 2040 scenarios due to hydropower reservoir construction and consequent decrease in peak flood levels.

For the most part flooding duration is from 32 to 64 days while small areas located upstream and downstream present higher duration floods (Figure 4).

The maximum flood depth map (Figure 5) shows that there is not much difference between the main scenarios for the flooding areas and the water levels for the peak flow events. However, low flow flooding changes a lot between the scenarios due to the mainstream dam construction and permanent water level increase as can be seen in the time series for the average flood depth and total flooded area (Figure 6 and Figure 8).

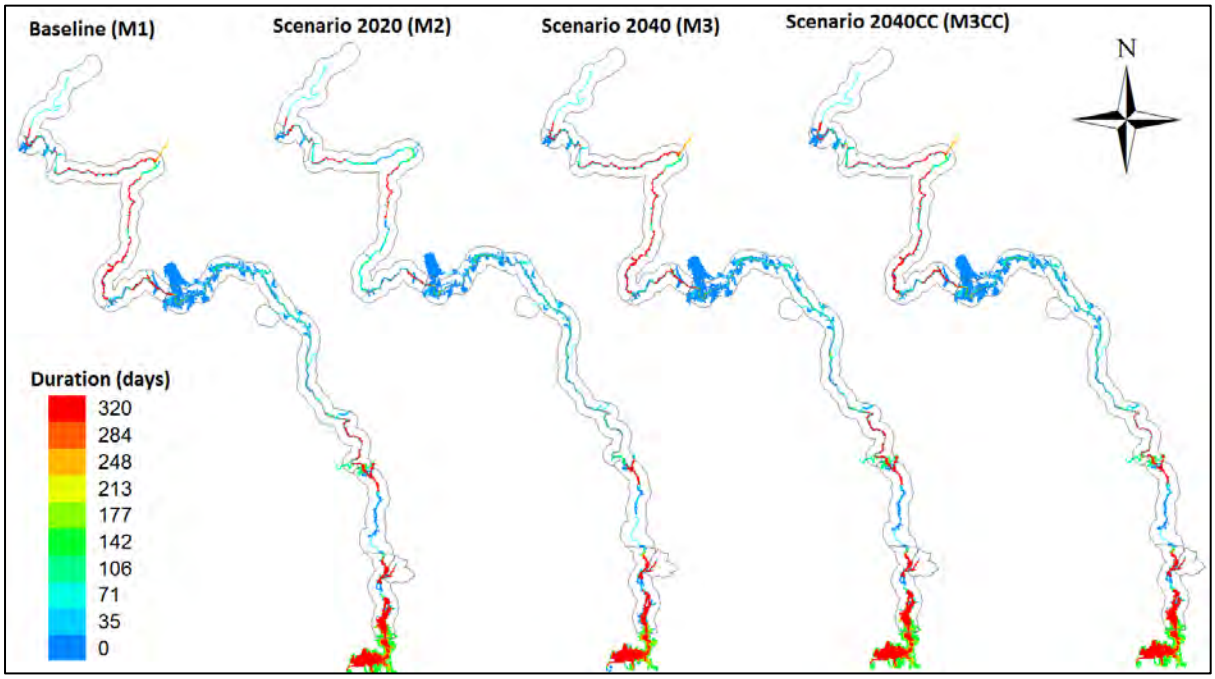

Figure 4. Map of flood duration for the three scenarios (Baseline, 2020 and 2040)

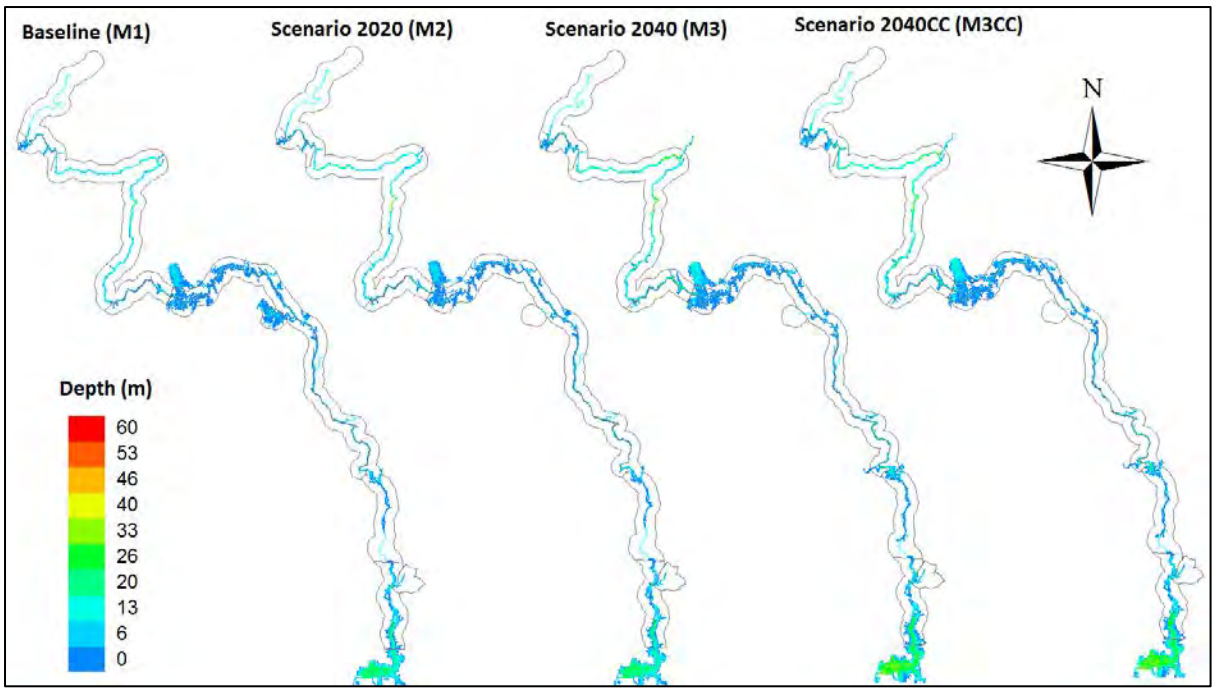

Figure 5. Map of maximum depth during floods for the three scenarios (Baseline, 2020 and 2040)

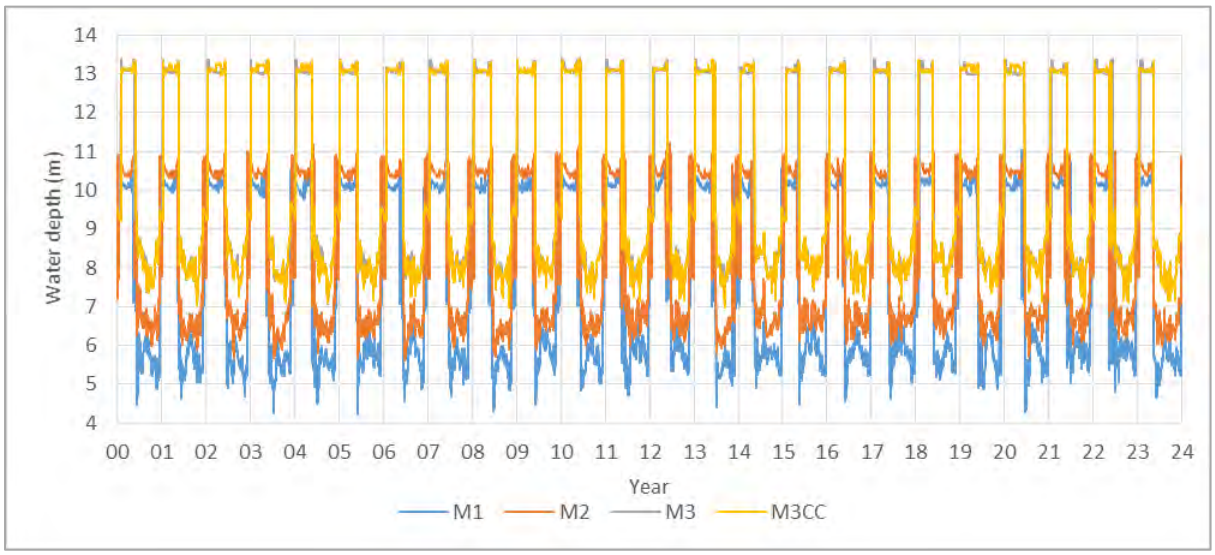

Figure 6. Spatially averaged daily water depth for the whole upper part of the Mekong River Basin (values include river channels).

Figure 6 shows spatially averaged daily water depth for the 24 simulation years. The figure illustrates inter-annual and dry/wet season variability. Due to the dam construction, mainstream reservoirs and dry season water release from tributary and China dams the mean water depth increases considerably reaching a maximum of 13 m for the whole basin for the M3 and M3CC main scenarios during the dry season. It is important to consider that this mean value corresponds to the whole basin and it does not represent the possible maximum depth in the basin. It should be also noted that the values are here affected by the river channel depths (model includes option to eliminate these in order to get floodplain values only but it is not utilized here). The high dry season water depths are caused by less flooding during the dry season and concentration of water in the river channels.

Figure 7 shows time-averaged water depths from Figure 6. The increased water depths in the future scenarios are caused by build-up of the mainstream reservoirs and increased discharge during the dry season caused by China and tributary dams.

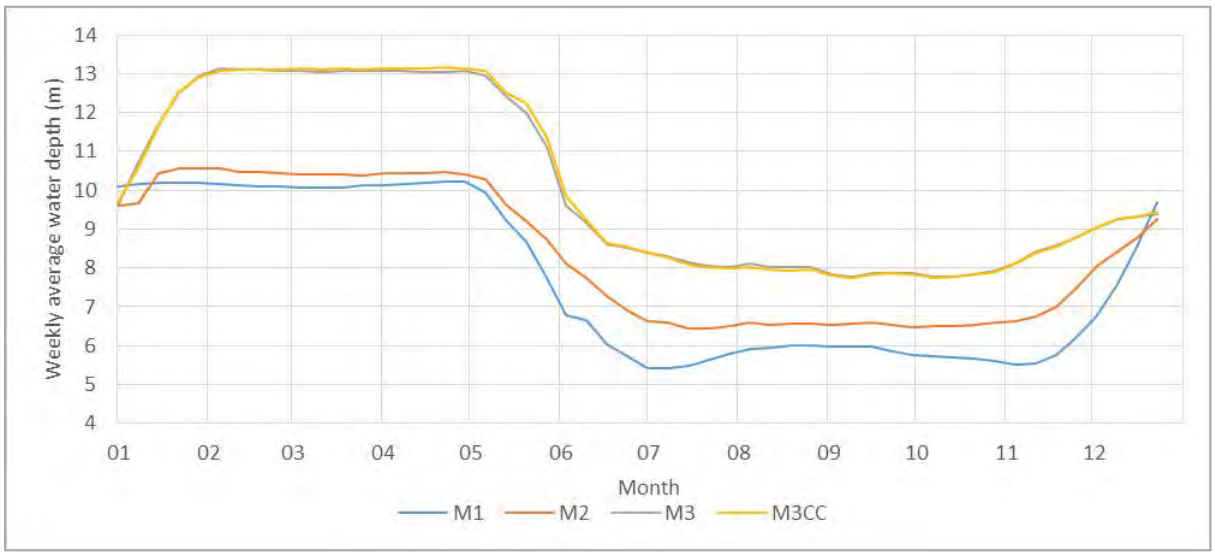

Figure 7. Weekly average water depth for the upper part of Mekong River. Observe that the depths represent different wet areas (compare to Figure 9).

The M3 and M3CC scenarios show large increase, about doubling, of the flooded area in the upper Mekong corridor. This is shown in the Figure 8 for daily flooded area. River channel is included in the flooded values.

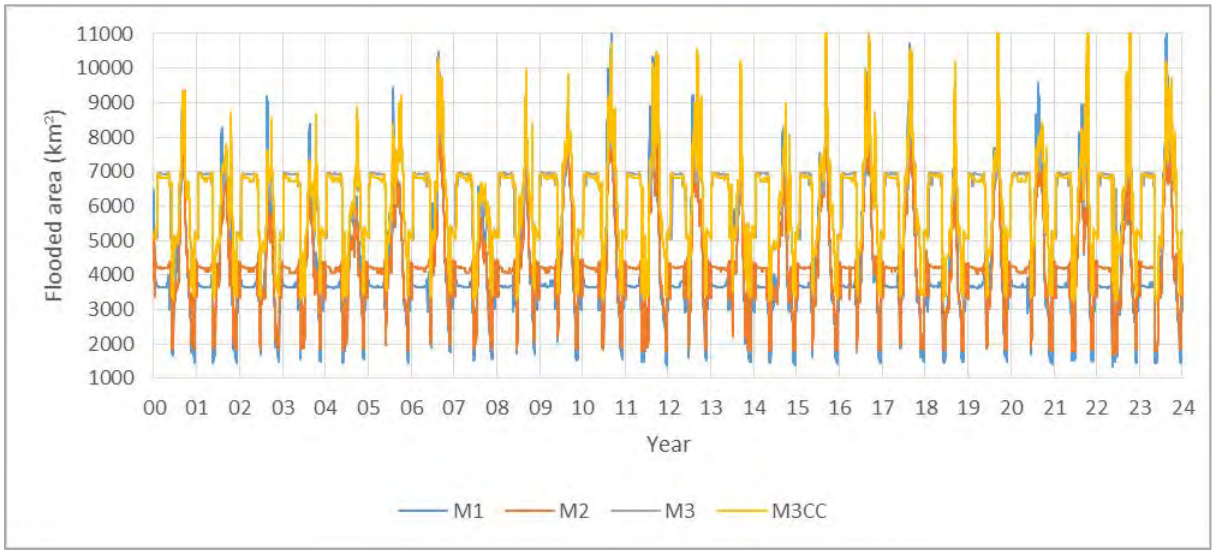

Figure 8. Total flooded area for the upper part of the Mekong River Basin (values include river area).

Figure 8 shows how the peak baseline (M1) floods are reduced due to water trapping by the reservoirs. It shows also impact of increased dry season flow caused by tributary and China dams as well as build-up of the mainstream reservoirs.

Time-averaged flooded area for the main scenarios is shown in Figure 9. In the 2040 the mainstream and tributary dams have full impact and the flooded area is nearly doubled other than the west season.

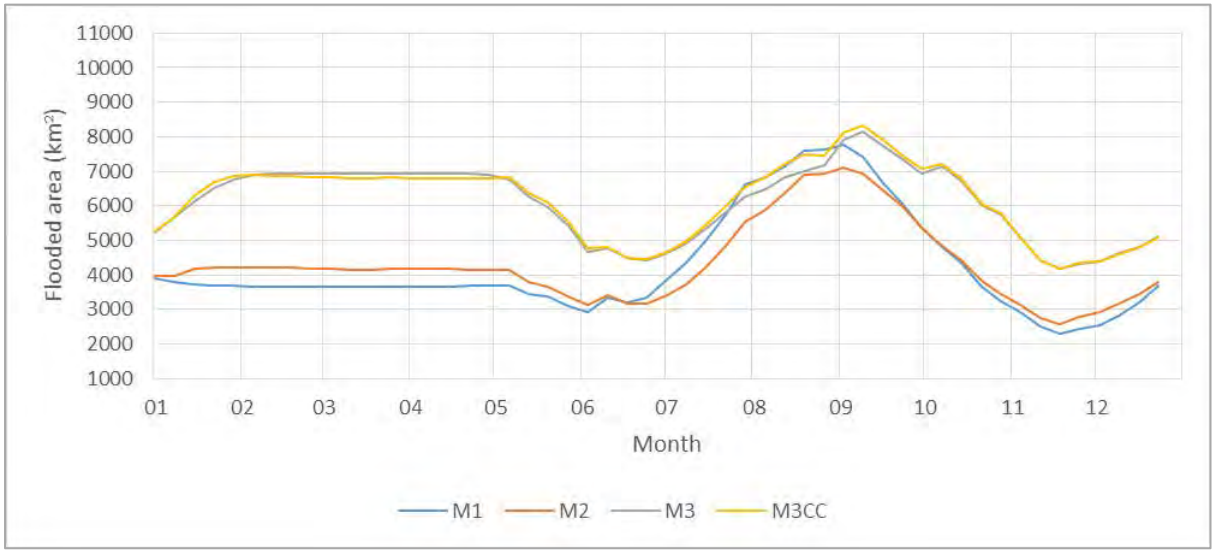

Figure 9. Weekly average flooded/wet area for the upper part of Mekong River.

Average flood depth the Zone 3A is shown in in Figure 10. The scenarios are clearly divided into two patches: the lower flood depths and higher inter-annual variation are connected to the scenarios M1, M2 and H1b with less hydropower development. Mainstream dams as well as decreased flood amplitudes stabilize flooding in the other scenarios. Building of the mainstream dams naturally also increases permanent flooding and flood depths.

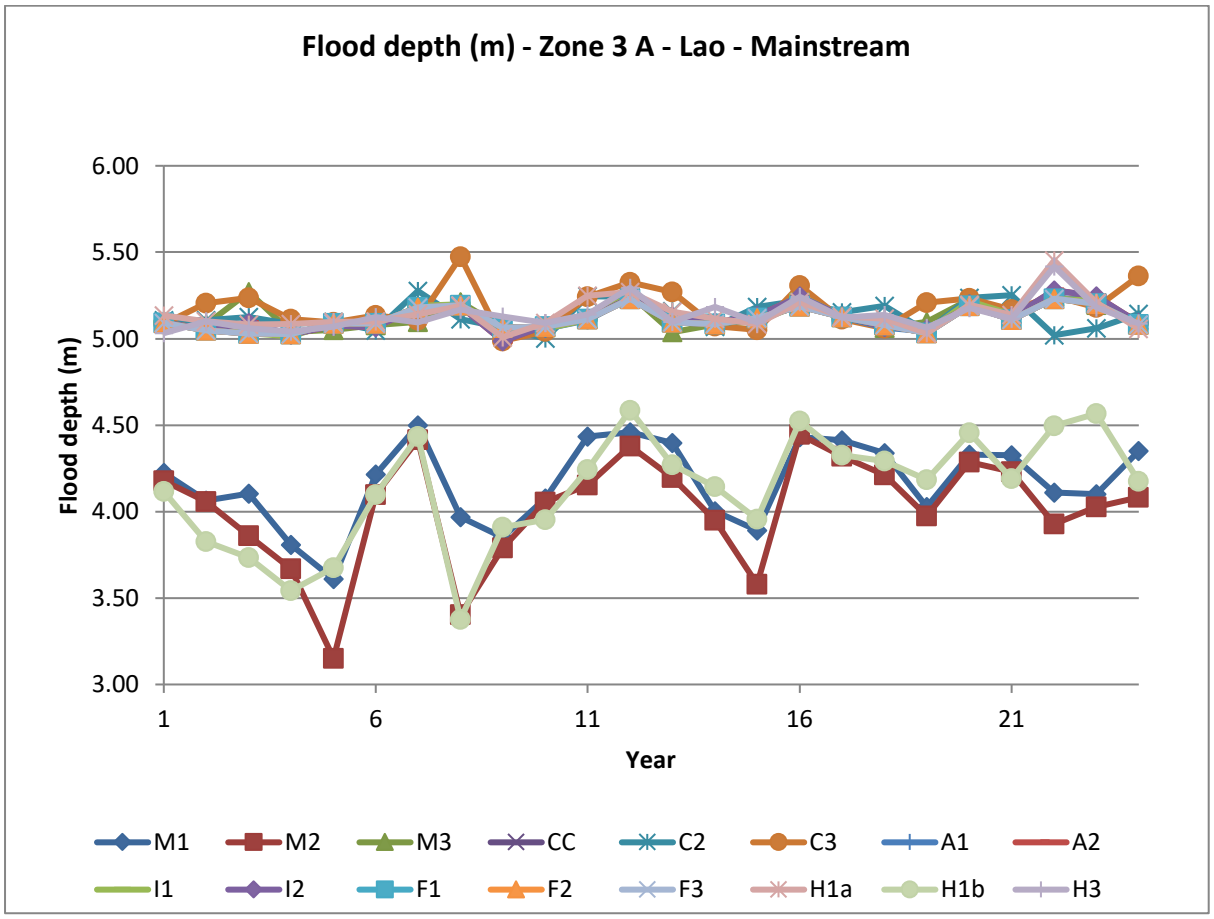

Figure 10. Annual variation of average flood depth in Zone 3A for all scenarios

Flooded areas show high inter-annual variation in all scenarios for the Zones 3A and 3B (Figure 12 and Figure 13). In Zone 2 with steeper river banks and limited flooded are the variation is less (Figure 11). Limited hydropower development in scenarios M1, M2 and H1b cause less flooding in Zone 2. M2 tends to have less flooding also in Zones 3A and 3B due to limited mainstream dams and lower flood peaks compared to the baseline. Scenario C3 shows reduced flooding in all scenarios due to dryer climatological conditions.

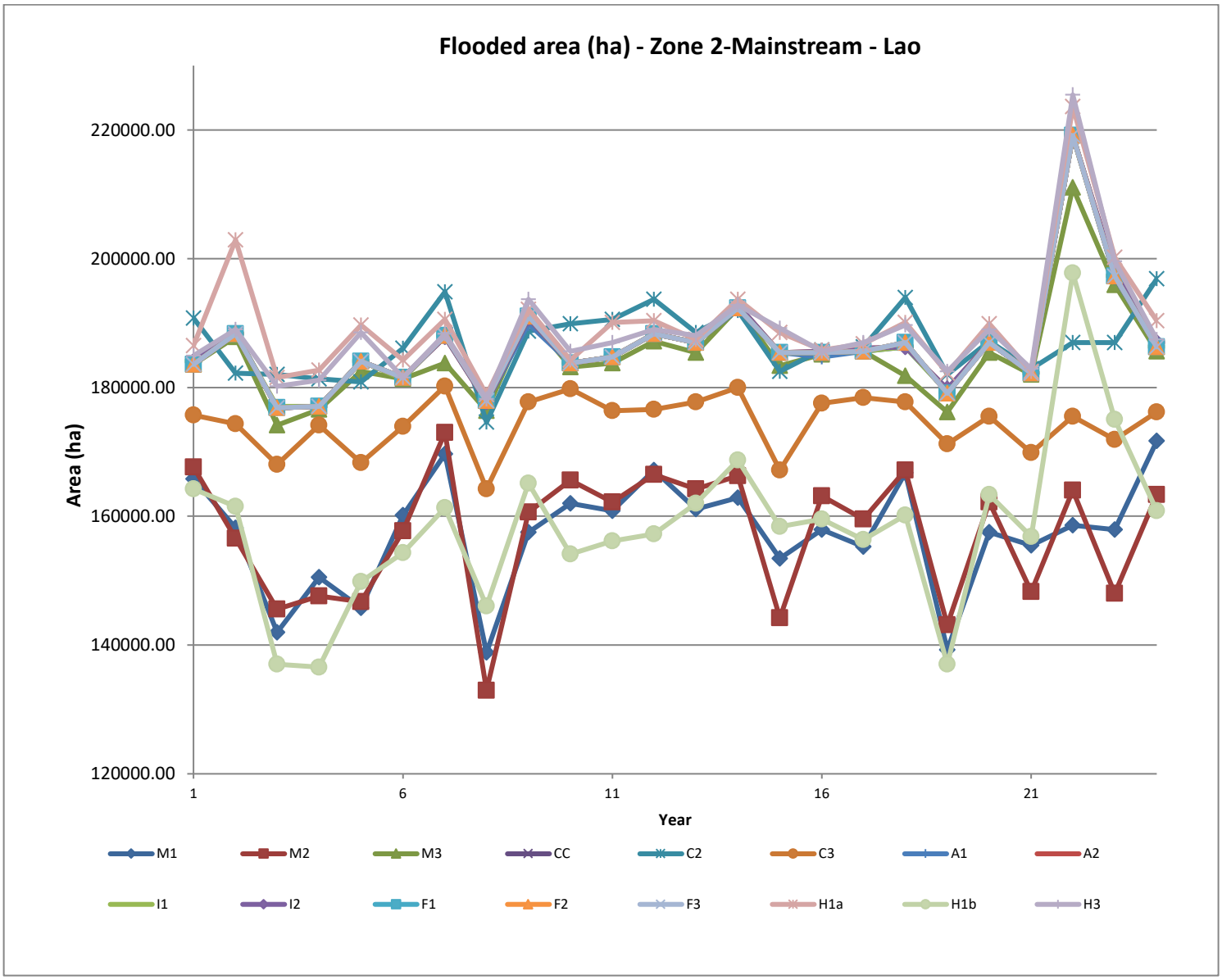

Figure 11. Annual variation of the flooded area in Zone 2 for all scenarios

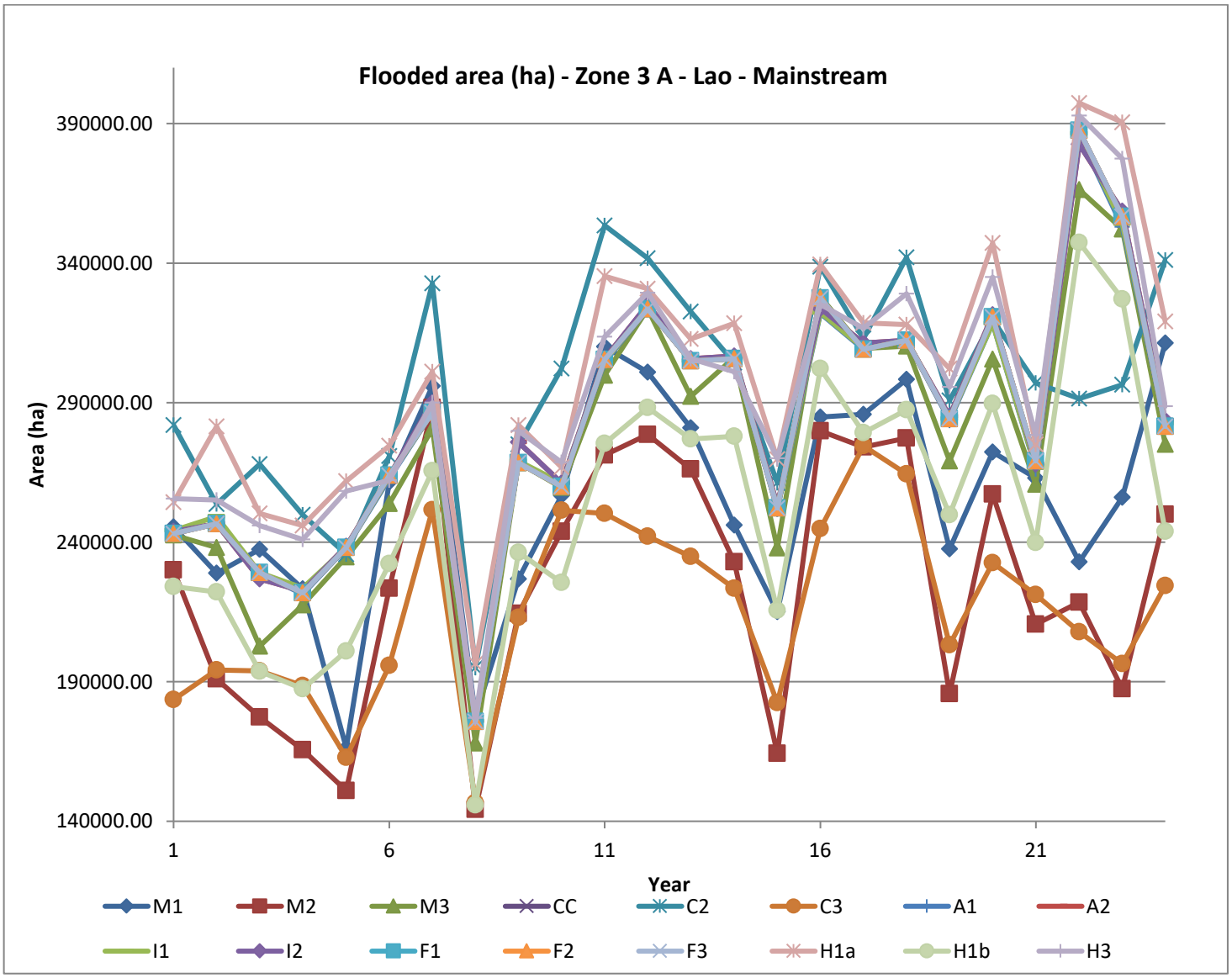

Figure 12. Annual variation of the flooded area in Zone 3A for all scenarios

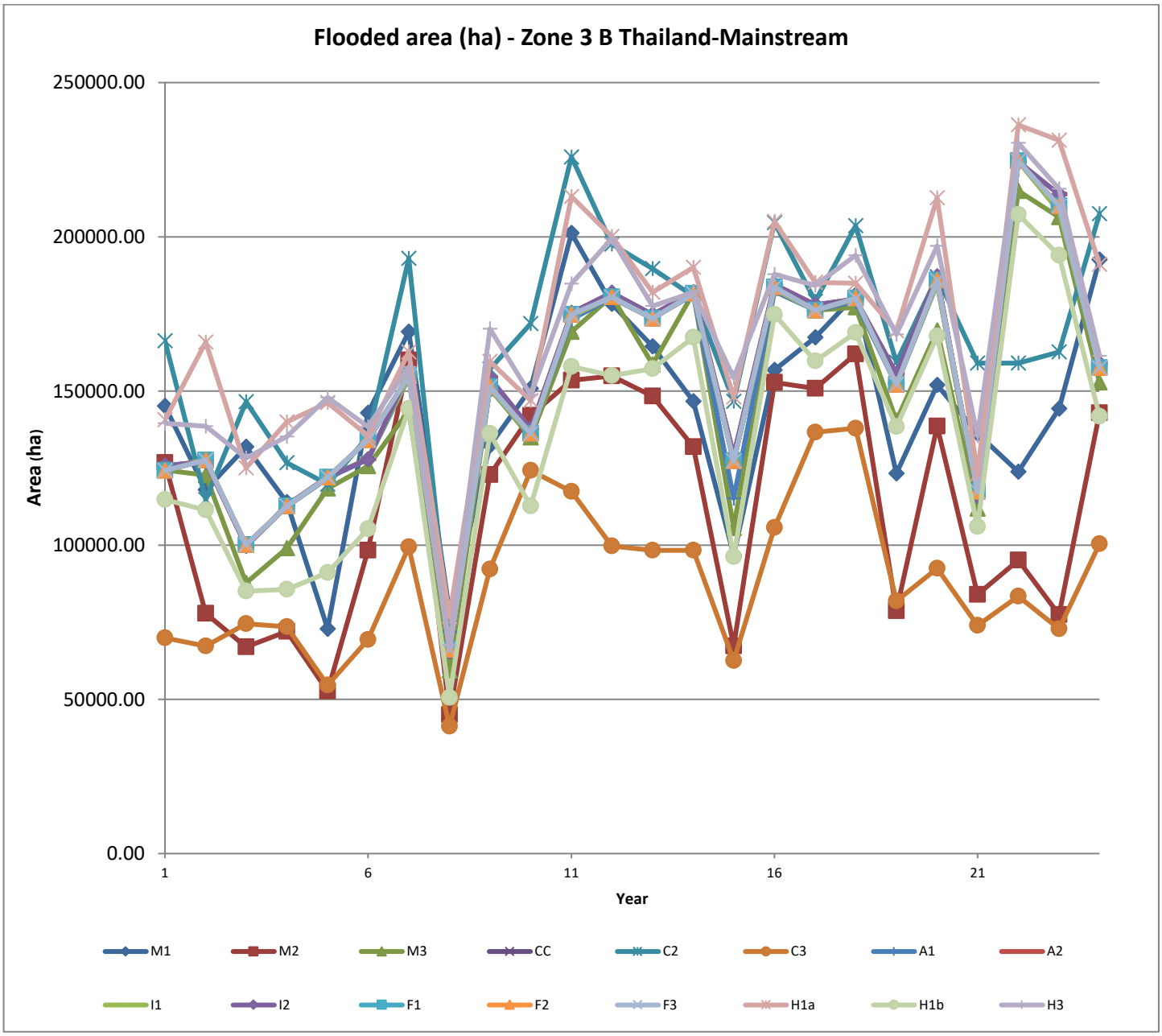

Figure 13. Annual variation of the flooded area in Zone 3B for all scenarios

4.2. Floodplain sedimentation

Floodplain sedimentation has strong correlation to flooding as it indicates both flooded area and flood duration. Floodplain sedimentation correlates strongly to sediment, nutrient and organic material loads; rice production; and fisheries production (see later chapters and ANNEX). In addition, decreased floodplain sedimentation may indicate change in balance between sedimentation and erosion processes. Only clay results are shown here as conclusions for silt are similar and clay can be considered good indicator for nutrient transport and soil fertility.

Average floodplain sedimentation in the Zones 2, 3A and 3B is shown in Figure 14. The sedimentation values vary greatly from location to location depending on the relief of the terrain as deeper river valleys, steeper river banks and limited floodplains decrease floodplain flooding and sedimentation. Flood duration plays also significant role here and especially in Zone 3A where flooded area is larger than in the Zones 2 and 3B but flood duration on the average smaller. Large sediment trapping by the reservoirs in M2, M3 and M3CC causes average sedimentation to collapse.

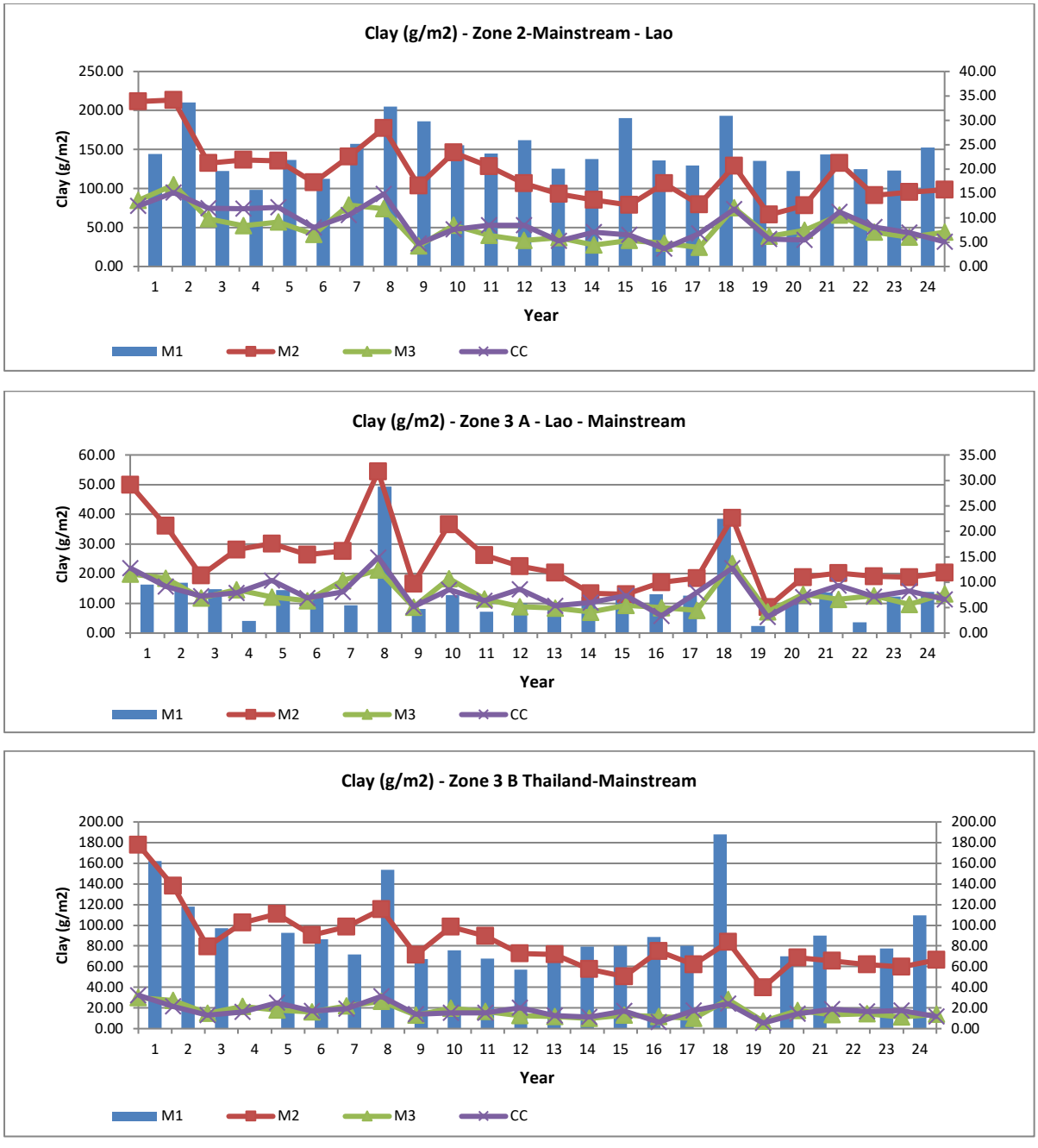

Figure 14. Annual variation of clay floodplain sedimentation for the main scenarios for Zones 2, 3A and 3B. Observe that scales are different for the bars (left scale) and for the time series (right scale).

Average annual sedimentation rates for all scenarios for the Zone 3B are shown in Figure 15. Considering the rather large uncertainties involved in sediment modelling no other conclusions can be

drawn from the figure other than that the sedimentation rate is much higher for the M1, M2 and H1b compared to the other scenarios.

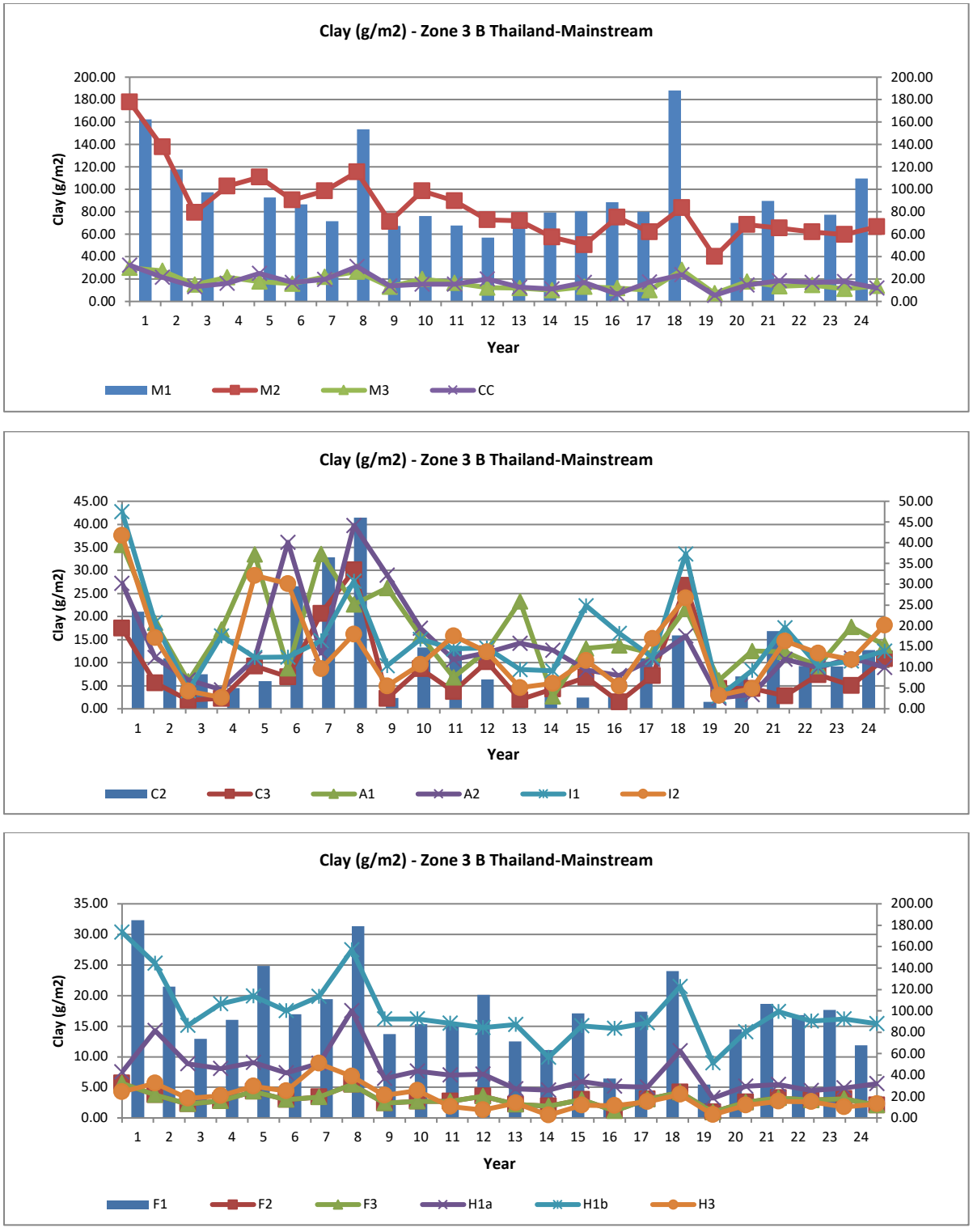

Figure 15. Annual variation of clay floodplain sedimentation for the all scenarios for Zone 3B. Observe that scales are different for the bars (left scale) and for the time series (right scale).

4.3. Rice production

In the model rice is impacted by climatic conditions (precipitation and temperature), sediment input to the paddies (soil fertility), flooding (soil water and flood damage), salinity, CO_2 concentration as well as hydrological characteristics of each paddy area such as water drainage dependent on slope and soil properties.

In the Figure 16 shows total non-irrigated rice production in the upper Kratie divided into the zones for the scenarios M1, M3, M3CC, C2, C3, A1 and A2. The other scenarios differ only slightly from these and are not shown. All the climate scenarios decrease production compare to the M3 due to more unfavourable conditions such as non-optimal temperatures, higher soil evaporation and decreased precipitation. The production decrease is most prominent in scenario C3 with consistently drier conditions. A1 and A2 have increased rice production compared to the M3 due to increased agricultural area.

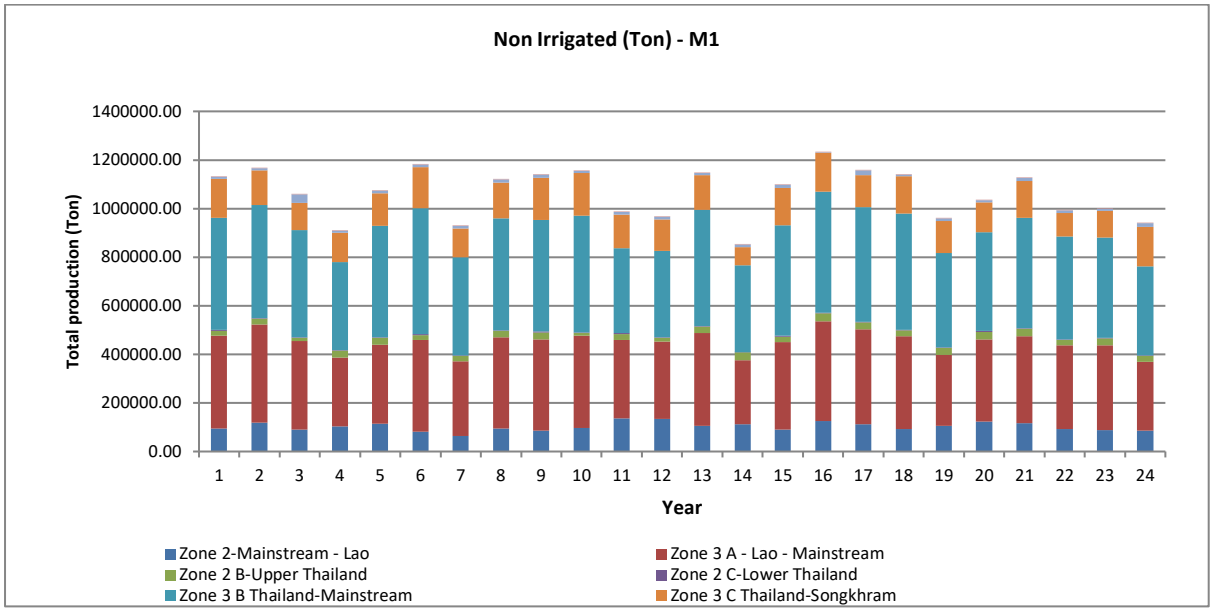

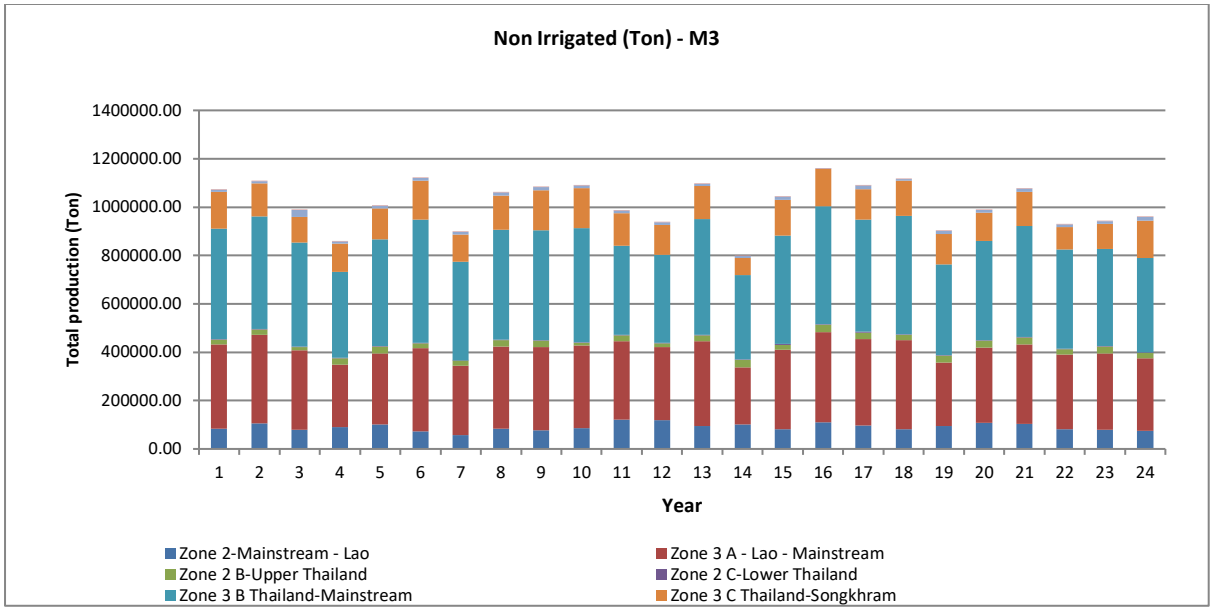

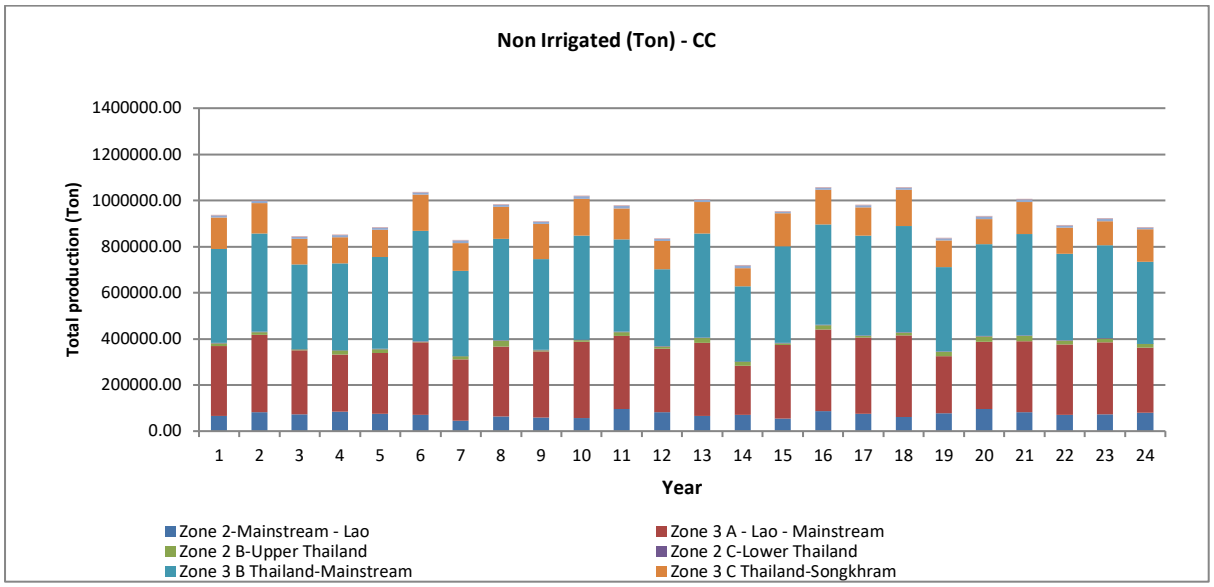
Non Irrigated (Ton) - CC
Total production (Ton)
1400000.00
1200000.00
1000000.00
800000.00
600000.00
400000.00
200000.00
0.00
1 2 3 4 5 6 7 8 9 10 11 12 13 14 15 16 17 18 19 20 21 22 23 24
Year
Zone 2-Mainstream - Lao
Zone 3 A - Lao - Mainstream
Zone 2 B-Upper Thailand
Zone 2 C-Lower Thailand
Zone 3 B Thailand-Mainstream
Zone 3 C Thailand-Songkhram

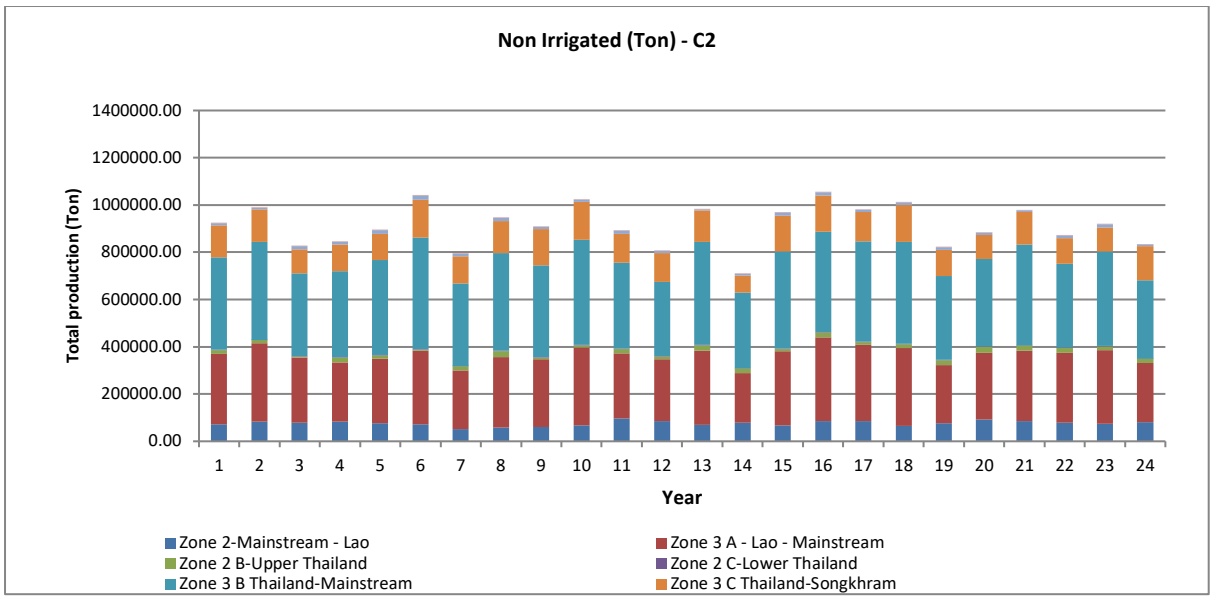
Non Irrigated (Ton) - C2
Total production (Ton)
1400000.00
1200000.00
1000000.00
800000.00
600000.00
400000.00
200000.00
0.00
1 2 3 4 5 6 7 8 9 10 11 12 13 14 15 16 17 18 19 20 21 22 23 24
Year
Zone 2-Mainstream - Lao
Zone 3 A - Lao - Mainstream
Zone 2 B-Upper Thailand
Zone 2 C-Lower Thailand
Zone 3 B Thailand-Mainstream
Zone 3 C Thailand-Songkhram

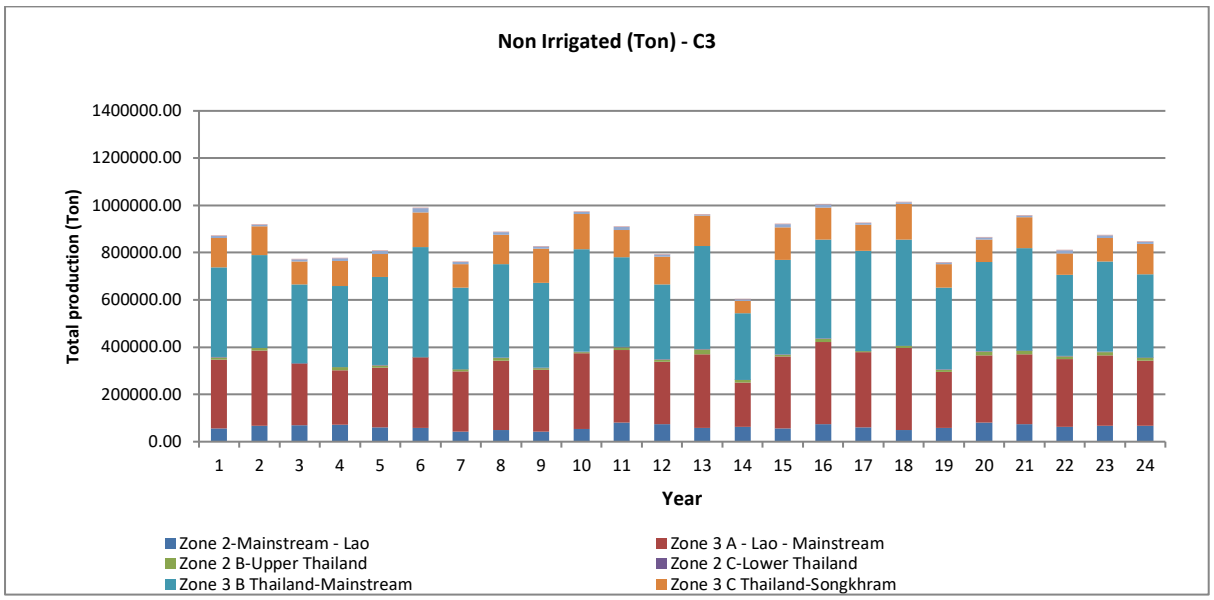
Non Irrigated (Ton) - C3
Total production (Ton)
1400000.00
1200000.00
1000000.00
800000.00
600000.00
400000.00
200000.00
0.00
1 2 3 4 5 6 7 8 9 10 11 12 13 14 15 16 17 18 19 20 21 22 23 24
Year
Zone 2-Mainstream - Lao
Zone 3 A - Lao - Mainstream
Zone 2 B-Upper Thailand
Zone 2 C-Lower Thailand
Zone 3 B Thailand-Mainstream
Zone 3 C Thailand-Songkhram

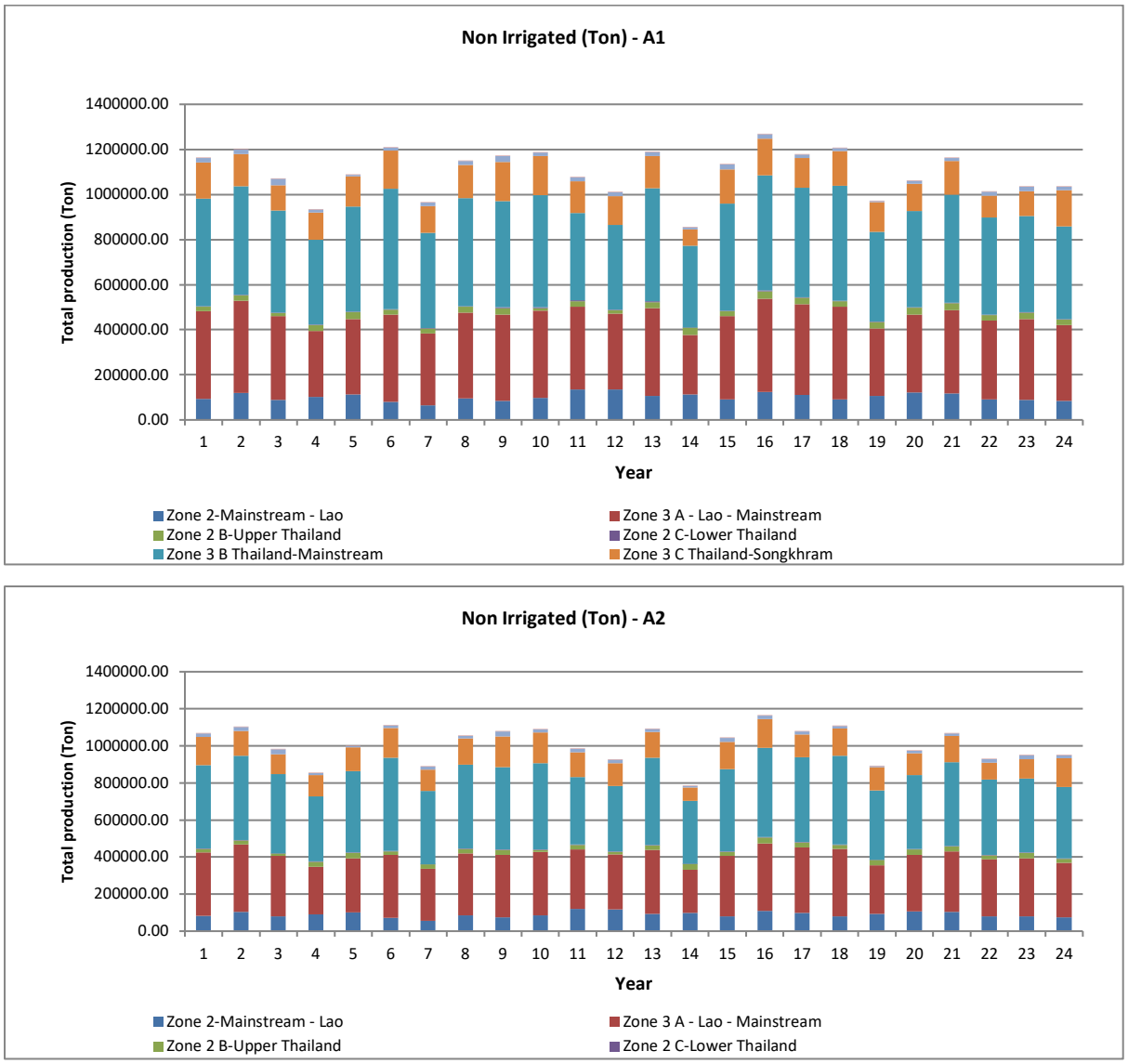

Figure 16. Annual variation of total rice production in the upper Kratie zones for the scenarios M1, M3, M3CC, M2, M3, A1 and A2.

The variation in non-irrigated rice production between the scenarios can be seen in the figures Figure 17- Figure 19. As explained above the largest differences are between the climate and agricultural area scenarios.

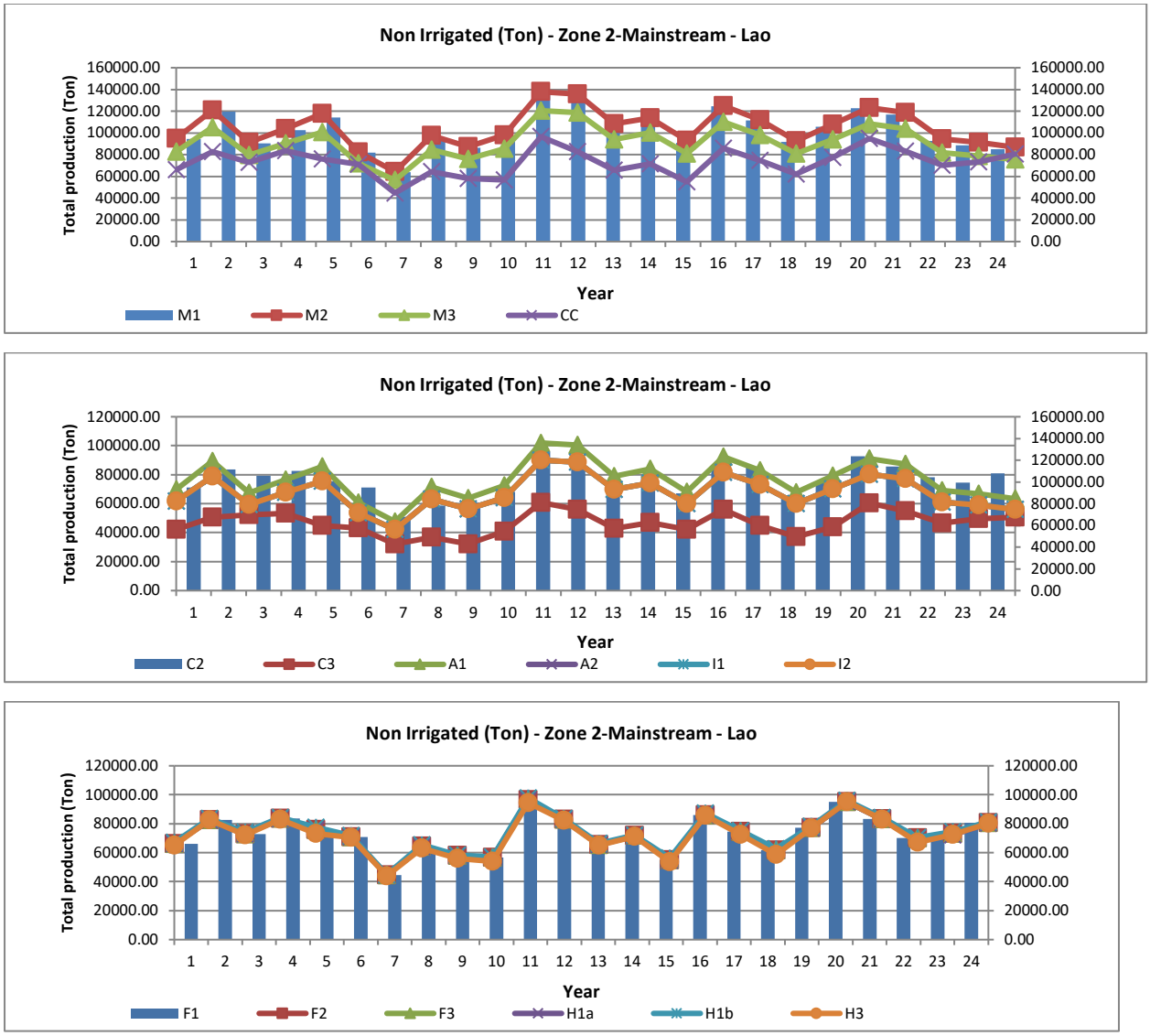

Figure 17. Annual variation of total rice production in the Zone 2 for all scenarios. Observe that scales are different for the bars (left scale) and for the time series (right scale).

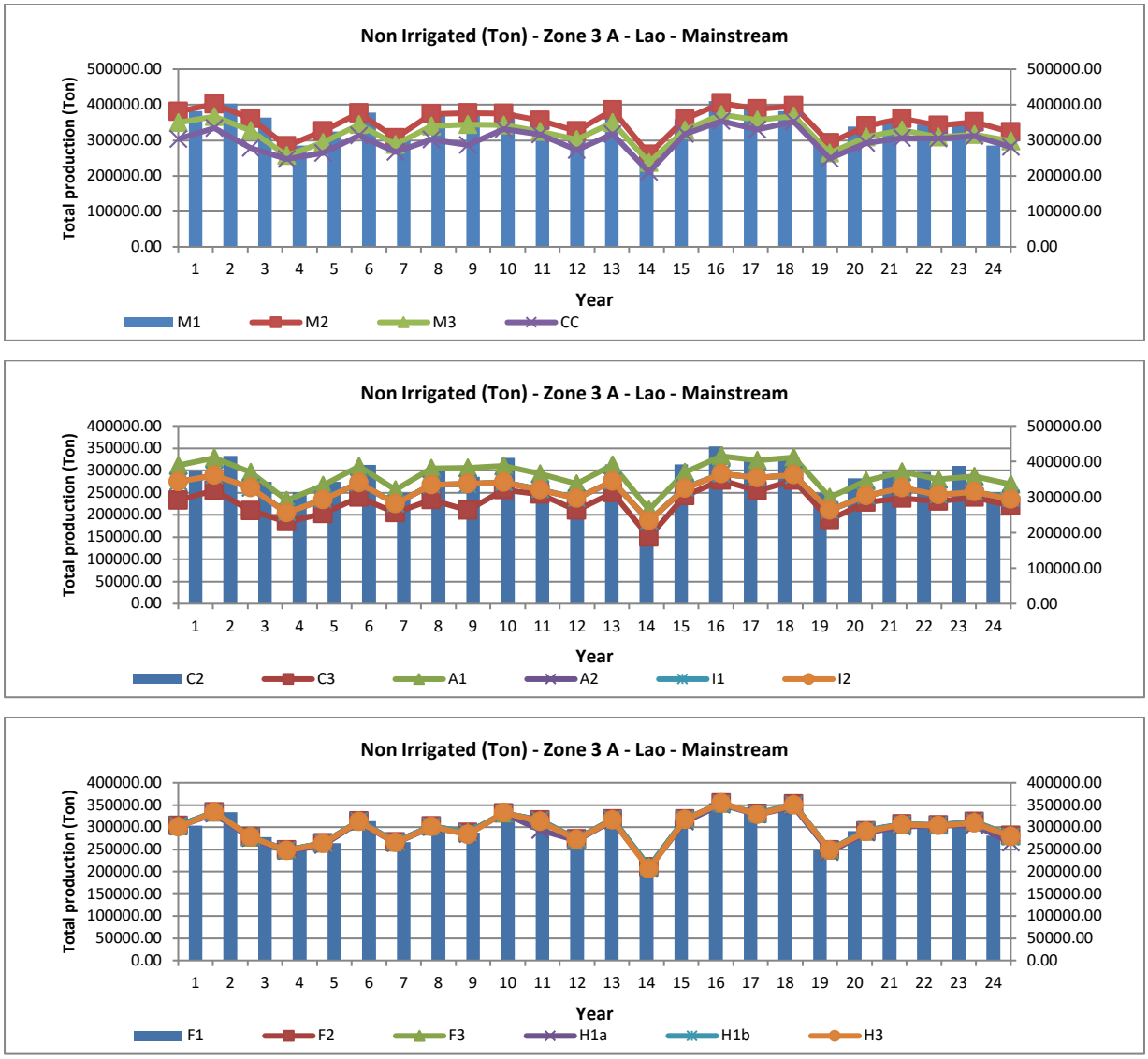

Figure 18. Annual variation of total rice production in the Zone 3A for all scenarios. Observe that scales are different for the bars (left scale) and for the time series (right scale).

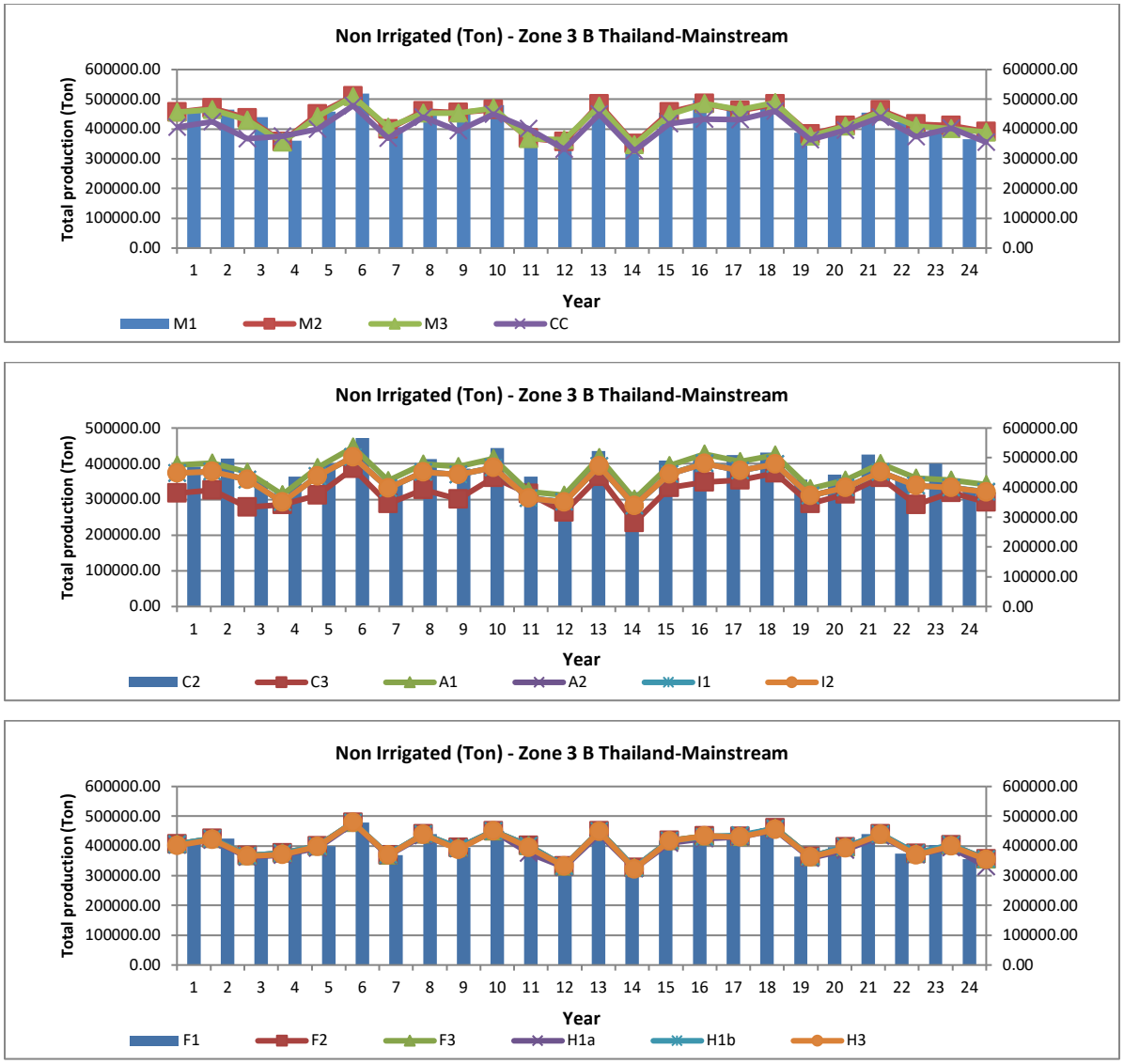

Figure 19. Annual variation of total rice production in the Zone 3B for all scenarios. Observe that scales are different for the bars (left scale) and for the time series (right scale).

4.4. Floodplain fisheries production

Upper LMB mainstream floodplains in the Council Study assessment corridor are quite limited and local fisheries production doesn't have as much importance as in the tributaries and in the lower LMB. The main catch in many locations is much more dependent on migratory fish from the tributaries and downstream than local population. In any case locally the fisheries can have some impact on food security and peoples' wellbeing.

Scenarios have impact on floodplain fisheries production in various ways: habitat change, migration barriers (dams), flood regime change and sediment, organic material and nutrient (alluvium) input. In the WUP-FIN modelling only flooding and sedimentation impacts due to hydropower regulation and sediment trapping are modelled. The alluvium input is impacted especially by hydropower reservoirs

and affects primary production and through it fisheries production. Fisheries production in the scenarios follows sedimentation in although not linearly (see Figure 76).

Figure 20 shows the main scenario impact compared to the baseline: the floodplain fisheries production in the upper Kratie impact assessment corridor is halved compared to the baseline. This is due to decreased sediment input to the floodplains and decreased primary production providing directly or indirectly to the fish growth. The production in M3 is not decreased in proportion to the sediment decrease between M2 and M3 because of the mainstream dam construction and increased permanently flooded area.

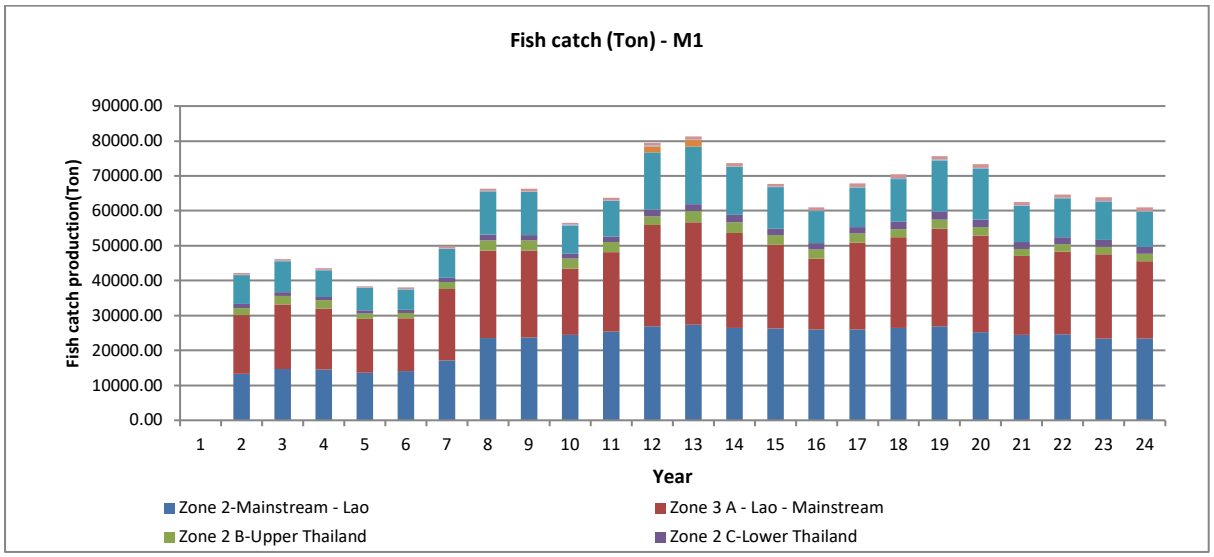

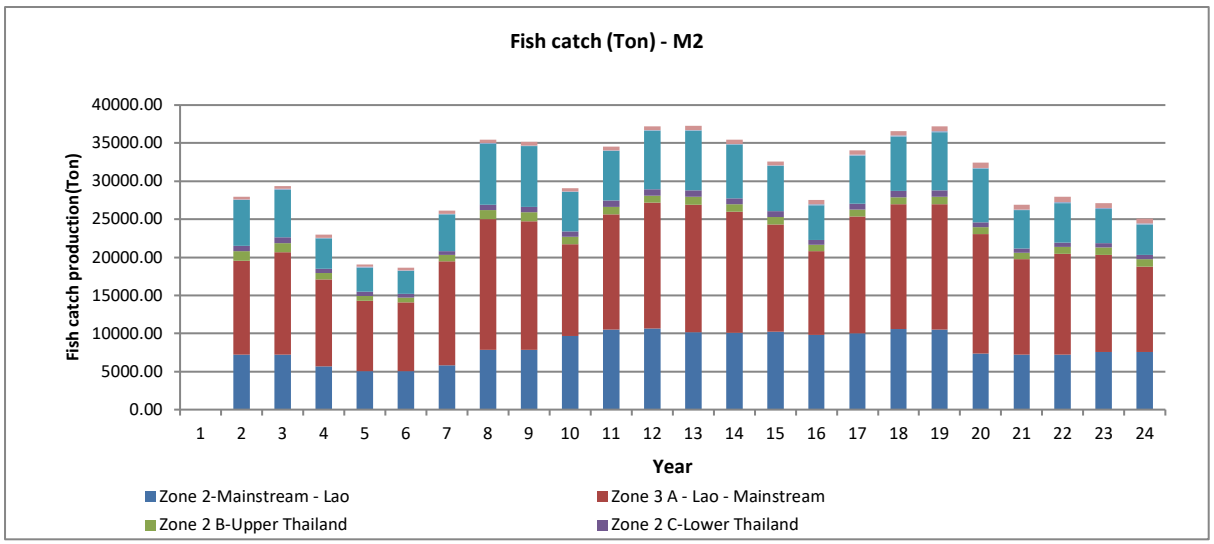

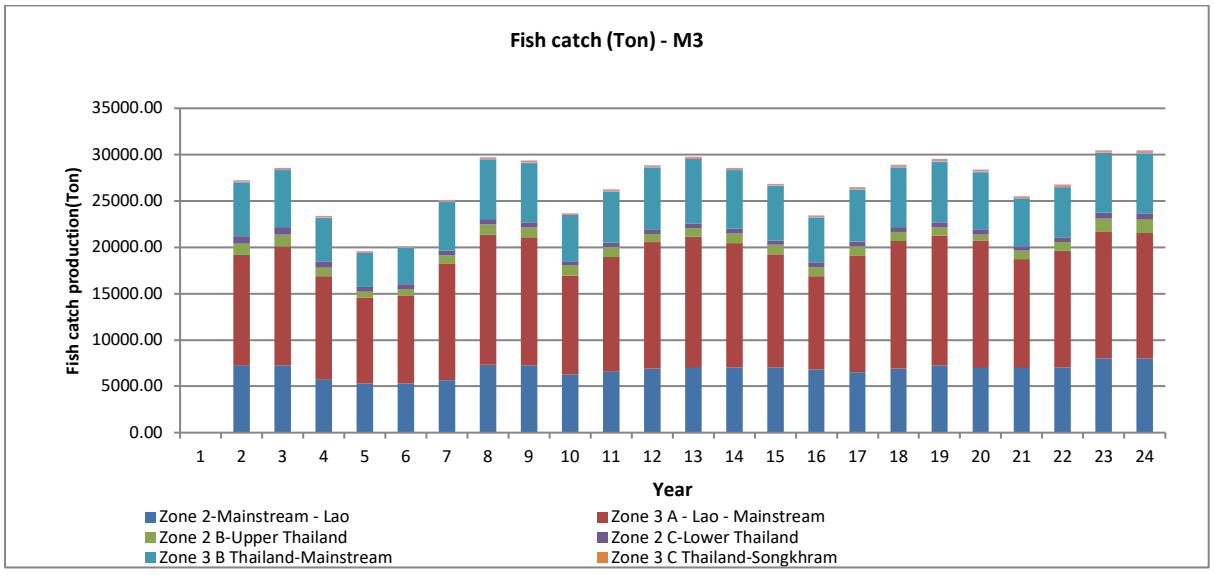

Figure 20. Annual variation of total floodplain fish production in the upstream Kratie impact corridor for the scenarios M1, M2 and M3.

Figure 21 shows the results of floodplain fish production for Zone 3A. Scenario C3 decreases further fish production compared to the other scenarios due to dryer conditions, decreased sediment transport and decreased flooding.

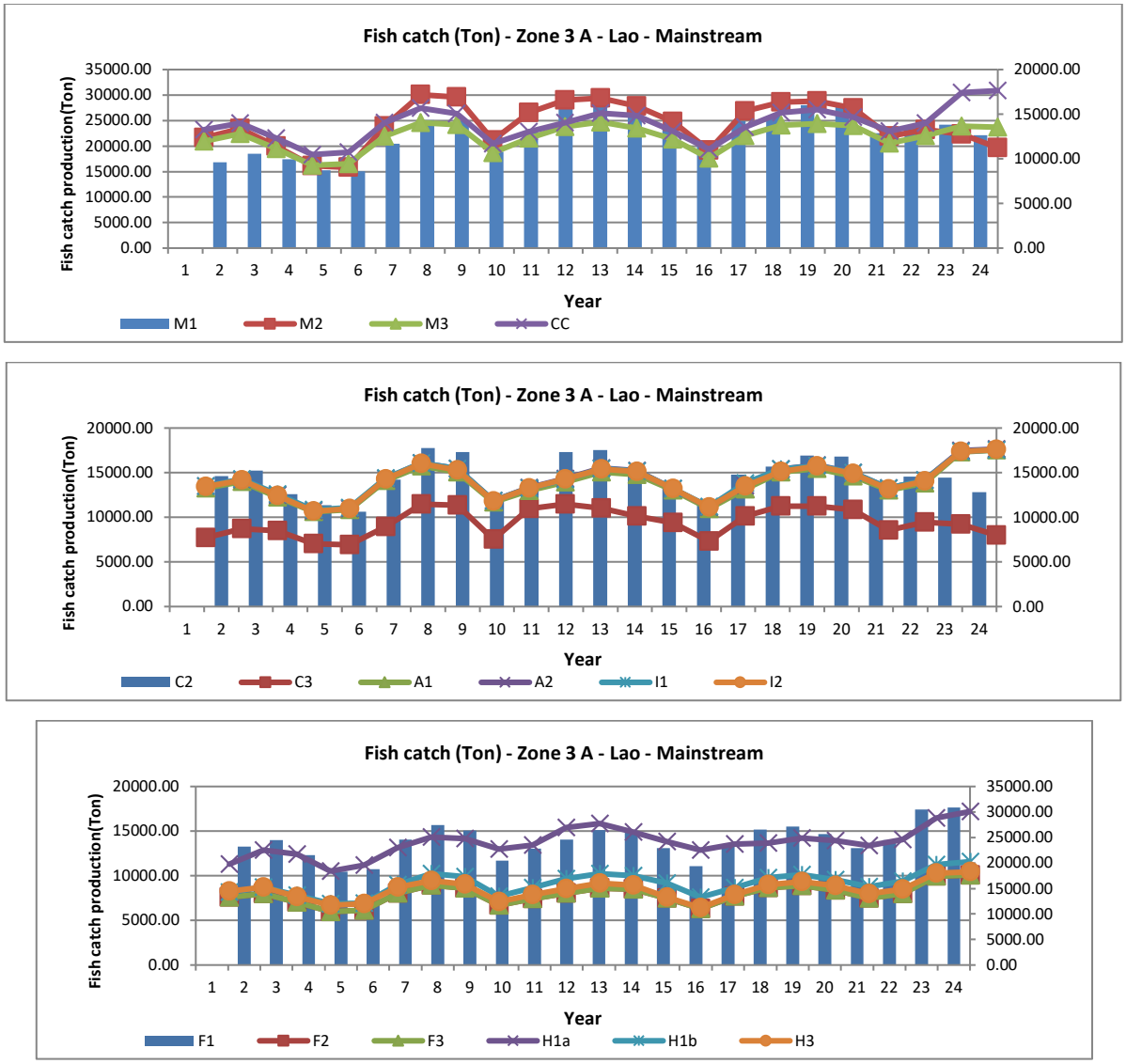

Figure 21. Total fish production in Zone 3A for all scenarios. Observe that scales are different for the bars (left scale) and for the time series (right scale).

5. Tonle Sap watershed scenario impacts

DSF modelling covers Tonle Sap watershed. This chapter focuses on complementary information on the climate change scenario impacts on water security, watershed erosion and crop yields. Special focus is on the climate change scenario C3 which is dryer and has larger impact than scenarios C1 and C2.

As no station climate projections for the Tonle Sap were not available precipitation projections have been computed with the IWRM modelling software based on the SIMCLIM projections obtained for Phnom Penh precipitation. SWAT projections have been available, but they are not for the original observation stations used in the IWRM model. An example of monthly average precipitation for the different climate scenarios is shown in Figure 22 for the Kampong Thom station for the year 1993. It can be seen that C3 is consistently drier than the other scenarios and October and November have increased precipitation for October and November compared to the baseline observed values.

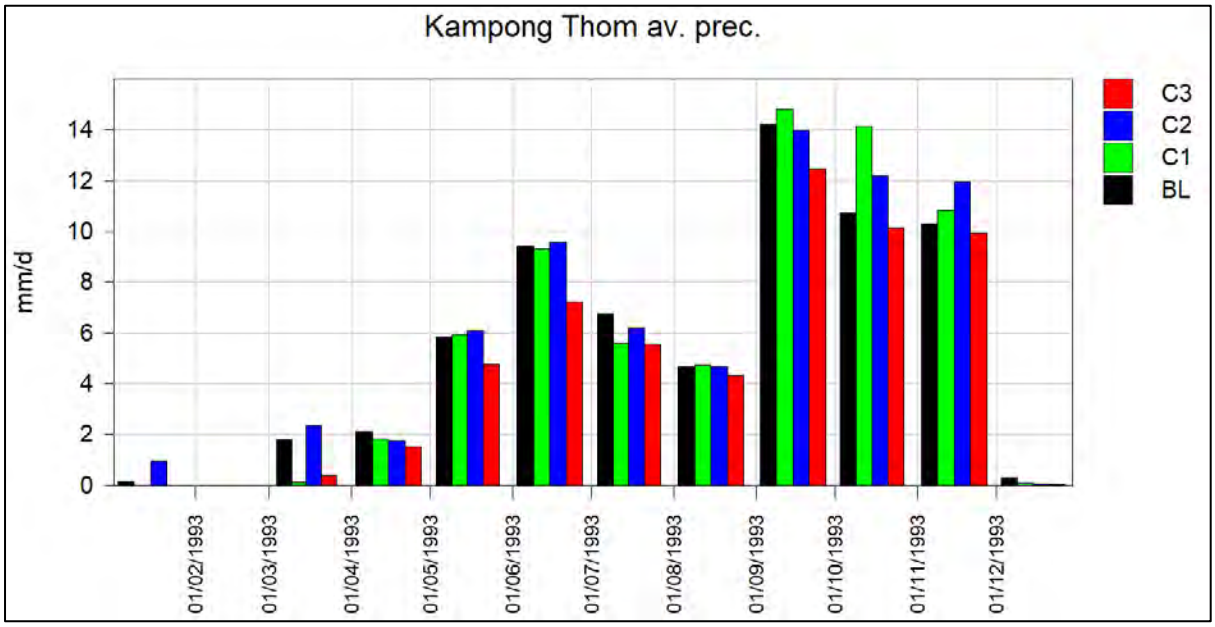

Figure 22. Kampong Thom average monthly rainfall during 1993. C1, C2 and C2 rainfall is projected from BL rainfall to the 2040 climate.

Decreased rainfall, hotter temperatures and increased evaporation affect the water security in the Tonle Sap watershed for the scenario C3. In Figure 23 shows dry season model soil layer 2 (0.2 m – 3 m) water content. The soil in scenario C3 is up to 50% drier than in the baseline.

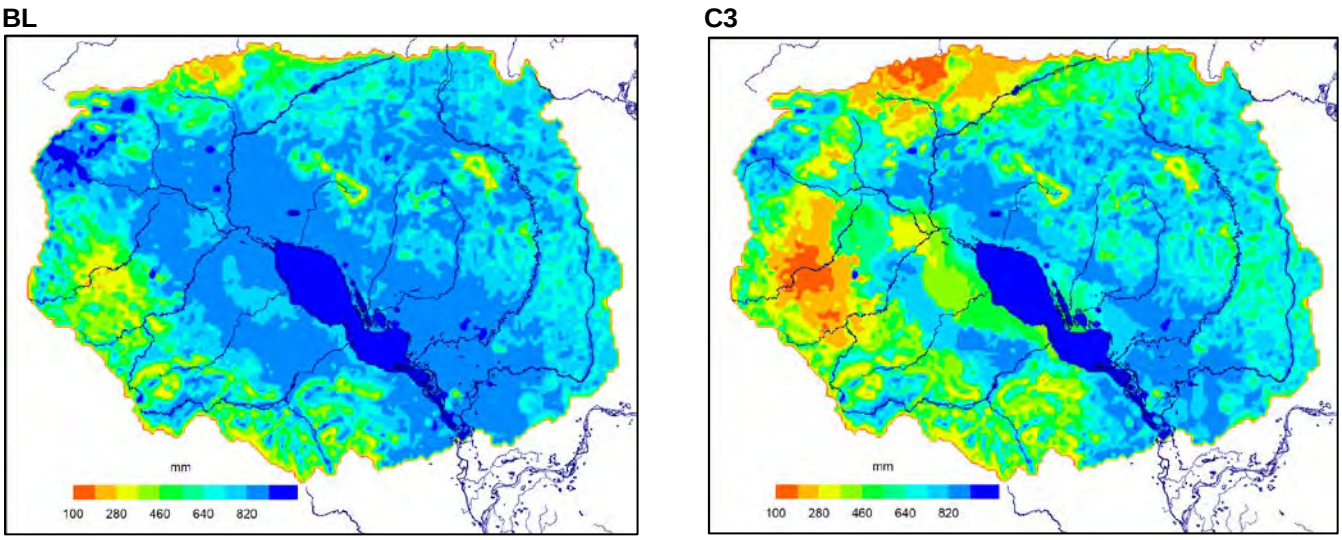

Figure 23. Model soil layer 2 (depth 0.2 m – 3 m) average water content for the dry season.

The drier conditions affect also groundwater as can be seen in the Figure 24: drier conditions drive groundwater deeper into the ground. It should be noted that the groundwater model has not been calibrated nor verified with monitoring data, so the results are illustrative and indicative only.

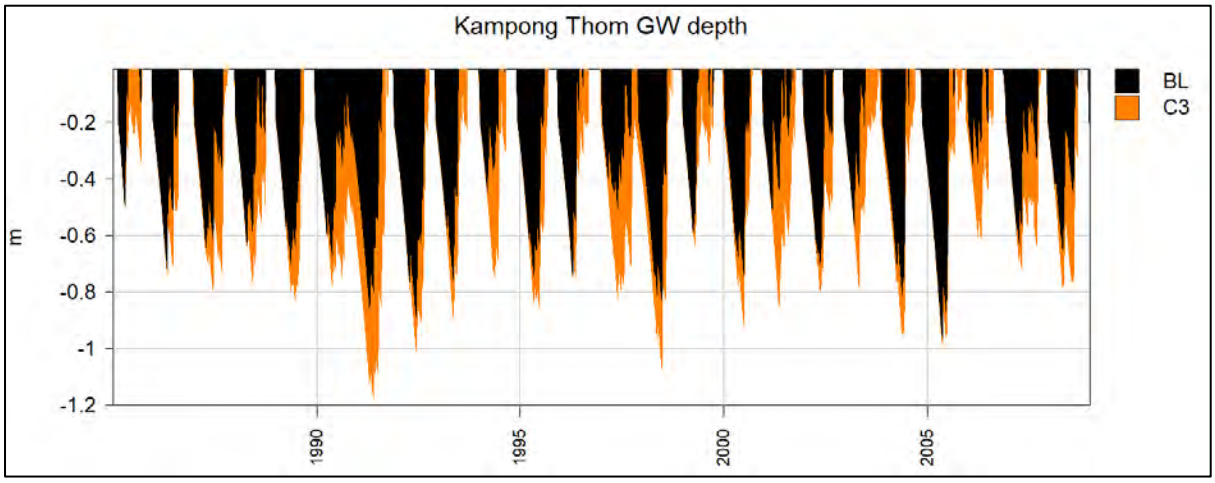

Figure 24. Groundwater depth in Kampong Thom for the baseline (BL) and C3 scenarios.

Rainfall affects soil erosion. Figure 25 shows Kampong Thom annual agricultural area erosion for climate change scenarios BL, M3CC, C2 and C3. C3 has consistently decreased erosion compared to the other scenarios.

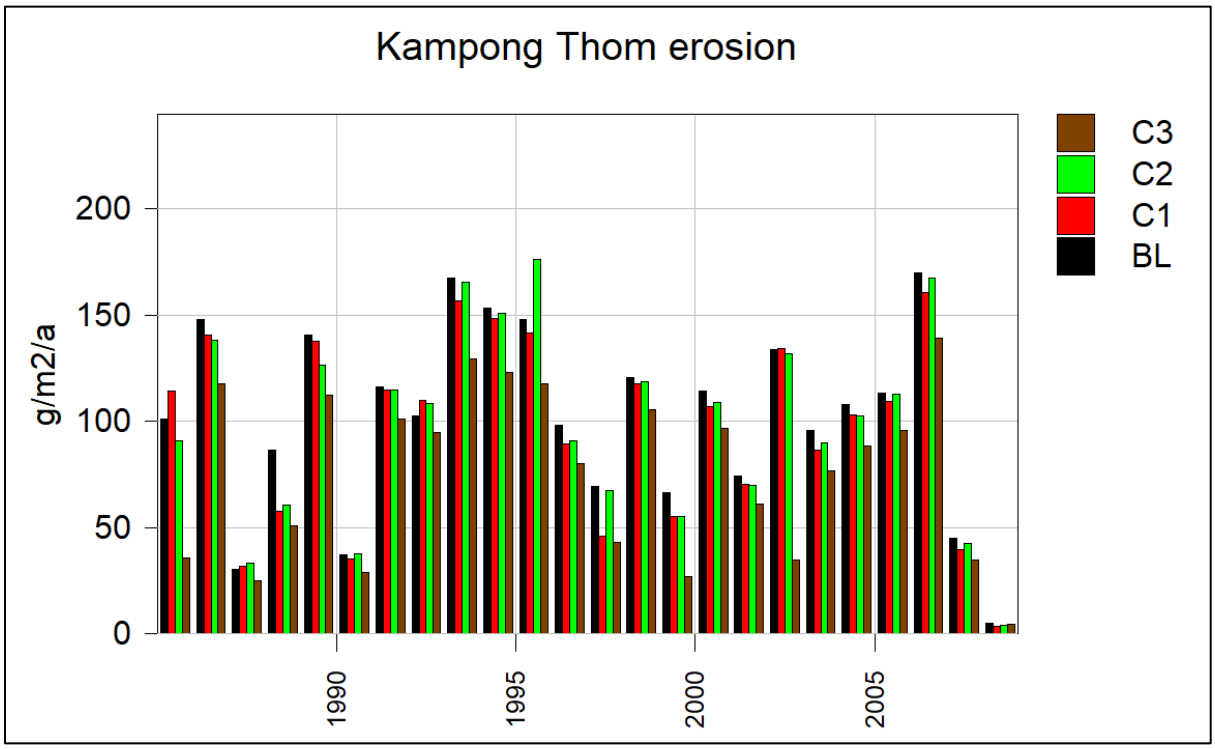

Figure 25. Kampong Thom annual agricultural area erosion for the climate scenarios BL, C1 (M3CC), C2 and C3.

Kampong Thom non-irrigated rice production is shown in Figure 26. The production shows rice failure for the years 1987, 1990 and 2008. Overall the climate scenarios C1, C2 and C3 have decreasing effect on production but the decrease is pronounced for C3. In the scenarios rice is planted mid-June.

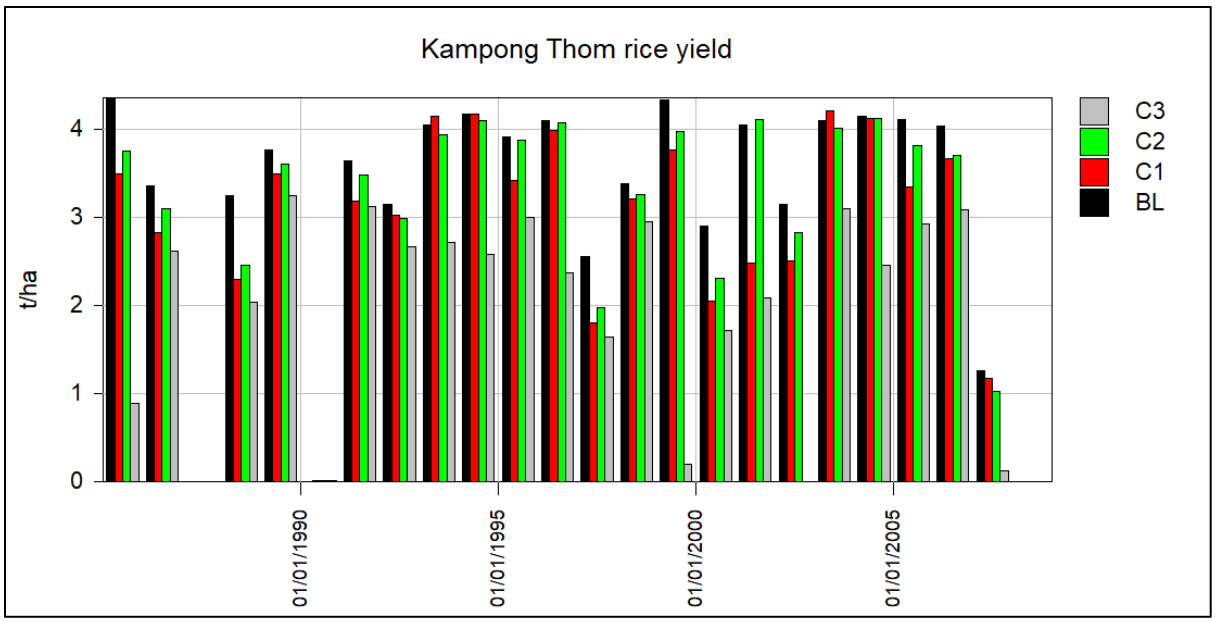

Figure 26. Kampong Thom rice production for the climate scenarios BL, C1 (M3CC), C2 and C3.

Figure 27 shows map of average non-irrigated rice production. The production decrease is pronounced and most critical in the South-Western part of the basin.

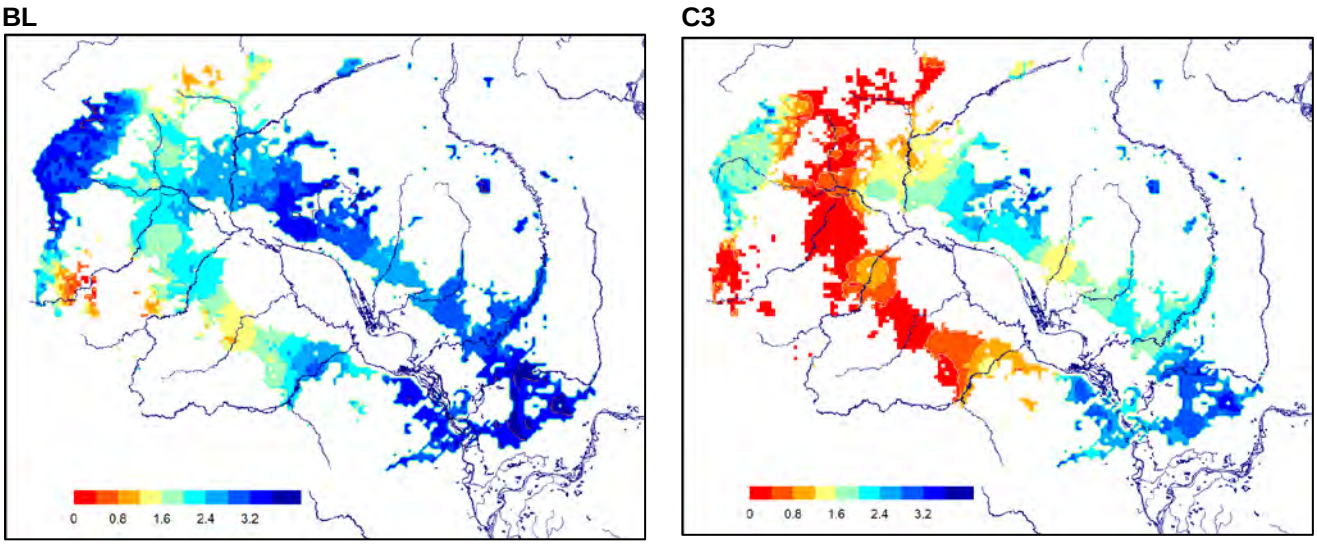

Figure 27. Average non-irrigated rice yields for mid-June planting.

Figure 27 and Figure 28 show irrigation demand in the baseline and change in the dry C3 climate scenario for dry and wet season rice. The wet season rice irrigation (Figure 27) is supplementary. The figures present irrigation demand as an average over the 24 CS simulation years. Both the baseline and irrigation demand and change in C3 are very heterogeneous. The wet season irrigation demand varies between 8000 m^3/ha for higher hilly area to 2000 m^3/ha to near-Mekong flat areas. The dry season irrigation demand varies between 15'000 m^3/s to 9000 m^3/s. The additional irrigation demand in C3 for wet season is 800 – 1800 m^3/s and for dry season 400 – 1100 m^3/s.

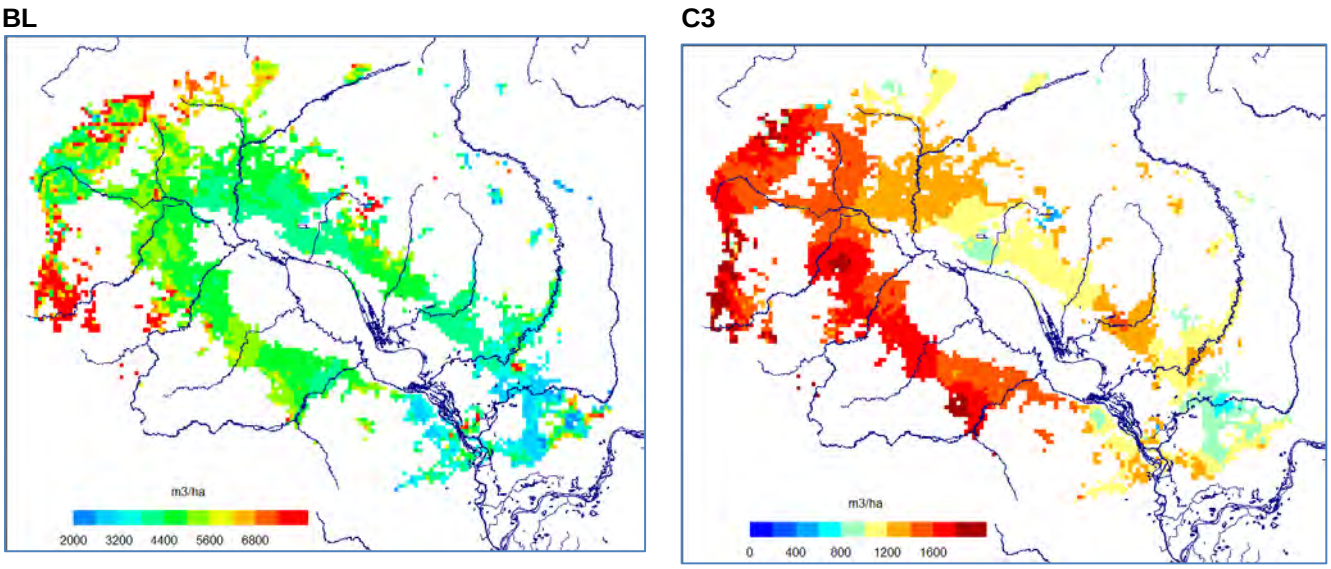

Figure 28. Average supplementary irrigation demand for rice planted in mid-June. Left baseline and right change in the dry C3 climate scenario.

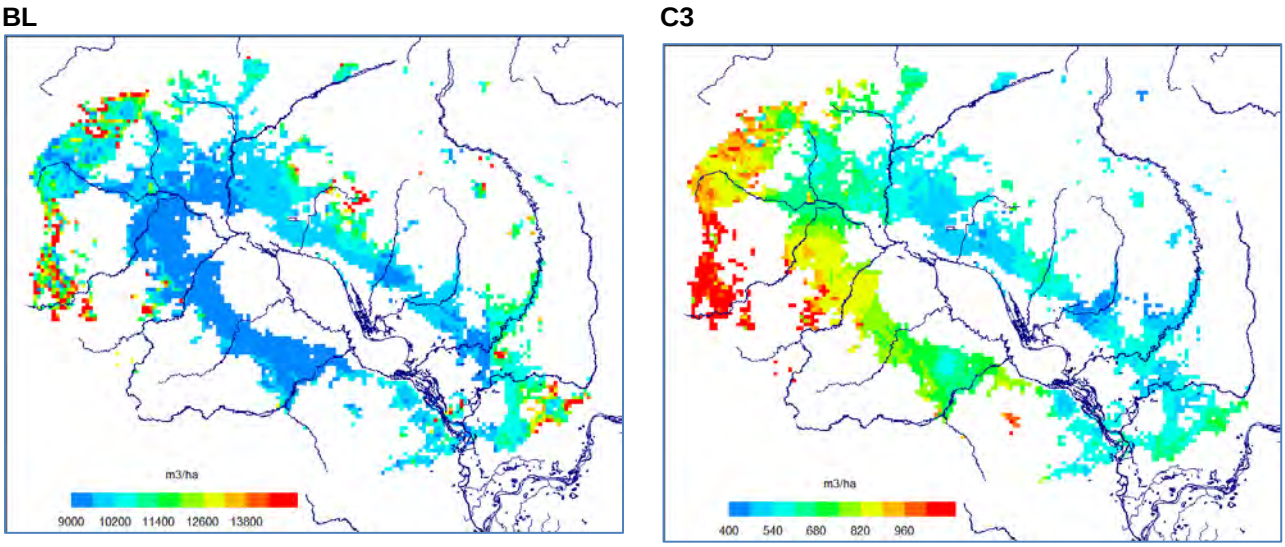

Figure 29. Average supplementary irrigation demand for rice planted in early January. Left baseline and right change in the dry C3 climate scenario.

6. Tonle Sap lake and floodplain scenario impacts

The main impact of scenarios to fish production occurs in Cambodia, Vietnamese Delta and the coastal areas. Tonle Sap is similarly affected by reduced alluvium (sediment, organic material and nutrients) input as the Delta although not as pronouncedly. However, in Cambodia and especially in the Tonle Sap socio-economic impact of reduced fish production is much more severe than in the Vietnamese Delta because population is more dependent on fisheries and less resilient to adapt in the reduced fisheries production. In the Delta the fisheries production has already suffered from local development and better economic conditions buffer fisheries losses.

Tonle Sap 3D hydrodynamic, water quality and fisheries model has been developed since 2001. The fish production depends on alluvium input, primary production, flooding, predation etc. The mode is described in detail in the ANNEX. Results of the model have been utilized by the bio-assessment (BioRA) including flooding, sediment, primary productivity (phytoplankton, periphyton, terrestrial) and oxygen. Here only fisheries assessment results are presented.

Figure 30 shows main scenario impacts on fisheries. It can be seen that production concentrates on specific areas where currents, wave action, sedimentation and resuspension transport alluvium. Sedimentation concentrates on the near-lake floodplains where submerged and over water vegetation dampens flow and wave action and net sedimentation is effective. In the lake proper suspended sediments maintain nutrients and phytoplankton production which is valuable food source for fish. When upstream sediment input to the lake is reduced in the development is reduced also the fish production suffers.

The inter-annual variation of Tonle Sap total fish production for the main scenarios is shown in Figure 31. Year-by-year variation is high. The most critical dry year fisheries production decreases from 250’000 t to 150’000 in the M3 and M3CC scenarios due to decreased sediment input.

BL

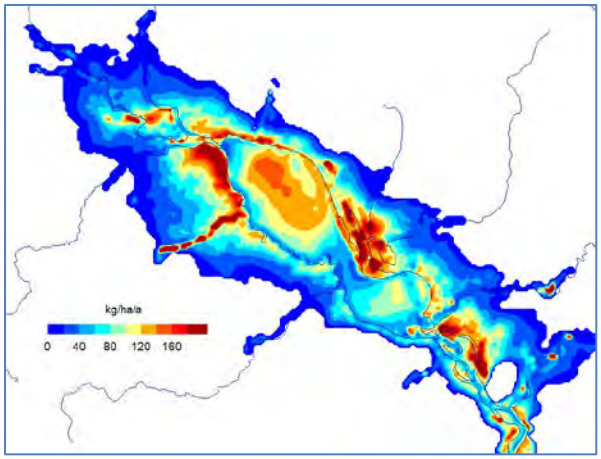

2020

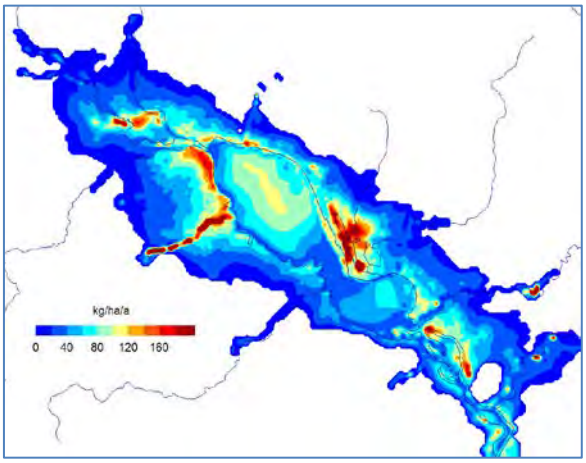

2040

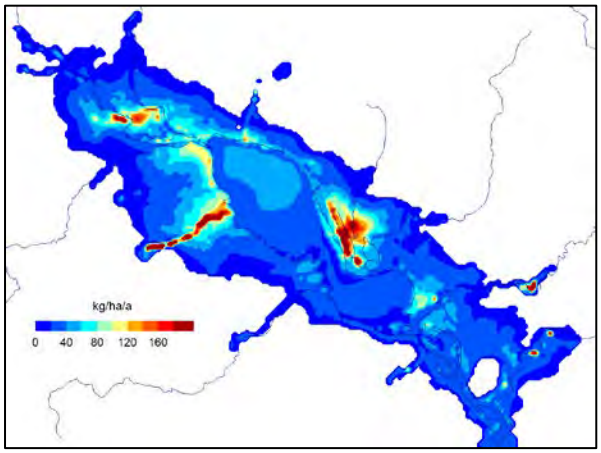

2040CC

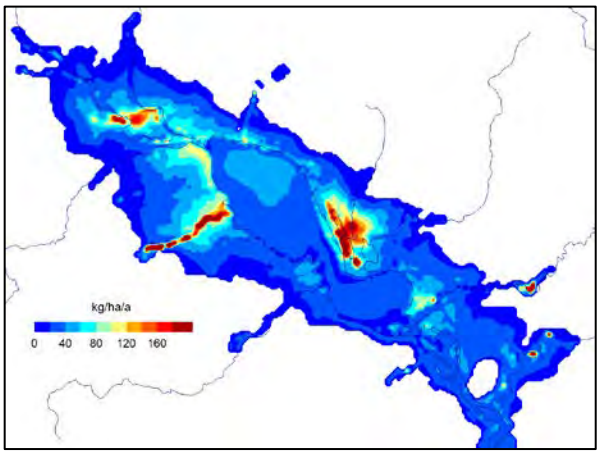

Figure 30. Main scenario average annual fisheries production.

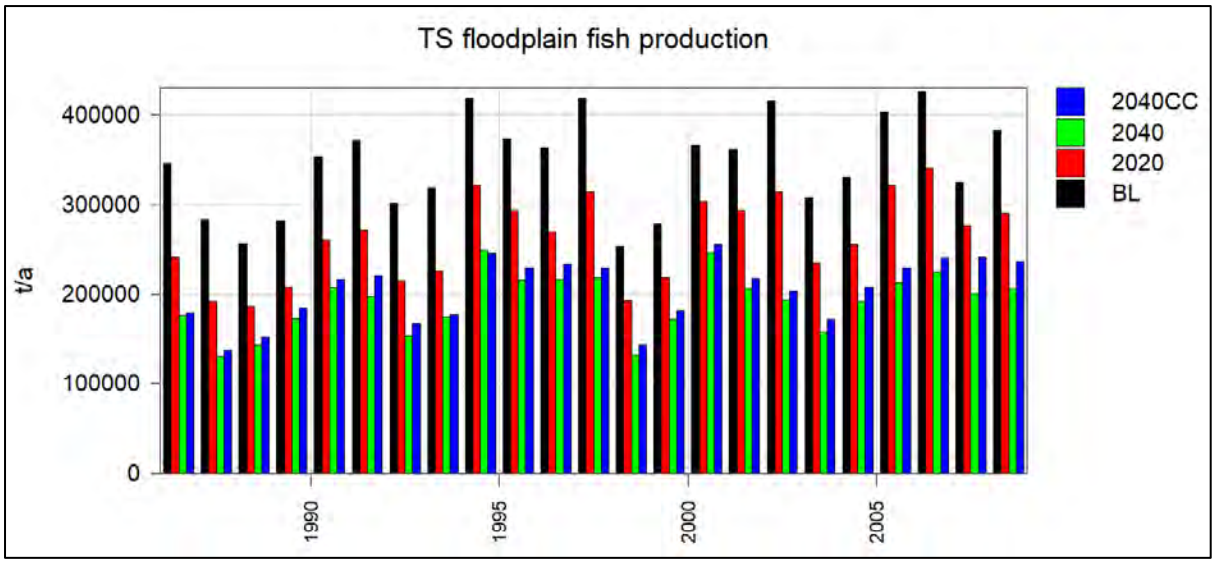

Figure 31. Main scenario annual fisheries production.

Tonle Sap fisheries production for all of the scenarios is shown in Figure 32 (floodplain) and Figure 33 (lake proper). In the floodplain 2040 scenarios (2040, 2040CC, C2 etc.) reduce fisheries production in the floodplain about 40%. In the lake proper reduction is about 70%. This is because floodplains are more influenced by the tributaries and have more buffer capacity for production whereas the lake is strongly affected from the Mekong. The exceptions for these reductions are H1a and H1b and to some extent H3 which maintain much better upstream sediments and Tonle Sap productivity.

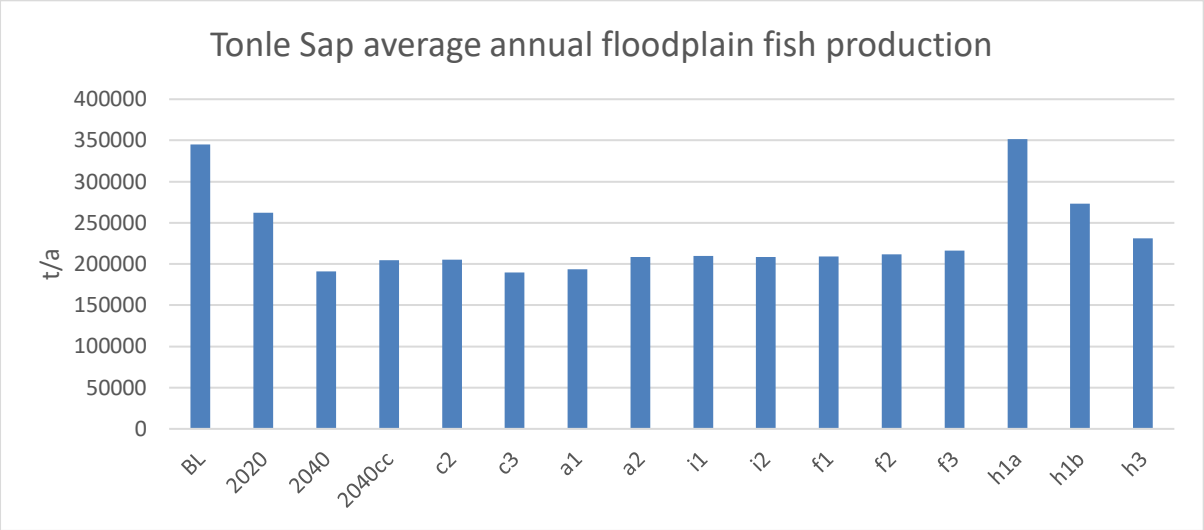

Figure 32. Tonle Sap average annual fisheries production for the floodplain

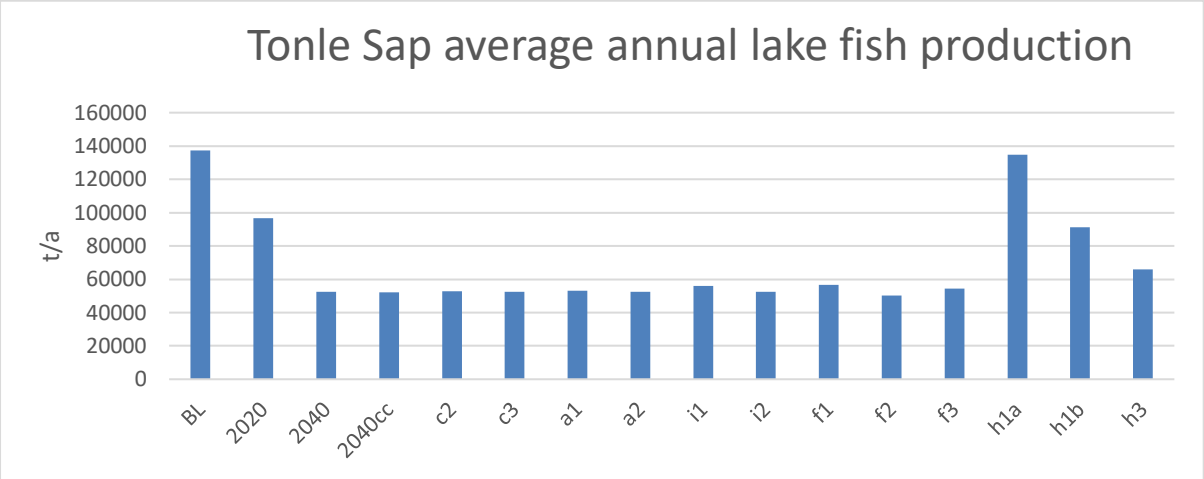

Figure 33. Tonle Sap average annual fisheries production for the lake

7. Cambodian floodplains and Delta scenario impacts

7.1. Factors affecting Delta conditions

This chapter presents some examples of the modelling results. Main part of the model results analysis and utilization comes through discipline (socio-economic and biological) and thematic/sector groups.

The lower part model approach is in principle same as for the upper part. Although the modelling approach is the same using combined ISIS and IWRM models, the characteristics of the upper and lower LMB are very different. The main difference is dominance of floodplains in the lower part.

Flooding

Figure 34 shows baseline flood duration and change in 2040 and 2040CC scenarios. For the most part flood duration decreases in the future development scenarios except for some areas in the flood periphery. Also, extreme flood events are reduced as the hydropower reservoirs store peak flood water (Figure 35, 2040 scenario). Climate change can on the other hand increase peak flooding even with the extensive hydropower development ((Figure 35, 2040CC scenario).

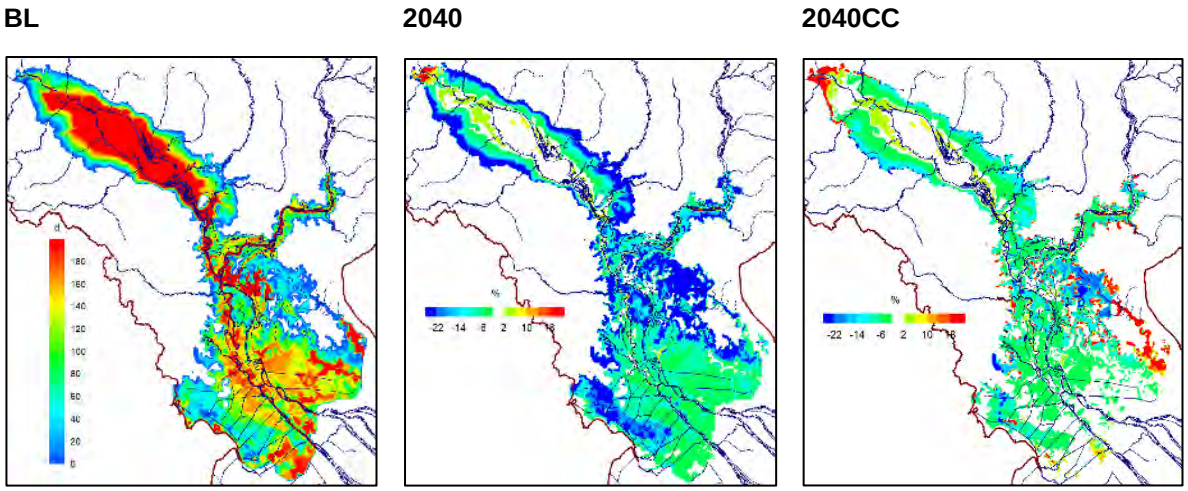

Figure 34. Average flood duration in the baseline (left), 2040 change (middle) and 2040CC change (right).

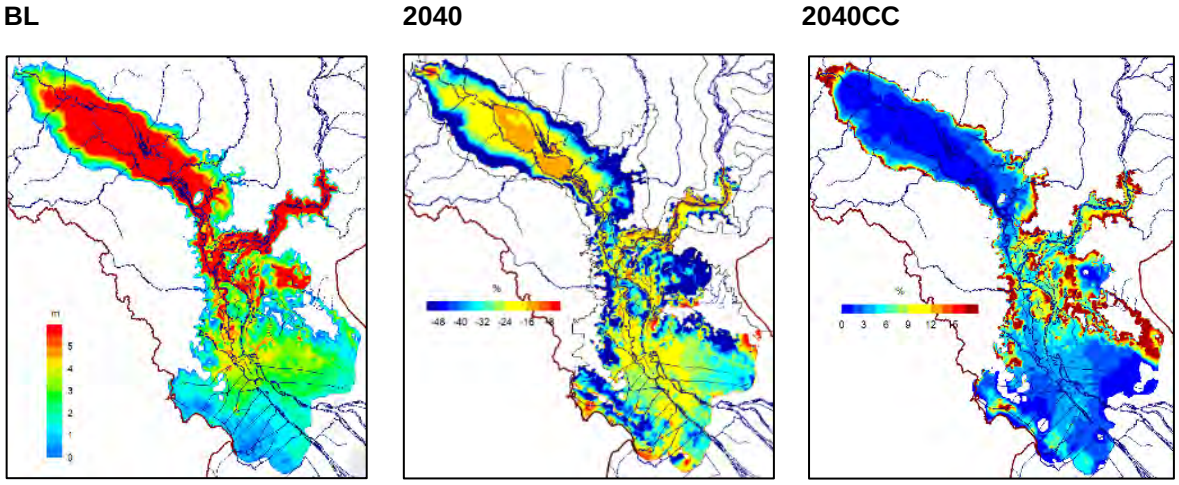

Figure 35. 100-year flood depths in the baseline (left), 2040 change (middle) and 2040CC change (right).

Flooding and rice production

Flooding is beneficial for rice production in providing fertile soil to paddies, flushing harmful substance from soils and recharging soil water. On the other hand too much flooding can slow down rice growth or damage it through long submersion. In Figure 36 shows rice yield when rice is planted mid-June and change for M3 scenario. The scenario is hypothetical in the sense that farmers would not plant rice when flood damages are expected but it illustrates clearly how hydropower development in M3 and other scenarios reduces flooding and increases yields for wet season rice not protected against flooding.

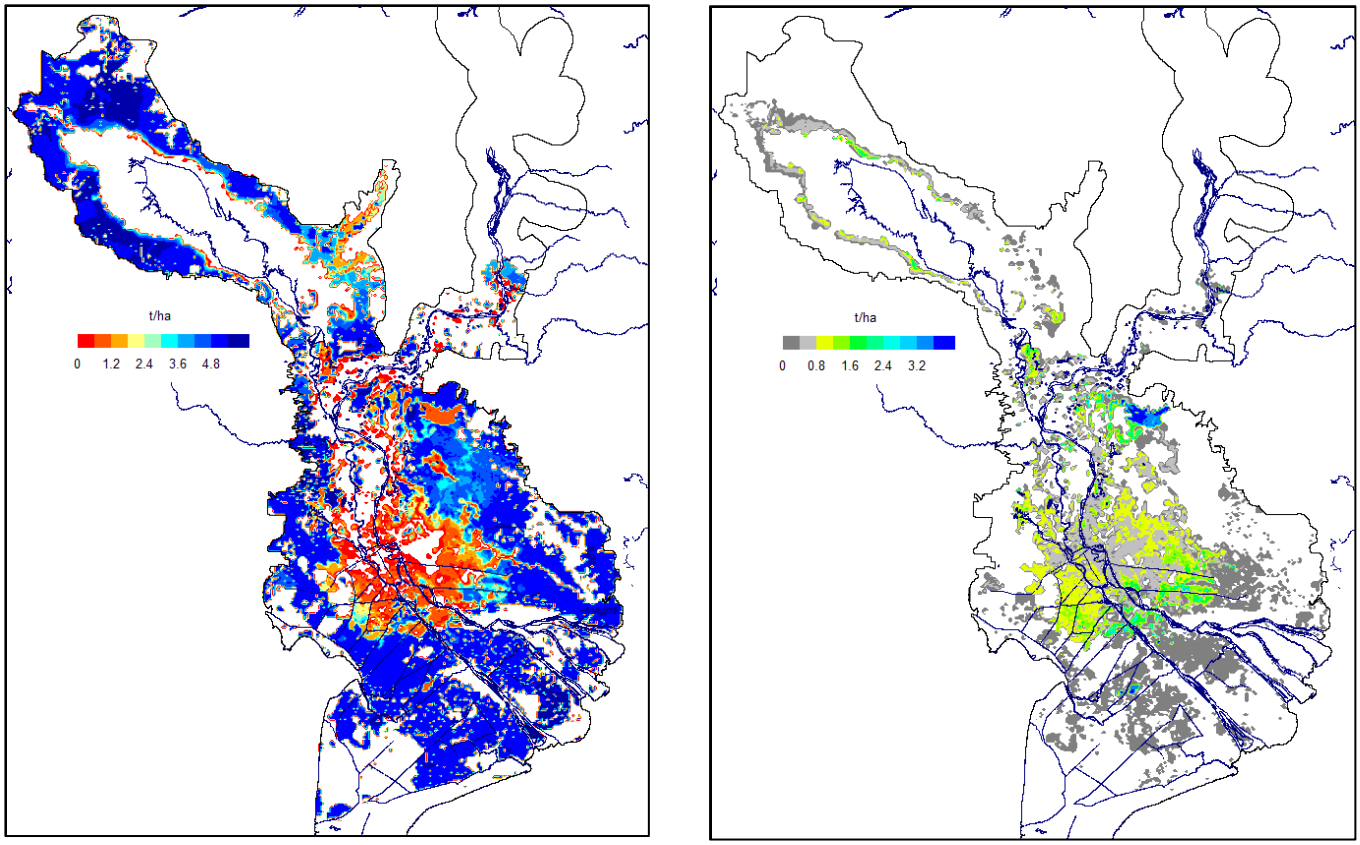

Figure 36. Flooding impact on no-flood protected rice production. Left baseline for rice planted mid-June and right yield increase in the M3 scenario.

Soil fertility and rice production

In addition to flooding rice production depends on soil fertility. Mekong alluvium (fertile sediments and organic material) improves soil quality and supplies nutrients to both natural and agricultural primary production. In agriculture lack of alluvium can be compensated through soil management and addition of fertilizers but they may be costly and time-consuming efforts. Only adding chemical fertilizers to paddies doesn't necessarily work in the long run as the soil quality tends to suffer reducing productivity.

Figure 37 shows how clay sedimentation is reduced in the M2 and M3 scenarios. In M2 sedimentation is third of the baseline and in M3 sedimentation is one tenth of that in M2. The reduction in rice

production between baseline and M3 is shown in Figure 38. In the flooded areas rice reduction is between 0.1 and 1 t/ha. It should be noted that flood damages are not included in this analysis.

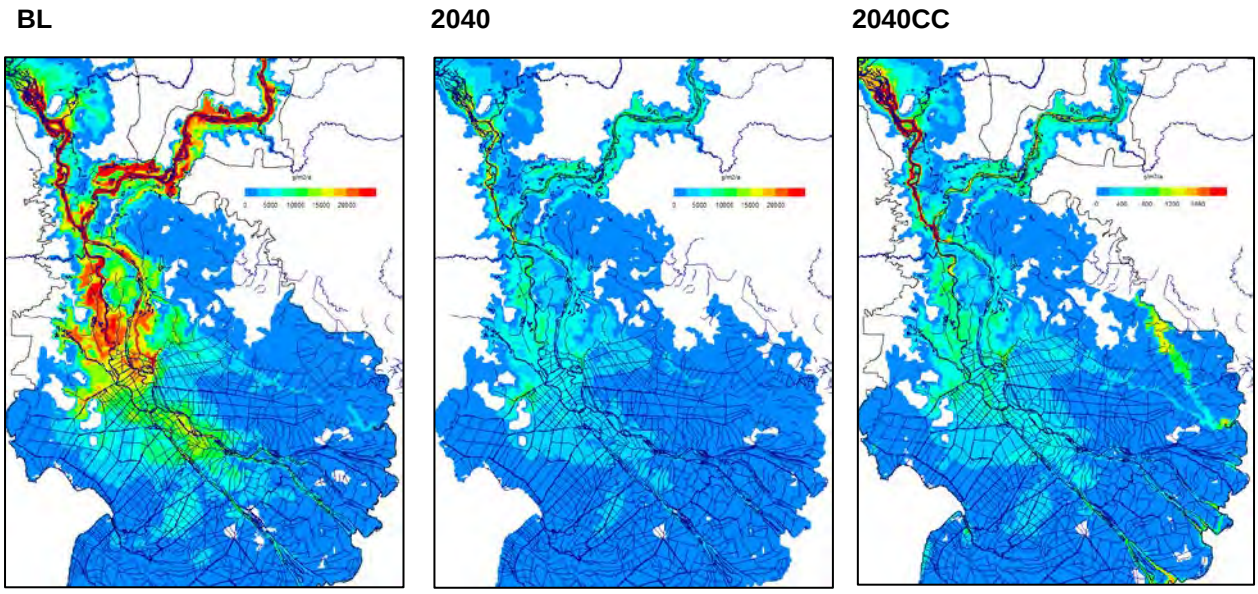

Figure 37. Sedimentation in the floodplains.

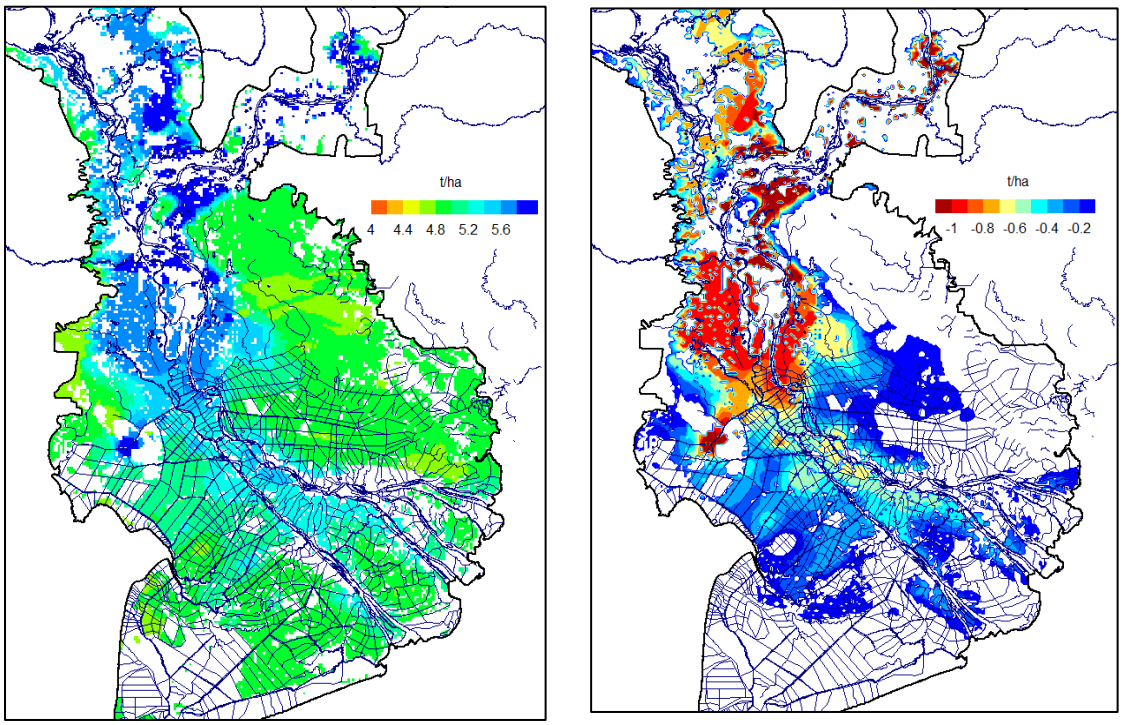

Figure 38. Sediment impact on rice production. Left baseline and right decrease of rice production in scenario M3. No flooding impact included.

Drought

Member countries assess drought larger problem than flooding as the countries have adapted living with floods and floods are essential for proper functioning of the Mekong system. There are many indicators for flooding also available from modelling such as crop yield. Figure 39 shows another indicator which is number of months when precipitation is less than half of potential evapotranspiration (PET). The main climate change scenario has only marginal impact on this indicator.

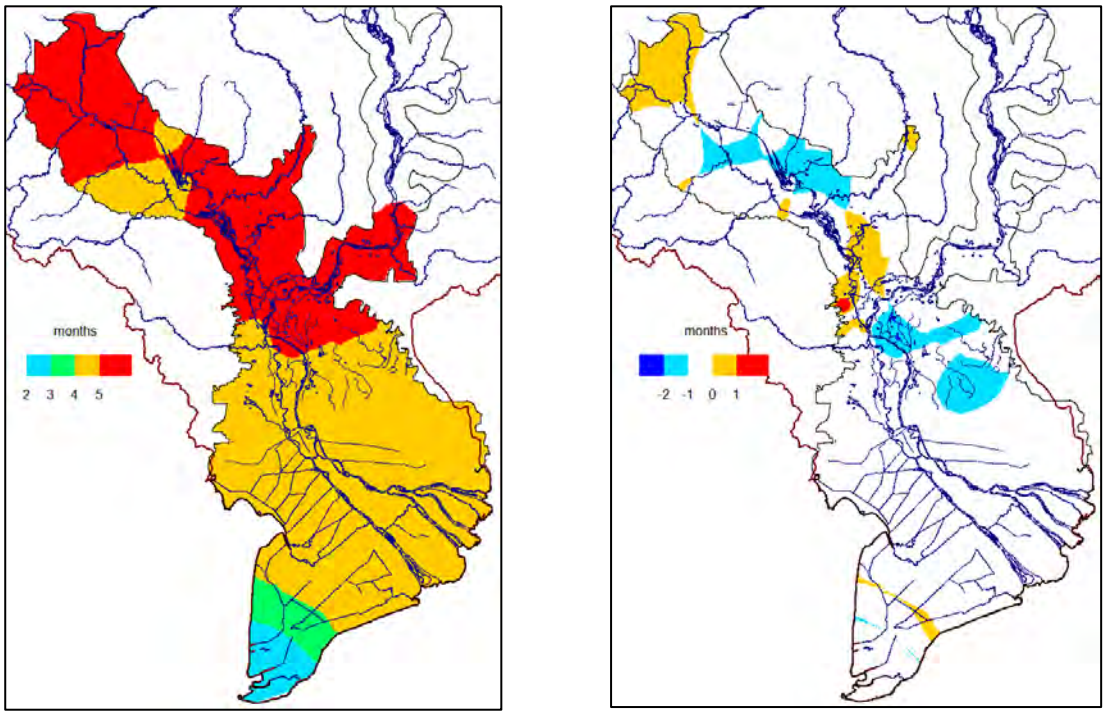

Figure 39. Average number of drought months in the baseline (left) and change in the 2040CC scenario.

Salinity intrusion and rice production

Future scenarios change salinity intrusion through changes in river discharges and sea level rise. This is shown in Figure 41 where the hydropower development in scenario M3 increases freshwater river discharge and lowers salinity.

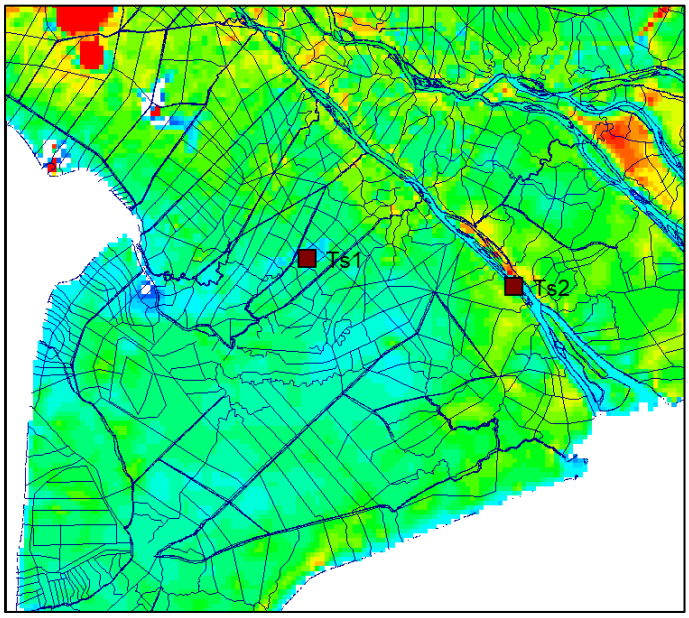

Figure 40. Salinity times series locations.

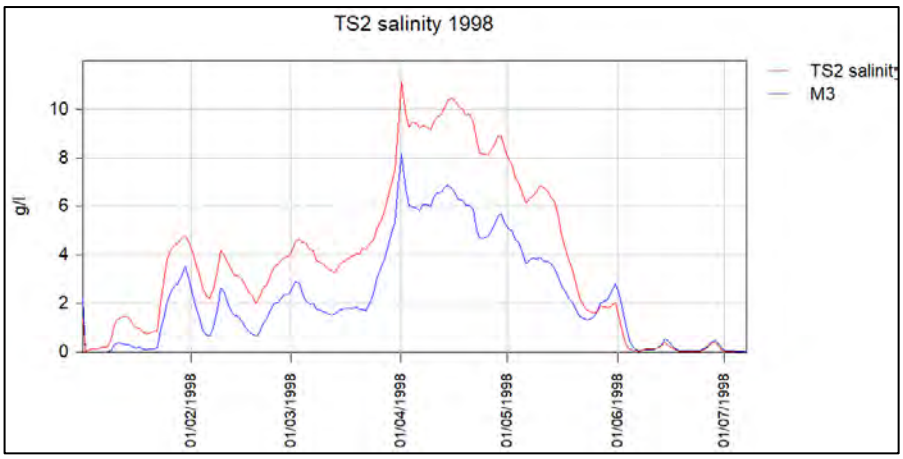

Figure 41. Salinity the Bassac River location TS2 (see Figure 40).

Because the discharge changes in the future scenarios also flooding changes. Figure 42 shows for location TS1 in the floodplains (see Figure 40) increased water level peaks in scenario M3. These increase average salinity in this specific location. Figure 43 shows on a map the effect of combined salinity and flooding changes on salinity index. The index is sum of flooding duration x salinity.

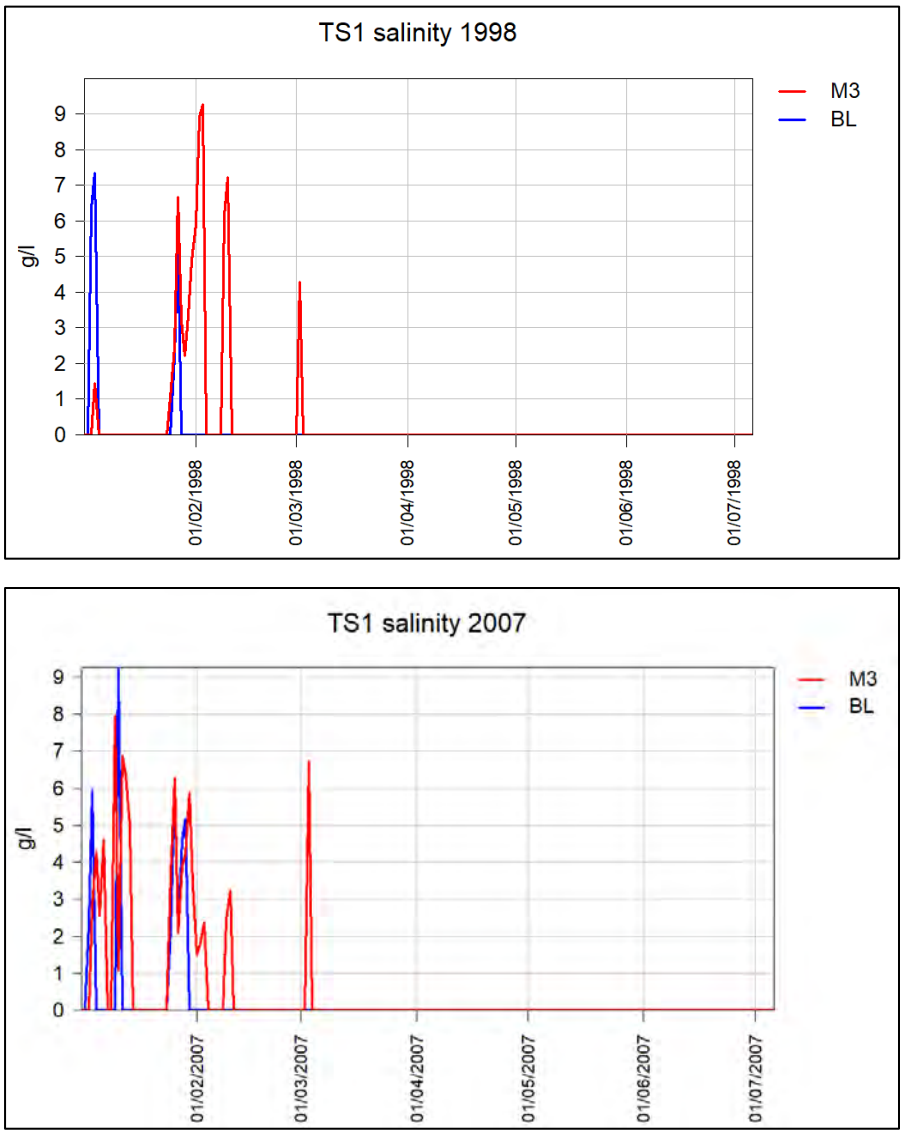

Figure 42. Salinity the Bassac River location TS2 (see Figure 40).

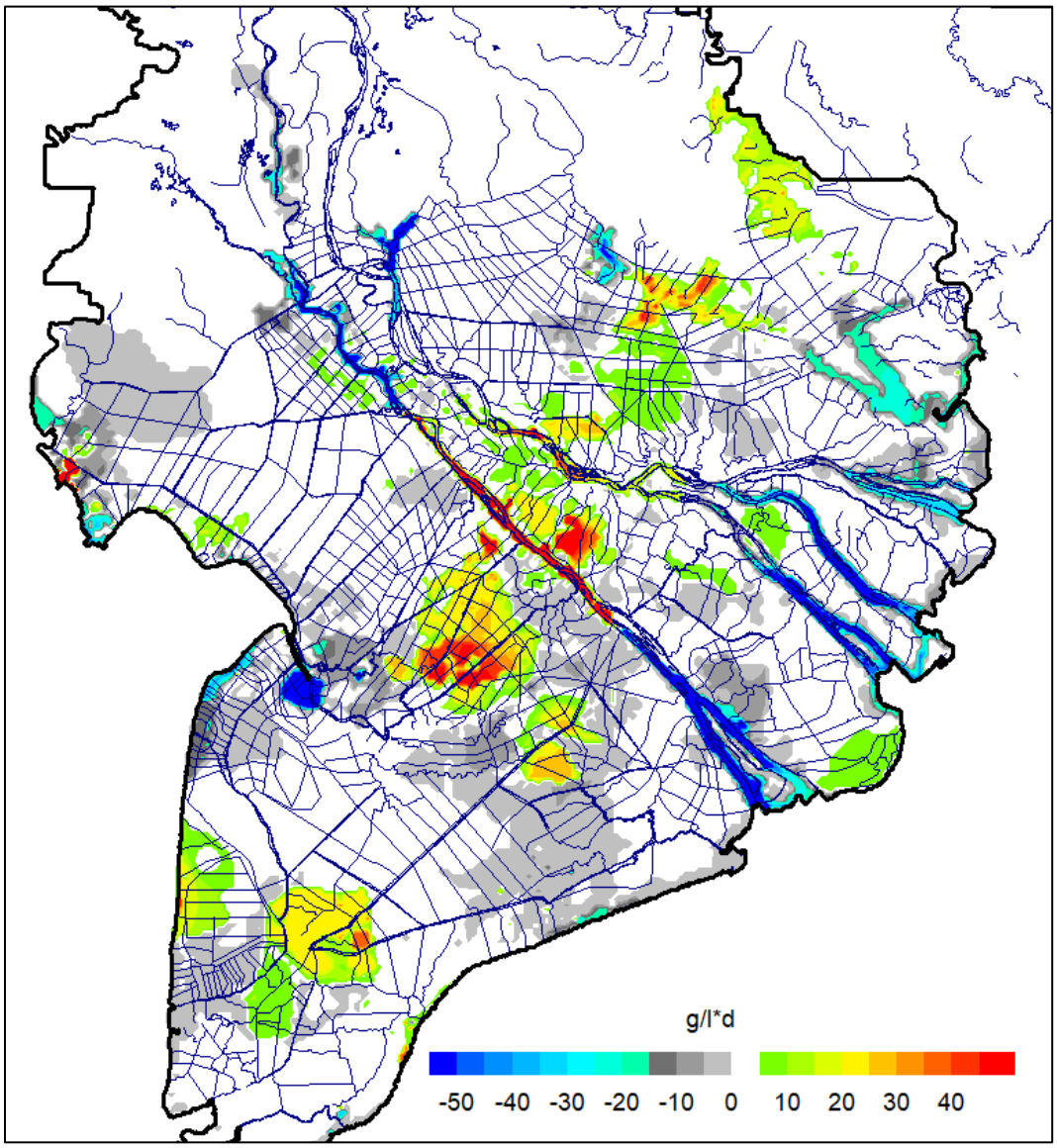

Figure 43. Areas of decreased (blue-grey) and increased salinity (green-red) during 1998 dry season. Salinity is described through index = flood duration x average salinity during flooding

Another way of looking at the salinity intrusion and its impacts is through average salinity only (Figure 44). This describes both flooded areas and irrigated paddies and other agricultural areas using river and channel water. Salinity changes are complex because of changing flood protection, water regulation, upstream flow and sea level rise.

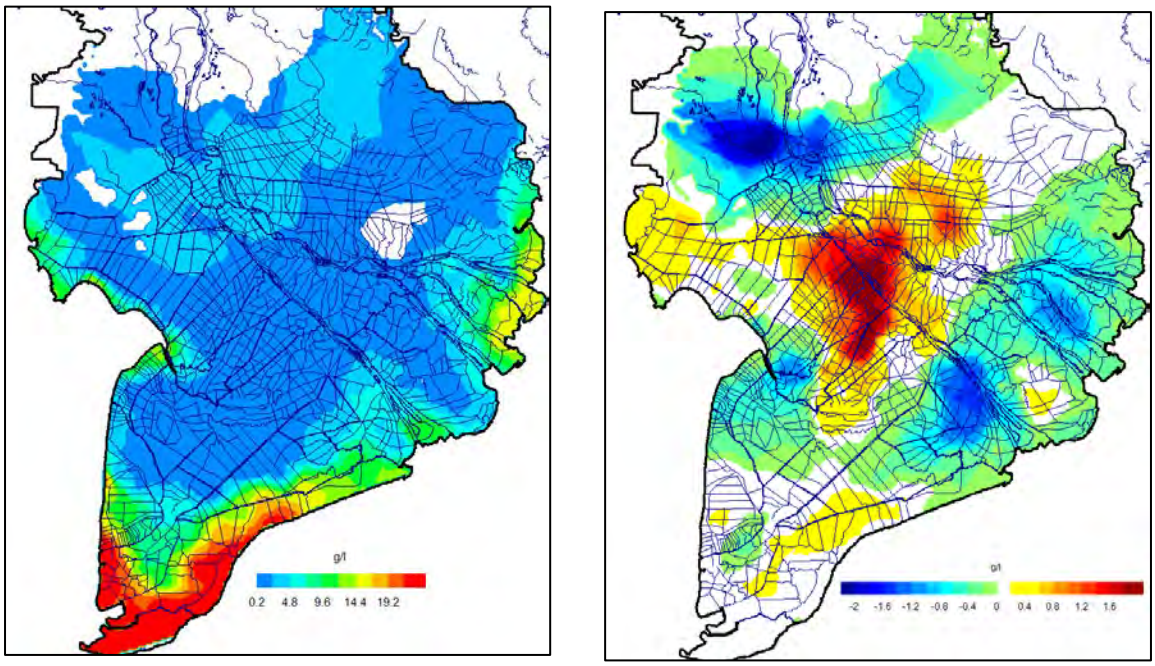

Figure 44. Average dry season baseline salinity in 1998 (left) and change in scenario M3.

Salinity intrusion in the Delta affects rice growth. Figure 45 shows change of dry season irrigated rice production in the Delta for the three main development scenarios. Due to increased dry season flow and decreased salinity intrusion (for the main part), there is small increase in dry season rice production. Interpretation of the results is not straightforward as sea level rise is included in 2040CC and not in 2040 scenario.

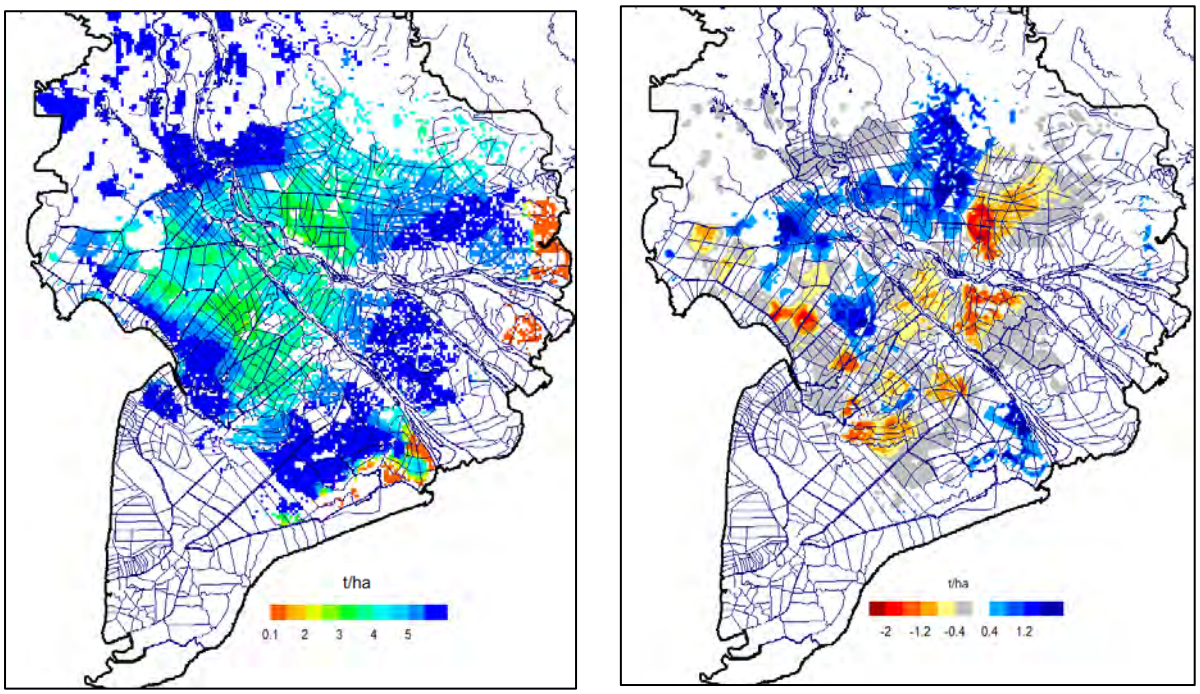

Figure 45. Baseline irrigated rice production in 1998 (left) and change in M3 scenario.

Fisheries production

Figure 46 shows large impact of decreased alluvium input in the future scenario fish production. 11. Fisheries production changes least in the area between Mekong Mainstream and the Tonle Sap River. In the central Cambodian floodplains fisheries production decreases up to 70% In the Vietnamese Delta production decreases 50% - 70%. In Vietnam the fisheries reduction needs to be considered in context of high water regulation, aquaculture production and economic resilience. Cambodia is much more vulnerable to the reduction than Vietnam through its high dependency on capture fisheries and less economic buffer capacity.

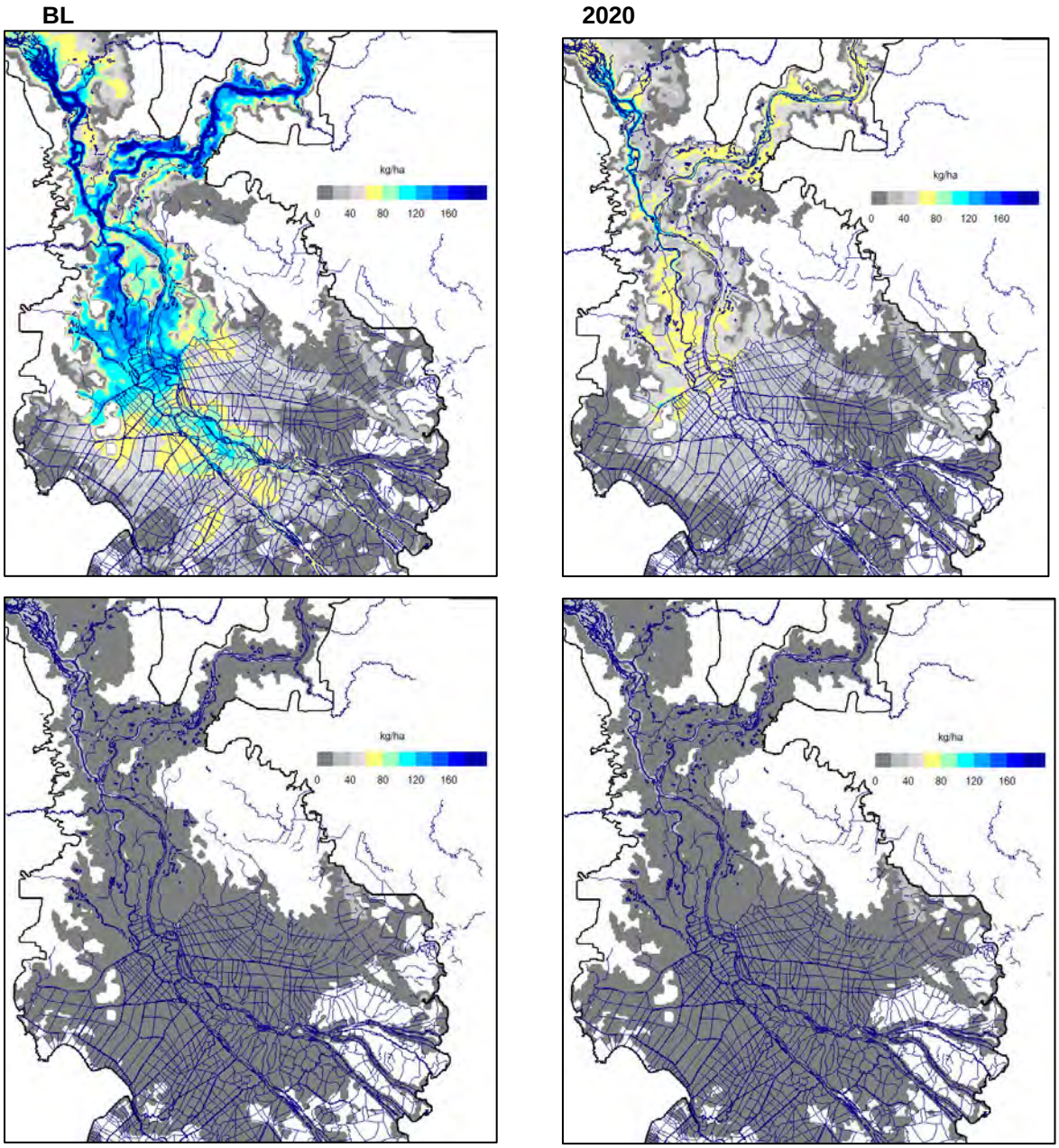

Figure 46. Baseline average floodplain fish production for the scenarios M1 - upper left (baseline), M2 – upper right (2020), M3 – lower left (2040) and M3CC - lower right (2040CC)

Shrimp production and saline and brackish water wild species

Shrimp aquaculture is only partly dependent on natural salinity as farmers can add salt to shrimp ponds. However, the shrimp growth indicates also conditions for brackish and saline water species in the wild. Figure 30 shows the complex changes in shrimp growth that reflect changes in upstream flow, flood protection, water regulation, sea level rise and salinity intrusion computed by the ISIS model.

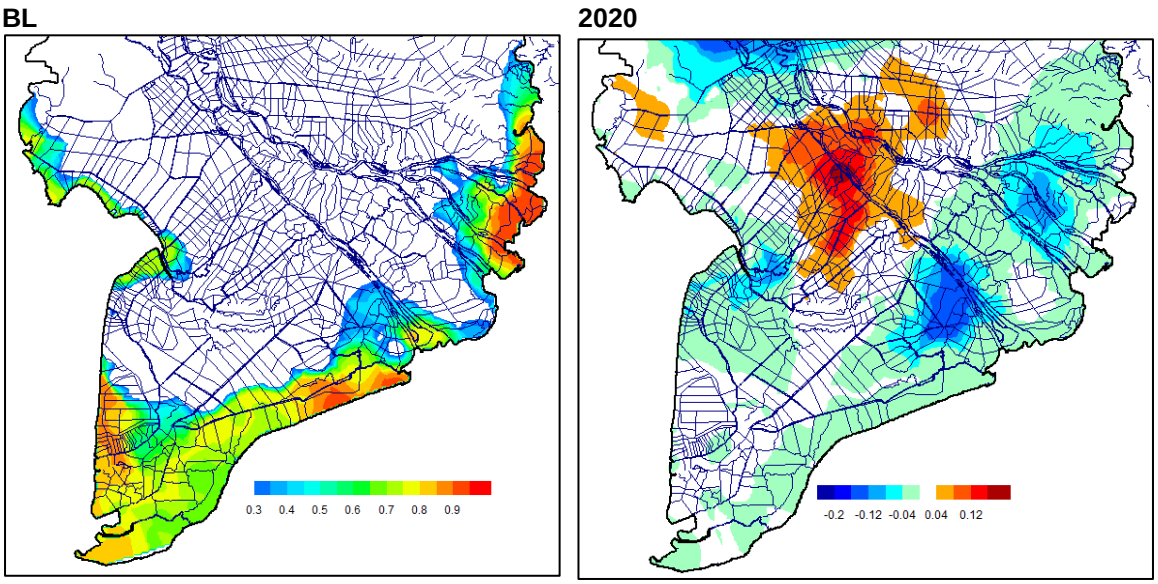

Figure 47. 1998 baseline average shrimp growth index (left) and change in the M3 scenario (right). Index 1 indicates maximum growth and index 0 no growth.

7.2. Scenario results for flooding characteristics

The results in this and subsequent chapters are presented for the Zones 4C (Cambodia from Kratie to Vietnam border), 6A (Vietnam Delta freshwater), 6B (central saline Vietnam Delta) and 6C (Cà Mau Peninsula) (see).

Flooded areas remain relatively constant for Zone 4C. In the coastal provinces sea level and flood protections affect flooding and flooded areas change more. The flooded areas are divided basically into two groups with and without sea level rise (Figure 48 and Figure 49). The former include here M1, M2, M3 and M3CC and the latter rest. The exception for the rule is flood protection scenario F1 which decreases flooding to the baseline level. It should be noted that in the model flooding areas depend on ISIS water levels in the river channels and are not affected directly by flood protections. This exaggerates flooding areas. In the future, when maps of flood protections become available, dykes can be implemented in the model.

Figure 48. Zone 6A annual flooded area

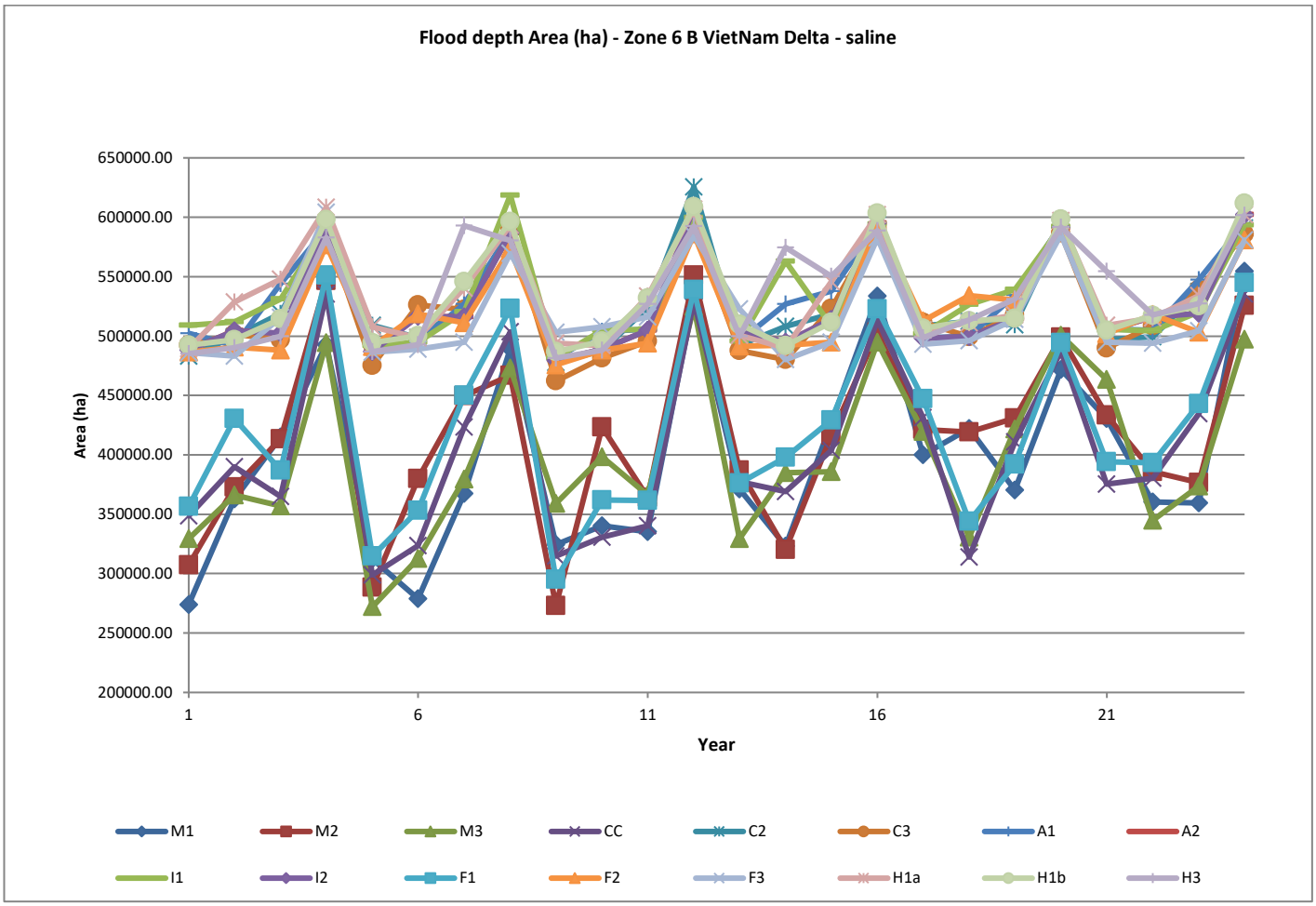

Figure 49. Zone 6B annual flooded area

Average annual flood depth for all scenarios is shown in Figure 50. Baseline has the highest average flood depth values whereas the dry C3 scenarios has lowest. Hydropower construction lowers the flooding depths.

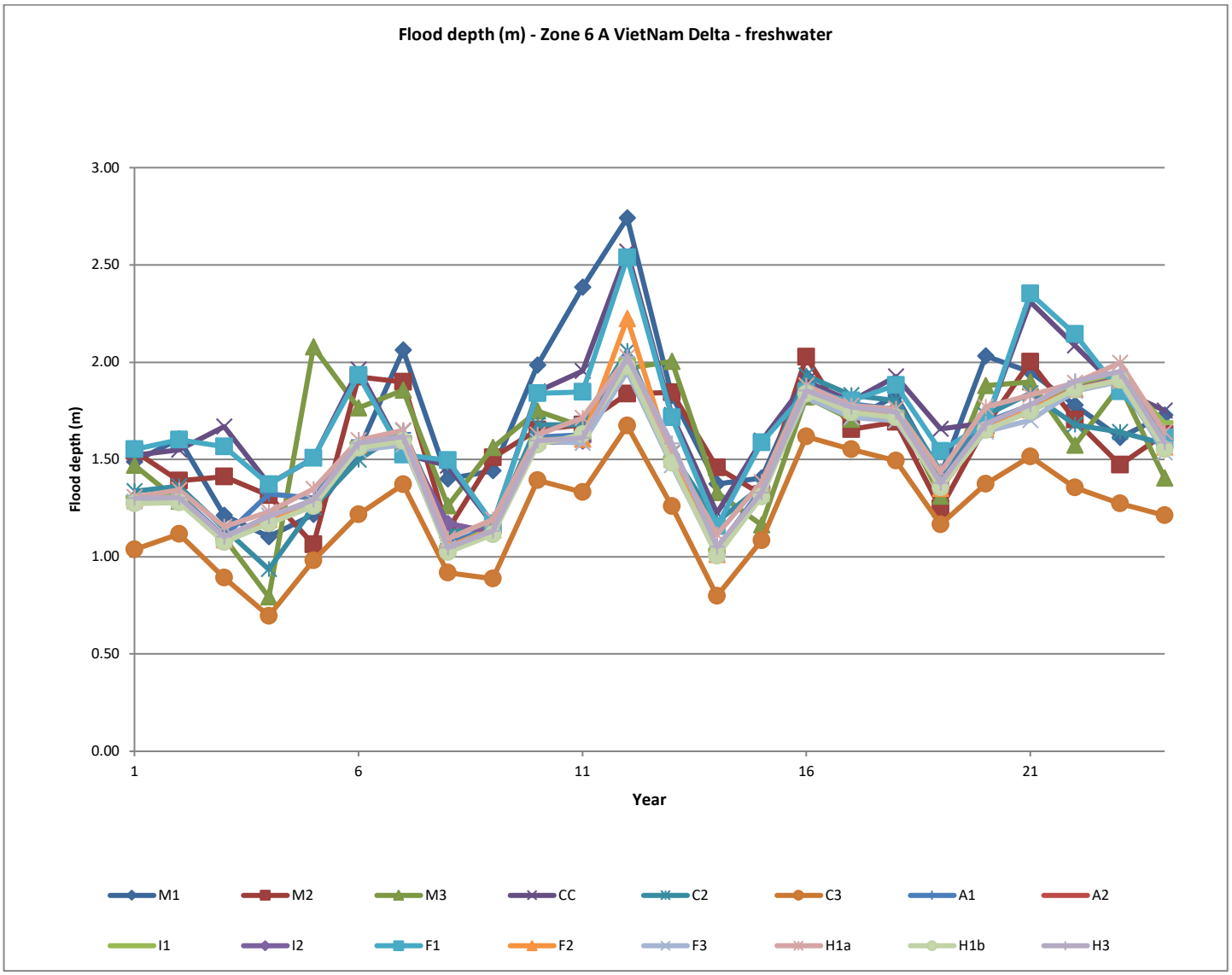

Figure 50. Average annual flood depth for Zone 6A.

7.3. Scenario results for sedimentation

Clay has been taken here as an indicator for overall sedimentation. It indicates soil fertility and Delta system productivity. Also silt and sand have been also computed with the model but as the productivity model has been calibrated for the clay only the other results are not presented.

Based on the Figure 51 the highest sedimentation rates in the Delta are in Zones 4C and 6A. This is logical as these are central areas having strongest impact from the Mekong. Scenario M2 collapses sedimentation rates about 70% and M3 further halves them. The M3CC climate change scenario slightly increases the rates compared to the M3 due to more intense rainfall and watershed erosion increasing downstream sediment loads. These very large changes in sediment input to the floodplains have major impact to the productivity of the Delta system as can be seen from the subsequent chapters for rice and fish production.

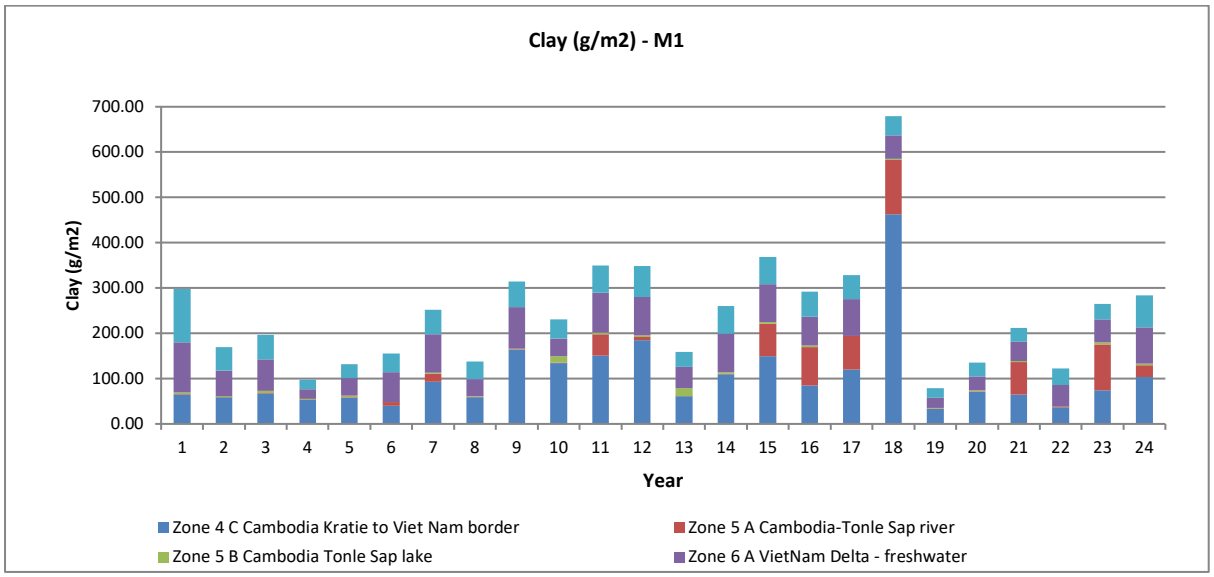
Clay (g/m2) - M1
700.00
600.00
500.00
400.00
300.00
200.00
100.00
0.00
Clay (g/m2)
1 2 3 4 5 6 7 8 9 10 11 12 13 14 15 16 17 18 19 20 21 22 23 24
Year
Zone 4 C Cambodia Kratie to Viet Nam border
Zone 5 A Cambodia-Tonle Sap river
Zone 5 B Cambodia Tonle Sap lake
Zone 6 A VietNam Delta - freshwater

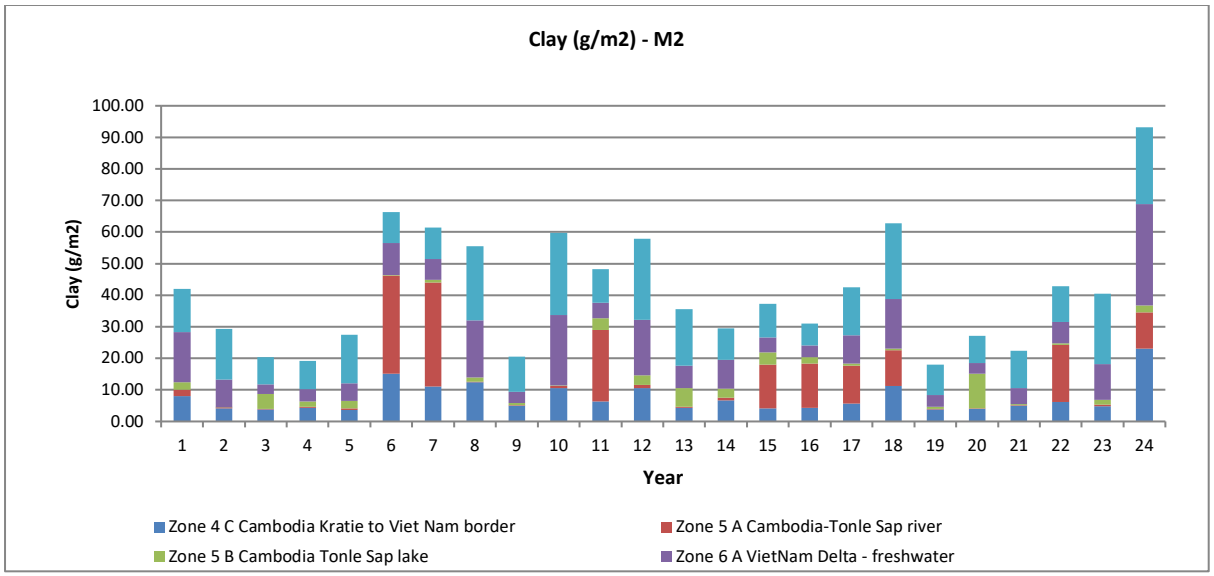
Clay (g/m2) - M2
100.00
90.00
80.00
70.00
60.00
50.00
40.00
30.00
20.00
10.00
0.00
Clay (g/m2)
1 2 3 4 5 6 7 8 9 10 11 12 13 14 15 16 17 18 19 20 21 22 23 24
Year
Zone 4 C Cambodia Kratie to Viet Nam border
Zone 5 A Cambodia-Tonle Sap river
Zone 5 B Cambodia Tonle Sap lake
Zone 6 A VietNam Delta - freshwater

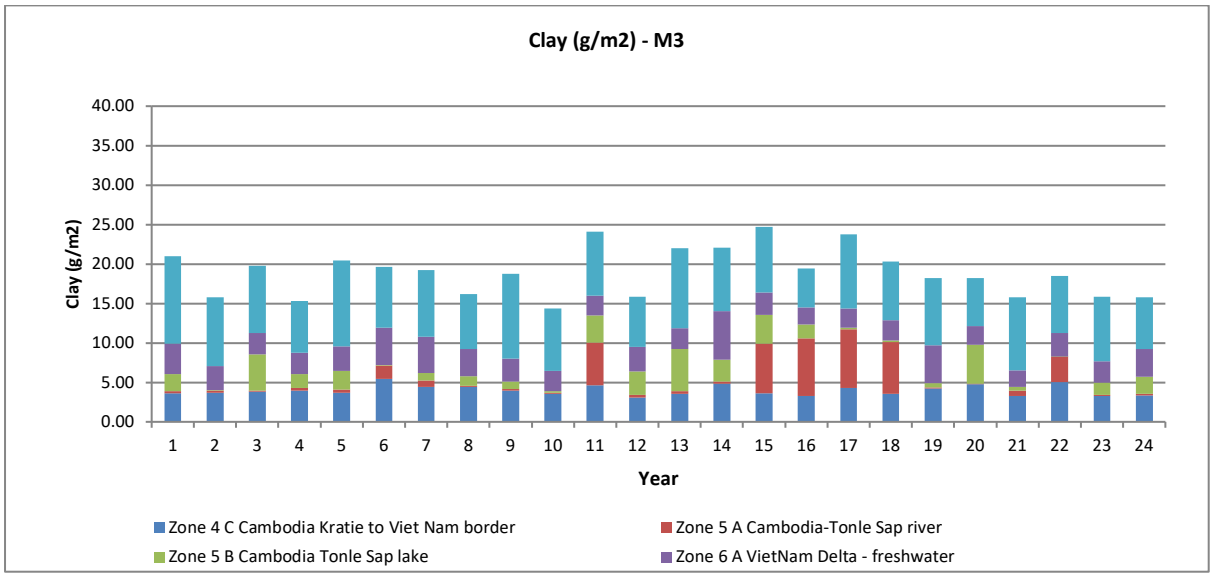
Clay (g/m2) - M3
40.00
35.00
30.00
25.00
20.00
15.00
10.00
5.00
0.00
Clay (g/m2)
1 2 3 4 5 6 7 8 9 10 11 12 13 14 15 16 17 18 19 20 21 22 23 24
Year
Zone 4 C Cambodia Kratie to Viet Nam border
Zone 5 A Cambodia-Tonle Sap river
Zone 5 B Cambodia Tonle Sap lake
Zone 6 A VietNam Delta - freshwater

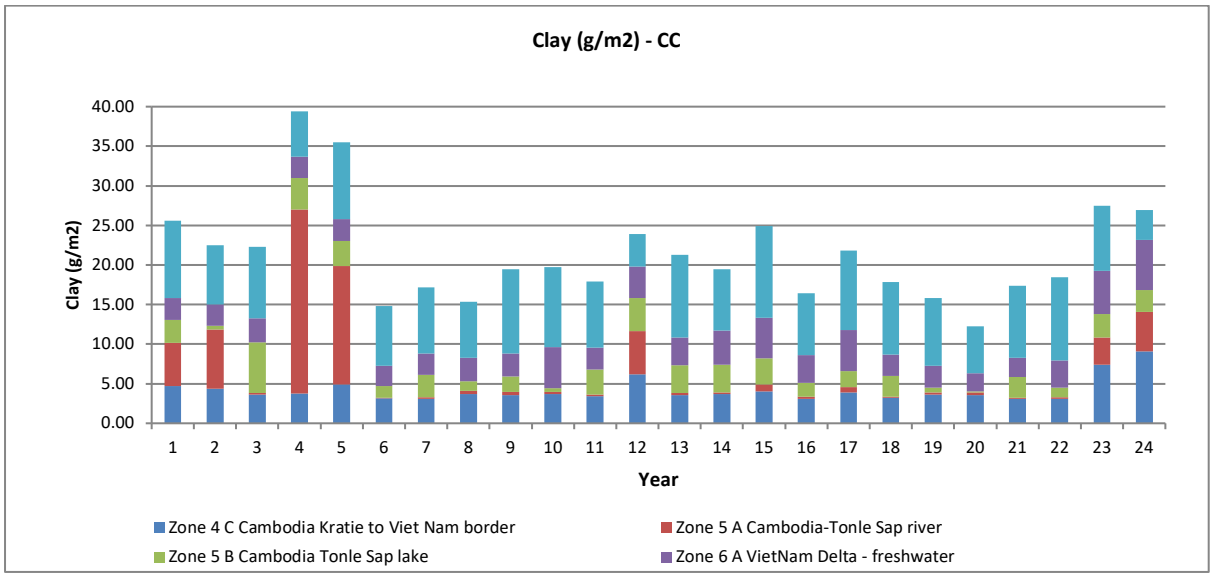

Figure 51. Annual variation of sedimentation rates for the main scenarios.

Clay annual sedimentation rates for the Zone 6A are shown in the Figure 52. Similar to the upstream results also downstream sediment inputs to the floodplains are maintained well with the H1a and H1b hydropower scenarios.

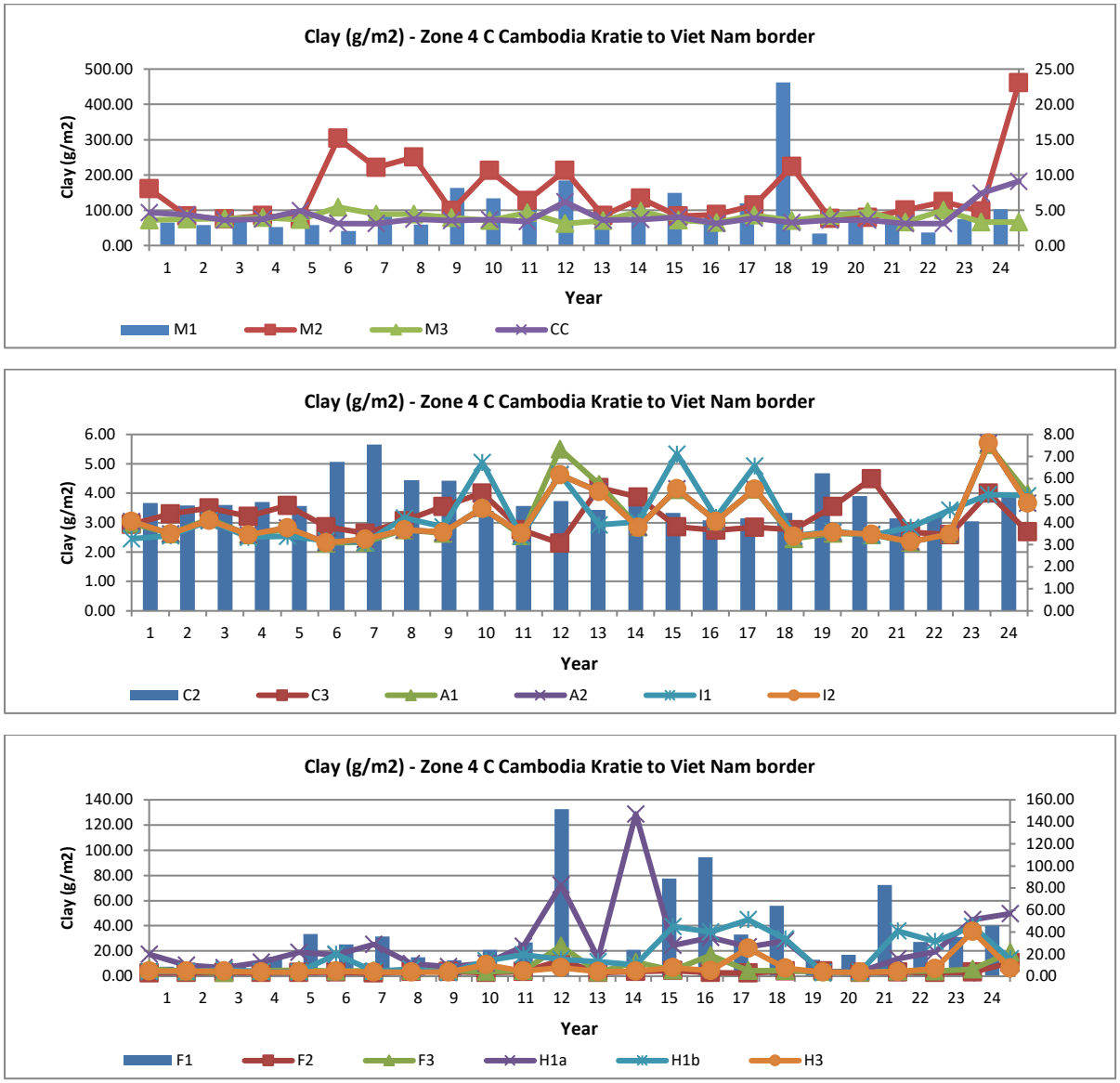

Figure 52. Annual variation of clay floodplain sedimentation for the all scenarios for Zone 6A. Observe that scales are different for the bars (left scale) and for the time series (right scale).

7.4. Scenario results for rice production

Combined Cambodia and Vietnam Delta annual non-irrigated rice production for the main scenarios is presented in Figure 53. Although flooding, sediment input and climate change have impact have impact on production, the change in agricultural area in Cambodia has by far largest impact between M1/M2 and M3/M3CC. In M3 and M3CC non-irrigated agriculture is transformed into irrigated one.

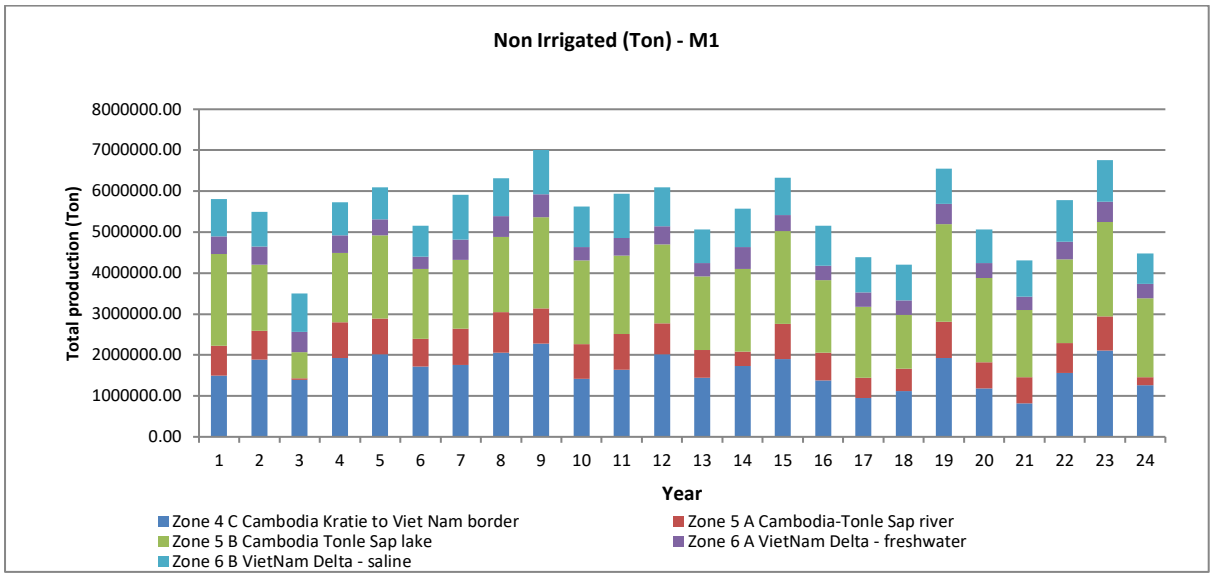

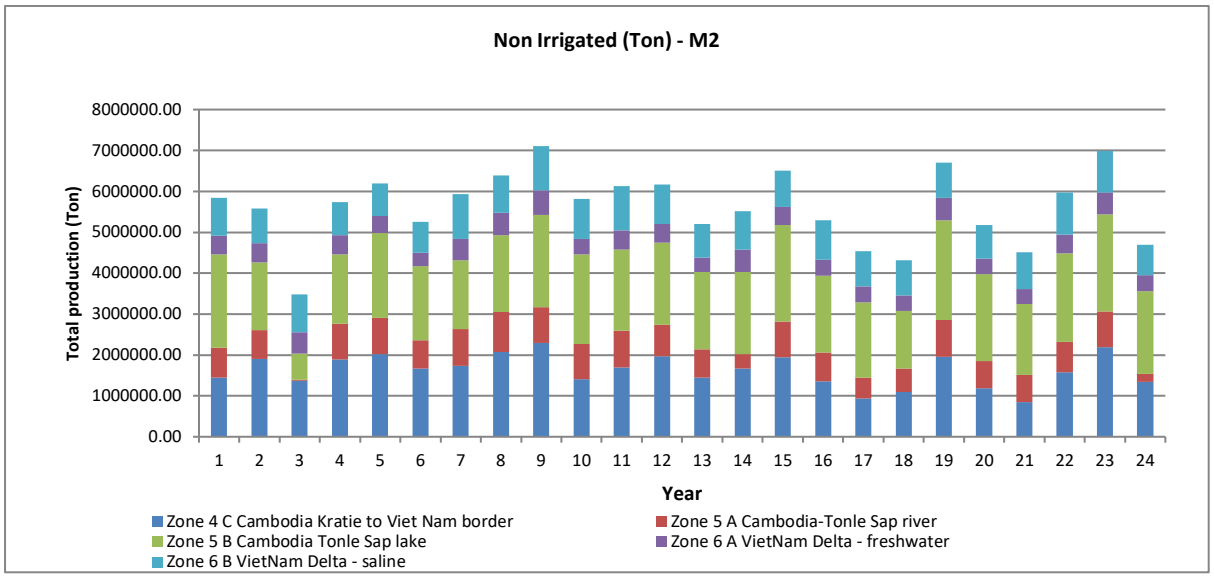

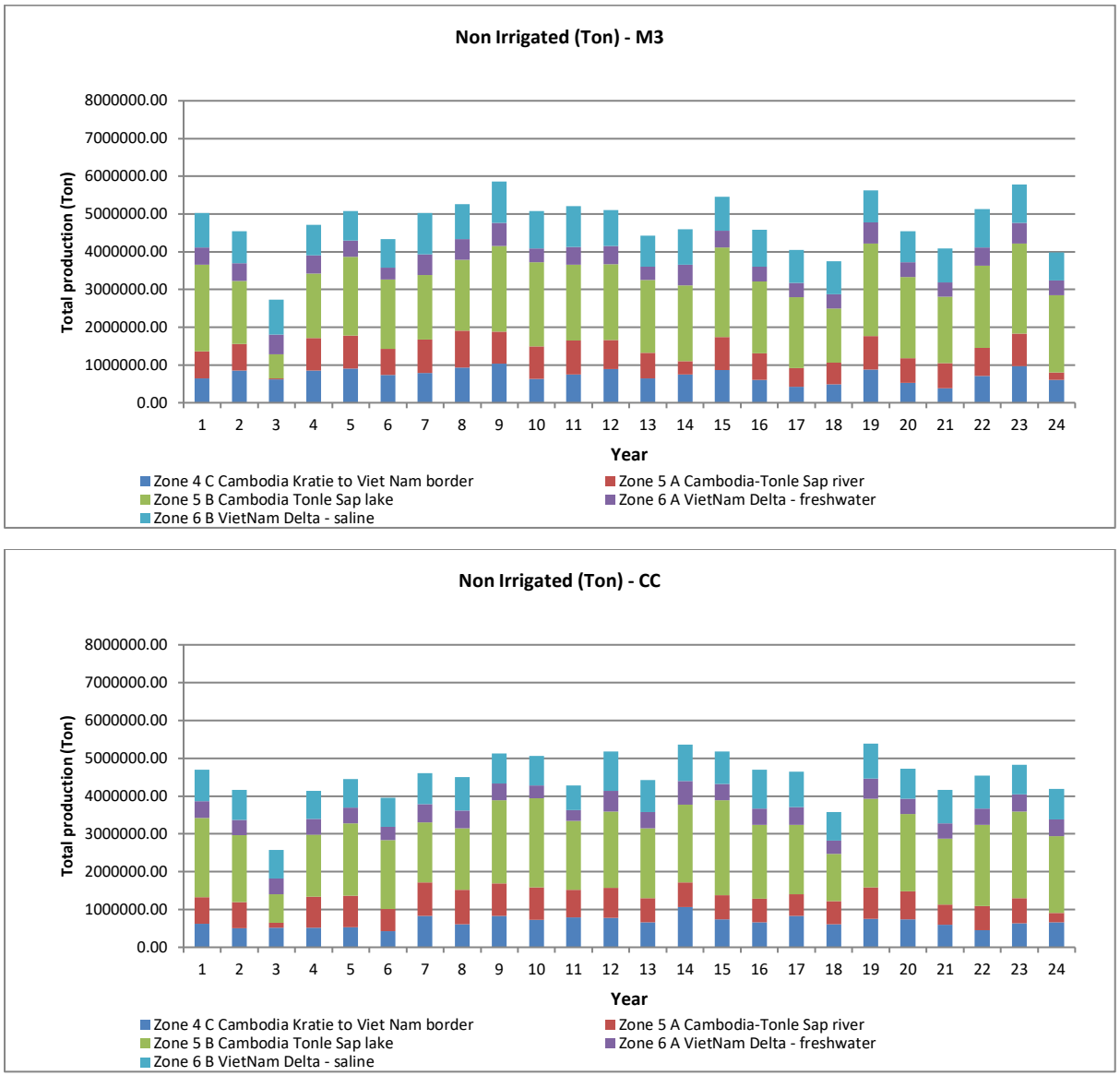

Figure 53. Annual variation of total Cambodia and Vietnam Delta non-irrigated rice production.

In the sub-scenarios scenario A1 stands out with very high rice production (Figure 54) for the Cambodian floodplains (Zone 4C). This is because of substantial irrigated agriculture area expansion in Cambodia for A1.

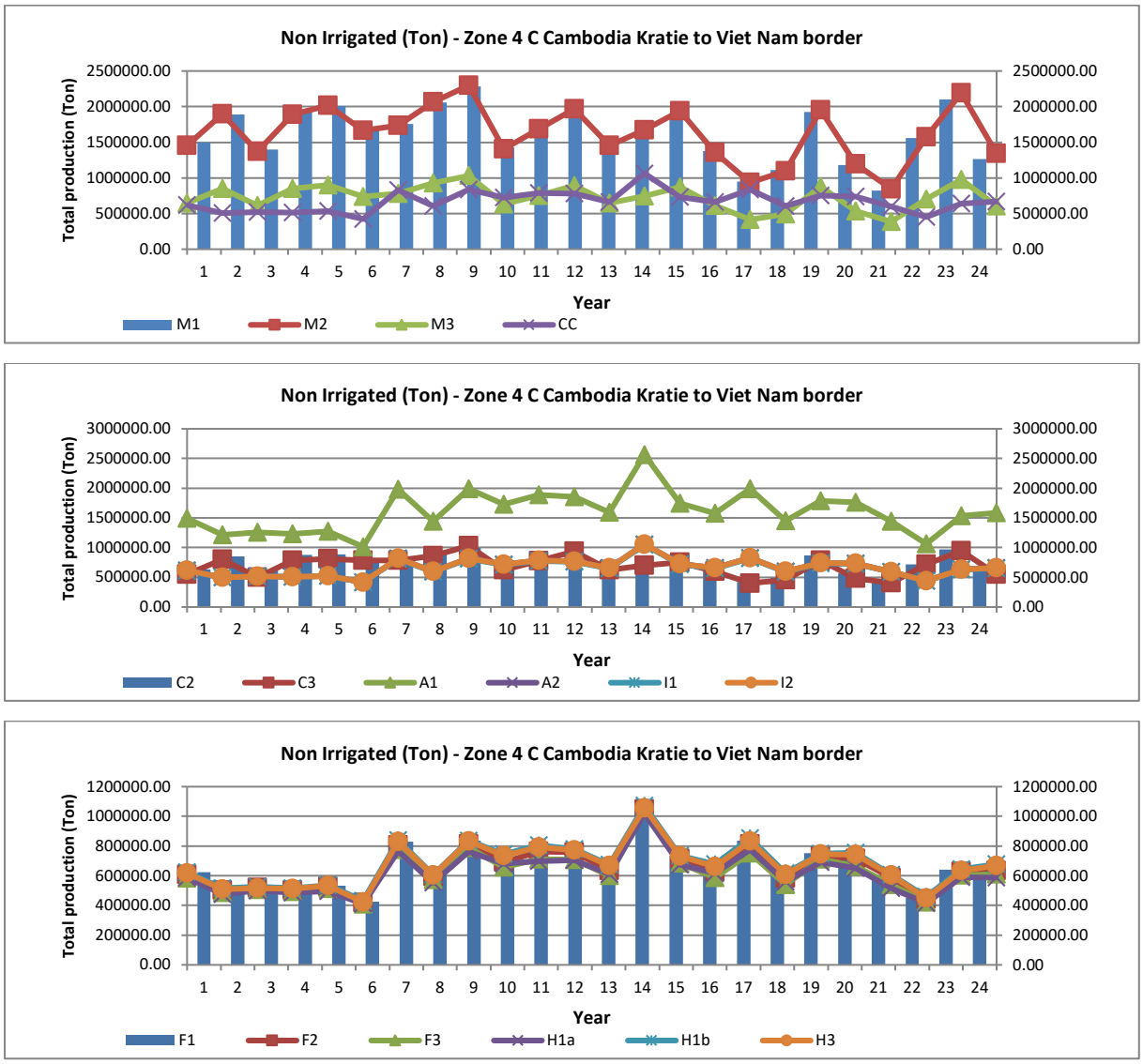

Figure 54. Sub-scenario rice production for non-irrigated rice for the Zone 4C. Observe that scales are different for the bars (left scale) and for the time series (right scale).

Irrigated rice production changes are minor in Cambodia and Vietnam Delta (Figure 55). In the main climate change scenario yields are slightly decreased because of temperature accelerated growth and consequent drop in yields.

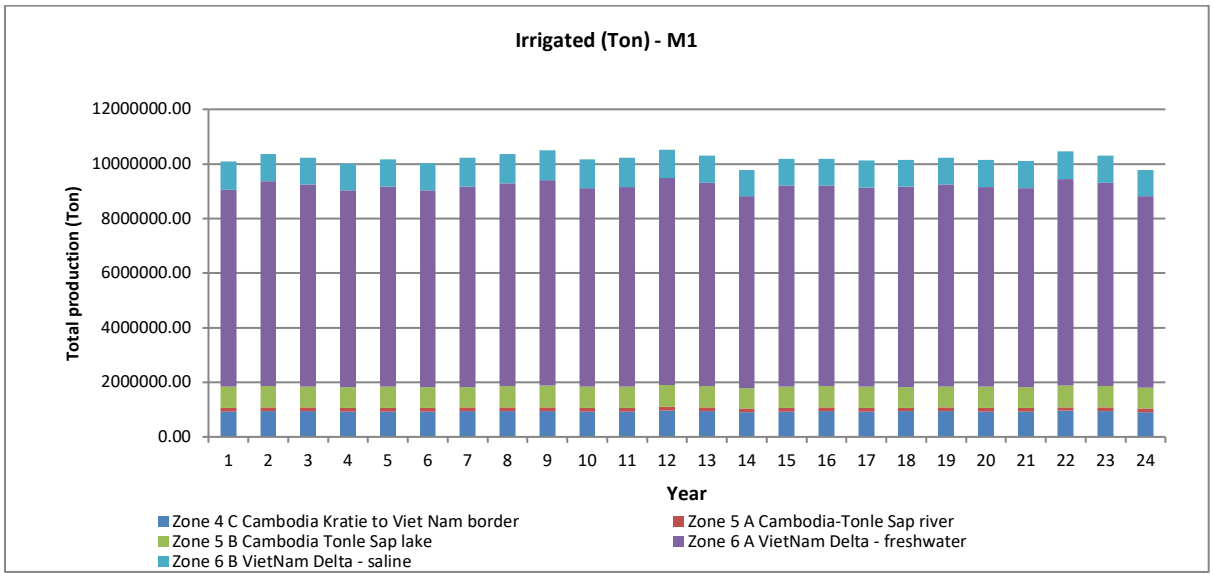
Irrigated (Ton) - M1
Total production (Ton)
12000000.00
10000000.00
8000000.00
6000000.00
4000000.00
2000000.00
0.00
1 2 3 4 5 6 7 8 9 10 11 12 13 14 15 16 17 18 19 20 21 22 23 24
Year
Zone 4 C Cambodia Kratie to Viet Nam border
Zone 5 A Cambodia-Tonle Sap river
Zone 5 B Cambodia Tonle Sap lake
Zone 6 A VietNam Delta - freshwater
Zone 6 B VietNam Delta - saline

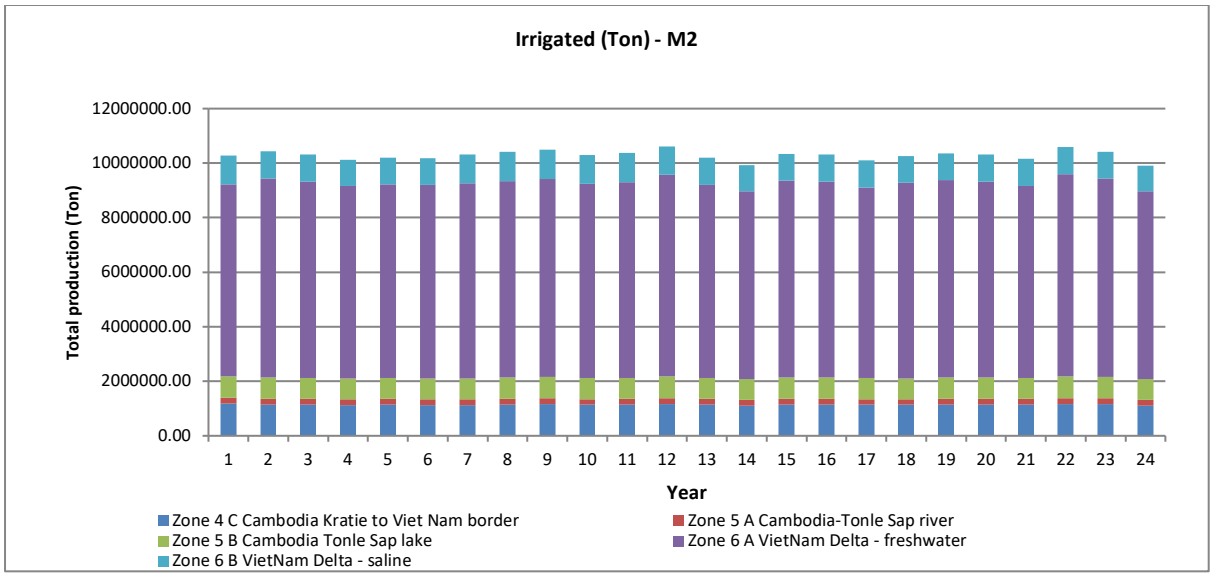
Irrigated (Ton) - M2
Total production (Ton)
12000000.00
10000000.00
8000000.00
6000000.00
4000000.00
2000000.00
0.00
1 2 3 4 5 6 7 8 9 10 11 12 13 14 15 16 17 18 19 20 21 22 23 24
Year
Zone 4 C Cambodia Kratie to Viet Nam border
Zone 5 A Cambodia-Tonle Sap river
Zone 5 B Cambodia Tonle Sap lake
Zone 6 A VietNam Delta - freshwater
Zone 6 B VietNam Delta - saline

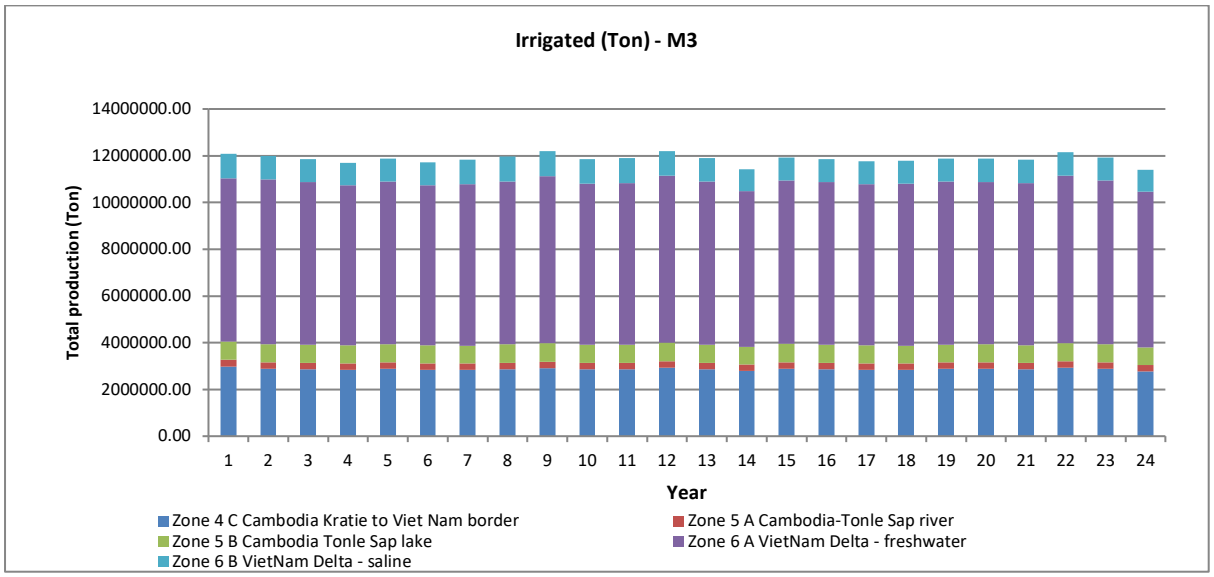
Irrigated (Ton) - M3
Total production (Ton)
14000000.00
12000000.00
10000000.00
8000000.00
6000000.00
4000000.00
2000000.00
0.00
1 2 3 4 5 6 7 8 9 10 11 12 13 14 15 16 17 18 19 20 21 22 23 24
Year
Zone 4 C Cambodia Kratie to Viet Nam border
Zone 5 A Cambodia-Tonle Sap river
Zone 5 B Cambodia Tonle Sap lake
Zone 6 A VietNam Delta - freshwater
Zone 6 B VietNam Delta - saline

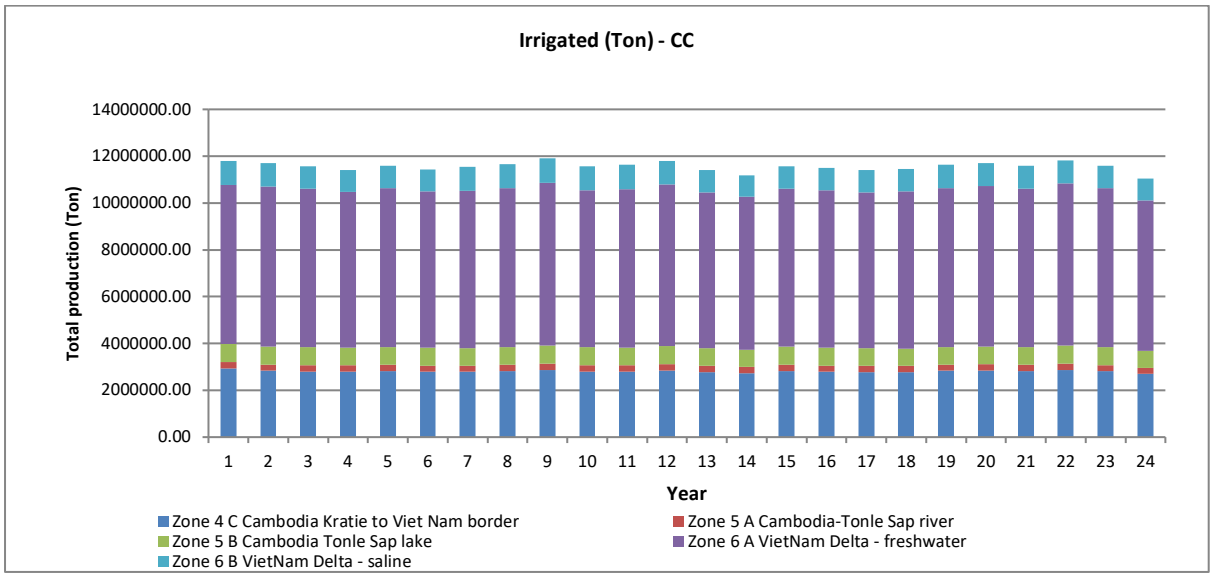

Figure 55. Annual variation of total Cambodia and Vietnam Delta irrigated rice production.

Similar to the main scenarios main changes in production are caused by land use change (Figure 56).

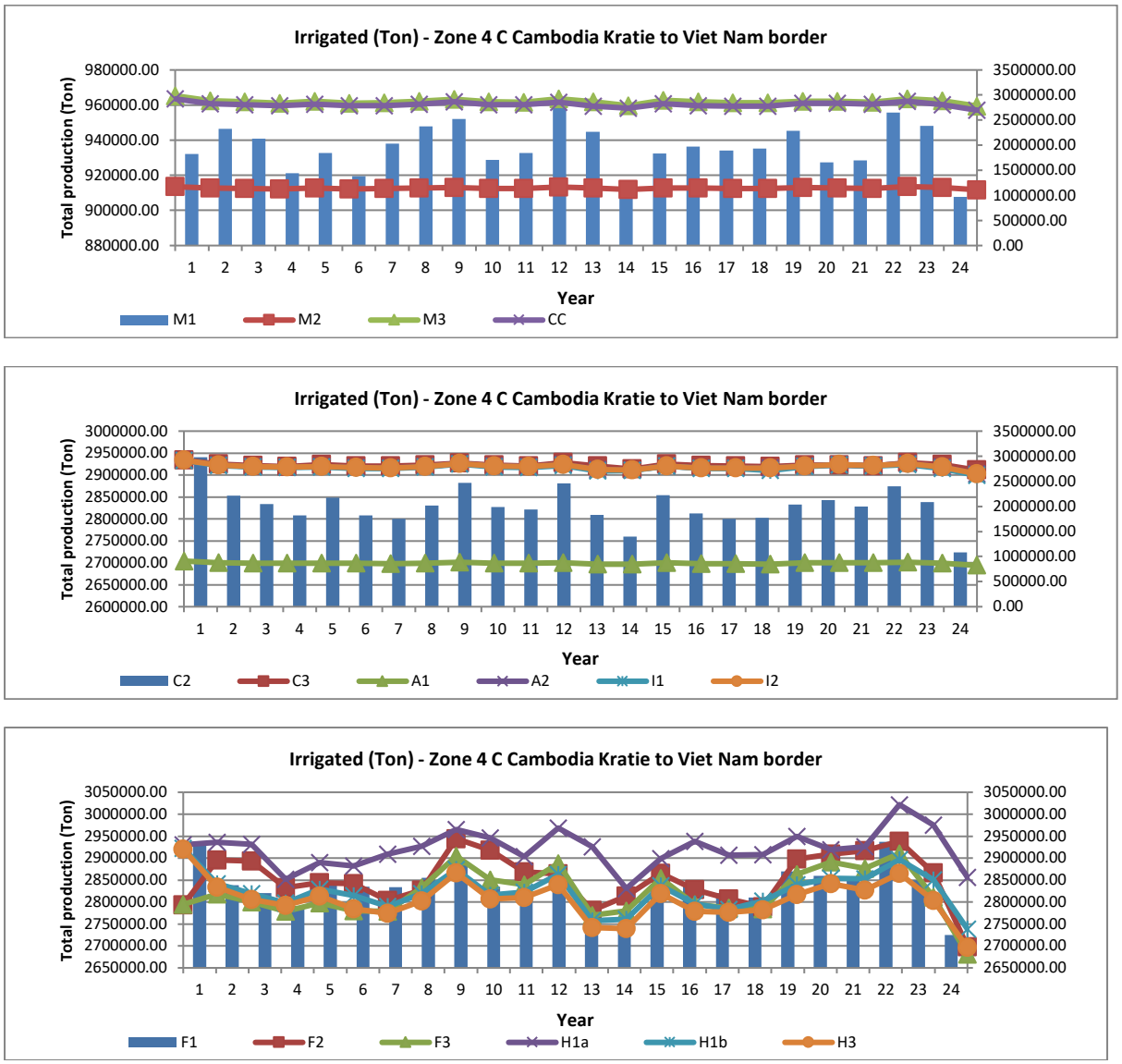

Figure 56. Sub-scenario rice production for non-irrigated rice for the Zone 4C. Observe that scales are different for the bars (left scale) and for the time series (right scale).

7.5. Scenario results for fisheries production

As discussed already in the previous chapters M2 reduces floodplain fisheries production 40% in the Cambodian floodplains and Delta and M3 and M3CC 70% compared to the baseline (Figure 57).

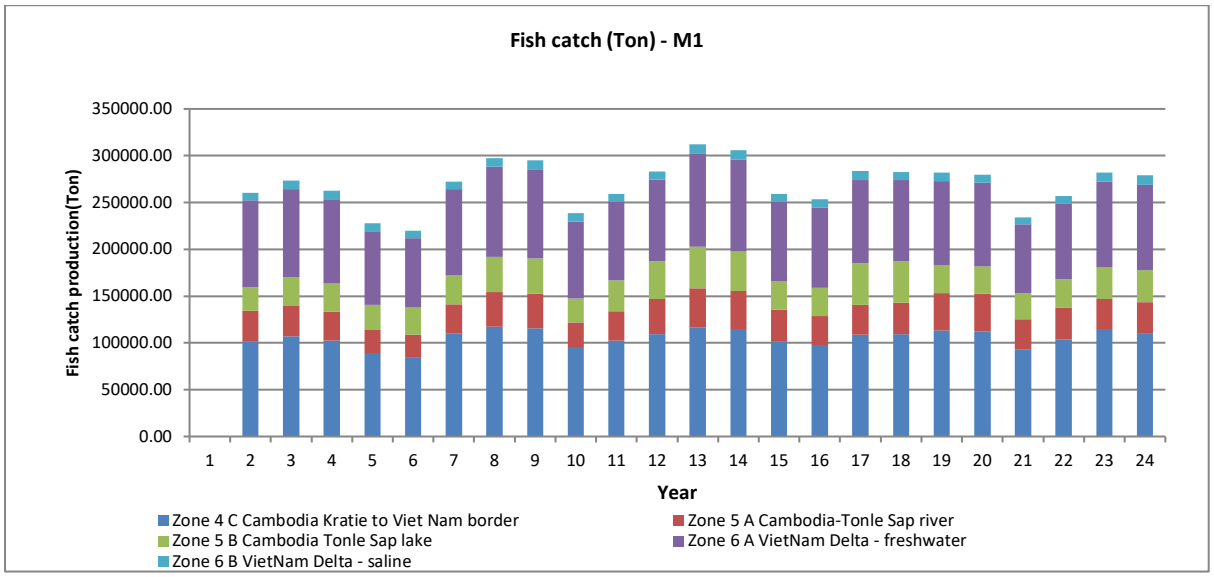

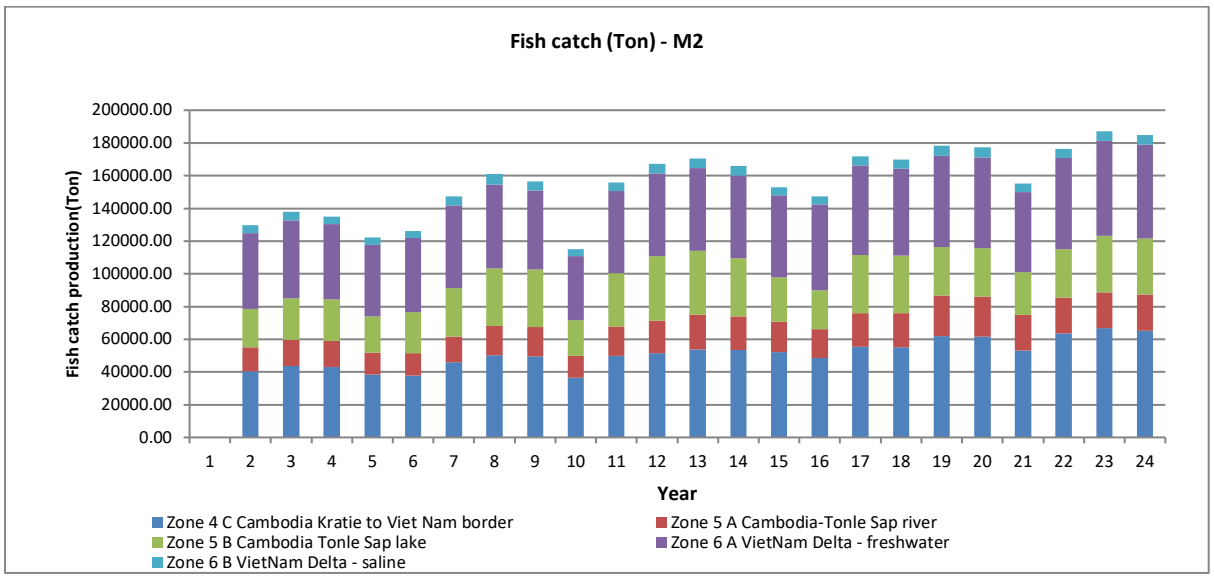

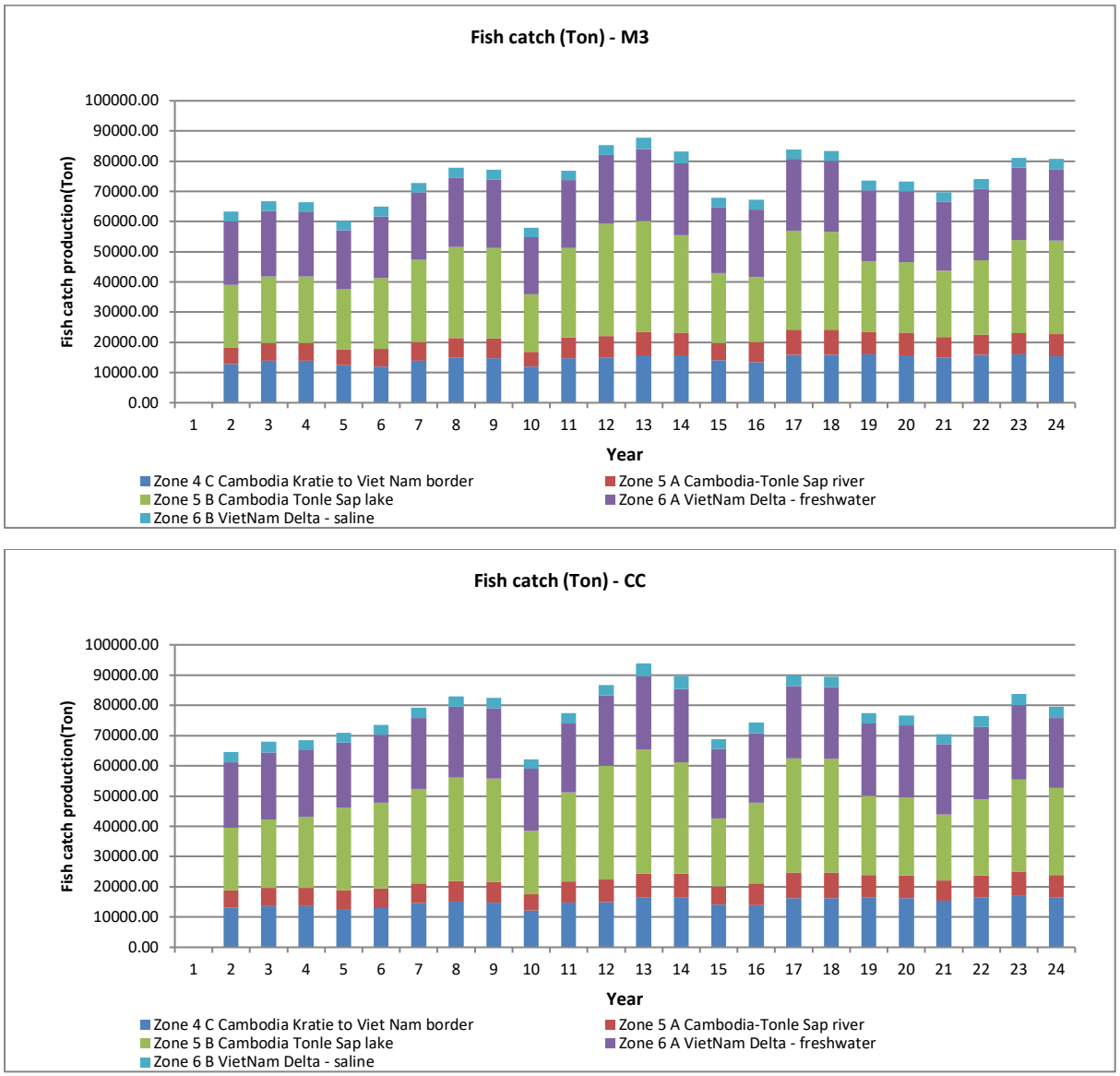

Figure 57. Annual variation of total Cambodia and Vietnam Delta floodplain fisheries production.

The H1a and H1b hydropower sub-scenarios maintain fertile sediment input to the Delta as well as fisheries production (Figure 58).

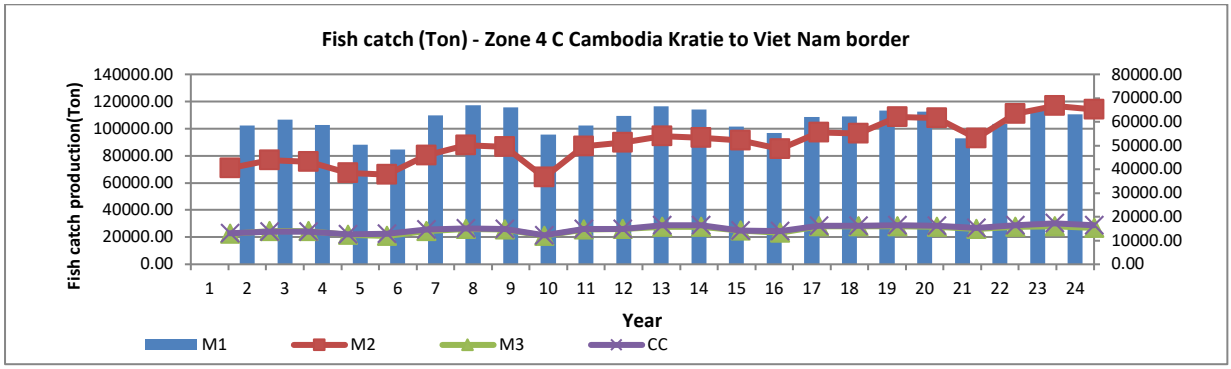

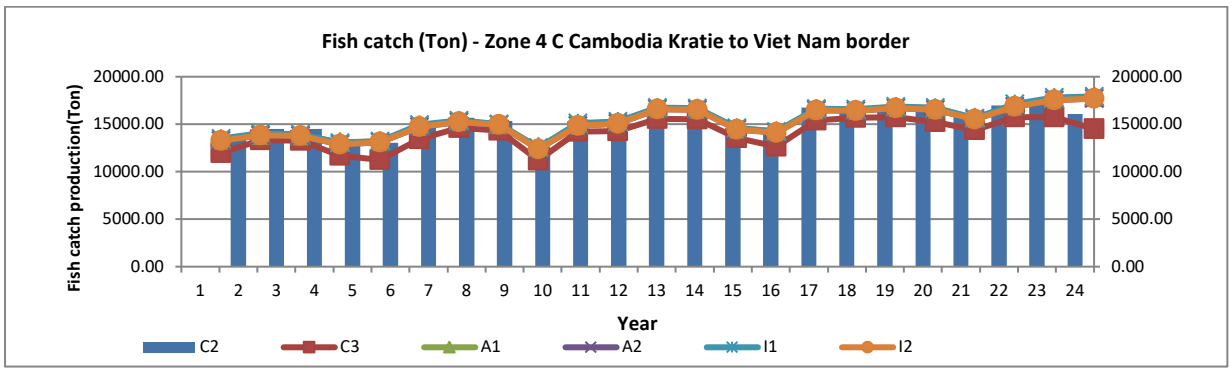

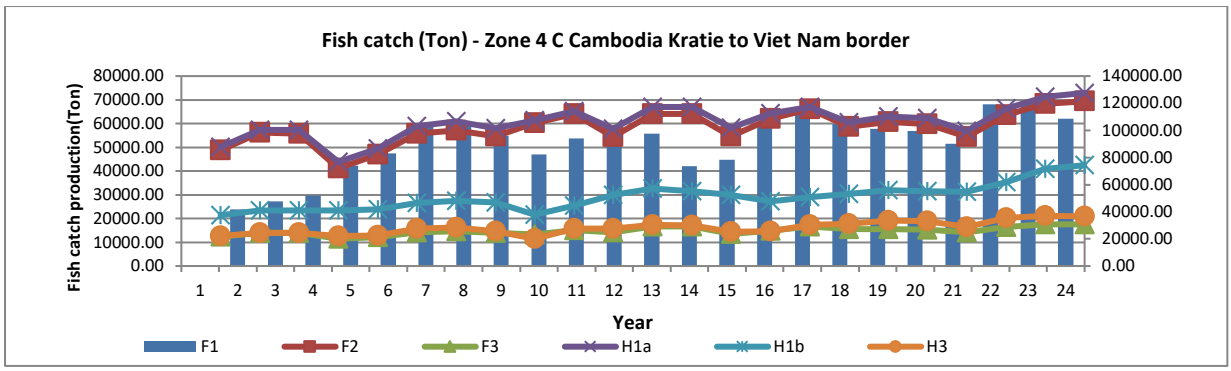

Figure 58. Sub-scenario fish production for the Zone 4C. Observe that scales are different for the bars (left scale) and for the time series (right scale).

8. Capacity building and Integrated Mekong Impact Assessment Tool (IMIAT)

8.1. The concept of geospatial enterprise information system

One of the key realisation during the entire Council Study work is that the majority of all data at MRC is geospatial, i.e. referring to a country, basin, areal zone or to a point of interest such as a monitoring station. Another realisation is that majority of the data is temporal. Moreover, some parts of the organization are producers of information (e.g. modelers, socio-economic experts), some are data consumers, i.e. gathering data, making synthesis and analysis, creating information for sector specialists and decision makers.

In a distributed organisation like MRC with its member countries, much of communication between the data producers and consumers happens through data, especially with spatial data. This creates obligations for the data, as people need to know from where to find data, what version of it is being used, who created it and when, how it was created, can it be published, when will the data be updated etc., in order to make communication itself successful. If communication fails, it creates significant inefficiency in the organisation and in case of MRC, can even have effect on policy decisions.

Geospatial and temporal data is most effectively managed in a Geographical Information System, GIS. The data in GIS may be stored in a database or it can be referenced as files. What's intuitive and effective from users´ point of view, the data can be accessed spatially (from a map) and map data with its attributes (tabular and time series data) can be accesses in one common user interface. GIS manages meta data for spatial and non-spatial information by nature, making possible to describe data sets in a similar way presented above, and also maintain versions of data.

Enterprise GIS is an architecture that integrates geospatial data and non-geospatial data and shares them across the organization. The basic idea of enterprise GIS is to address the needs of departments collectively instead of individually. The development of one comprehensive infrastructure minimizes potential conflicts and misunderstandings and can result in significant cost savings and organization performance improvements.

Enterprise GIS can even be expanded to serve organization's clients and stakeholders. In MRC's case those stakeholders can mean member country non-technical experts and policy decision makers or even public engagement. Data in the geodatabase can be published on the web with web services. Web clients (web browser applications) can provide advanced functionality for data access and visualisation. Web services and underlying database may be hosted locally or on the cloud, i.e. with an external hosting service provider.

It's notable that all applications in need of spatial or simply map data as files can access a common geodatabase, i.e. it's not limited to serve GIS software. The geodatabase can function as a spatially accessible catalogue for applications and / or their users.

All software components for building an enterprise geodatabase, spatial web services and web clients are available on open source basis.

8.2. Development needs for council study impact assessment tools

MRC Council Study has accomplished major advances in assessing Mekong Basin social, economic and environmental conditions and development impacts on them. The technical advances include

- monitoring data utilization;
- modelling; and
- discipline and thematic assessment methodology and tools.

The results of the CS main scenario assessment prove that the different assessment components and tools support each other well and provide information relevant up to the highest policy level in the region. Consequently, there is a need to consolidate the developments, methodology and results for

- country capacity building;
- update of the CS with improved data; and
- expanded use and user base of the CS tools.

At the moment CS methodology and tools can be utilized mostly by experts and there is need for capacity building and development of an easy to use Council Study platform including information, models and results processing and interpretation tools.

World Bank and Australian Water Partnership have been conducting review of the MRC data and modelling tools. The main conclusions show clearly that they are outdated and their use is constrained. The constrained use of MRC data and modelling tools refers to

- Limited utility of MRC technical work on country planning and policy level
- Limited support for non-technical experts´ problem solving
- Data availability in large & distributed organisation
- No common platform for data management, data maintenance and meta data
- Capacity building for the member countries needs improvement

During the MRC and World Bank meeting in Bangkok 5 – 6 July 2017 (Regional Workshop on Water Resources Modelling in the Mekong River Basin: Developing Synergies between National and the Mekong River Basin Modelling Program) the Member Countries acknowledged the review team findings and endorsed development of the MRC modelling and data systems.

The MRC Planning Division is engaged in developing hydropower strategy for the Mekong. It requires powerful but at the same time easy to use tool to be utilized for stakeholder planning and deliberation.

8.3. Development objectives with implementation notes

The main objectives for an Integrated Mekong Impact Assessment Tool (IMIAT) are

- Combine the current Council Study tools and results into a single application platform
- Focus on problem solving and true cross-sectoral planning
- Promote spatial planning approach and web technology
- Provide easy-to-use tools for sector specialists and decision makers
- Facilitates capacity building for member countries

- Provide a unified data storage platform for data access, management, maintenance, distribution and analysis in form of an enterprise geodatabase
- With the geodatabase, provide technical teams better means of data service and communication

The current MRC Council Study impact assessment tool framework consist of the following components:

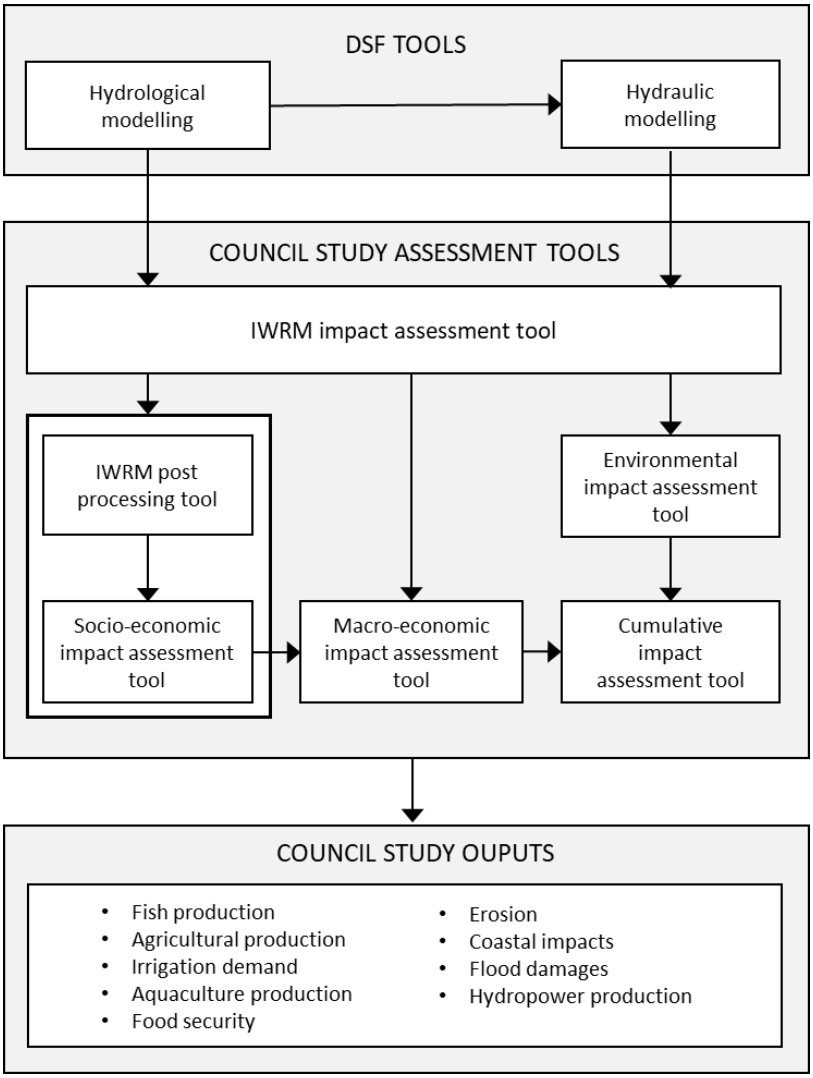

Figure 59. MRC Council Study assessment tool framework

The Council Study assessment tools are ran internally at MRC (Figure 60). Data storage for the results is currently based on dedicated files on the file system. Version management and meta data of outputs is manual.

The obvious development steps towards an enterprise information system are

- harmonize and stabilize the data interfaces between the assessment components;
- transform data input and output into database with added meta data; and
- make the data flow automatic between the components in order to provide software controlled workflows

in order to

- facilitate a unified data storage platform for data access, management, maintenance, distribution and analysis in form of an enterprise geodatabase and
- Combine the current Council Study tools and results into a single application platform.

When operational data is stored into enterprise geodatabase, it's essential to attach meta data to the actual data. When data storing into geodatabase is controlled in the process, it also makes possible to make uniform queries based on the meta data, e.g. reference, creation date, creator, version, creation method, access rights etc.

Once a common enterprise database has been established, it creates a common basis for information sharing throughout the organization and to the stakeholders, using web services. For the publishing, a secondary publishing database is being created. Standardized and automated processes will be created to extract publishable data from the enterprise database to the publishing database.

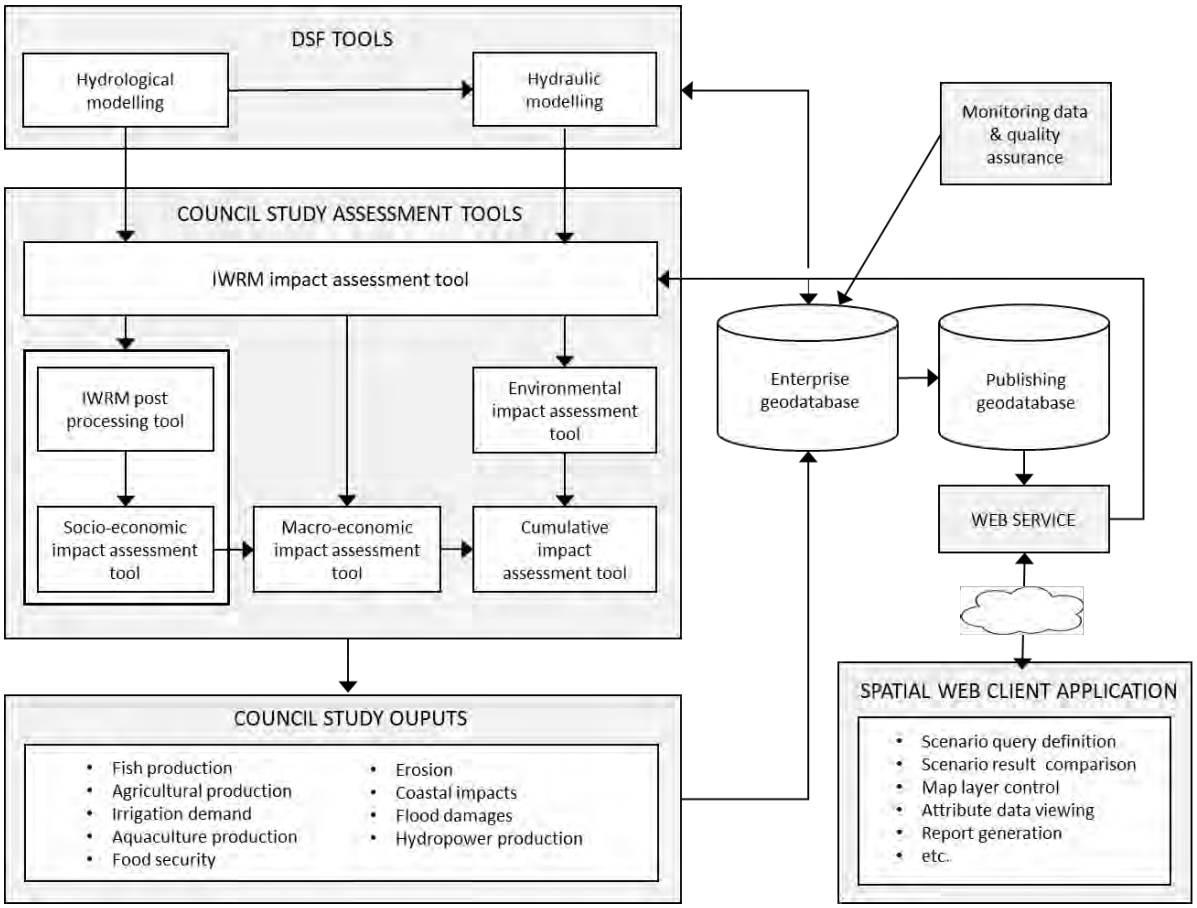

Figure 60. Council Study Assessment Tools with enterprise geodatabase and web service

Web service is communicating with a web client running on a web browser. Web browser application is providing easy-to-use tools for users. The functionality of the web client application would include, as an example:

- Map layer selection and visibility control
- Selecting of map objects and (tabular) attribute data viewing

- Scenario definitions, which the system will run on-the-fly
- Scenario result comparison
- Spatial animation viewing
- Report generation

It's notable, that when running scenarios on-the-fly the assessment tools must be able to run in batch mode, i.e. without user interference. It has been verified that the IWRM Impact Assessment Tool and its post-processing tool combined with the socio-economic impact assessment tool can provide batch operation mode.

When implemented to the level described above, the Integrated Mekong Impact Assessment Tool framework would facilitate improved knowledge transfer and capacity building especially because the system

- Focuses on problem solving and planning instead of learning modelling tools
- Is easy and intuitive to use (web access, map user interface)
- Provides transparency and improved understanding of processes and causal relations
- Facilitates spatial insights and interpretations
- Open access to software and data enables transfer to the member countries and member country participation in the system development
- Facilitates truly integrated approach for cross-sectoral planning.

As can be found the implementation notes here are on overall level, but on the other hand based on current Council Study assessment tool capabilities, proven technology and experience of similar systems and system implementation. Taking account of the complexity of the MRC Council Study assessment tool framework as a whole, the numerous variation of output options and the real-life challenges in a distributed organisation, it would be a practical to approach the system planning and implementation using agile development method, i.e. building a proof-of-concept demo with limited functionality and capacity, move forward with demo evaluation and feedback before proceeding to a production system definition and implementation phases.

8.4. Capacity building with eLearning extension

IMIAT framework could be completed to provide modern eLearning services both to MRC, its member countries, other stakeholder or to external, possibly paying customers.

The basic idea of an eLearning concept is to provide new or existing users of the IMIAT a course tray on the web, with which the users can take the courses in their own pace, proceed systematically and achieve knowledge level targets set by eLearning portal administrators, keeping in mind different user groups and their needs. The courses can be organized into learning paths, covering a specific assessment tool or methods for specific discipline problem solving.

The course material will be based on video material, prepared into logically organized lessons. The course material is produced by recording usage of the assessment tools with selected training data. The benefits of utilizing eLearning platform with the IMIAT in brief are

- new users (e.g. new employees) will have a well-organized familiarization to the system

- training is flexible and efficient, there's no need to organized traditional training sessions tight to location and dates
- The concept of using eLearning would free expert resources from basic training tasks
- Member countries can organize their training materials independently, with local data sets
- The standardized training materials can be more easily localized
- The training paths can be customized for different user groups (e.g technical, sector specialists, system administrators)
- Information and knowledge regarding IMIAT will increase cumulatively as the course tray and the training paths evolve over time
- Information and knowledge is no longer person dependent

The concept of using eLearning does not rule out traditional training but should be considered as a complementary method. An eLearning platform for MRC can implemented based on open source components.

9. References

Jorma Koponen, Dirk Lamberts, Juha Sarkkula, Arto Inkala, Wolfgang Junk, Ashley Halls, Mrigesh Kshatriya (2010) Productivity and Fisheries Report, Mekong River Commission/ Information and Knowledge Management Programme.

Modelling Framework for the Council Study (April 2015), MRC Information and Knowledge Management Programme.

M. Shahjahan Mondal, Abul Fazal M. Saleh, Md. Abdur Razzaque Akanda, Sujit K. Biswas, Abu Zofar Md. Moslehuddin, Sinora Zaman, Attila N. Lazar, Derek Clarke (2015) Simulating yield response of rice to salinity stress with the AquaCrop model, Environ Sci Process Impacts. 2015 Jun;17(6):1118-26.

Raes, D, P. Steduto, T.C. Hsiao, and E. Fereres, 2009. AquaCrop-The FAO crop model to simulate yield response to water. FAO, Rome, Italy.

Dirk Raes, Pasquale Steduto, Theodore C. Hsiao, and Elias Fereres (2012) AquaCrop Version 4.0 Reference Manual, FAO, Land and Water Division.

James A. Wyban, James N. Sweeney (1991) Intensive shrimp production technology : the Oceanic Institute shrimp manual. Redmond, Washington : Argent Chemical Laborities, 158 pages.

1. Annex 1 - Overview of the IWRM modelling approach

1.1. Council Study Modelling Objectives

The MRC Council Study overall objectives are:

1. Triple bottom line - further understand the environmental, social and economic (both positive and negative) consequences of water resources development;
2. Enhance the BDP process to support Member Countries in the sustainable development of the basin; and
3. Promote technology transfer and capacity building.

The Council Study Hydrologic Assessment Discipline Team led by the Information and Knowledge Management Programme (IKMP) is responsible for carrying out the hydrologic, hydraulic, sediment transport, and water quality modelling required to support the assessment of environmental and socio-economic impacts associated with water resources developments in six thematic areas or development sectors. The six thematic areas include hydropower, irrigation, agriculture and land use change, domestic and industrial water use, navigation, and flood protection. The water resources development impacts will be studied in relation to the climate change also.

Council Study modelling specific objectives for the first phase are to:

1. Support Council Study Discipline and Thematic Teams by data collection and analysis, provision and interpretation of modelling data, consultation and report writing
2. Provide evidence based and quantitative information on Mekong development impacts
3. Identify main (quantitative) knowledge gaps.

1.2. Specific IWRM Modelling Objectives

MRC TACT (Technical Assistance and Coordination Team) accepted the proposal to engage WUP-FIN (MRC Water Utilisation Programme Finnish Component) Team and MRC Toolbox WUP-FIN models to support the Council Study. MRC Council Study modelling consists of two complementary parts: the WUP-A DSF (Decision Support System) for hydrologically related parameters, sediments and nutrients and WUP-FIN impact modelling for environmental and socio-economic related parameters such as fish, aquaculture, agriculture, land use and coastal impacts.

The primary objective of the WUP-FIN modelling is *to provide complementary and quantitative data for the Council Study environmental and socio-economic impact assessment as part of the Council Study modelling effort*.

The secondary objective of the WUP-FIN modelling activity at the IKMP is to *improve the MRC Countries' capacity to use WUP-FIN tools and results*.

The term IWRM modelling, that is Integrated Water Resources Management modelling, is introduced here as it is more widely used than WUP-FIN and in order to emphasize the integrated nature of the modelling. The integration is both cross-sectorial (environmental-social-economic) and cross-model (DSF/WUP-FIN).

1.3. Modelling scope

The Council Study Modelling Framework is detailed in the document "Modelling Framework for the Council Study" dated 9th April 2015. It is based on the Concept Note "Modelling Approach in Support of the Council Study" dated 15th of January 2015. The Modelling Framework has been approved by the MRC Countries and the Council Study Modelling Team has been following it closely in the modelling implementation. It has been agreed by the Member Countries that the assessment of positive and negative impacts will be conducted in:

- A corridor on both sides of the mainstream from Chinese border to Kratie for Thailand and Lao PDR boundary delimitated (Zones 2 – 3)
- The Cambodian floodplains including Tonle Sap River and Lake (Zones 4 - 5)
- The Vietnamese Delta and coastal areas directly influenced by the Mekong estuary (Zone 5)

The assessment area corresponds to MRCS SIMVA zones except for the Vietnam Delta Zone 6 C that includes Ca Mau Peninsula (Figure 61).

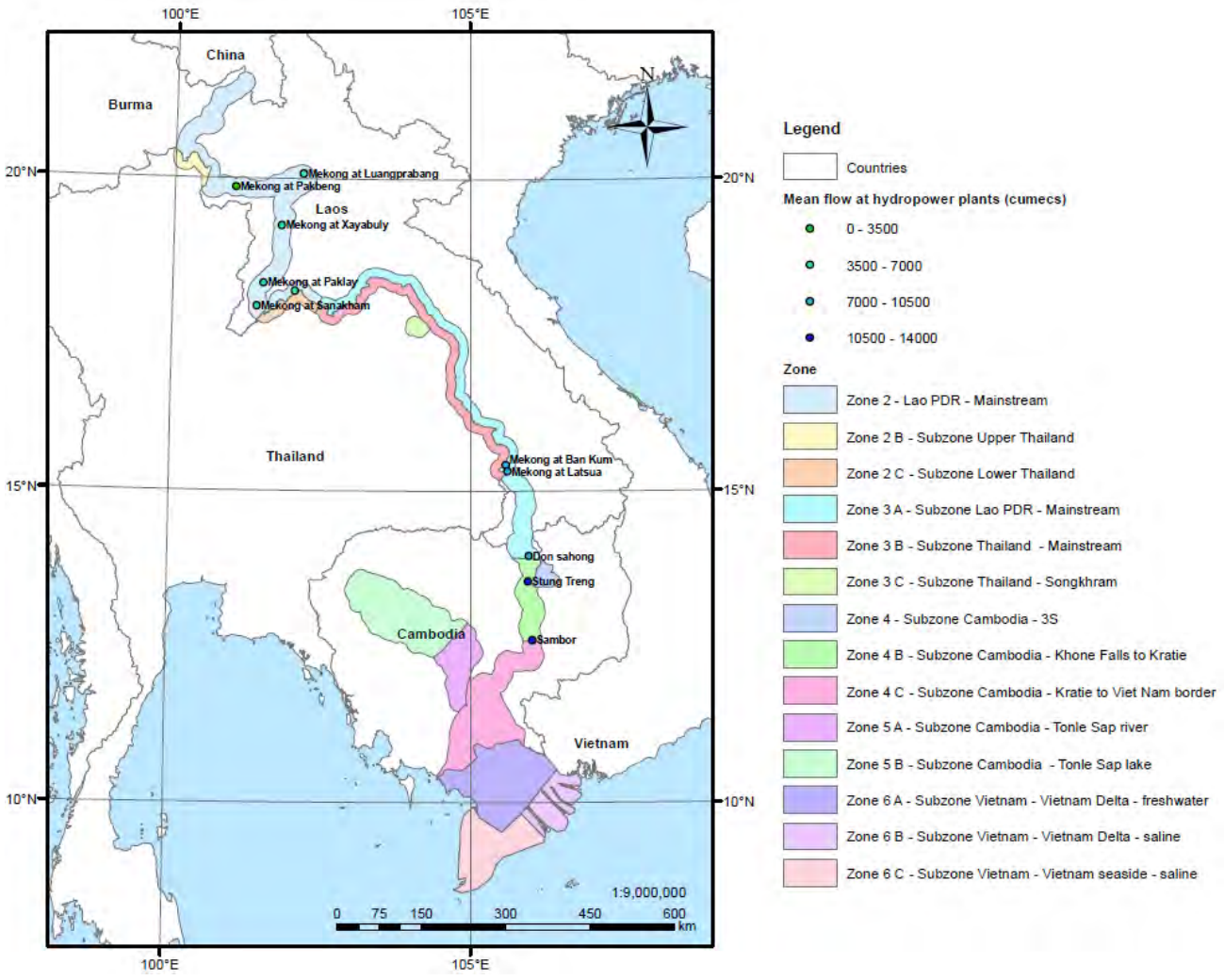

Figure 61. Council Study impact assessment and socio economic assessment areas

The description of each SIMVA zone is given in Table 1.

Table 1. Description of the SIMVA zones used in the model analysis and socio-economic study

SIMVA Hydro-ecological zone	Description: IBFM	Description: SIMVA	Social survey Sub-zones	Description
Zone 2	From Chinese border to Vientiane (Upstream)	From Chinese border to Vientiane (Upstream)	Zone 2 - Lao - Mainstream	Lao PDR side of Zone 2
			Zone 2 B - Subzone Upper Thailand	Thai side of Zone 2 in 2 significantly different Sub-zones: Upper stream in Chiang Rai and Phayao Provinces and Lower stream west of Vientiane in Loei and Nong Khai provinces
			Zone 2 C - Subzone Lower Thailand	
Zone 3	From Vientiane to Pakse	From Vientiane to Lao-Cambodian border	Zone 3 A - Subzone Lao - Mainstream	Lao side of zone 3 along the Mekong mainstream (incl. Vientiane)
			Zone 3 B - Subzone Thailand - Mainstream	Thai side of zone 3 along Mekong mainstream
			Zone 3 C - Subzone Thailand - Songkhram	App. 40 km upstream from confluence of Songkhram and Mekong – wetland areas and undammed river
Zone 4	From Pakse to Kratie	From Lao-Cambodian border to Cambodian Viet Namese border	Zone 4 B - Subzone Cambodia - 3S	App. 40 km from confluence of 3S and Mekong – undammed river, special eco-system
			Zone 4 A - Subzone Cambodia - Khone Falls to Kratie	Along Mekong mainstream down to start of floodplain
			Zone 4 C - Subzone Cambodia - Kratie to Viet Nam border	A 15 km zone around the maximum flooded area on the floodplain along the Mekong mainstream and Bassac east and south of Phnom Penh
Zone 5	From Kratie to Phnom Penh (upstream), incl. Tonle Sap	From Phnom Penh up to and including Tonle Sap lake	Zone 5 A - Subzone Cambodia - Tonle Sap river	The socio-eco system of Tonle Sap river is considered different from the Lake so a special subzone has been drawn
			Zone 5 B - Subzone Cambodia - Tonle Sap lake	The area is defined as 15 km around the maximum flooded area (in year 2000)
Zone 6	From Phnom Penh to Mekong Delta.	From Cambodian-Viet Namese border to sea - the Mekong Delta	Zone 6 A - Subzone Viet Nam - Mekong Delta - freshwater	The subzone covers the area of the Mekong Delta which has freshwater
			Zone 6 B - Subzone Viet Nam - Mekong Delta - saline	The saline subzone has special characteristics such as problems with saline intrusion

To support Bio- and socio-economic assessment the IWRM modelling has been applied in the corridor for:

- BioRA specific flood indicators
- Floodplain sedimentation for clay, silt, sand and nutrients
- Fisheries production
- Agricultural productivity
- Aquaculture (shrimp) production.

The IWRM corridor impact modelling is based on uses ISIS discharge, water level, sediment and nutrient results. It should be noted that this modelling focuses on environmental and socio-economic indicators and has been applied only for complementary assessment necessary for the discipline and thematic teams.

In the Tonle Sap comprehensive water quality modelling have been implemented including detailed sediment processes, nutrient dynamics, primary productivity, dissolved oxygen and fisheries productivity. The coastal modelling includes coastal flooding, salinity intrusion, sediment transport, bed erosion and fishery productivity.

The IWRM model application is presented in Figure 62.

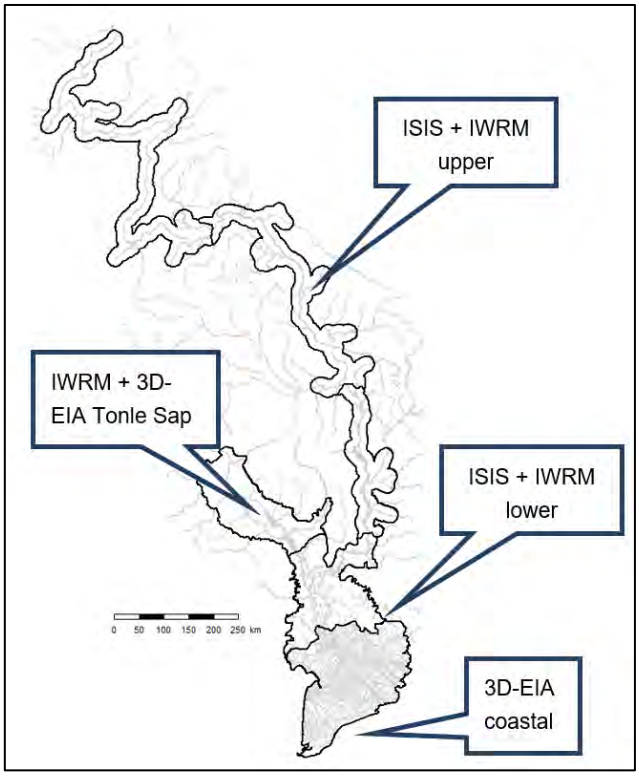

Figure 62. IWRM (integrated ISIS and WUP-FIN) model application areas

1.4. Floodplain fisheries, agriculture and aquaculture modelling

The IWRM modelling approach is based on flooding approximation using ISIS water levels (or any other water level information) in the channels as starting point and spreading flood from them based on terrain. The Halcrow DeltaMapper software for ISIS flood and salinity mapping differs from this approach as it builds TIN (Triangular Irregular Network) based on the location of the ISIS nodes (Figure 63) and interpolates the results into a regular raster grid. The TIN approach can be used to produce individual flood and concentration maps but it requires too much data to be practical in day-to-day modelling for long time series.

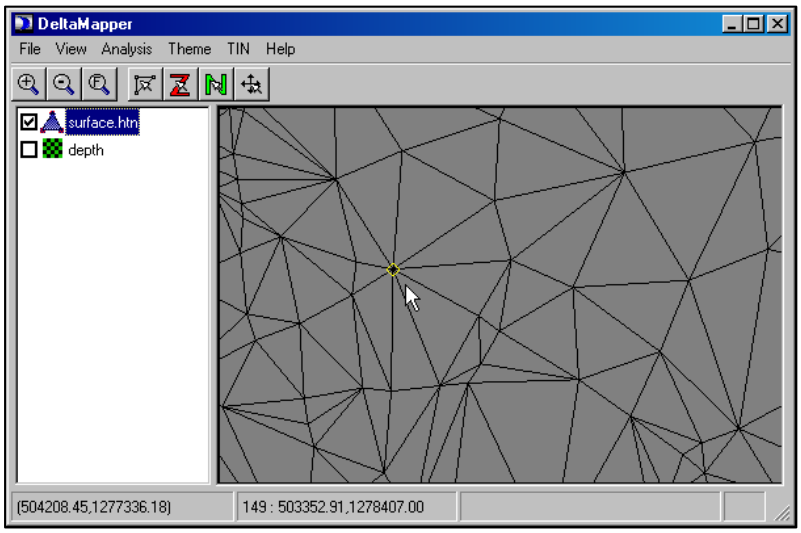

Figure 63. TIN (Triangular Irregular Network) of ISIS nodes used for the interpolation in the Halcrow DeltaMapper (from Decision Support Framework User Guides, DSF 210, DeltaMapper)

Dykes can be implemented in the IWRM model either as part of the floodpoint data (Figure 64) or embedded in the model DEM. Unfortunately dyke and other infrastructure data is lacking and has not been implemented so far. Consequently, the flooding is indicative in the model and exaggerates the real flood extent. This is especially true for the flood protection scenarios which increase water levels in the river channels. On the other hand flood protections tend to increase flooding in upstream so the current model results represent worst case scenario.

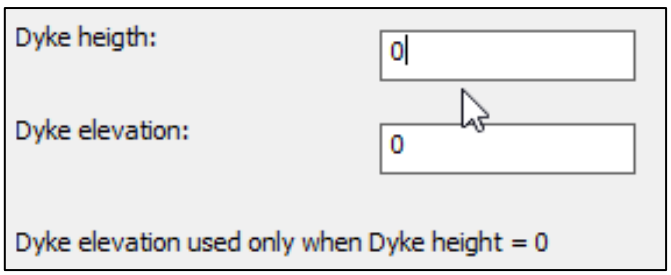

Figure 64. Dyke information in the floodpoints.

Floodplain modelling has been divided into two areas: upstream and downstream of Kratie. Figure 65 shows upper part assessment model grid land use and ISIS nodes where ISIS model stage and sediment concentrations are used. ISIS water level mapping to the floodplains is computed as water transport from ISIS points to the surrounding areas as defined by the DEM (Figure 66). Model spatial data includes corrected MRC DEM, soil classification and 2010 Land Cover.

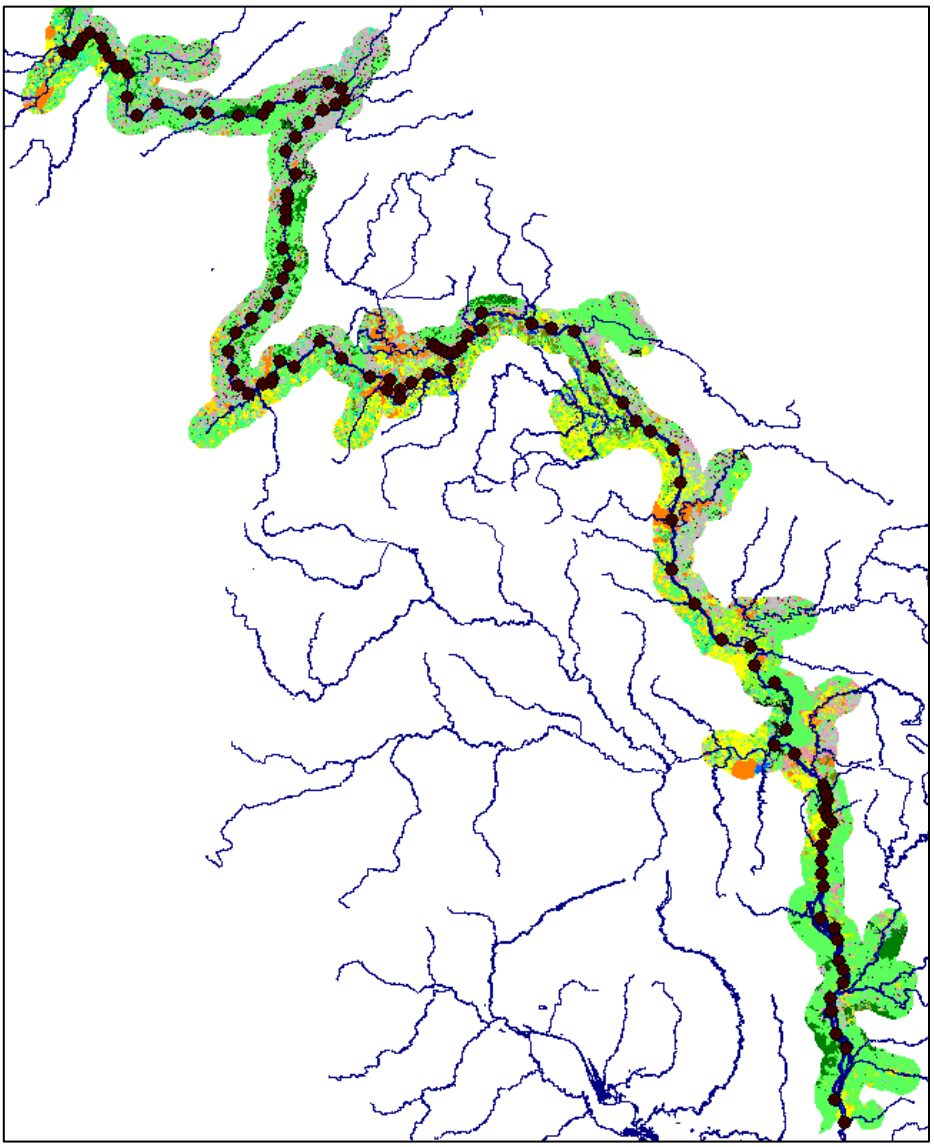

Figure 65. Upper model area corresponding to the Council Study impact assessment area (SIMVA zone). Brown markers are locations where ISIS data is used and colours correspond to the MRC 2010 land cover classes.

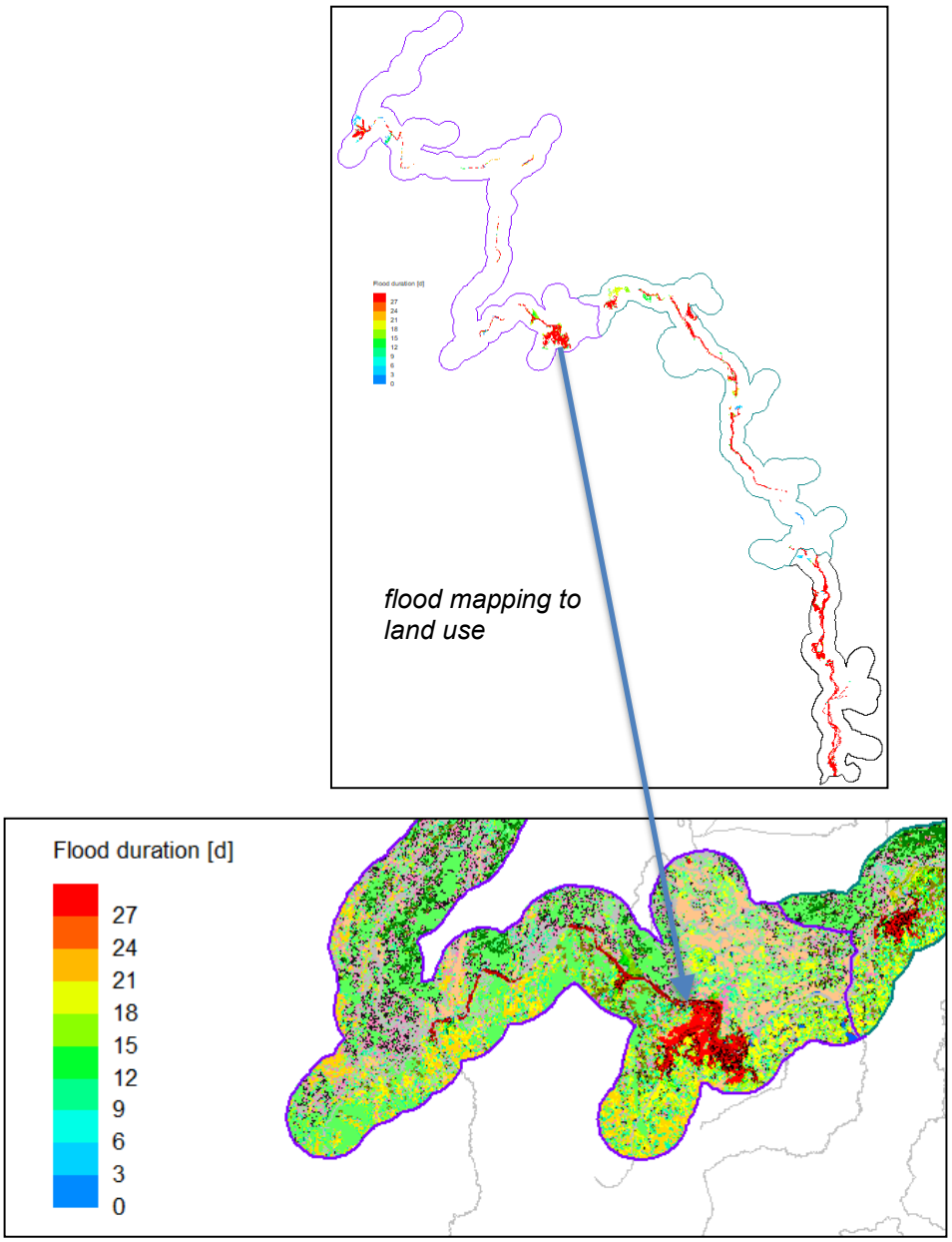

Figure 66. Flood mapping from ISIS mainstream points to the floodplains.

Corresponding model set-up for the lower part is shown in Figure 67. More than 250 ISIS nodes are used in the model. ISIS Delta model has about 5000 nodes but it would be impossible to utilize all of them for the impact modelling. The IWRM Delta assessment model spreads flood in between the nodes based on the model DEM.

Upper model resolution is 1'500 m and lower model 1'250 m. These result correspondingly to 40'000 and 58'000 active grid cells. For the agriculture areas there are 31'000 additional grid cells in the lower model. With these resolutions model computation times are reasonable, for instance the Council Study 24 year assessment period is computed in about 4.5 hours.

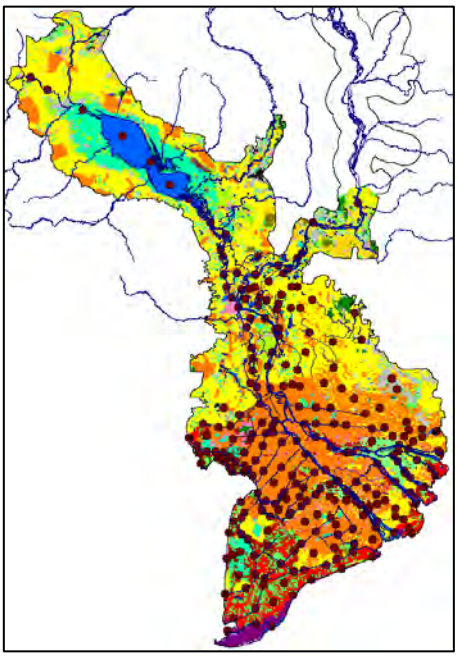

Figure 67. Delta model land use and used ISIS nodes (brown markers). Orange areas are irrigated agriculture and yellow ones non-irrigated agriculture.

MRC 2010 land cover data doesn't differentiate between irrigated and non-irrigated agriculture. For irrigated areas BDP2 irrigation area maps have been used. In Vietnam only provincial level total irrigation area data was available and for that reason irrigation area locations have been estimated by the WUP-FIN Team (Figure 69).

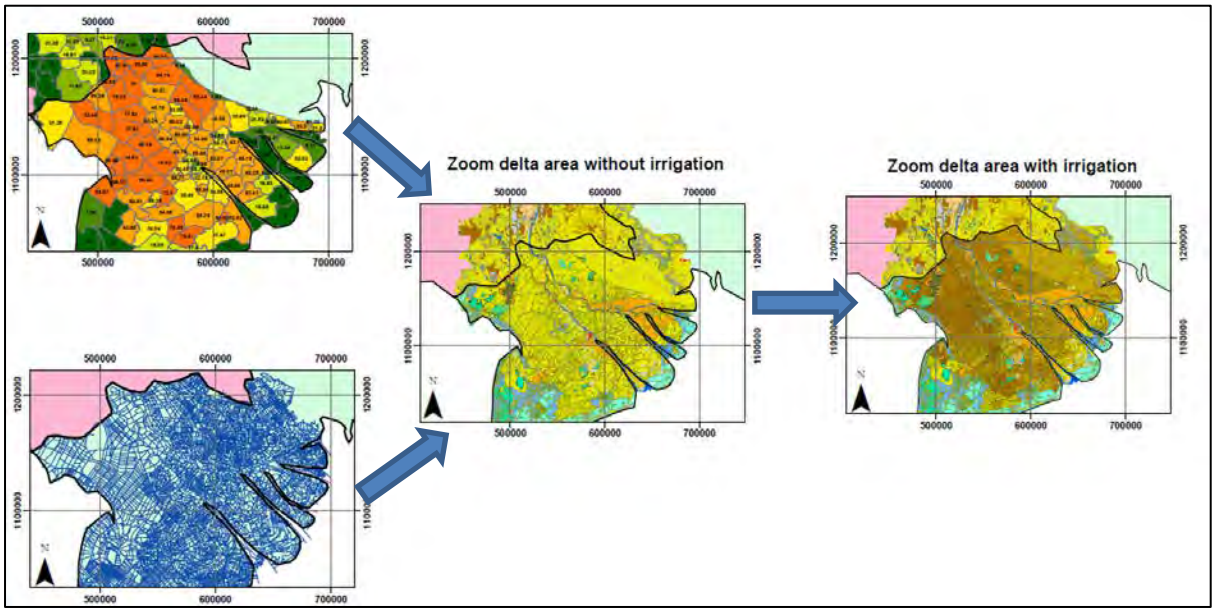

Figure 68. Generation of model irrigation areas in the Delta based on the BDP2 provincial data (upper left figure), irrigation channel network (lower left figure) and the MRC 2010 land cover (middle figure).

The resulting land use map is shown in detail in Figure 69.

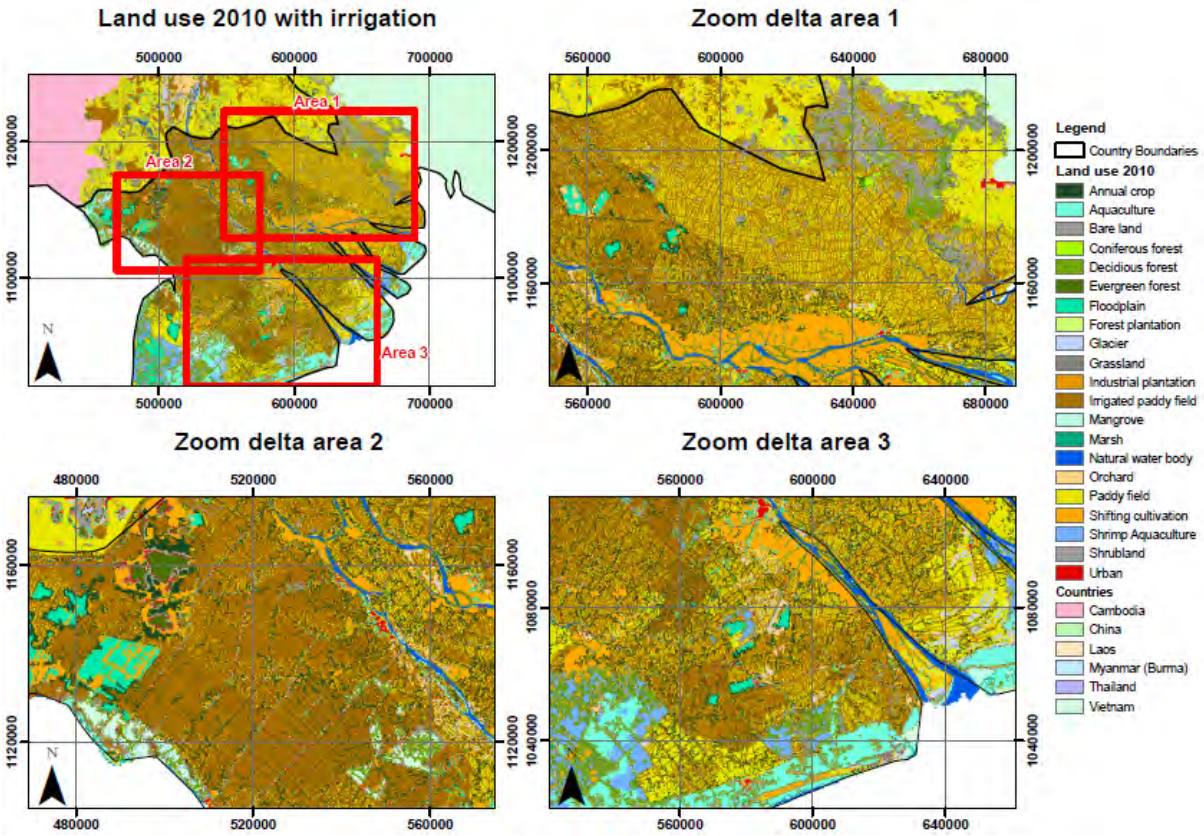

Figure 69. Details of the generated irrigation areas in the Delta.

The Hydrologic variables as rainfall and temperature are computed for the impact corridor for agriculture analysis which are yield production and irrigation demand. DSF KB (Knowledge Base) in the corridor has been used to set up the model, transforming and projecting information according to the base information used in the seed models for the impact assessment model as shown in Figure 70, Figure 71 and Figure 72.

Upper Mekong River used imported SWAT precipitation data from the results of the hydrologic model considering climate change conditions as shown in Figure 73.

The rainfall and temperature values have been corrected to be compared with the station data and to conduct climate projections for the climate change scenarios. In the upper part temperatures for the climate scenarios have been scaled using the SIMCLIM monthly scaling factors prepared by the modelling team.

The lower Mekong River the rainfall information was extracted from ISIS stations as shown in Figure 72 and supplemented with additional rainfall stations for Tonle Sap and NCEP temperature stations.

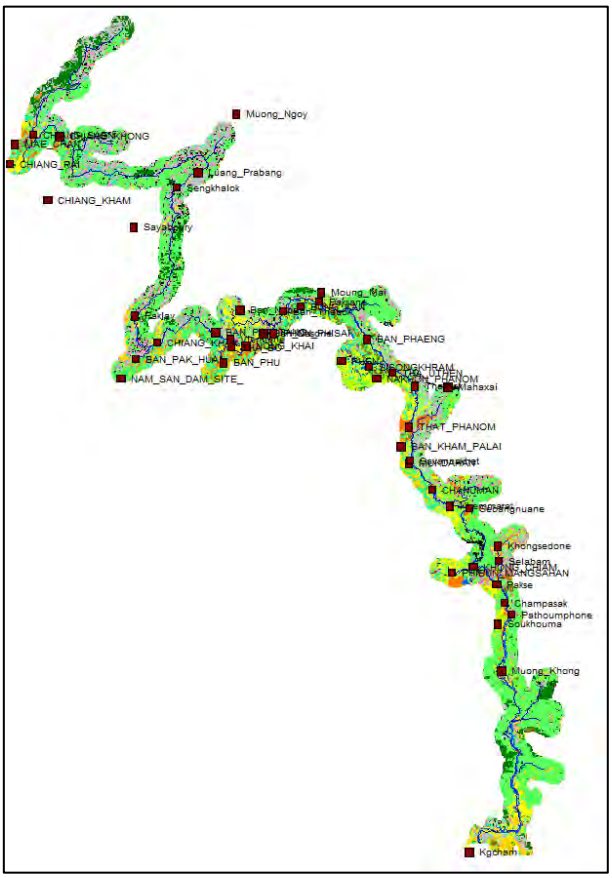

Figure 70. Rainfall stations used in the upper IWRM model.

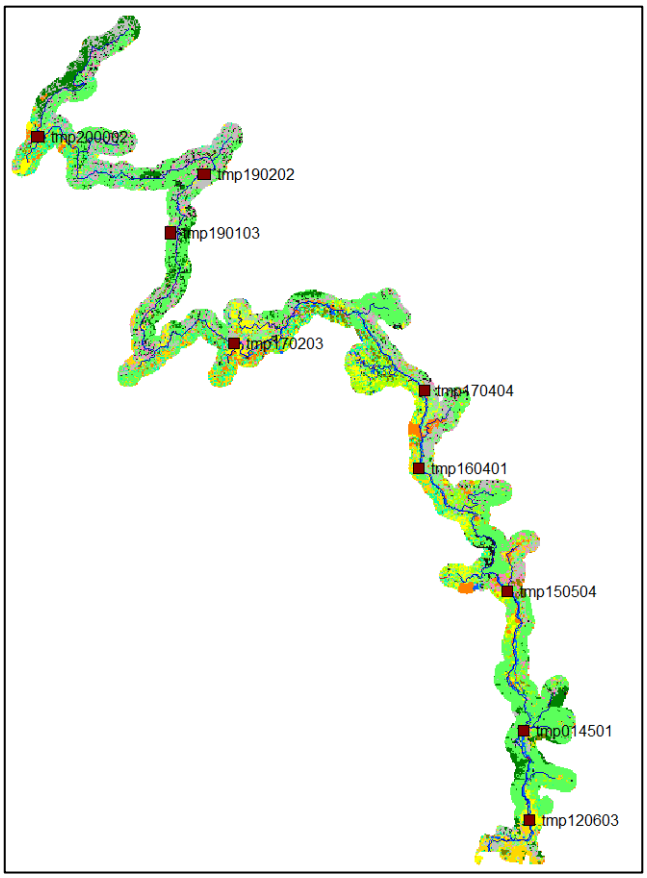

Figure 71. Temperature stations used in the upper IWRM model.

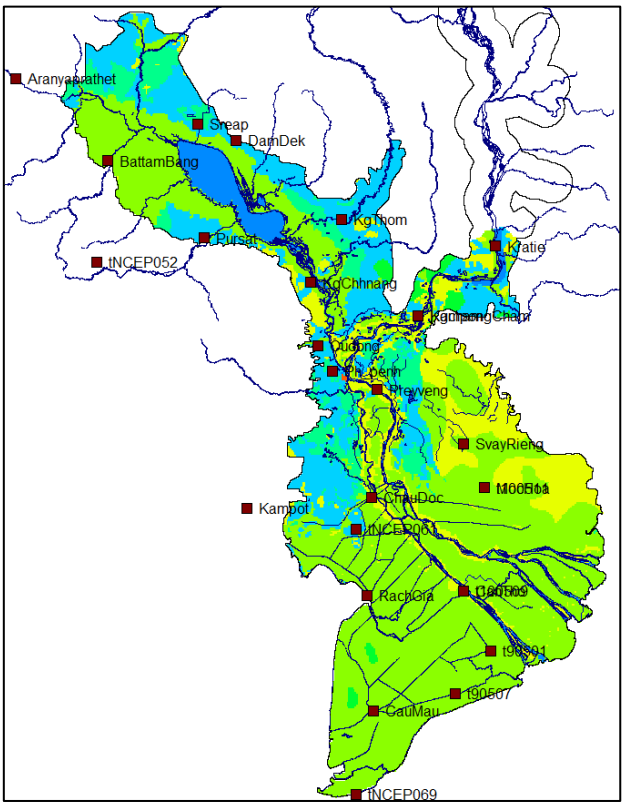

Figure 72. Delta model weather stations and soil classification.

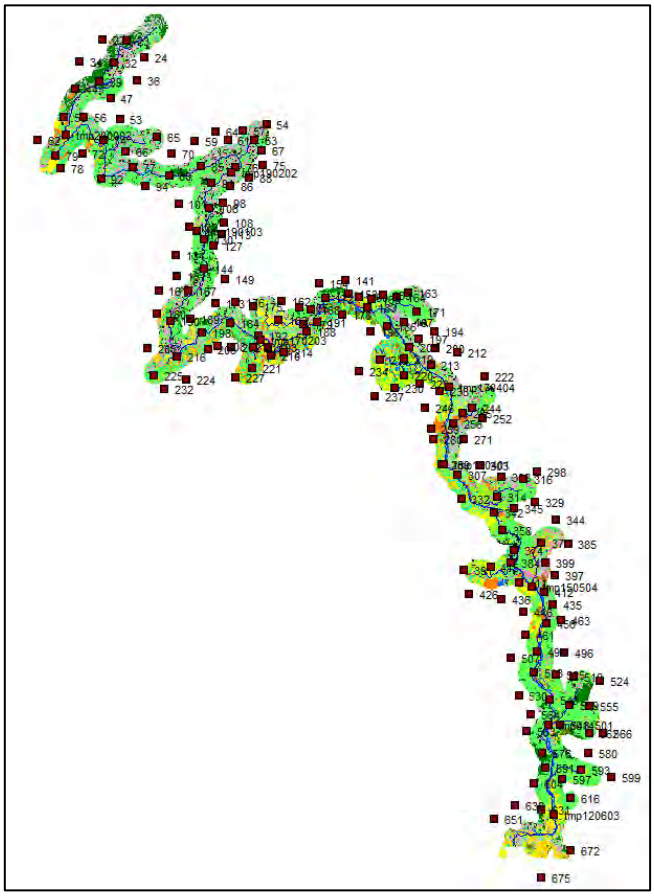

Figure 73. SWAT sub-area centroids for rainfall data.

1.4.1. Generalized floodplain sedimentation and fisheries production modelling

Because the IWRM model uses hydrodynamic model such as ISIS or monitoring data for the water levels its flood propagation approximates a real 2D/3D flood propagation and material transport process. Consequently, the floodplain sedimentation needs to be adjusted to a real value. 3D model for Xe Bang Fai and Tonle Sap floodplains has been used for the adjustment (Figure 74).

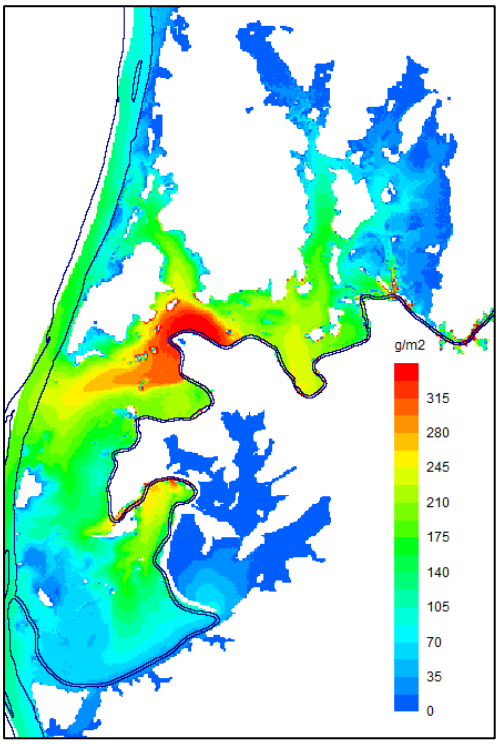

Figure 74. 3D model floodplain silt sedimentation during period 1.9.2000 – 14.9.2000 used to adjust the IWRM model sedimentation.

It seems that fisheries production can be correlated with annual floodplain sedimentation with high reliability as evidenced by the MRC Fisheries Programme Tonle Sap Dai fishery analysis (Figure 75). The relation between sedimentation, primary production and total fisheries production has been quantified in collaboration with the MRC FP and Max Plank Institute Amazon research group (ref. WUP-FIN Baseline Report 2016).

During the Council Study the 3D model has been re-calibrated to describe more accurately the chain alluvium – primary production – fisheries production. Alluvium is here fertile material consisting sediments, nutrients and organic material. Primary production has been divided into lake and floodplain production consisting phytoplankton, periphyton and flooded terrestrial production. Finally it has been possible to generalize floodplain fish production using annual floodplain sedimentation (Figure 76). This relation computed by the 3D model has been used for rest of the Delta and Cambodian floodplains. It has not been possible to derive corresponding relation for the lake so the relation is applicable only for the floodplains.

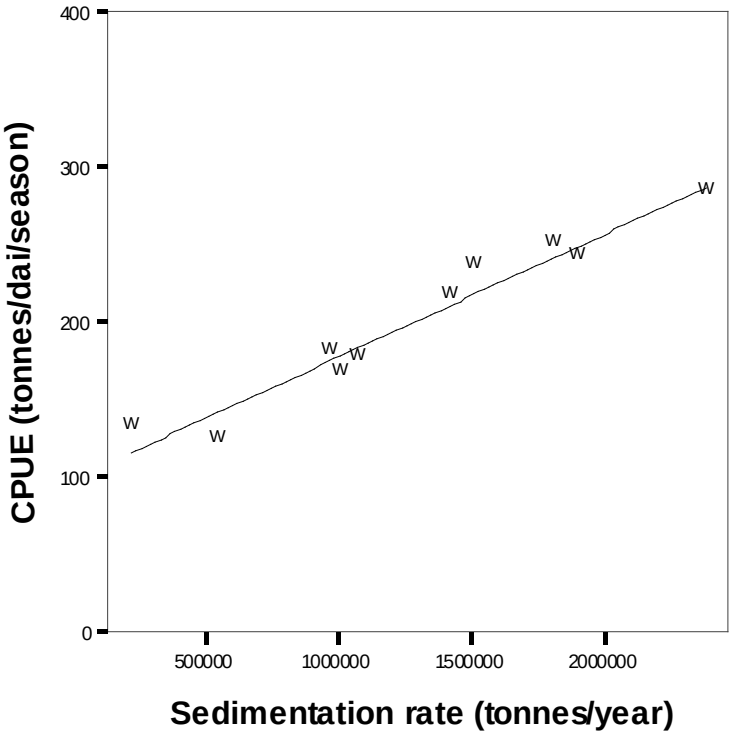

Figure 75. Monitored Dai fishery biomass index plotted as a linear function of rate of 3D Tonle Sap model floodplain sedimentation with fitted regression models. CPUE = 98.65 + 7.929E-05 x Sediment rate (d.f =10; R2 = 0.95; p < 0.001). Halls et al. 2010.

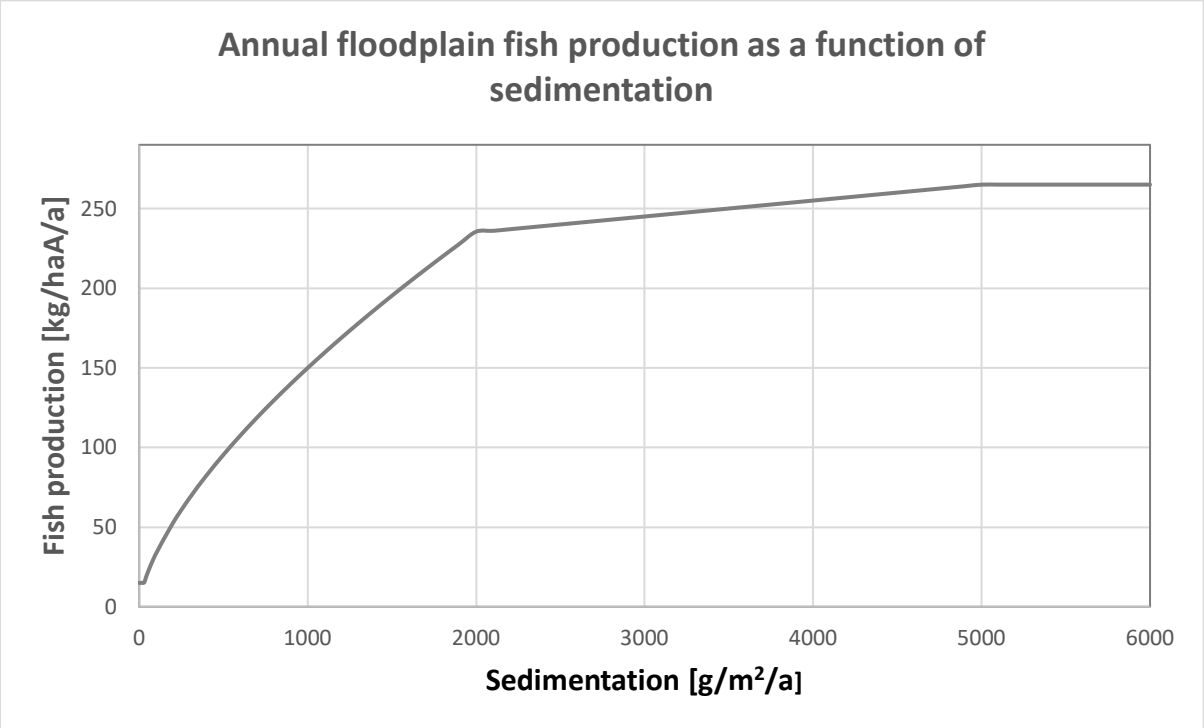

Figure 76. Tonle Sap floodplain fish production dependency on annual sedimentation. Statistical analysis based on Tonle Sap 3D model computed floodplain sedimentation, primary production and fisheries production.

Annual average 3D and IWRM model fish production is shown in Figure 77 and Figure 78. The figures show that the 3D model computed floodplain fish production can be estimated using the IWRM computed floodplain sedimentation.

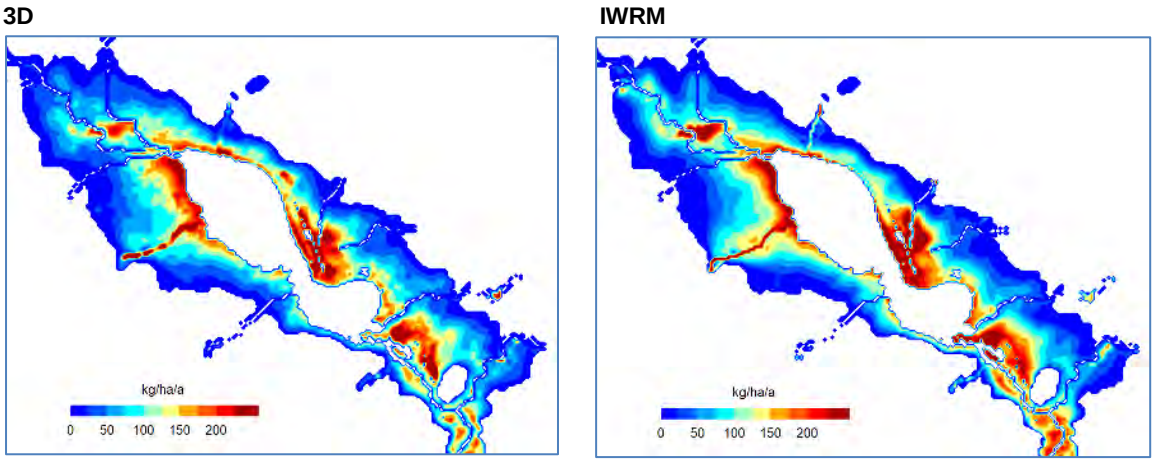

Figure 77. Tonle Sap floodplain fish production computed with the 3D model (left) and approximation with the IWRM model using sedimentation only (right).

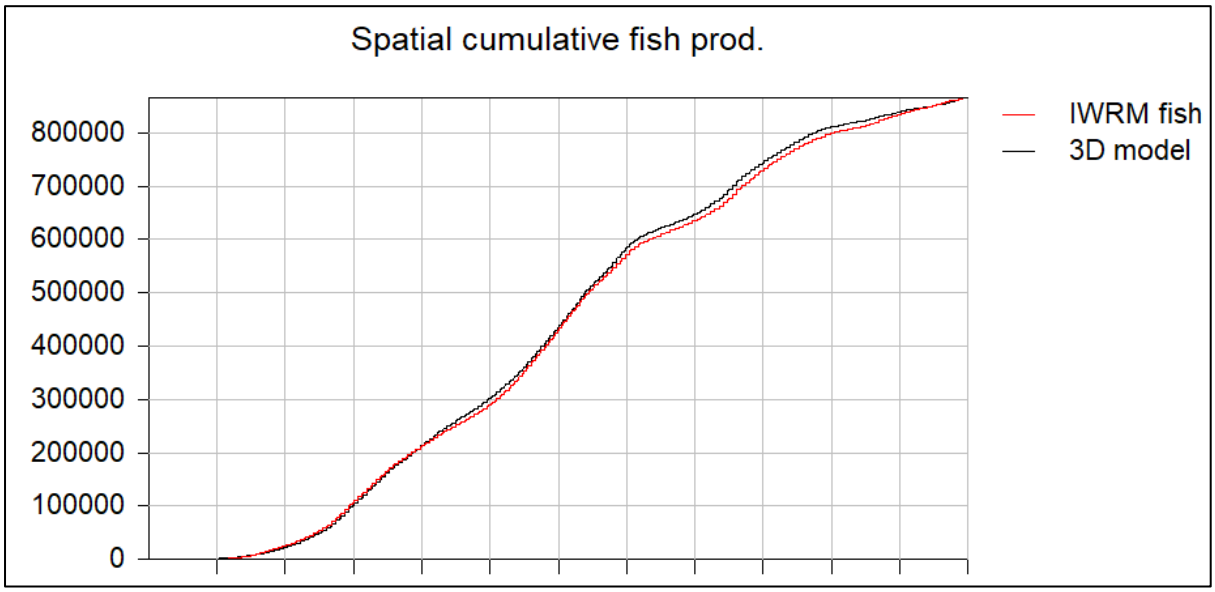

Figure 78. Comparison of 3D and IWRM computed Tonle Sap floodplain fish production. Cumulative fish production summing over model grid cells.

1.4.2. Agriculture modelling

Crop yield modelling is undertaken by integrating the FAO AquaCrop model within the IWRM distributed hydrological model. The AquaCrop model provides a framework and the algorithms to calculate crop yield based on climate, crop, soil, field management, and irrigation management. Each crop area within a base grid cell is assigned its own sub-cell and computed with full hydrology including infiltration, soil moisture and lateral surface and soil water flow, as well as the additional AquaCrop calculations. Characteristics of the model are:

- fully integrated with distributed hydrological modelling and water resources management modelling
- is a physiological plant growth model; in contrast earlier FAO CropWat used in the IQQM is hydrological crop model
- AquaCrop focuses on water stress
- suitable and detailed for irrigation demand, drought and climate change assessments
- simple data requirements - soil properties are usually not well known and AquaCrop has only one soil stress/soil fertility parameter to calibrate.

Further details of the AquaCrop model implementation can be found in the ANNEX.

In the Council Study modelling soil fertility/soil stress is linked with floodplain alluvium sedimentation computed by the model. Tonle Sap 3D primary productivity model has been used to derive relation between sedimentation and soil fertility.

Other factors than the alluvium affecting crop yields are flooding, droughts, climate change in general and salinity. In the AquaCrop model impact of soil salinity on crop growth is described with a salinity (soil) stress function:

$$K_{Salt} = 1 - \frac{e^{S_{rel} f_{shape}} - 1}{e^{f_{shape}} - 1} \quad \text{(Equation 1)}$$

$$S_{rel} = (C - ECe_n)/(ECe_x - ECe_n) \quad \text{(Equation 2)}$$

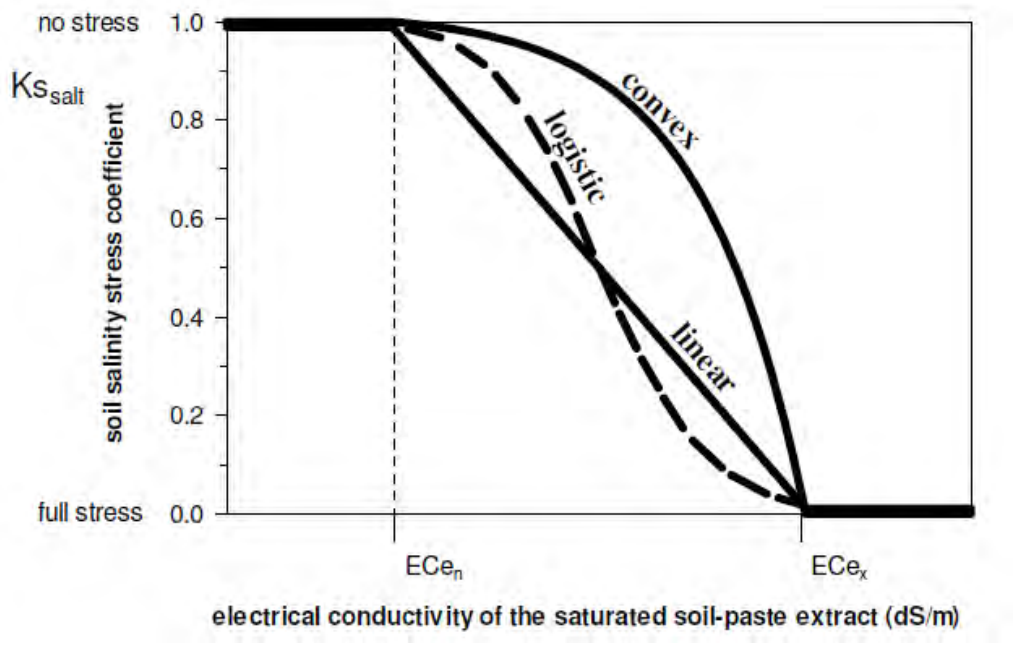

Figure 79. FAO AquaCrop salinity stress function (Raes et al. 2012). Original FAO stress function shape function is linear. Calibrated shapes are convex.

Mondal et al. (2015) have calibrated the salinity stress function in Bangladesh. The original crop yield data has been used to calibrate the Delta Impact Model with weather data corresponding to the Mekong Delta climate conditions. The original FAO and calibrated parameters are shown in the Table 2.

Table 2. Original FAO and calibrated climate conditions

Paremeter	FAO	Mondal et al.	IWRM Model
ECe_n [dS/m]	3	2	0.5
ECe_x [dS/m]	11	10	10
f_{shape}	0	2.4	1.4

Their corresponding crop yields are shown in the Figure 80.

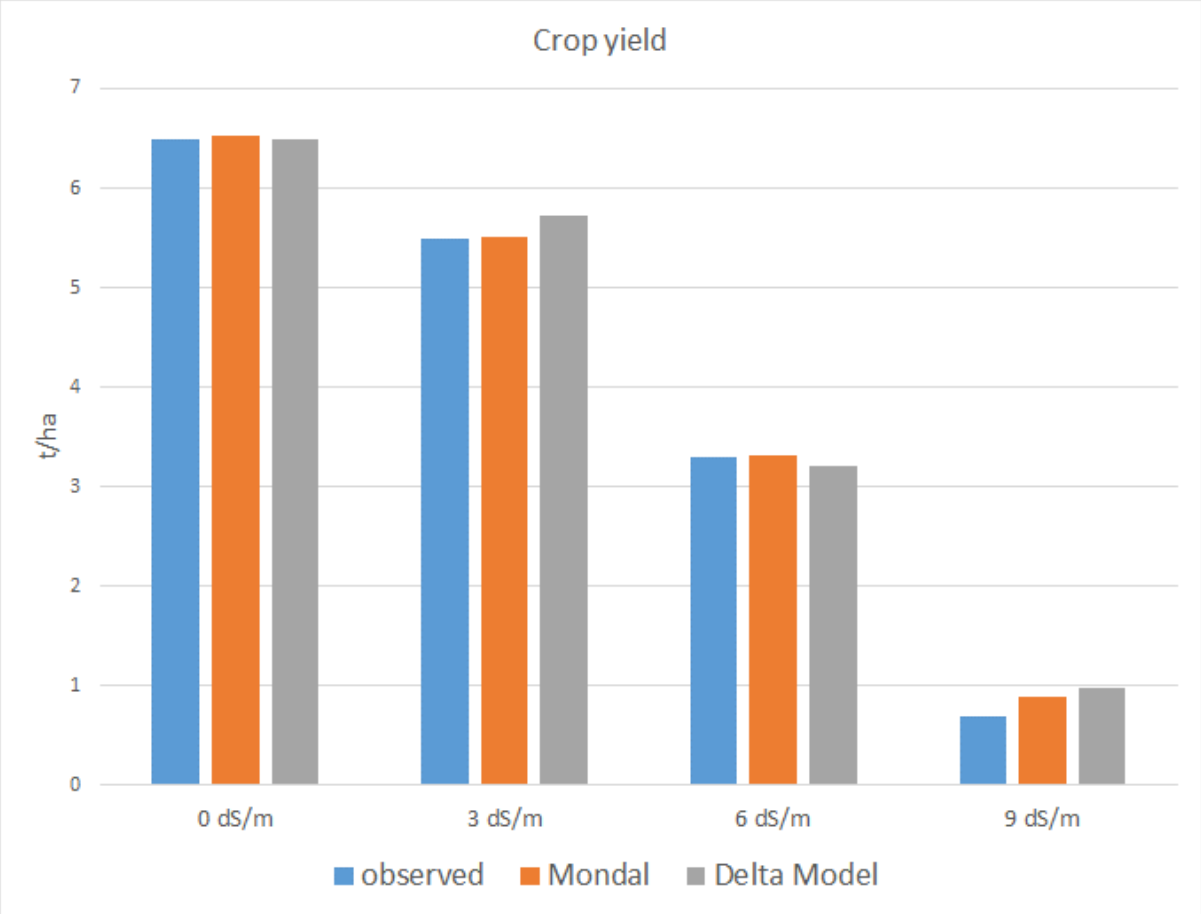

Figure 80. Comparison between observed (blue bars), Mondal AquaCrop (orange bars) and Delta Impact Model (grey bars) rice crop yields for different salinity treatments.

1.4.3. Aquaculture modelling

Penaeus vannamei is a common aquaculture shrimp used in the IWRM as an indicator saline water aquaculture species. It tolerates a wide range of salinities, from 0.5-45 ppt, is comfortable at 7-34 ppt, but grows particularly well at low salinities of around 10-15 ppt where the environment and the blood

are isosmotic (Wyban et al. 1991). The species and the salinity ranges have been taken as a basis for the Delta shrimp growth indexing. No actual aquaculture yields are computed as they depend on specific species, temperature, diseases, nutrition, added salt, flushing etc. Instead an environmental salinity dependent index is provided based on Penaeus vannamei preferences. The index is computed every day for each grid cell, summed and at the end of the computation converted to 0 to 1 scale where 0 signifies no growth and 1 maximum salinity dependent growth. The shape of the index function is:

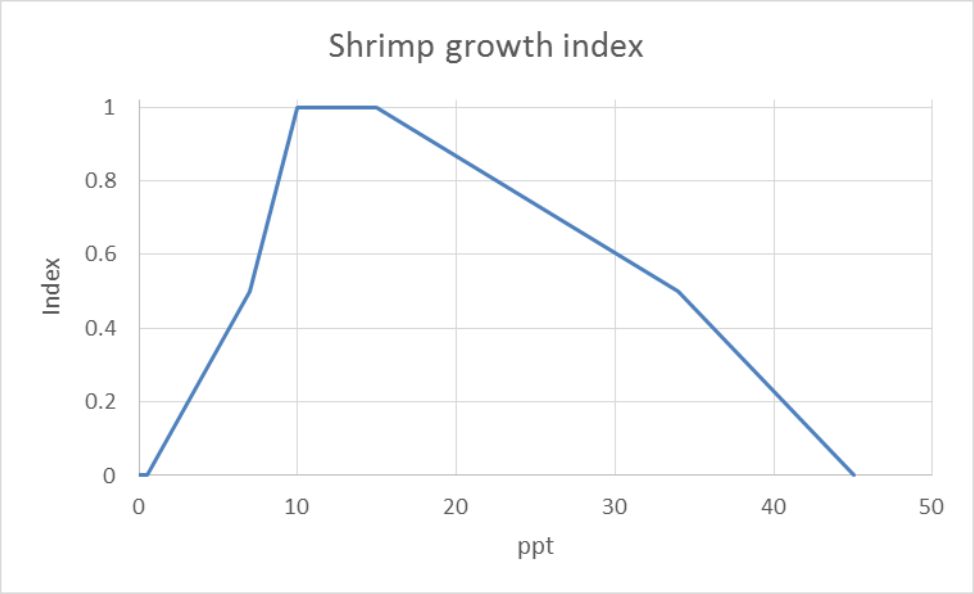

Figure 81. Shape of the *Penaeus vannamei* salinity dependent growth index.

1.5. Lake and coastal modelling

The 3D-EIA model is a general purpose hydrodynamic, water quality and productivity model for reservoirs, lakes, river channels, floodplains and coastal areas for 1D, 2D and 3D combined modelling. The Tonle Sap implementation is shown in Figure 82. Details of the 3D model implementation and calibration can be found in the ANNEX.

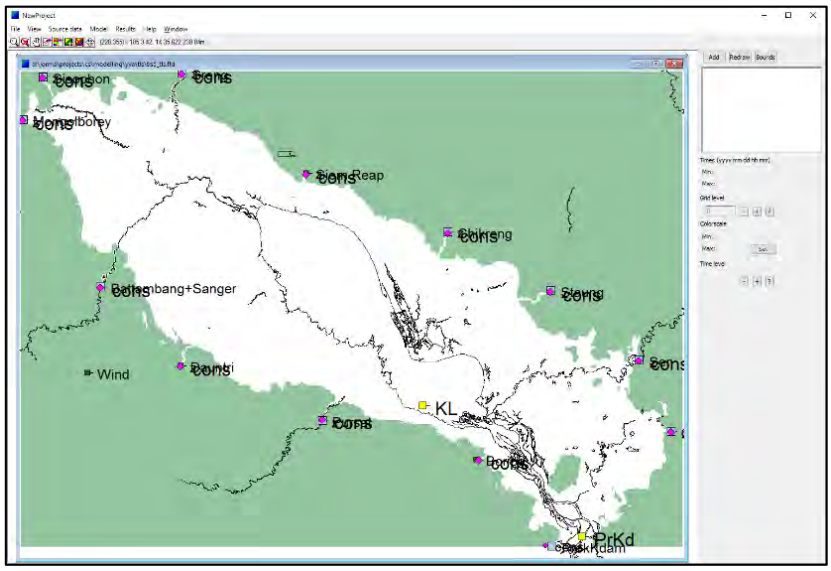

Figure 82. Tonle Sap 3D-EIA model user interface.

The sea area model covers whole South Sea focusing on the Mekong coastal area:

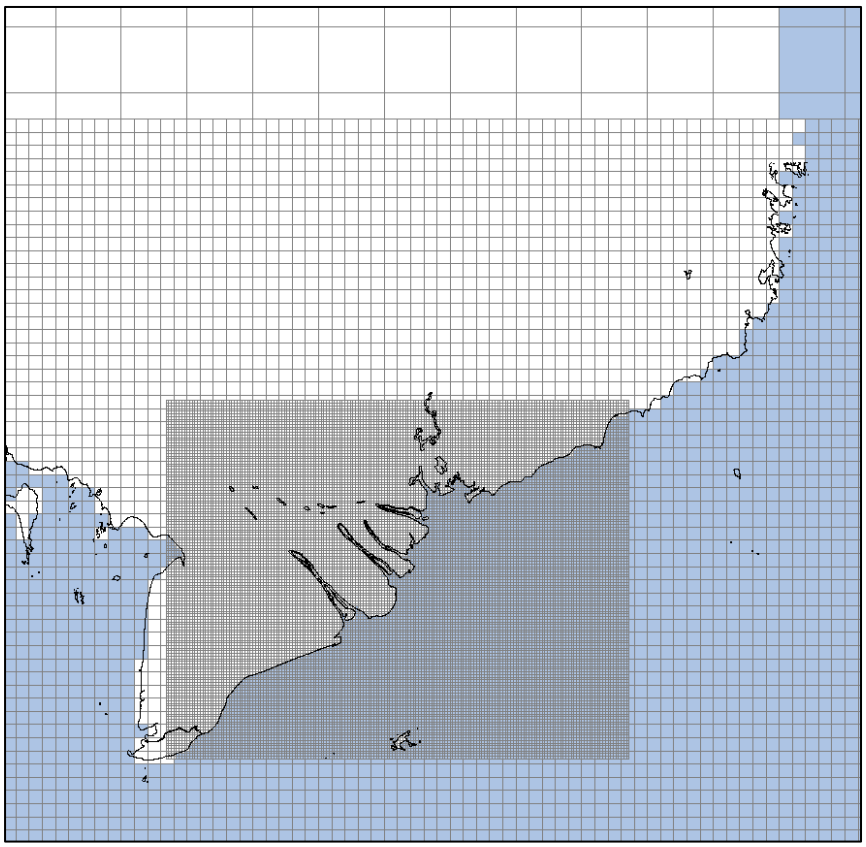

Figure 83. South Sea 3D-EIA model focusing high resolution nested model on the coast. Nested model grid sizes are 2 km, 10 km and 50 km.

An example of 3D model computed erosion is given in Figure 84. Further results of the coastal model are presented in the WUP-FIN Coastal Modelling Report.

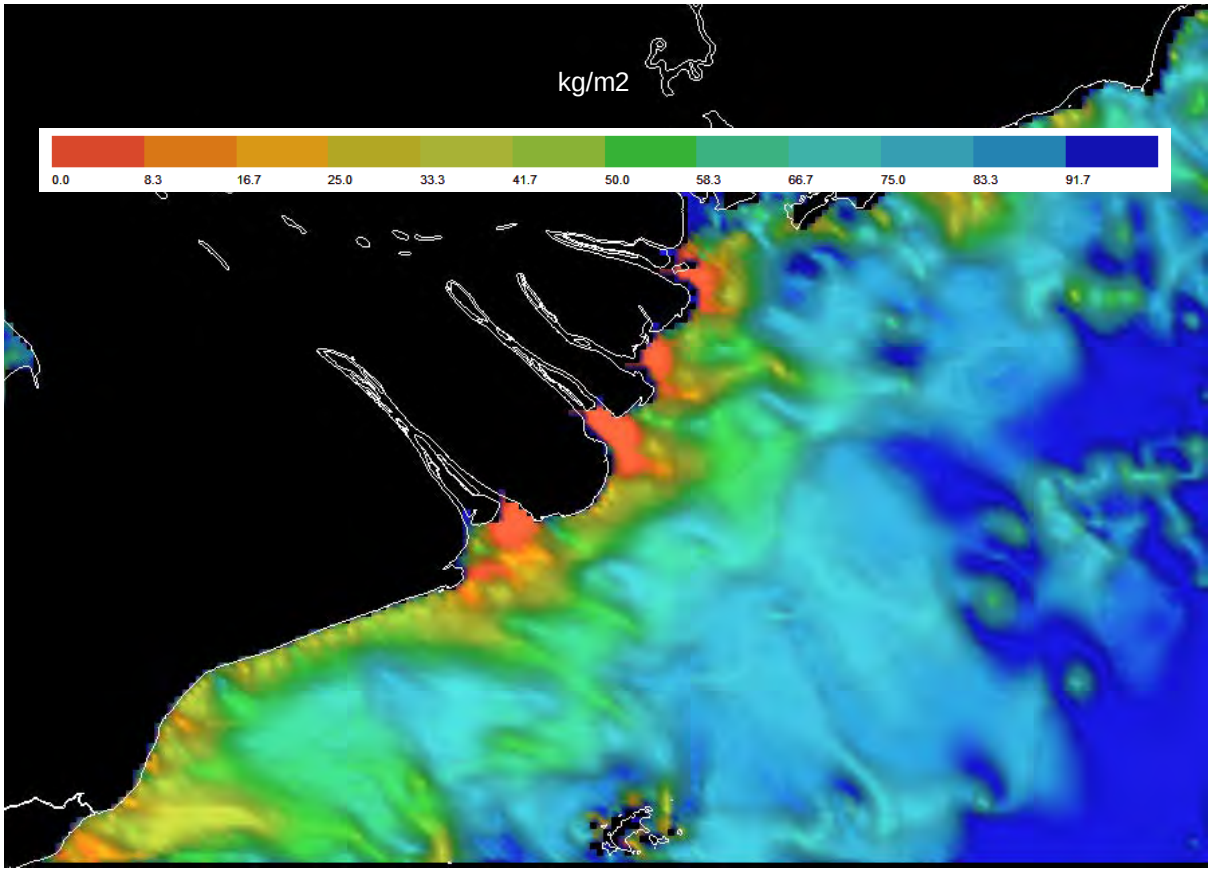

Figure 84. 3D model computed erosion off the Mekong coast.

A detailed 3D water quality model for computation of nutrient processes in the Tonle Sap Lake has been implemented in addition to the 3D-EIA hydrodynamic, water quality and productivity model. The dedicated 3D water quality model uses the pre-computed flow fields to speed up water quality computation. The model has been originally developed for hydropower reservoir modelling but is applicable also to natural lakes such as the Tonle Sap. The model and initial results are presented in the ANNEX.

1.6. Linking to the ecological assessment (BioRA)

1.6.1. BioRA modelling approach

Figure 85. BioRA Council Study Focal Areas.

BioRA Focal Areas are shown in Figure 85. IWRM modelling has been implemented in FA3 and FA5 – FA8. For these and FA1, FA2 and FA4 ISIS results have been provided.

For BioRA the model uses approximate floodplain sedimentation formula (source Robin Ellis, Dynamic SedNet Component Model Reference Guide, 2014):

$$FD_{fs}(kg) = I_f * \left(\frac{Q_f}{Q_L}\right) * \left(1 - e^{\frac{-v_p * A_f}{Q_f}}\right) \quad \text{(Equation 1)}$$

Where:

- Q_L = daily discharge (m3/s)
- Q_{bf} = Bank Full Flow (determined during parameterisation) (m^3/s)
- $Q_f = Q_L - Q_{bf}$ (m^3/s)
- I_f = daily fine sediment supply (kg)
- A_f = floodplain area (m^2)
- v_p = settling velocity (m/s), default for clay 0.0007.

The IWRM/VMOD model implementation differs from this formulation by computing Bank Full Flow and not giving it as a parameter. Different settling velocity is used for clay, silt and sand. Figure 86 presents model setup for floodplain sedimentation simulation in case river discharge and sediment load time series are utilized.

It should be noted that the approach is not used for the lower Delta model which is much more complex area. Instead flood propagation approach described in the previous chapter is used.

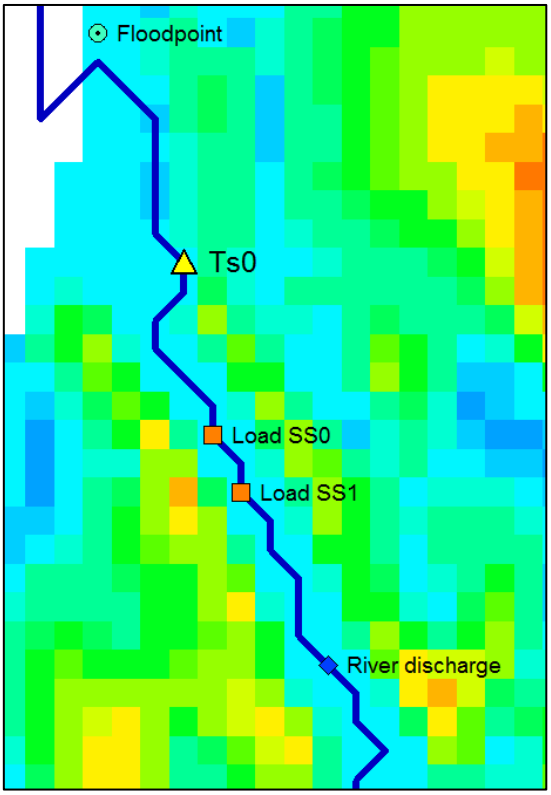

Figure 86. Model set up for floodplain sediment computation. SS0 = clay load, SS1 = silt load. Flood point provides water level information and can be obtained from ISIS or measurements.

Specific flooding, sedimentation, nutrient and salinity indicators have been provided for each of the focal areas. Examples of the areas are shown in Figure 87 and Figure 88.

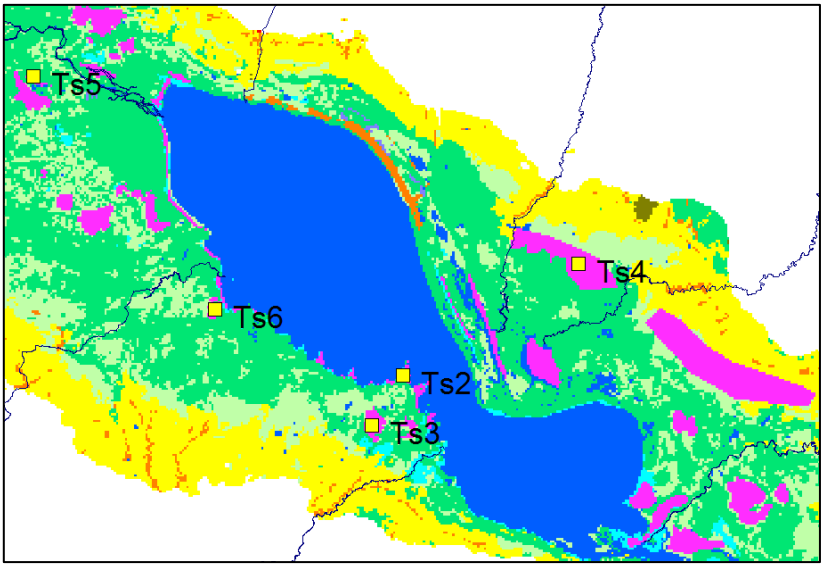

Figure 87. Location of the model output points for BioRA sample vegetation areas (purple areas).

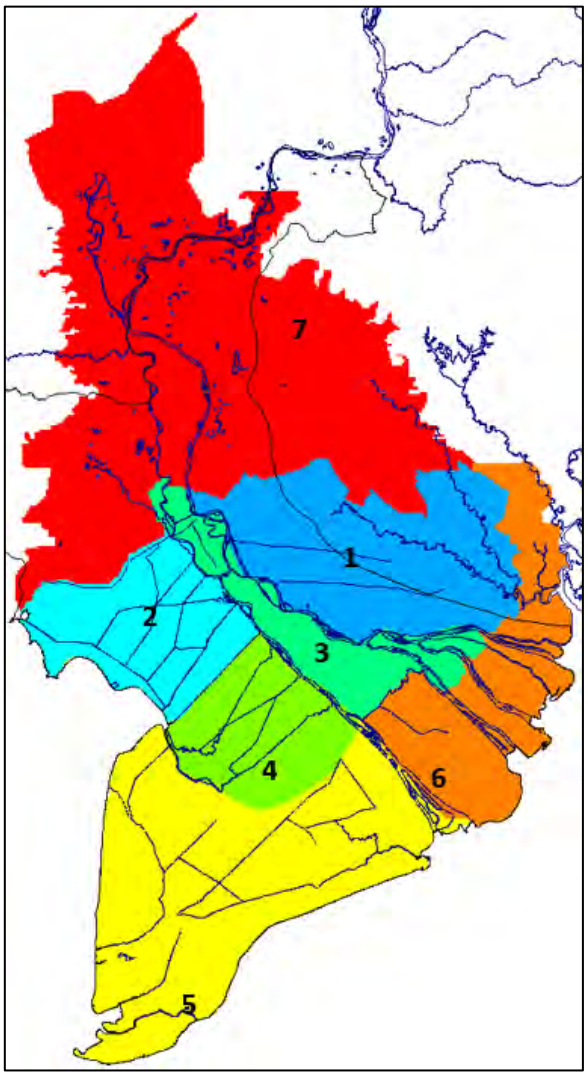

Figure 88.Definition of the Delta model BioRA output areas. Different indicators and average daily time series have been provided for each of the areas.

It has been possible to distinguish between the different vegetation types based on a simple flooding index:

$$I_{fl} = H_{fl} * A_{fl}/A_{max}$$

- I_{fl} = flooding index
- H_{fl} = average flooding depth in any given day
- A_{fl} = flooded area in any given day
- A_{max} = maximum flooded area

When the index is accumulated over a flooding period the different vegetation types can be distinguished:

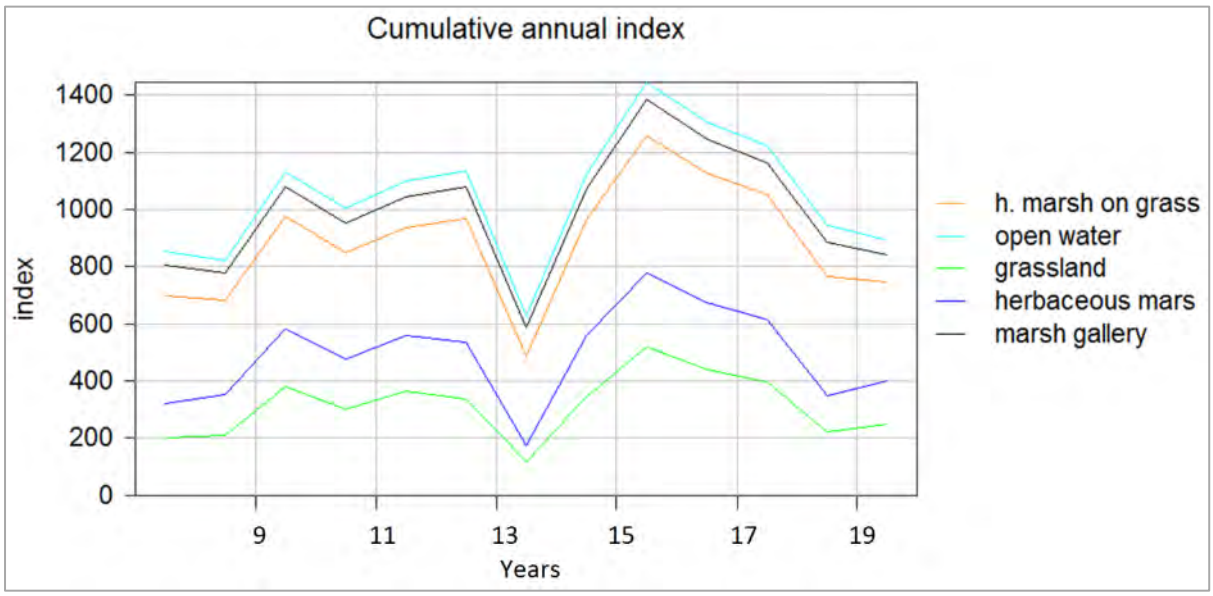

Figure 89. Cumulative annual indexes for the BioRA vegetation types.

This index will be used to indicate Mekong wetlands and their change in the future development scenarios.

1.6.2. Model outputs for BioRA

In the upper LMB IWRM modelling results have been prepared for the BioRA for **Nam Songkhram (only baseline), Xe Bang Fai and Kampong Cham**. The flood conditions are very variable depending on a hydrological year as can be seen from Figure 90. Consequently, also sedimentation and floodplain productivity vary significantly depending on a hydrological year.

Kampong Cham flooded area and daily floodplain silt sedimentation are shown in Figure 91 and Figure 92 respectively. Future scenarios differ significantly from the baseline as sedimentation is reduced and flooding delayed. Late wet season flooding is increased significantly in the main climate scenario case when baseline and other main scenarios are practically the same during the late season.

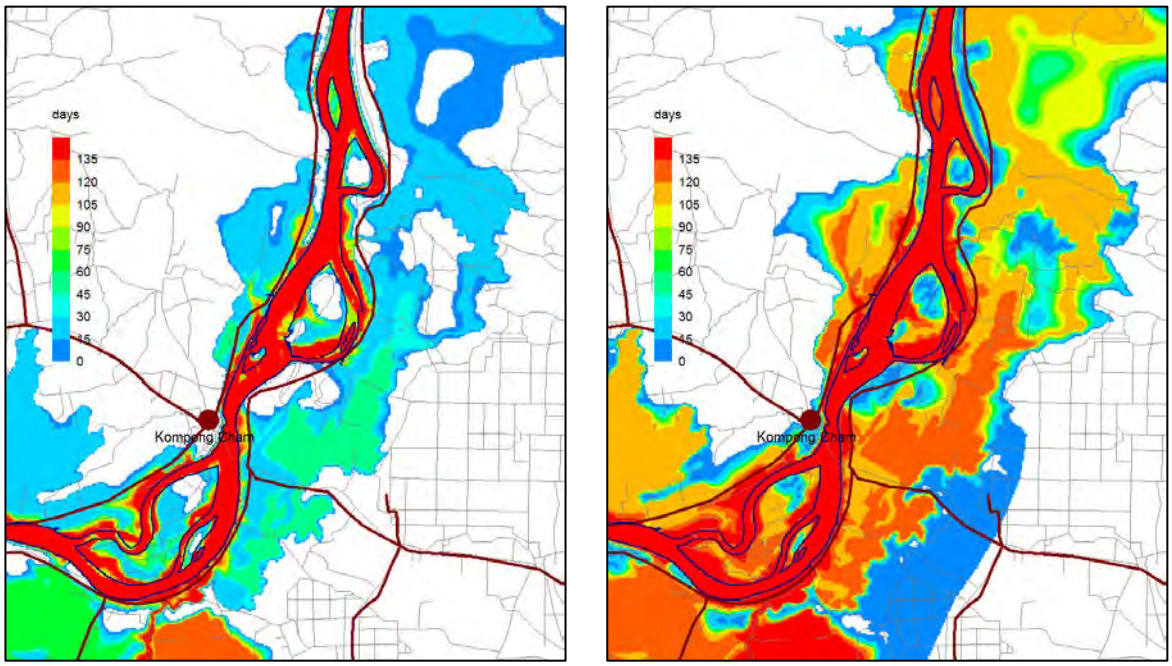

Figure 90. Flood duration in during driest year 1998 (left) and wettest year 1996 (right).

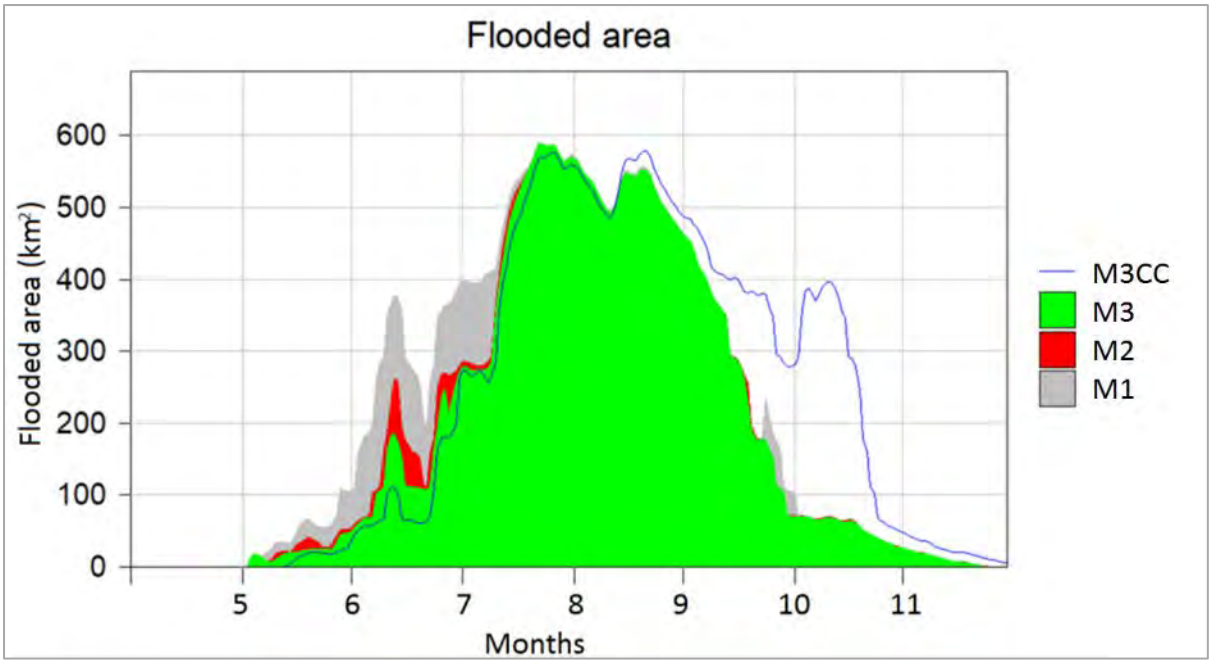

Figure 91. Kampong Cham flooded area in the main scenarios.

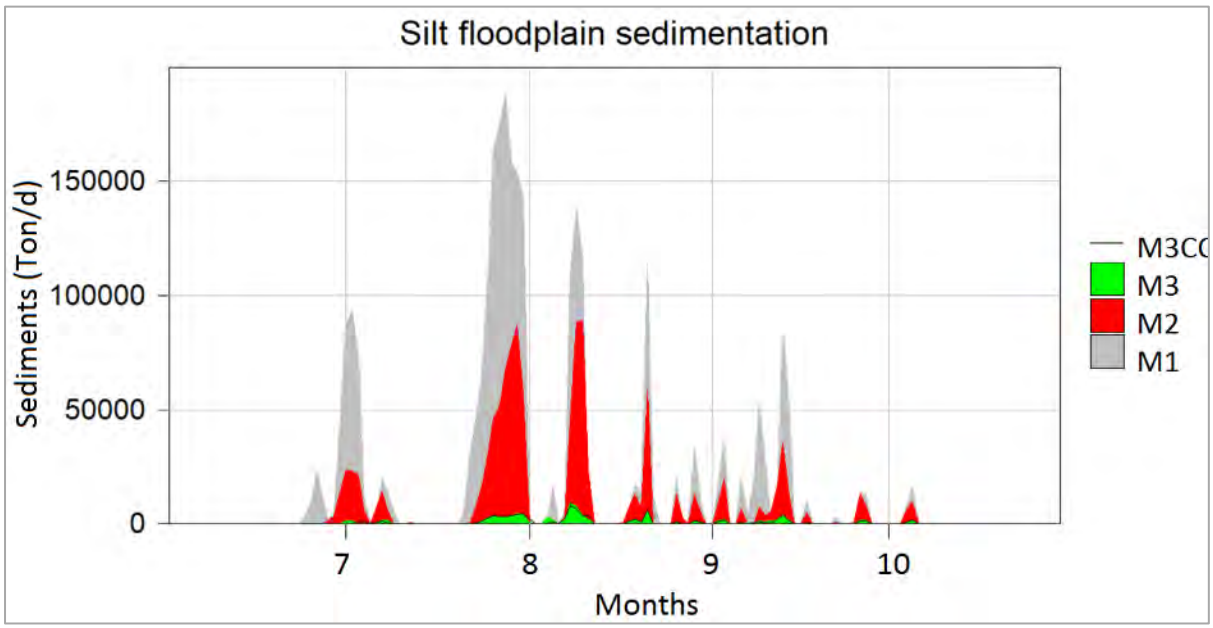

Figure 92. Kampong Cham total daily floodplain sedimentation for main scenarios.

Following indicators have been provided for BioRA for **Tonle Sap** ecological analysis:

- WL = AVERAGE WATER LEVEL (m)
- WD = AVERAGE WATER DEPTH (m)
- WA = WATER AREA (km2)
- WV = WATER VOLUME (km3)
- TP = TOTAL PRIMARY PRODUCTION (tC/d)
- PER = PERIPHYTON PRODUCTION (tC/d)
- PHY = PHYTOPLANKTON PRODUCTION (tC/d)
- TER = TERRESTRIAL PRODUCTION IN AQUATIC PHASE (tC/d)
- SEDB = TOTAL SEDIMENTATION (t/d)
- OX0 = AREA OF OXYGEN VERTICAL AVERAGE 0 - 2 MG/L (km2)
- OX2 = AREA OF OXYGEN VERTICAL AVERAGE 2 - 4 MG/L (km2)
- OX4 = AREA OF OXYGEN VERTICAL AVERAGE > 4 MG/L (km2)
- SECC = AVERAGE SECCHI DEPTH (m)
- EUPHVOL = EUPHOTIC VOLUME (km3)
- Fphy = Daily fish production sustained by phytoplankton (t/d)
- Fper = Daily fish production sustained by periphyton (t/d)
- Fter = Daily fish production sustained by terrestrial flooded vegatation (t/d)
- Ftot = Total daily fish production (t/d)

These indicators are provided separately for the lake proper and the floodplains as the processes and indicator values are fundamentally different in them.

In addition to the 3D model indicators simple flood depth and area indicators have been prepared for BioRA Tonle Sap assessment. An example is shown in the table below.

Table 3. Example of Tonle Sapflood indicator output for the Bio-assessment. Table shows baseline flood area indicators.

	Flood area							
	Depth < 3.5 m					Depth > 3.5 m		
	Peak	Av	Max	Cumul		Peak	Av	Max	Cumul
year	d	m	m	m		d	m	m	m
1985	118	2965	4958	895415		65	1672	3267	247420
1986	151	2962	4961	900380		62	2020	3639	298900
1987	133	2748	4764	769392		40	1348	2288	160373
1988	148	2866	4795	857005		79	1211	1755	164636
1989	131	2900	4961	875709		64	1682	2806	242274
1990	94	3306	4951	988629		84	2182	3976	381776
1991	159	3132	4958	939481		68	2551	4764	413336
1992	123	2646	4764	740967		49	1373	2240	164723
1993	109	2891	4882	835398		55	1497	2535	211007
1994	90	3169	4958	960065		78	2562	4993	427815
1995	94	3187	4947	949588		71	2674	5066	441194
1996	120	3008	4960	1016693		67	2772	5276	482364
1997	222	2538	4956	911063		63	2327	4070	353688
1998	104	2705	4744	768168		48	1151	2239	139300
1999	171	3292	4962	1066564		88	1859	3515	345726
2000	102	3237	4961	1123297		101	3013	5590	602658
2001	99	3206	4943	984182		79	2717	5157	494554
2002	167	3342	4958	999125		75	2695	5284	474293
2003	116	2722	4954	851985		58	1782	3501	245950
2004	151	3038	4957	890058		61	2443	4877	359160
2005	76	3267	4952	921239		57	2728	4998	433748
2006	173	2961	4957	959437		79	2635	4735	437439
2007	193	3002	4959	999712		80	2311	4326	385928
2008	195	3457	4958	874700		82	2581	4212	420702

Delta flooding, sediment, nutrient and salinity indicators have been developed together in collaboration between the modelling and BioRA teams. Examples of the indicators provided to BioRA assessment are shown in Table 4 and Table 5.

Table 4. Part of flood indicator output for the Bio-assessment.

Year and area	Flood areas km^2					
	0.05-0.3 m	0.3-0.55 m < 110 d	0.3-0.55 m > 110 d	> 0.55 m dry season	> 200 d	> 2.75 m
1985						
1	5708	5821	0	33	196	12
2	3220	2611	0	1	0	0
3	2785	2431	1	14	123	6
4	3009	1744	0	0	0	0
5	4978	2614	1031	265	2454	2
6	2147	1328	522	67	1010	0
7	6848	7037	14	171	606	2471
1986						
1	5845	6050	0	49	196	31
2	3121	2731	0	6	0	1
3	2727	2428	0	16	124	15
4	3082	1816	2	0	0	0
5	4773	2573	1084	266	2461	225
6	2460	1317	524	82	1077	0
7	7729	7873	21	207	925	3152
1987						
1	5566	5511	0	24	193	1
2	2455	2070	0	0	0	0
3	2692	2255	2	12	120	1
4	2755	1507	0	0	0	22
5	4868	3177	1079	265	2458	91
6	2167	1566	588	75	1098	138
7	6375	6553	11	159	840	2124
1988						
1	4996	4552	0	31	194	0
2	2306	1921	0	3	0	0
3	2398	1791	1	14	122	0

Table 5. Salinity indicator output for the Bio-assessment.

	>4 g/l 1-4 m	>4 g/l 4-6 m	>4 g/l >6 m	<4 g/l	<1 g/l	av	max	min	>20 g/l	>20 g/l >1 m
	km^2	km^2	km^2	km^2	km^2	g/l	g/l	g/l	km^2	km^2
1998										
1	173	0	0	7551	7142	1.03	9.67	0	0	0
2	0	0	0	4918	4884	2.73	11.59	0	0	0
3	100	0	0	3526	3445	1.00	9.58	0	0	0
4	12	0	0	3837	2886	1.57	20.00	0	0	0
5	1197	1838	310	7881	7103	9.47	32.57	0	3201	1965
6	1011	542	153	4463	4338	8.17	27.55	0	720	185
7	0	0	0	24477	24474	0.22	11.24	0	0	0
2007										
1	186	0	0	7326	6974	0.98	9.96	0	0	0
2	0	0	0	4922	4841	1.62	7.59	0	0	0
3	121	0	0	3515	3431	0.98	9.80	0	0	0
4	11	0	0	3185	2814	1.30	19.53	0	0	0
5	754	1851	287	7831	6981	8.69	32.57	0	3183	1955
6	882	490	149	4635	4292	7.24	27.11	0	723	169
7	0	0	0	24467	24464	0.11	9.96	0	0	0

1.7. Linking to the social and economic assessment

Socio-economic analysis requires detailed information on production for the many SIMVA zones (Figure 61). Originally the data processing was planned to be implemented similar to the BioRA analysis where indicators are processed for areas defined by land use or other classification inside the model. As this would require model tailoring and use of many additional land use classes it is not very general nor practical method. Instead automated GIS preprocessing was developed that is general and flexible to include new processing requirements. A statistical processing system was implemented in the model (Figure 93) that produces statistical ESRI ASC-maps of required frequency that are processed automatically by GIS. At the same time model produces binary statistics data that can be animated and processed within the model user interface (Figure 94).

Powerful GIS and Excel post-processing system has been developed utilizing the model ASC output files. The system is largely automated and includes user interface for easy configuration. Any areas can be selected for processing and the system prepares automatically the socio-economic analysis tables (Table 6 and Table 7). At the same time the system prepares the output in graphical format for ease of checking the model results and for reporting (Table 8).

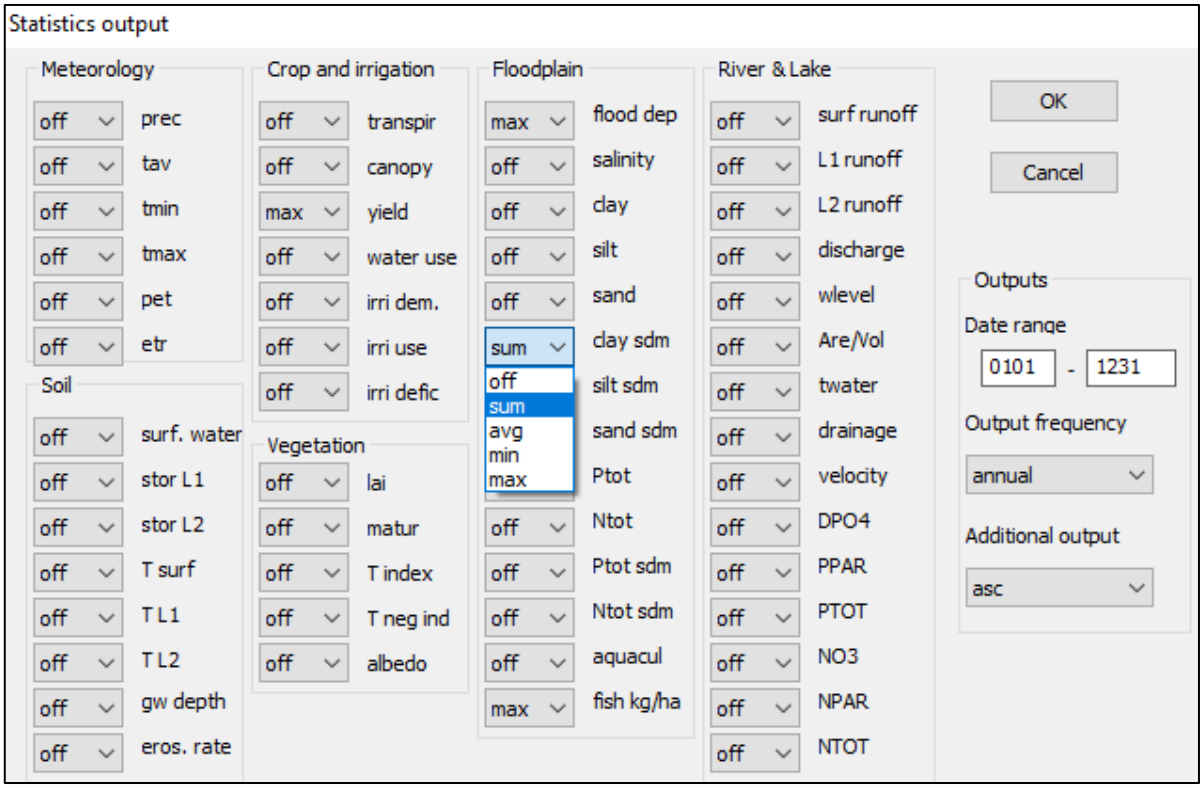

Figure 93. Model dialogue window for defining statistics outputs and formats.

Figure 94. Model statistics viewing and processing window.

Examples of the model socio-economic tabular outputs are given in Table 2 and Table 3.

Table 6. Part of model socio-economic output table.

Open	Zone 3 B Thailand-Mainstream							
M1	**Population**	**fish (Ton)**	**OAA (Ton)**	**Aquaculture (Ton)**	**Cattle/Buffalo (Ton)**	**Goats (Ton)**	**Pigs (Ton)**	**Poultry (Ton)**
1	739086.28	66536.29	15991.76	19000.00	6719.23	1372.27	150944.58	10445452.25
2	739581.37	68334.18	16007.75	19380.00	6732.67	1399.72	158491.81	10863270.34
3	740092.05	65999.52	16023.76	19767.60	6746.13	1427.71	166416.40	11297801.15
4	740618.34	65317.73	16039.78	20162.95	6759.62	1456.27	174737.22	11749713.20
5	741160.23	64032.33	16055.82	20566.21	6773.14	1485.39	183474.08	12219701.72
6	741717.72	68137.00	16071.88	20977.54	6786.69	1515.10	192647.79	12708489.79
7	742290.81	70654.24	16087.95	21397.09	6800.26	1545.40	202280.17	13216829.38
8	742879.50	67144.42	16104.04	21825.03	6813.86	1576.31	212394.18	13745502.56
9	743483.79	67565.34	16120.14	22261.53	6827.49	1607.84	223013.89	14295322.66
10	744103.68	70429.20	16136.26	22706.76	6841.15	1639.99	234164.59	14867135.57
11	744739.18	72567.79	16152.40	23160.89	6854.83	1672.79	245872.82	15461820.99
12	745390.27	73457.56	16168.55	23624.11	6868.54	1706.25	258166.46	16080293.83
13	746056.96	75331.38	16184.72	24096.59	6882.28	1740.37	271074.78	16723505.58
14	746739.26	75511.76	16200.90	24578.53	6896.04	1775.18	284628.52	17392445.81
15	747437.16	72764.19	16217.10	25070.10	6909.83	1810.68	298859.95	18088143.64
16	748150.65	74531.73	16233.32	25571.50	6923.65	1846.90	313802.94	18811669.38
17	748879.75	75759.03	16249.55	26082.93	6937.50	1883.84	329493.09	19564136.16
18	749624.45	76655.06	16265.80	26604.59	6951.37	1921.51	345967.74	20346701.61
19	750384.75	75911.44	16282.07	27136.68	6965.28	1959.94	363266.13	21160569.67
20	751160.65	75074.71	16298.35	27679.41	6979.21	1999.14	381429.44	22006992.46
21	751952.15	75059.05	16314.65	28233.00	6993.17	2039.12	400500.91	22887272.16
22	752759.25	77080.53	16330.96	28797.66	7007.15	2079.91	420525.96	23802763.04
23	753581.96	74063.78	16347.30	29373.61	7021.17	2121.50	441552.25	24754873.56
24	754420.26	80585.55	16363.64	29961.09	7035.21	2163.94	463629.87	25745068.51
M2	**Population**	**fish (Ton)**	**OAA (Ton**	**Aquaculture (Ton)**	**Cattle/Buffalo (Ton**	**Goats (Ton**	**Pigs (Ton**	**Poultry (Ton**
1	739086.28	65624.90	14392.58	19000.00	6719.23	1372.27	150944.58	10445452.25
2	739581.37	63378.37	14406.97	19380.00	6732.67	1399.72	158491.81	10863270.34
3	740092.05	58943.63	14421.38	19767.60	6746.13	1427.71	166416.40	11297801.15
4	740618.34	57936.46	14435.80	20162.95	6759.62	1456.27	174737.22	11749713.20
5	741160.23	56536.62	14450.24	20566.21	6773.14	1485.39	183474.08	12219701.72
6	741717.72	58339.48	14464.69	20977.54	6786.69	1515.10	192647.79	12708489.79
7	742290.81	58872.75	14479.15	21397.09	6800.26	1545.40	202280.17	13216829.38
8	742879.50	55170.24	14493.63	21825.03	6813.86	1576.31	212394.18	13745502.56
9	743483.79	53573.24	14508.13	22261.53	6827.49	1607.84	223013.89	14295322.66
10	744103.68	55273.99	14522.63	22706.76	6841.15	1639.99	234164.59	14867135.57
11	744739.18	56028.00	14537.16	23160.89	6854.83	1672.79	245872.82	15461820.99
12	745390.27	56245.29	14551.69	23624.11	6868.54	1706.25	258166.46	16080293.83
13	746056.96	56174.41	14566.25	24096.59	6882.28	1740.37	271074.78	16723505.58
14	746739.26	55243.99	14580.81	24578.53	6896.04	1775.18	284628.52	17392445.81
15	747437.16	54194.68	14595.39	25070.10	6909.83	1810.68	298859.95	18088143.64
16	748150.65	56576.86	14609.99	25571.50	6923.65	1846.90	313802.94	18811669.38
17	748879.75	57641.31	14624.60	26082.93	6937.50	1883.84	329493.09	19564136.16
18	749624.45	57939.10	14639.22	26604.59	6951.37	1921.51	345967.74	20346701.61
19	750384.75	52971.69	14653.86	27136.68	6965.28	1959.94	363266.13	21160569.67
20	751160.65	55098.39	14668.52	27679.41	6979.21	1999.14	381429.44	22006992.46
21	751952.15	55821.44	14683.18	28233.00	6993.17	2039.12	400500.91	22887272.16
22	752759.25	56283.37	14697.87	28797.66	7007.15	2079.91	420525.96	23802763.04
23	753581.96	55207.42	14712.57	29373.61	7021.17	2121.50	441552.25	24754873.56
24	754420.26	58140.79	14727.28	29961.09	7035.21	2163.94	463629.87	25745068.51
M3	**Population**	**fish (Ton)**	**OAA (Ton**	**Aquaculture (Ton)**	**Cattle/Buffalo (Ton**	**Goats (Ton**	**Pigs (Ton**	**Poultry (Ton**
1	739086.28	66586.82	11993.82	19000.00	6719.23	1372.27	150944.58	10445452.25
2	739581.37	51123.33	12005.81	19380.00	6732.67	1399.72	158491.81	10863270.34
3	740092.05	44712.18	12017.82	19767.60	6746.13	1427.71	166416.40	11297801.15
4	740618.34	42265.90	12029.84	20162.95	6759.62	1456.27	174737.22	11749713.20
5	741160.23	38942.59	12041.87	20566.21	6773.14	1485.39	183474.08	12219701.72
6	741717.72	39143.54	12053.91	20977.54	6786.69	1515.10	192647.79	12708489.79
7	742290.81	39040.17	12065.96	21397.09	6800.26	1545.40	202280.17	13216829.38
8	742879.50	35137.56	12078.03	21825.03	6813.86	1576.31	212394.18	13745502.56
9	743483.79	32955.84	12090.11	22261.53	6827.49	1607.84	223013.89	14295322.66
10	744103.68	34265.71	12102.20	22706.76	6841.15	1639.99	234164.59	14867135.57

Table 7. Part of model socio-economic output table.

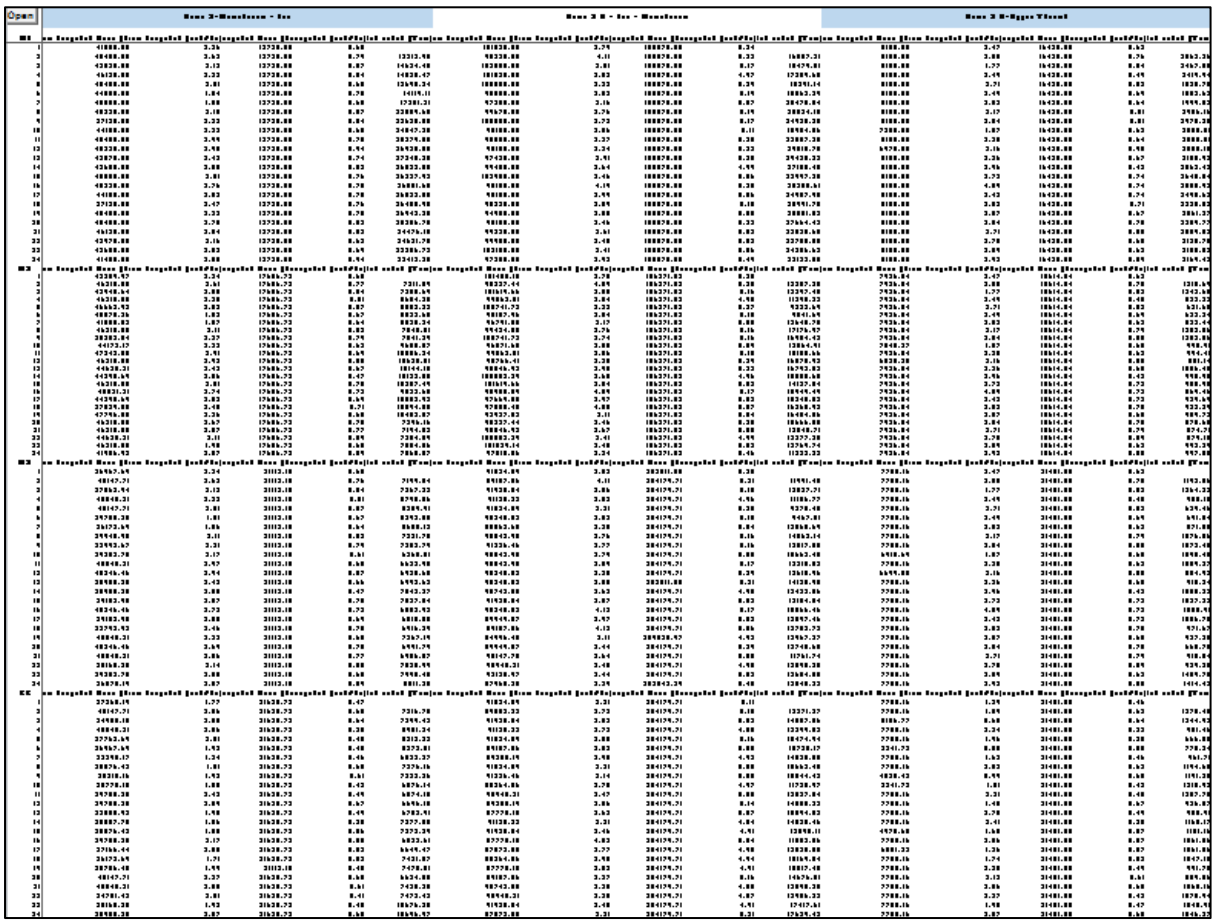

Table 8. Part of model socio-economic graphic outputs.

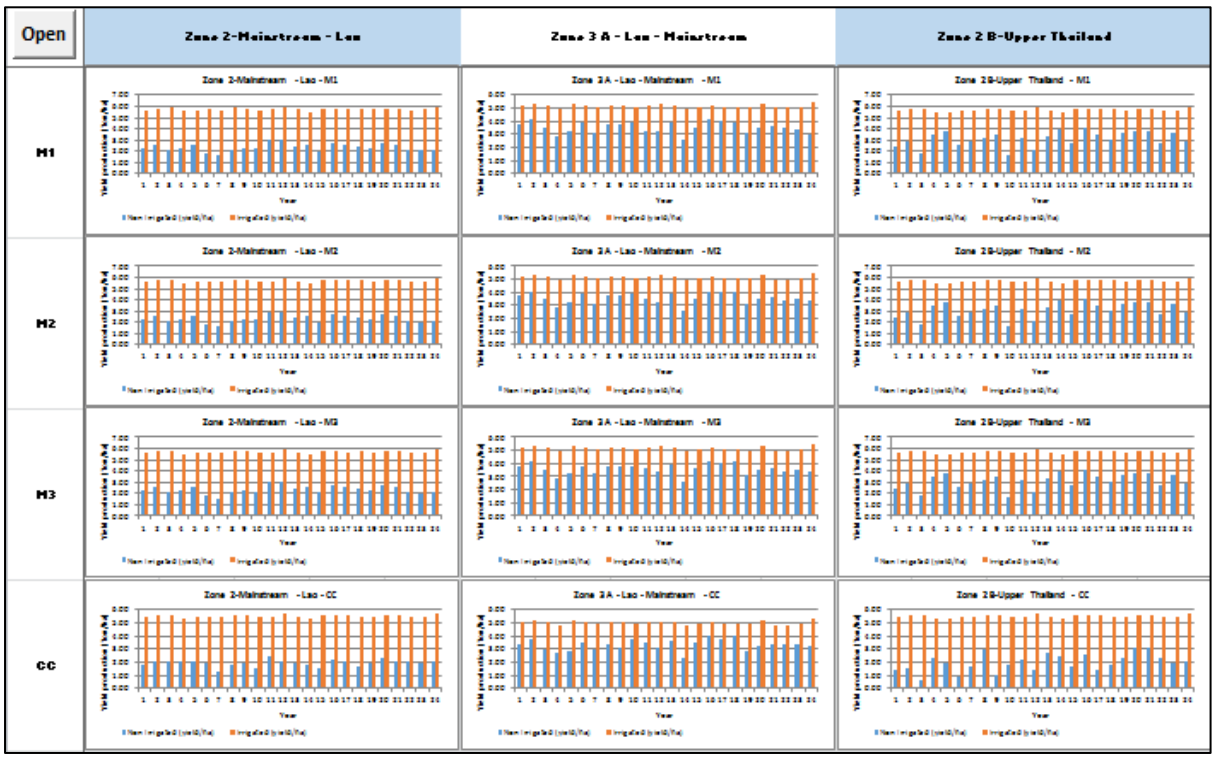

Model indicator processing for the lower LMB uses same methodology as for the upper part. An example of the model results provided to the socio-economic team is shown in Table 4.

Table 9. Example Delta model outputs for the socio-economic assessment.

Open	Zone 6 A VietNam Delta - freshwater				
M1	**Non Irrigated Area (ha)**	**Non Irrigated (Ton/ha)**	**Irrigated Area (ha)**	**Irrigated (Ton/ha)**	**Fish catch (Ton**
1	105000.00	4.10	1240470.00	5.79	
2	101563.00	4.26	1233750.00	6.06	102432.74
3	107656.00	4.65	1234690.00	6.04	121548.08
4	107813.00	4.04	1234530.00	5.84	120748.10
5	103906.00	3.75	1236410.00	5.94	90910.73
6	93750.00	3.22	1234370.00	5.91	104853.13
7	96093.70	5.05	1232660.00	5.99	123302.28
8	107969.00	4.62	1231090.00	6.08	128951.90
9	102344.00	5.41	1237810.00	6.16	130443.22
10	81406.30	4.03	1235000.00	5.95	116369.24
11	104375.00	4.16	1234690.00	6.01	124960.51
12	104063.00	4.17	1229840.00	6.29	142659.43
13	95156.20	3.38	1227190.00	6.25	164695.43
14	107813.00	4.98	1233440.00	5.75	162361.40
15	104375.00	3.86	1232500.00	5.98	116757.03
16	68125.00	5.18	1230000.00	6.21	169268.63
17	89843.80	3.91	1228440.00	6.01	173591.82
18	82187.50	4.16	1229370.00	6.01	125162.10
19	105781.00	4.71	1227970.00	6.11	134687.50
20	105625.00	3.37	1234220.00	6.00	134076.41
21	106094.00	3.07	1234370.00	5.98	112638.37
22	95468.70	4.38	1229530.00	6.33	150010.77
23	106250.00	4.69	1231870.00	6.23	161781.13
24	100469.00	3.44	1228750.00	5.83	161557.81
M2	**Non Irrigated Area (ha)**	**Non Irrigated (Ton/ha)**	**Irrigated Area (ha)**	**Irrigated (Ton/ha)**	**Fish catch (Ton**
1	107031.00	4.23	1231555.16	5.79	
2	105937.00	4.40	1227187.38	5.94	59479.04
3	109375.00	4.74	1226569.11	5.87	62330.42
4	108750.00	4.25	1230149.09	5.75	64006.62
5	107344.00	3.96	1229062.13	5.89	63764.74
6	100312.00	3.19	1228433.89	5.80	69260.93
7	102969.00	5.11	1225322.59	5.90	90110.12
8	109219.00	4.92	1224385.22	5.94	92360.82
9	107969.00	5.55	1231555.16	5.99	80253.52
10	88750.00	4.07	1230149.09	5.79	59045.67
11	107813.00	4.35	1226409.55	5.89	83270.66
12	106875.00	4.36	1223766.95	6.09	83373.59
13	103750.00	3.43	1221273.92	5.96	84012.68
14	109219.00	5.01	1227815.62	5.64	79309.94
15	104531.00	4.16	1224694.35	5.89	72284.22
16	73593.70	5.14	1224076.08	5.92	83042.78
17	96093.70	3.95	1222989.12	5.91	97805.50
18	87343.80	4.20	1223298.26	5.93	97165.36
19	108438.00	5.05	1223138.70	5.97	94010.85
20	107813.00	3.60	1227656.07	5.89	93004.46
21	107813.00	3.44	1228433.89	5.88	77375.94
22	104688.00	4.44	1223138.70	6.14	97498.06
23	108281.00	4.98	1224694.35	6.02	101215.69
24	104531.00	3.72	1223298.26	5.67	99472.12
M3	**Non Irrigated Area (ha)**	**Non Irrigated (yield/ha)**	**Irrigated Area (ha)**	**Irrigated (yield/ha)**	**Fish catch (Ton**
1	107500.00	4.24	1201085.75	5.79	
2	107031.00	4.42	1195162.22	5.85	23286.93
3	109375.00	4.76	1195765.27	5.79	24019.57
4	108906.00	4.33	1198051.03	5.68	23973.11
5	108438.00	3.97	1196378.05	5.80	22570.59
6	100937.00	3.22	1197292.35	5.72	31914.17
7	105781.00	5.10	1195006.59	5.80	48813.02
8	109531.00	4.98	1194247.91	5.86	51462.34
9	108594.00	5.61	1200784.22	5.95	50364.85

2. Annex 2 - Tonle Sap watershed hydrological and water quality modelling

The Working Paper “Modelling Framework for the Council Study” states about VMOD (the hydrological component of the IWRM model) that “Tonle Sap VMOD will provide sediment and nutrient loads to the Tonle Sap Lake model” and “VMOD: backup in case SWAT/IQQM not be able to provide some WQ parameters for Water quality EIA need in Tonle Sap.” As the delivery of the final SWAT results was delayed until August 2016 the results could be used for the lake model calibration that occurred almost one year earlier. 3D model re-calibration using SWAT results can be considered when SWAT results are improved further as shown later in this chapter.

2.1. Land Use

The discussion in this chapter relates also to the land use for the 3D lake model.

For compatibility with the DSF models the MRC 2003 land cover data has been used for the hydrological IWRM/VMOD Tonle Sap model. However, for impact modelling new 2010 land use data has been used because it can be considered to be closer to 2007 baseline and to be more accurate. The 2003 data has also major issues in the Delta and can’t be used there without major modifications.

MRC Land Cover maps for 2003 and 2010 are compared in **Figure 95**. It can be seen that agricultural expansion is occurring to the Tonle Sap floodplains and forest areas.

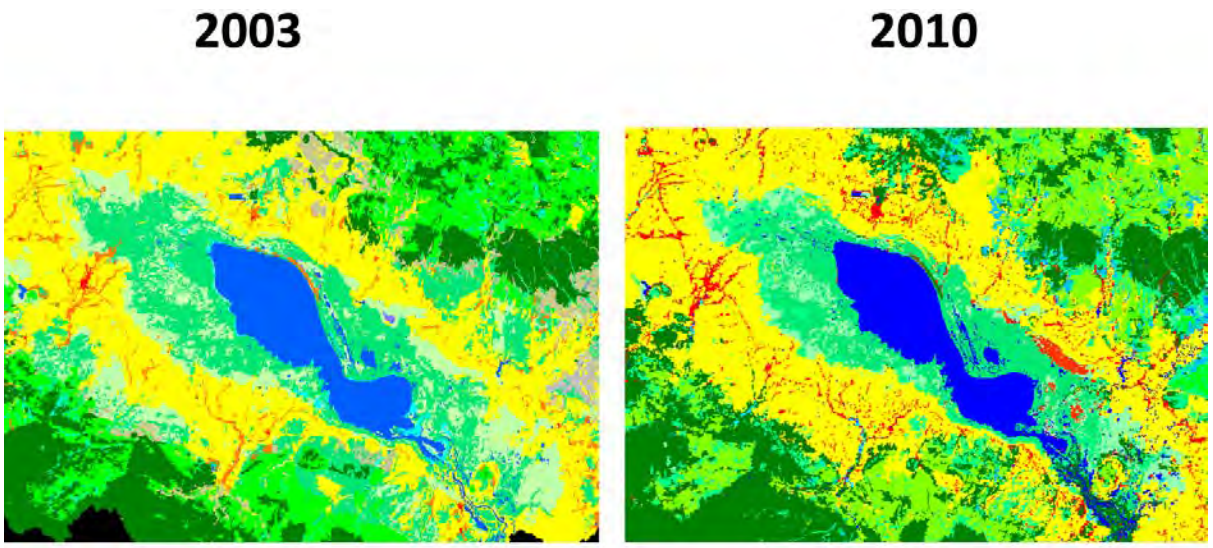

Figure 95. MRC Land Cover maps for 2003 and 2010. Observe that the classification is different.

The 2003 and 2010 land cover classifications are not identical. The classes relevant for Tonle Sap are compared in Table 3.

Table 3. MRC Land Cover 2003 and 2010 classification relevant for the Tonle Sap

MRC 2003 Land Cover	MRC 2010 Land Cover
Water	Annual Crop
Paddy	Paddy Rice Rotated with Annual Crop
Deciduous forest	Shifting Cultivation
Evergreen forest	Orchard
Field crop	Flooded Forest
Built-up area	Grassland
Industrial plantation	Shrubland
Swidden cultivation	Urban Area
Orchard	Bare Land
Flooded forest	Industrial Plantation
Grassland	Deciduous Forest
Shrubland	Evergreen Forest
Barren land/Rocky hill	Forest Plantation
Bamboo forest	Bamboo Forest
Marsh and Swamp	Coniferous Forest
Forest plantation	Mangrove
Coniferous forest	Marshes/Swamp Area
	Aquaculture
	Aquaculture (Shrimp) Rotated with Paddy Rice
	Waterbody

Number of original MRC land use classes can be combined (reclassified) into hydrological model classes (**Figure 96**). This simplification facilitates model calibration as calibration values for other areas can be utilized and number of land use classes to be calibrated is reduced.

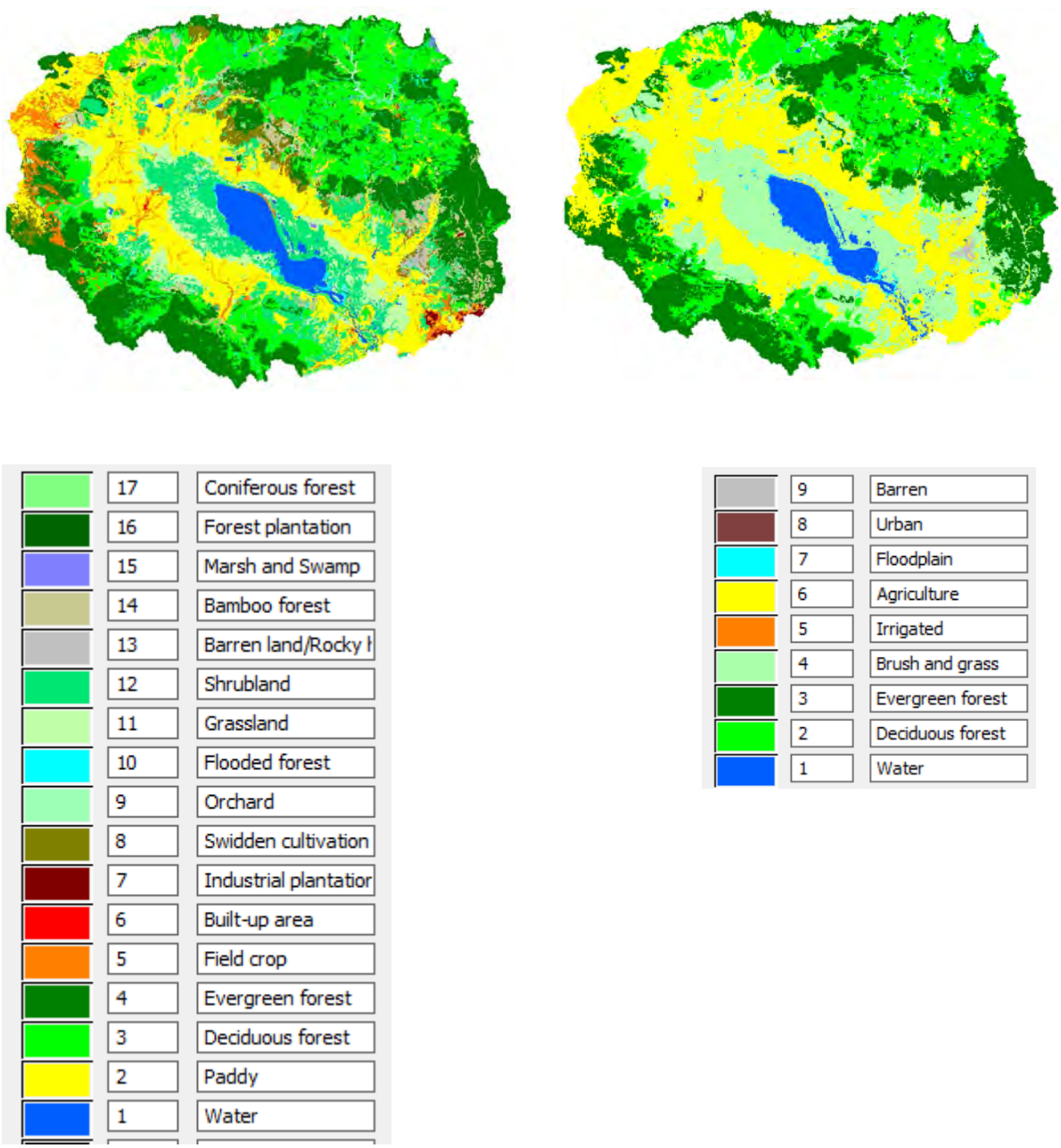

Figure 96. Simplification of the original MRC 2003 land use classes (left) into the model standard hydrological land use classes (right).

2.2. Soil classification

MRC soil classification is similar although less detailed than what is nationally available (**Error! Reference source not found.**). However, the differences are not significant when the soil classes are reclassified for the model

).

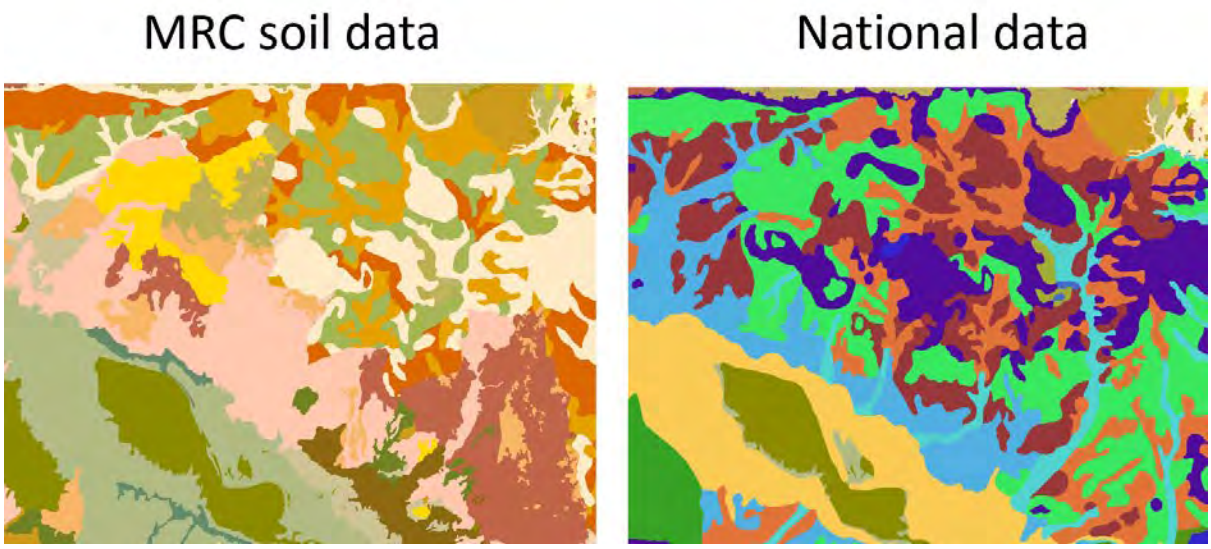

Figure 97. Original soil classification.

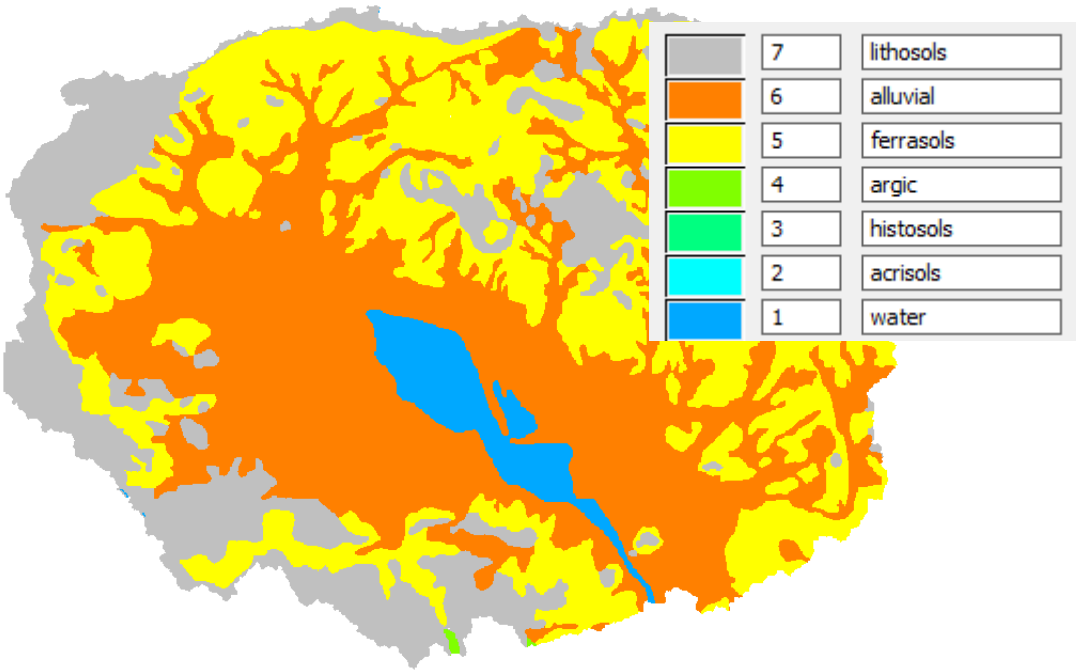

Figure 98. Soil reclassification for the IWRM/VMOD.

2.3. Weather data

The weather data used in the model consists of the **original** gap-filled MRC Modelling Knowledge Base (KB) rainfall and daily temperature data (**Figure 99**). It should be observed that this is not the same as the interpolated data used in the SWAT model.

Each station in the IWRM/VMOD is assigned elevation either from the model DEM or, when outside of the model area, separately. The elevations are used to height-correct both rainfall and temperature. 3 nearest stations are used for interpolating the weather for each model grid cell.

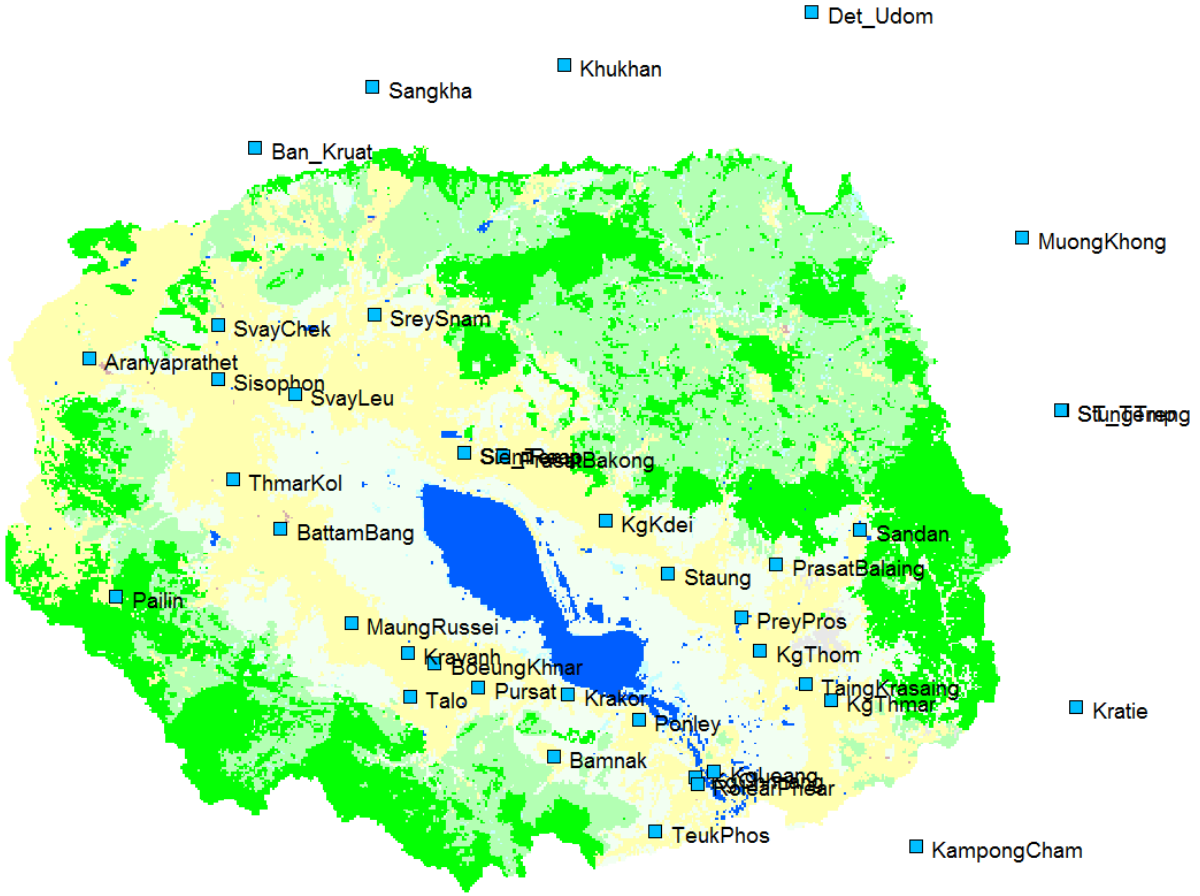

Figure 99. Tonle Sap IWRM/VMOD model rainfall and temperature data from the IKMP Modelling KB (Knowledge Base).

To facilitate import of large number of stations KB data import tool was developed for the IWRM/VMOD. It requires csv-file of the station names and coordinates (**Figure 100**) as these are not available in the KB data dump. After that tool “Create txd files (MRC hydromet csv)” can be used to import the station data (**Figure 101**).

Saang	110519	11.35	105.25
Bar_Phnom	110520	11.25	105.4
Kampong_Leav	110521	11.49	105.34
Kompong_Trabel	110522		
Mesaing	110523	11.33	105.55
Peam_Ror	110524	11.31	105.28
Pear_Raing_	110525	11.66	105.23
Chroy_Thmar	110526	11.902	105.47
Mimot	110605	11.84	106.19
Chalang	110606	11.783	106.117
Kantroy	110607	11.75	106.283
Peam_Chikang	110608	11.951	105.267
Pailin	120202	12.859	102.618
Chamlong_Kuoy	120205	12.713	102.96
Treng	120206	12.841	102.921
Rattanak_Mondo	120213	12.817	102.617
Tuol_Krous	120301	12.361	104.526
Pursat	120302	12.55	103.9
Maung_Russey	120303	12.771	103.45
Dap_Bat	120304	12.343	103.787
Raing_Kesey	120305	12.967	103.25
Leach	120306	12.35	103.767
Talo	120309	12.519	103.659
Cheang_Meanch	120311	12.877	103.105

Figure 100. Data format for the station name and location data required for KB data import.

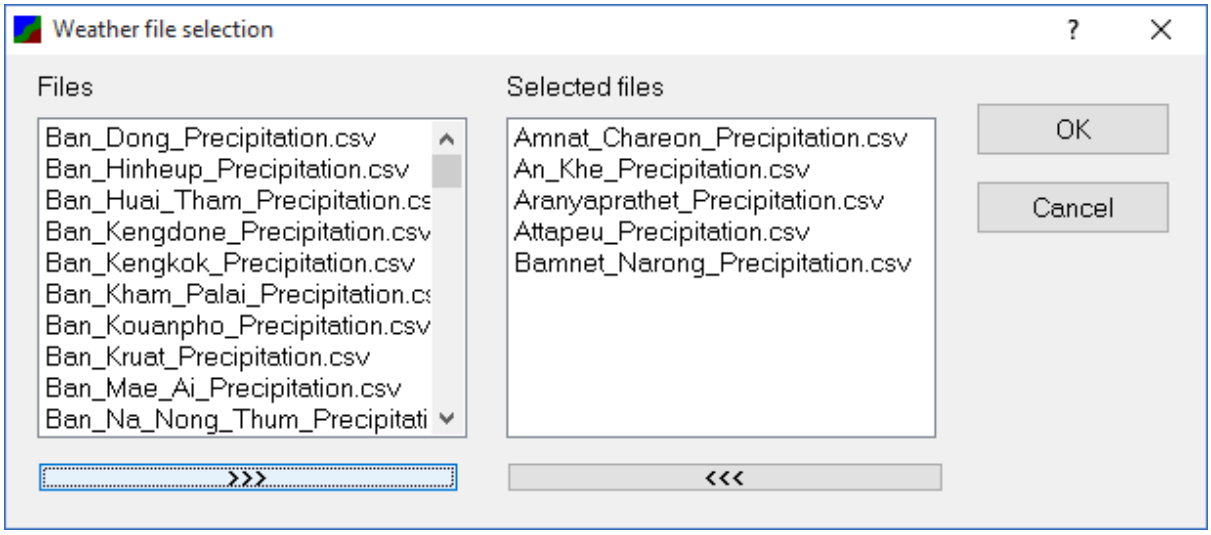

Figure 101. Selection of station data to be imported to the model.

Following MRC discharge stations have been used for the model calibration:

- Btrakuon (Pursat)
- Sangker
- Mongol Borei
- Chinit
- Sen
- Sisophon
- Sreng.

As have been observed already during the WUP-project by the different modelling teams (WUP-A, WUP-JICA and WUP-FIN) not all of the stations are suitable for calibration because data quality or coverage issues. This applies both to discharge and meteorological data.

2.4. Tributary and lake water quality data

For the IWRM/VMOD only tributary water quality data has been used for calibration. But it is convenient to present also the Lake monitoring database here as it is integrated with the tributaries data.

Primarily the WUP-FIN monitoring database for 2001 – 2003 has been used in the calibration. This is because of sampling quality concerns for the longer term MRC sediment sampling, patchy nutrient data availability and very high temporal and spatial resolution of the WUP-FIN data which reveals how much inherent temporal and spatial variability/randomness is included in the sampling.

The characteristics of the WUP-FIN sampling are:

- Data collected 2001 - 2002
- Two intercalibrations
- 1100 water quality samples (see **Figure 102** for the main stations)
- Automatic recording stations in 8 locations (see **Figure 103**)
- DO (Dissolved Oxygen) probe results
- Wet season 2001 sampling covers 90% of the incoming small tributary water.

The analysed parameters are:

- Temperature, Secchi-depth, turbidity, TSS
- COD, Si, pH, alkalinity, Ca
- PO4, TotP
- NO3-N, NO2-N, NH4-N, TotN
- Bio-available sediment phosphorus
- Chlorophyll-a, biomass, zooplankton
- Laser analysis of grain size distribution in water samples including sonification.

View of the Tonle Sap hydromet database where all hydromet and water quality sampling and GIS data is included is shown in **Figure 104**.

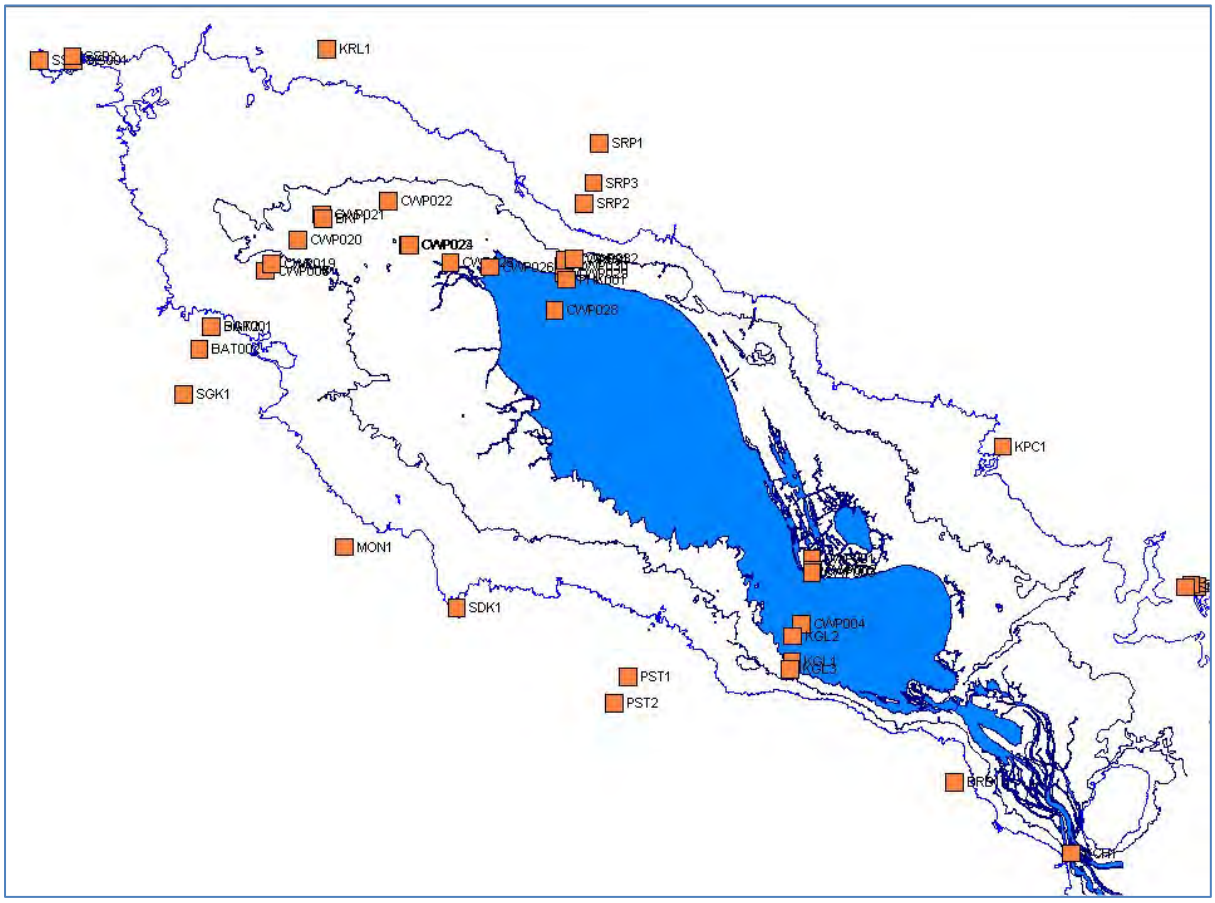

Figure 102. Main WUP-FIN water quality sampling stations.

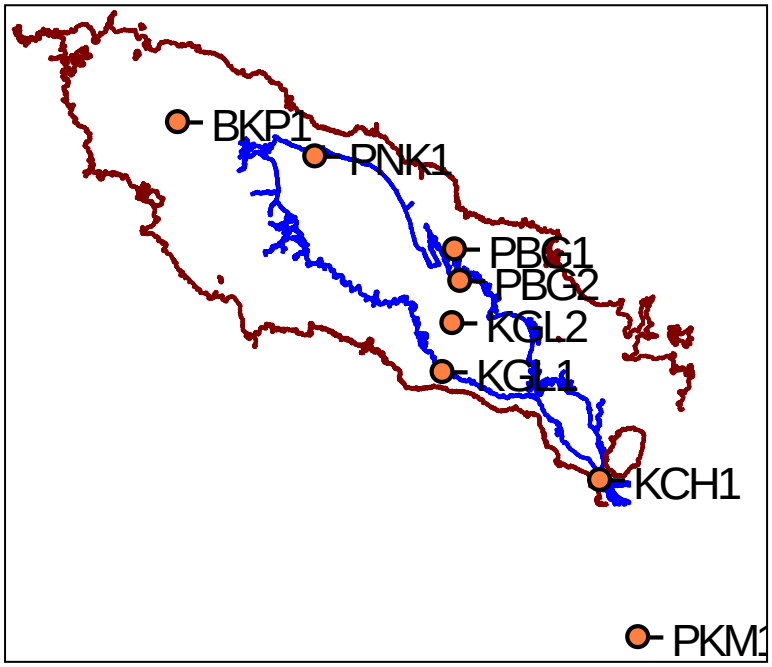

Figure 103. Recording water quality sites.

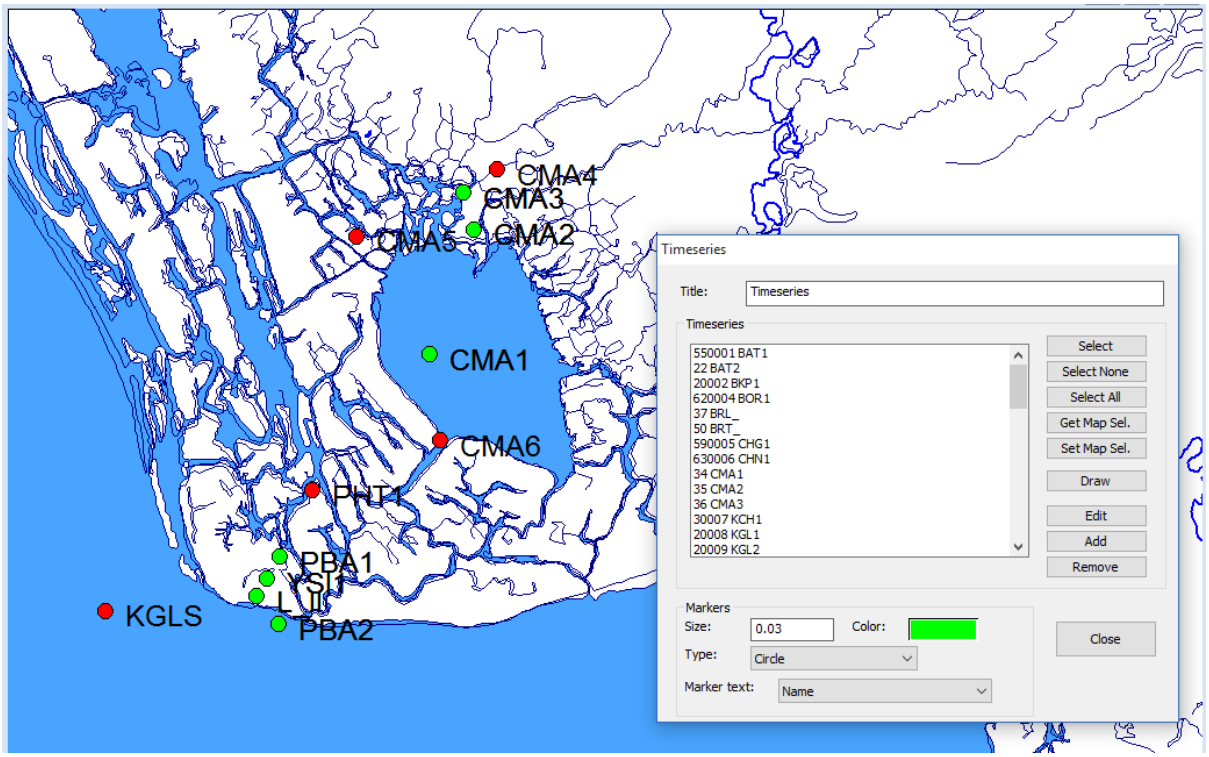

Figure 104. View of the Tonle Sap monitoring database user interface.

Carbonne et al. (1963) comprehensive Tonle Sap water and sediment balance study would be excellent data for model calibration but unfortunately meteorological data is not readily available for so early period.

Water quality modelling in the Nam Ngum Basin has been the foundation of the Tonle Sap water quality modelling (Kallio 2015), **Figure 105** and **Figure 106**.

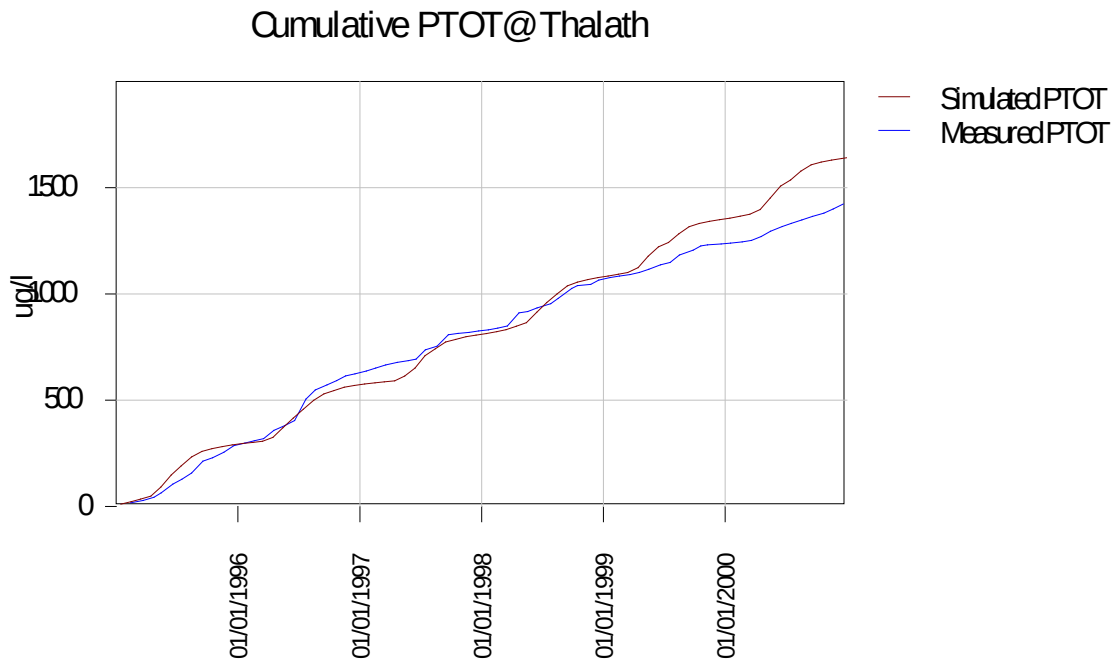

Figure 105. Cumulative modelled and measured phosphorus concentrations in Thalath, Nam Ngum Basin.

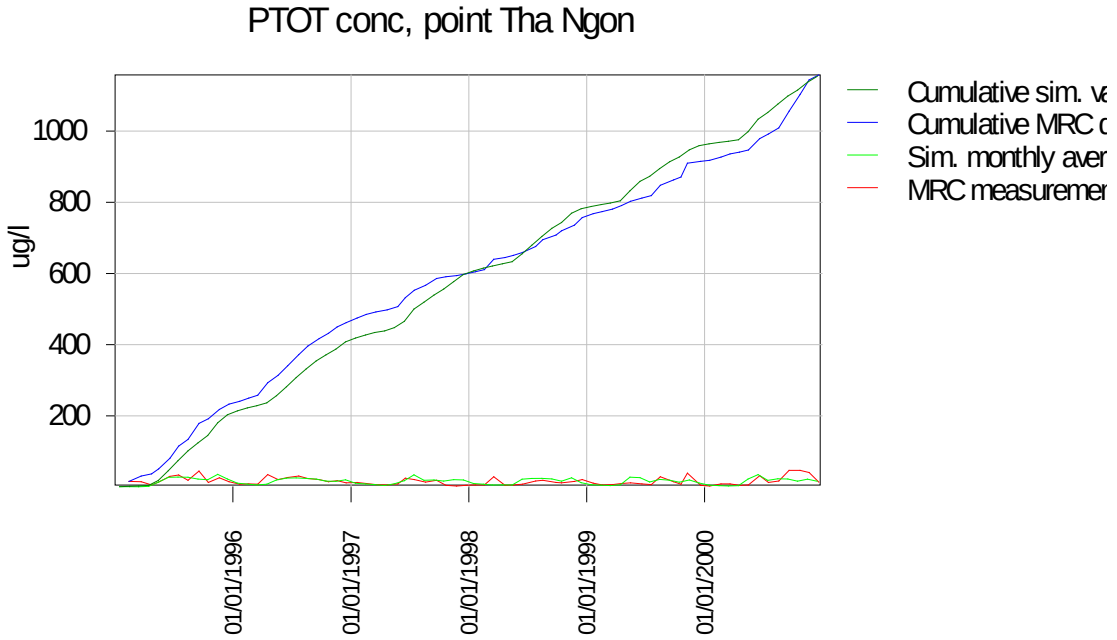

Figure 106. Cumulative modelled and measured phosphorus concentrations in Tha Ngon, Nam Ngum Basin.

2.5. Hydrological model calibration

The major Tonle Sap tributaries with most comprehensive and consistent data were selected for calibration and comparison (Chinit, Sen and Sreng; **Figure 107**). The three tributaries cover large part of the watershed. Both recalibrated SWAT and IWRM/VMOD results have been compared to the observations. Also fully lumped HBV results are presented for Sen for comparison with the distributed IWRM/VMOD and semi-distributed SWAT.

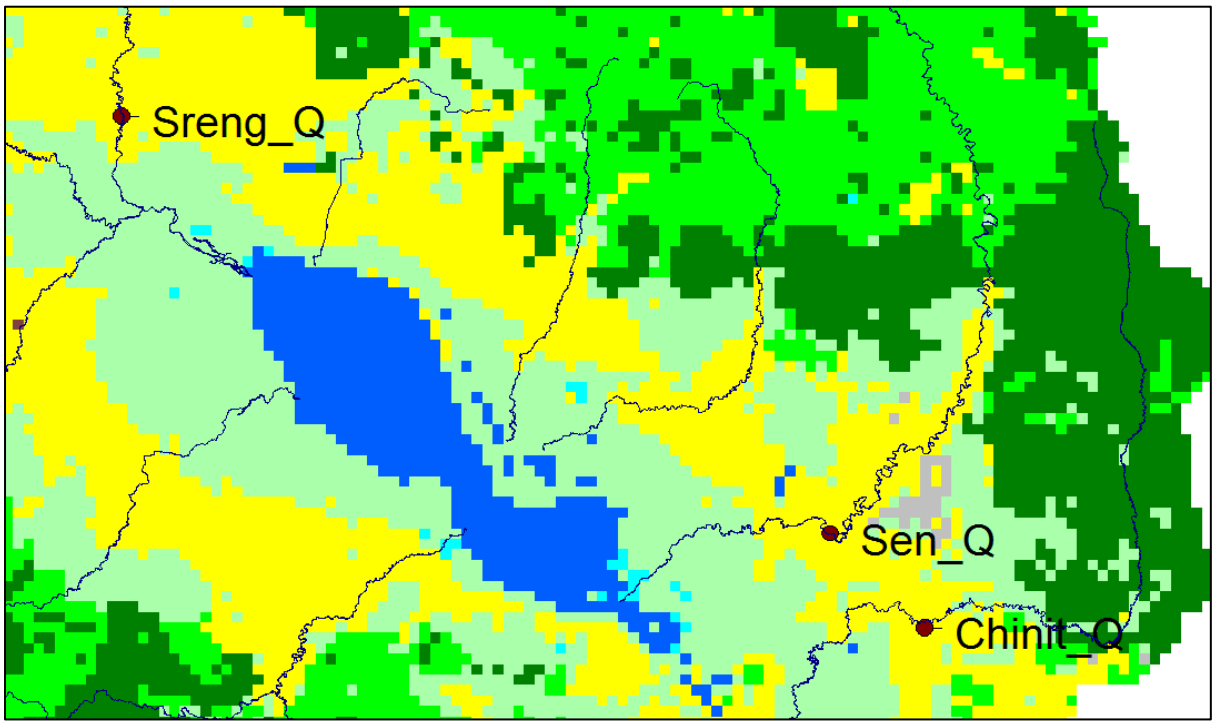

Figure 107. Main calibration locations.

SWAT results represent the whole basin and are not directly comparable for Kampong Thmar that represents major part but not the whole watershed (**Figure 108**).

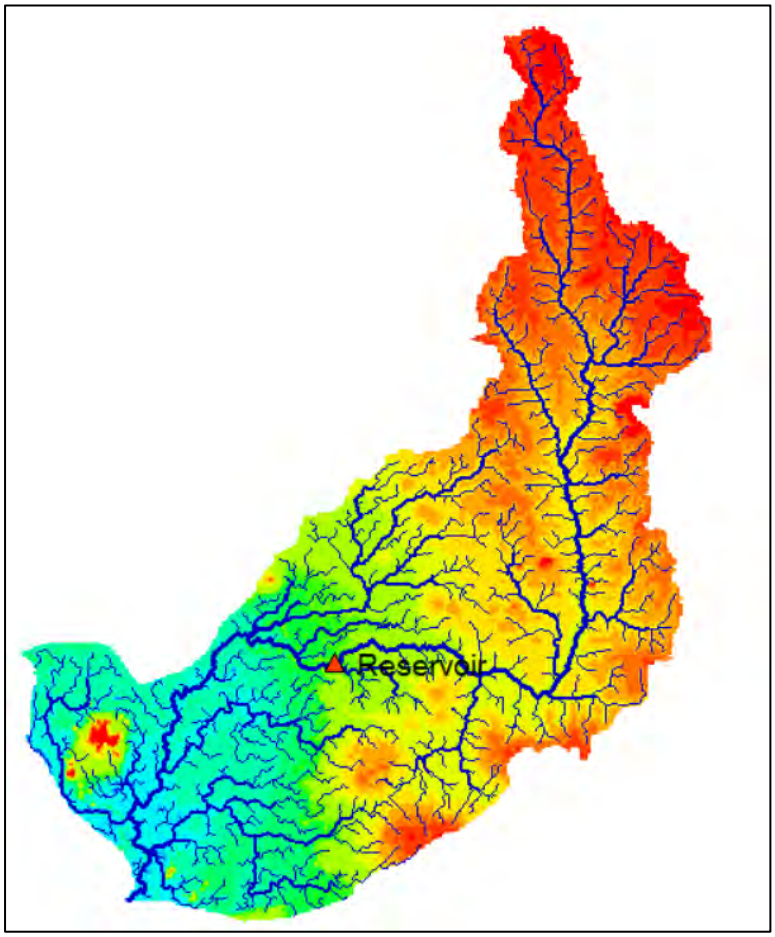

Figure 108. Chinit watershed and Kampong Thmar reservoir. The discharge observation station is located closely downstream of the reservoir.

Comparison between simulated and observed flow is presented in **Figure 109** - **Figure 111**.

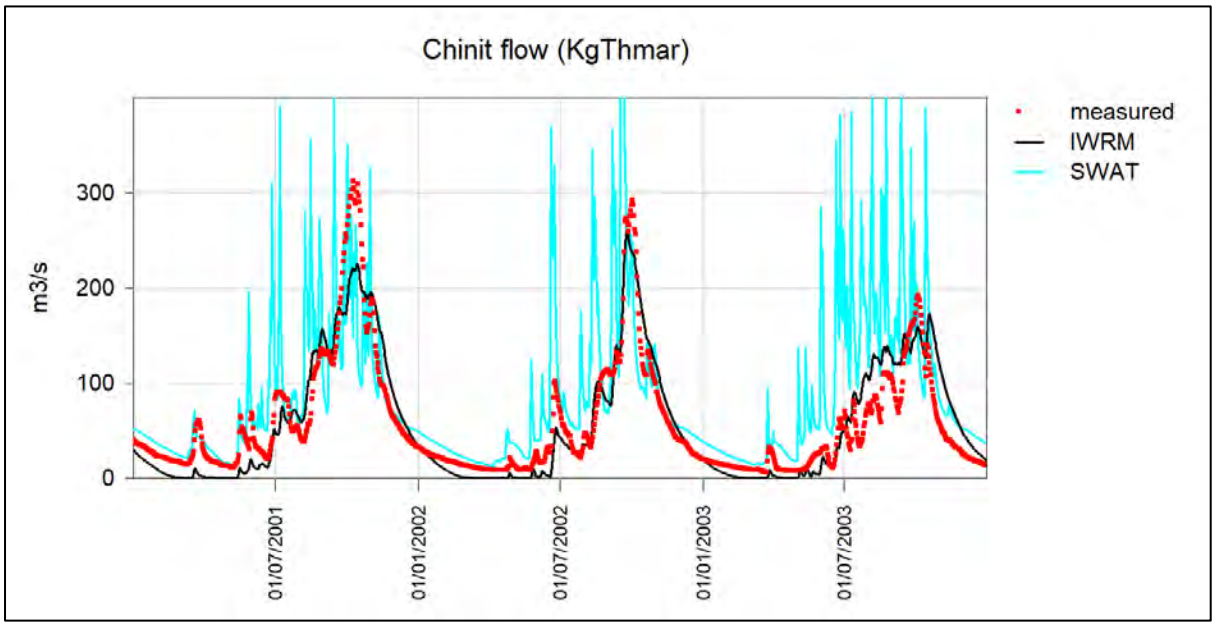

Figure 109. Measured (red line) and IWRM/VMOD modelled (black line) discharge for Chinit Basin. Comparison with SWAT computed flow (light blue line).

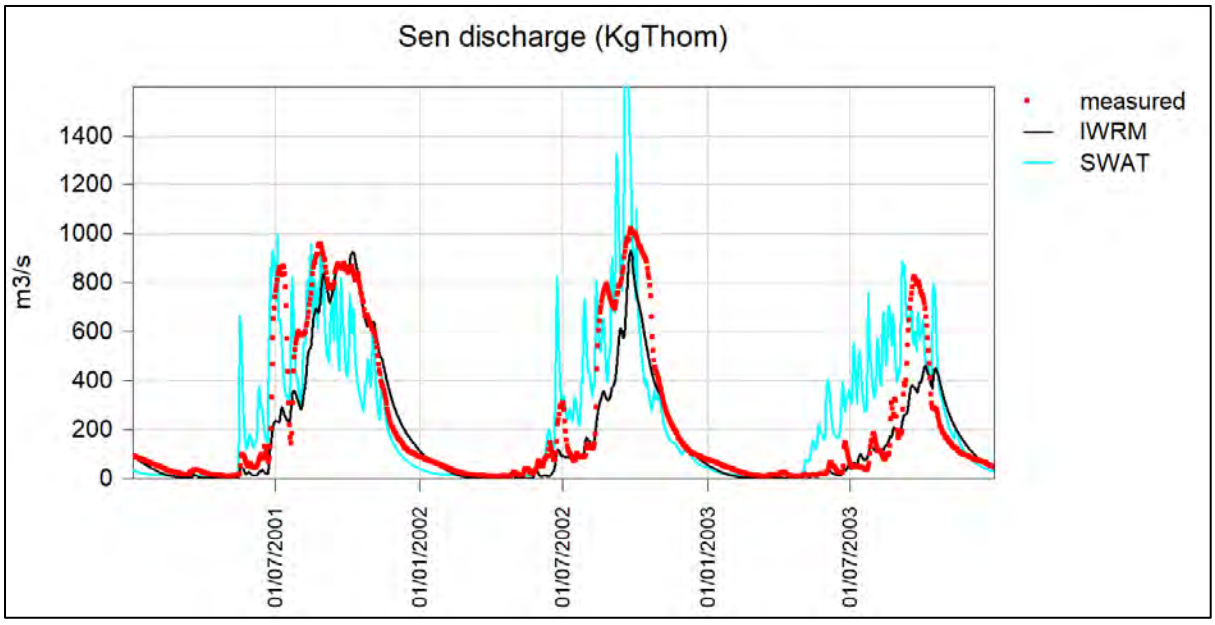

Figure 110. Measured (red line) and IWRM/VMOD modelled (black line) discharge for Sen Basin. Comparison with SWAT computed flow (light blue line).

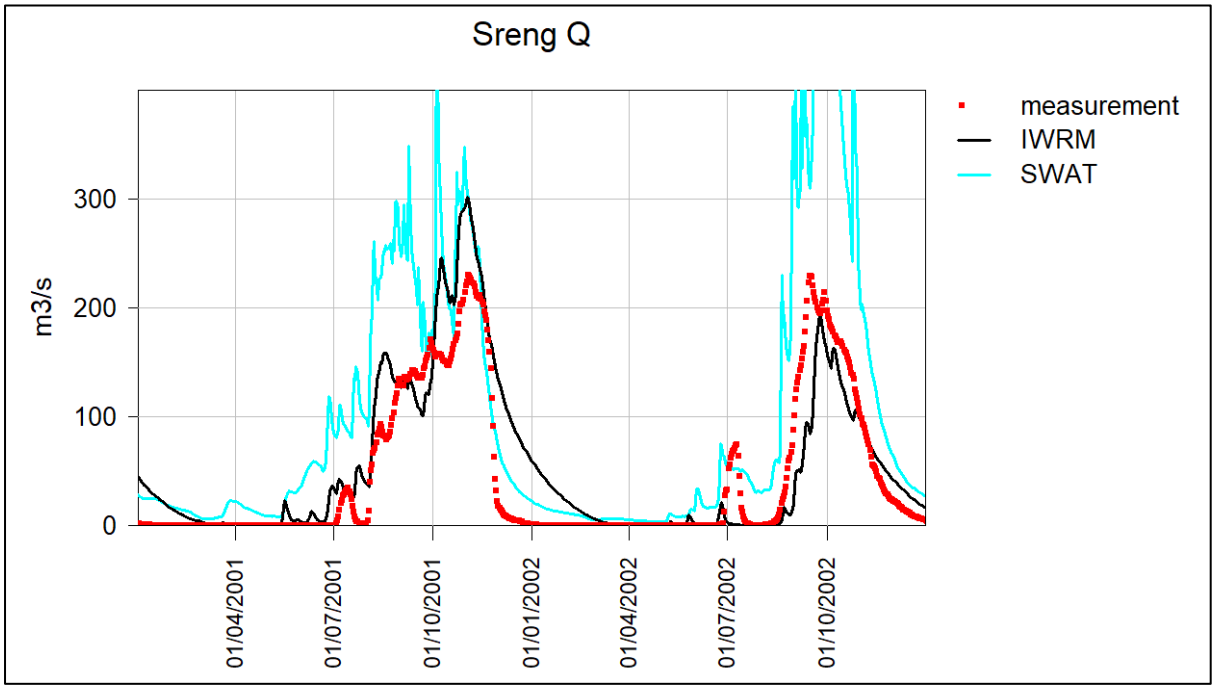

Figure 111. Measured (red line) and IWRM/VMOD modelled (black line) discharge for Sreng Basin.

Figure 112 shows results from a simple lumped HBV model (part of the WUP-FIN modelling tools) compared with the IWRM model and measurements. In case of small watersheds lumped model results can be quite satisfactory if only watershed outflow is required. However, lumped models and not suitable for physically based modelling required for instance for erosion.

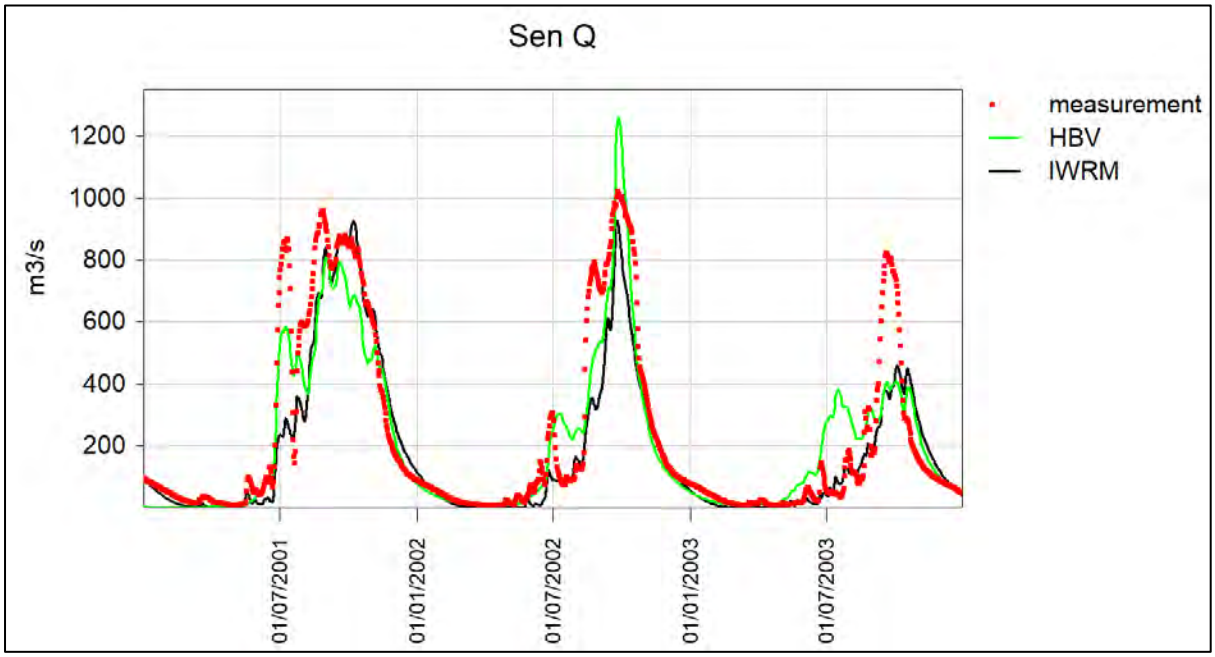

Figure 112. Observed flow (red dots) compared to HBV lumped model (black line) in Sen.

The overall conclusion of the calibration results is that IWRM/VMOD replicates observed flow reasonably well although some years are better represented than the others. The main cause of the

discrepancies between modelled and observed flow is that large part of the calibration basins presented here are not covered by rainfall observation stations. There are some stations north of the basins in Thailand but they are separated by a mountain range and represent different climatic conditions. Interpolating rainfall between near-Lake stations and those in Thailand is obviously not sufficient to represent accurately the very variable rainfall in the Tonle Sap watershed.

2.6. Water quality calibration

Water quality was calibrated for Chinit and Sen basins as they have most comprehensive monitoring data. Also SWAT has been calibrated in these basins so comparison between the models is straightforward. MRCS monitored discharge and WUP-FIN monitored water quality have been used to estimate sediment and nutrient loads for comparison with the models below.

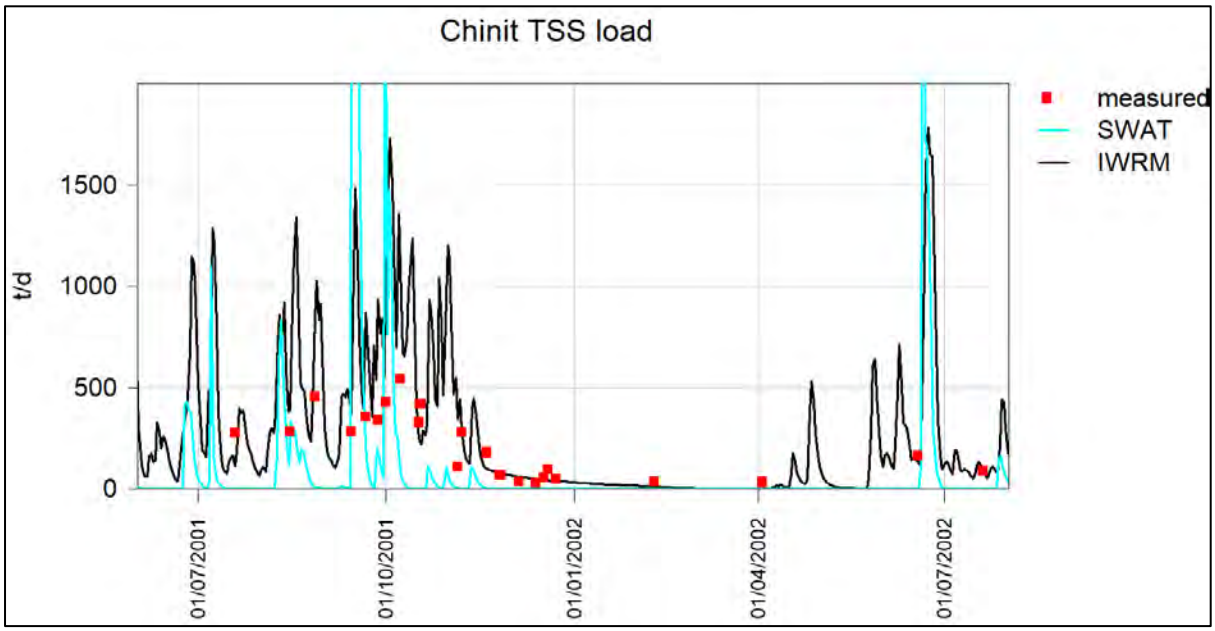

Figure 113. Observed (red squares) and VMOD (black line) and SWAT (blue line) modelled Total Suspended Solids (TSS) loads in Chinit.

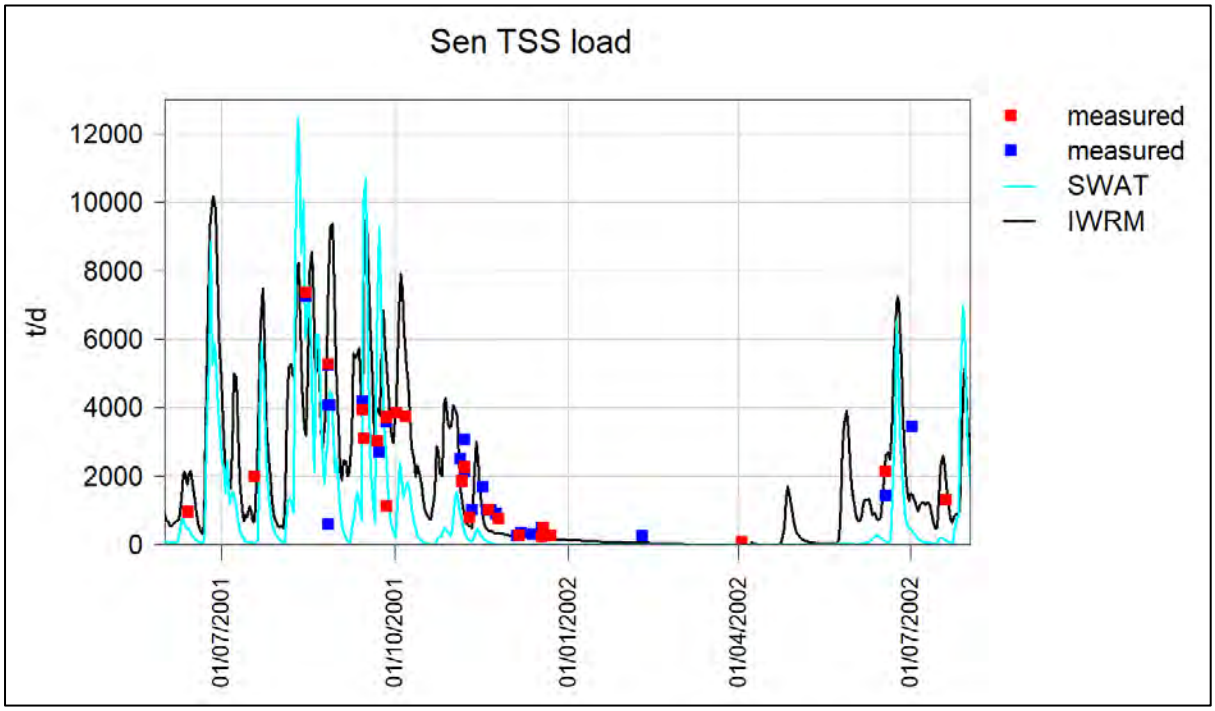

Figure 114. Observed and SWAT (blue line) and VMOD (black line) modelled Total Suspended Solids (TSS) loads in Sen. Red and blue squares are observations from different nearby stations.

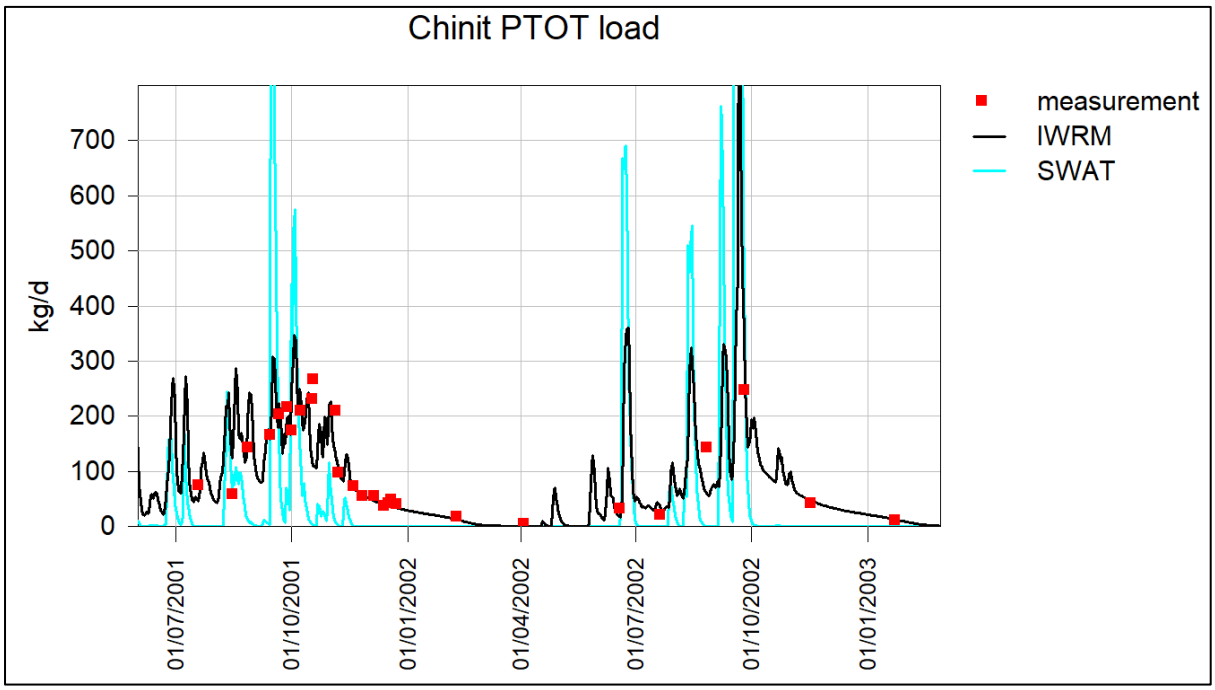

Figure 115. Observed (red squares) and VMOD modelled (black line) Total Phosphorus (TOTP) loads in Chinit. Comparison with the SWAT (blue line).

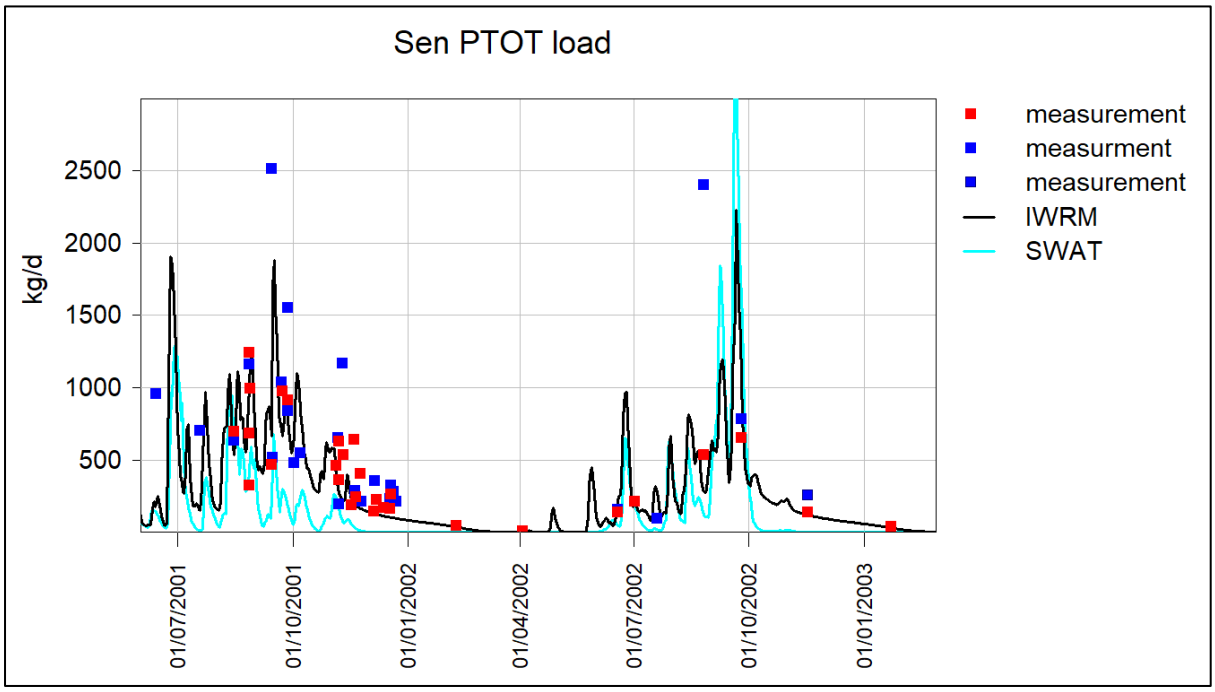

Figure 116. Observed and VMOD modelled (black line) Total Phosphorus (TOTP) laods in Sen. Red and green squares are from different nearby stations. Comparison with the SWAT (blue line).

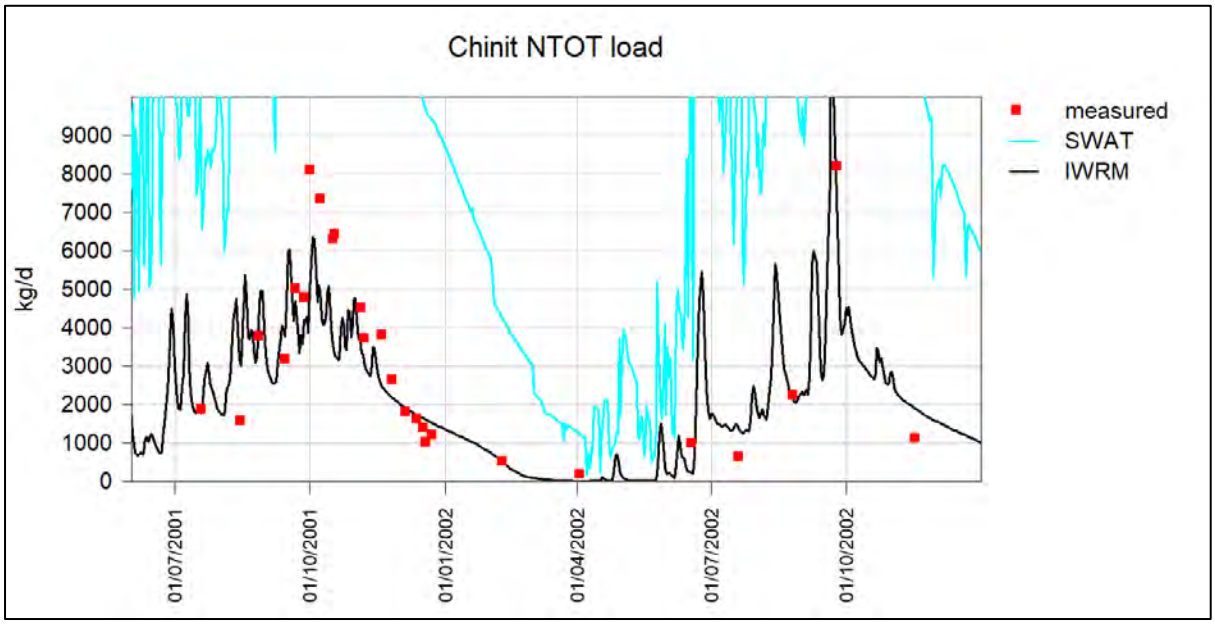

Figure 117. Observed (red squares) and VMOD modelled (black line) Total Nitrogen (TOTN) concentrations in Chinit. Comparison with the SWAT (blue line).

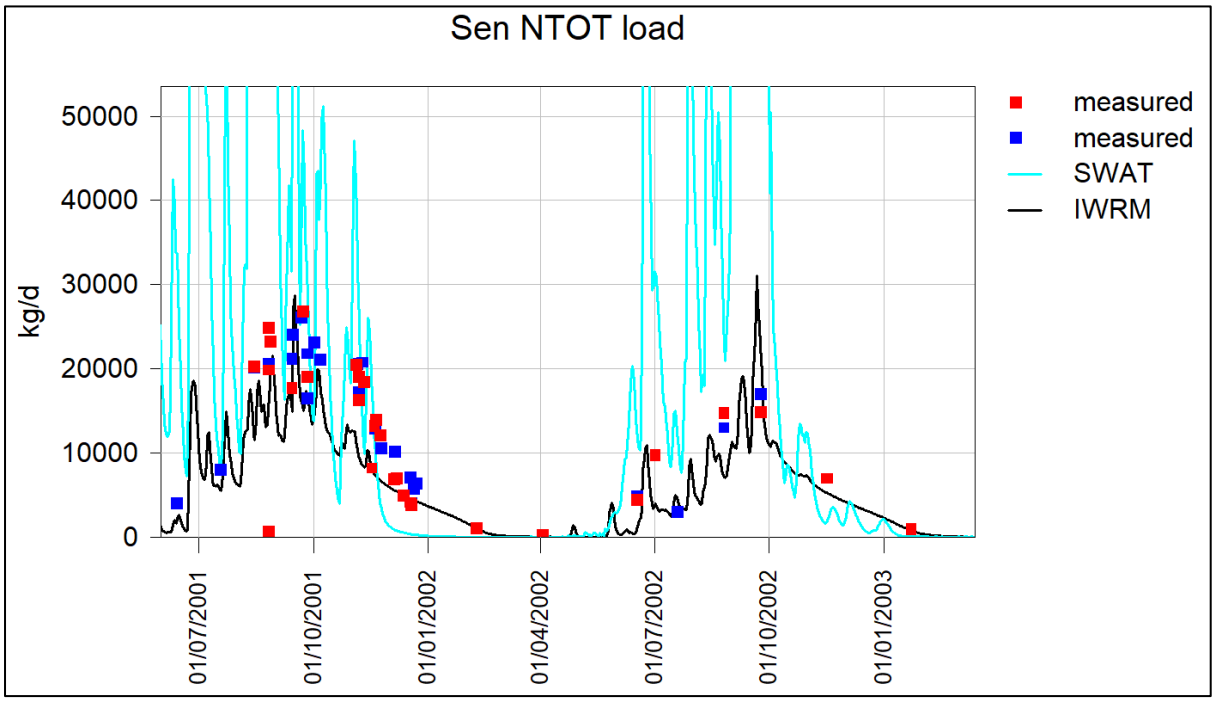

Figure 118. Observed (red squares) and VMOD modelled (black line) Total Nitrogen (TOTN) loads in Sen. Comparison with the SWAT (blue line).

The WUP-FIN water quality monitoring results show the high spatial and temporal variability of Total Suspended Solids (TSS) and phosphorus. Compared to the measured values VMOD reproduces the Tonle Sap watershed water quality seasonal cycles and variability reasonable well. Overall, but based on limited observation data, it can be concluded that VMOD produces sediment and nutrient loads in line with observations.

To test the important river channel deposition and erosion terms in SWAT they were also implemented in the VMOD (**Figure 119**). The difference between SWAT and VMOD is that the latter calculates deposition and erosion/resuspension processes as mass balances so that no material is created or destroyed. The mass balance approach doesn't seem to improve the modelling results, at least not in the Tonle Sap case.

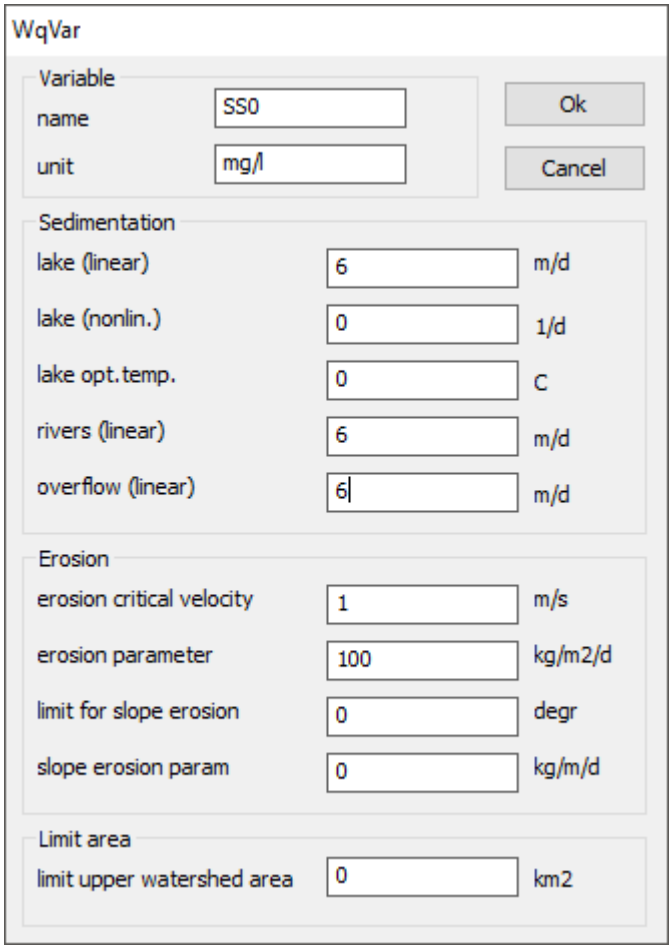

Figure 119. VMOD definitions for settling/sedimentation and erosion/resuspension.

3. Annex 3 - Tonle Sap Lake and floodplain hydrodynamic and productivity modelling

Description and validation for the 3D-EIA model is presented in ANNEX II - III. In this chapter Tonle Sap model topographic data and main calibration results are shown.

3.1. Tonle Sap topographic data

The 3D-EA model land use and calibration data are presented in the previous chapter. Here only the topographic data is discussed.

Tonle Sap topographic data consists of:

- For the floodplain Certeza survey 1964
- For the lake FINNMAP MRC Hydrographic Atlas survey data (**Figure 120**)
- Other areas MRC DEM
- Compared with Radarsat (**Figure 121**) and more recent ground survey data (**Figure 122** and **Figure 123**).

Comparison between the Certeza, Radarsat and more recent ground survey data shows that Certeza data continues to be reliable and that erosive or dipositive processes have not significantly altered the topography of the Tonle Sap Lake or the floodplain.

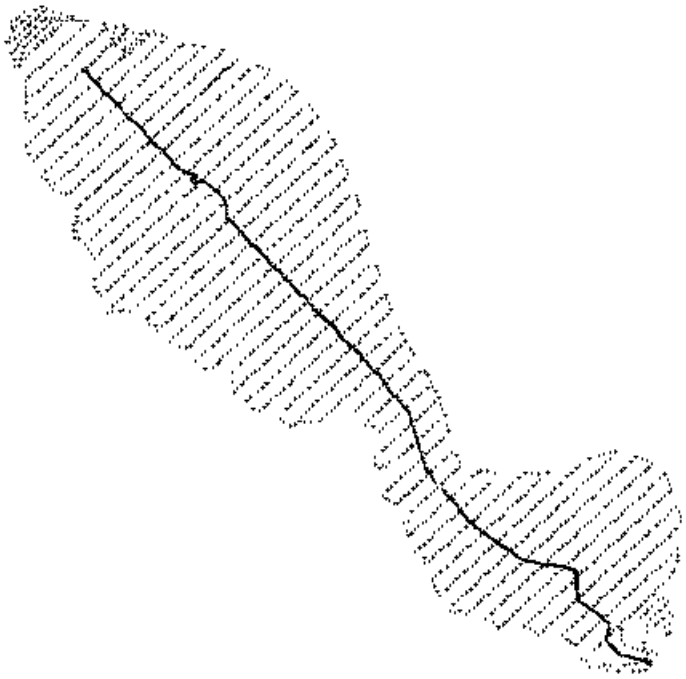

Figure 120. FINNMAP Tonle Sap Lake bathymetric survey in 1998 showing survey points.

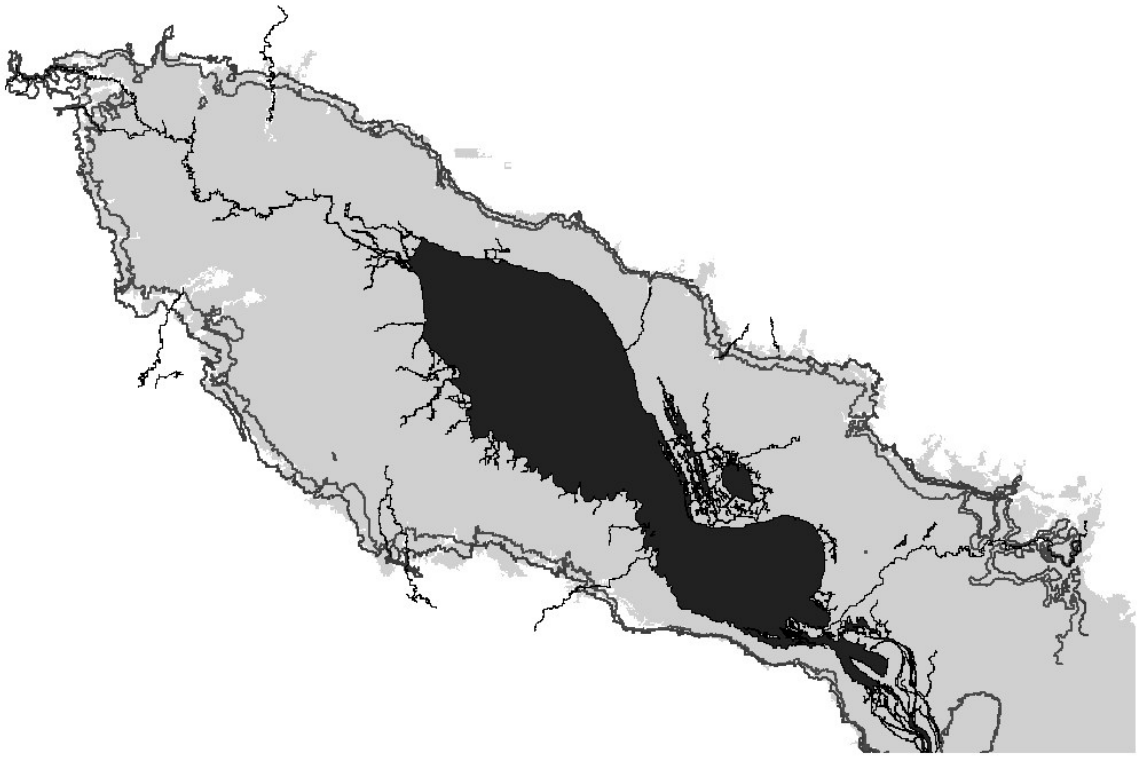

Figure 121. Certeza 9 m and 10 m ground elevation lines compared to Radarsat remote sensing data. Grey area Radarsat for water level 9.5 m (J. Himel/ Aruna Technologies).

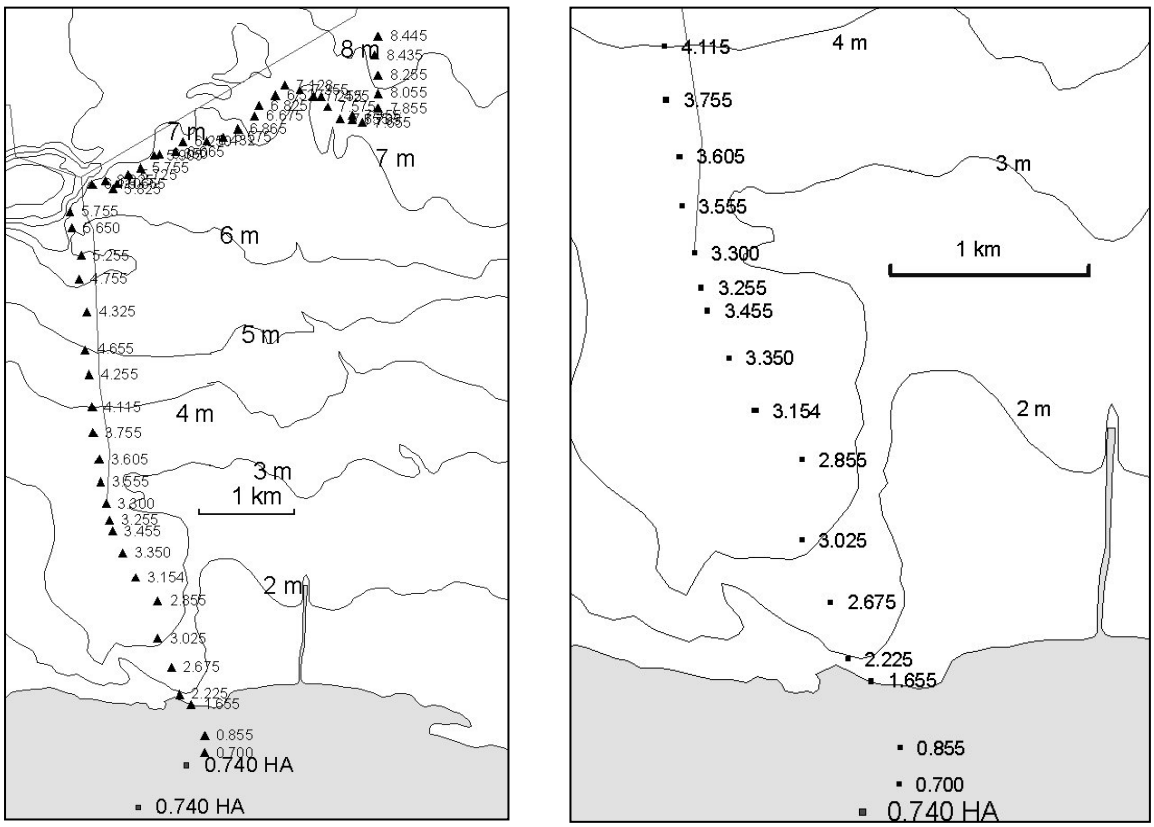

Figure 122. Overview of the lower survey line (left). Detailed view of the lower part of the survey (right). HA after the numerical value signifies Hydrographic Atlas 1998 values. Otherwise numerical values are by Seang (1998). Contour lines digitized by MRCS from the Certeza maps.

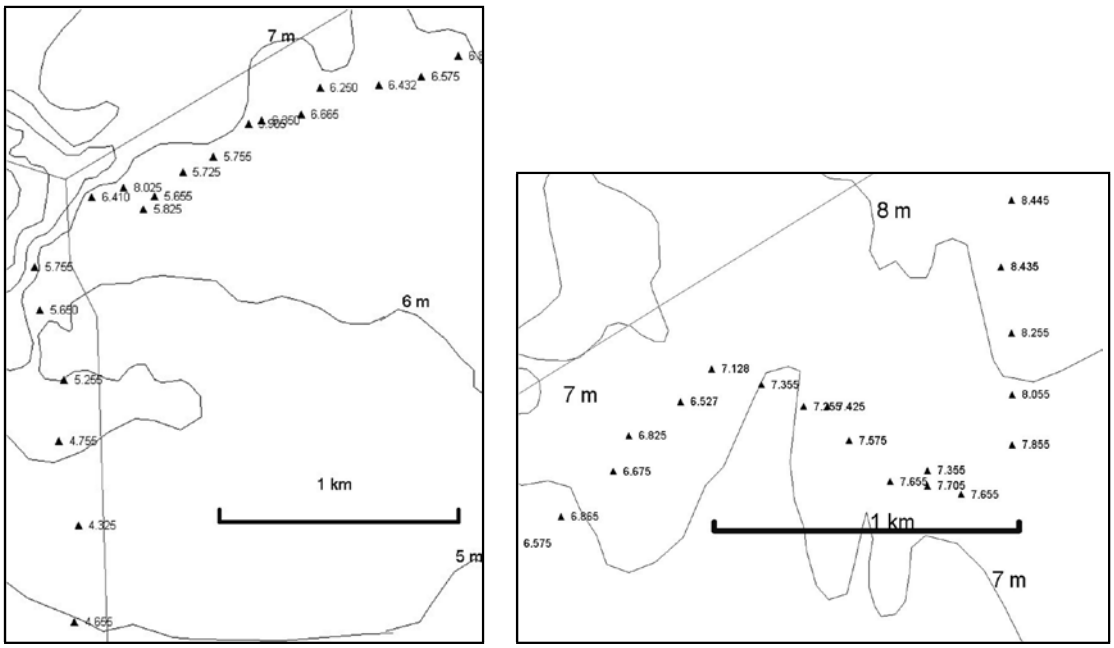

Figure 123. Middle (left) and upper (right) part of the Seang (1998) survey data compared with the Certeza survey contour lines.

Recent high resolution (at least horizontally) national data is available for modelling. The data has been compared around Tonle Sap to the Certeza survey data. It appears that there is need in the new data to process vegetation impacts as the paddies and water have have less error than forested areas. It may be also possible that there has been an error in processing original data into raster DEM and the error is highest in areas with high terrain gradients. Because of the errors in the high resolution data it has not been utilised in the modelling.

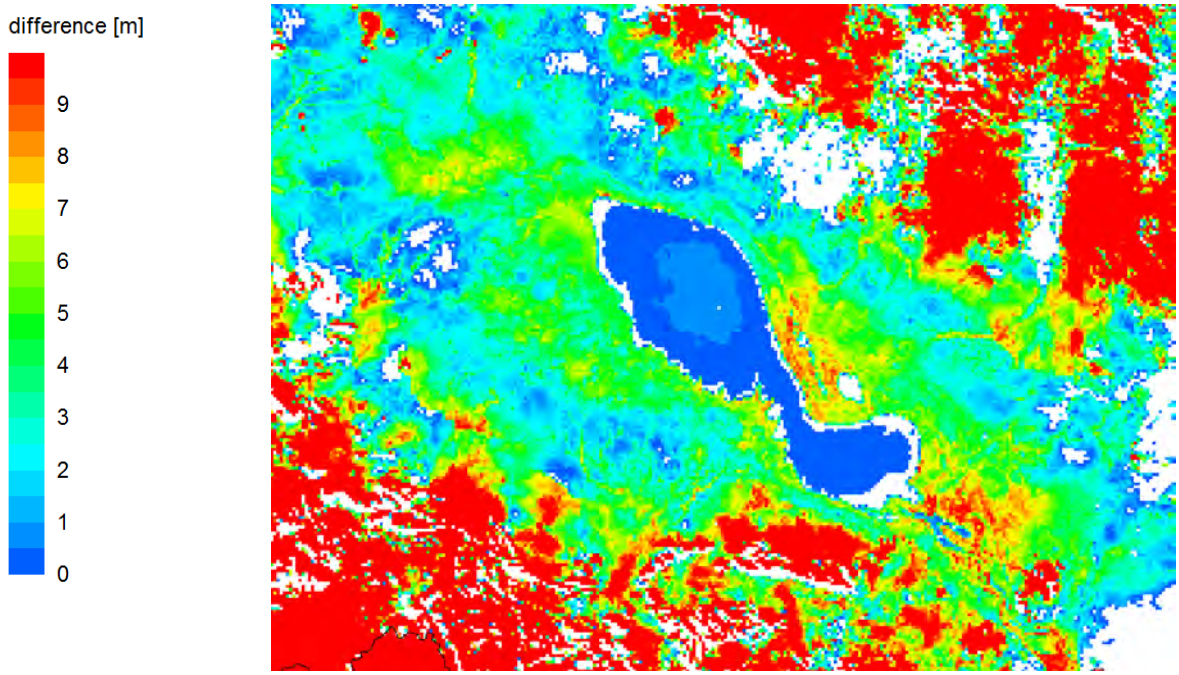

Figure 124. Difference in ground elevations between new national high resolution topographic data and the Certeza survey data (new – Certeza).

Figure 125 presents difference between original Certeza derived DEM and the MRC DEM. The error stems from the fact that the MRC DEM is in integer numbers. Because of the large differences between the datasets the original decimal data has been used for the DEM.

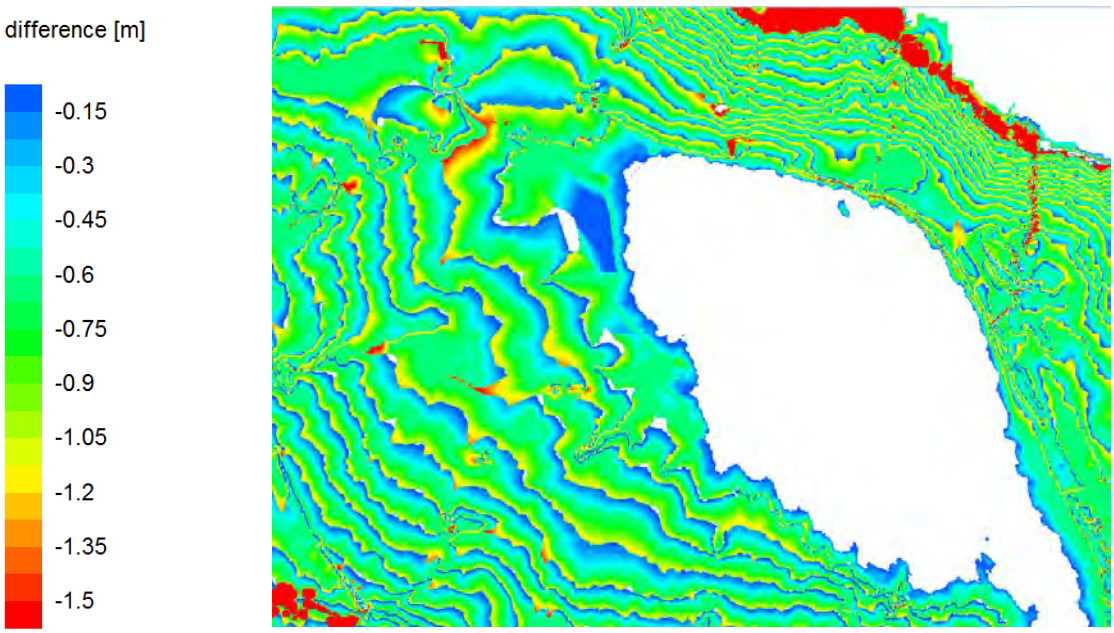

Figure 126. Difference in ground elevations between MRC DEM and the original Certeza survey based DEM (MRC – Certeza).

The Certeza derived decimal number DEM as well as the MRC 2010 were used to update the old 1 km grid size model and to generate a new 500 m resolution model (**Figure 127**). The 500 m resolution model has 176'000 grid cells.

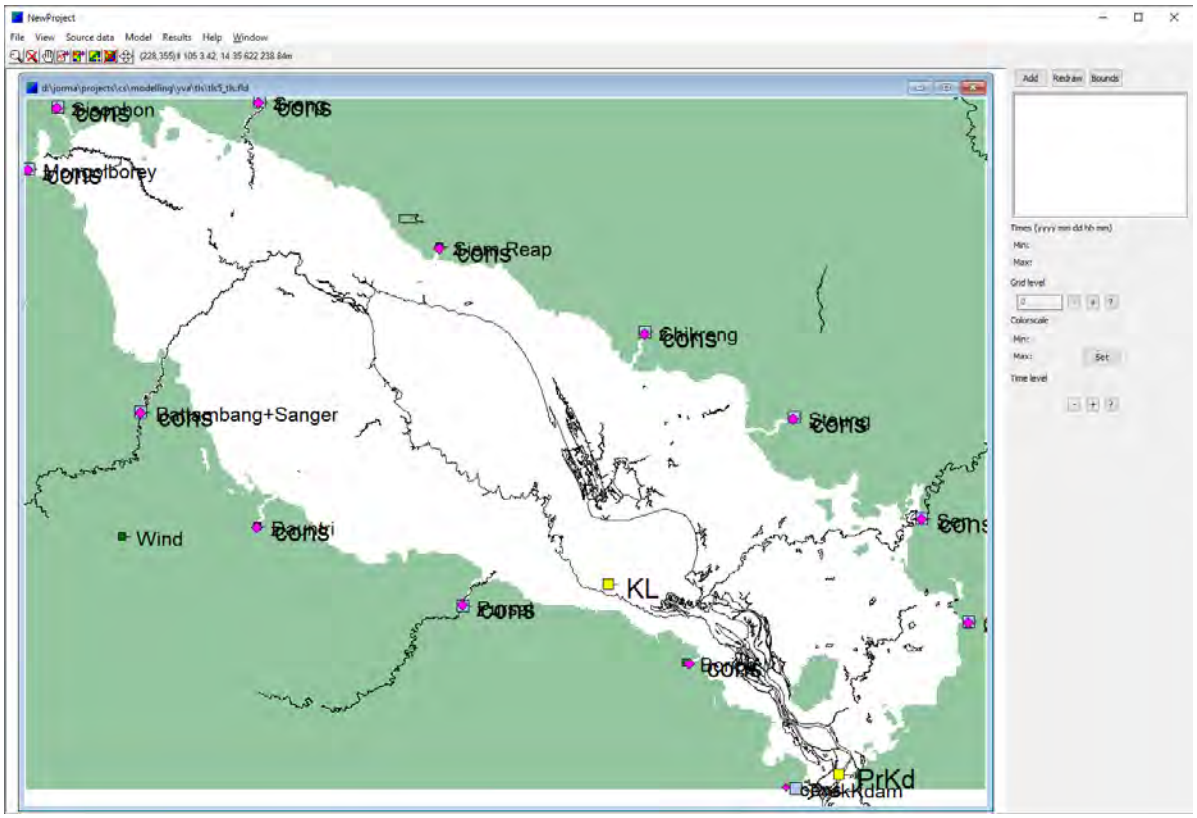

Figure 127. 500 m grid resolution Tonle Sap 3D-EIA model.

3.2. Tonle Sap hydrodynamic modelling development and calibration

Tonle Sap hydrodynamic model principles and validation is presented in ANNEX II. The ANNEX focuses on flood modelling validation as it is the to a large extent basis for the sediment, water quality and productivity modelling. In this chapter Tonle Sap hydrodynamic 3D model development and calibration are described.

For the model development and calibration precipitation and evaporation data in the lake area was obtained from Aphrodite precipitation database (Add Ref), using average of three database precipitation data points. Evaporation was obtained from the Mekong basin 5km resolution VMOD model (Sarkkula et al. 2010). The flow model was first calibrated using Prek Kdam water level at the Tonle Sap river boundary. Tributary flows and evaporation were included in the computation. The average tributary inflow was obtained from measured and estimated water balances (Kummu et al. 2008) and applying timing for the flows for each tributary.

During the testing phase of the model it became evident that low water modelling, that is the driest period when Tonle Sap is emptying, didn't represent the water balance well. Because of this too high friction in the Lake and Tonle Sap River was reduced.

Connected with flooding/drying model improvement, representation of flood flow in areas with high ground elevation gradients such as in the Tonle Sap River was improved. The 3D model grid structure is shown in **Figure 128**. The grid is actually formed of two interleaved grids – one for concentrations, density and water levels and one for velocity components. Wetting (flooding) and drying of the grid cells is problematic when high gradients are present and for instance ground elevation in one of the corner points is much higher than in the others preventing flooding although the corner point would be needed for the velocity computation. Previous flooding algorithm smoothed the pressure grid ground elevations and also forced artificially flooding which created less stable solution. In the new flooding algorithm neither one of these approximations are needed making the representation of the topography more accurate and improving stability.

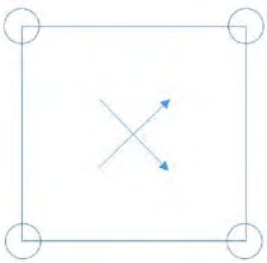

Figure 128. 3D-EIA model grid structure. Rotated velocity components are computed in the middle of the basic grid cell. On the corners secondary grid is formed where pressure terms (density and water elevation) are computed.

A flow computation model was setup for the Lake area. The model area is shown below, and it contains the lake Tonle Sap area up to flood level +12m. Southern boundary of the model is somewhat north from Prek Dam. The model grid resolution was 500 m. 10 m was added to the

ground elevations to eliminate negative depths in the Tonle Sap River and 10 m needs to be subtracted from the computed water elevations to get MSL values.

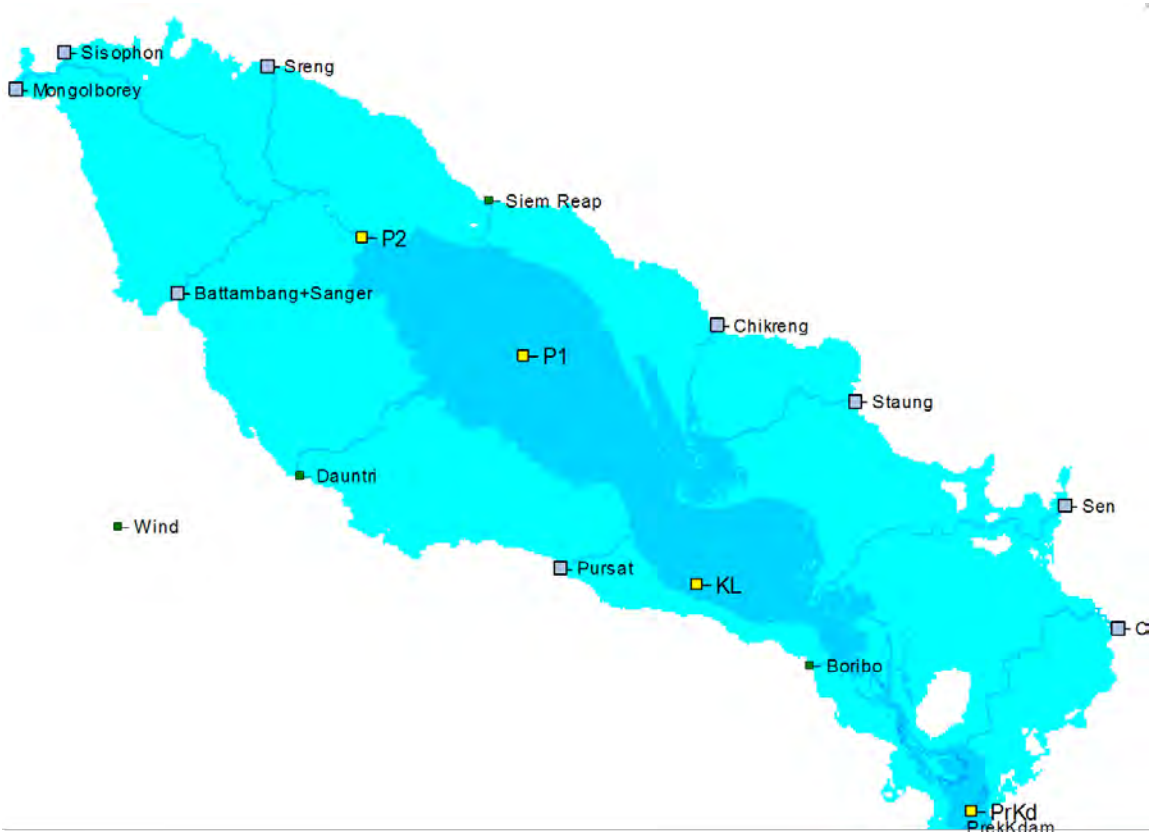

Figure 129. Set up of the Tonle Sap 3D model grid for testing and calibration. Water level +12m and +2m shown with different colors. Inflows shown with blue rectangles.

The model computational time steps were:

- External (2D) 20 s; this time step is also for direct 3D momentum equation solution
- Internal (3D) 60 s
- Bottom friction 120 s
- Advection (substance transport) 360 s
- Settling 360 s
- Flooding 2000 s.

The model has two computation modes: external/internal (see Simons 1980) and direct solution of the 3D momentum equations.

As a first estimate a linear bottom friction 0.01 was used in the computation. Wind friction coefficient was set to 0.0012 which is a standard value based on numerous modelling studies verified with flow measurements. First test of the model was to check whether the model grid in the mouth of the Tonle Sap River was sufficiently deep. Based on the model results the bathymetry was corrected in the mouth area (**Figure 130**).

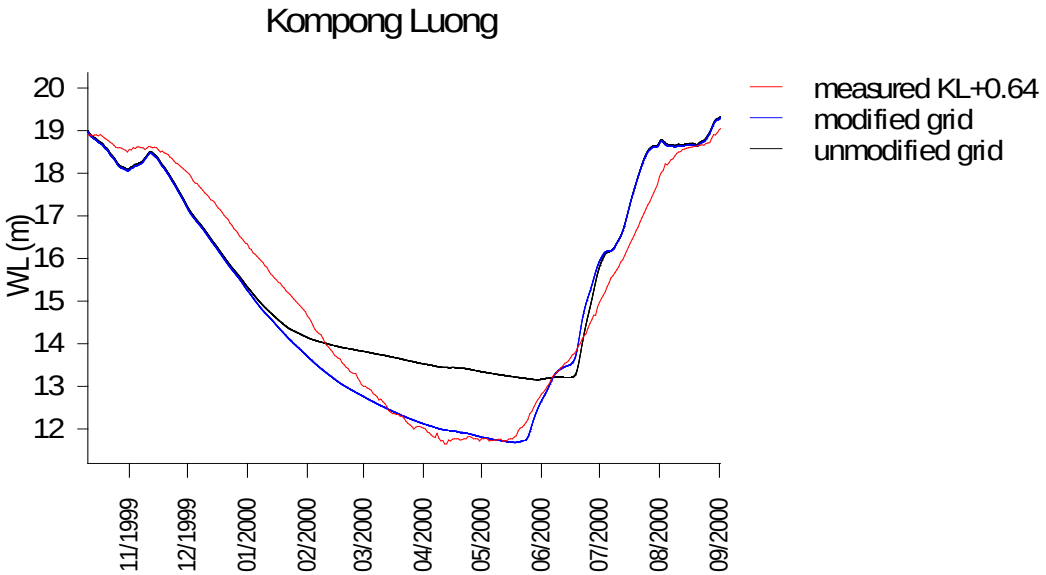

Figure 130. Water level at Kompong Luong (Tonle Sap) Year 2000 with and without Tonle Sap River mouth grid depth modification. (Subtract 10 m from the water levels to get MSL values.)

Next, the bottom friction coefficient was tested (**Figure 131**). Too large friction coefficient clearly weakens the model fit to results. Linear friction value of 0.01 was confirmed to be optimal value for best fit.

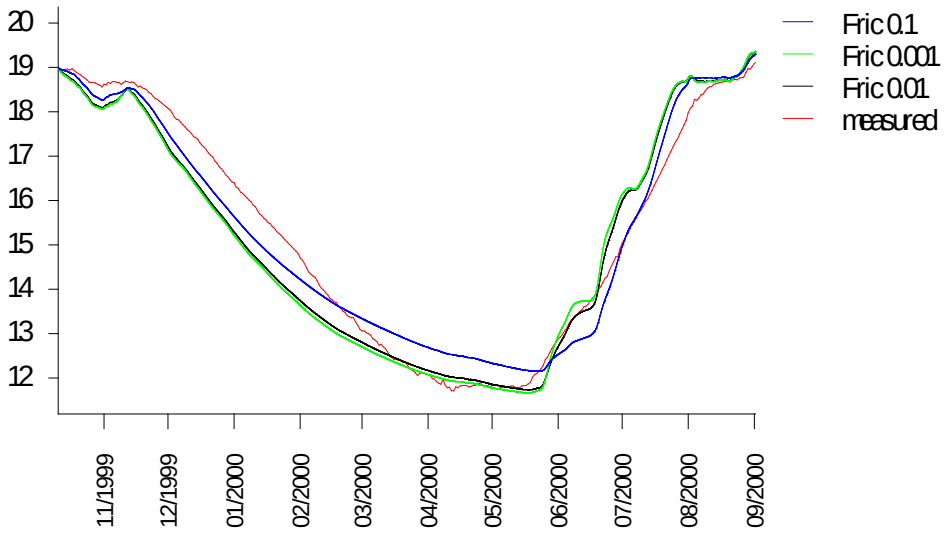

Figure 131. Effect of linear friction coefficient; water level at Kompong Luong for values 0.1, 0.01 and 0.001. (Subtract 10 m from the water levels to get MSL values.)

Effect of precipitation and evaporation was tested, by leaving the evaporation out from the computation (**Figure 132**). In the calibration computation the evaporation does have only a small effect to the model water level. Part of the results is explained by the dominating effect of water level boundary condition at the Tonle Sap river boundary, but overall effect of the evaporation and precipitation to the lake water area is mainly in dry season, where the water level of the lake is reduced.

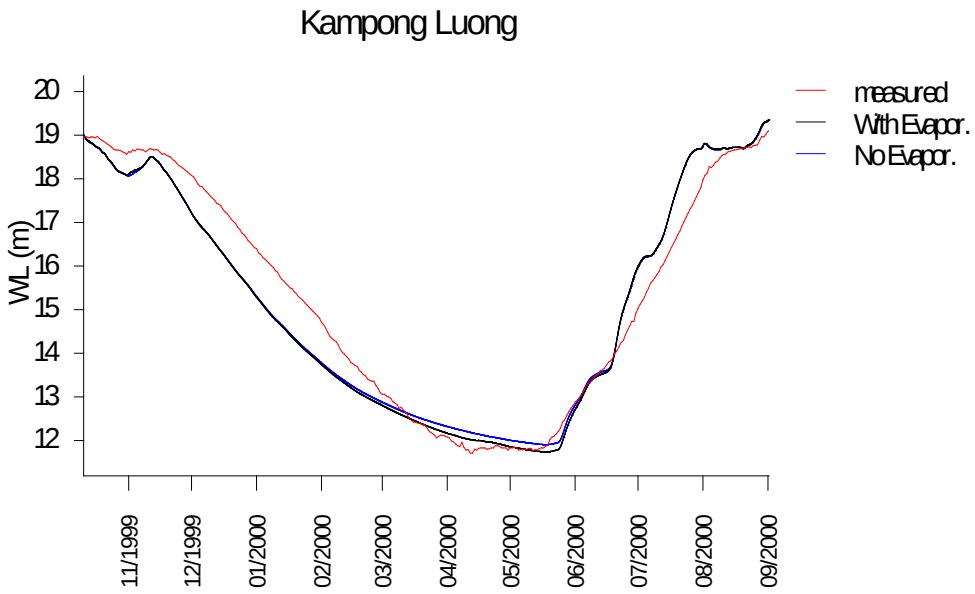

Figure 132. Effect of evaporation & precipitation to water level at Kompong Luong (evaporation & precipitation from VMOD Aphrodite model run; potential evaporation as an average of three points on the dry season lake area). (Subtract 10 m from the water levels to get MSL values.)

To calibrate the inflows, the boundary condition at the Tonle Sap river boundary was changed to inflow and outflow data computed using ISIS model (**Figure 133**). Using the ISIS data the water level change (decrease) was not large enough. Also real maximum flood water levels are not reached with ISIS. Supposing the lake volume is approximately correct, the outflow from lake is then too large, as evaporation cannot modify the water level too much. Several coefficients were tested to correct the ISIS flow, and for the test year value 1.3 gave approximately correct water level decrease. However, it should be noted that the flow calibration depends also on tributary flows.

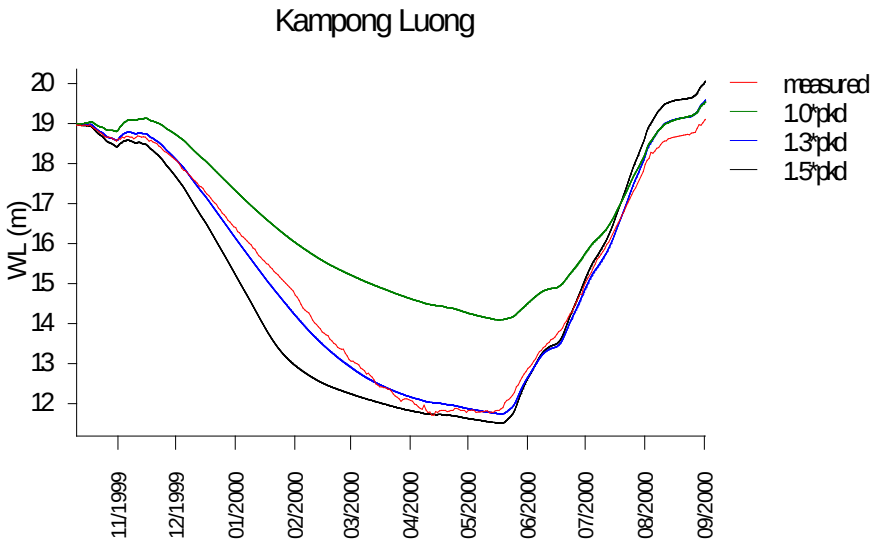

Figure 133. Water level using Preak Kdam flow computed using ISIS model; best fit with 30% increased ISIS flow. (Subtract 10 m from the water levels to get MSL values.)

A three-year period was computed using the ISIS in- and outflows. The results was checked against measured water levels at Kampong Luong. Only the year 2001 flood season results show good agreement with the measured water levels. A revision of the inflow data and tributary flows is therefore needed.

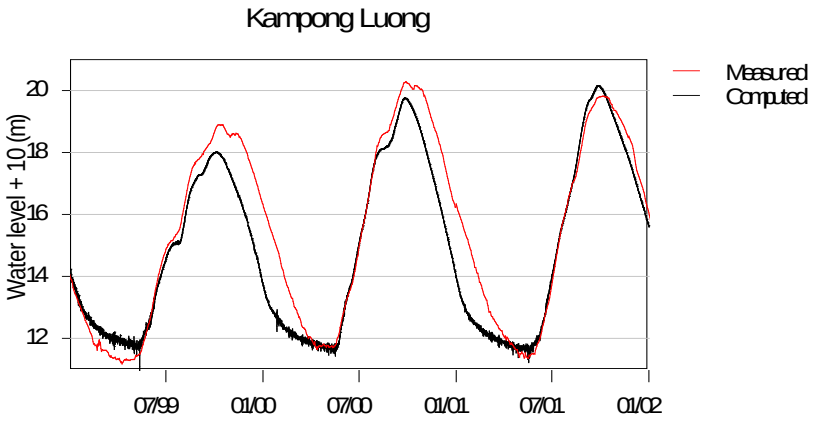

Figure 134. Water level for three years computed using Preak Kdam flow from ISIS model, flow multiplier 1.5. (Subtract 10 m from the water levels to get MSL values.)

3.3. Tonle Sap Lake and floodplain sediment calibration results

The Total Suspended Solids (TSS) were calibrated using the WUP-FIN water quality database used also for the watershed model calibration. Four calibration points were selected: two in the Lake proper and tow in the floodplain (**Figure 135**). Settling/sedimentation coefficient optimal value was found to be 21 cm/d in contrast to previous value 7 cm/d. Which one would work better for floodplain productivity would need to be verified with actual floodplain sedimentation, primary production and fisheries monitoring results. Both values are used for sedimentation and productivity mapping below but the sediment calibration time series are shown only for 21 cm/d value.

The calibration results are presented in **Figure 136** - **Figure 139**. In most of the figures both surface and deeper water layer concentrations are shown. The model replicates the observed data quite well considering the very high spatial and temporal variability of TSS. Also inflow concentrations have been estimated from available data and the results are expected to be improved when calibrated watershed model data is used.

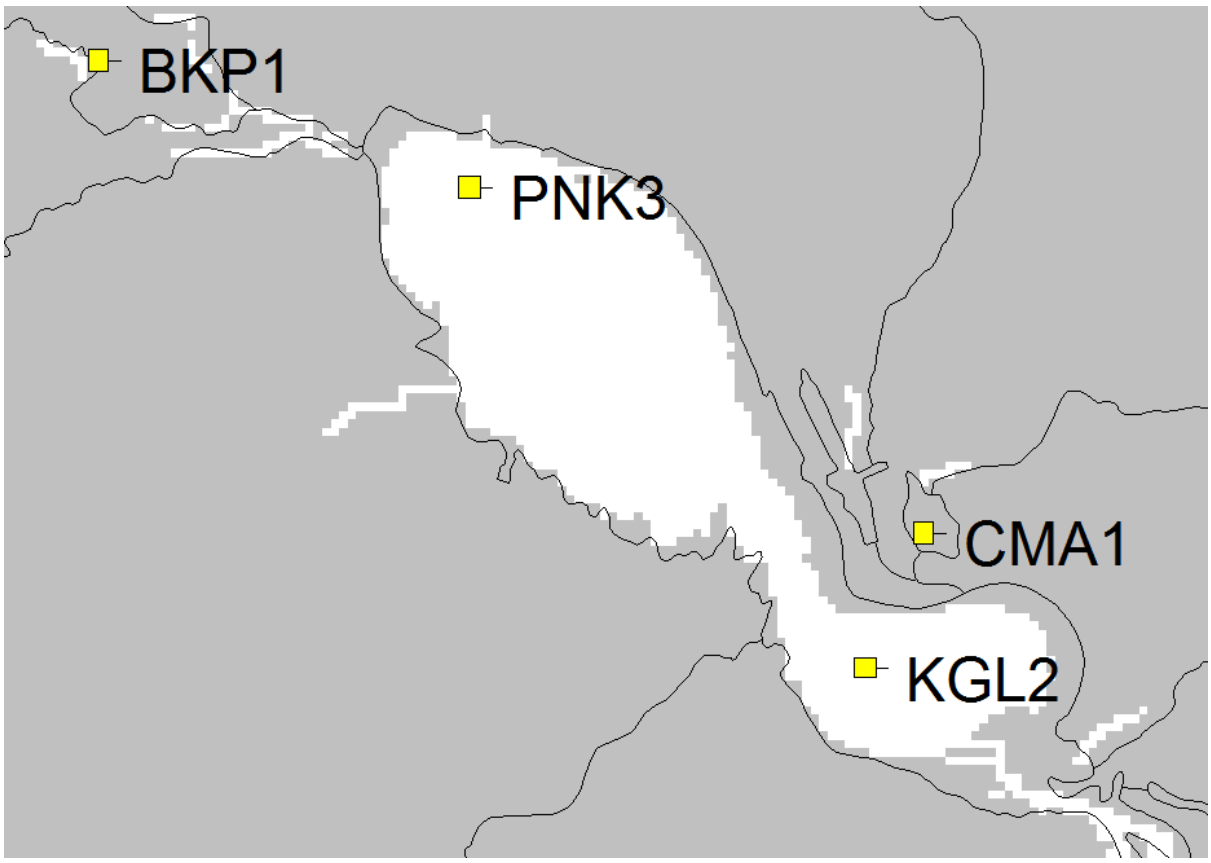

Figure 135. Location of the TSS (Total Suspended Solids) model calibration points.

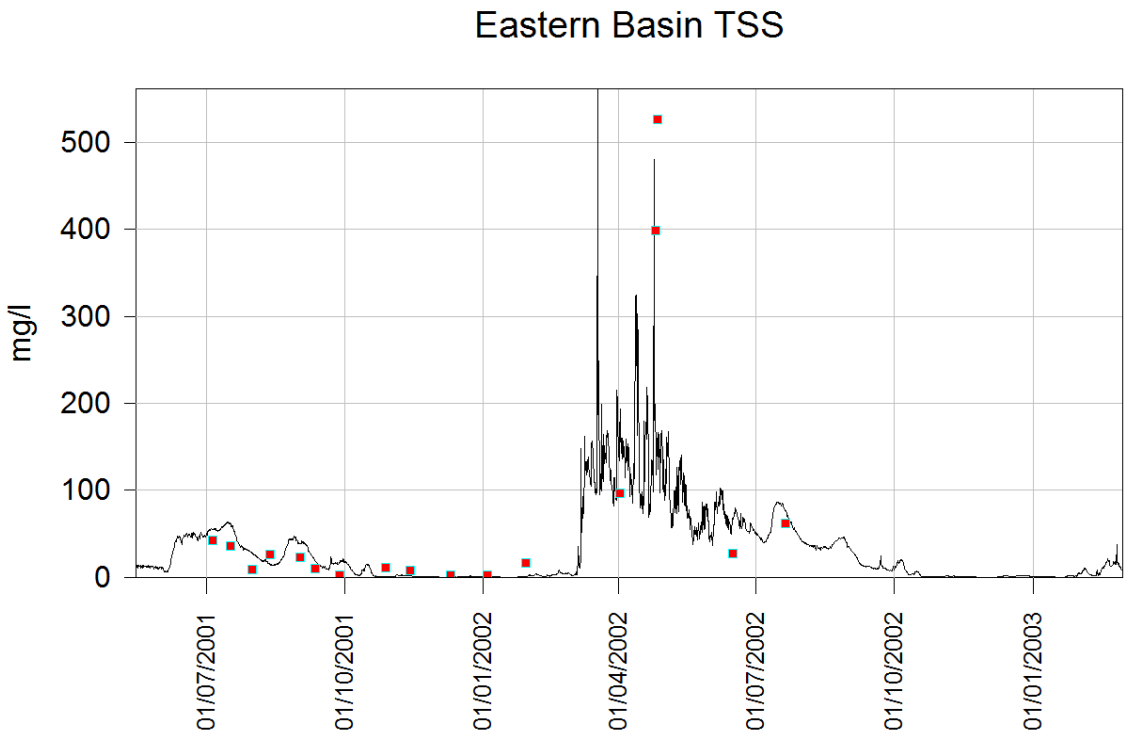

Figure 136. Eastern Basin (KGL2) modelled and measured TSS concentrations.

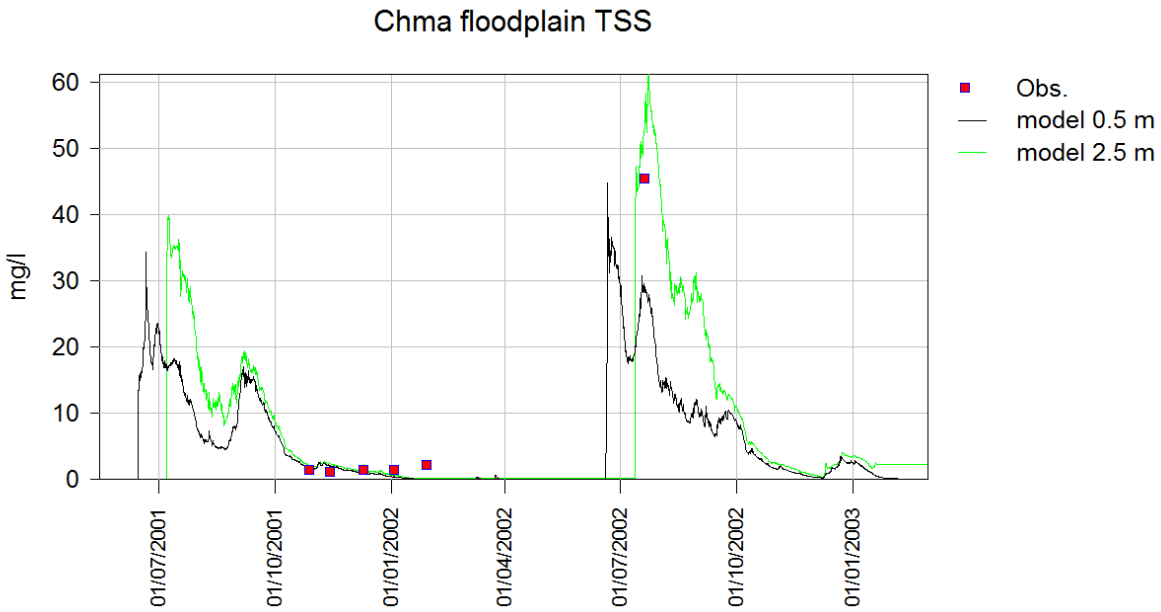

Figure 137. Eastern Basin floodplain (CMA1) modelled and measured TSS concentrations.

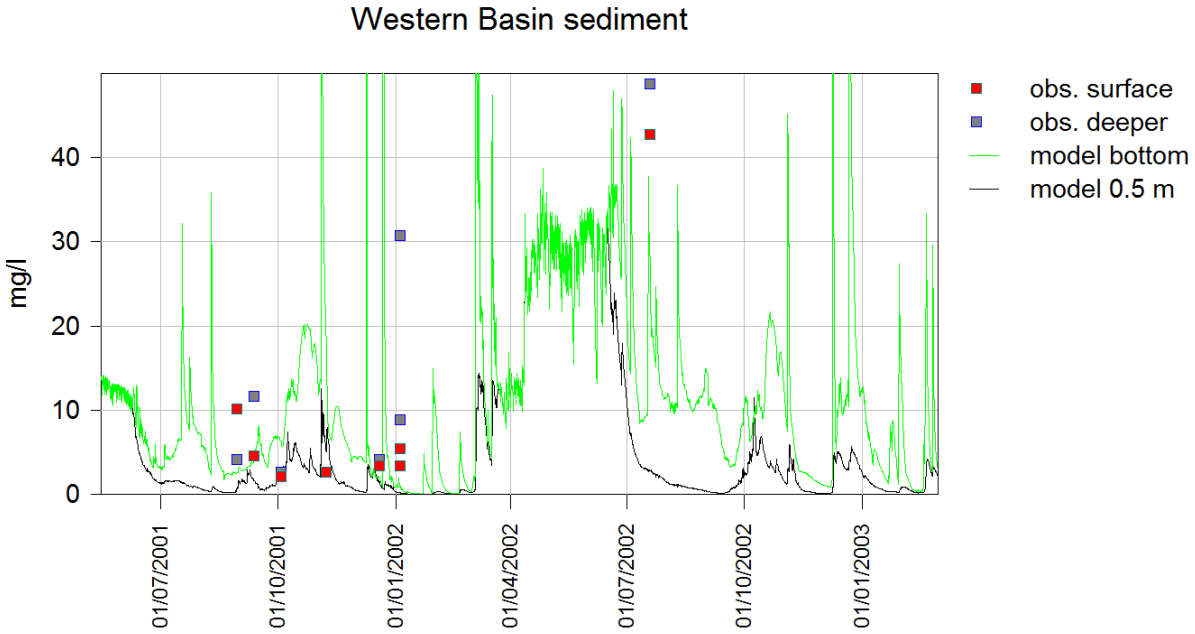

Figure 138. Western Basin (PNK3) modelled and measured TSS concentrations.

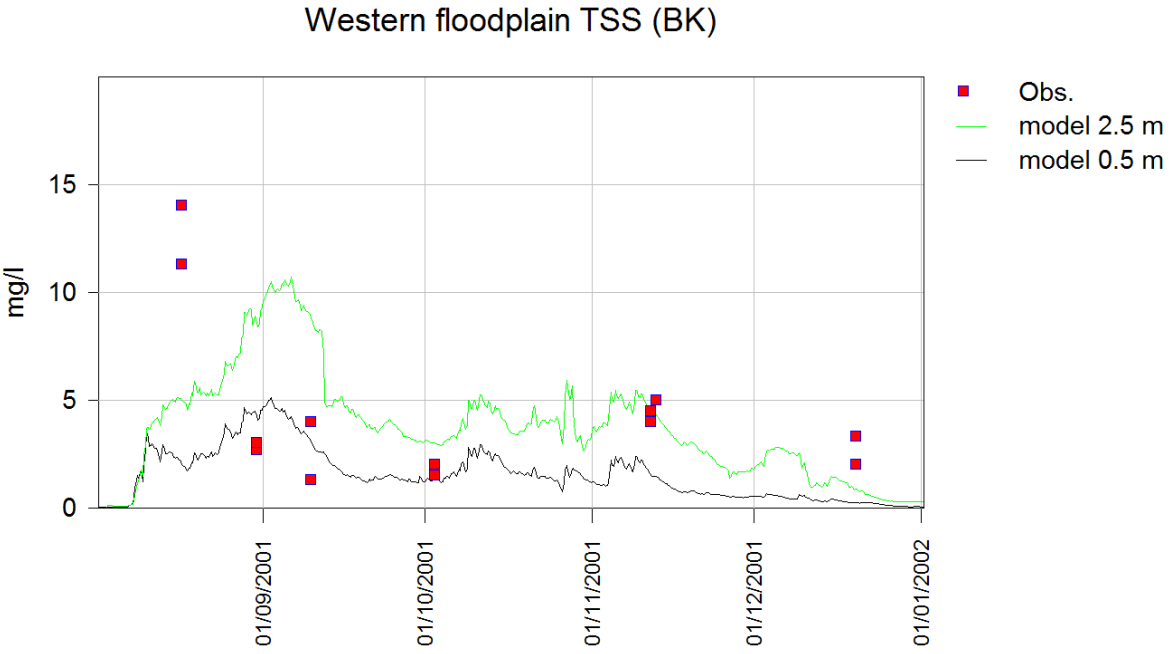

Figure 139. Western Basin floodplain (BKP1) modelled and measured TSS concentrations.

Modelled floodplain sedimentation is shown in **Figure 140**. Direct floodplain sedimentation measurements have not been used, but it can be easily verified through water quality (water is very clear further away from the Lake proper in the floodplain) and natural levee formations near the Lake edge that model sedimentation pattern follows real one. In the Lake proper net sedimentation is minimal which is also confirmed also by core samples (Tsukawaki 1997). In addition to sedimentation the flood duration of course impacts sedimentation so that upper floodplain is flooded much less than the lower reaches (**Figure 141**).

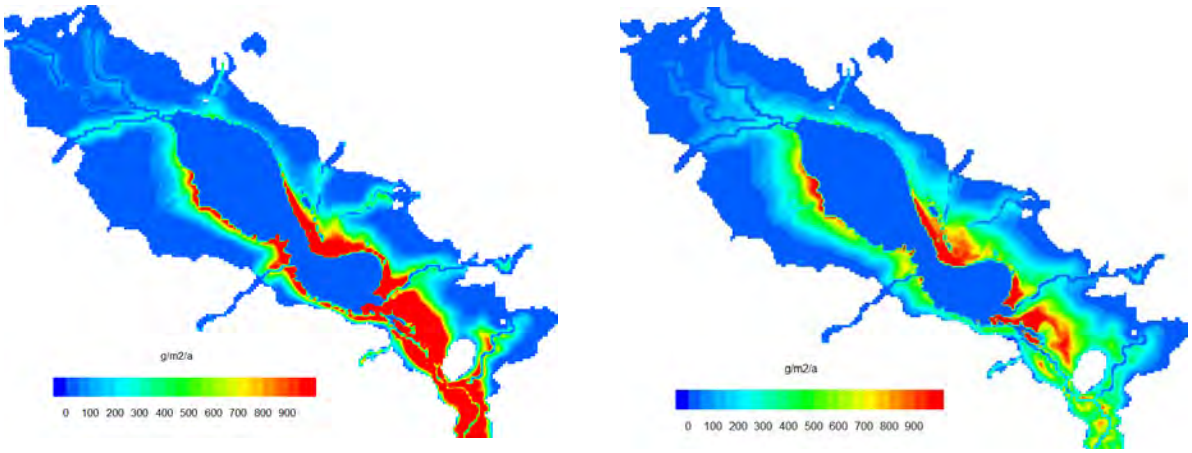

Figure 140. Tonle Sap floodplain 2005 modelled sedimentation. Left sedimentation coefficient 21 cm/d and right 7 cm/d.

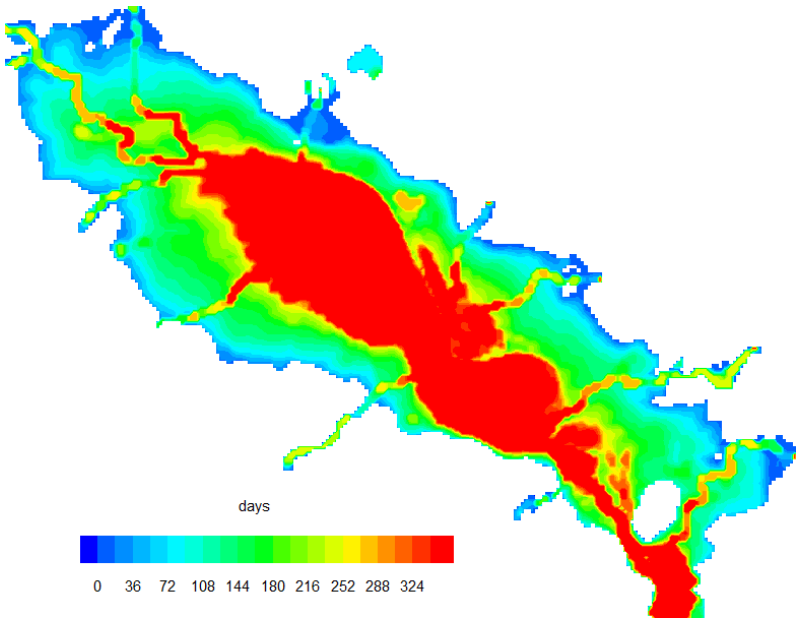

Figure 141. Tonle Sap 2005 flood duration.

3.4. Dissolved oxygen and productivity

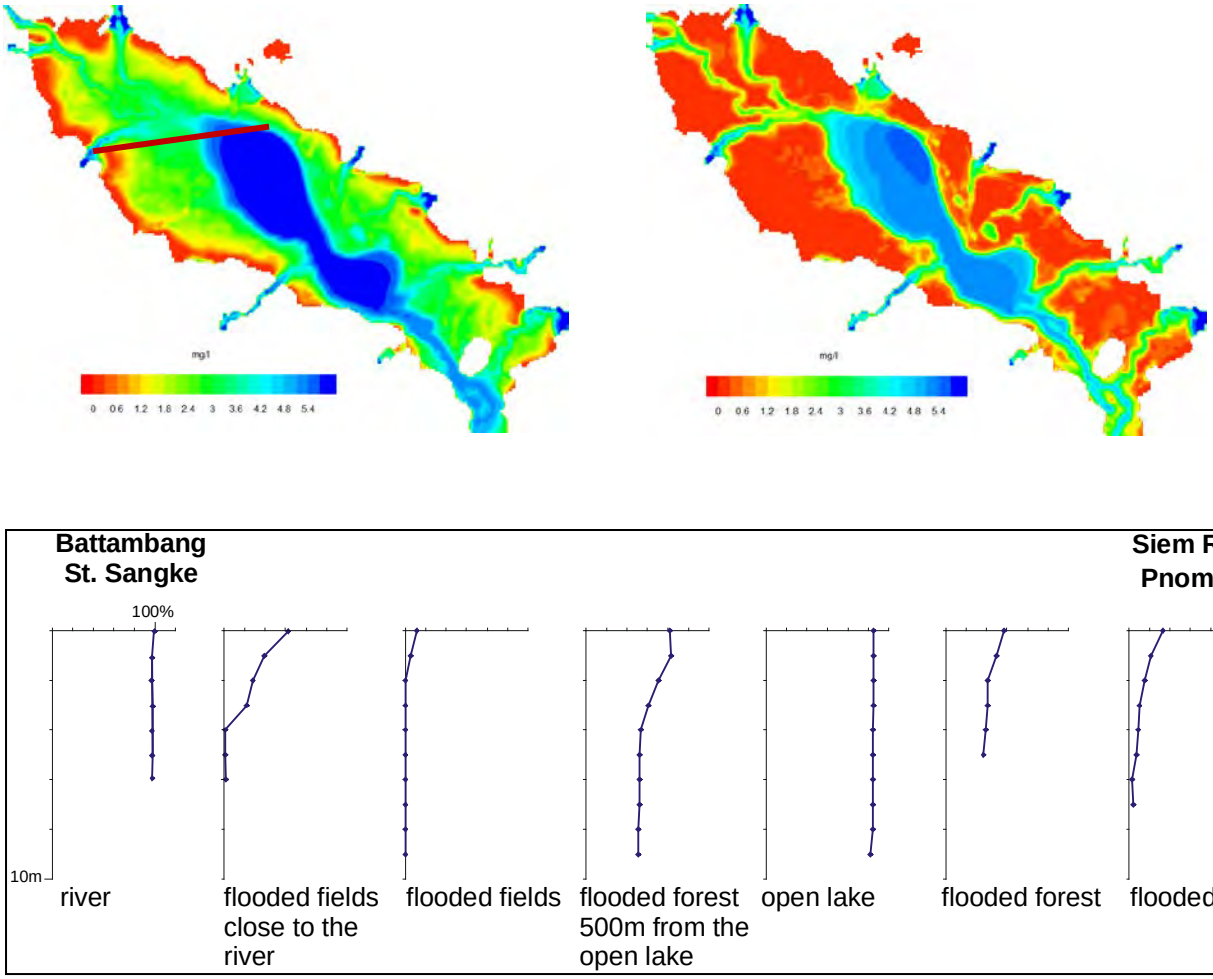

Figure 142. Tonle Sap 2002 computed time averaged near-surface and near-bottom dissolved oxygen (upper figures) compared with measured oxygen saturation profiles (lower figures). Brown line in the model figure shows the measurement section.

The oxygen calibration result is shown in **Figure 142**. Dissolved Oxygen (DO) saturation profiles are from the cross section drawn on the map. Model results are from mid-depth in varying depth water columns. Both in the model and in the measurements the DO values are good in the rivers and in the Lake proper deteriorating in the floodplain. Large parts of the floodplain in the model are DO poor or anoxic which has been also confirmed through sampling and using DO probe.

Figure 143 shows total primary production (phytoplankton, periphyton and mobilized terrestrial production) and **Figure 144** potential fisheries production. The largest fisheries production areas in the model are comparable to the common understanding of the highest production areas and fishing lots, at least for the 7 cm/d settling velocity and in the past when the fishing lot system was in place.

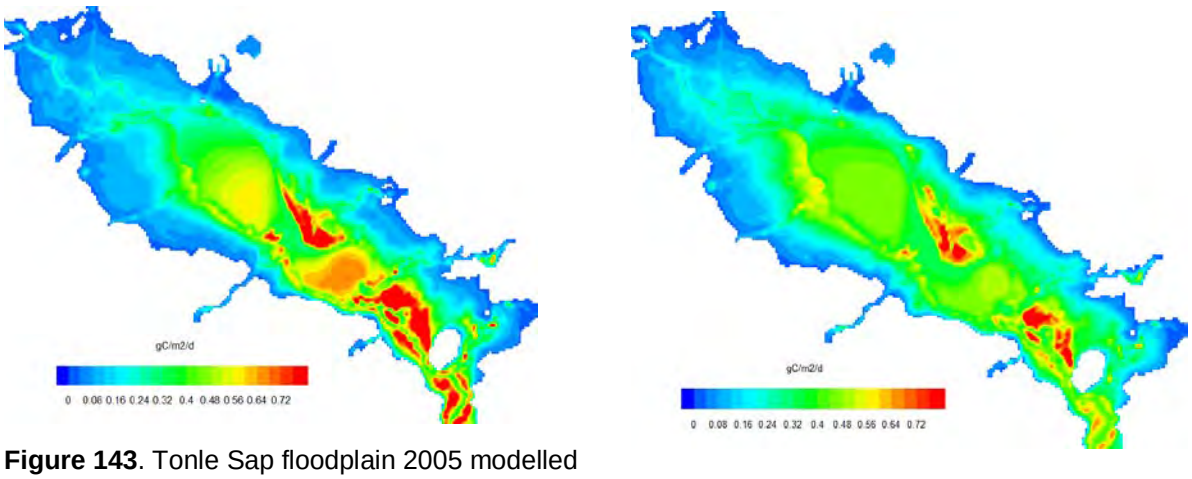

Figure 143. Tonle Sap floodplain 2005 modelled total primary production. Left sedimentation coefficient 21 cm/d and right 7 cm/d.

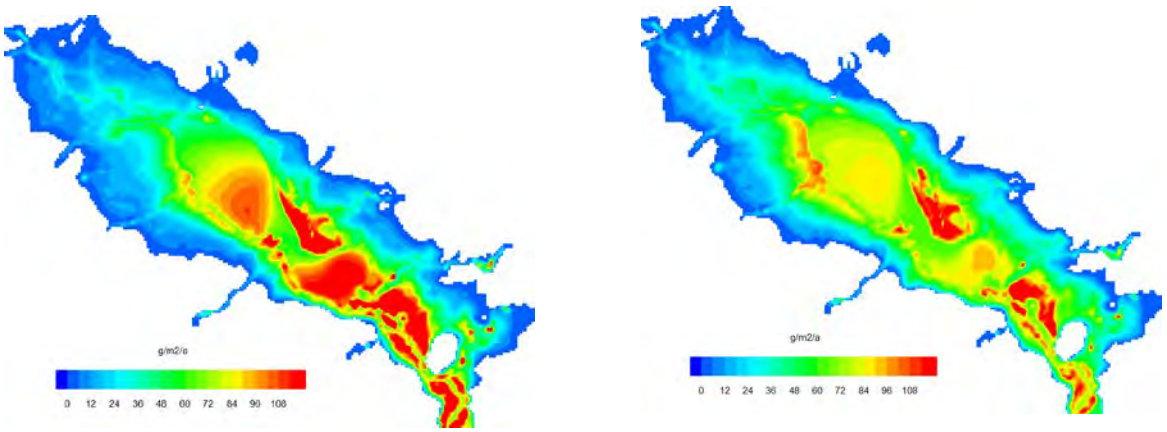

Figure 144. Tonle Sap floodplain 2005 modelled fisheries production. Left sedimentation coefficient 21 cm/d and right 7 cm/d.

It is interesting to compare the relatively high flood year 2005 sedimentation and productivity to the extremely dry year 1998 (**Figure 145**). It can be seen that hydrological and sediment conditions have dramatic impact on the Lake productivity.

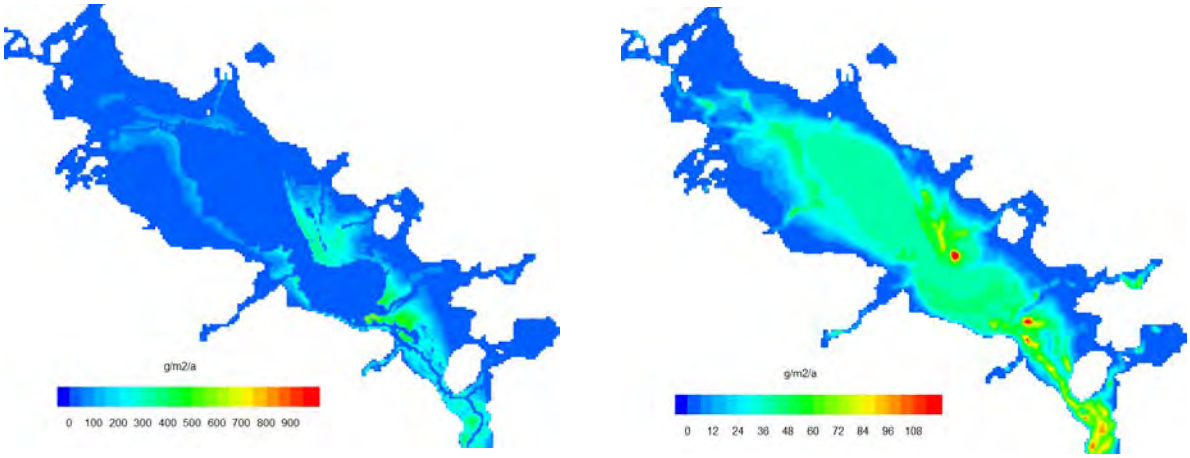

Figure 145. Tonle Sap floodplain 1998 modelled sedimentation (left) and fisheries production (right). Sedimentation coefficient 7 cm/d.

4. Annex 4 - Tonle Sap Lake and floodplain nutrient cycle modelling

Description and validation for the 3D-EIA WQ (Water Quality) model is presented in ANNEX IV. Here Tonle Sap application data, construction and testing and calibration results are presented.

The 3D-EIA model includes basic water quality and productivity modelling capacity. The main objective of the 3D WQ model is to model nutrient cycle, that is **how nutrients circulate between water, biota and bottom and how they affect primary (and fisheries) production**. The 3D hydrodynamic model simply assumes that all primary production is dependent on sediment phosphorus through a simple function. As the Delta productivity impacts need to be assessed reliably it is of utmost importance to verify the nutrient cycle and productivity through robust modelling. A secondary but very important objective is to **develop methodology for reservoir nutrient trapping**. The 3D-EIA model can be applied to the reservoirs in a straightforward way. As a matter of fact it has specialized technology for efficient reservoir water quality modelling over decades long operation.

The 3D WQ modelling is not required by the original Council Study Modelling Framework. The 3D WQ model development has been provided to the Council Study as an additional service to strengthen MRCS modelling suite for the Council Study. The model development work is at its final stages and will complete necessary foundation for advanced nutrient and productivity modelling. However, further work will be needed to bring the model to a fully tested, calibrated and operational stage.

It should be noted that the 3D-EIA WQ model is dedicated water quality model which doesn't include hydrodynamics other than using pre-computed flow fields. The water quality model presented in this chapter uses 500 m grid cell size. Extensive use of the hydrodynamic 3D model would be too slow with this grid resolution but it is feasible for the water quality model that uses pre-computed flow fields.

4.1. Model grid

Water level in the model is presented as depth from surface, so compared to ground elevation scale the model depth scale is upside down. Model zero water level is set to 12m elevation. To get model grid elevation from the ground elevation, use formula

$$d = 12 - \text{round}(e),$$

d = model depth (m)
e = ground elevation (m),
round()=rounding to nearest integer value

Water level can be converted to model water level using following formulation

$$h_{Mod} = 11.5 - h_{Obs}$$

h_{Mod} = model water level
h_{Obs}= observed water level (Kampong Luong + 0.64)

In the flow model 10m is added to all elevations, so 22 must be used instead of 12 to in the above formula to convert from flow model elevation to water quality model depth.

The volume of the water quality grid closely follows the volume obtained from 500 m resolution DEM (**Figure 147**). There is, however, a cumulative error so at the 12m water level the volume is about 1% too small. The model grid is shown in **Figure 146**.

The model is setup so that the lowest possible water level is 1.0m. Highest possible water level is not limited, but the grid volume is correct up to level +12m.

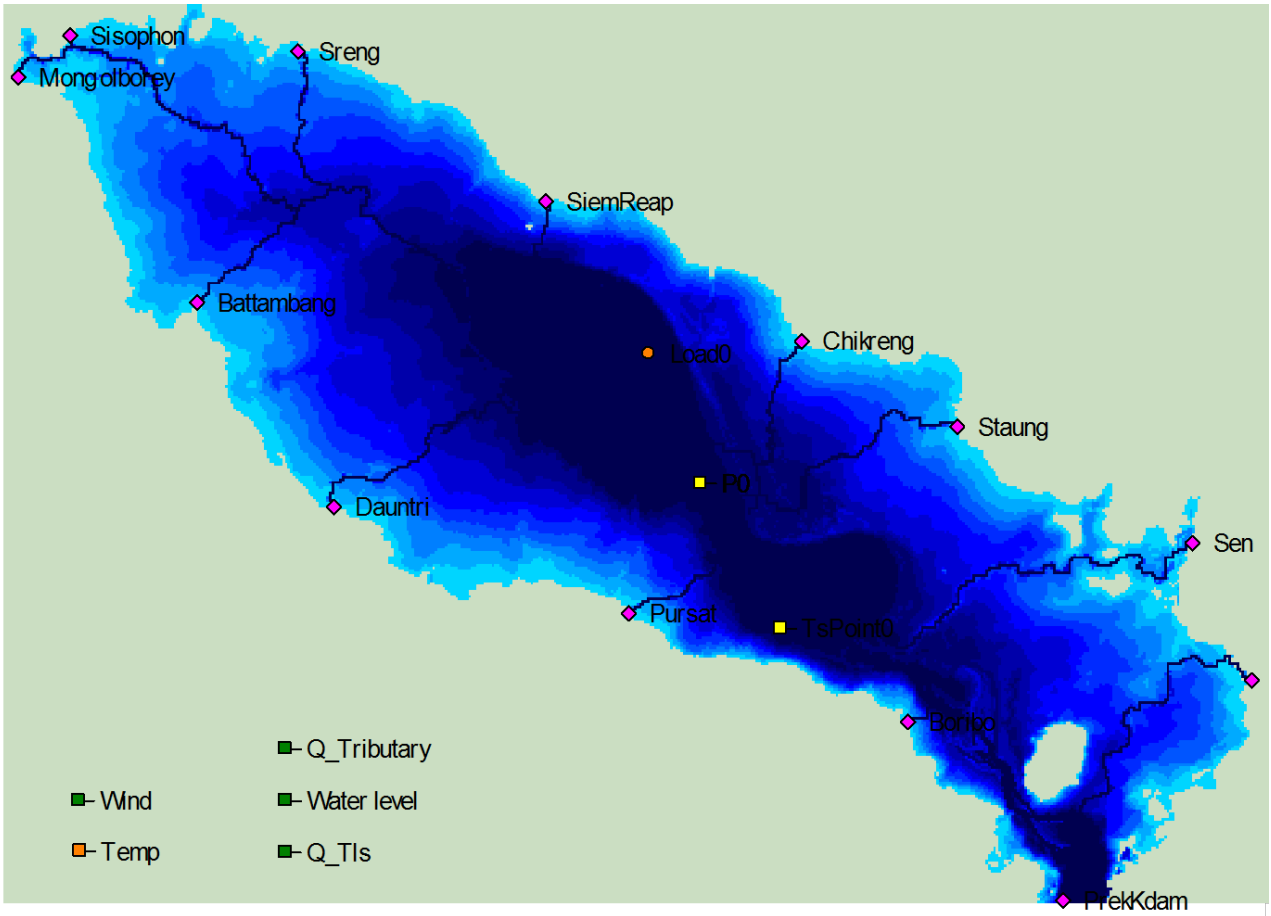

Figure 146. Water quality model setup showing inflows and depths of the model grid.

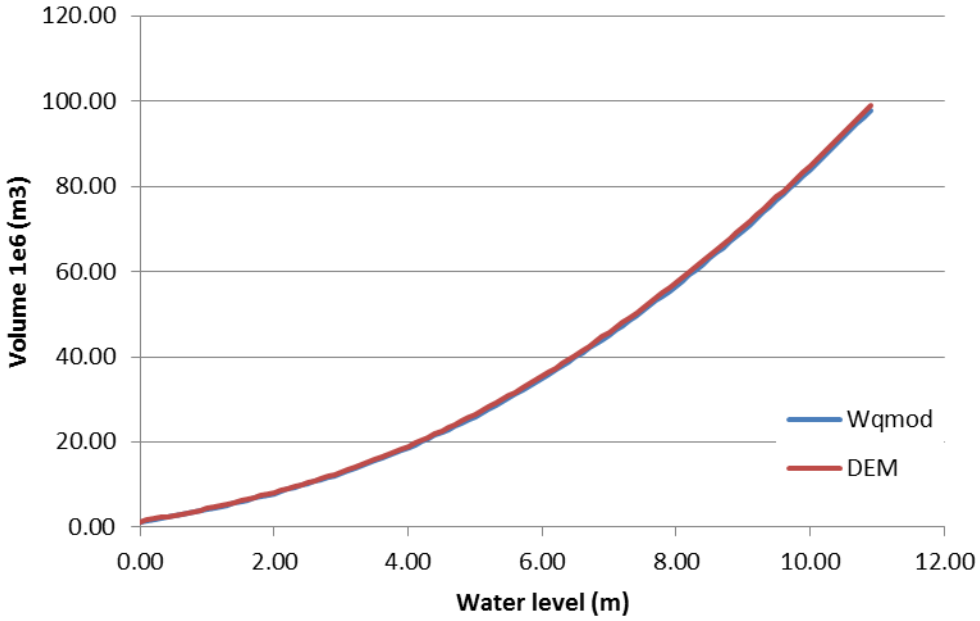

Figure 147. Water quality model grid volume, and volume computed from elevation model.

4.2. On the computation of water flows and water level

Depth levels in the water quality model are stepped with 1m interval. For each depth level a separate set of flow fields are computed, describing the effect of Tonle Sap River, tributary rivers, and wind to the total flow in the lake. The Tonle Sap model uses a total of 12 different water levels and corresponding flow field sets. To obtain a flow state for given water level, boundary flow, and wind conditions, first the flow field set corresponding the given water level is selected, after which the flow fields are combined to obtain flow state in the lake for given boundary flow and wind conditions. During computation the water level increases gradually. When the water level is at the boundary of two depth levels, the set of flow fields used to compute the water flow is changed.

4.3. Model parameters

In the model the option “Calculate water levels” must be active. This option defines that the water level is computed using the given in- and outflow data, e.g. Tonle Sap river and tributary flows.

4.4. Boundary flows

The main in and outflow to Lake Tonle Sap is through the Tonle Sap river. During large floods part of the inflowing water may also flow over the floodplain, but this in not accounted separately in the model. Other inflows include 12 main tributary rivers, the locations of which are shown in **Figure 146**.

Compared to water level, the inflows do not match correctly the observed water level, e.g. when inflows are used in the water quality model, the resulting water level does not match the observed water level accurately. As first approximation, the incoming flow from Tonle Sap River is computed using the water level and tributary discharges so that the amount of inflow from Tonle Sap River and water level match correctly. Computed flow is shown in **Figure 148** along with the ISIS modelled flow. Both flows are quite similar, even though there are also some differences. Note that the river Tonle Sap flows in two directions, the flow to the lake is positive, and flow out from lake is negative.

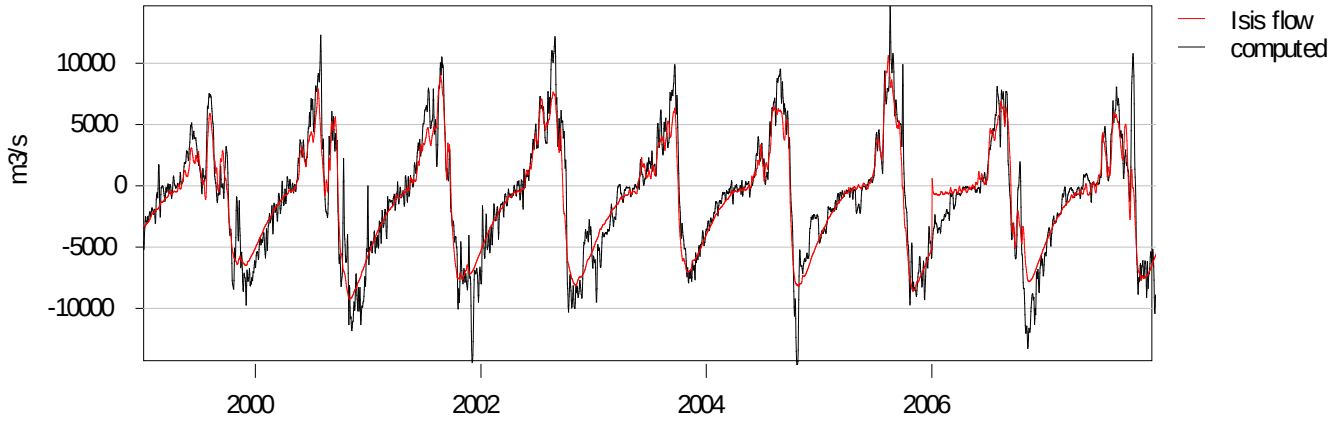

Figure 148. Corrected flow from Tonle Sap River to the Lake compared with the flow from ISIS-model.

Tributary discharges are estimated in the model using base discharge which is scaled to obtain a discharge for a specific river. To obtain a flow for a given tributary, the base discharge is multiplied by average discharge of that tributary. The tributaries used in the model and corresponding average discharges are listed in Table 4 (Sarkkula et al. 2006)

The tributary base discharge time-series is shown in **Figure 149**.

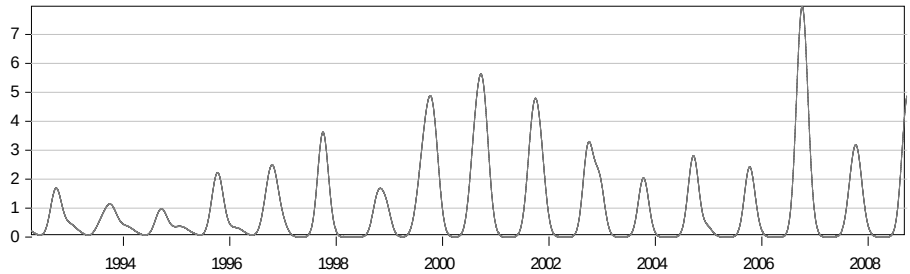

Figure 149. Tributary base discharge, scaled so that the average discharge is 1 m3/s

Table 4. Tributary rivers and average annual discharges (from 1993-2007 data)

River	km3/a	%	m3/s (avg)
Chinit	3.46	14.4	109.7
Sen	5.84	24.2	185.2
Staung	1	4.1	31.7
Chikreng	0.73	3.0	23.1
SiemReap	1.16	4.8	36.8
Sreng	1.75	7.3	55.5
Sisophon	0.57	2.4	18.1
MongolBorey	1.34	5.6	42.5
BattamBang	2.73	11.3	86.6
Pursat	2.63	10.9	83.4
Boribo	2.46	10.2	78.0
Dauntri	0.44	1.8	14.0
total	24.11	100.0	764.5

As the water level changes, the location at which the tributary flow enters the lake moves along the river channel. In the model this behavior has to be implemented in a somewhat complicated manner by defining a separate location for each discharge entry point and water level. **Figure 150** shows an example of the locations of discharge entry points, there is one point for each of the 11 possible water levels. When the model is run only the discharge point corresponding to the current water level in the model is active.

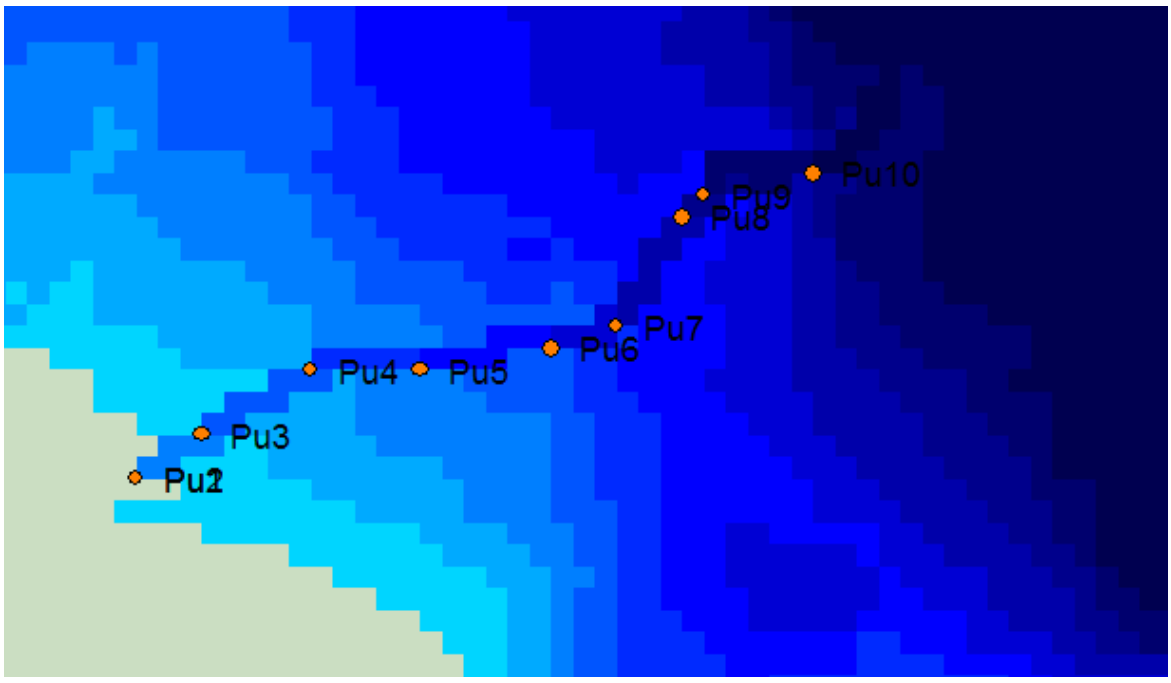

Figure 150. An example of tributary discharge entry points locations corresponding to different water levels for a tributary river (Pursat).

4.5. Loads

The model computes the concentrations of defined water quality variables, e.g. total suspended sediment (SEDI), total phosphorus (PTOT), and total nitrogen (NTOT) in the modelled area. In order to compute the water quality, incoming loads of the computed variables must be given for the model. Loads may come from different sources, such as inflowing rivers, point sources on the lake, atmospheric load, and loads from the lake bottom.

4.5.1. Tributary river load setup

The tributary river loads are defined in the model as point loads at the river inlet location. Loads are expressed in units of kilograms per day (PTOT, NTOT) or tons per day (SEDI). The load does not depend explicitly on river discharge, instead the load is computed beforehand from concentration and river discharge, and the resulting load is then put to the model. This method allows accurate definition of the amount of load that end up to the lake.

The moving water level brings with it some complications, as the location of the river inlet to the lake depends on the water level. Therefore the tributary loads are defined in the model similarly as tributary discharge entry points, e.g. for each water level there is a separate load point. **Figure 150** shows an example of point locations defined for a single tributary river.

The model has a specific loading type, that is active at specific water level only (the type is “wldependent” in the model load type selections). Load area top layer value (z0) defines the water level where the load is active. This way, by defining a separate load point for each water level (for all 11 possible z0 values), the load point moves as the water level varies.

4.5.2. River Tonle Sap load setup

The Tonle Sap River is deep enough so that there is water at all water levels at the main river channel. Therefore the load location stays in same locations at all water levels. Instead of load (unit kg/d), the Tonle Sap river load is defined as concentration of the given substance in the incoming water (unit mg/l). For large inflows this is usually the easier method to define incoming water quality.

Tributary river load points and Tonle Sap river concentration points (Prek Kdam) are shown in **Figure 151**.

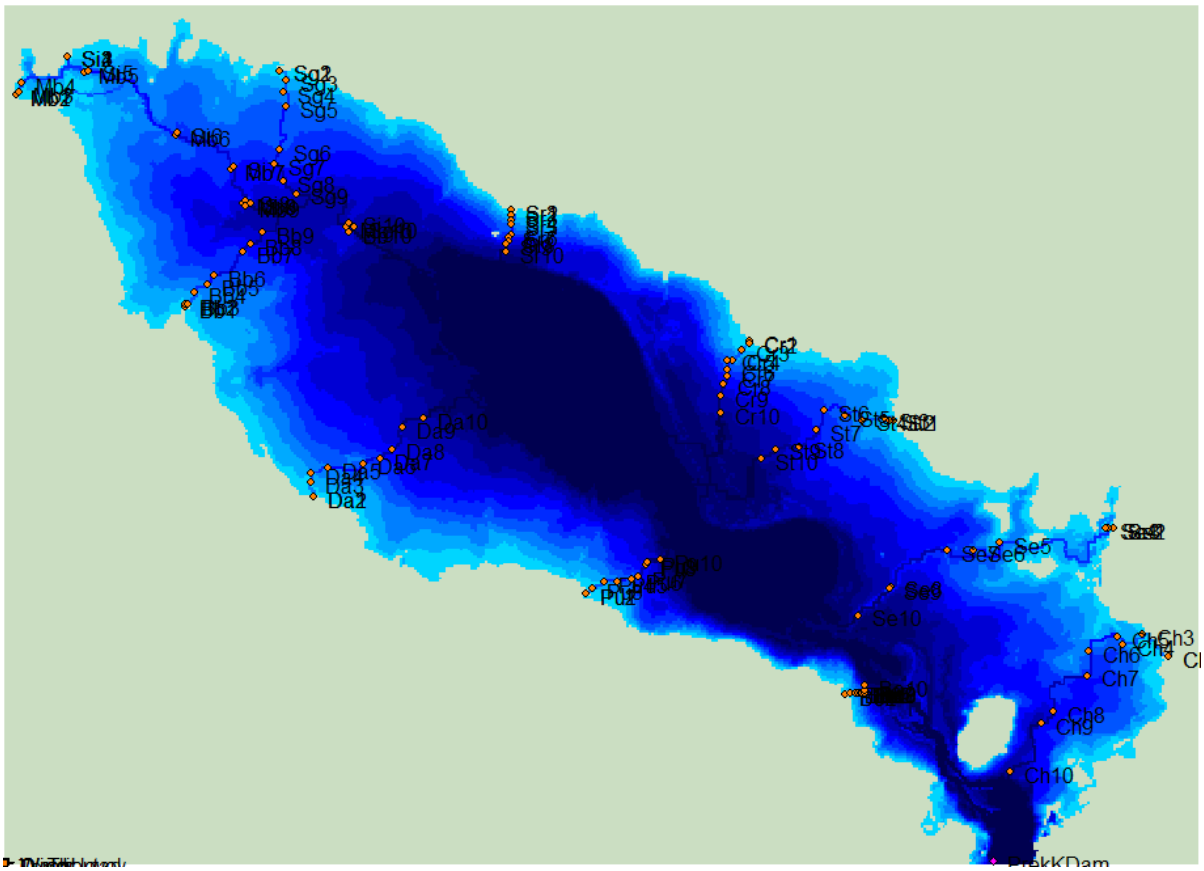

Figure 151. Model grid with tributary loads and River Tonle Sap concentration.

4.6. Tributary loads

Tributary loads to the model are computed using a catchment model. The points for which the catchment model computes the loads (points L1-L7, shown in **Figure 152**) do not correspond to the tributary river locations used in the water quality model. Therefore the load values for each tributary river had to be separately computed from the load values given by the catchment model. Computation formulas used to obtain the loads for tributary rivers from to loads at points L1-L7 are shown in the Table 5. Note that values for L1-L7 are differences of the loads between the two load points. If two loads are from same catchment model load point the loads are shared using the ratio between average discharges of the tributary rivers.

4.7. Estimation of inflow concentrations from Tonle Sap River

Inflow concentrations to the lake from Tonle Sap River were estimated from a small set of measurement data obtained during years 2001-2002. Estimate was needed for each day of the computation, therefore measurement data could not be used directly. Instead a relation of concentration with the inflow was attempted.

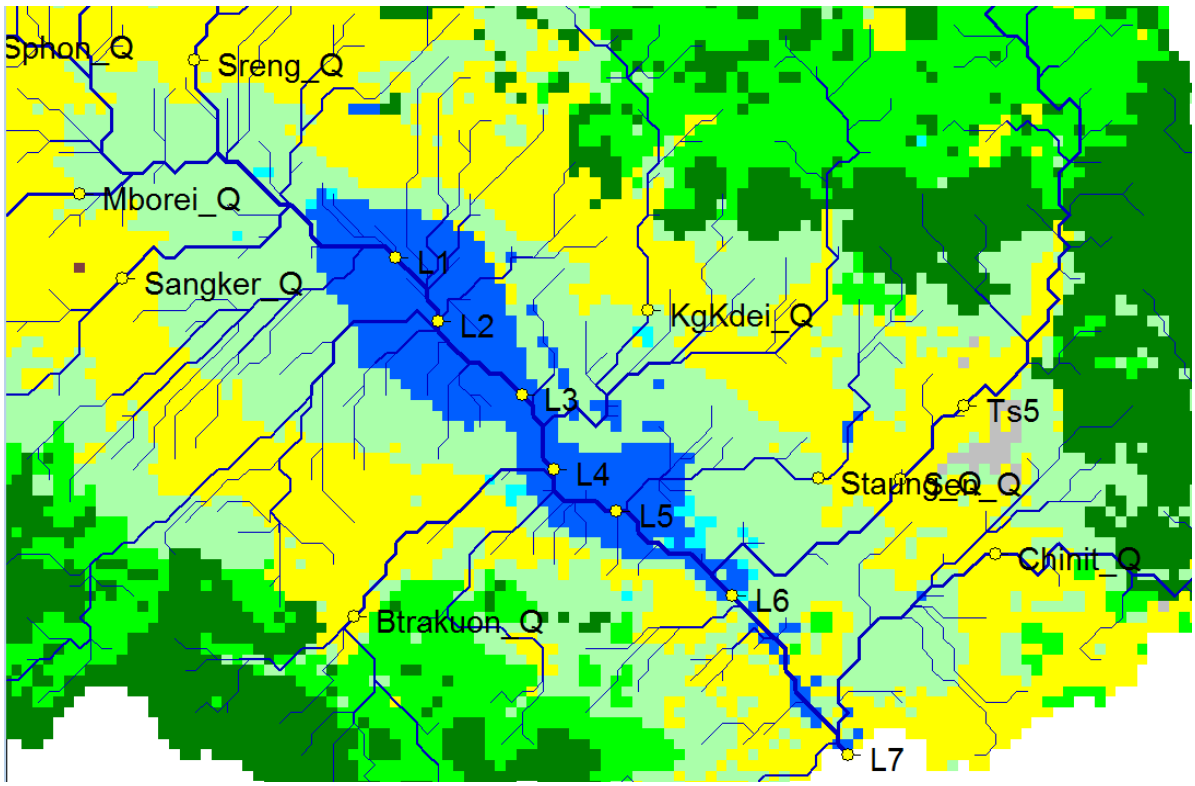

Figure 152. Catchment model tributary load locations in the Tonle Sap catchment (L1-L7).

Table 5. Tributary loads, computation method

River	*Q (m3/s)*	*Formula*
Chinit	109.7	*L7 * 0.585*
Sen	185.2	*L6*
Staung	31.7	*L4 * 0.578*
Chikreng	23.1	*L4 * 0.422*
SiemReap	36.8	*L2*
Sreng	55.5	*L1 *0.274*
Sisophon	18.1	*L1 *0.089*
MongolBorey	42.5	*L1 *0.210*
BattamBang	86.6	*L1 *0.427*
Pursat	83.4	*L5*
Boribo	78.0	*L7 *0.415*
Dauntri	14.0	*L3*
total	764.5	

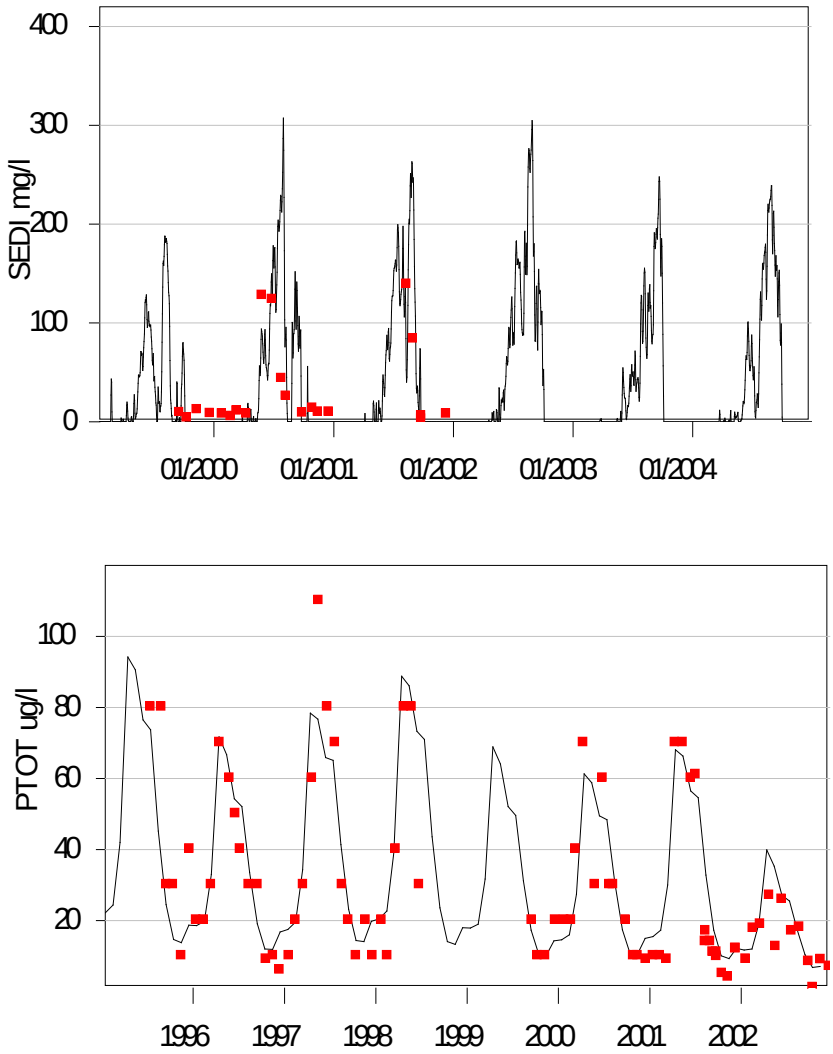

Figure 153. Estimated total sediment (upper) and phosphorus (lower) concentrations with measurements at Kampong Chhanng, measured values as dots.

Sediment concentration was estimated according to Lu et al., and adjusted with measurement data, using a simplified formulation TSS = 0.025 * Q_{PK}, where Q_{PK} is the inflow to Tonle Sap at Prek Kdam and TSS is the suspended solids concentration in mg/l. The estimate is valid for inflow period only.

Total phosphorus did not have clear relation to inflow discharge. Therefore the inflow concentration was estimated using average monthly concentration from the period from which data was available, which was then replicated for the computation period, and multiplied by the annual average concentration data. The resulting time series had r^2 fit of 0.74 with the measurement data. The estimated inflow PTOT concentration is shown in **Figure 153**.

Incoming NTOT was estimated from measured NO23 and measured NH4 data. It was assumed that Dissolved inorganic part (NO23+NH4) of the nitrogen was 50% of the total (Lewis et al., 1999), so to obtain the NTOT the N023 and NH4 fractions were summed together and multiplied by two. Similarly as for PTOT, the monthly average values computed from the whole measurement period multiplied by

the annual average measurement values were used as concentration values. The result is shown in **Figure 154**.

The NH4 and NO23 parts did not correlate well, the measurement average of NH4 concentration was 60 ug/l, and the NO23 concentration was 290 mg/l.

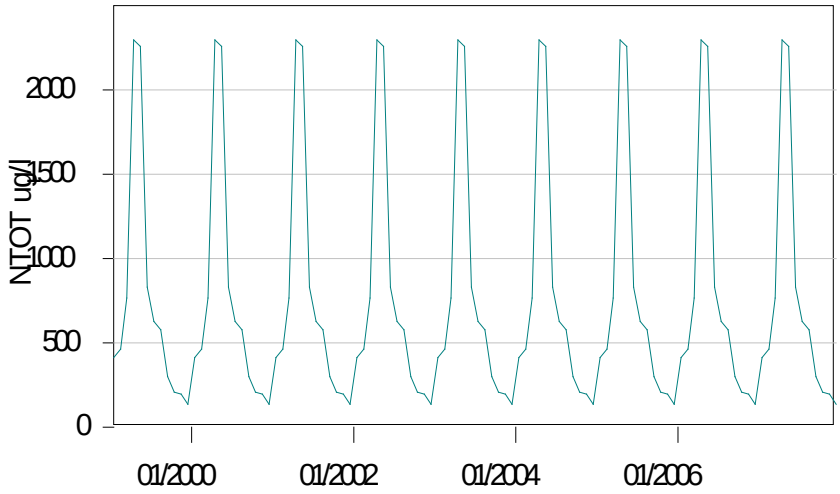

Figure 154. NTOT concentration for inflow to Tonle Sap, computed from measurements at Kampong Chhnang.

Based on measurement data from the period 09/1999 – 12/2002 at Kampong Chhnang the PO4P/TOTP relation is PO4P = 0.73 * TOTP (two outlier points were dropped from the regression, possible mistake in the input data, R2=0.94). **Figure 155** shows the relation of PTOT and PO4P data. The fraction of PO4 is rather large.

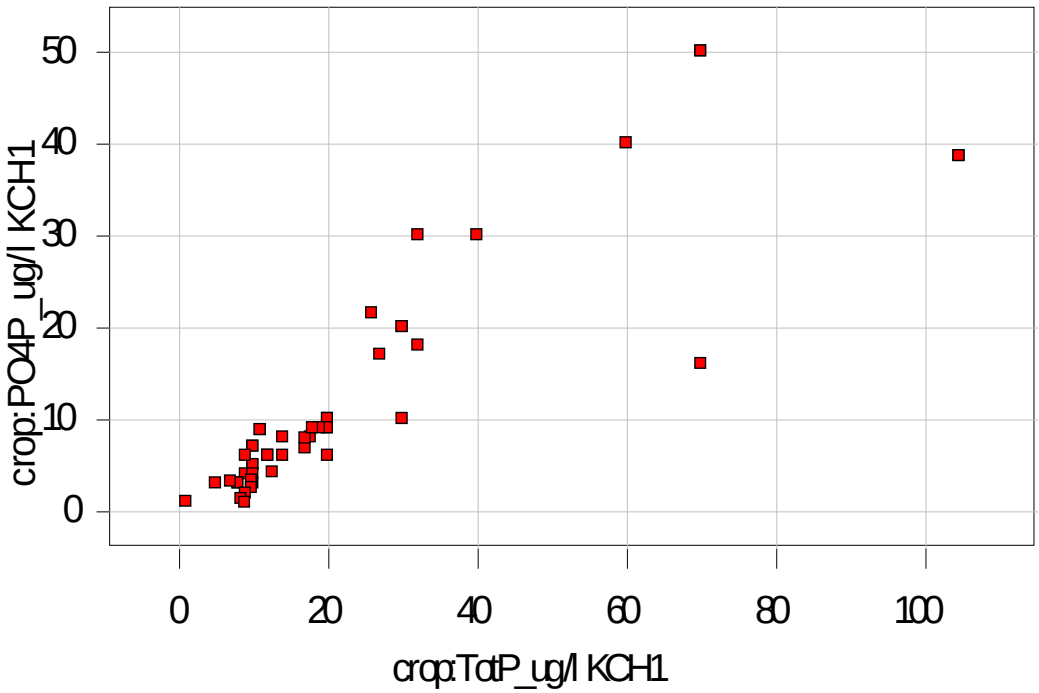

Figure 155. Relation of PTOT concentration to PO4P concentration at Kampong Chhnanng.

4.8. Resuspension of sediment from lake bottom

As a first guess, the resuspension from lake bottom was estimated using following formulation

$R = C\,(u^{e1} - u_{cr}^{e1})^{e2}$, when $u>u_{cr}$ otherwise 0

where R = amount of resuspended sediment, C=coefficient, u=average flow speed at bottom layer, u_{cr} =critical velocity and e1 and e2 are exponent value that must be calibrated. Resuspension was used for PTOT and SEDI variables. Following parametrization was used: e1=2, e2=2, u_{cr} = 6 cm/s. Constant C was set separately for each variable.

4.9. Results

The model works at demonstration level and these preliminary results are presented to show the model behavior with the estimated input loads. Test computation period was from 04/1999 to 04/2003. There were some missing loads, such as atmospheric load and possible point loads from the villages and cities around the lake. Lake internal processes are taken into account only at very coarse level, by including constant settling, sedimentation and flow speed dependent bottom load to the model.

The water level used by the model is shown in **Figure 156**. During the low water period the water level stays too high, the difference on year 2002 dry season is about 0.9m.

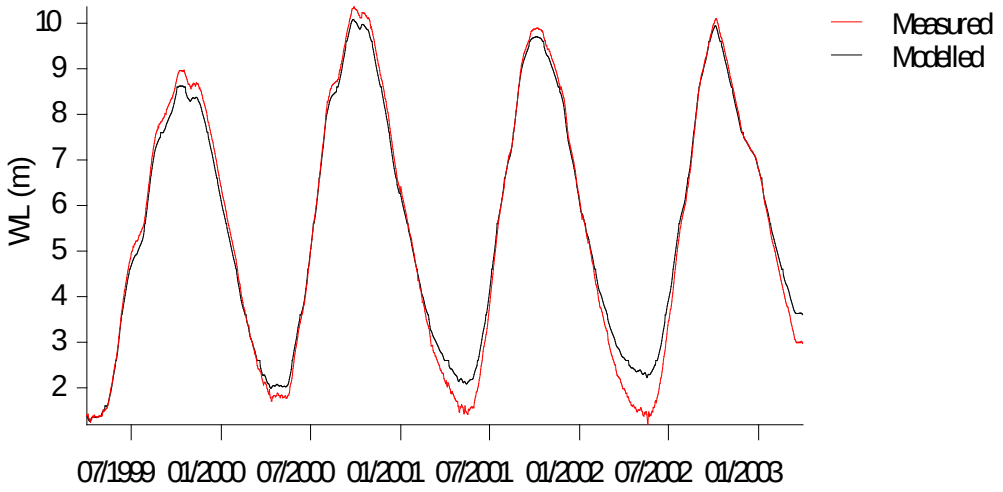

Figure 156. Computed and measured water levels.

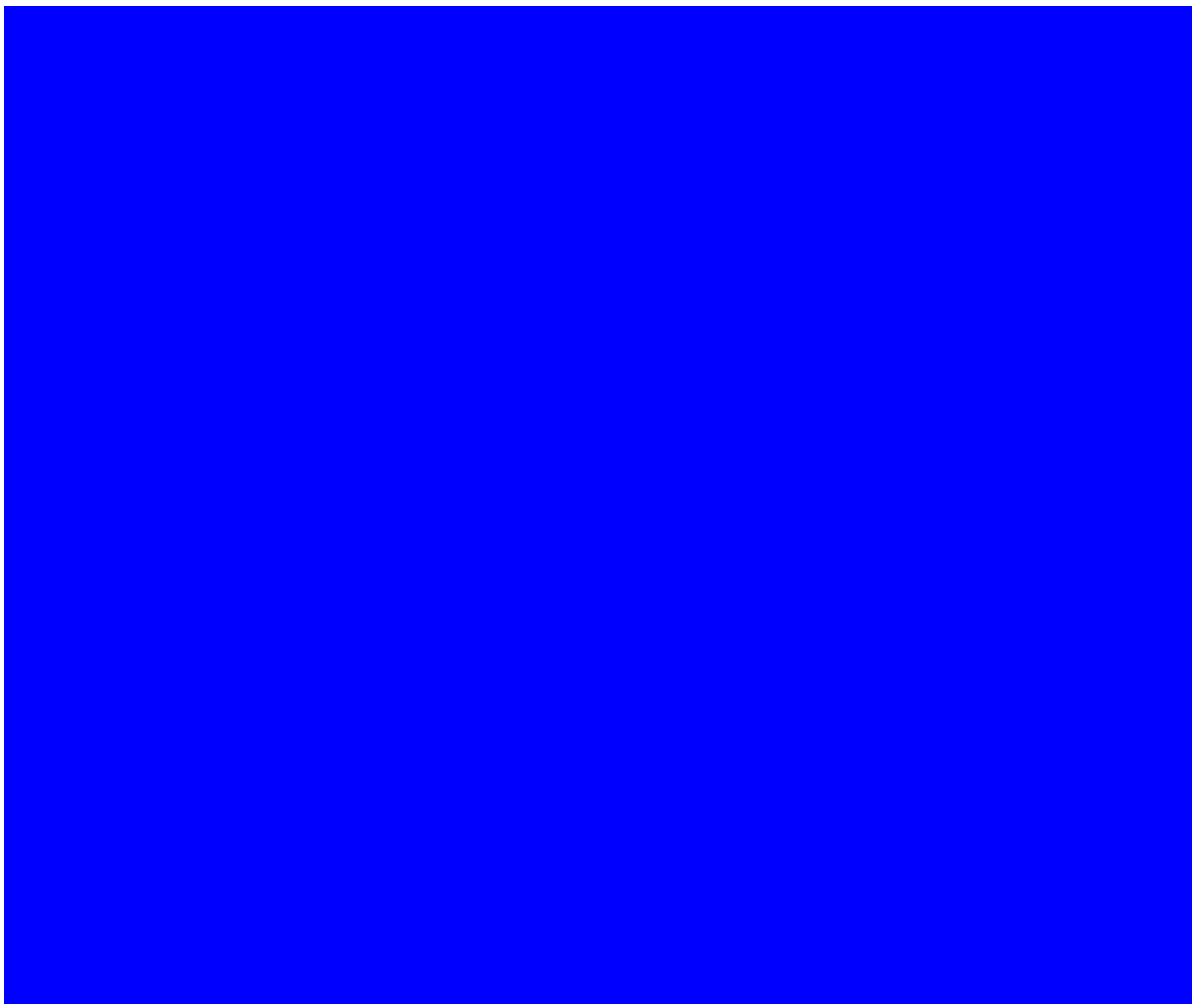

Figure 157. Measurement point locations, KGL1, KGL2 and PNK3 used in analysis.

4.9.1. Sediment

The sediment settling speed was set to 20 cm/d and sedimentation to 5 cm/d, and bottom load to 0.001. Preliminary sediment computation results are shown in **Figure 158**. Location of points is shown in **Figure 157**.

The results show some similarities with measurement data, high concentration during low water are partly replicated by the resuspension. However the behavior of the eastern part of the lake does not correlate well with the measurement data.

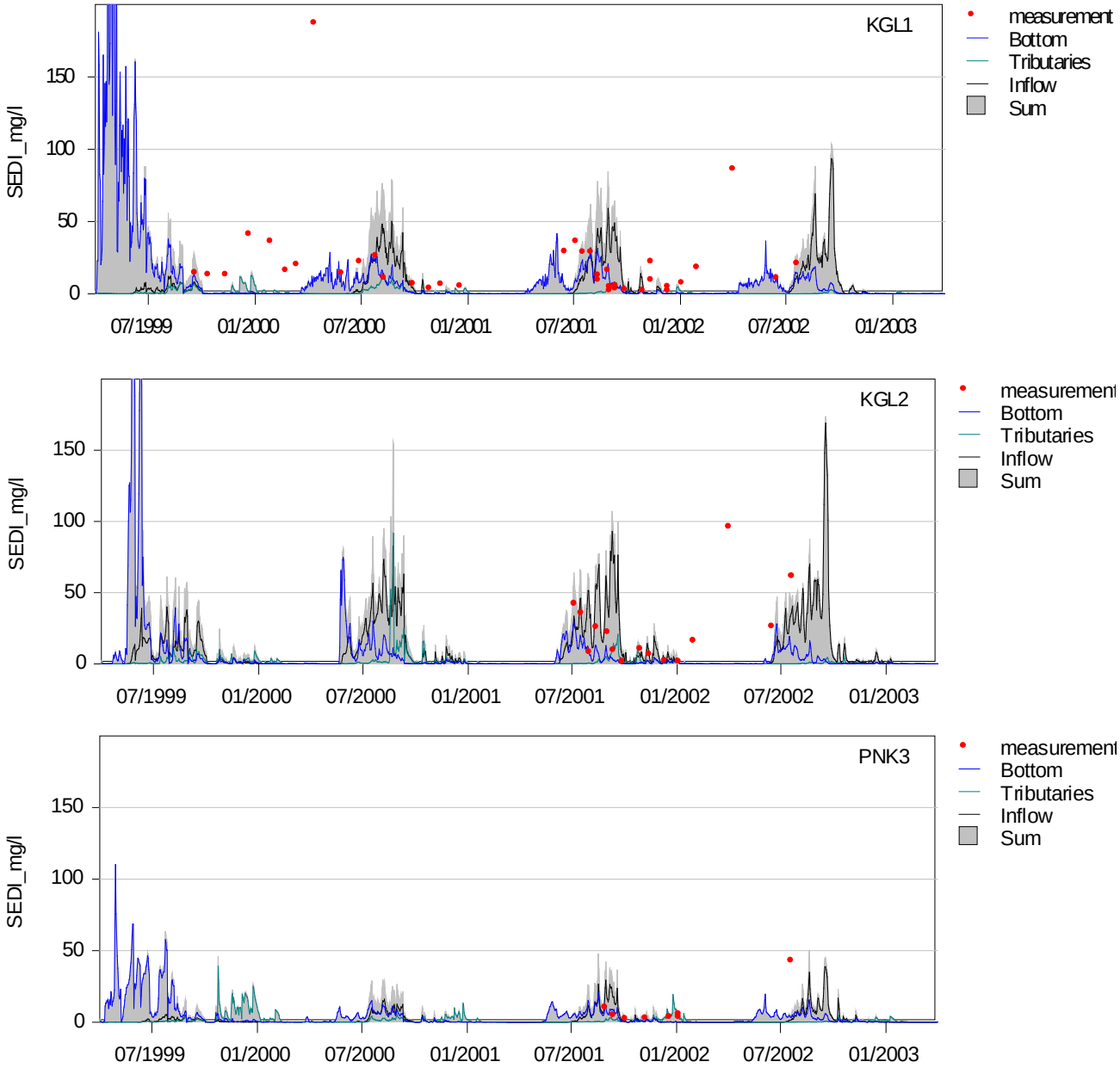

Figure 158. Preliminary TSS concentrations and contribution of different load factors at three measurement points, KGL1, KGL2 and PNK3 (). Grey area is the sum of bottom + tributaries + Tonle Sap River inflow contributed sediments.

4.9.2. Total phosphorus

Settling and sedimentation speed were set to 5 cm/d and 1.25 cm/d correspondingly. Resuspension load was 0.0025. Preliminary PTOT results are shown in **Figure 159**.

Overall the measurement data shows quick variations of PTOT, which are not clearly replicated in the model. The PTOT values are generally too large, which may be due to removal of soluble fraction by biological activity or too low PTOT settling rate. The large fraction of PO4 points to the first explanation.

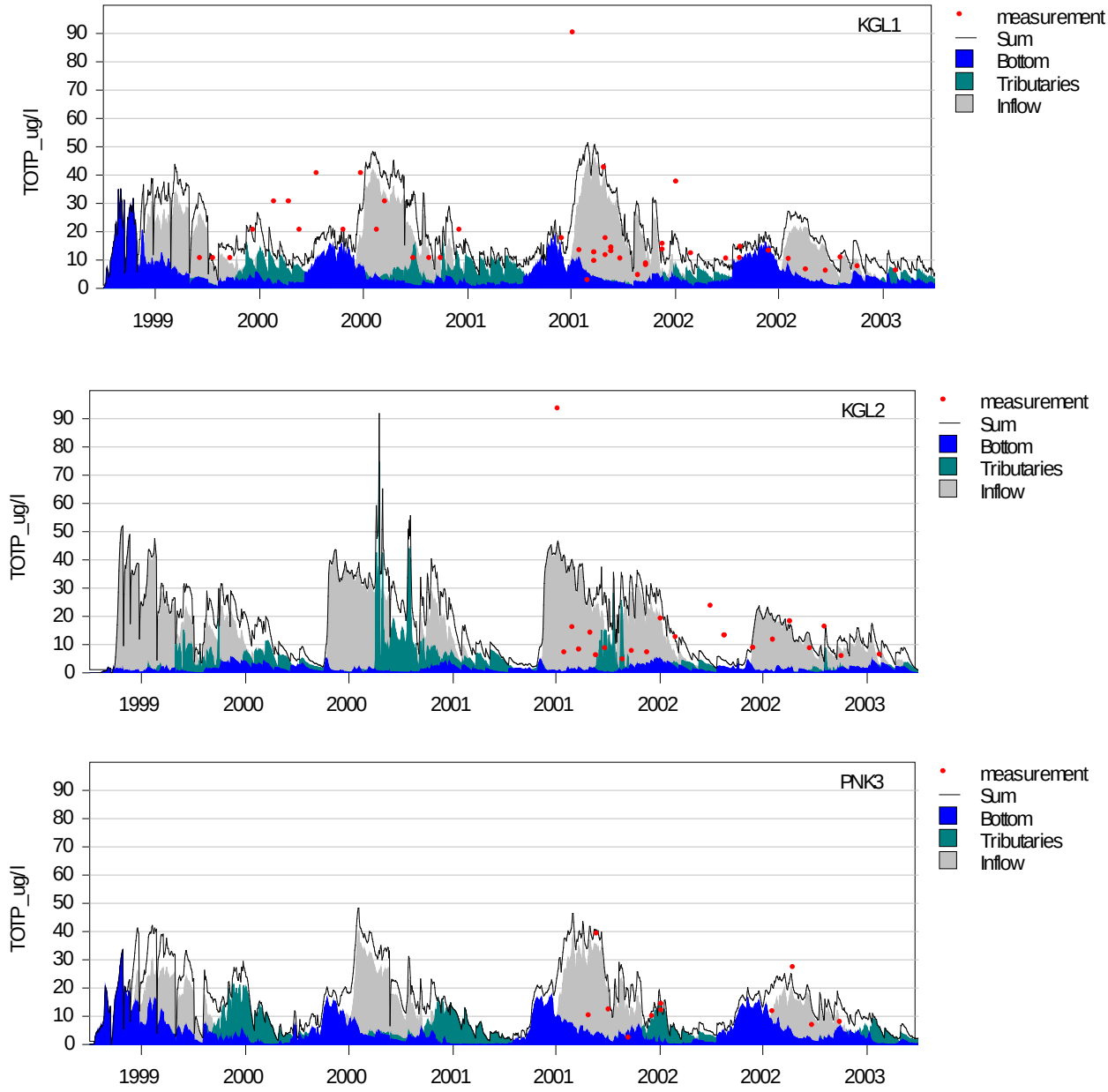

Figure 159. Preliminary PTOT concentrations and contribution of different load factors at three measurement points, KGL1, KGL2 and PNK3. Black line is the sum of bottom + tributaries + Tonle Sap River inflow contributed phosphorus.

4.10. Conclusion and further work

The EIA water quality model has been set up for the Tonle Sap Lake, and it works at demonstration level with given input data. The presented work creates a base model that can be improved and extended to include further factors affecting the water quality in the lake, such as biological activity and atmospheric loads. The model clearly requires refinement of necessary input data and further calibration, as the fit between model results and available measurement data is not good. Additionally the computation period should be extended.

5. Annex 5 - Delta Impact Modelling

The rationale behind the Delta Impact Modelling is:

- Use mapping instead of fully physical modelling to enable Cambodian Floodplains and Vietnam Delta modelling with limited resources;
- Use of the existing models (ISIS) as a basis for the mapping; when model results are not available also monitoring results can be used;
- Next phase construct 1D/2D/3D hydrodynamic model for the channel and river network, floodplains, Delta and the coastal areas for fully physical approach. The approach is required for flooding but also for instance for more accurate sedimentation as it depends on flood flow, not only on flood mapping information.

The methodology is working well as demonstrated by the results in this chapter. However, more ISIS data needs to be included especially in Ca Mau, along the Mekong mainstream and in areas with high salinity and flood depth gradients. This work will be re-commence once the National Modellers are again engaged in the Council Study modelling.

5.1. Impact model construction

The Delta Impact Model (DIM) methodology depends on spreading flood from Floodpoints following terrain. The function for flood mapping is not hydrodynamic, in other words there is no actual flow involved and the mapping function describes where water would eventually end up given the water level in a floodpoint. Water level data is obtained from ISIS nodes as well as for sedimentation discharge (see the algorithm in BioRA Modelling Report) and for agri- and aquaculture salinity.

The ISIS model has 5’500 grid nodes in the Lower Mekong Basin application and it would take too much storage to store hourly data for all of them. Hourly data is required especially near the coast where tidal forcing is important. Because of this the user needs first to define output nodes in ISIS and run then the model for hourly outputs. The Delta Impact Model under the VMOD modelling framework includes a tool to import the resulting ISIS csv-data (see figure below) automatically to the DIM.

Output data from file D:\ISIS_LMB_BL2007\ISIS_BASELINE\ISIS_LMB.ZZN
Selected output data from time (hr): 113958
to time (hr): 122724

Stage

Time (hr)	HAM3350(	VCT06000	CMB6970(	LT727001	TRA00000	KimQui-1[	108	RRE24000
19980101 0600	1.182	1.03	0.958	0.175	1.016	0.169	0.982	0.388
19980101 0700	1.205	1.066	0.971	0.184	1.073	0.171	1	0.4
19980101 0800	1.297	1.119	1.103	0.204	1.127	0.308	1.078	0.413
19980101 0900	1.394	1.188	1.238	0.246	1.185	0.437	1.195	0.435
19980101 1000	1.329	1.216	1.343	0.304	1.237	0.568	1.27	0.469
19980101 1100	1.034	1.132	1.205	0.36	1.245	0.64	1.198	0.508
19980101 1200	0.599	0.904	0.941	0.412	1.167	0.65	0.947	0.533
19980101 1300	0.117	0.593	0.605	0.452	1.012	0.523	0.596	0.525
19980101 1400	-0.349	0.27	0.292	0.465	0.815	0.362	0.241	0.452
19980101 1500	-0.763	-0.0437	0.0557	0.442	0.596	0.23	-0.0823	0.319
19980101 1600	-1.109	-0.306	-0.122	0.382	0.378	0.1	-0.376	0.183
19980101 1700	-1.375	-0.52	-0.283	0.305	0.165	-0.00786	-0.613	0.059

Figure 160. ISIS hourly water level output for selected nodes.

DIM has been implemented with two grids: 1 km resolution for rice and 500 m for the other parameters. The 1 km grid has 65'000 basic grid cells and 14'000 additional ones for near-coast agricultural areas. The 500 m resolution grid has 260'000 grid cells. The reason why the 1 km resolution is applied for rice instead the 500 m one is computation time: whereas the 1 km grid computation takes 1.5 minutes the 500 m agricultural simulation takes 10 h! The reason for such large difference must be in the memory handling – the smaller grid size enables faster memory access, probably fast cache. Finding out the exact cause and improving large grid computation efficiency will be done in the future.

The DIM model floodpoints based on selected ISIS nodes are shown in **Figure 161** - **Figure 163**. **Figure 161** shows the flooding and sedimentation simulation floodpoints and **Figure 163** salinity, rice and shrimp simulation floodpoints. The reason why there are two sets of floodpoints is because flooding is limited in the Delta by dykes and gates whereas the salinity intrusion follows the river and channel network from the sea. A barrier has been built in the model to limit flooding (**Figure 162**). It follows ISIS flood mapping practice.

As noted above the floodpoint coverage needs to be improved. Some attempt has been done to increase floodpoints through interpolating between nodes (floodpoints with "av" in their name) but these should be replaced in the future with ISIS node data.

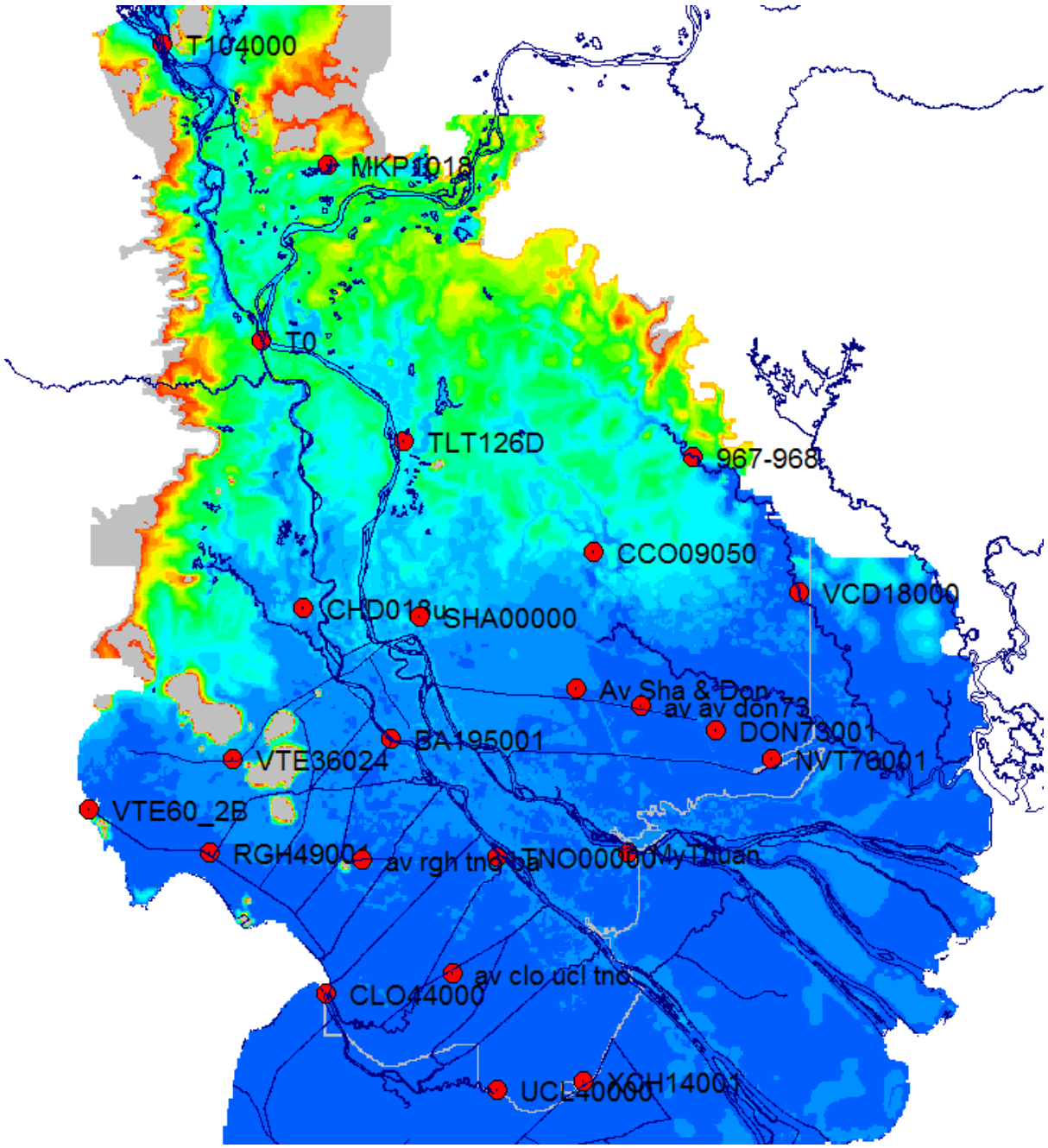

Figure 161. Model floodpoints for flood and sedimentation mapping. The floodpoint names are based on ISIS names.

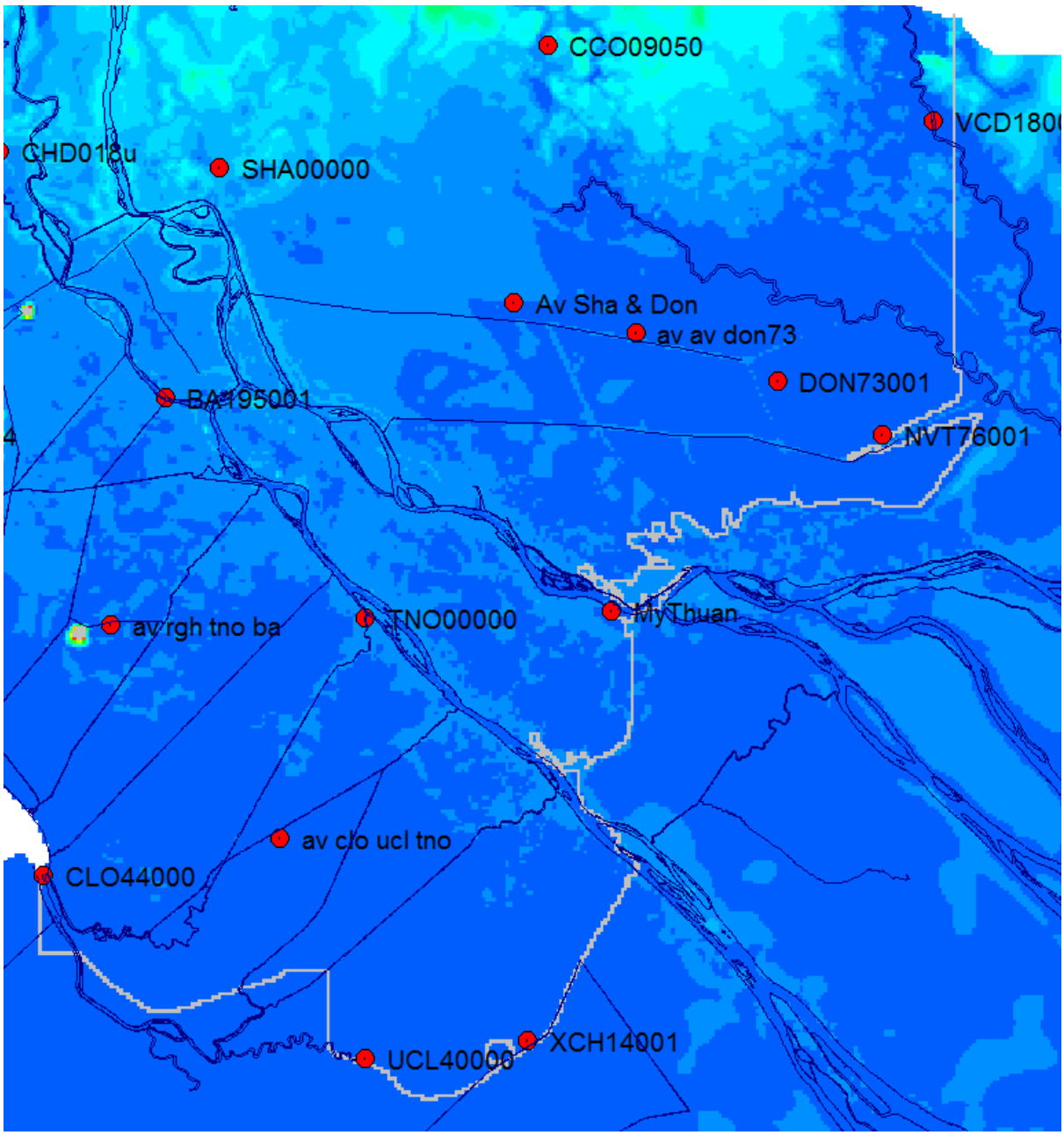

Figure 162. Flooding barrier (grey line) to limit flood extent in the model.

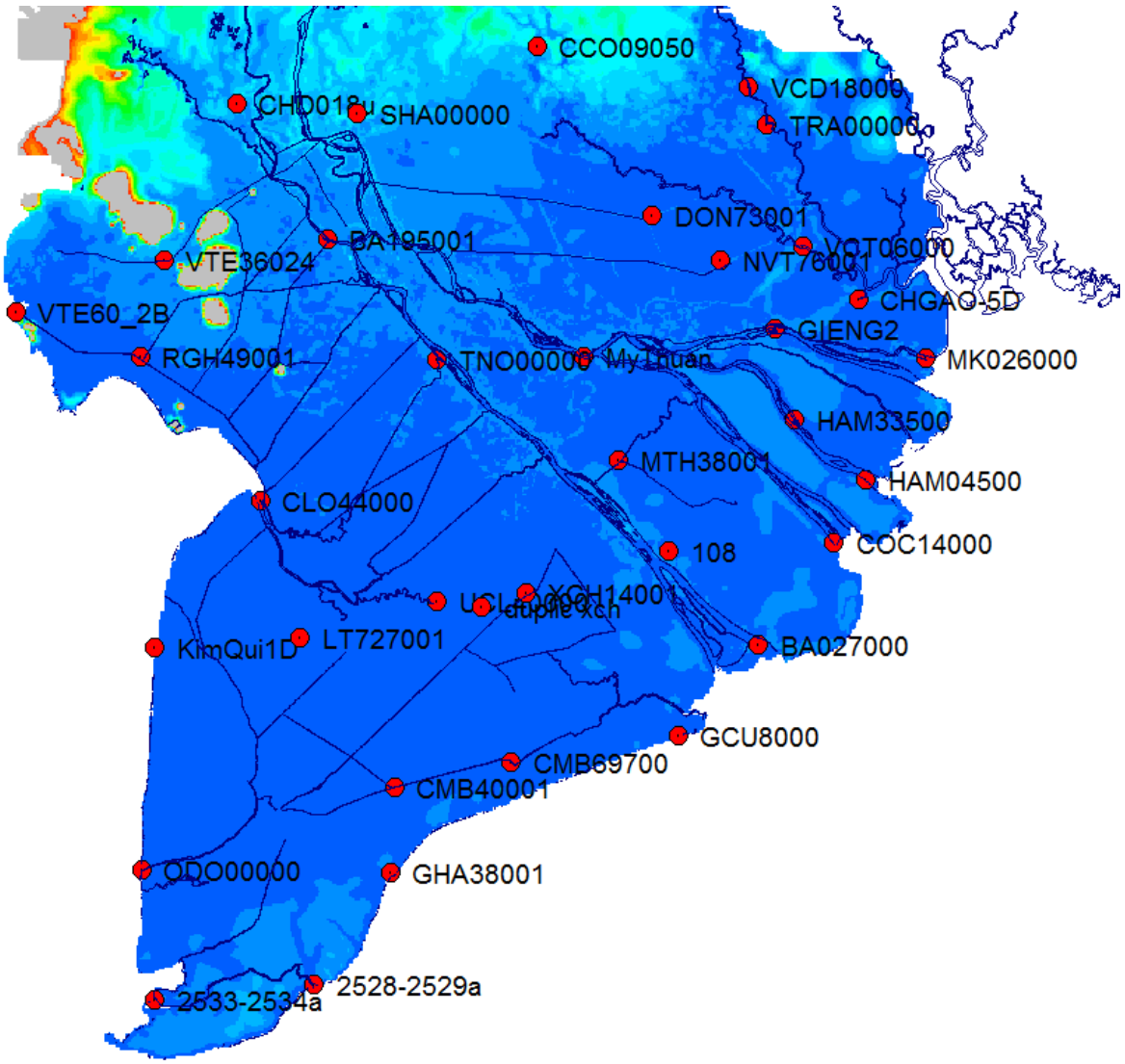

Figure 163. Model floodpoints for salinity, rice and shrimp mapping. The floodpoint names are based on ISIS names.

Modelling Team has analysed available sediment and water quality information from different stations with the USGS LOADEST tool. Summary water and sediment balances for 1985 – 2008 and 2009 – 2013 are presented in **Figure 164**. These could be used for the model inputs but direct use of the monitoring results show that LOADEST results are not representing material balances properly (**Figure 164** - **Figure 168**).

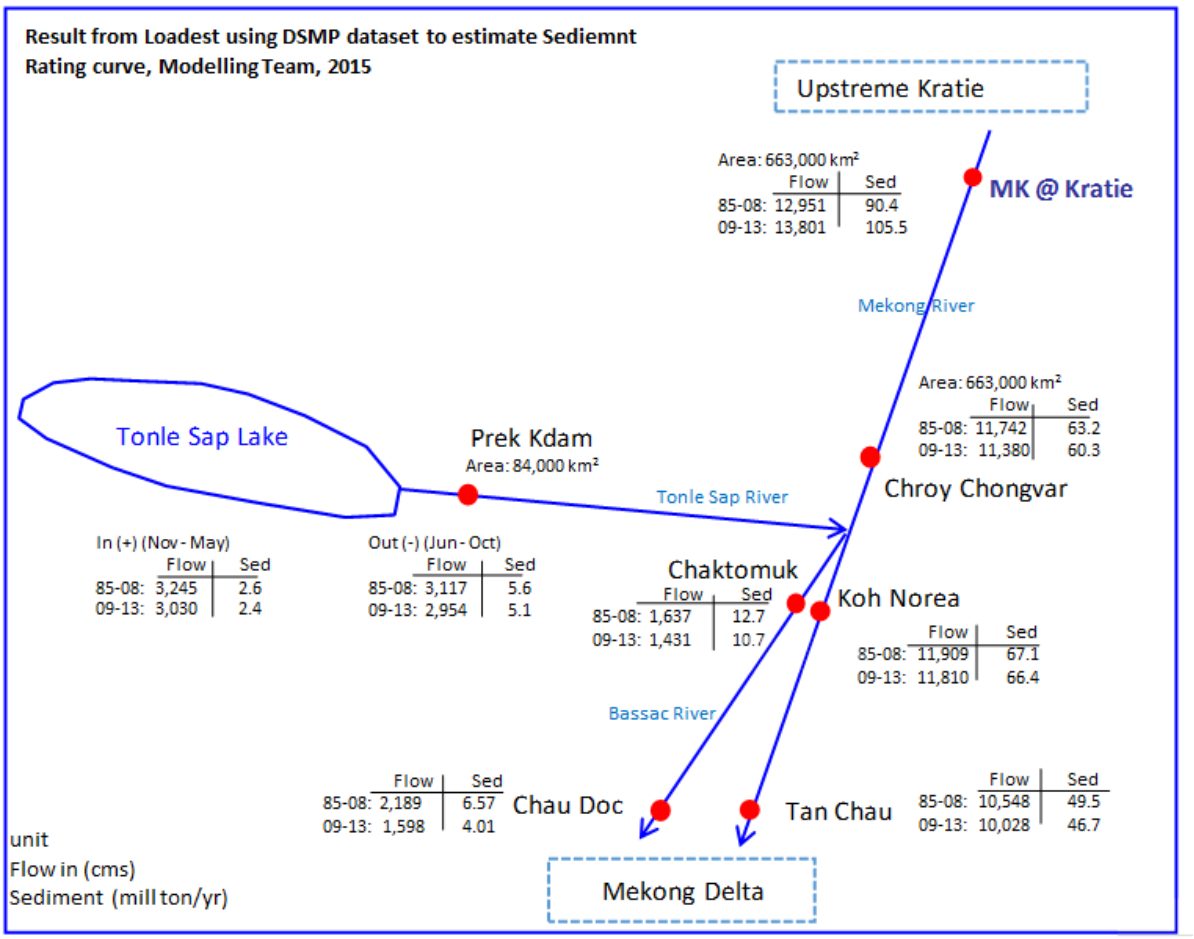

Figure 164. Summary water and sediment balances for 1985 – 2008 and 2009 – 2013 for the Delta.

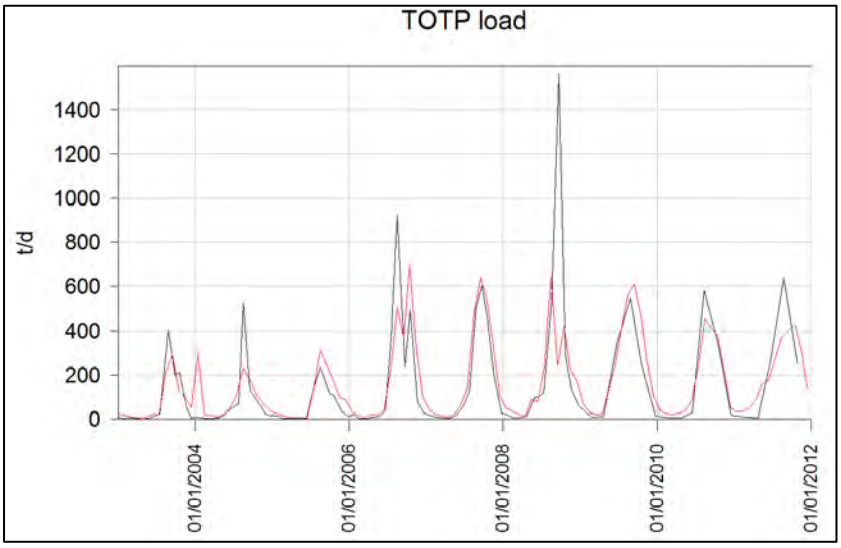

Figure 165. Chroy Changvar (black) and combined Chau Doc + Neak Luong loads computed from observed concentrations and ISIS flows. Other than 3 – 4 peaks the masses are in balance.

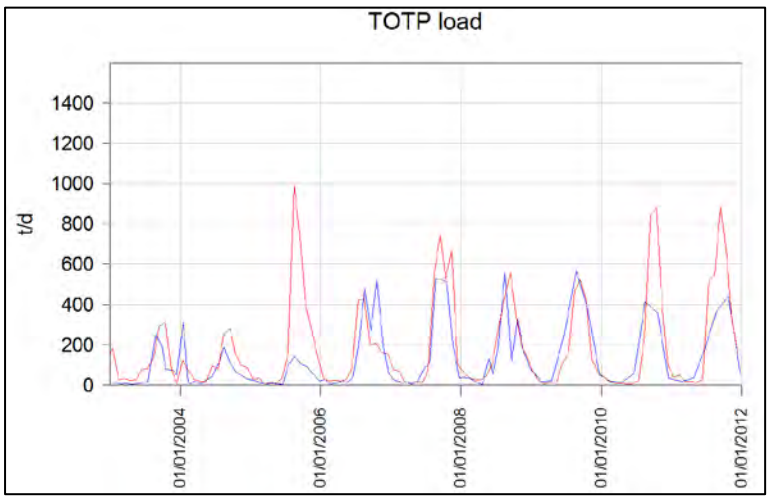

Figure 166. Neak Luong (blue) and Tan Chau (red) loads computed from observed concentrations and ISIS flows. Higher values in Tan Chau occur in August – October and may indicate impact of the overland flow.

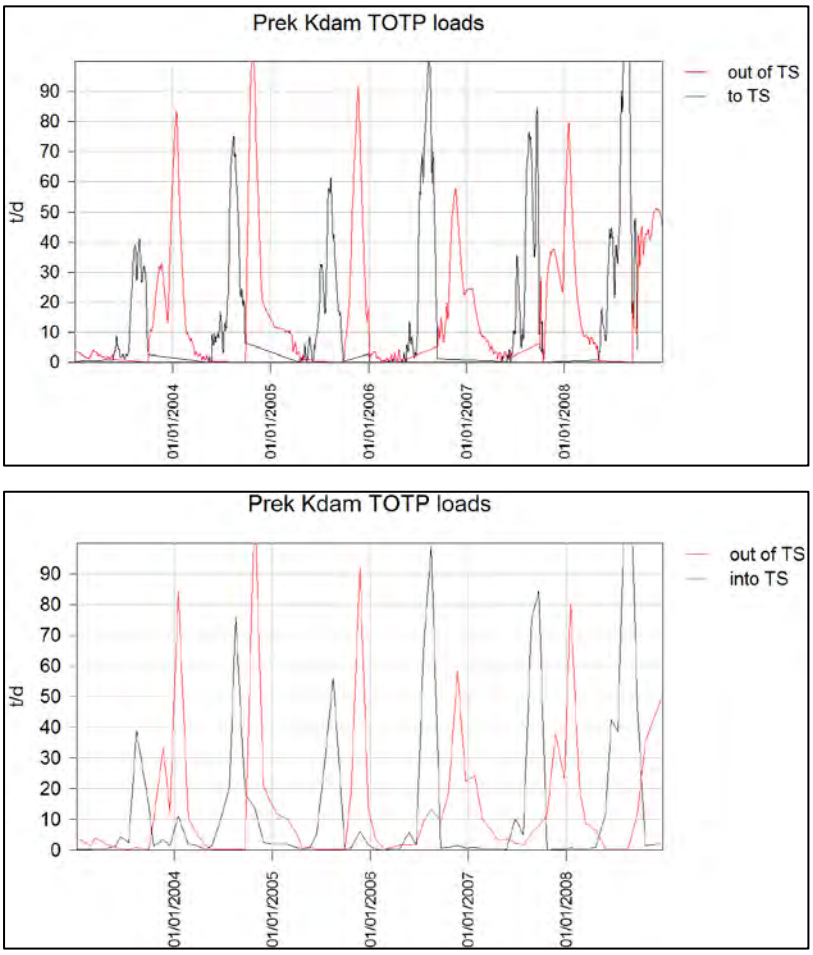

Figure 167. Prek Kdam into Tonle Sap (black) and out of Tonle Sap (red) loads computed from observed concentrations and ISIS flows. These have only minor effect on the overall Mekong mass balances. Above figure estimated loads for all days, lower figure only observation days.

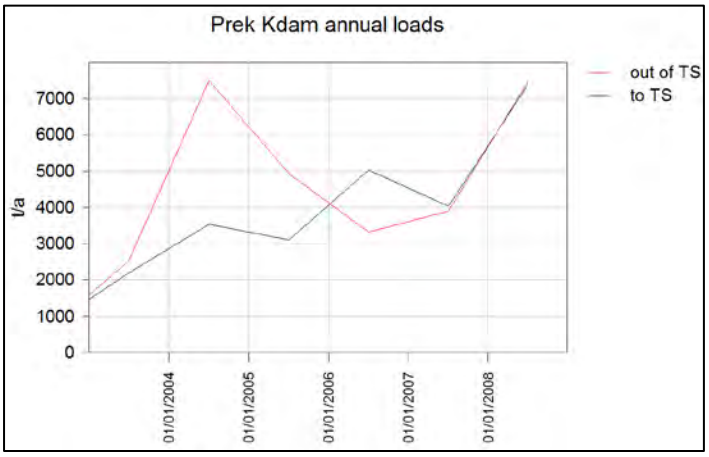

Figure 168. Estimated annual Prek Kdam TOTP loads. The loads are more or less in balance.

5.2. Mapping of sedimentation and water quality

When water level, discharge, salinity, sediment and nutrient time series are provided in the floodpoints, sedimentation and water quality maps as well as point time series are produced by the model. The water level, discharge and salinity time series are obtained in the example from ISIS nodes. The clay time series are based on the Kratie LOADEST rating curve processed by the Council Study Modelling Team. ISIS sediment and nutrient results will be added to the floodpoints when they are available. Temperature, dissolved oxygen (DO) and carbon (C) time series are currently not used in the model although it is possible to define time series for them.

Each constituent (salinity, sediments and nutrients) have three parameters: Invw (inverse weighting coefficient), Set (settling coefficient m/d) and Dec (decay coefficient 1/d) but decay is not implemented for the constituents used currently. The Invw coefficient is intended to approximate decrease of concentrations further away from the floodpoints:

$$\frac{1}{e^{a\Delta xv}}$$

- a = inverse coefficient (Invw) [0.001 m2 d]
- Δx = distance from a floodpoint [km]
- v = settling coefficient [m/d].

The approximation is implemented because the mapping function just interpolates concentrations between the floodpoints without taking into account actual transport and sedimentation processes.

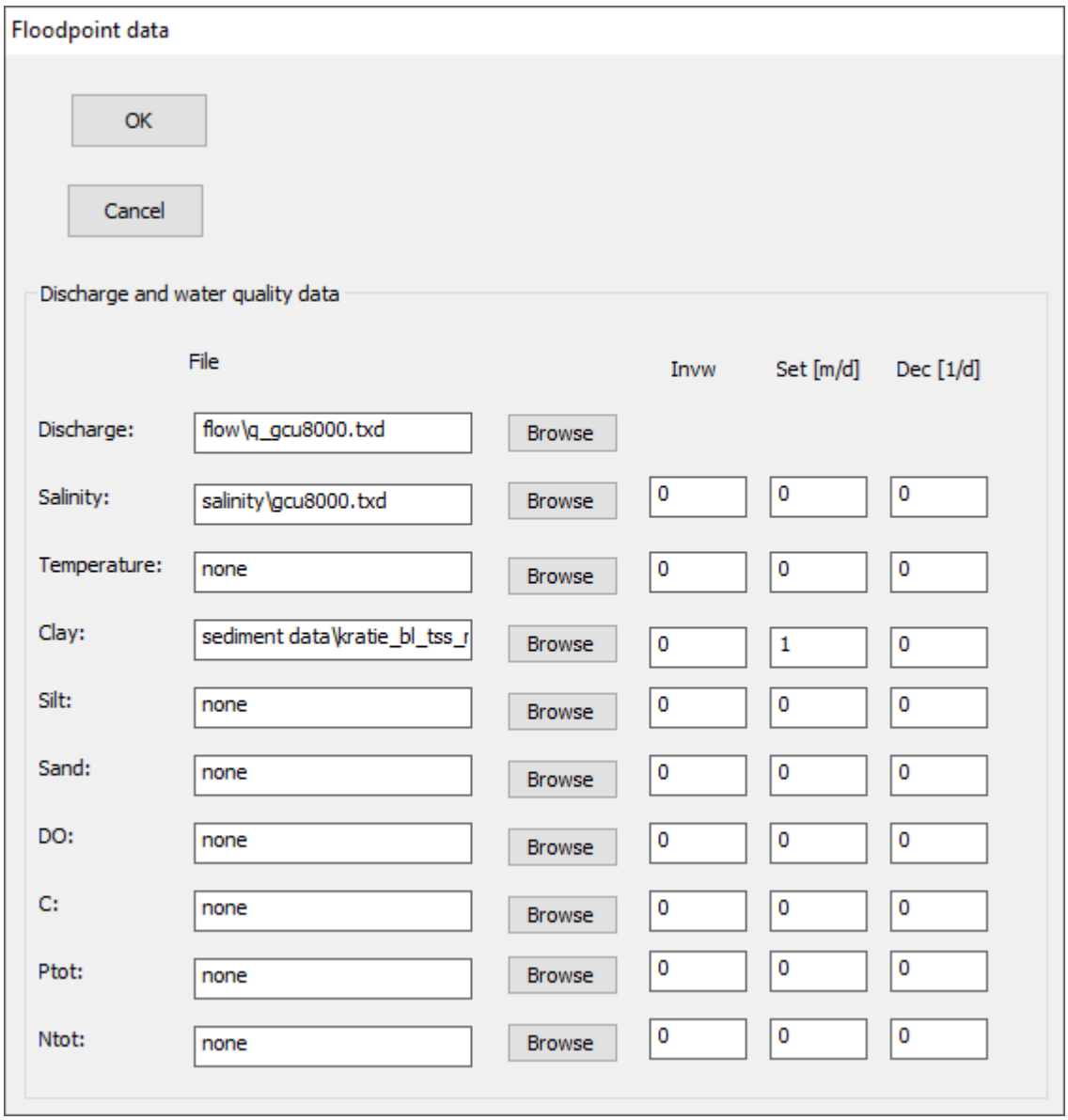

Figure 169. Time series definitions for sedimentation and water quality mapping.

Sedimentation on the floodplains is estimated first based on the interpolated concentration fields and then scaled based on the total bulk sedimentation estimate presented in the previous chapter.

It is possible to account for upstream sedimentation in floodpoints through indexing the floodpoints. If upstream floodpoint index is given the upstream sedimentation around the upstream point affects the downstream point concentration and load.

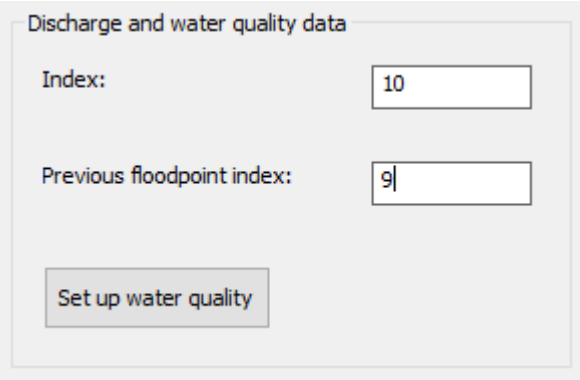

Figure 170. Floodpoint indexing for taking into account upstream sedimentation on concentrations and loads.

In addition to the bulk clay, silt and sand sedimentation time series user has, provided the (ISIS) time series have been provided for the mapping, possibility to produce time series of concentrations and sedimentation. User can also draw corresponding maps (**Figure 171**).

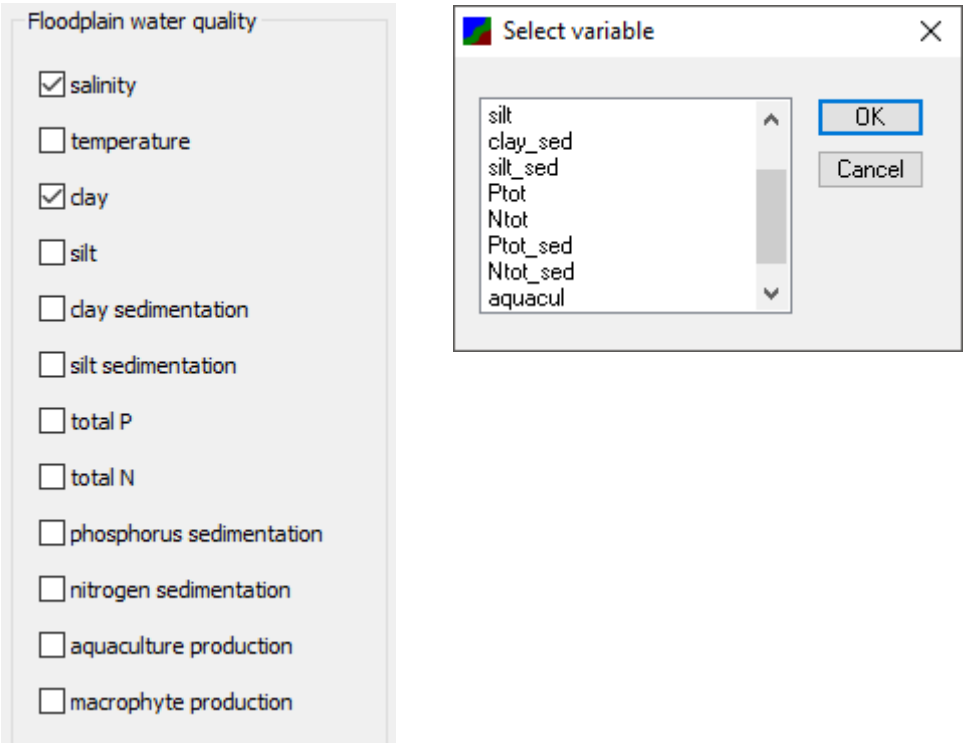

Figure 171. Selection of water quality concentration and sedimentation time series (left) and corresponding maps (right). Also aquaculture growth index is available.

5.3. Rice and aquaculture impact mapping

The current version of the model computes salinity impacts on aquaculture (shrimp) and rice productivity. It would be important to take into account also sedimentation impacts on soil fertility and

agricultural productivity. This requires the next model version that is based on flow as actual sedimentation of paddies and floodplains depends on both transport and concentration.

ISIS computes salinity in units g/l. This can be directly used for aquaculture growth index calculation but the FAO AquaCrop growth function requires salinity given as conductivity. The practical salinity (PSU, Practical Salinity Unit) is determined from empirical relationships between temperature and the conductivity ratio of a sample (Fofonoff et at. 1983, UNESCO). Using the UNESCO equation and ignoring impact of temperature gives for salinity *S* [PSU] using conductivity *C* [dS/m]:

$$S = 0.008 - 0.1692 * \sqrt{R} + 25.3851\,R + 14.0941 * R^{1.5} - 7.0261 * R^2 + 2.7081 * R^{2.5}$$

$$R = \frac{C}{53.02}$$

The equation is reversed with the Newton-Raphson method for conductivity.

In the AquaCrop model impact of soil salinity on crop growth is described with a salinity (soil) stress function:

$$K_{Salt} = 1 - \frac{e^{S_{rel} f_{shape}} - 1}{e^{f_{shape}} - 1}$$

$$S_{rel} = (C - ECe_n)/(ECe_x - ECe_n)$$

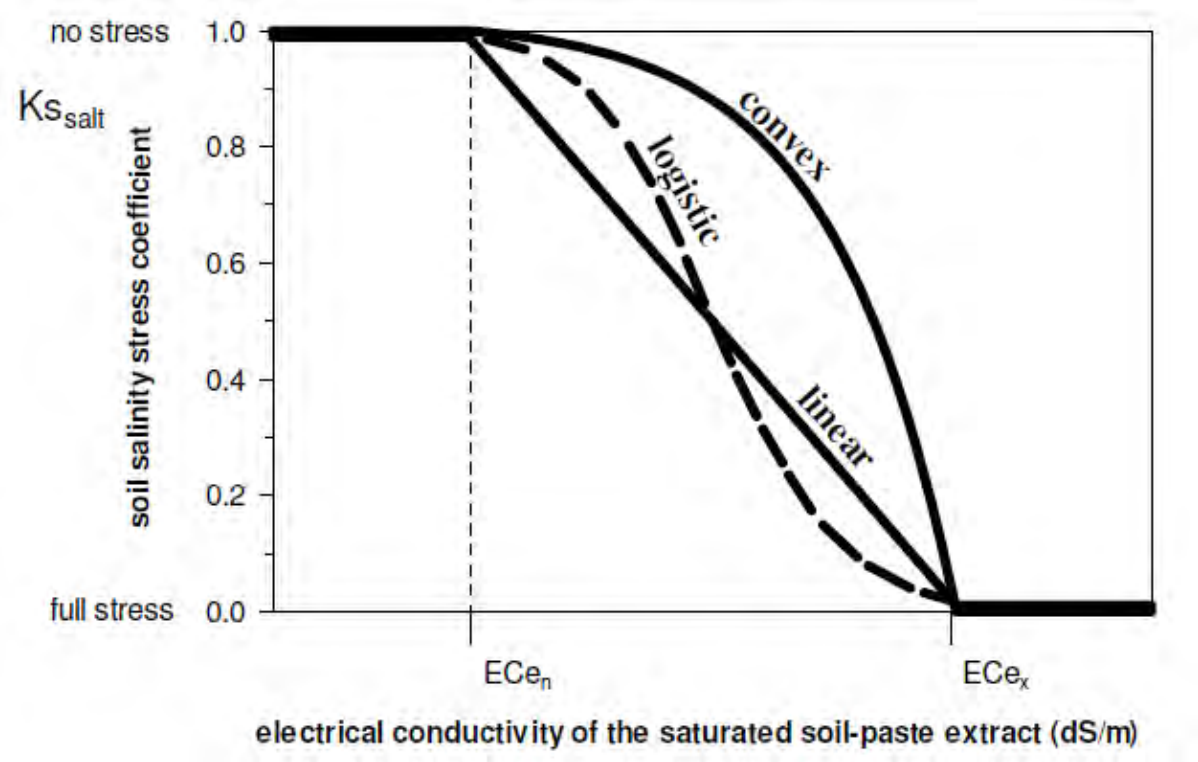

Figure 172. FAO AquaCrop salinity stress function (Raes et al. 2012). Original FAO stress function shape function is linear. Calibrated shapes are convex.

Mondal et al. (2015) have calibrated the salinity stress function in Bangladesh. The original crop yield data has been used to calibrate the Delta Impact Model with weather data corresponding to the Mekong Delta climate conditions. The original FAO and calibrated parameters are:

Paremeter	FAO	Mondal et al.	Delta Impact Model
ECe_n [dS/m]	3	2	0.5
ECe_x [dS/m]	11	10	10
f_{shape}	0	2.4	1.4

In the Mondal et al. report there seems to be inconsistency in the reported salinity treatments as 12 dS/m treatment (reported as “T4”) should give 0-yield when in the bar chart the model yield is 0.9 t/ha. Similarly 9 dS/m treatment should give very low yield as the treatment is close to maximum stress. However, in that case the reported model yield is 3.3 t/ha, that is half of the maximum yield. Because of the inconsistency 3 dS/m has been subtracted from the original bar chart conductivities in the chart below comparing modelled and observed yields:

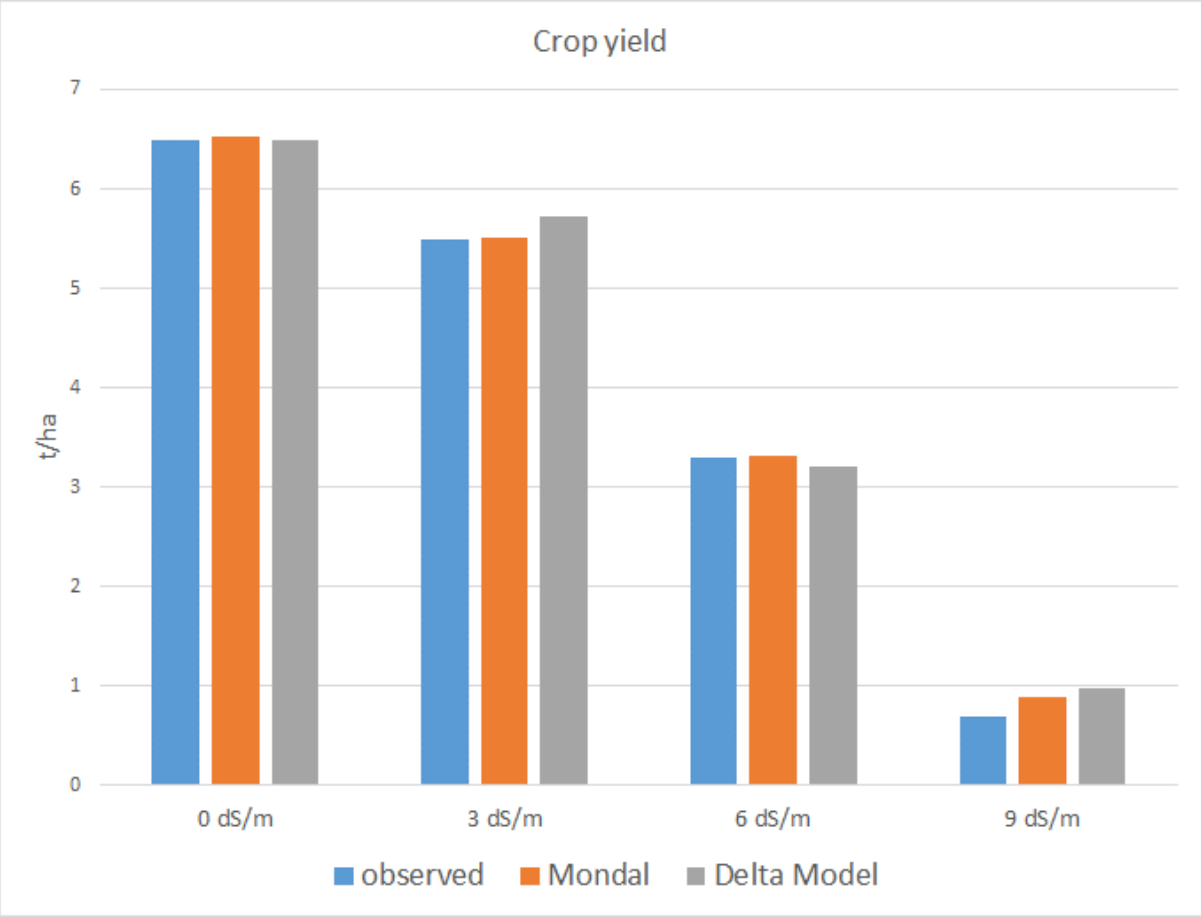

Figure 173. Comparison between observed (blue bars), Mondal AquaCrop (orange bars) and Delta Impact Model (grey bars) rice crop yields for different salinity treatments.

Penaeus vannamei (common aquaculture shrimp) tolerates a wide range of salinities, from 0.5-45 ppt, is comfortable at 7-34 ppt, but grows particularly well at low salinities of around 10-15 ppt where the environment and the blood are isosmotic (Wyban et al. 1991). The species and the salinity ranges have been taken as a basis for the Delta shrimp growth indexing. No actual aquaculture yields are computed as they depend on specific species, temperature, diseases, nutrition, added salt, flushing etc. Instead an environmental salinity dependent index is provided based on Penaeus vannamei preferences. The index is computed every day for each grid cell, summed and at the end of the computation converted to 0 to 1 scale where 0 signifies no growth and 1 maximum salinity dependent growth. The shape of the index function is shown in **Figure 174**.

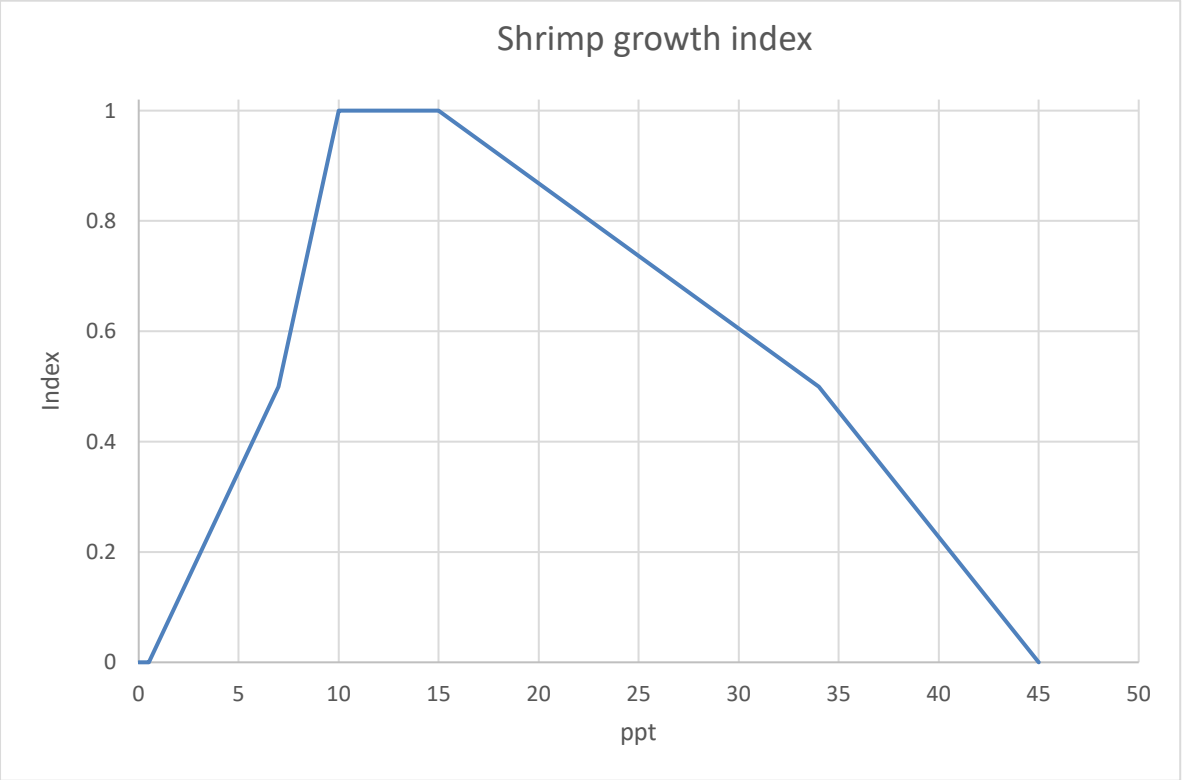

Figure 174. Shape of the *Penaeus vannamei* salinity dependent growth index.

6. Annex 6- IWRM/VMOD Model Description and Validation

In this and some subsequent chapters Xe Bang Fai watershed has been used as a validation area for the models. Also the models have been partly developed in the Xe Bang Fai. The justification for use of the Xe Bang Fai are:

- Different model area compared to the model application and calibration areas (Zone 4 and Zone 5) provides more convincing validation.
- Lower Xe Bang Fai that has been mostly used for validation is geographically more constrained than the large and complex Tonle Sap and Delta systems; this facilitates both model development and validation of specific models and processes.
- Good quality data is available for Xe Bang Fai. This applies especially for recent ortophoto based high resolution (5 m) DEM facilitating flood modelling.
- Previous national World Bank and FMMP sponsored modelling work provides good basis for model development and validation.

It needs to be emphasized that Xe Bang Fai modelling results have not been used for any other purposes than WUP-FIN consultant internal model development and validation.

6.1. Model development history

The IWRM model family has been developed by the Environmental Impact Assessment Centre of Finland (EIA). EIA is an independent research company which develops and applies state of the art surface water models. EIA have developed models for watersheds, rivers, lakes, coastal areas, the ocean and the atmosphere. EIA models have been applied to 300 different locations round the world since 1974 (ref. EIA Models). The model family developed by EIA includes the following models and supporting software:

- **IWRM/VMOD:** A grid-based distributed hydrological model that can be used to compute discharge and water quality in river basins (*the focus of this modelling guide*);
- **IWRM 1D/2D/3D:** Hydrodynamic model suitable for advanced 3D and coupled 1D/2D/3D surface water modelling. Example model applications include assessments of wetland productivity, reservoir water quality and sediment flushing, power plant thermal releases, and computation of surface currents for oil spill release forecasting;
- **IWRM WQ 3D**: Specialized water quality model that uses flow data generated by the 3D hydrodynamic model. Typical applications include computation of release, transport and reactions of sediments, nutrients or other substances (e.g. eutrophication) in inland or coastal waters;
- **EIA HBV**: A lumped hydrological model. The EIA HBV model is a modified version of the original Swedish Meteorological and Hydrological Institute HBV (Hydrologiska Byråns Vattenbalansavdelning) model. The model is a “very rapid” assessment model typically used to analyse sub-basin outflow; and
- **RLGIS**: GIS software tool for watershed monitoring and management as well as handling spatial data for hydrological model grid creation.

Examples of the different modelling tools are shown in **Figure 175** and **Figure 176**. The main WUP-FIN models are included in the MRC Toolbox.

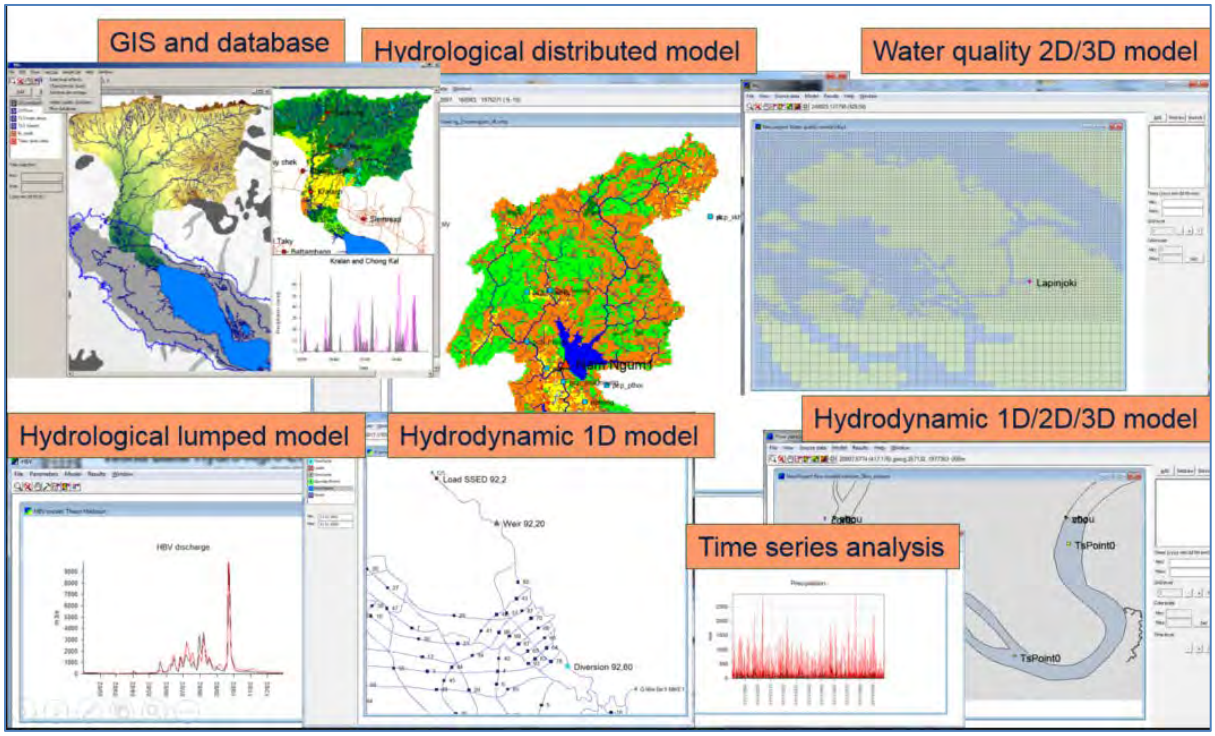

Figure 175. Main WUP-FIN modelling tools.

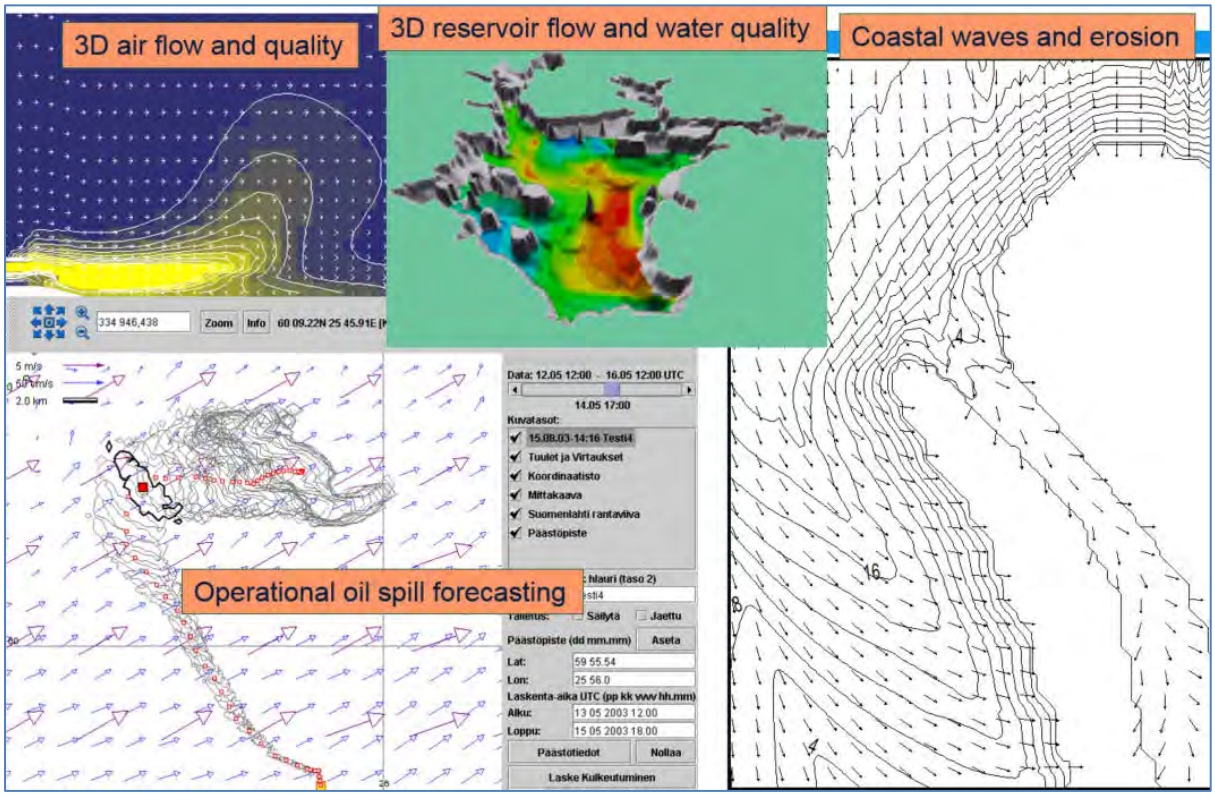

Figure 176. Additional WUP-FIN modelling tools.

User interface for the three main components of the WUP-FIN modelling system are shown in **Figure 177**, **Figure 178** and **Figure 179**. They are the GIS support software and hydrodynamic and hydrological model systems.

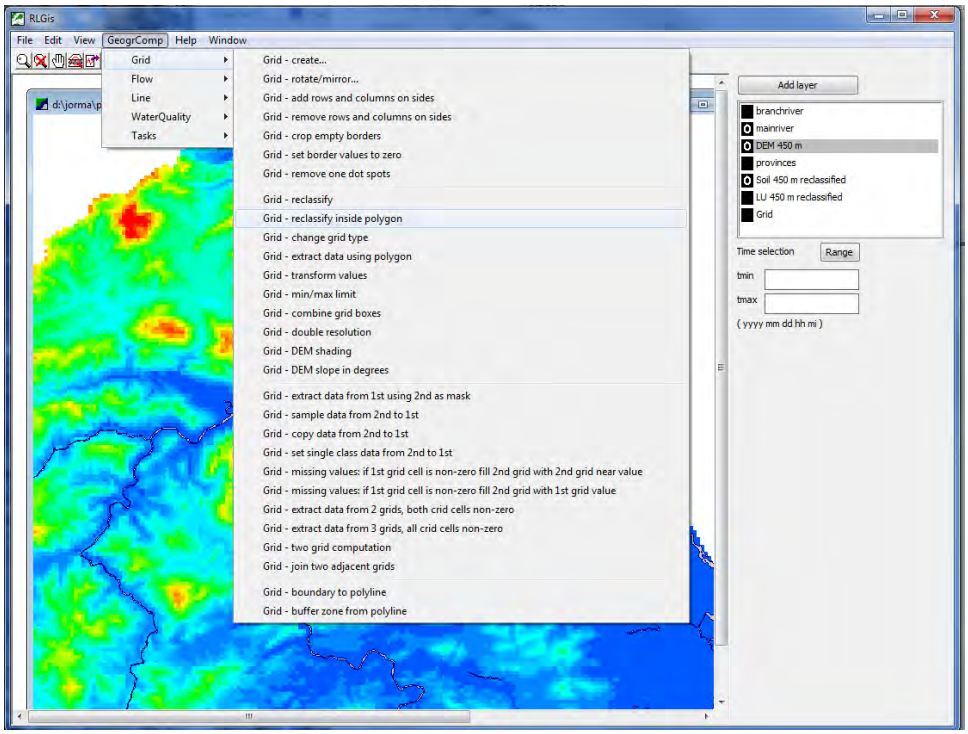

Figure 177. WUP-FIN RLGis software for GIS, modelling support, graphical monitoring database construct and watershed management support functions.

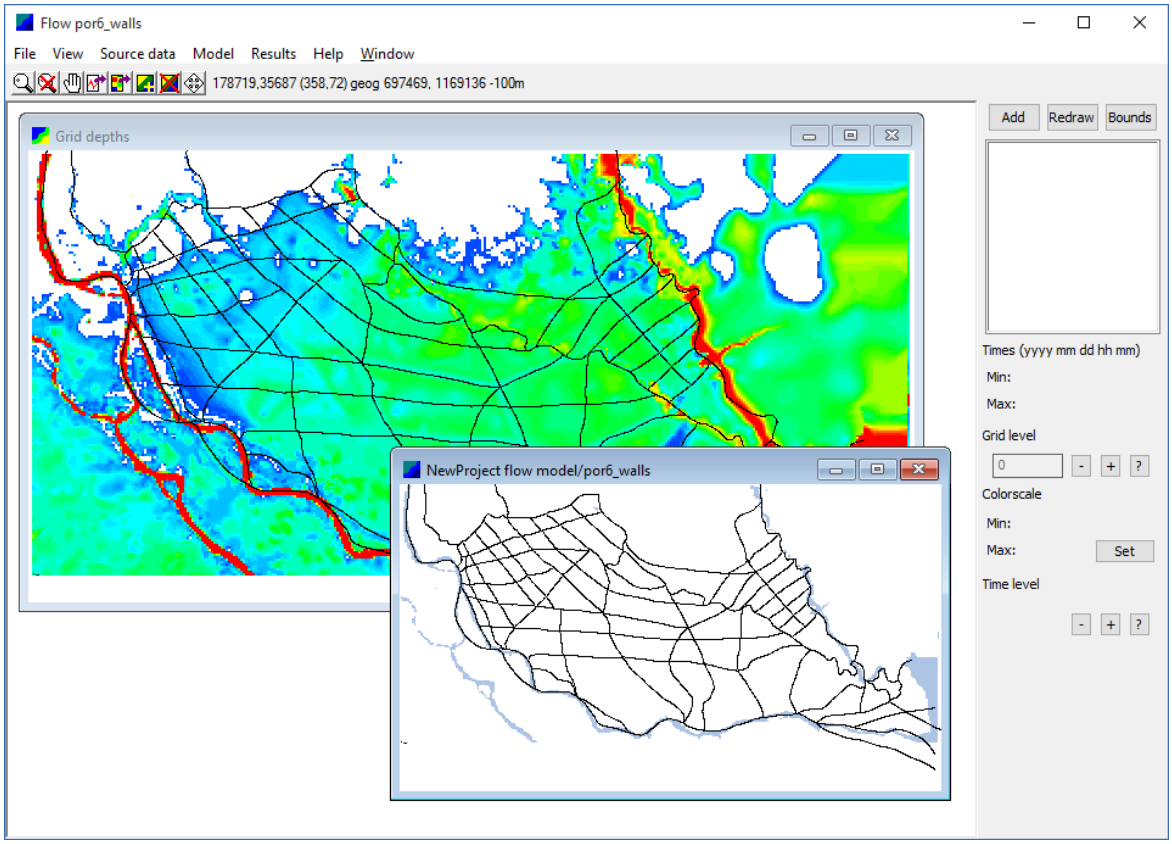

Figure 178. WUP-FIN 3D-EIA hydrodynamic model for flow, flooding, water quality, fish and erosion. Figure shows coupled 1D/3D model user interface for the Plain of Reeds.

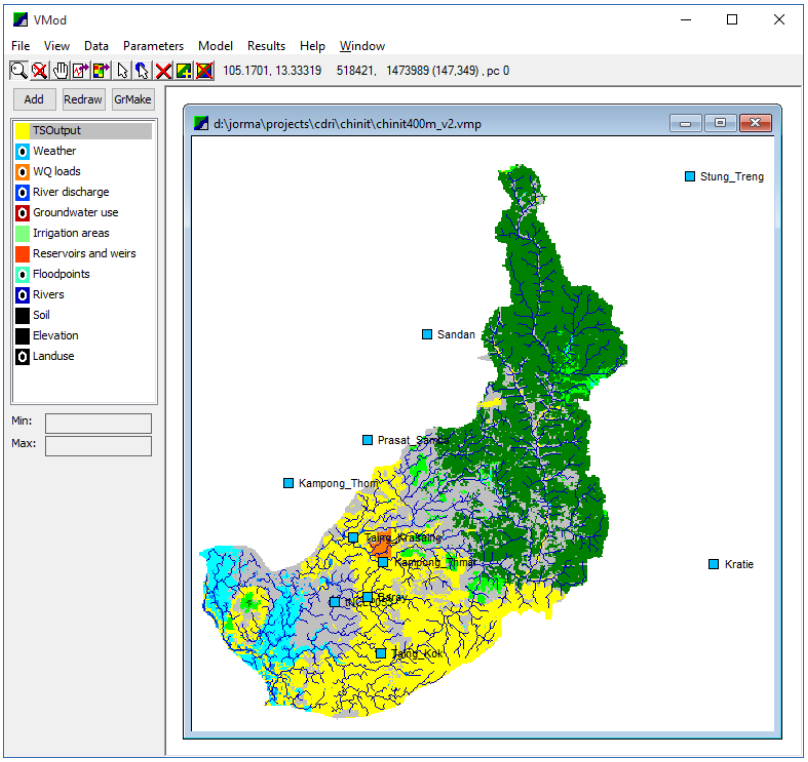

Figure 179. WUP-FIN IWRM/VMOD distributed hydrological model for water quality, erosion, agriculture, hydropower etc.

The WUP-FIN modelling system ("Hydrology and flow") together with main outputs ("Environment") and socio-economic uses ("Socio-economics") is shown schematically in **Figure 180**. The modelling system can be divided into two components:

1. IWRM/VMOD (also HAE/VMOD in World Bank context) distributed hydrological model with comprehensive water management, farming system, erosion, hydropower and climate change sub-components; simple flooding is included for crop impact modelling (see figure below).
2. Combined EIA-1D/2D/3D hydrodynamic model for flooding, erosion, water quality, primary productivity and fisheries productivity.

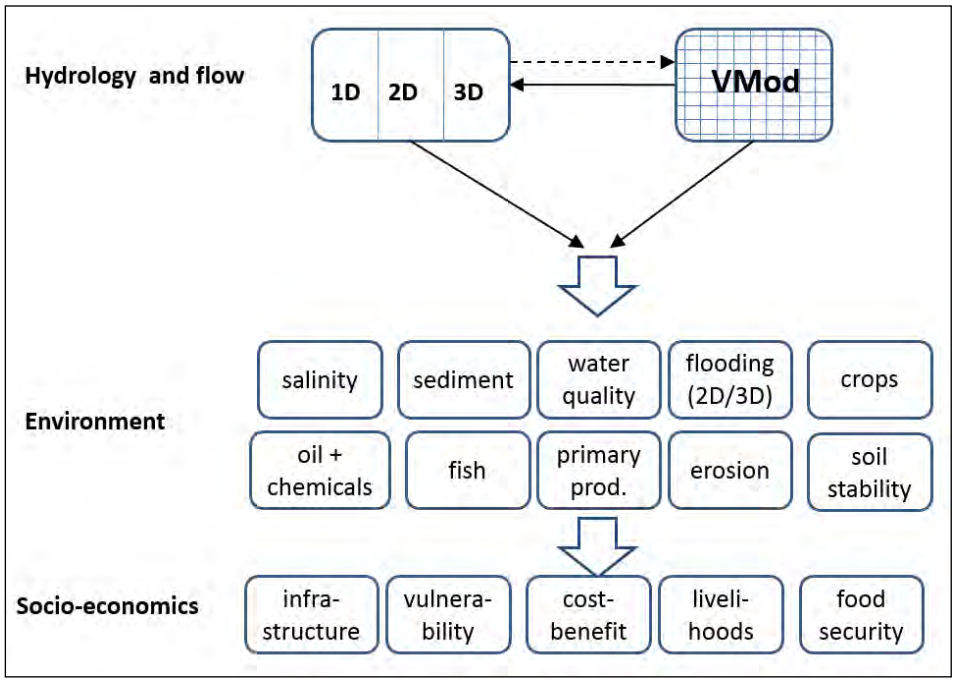

Figure 180. Schematic representation of the WUP-FIN modelling tools.

The development history of the WUP-FIN modelling tools is summarised below.

Early WUP-FIN history

1974 – 1990 2D flow and water quality modelling (Technical Research Centre of Finland -VTT)

1983 – 2015 3D flow and WQ modelling (VTT, EIA Ltd)

2000 European Union watershed management system RiverLive for authorities, became model support GIS system

Mekong WUP-FIN history

2001 – 2008 MRC modelling support (total value $5.5 million USD)

2009 – 2010 IWRM modelling at the MRC

2011 – 2012 World Bank project for climate change modelling in Lao PDR

2011 – 2015 large number of sector projects (power plants, roads, agriculture, disaster management, climate change etc.)

The models have been developed to support engineering, consultancy and impact assessment. Since 2008 the IWRM/VMOD watershed model has been made increasing available to and tested with the Mekong modelling users. The phases of the IWRM/VMOD model user interface development have been:

- 1994 – 2008 mostly in-house expert tool with some training for the MRC Member Countries
- 2008 – 2010 user interface development in connection with the MRC country model training
- 2011 – 2013 World Bank HAE project with additional user interface development
- 2014 finalisation of the user interface resulting in more user friendly and robust software.

The robustness of the software has been achieved through software based checking of input data and user actions and guidance to a user. The earlier model versions assumed expertise in model use whereas the newer version is able to check and notify about typical errors in data and user controls. In the user interface development work the Mekong Countries' role has been essential as initial and beta testing community. Other recent tools that facilitate IWRM/VMOD model use are:

- context sensitive help
- automated calibration
- parameter library for different types of watersheds
- tools for creating consistent datasets for grid generation
- established procedures and detailed instructions for reclassification, calibration and other tasks
- detailed instructions for scenario set-up.

The long and thorough development phase together with the users has brought along following benefits:

- tools adaptation to the local conditions
- model data requirements are adapted to the available data
- added functionality including 3D flooding, fisheries, crops, hydropower, advanced climate change downscaling etc.
- added functionality such as large number of GIS, data processing, analysis and visualisation tools
- user friendly and robust software.

Table 1 and 2 lists the WUP-FIN model use in the Mekong region. 32 VMOD and 3D-EIA modelling projects have been implemented in the region in between 2001 and 2015.

Table 1. Mekong basin and region VMOD applications.

Application	Client	Area	Year	Indicators and issues
Hydropower impacts, DMS	MRC/IKMP	Mekong Basin	2008 - 2010	Flow, sediment, water quality, primary production, fisheries production, sosio-economics
CC Adaptation, Mekong ARCC	USAID	Mekong Basin	2012-2013	Ecosystem and farming vulnerability for CC, crop suitability changes
Road and bridge climate proofing	Vietnam Government, ADB	Cao Lanh and Vam Cong Bridges and connecting road	2011 - 2012	Upstream impacts on flow, scouring and flooding
Gas power plant construction	Vietnam Government, ADB	Mekong	2010	Upstream impacts on flow and flooding
CC risk screening	WB	Delta	2014 - 2015	Upstream impacts on flow and sediment; Delta impacts on salinity,l agriculture, fisheries, aquaculture and coastal erosion
Research	Academic	Mekong Basin	2013 - 2014	Use of global datasets for modelling
Watershed management	GIZ	Nam Ton, Laos	2007	Sediment, flow
Watershed management	Academic	Nam Ngum, Laos	2012 - 2014	WQ, hydropower, irrigation, mining
Hydropower management	KENSAI, ADB	Nam Ngiep, Laos	2014	CC, dam safety, cascade management, economics, sedimentation
CC adaptation, Hydro-Agro-Economic Model for CC Adaptation	Lao Government, WB	Central Laos and Thailand	2011-2013	CC adaptation, farming planning on basin, provincial and village levels
Flood management	MRC	Nam Songkhram	2004 - 2007	Fisheries, flood control
Watershed management	MRC + TNMC	Nam Pong	2013 - 2015	Reservoir and irrigation management
Flood management	Lao Government, WB	Xe Bang Fai	2014 - 2015	Infrastructure design and planning, upstream watershed management
Rural planning, especially transport	Cambodia Government, NDF	Whole Cambodia + Kampong Thom + 5 Islands	2012 - 2013	CC impacts, rural road planning
CC adaptation	CDRI, CIDA	Stung Chinit, Pursat, Stung Chrey Bak	2013 - 2015	Livelihoods and village level adaptation to CC
Cascade management	WLE Mekong	3S	2010 - 2013	water, food and energy trade-offs in a cascade of multi-purpose reservoirs
Mekong region				
CC adaptation	Vietnam Government, ADB	Da Nang and Thanh Hoa	2011 - 2014	Multi-sector CC impacts
Watershed and flood management	Thailand Government, ADB	Yom	2014 - 2015	Agriculture, reservoirs, land use management, flood control
Model testing	MRC	Mae Chaem, Khuwae Noi	2004 - 2007	Hydrological model testing with extensive data

Table 2. Mekong basin 3D-EIA applications.

Application	Client	Area	Year	Indicators and issues
Reservoir management	MRC	Xayaburi (part)	2010	reservoir sedimentation and water quality
Erosion management	MRC	Vientiane	2004 - 2007	Mekong River bank erosion
Flood management	MRC	Nam Songkhram	2004 - 2007	Mekong backwater, effectiveness of planned flood protection measures
Flood control design	Laos, WB	Xe Bang Fai	2014 - 2015	Upstream impacts (land use, hydropower), climate change, drainage blocking, effectiveness of flood protection measures
Climate change and flooding	Academic	Mekong downstream Kratie	2009	Climate change impact on Lower Mekong Basin flooding
Development impacts	MRC	Tonle Sap	2001 - 2010	Sediment trapping by hydropower, primary production, fisheries production, water quality, habitat change, floodplain productivity, sosio-economic questions
Dredging feasibility	MRC/NAV	Tonle Sap	2007	Navigational channel feasibility study
River junktion management	MRC	Chaktomuk	2004-2007	Bank erosion, fish larvae drift, sand mining
Floodplain water quality and sedimentation	MRC	Plain of Reeds	2004-2007	Acidity flushing, overland flow and its sediment and nutrient input, harmful substance spreading; integrated 1D/2D/3D
River bank protection	MRC	Tan Chau	2004 - 2007	river bank erosion
Road and bridge climate proofing	Vietnam, ADB	Cao Lanh and Vam Cong Bridges and connecting road	2011 - 2012	Flooding, wave action, scouring
Gas power plant construction	Vietnam, ADB	Mekong	2010	Coolant water intake temperature, coolant recirculation to intake, coolant impacts, flooding
Salinity intrusion prevention	MRC	Tieu River Mouth	2004 - 2007	Sea level rise and dredging impacts on salinity intrusion (density flow!), harmfull substance spreading

6.2. Distributed and lumped modelling

The IWRM/VMOD modelling tool is a physically based distributed hydrological model that enables users to test the hydrological impact of water resource management development alternatives in the context of a whole basin. In this way the water management development activities planned in a basin can be tested together and separately to understand their individual and cumulative effects.

Hydrological models are simplified conceptual representations of part/s of the hydrological cycle. The IWRM/VMOD modelling tool is physically based because it represents the physical processes observed in the real world through sets of equations. This is in contrast to stochastic models which are based on statistics linking inputs to outputs. Physically based models are more appropriate for use in IWRM planning (Global Water Partnership 2000) because they give insight into the hydrological processes occurring and allow alterations to the model that can represent alternative planning scenarios.

The model is considered distributed because the entire catchment of interest is represented by a grid of evenly spaced cells, each with its own set of characteristics. This is in contrast to a lumped model which assigns the same set of characteristics to areas that are grouped together (**Figure 181**). Distributed models have transparent and detailed one-to-one correspondence to the basin characteristics (topography, river network, landuse, soil) and are therefore more appropriate for use in IWRM planning applications than lumped or semi-lumped/distributed models. Lumped models are restricted in their capacity to incorporate scenarios such as land use change or reservoir sediment management.

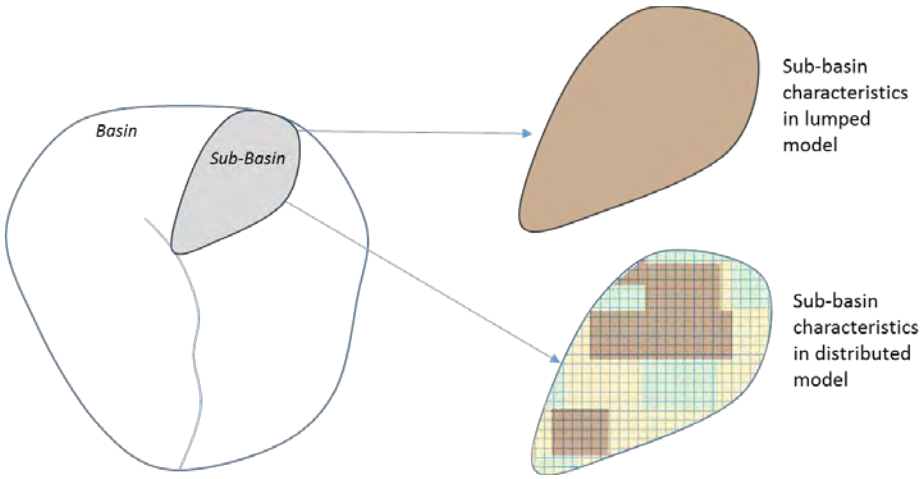

Figure 181. The IWRM/VMOD modelling tool is a distributed model which reproduces the hydrological processes more faithfully than lumped models

Advantages of distributed modelling can be summarized as:

- model has one-to-one correspondence to the basin characteristics; this improves model transparency (“WYSIWYG What-You-See-Is-What-You-Get”) as well as compatibility with GIS for both model inputs and outputs
- easy to set water management options as the model structure takes care of basic setup

- detailed basin characteristics enabling more comprehensive watershed scenario and management modelling
- physical erosion modelling
- flood modelling option (see next chapter).

There are semi-lumped or semi-distributed hydrological models in between the conceptual and fully distributed hydrological ones. The most popular globally is SWAT hydrological, sediment and water quality model. SWAT aggregates and conceptualises sub-watersheds into a few HRUs (Hydrological Response Units). For instance the MRCS Mekong SWAT application has 880 HRUs when the distributed IWRM/VMOD model has 40'000 – 1'000'000 grid cells depending on the model version.

6.3. VMOD model components

The IWRM/VMOD modelling tool consists of the distributed hydrological base model and several coupled components. Each component is flexible so that management alternatives can be incorporated into the model and assessed. The relevant model components for supporting IWRM include:

Hydrology which enables analysis of the impact of land use changes, water conservation measures and climate change;

River flow which enables analysis of water availability, hydropower operations, flooding and flood management;

Flooding which enables utilization of water level data from various sources for flood mapping and impact assessment;

Sediments and erosion which enables analysis of soil conservation measures and reservoir sediment trapping; latest model version includes also in-stream erosion and sedimentation (mass-balance approach) and special steep slope erosion for high-erosion mountainous areas;

Water quality which enables assessment of dissolved and particulate nutrients for both river channels and floodplains and impact of dam trapping;

Reservoir operations which enables analysis of the impact of construction and operation of reservoirs and other water storage infrastructure;

I**rrigation and crop yield** which enables analysis of altering irrigation and crop planting regimes.

New modules for **flooding, salinity, aquaculture and floodplain sedimentation and water quality** are discussed in the Delta Impact Assessment chapter below.

A detailed description of the model computation methods and model equations can be found in the IWRM/VMOD model manual (Koponen et al. 2010) and in the Help menu provided within the software. The following sections provide a summary of the key computation methods for each component of the model. The model manual can be referred to for more detail.

6.4. Hydrology

The hydrological base model is a physically based model. It simulates the actual physical processes behind a basin hydrological regime for each grid cell in the model and for each time step under analysis based on parameters like evapotranspiration (*petcorr)*, rainfall (*rainmult*), overland flow (*mnover)*, infiltration rate (*infkz*), leaf-area index (*lai)* and field capacity (*thf)* (**Figure 182**). As the model simulates the actual physical processes occurring it can incorporate management options such as conjunctive use, small scale storages, soil and water conservation measures, reforestation and irrigation schemes.

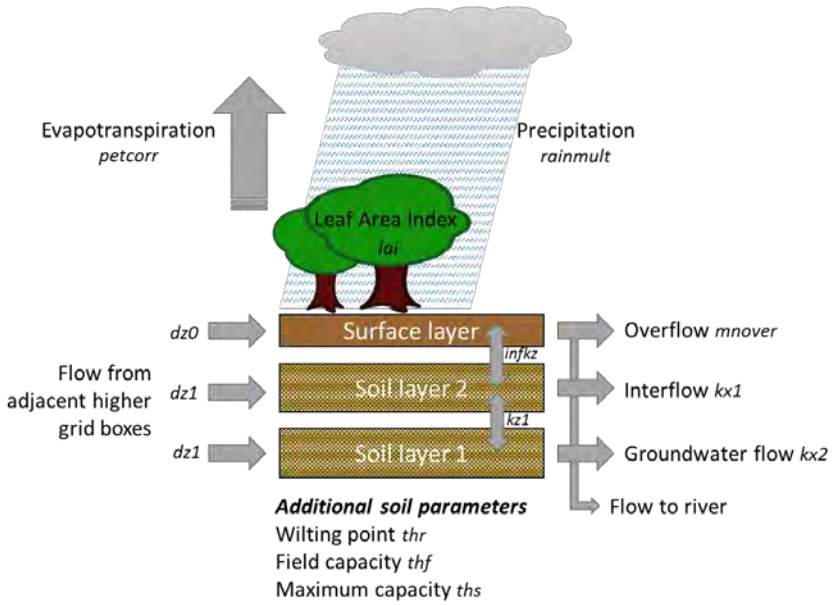

Figure 182. IWRM/VMOD model rainfall runoff key computational parameters (revised from Koponen et al, 2010).

For each time step the model first interpolates meteorological data to each grid cell using height correction where required. Then in the surface model, interception is estimated using a simple storage model and vegetation leaf area index. Infiltration is computed using the Green-Ampt model and possible overflow is accumulated into pond storage and surface runoff. Evaporation is estimated using potential evaporation, pond and interception storages, soil moisture, and vegetation data in each grid cell. For surface runoff the amount of water leaving from the grid cell to the next lower grid cell or to a river depends on ground surface flow resistance and ground slope. The water leaving from each grid cell can continue on to a river in the grid cell or to a lower grid cell determined by the flow direction net.

6.5. River flow

The flow direction net is a representation of the direction of flow from each grid cell (**Figure 183**). It is calculated from model grid elevations and digitized river network. For each grid cell in the model the flow network shows to which adjacent grid cell, or river network, water exiting the cell will flow to.

Through the river network the entire watershed is linked to a single outflow point, meaning that rainfall falling on any part of the catchment can be routed to the basin outlet.

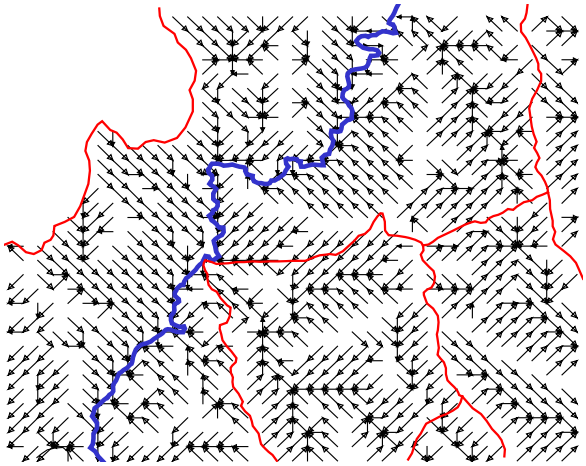

Figure 183. Example flow direction net, each black arrow represents a grid cell and the direction that water will flow out of the grid cell. The blue line represents a main river and the red lines are the watershed boundaries (Koponen et al, 2010).

The river flow computation is based on kinematic wave approximation of the St. Venant equations (flow speed depends only on slope and flow depth). When possible, actual cross section data can be used. If cross-section data is not available then it can be estimated using typical trapezoid river cross sections (**Figure 184**). The river model is solved numerically from upstream cells to downstream, so downstream surface height does not affect the upstream flows. This method enables use of a reasonably large time step and therefore shortens computation times but water level calculation in flat areas requires 1D or coupled 1D/2D/3D modelling. A more complete approximation taking into account water levels (backwater effect) is an option in the model but it requires quite short computational time step.

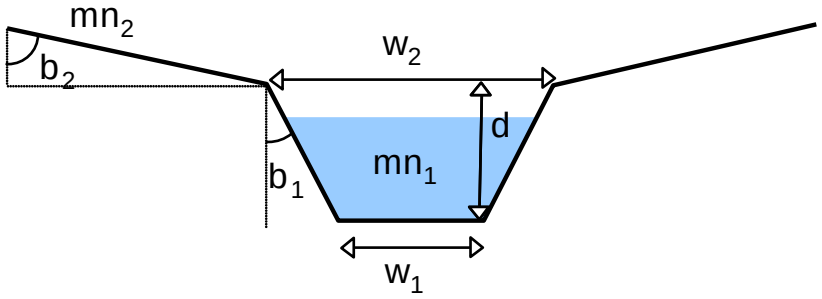

Figure 184. Trapezoidal river channel cross section approximation. *d = river bank height (m); w_1 = river bottom width (m); w_2 = river width at bank height = w_1 + 2d tan (b_1); b_1 = river bank slope (tan); b_2 = floodplain slope (tan); mn_1 = Manning's friction parameter for river channel; mn_2 = Manning's friction parameter for floodplain*

6.6. Flood simulation

Because of the IWRM/VMOD model represents the physical characteristics and processes in the watershed including river channels it is possible to use the model, with important limitations, for water level simulation. As the model includes the flood mapping software it is straightforward to use the computed water levels for flood mapping. The water level simulation works for areas with sufficient bed slope. That is flat areas should not be modelled with this technique. The model also includes back-water option for flow simulation in flat areas but it has proven to be too unstable for practical work.

Simulation of water levels requires adjustment of model river cross sections in places where water levels are required (**Figure 184**). The dimensions are obtained during the model construction phase based on discharge and statistically derived dependency on channel dimensions on flow. For the water level calibration only two main parameters need to be modified: for low flow river bed width w_1 and/ or river depth d and for flood flow the floodplain slope b_2. With the adjusted cross sections the observed water levels can be modelled even with better accuracy than flow ().

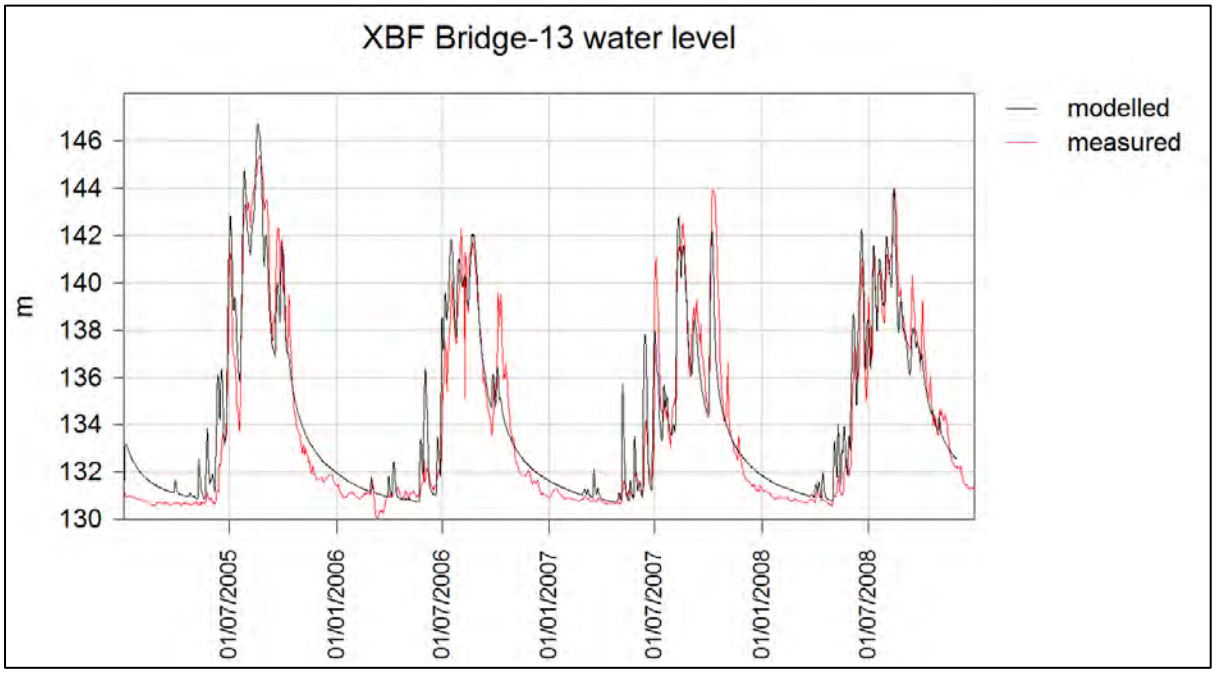

Figure 185. Comparison of simulated (black) and observed (red) water levels. Simulated water levels are computed by the distributed hydrological model.

6.7. Erosion

Watersheds can be eroded by wind, precipitation, water flow, ice and vegetation. Constant erosion component takes into account average impact of wind, ice and vegetation. Precipitation and flow initiated erosion is considered in the current IWRM/VMOD model through physical modelling because they are typically the main drivers of erosion. The processes of erosion by precipitation and water flow are as follows. Soil particles are detached when the impact of raindrops or the erosive force of flowing

water is in excess of the ability of the soil to resist erosion. Sediment particles are then transported downhill by raindrop splash and overland flow. Once in motion, deposition of suspended soil particles, either in the catchment or the river network, occurs when the weight of the particle exceeds the forces tending to move it. This condition is often expressed as the sediment load exceeding sediment transport capacity.

Morgan, Morgan and Finney (1984) provide a widely used and simple empirical erosion formulation of the rainfall and water flow drivers of watershed erosion. The formulation divides the erosion process into raindrop and surface runoff based components (**Figure 186**). To identify the erosion rate of a watershed, the formulation compares the predictions of total detachment by rain drops (F) and surface runoff (H) with the transport capacity of runoff (TC). The lower value of the two is taken as the actual erosion rate. Advantages of the Morgan, Morgan and Finney (1984) formulation include:

- Suitable for steep slope conditions (the model was developed to predict soil loss from hill slopes);
- Conceptually simple and corresponds to an intuitive understanding of erosion process;
- Addresses recent advances in understanding of erosion process;
- Physically based empirical model; and
- Requires less data than most erosion predictive models.

The IWRM/VMOD modelling tool uses a slightly revised and updated version of the Morgan, Morgan and Finney (1984) formulation which takes into account canopy height, leaf drainage and a more detailed description of soil particle detachment by water flow.

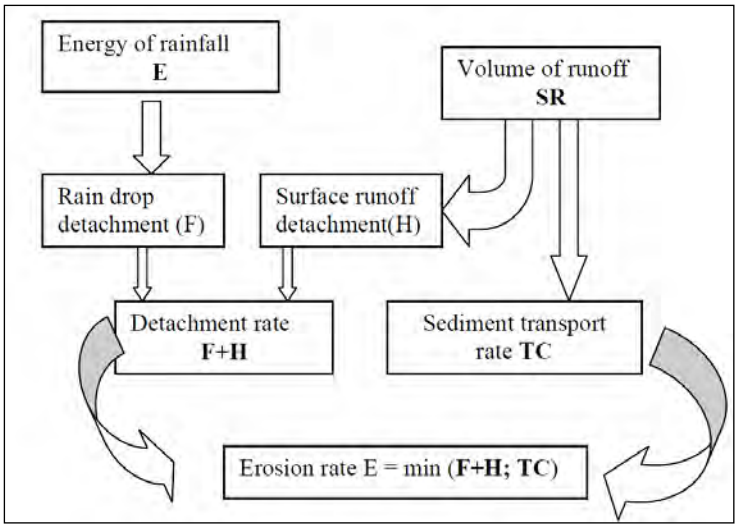

Figure 186. Watershed erosion model concept described by Morgan, Morgan and Finney (1984) (*ibid*)

In addition to the standard land based erosion model IWRM/VMOD includes special modules for mountain slope and in-channel erosion.

6.8. Water quality

The water quality model has four standard variables including sediment components:

- DPO4 - soluble phosphate phosphorus
- PPAR - particulate phosphorus
- NO3 – dissolved nitrogen
- NPAR – particulate nitrogen
- SS0 - clay
- SS1 - silt
- SS2 -sand.

The selection of the nutrient components follows DHI findings (Study on the Impacts of Mainstream Hydropower on the Mekong River, Draft Baseline Assessment Report, 2015); “Monitoring data from the Additional Sediment and Nutrient Studies from the dry season of 2014 indicates that 80 to 90 % of the Total Phosphorus is adhered and transported with the sediments, with increasing content of phosphorus from the Chinese border until the Mekong Delta where the sediments are saturated with phosphorus… Measurements related to nitrogen shows that most nitrogen is found as dissolved nitrite, nitrate and ammonia, with only 20% being adhered to, and transported with sediments.” About 80% of the nitrogen is inorganic and NO3 is taken to represent this fraction.

Recently DOC (Dissolved Organic Carbon), BOD (Biological Oxygen Demand), COD (Chemical Oxygen Demand), DO (Dissolved Oxygen) NH4 (ammonium) as well as contaminants have been added to the model. When needed these can be readily implemented.

The water quality loads can be given either as diffuse or point loads. The diffuse loads depend on land use as well as with different water components (surface runoff, soil layer flow, drain/ditches). The soluble phosphorus (DPO_4) can be assumed to be mainly from fields, point sources and population load. In forested areas the soluble phosphorus is mainly from decomposing organic matter. The characteristic sediment concentrations are modified based on soil types and specifically their clay, silt, sand and organic material content shown below. The relative differences between soil types correspond to values reported by Havlin (2004):

- 0.43 for clay
- 1.00 for silt
- 1.40 for sand
- 2.33 for peat or other organic soils.

After the loads sedimentation/absorption parameters are defined for each variable and water type (lake, river, overland flow).

6.9. Lakes and Reservoirs

Lakes and reservoirs are handled separately. Any set of neighbouring grid cells can be set to be a lake or reservoir (**Figure 187**). Each lake or reservoir is treated as storage that keeps account of the water level as a difference from the reference water level. Water level changes are linearly related to volume changes, which are computed from inflow, outflow, precipitation, evaporation, seepage and

water extraction (for example, for irrigation). Outflow from a lake is computed as a function of the water height using river section equations. Outflow from a reservoir is determined by given time series or regulation rule that can be determined on monthly, weekly and daily basis. Evaporation from lakes and reservoirs occurs at the potential rate.

The reservoir operations component of the IWRM/VMOD modelling tool allows the user to incorporate reservoirs construction at any point in the basin and to test the impact of operations rules (monthly, weekly and daily) for existing and new reservoirs. When reservoir volume changes are included the sedimentation/erosion process leads to a pseudo stable state where erosion and sedimentation are in balance over longer time periods.

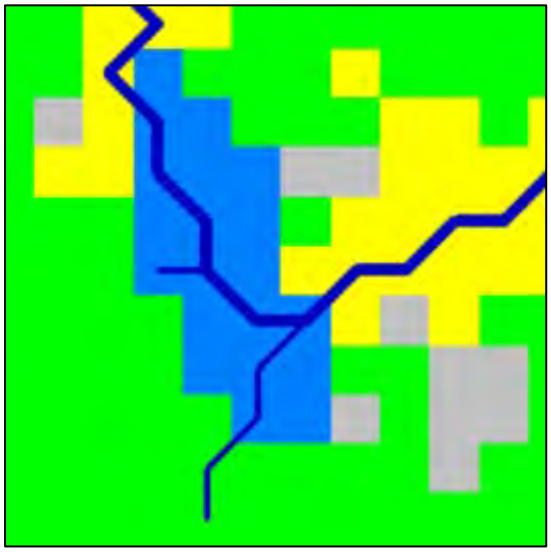

Figure 187. Representation of a lake in the model interface. The lake cells are shown in light blue.

6.10. Irrigation and crop yield

Crop yield modelling is undertaken by integrating the FAO AquaCrop model within the IWRM/VMOD distributed hydrological model. The AquaCrop model provides a framework and the algorithms to calculate crop yield based on climate, crop, soil, field management, and irrigation management (**Figure 188**; Raes et al. 2009). Each crop area within a base grid cell is assigned its own sub-cell and computed with full hydrology including infiltration, soil moisture and lateral surface and soil water flow, as well as the additional AquaCrop calculations. The VMOD/AquaCrop model benefits are:

- fully integrated with distributed hydrological modelling and water resources management modelling
- is a physiological plant growth model; in contrast earlier FAO CropWat is hydrological crop model
- AquaCrop focuses on water stress
- suitable and detailed for irrigation demand, drought and climate change assessments
- simple data requirements - soil properties are usually not well known and AquaCrop has only one soil stress/soil fertility parameter to calibrate.

Using the agro-ecological component of the IWRM/VMOD modelling tool, users can alter agricultural area hydrological parameters and farming parameters to test the impact of management activities such as irrigation efficiency improvements and changing crop patterns.

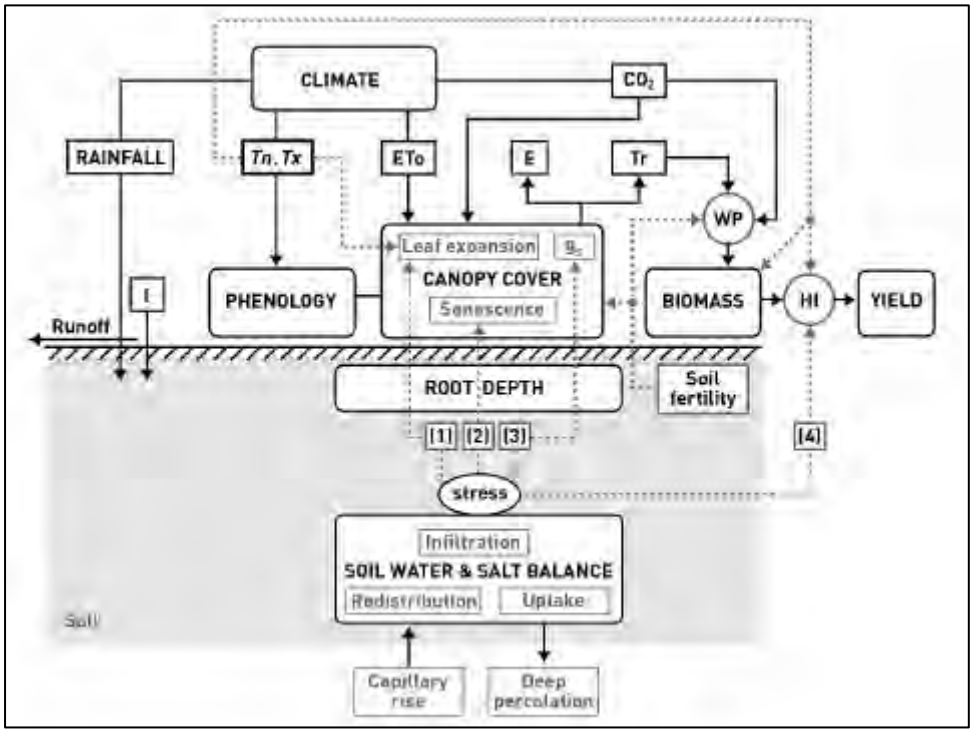

Figure 188. FAO AquaCrop flow chart indicating the main parameters affecting crop yield (Raes et al. 2009).

6.11. Reservoir sediment trapping validation

VMOD reservoir module can read IQQM files and set up the reservoir characteristics including monthly volume-discharge curves based on them. Additionally user can define daily and weekly release patterns as well environmental flows. Sediment trapping takes into account sedimentation, erosion, basin dimensions and sediment trapping effect on reservoir volume:

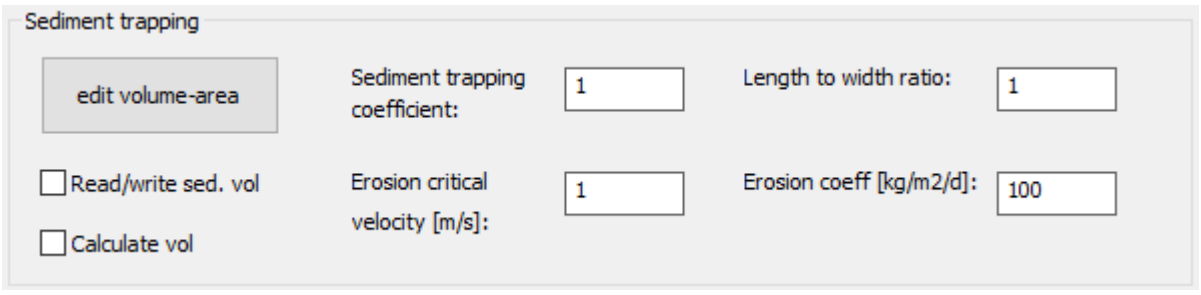

Figure 189. VMOD reservoir model sediment related parameters.

Council Study principal tool for sediment trapping modelling will be eWater SOURCE. During the SOURCE development phase the VMOD sediment trapping results and Brune curve data were compared with the VMOD results. VMOD was test for reservoir sediment trapping in 4 cases and compared with the empirical Brune data. The cases are:

1. Reservoir with 1000 Ml storage volume, 1'000 m^3/s inflow and 10 m depth
2. Reservoir with 1000 Ml storage volume, 10'000 m^3/s inflow and 10 m depth
3. Reservoir with 1000 Ml storage volume, 100 m^3/s inflow and 10 m depth
4. Reservoir with 1000 Ml storage volume , 100 m^3/s inflow and 5 m depth

In all cases incoming sediment concentration is 100 mg/l for clay, silt and sand.

The purpose was to test how model results fit with the Brune curve and how reservoir depth affects sedimentation: "shallow sediment-retention basins … can operate much more efficiently than indicated by the curve."

A small model area is used for testing (**Figure 190**). River discharge is fixed with the "River discharge" control point. Sediment load is given separately for clay, silt and sand (3 "Load SS" control points). Load is changed for each discharge to maintain 100 mg/l concentrations. Reservoir rating curve is changed so that for each discharge case the storage volume is 1'000'0000 Ml.

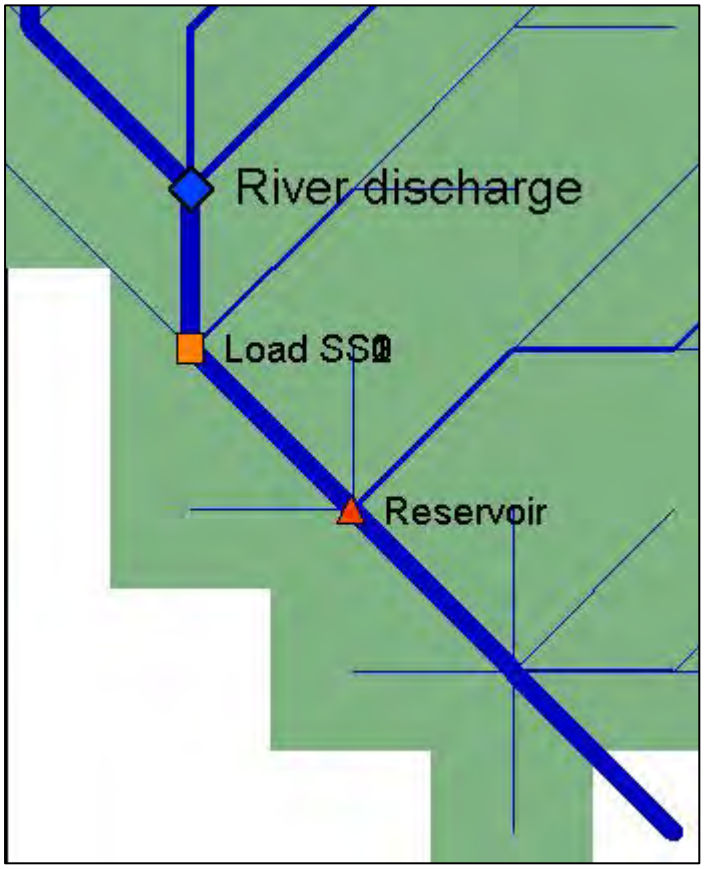

Figure 190. Model setup for reservoir sediment trapping.

Three time series points are defined below the reservoir (T0), in the reservoir (T1) and upstream the reservoir (T2):

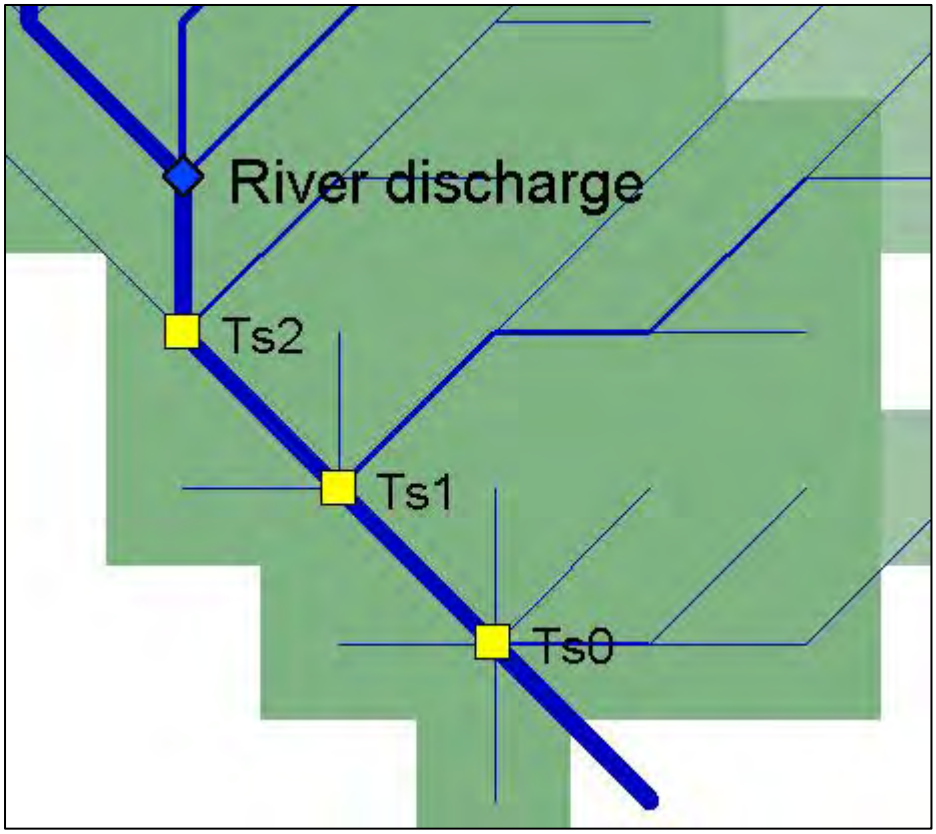

Figure 191. Model time series output points.

Clay, silt and sand concentrations are plotted below for different discharges and reservoir depths:

Discharge 1'000 m^3/s

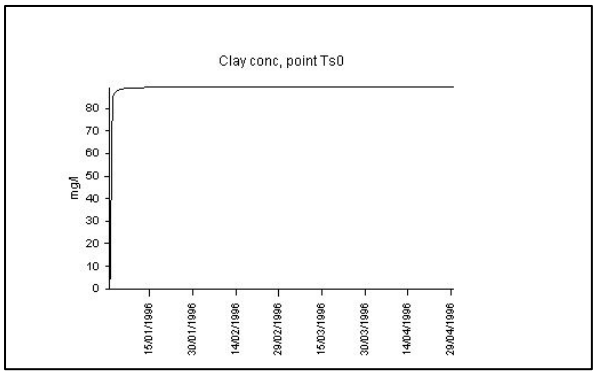

Discharge 10'000 m^3/s

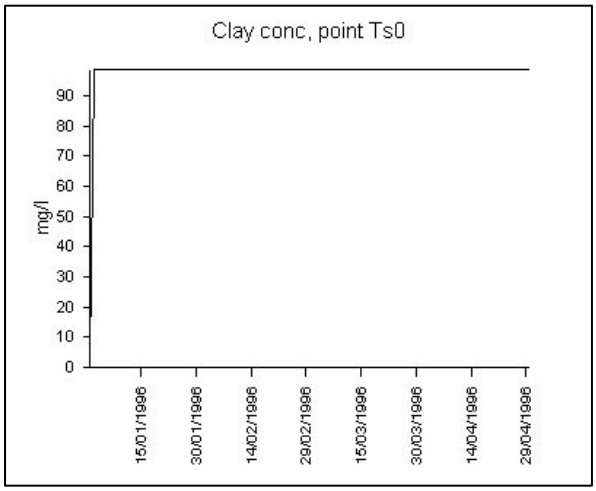

Discharge 100 m^3/s

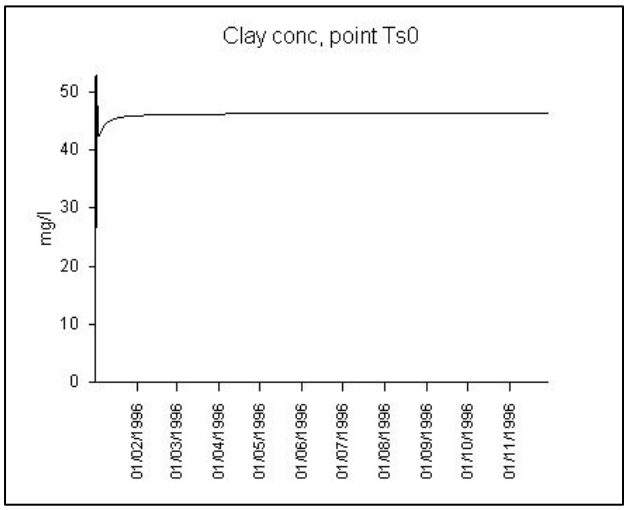

Discharge 100 m^3/s, half depth (5 m)

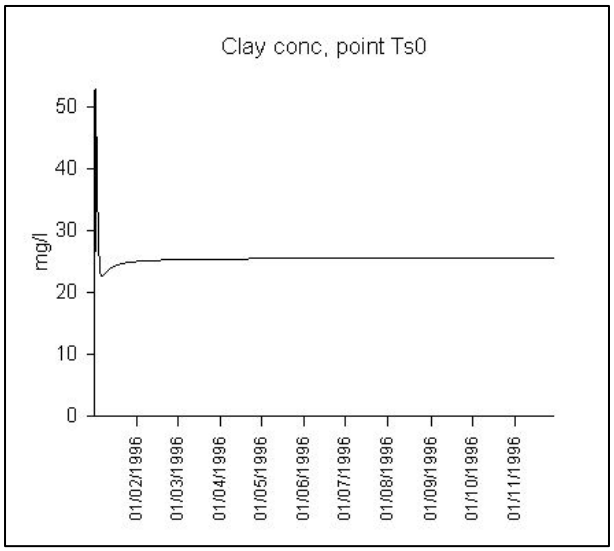

Discharge 1'000 m^3/s

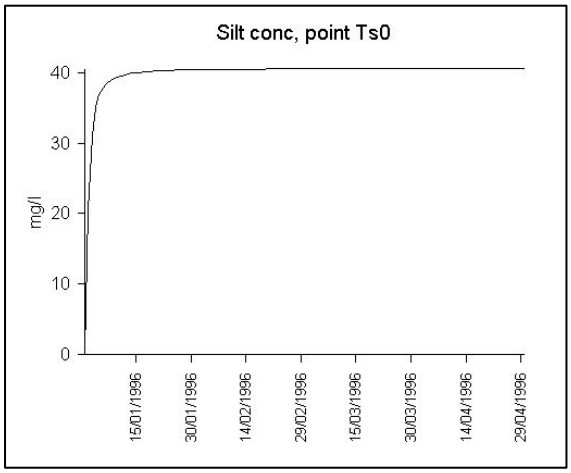

Discharge 10'000 m^3/s

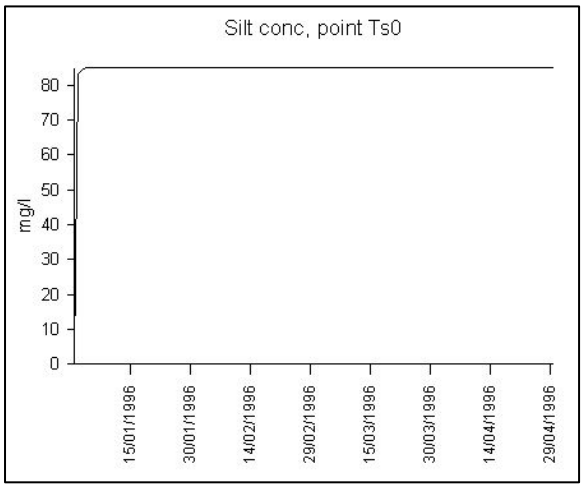

Discharge 100 m^3/s

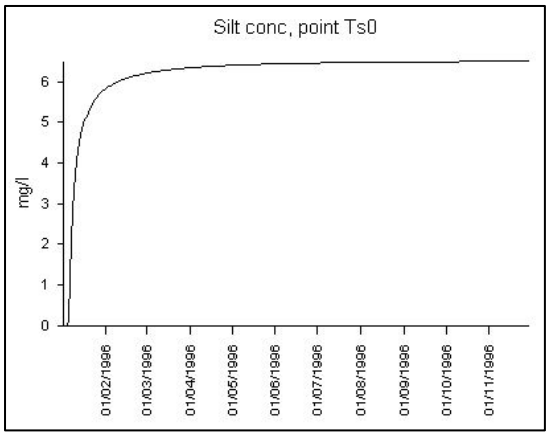

Discharge 100 m^3/s, half depth (5 m)

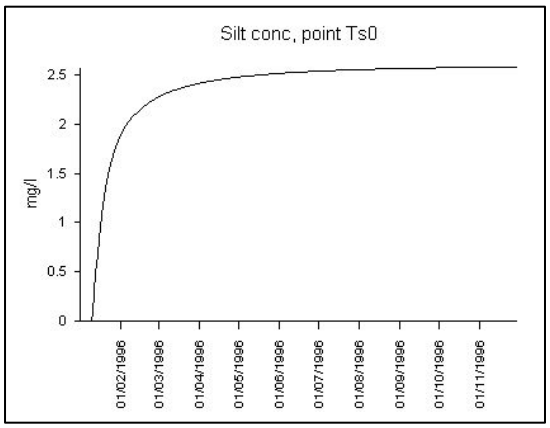

Discharge 1'000 m^3/s

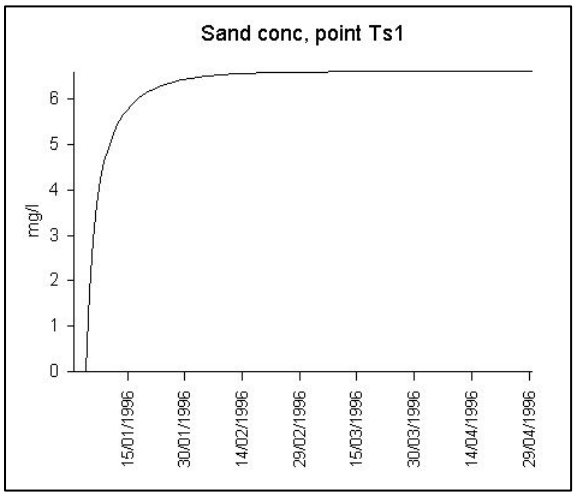

Discharge 10'000 m^3/s

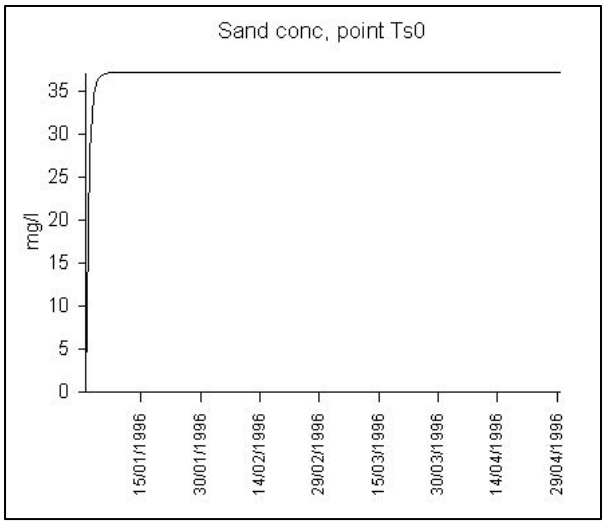

Discharge 100 m^3/s

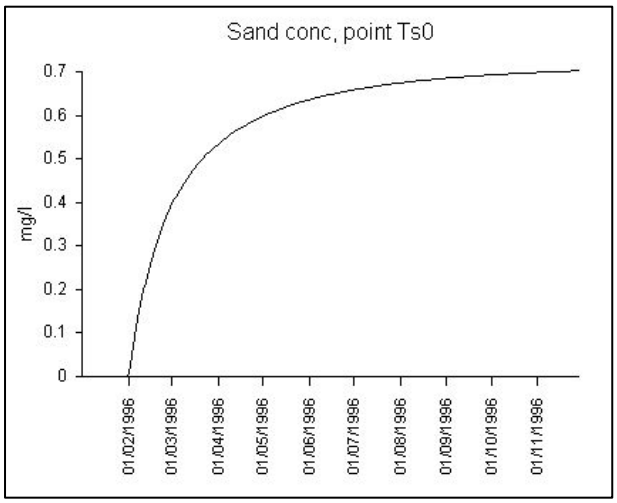

Discharge 100 m^3/s, half depth (5 m)

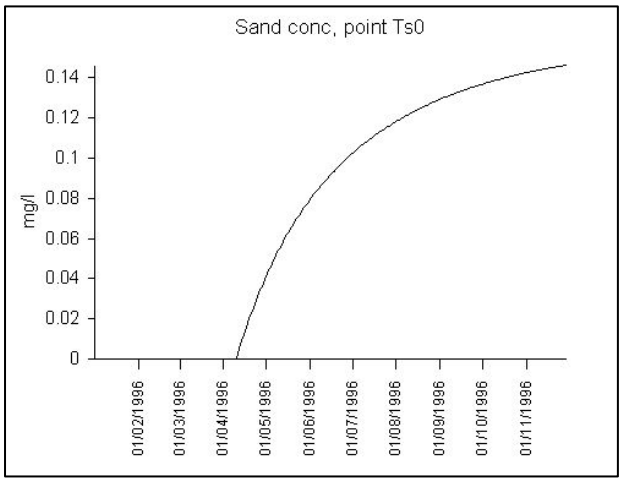

Following table summarises comparison between empirical sediment trapping efficiencies by Brune and model results. C:I is the ration between the reservoir volume (m^3) and annual cumulative flow (m^3).

Table 6. Comparison of trapping efficiencies between the Brune curve and IWRM/VMOD model.

	C:I 0.003	C:I 0.03	C:I 0.3	C:I 0.03 half depth
Bourne min	5%	60%	90%	
Bourne max	35%	80%	100%	
Clay	1%	11%	54%	25%
Silt	15%	60%	93%	99%
Sand	37%	93%	99%	100%

Model results for silt and sand trapping efficiencies are rather well within the scope of the Brune curve. However the clay is trapped clearly less in the model than the range given by Brune. It should be noted that decreasing the reservoir depth (last column) clay sedimentation becomes much more efficient as has been also observed in practice: “shallow sediment-retention basins designed for the express purpose of trapping sediment can operate much more efficiently than indicated by the [Brune] curve. For instance, the All-American Canal desilting basins in Arizona would have negligible sediment trapping efficiency based on their C/I ratio, but the basins operate at a trapping efficiency of 91.7 percent.” (Enbarasan 2015).

Both linear and non-linear fitting were done for the original Brune data to facilitate definition of SOURCE sediment trapping algorithm:

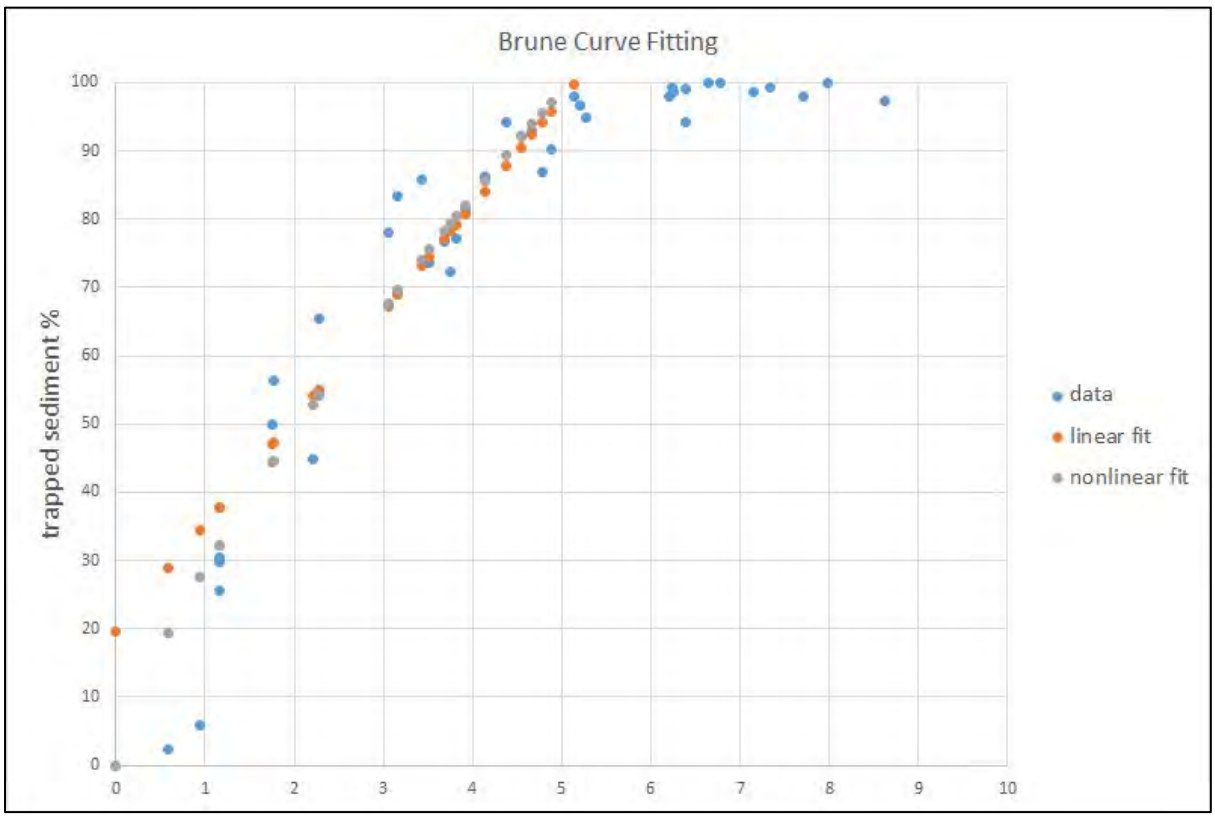

Figure 192. Best fit for Brune original data (blue dots). Linear fit (orange dots) y = 19.70+15.59*x, nonlinear fit y = $28.83*x^{0.766}$, x = ln(I)+ 6.438, I = Brune Capacity:Inflow ratio [acre-feet of capacity per acre-feet of annual flow]. Observe that after x = 5 trapping efficiency is practically 100%.

6.12. Sediment trapping case study for the Mekong

Mekong sediments and more generally alluvium (sediments together with nutrients and organic material) have major importance for maintaining land mass and sustaining natural and agricultural productivity. Because of this complementary sediment and reservoir trapping study reported here has been conducted. The study focuses on grain size distribution impact on sedimentation and to establish time scales for reservoir filling and sediment trapping. The study supports Council Study impact assessment and modelling results analysis but is not intended to replace the main DSF sediment and reservoir modelling.

The reservoir modelling data is based on the DSF IQQM data on reservoir volumes, shapes and operations. In addition following parameters are defined for each reservoirs:

- Length to width ratio
- Erosion rate (kg/m2/d) at the critical (shear) velocity
- Sediment trapping coefficient
- Erosion critical velocity for clay, silt and sand (m/s).

Incoming water volumes and clay, silt and sand loads are computed with the IWRM distributed model. In the reservoir water volume changes, sediment volume changes, sediment transport, sedimentation and resuspension are computed (**Figure 193**).

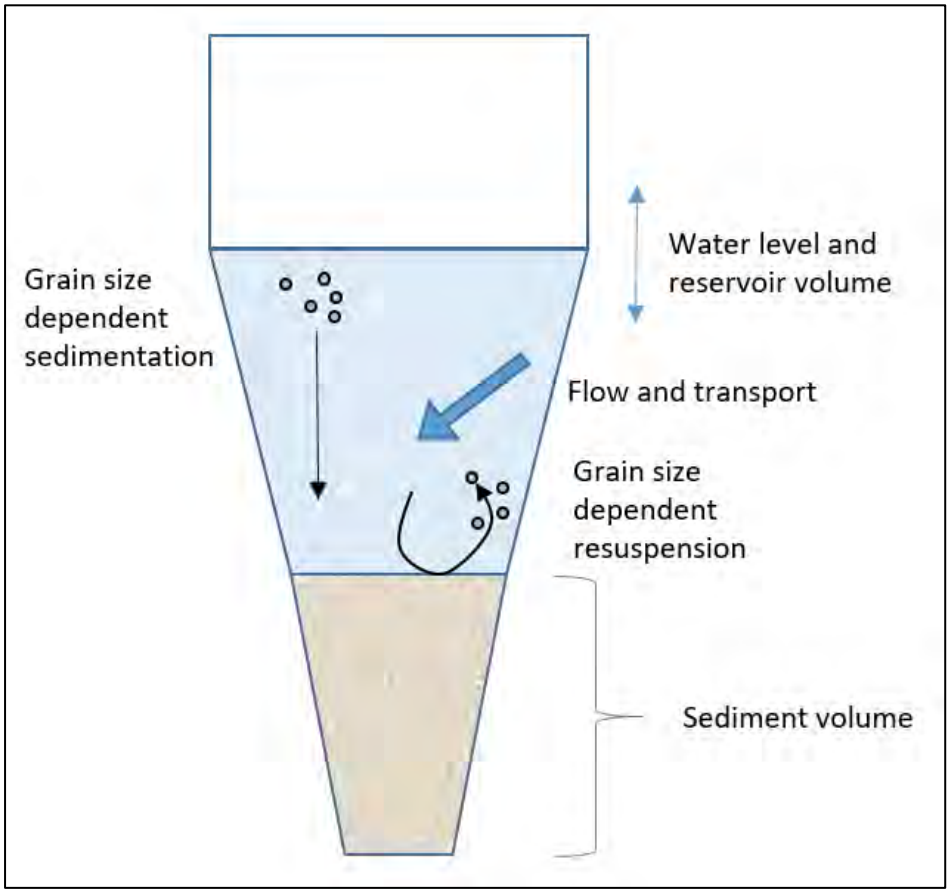

Figure 193. Reservoir model used in the study.

6.12.1. Model calibration

The watershed model was calibrated for the pre-dam conditions and the reservoir model for Manwan sediment trapping. Because lack of grain size distribution data in the pre-dam conditions, it has been assumed that earlier sediment monitoring results and mass balance estimates account mainly clay and silt. Consequently model clay and silt have been calibrated on the sediment monitoring data but sand is accounted for in the Manwan sediment trapping. It would be important in the future to analyze available grain size data and to improve grain distribution especially for the mountainous areas. In the sediment trapping two options are available: either use high critical velocity numbers signifying strong sediment consolidation or use lower values. Both of these options have been used. For strong consolidation 1 m/s critical velocity has been prescribed for all sediment fractions. For weak consolidation 0.01 m/s, 0.1 m/s and 1 m/s for clay, silt and sand have been used.

China sediment load in Chiang Saen has been calibrated based on three sources:

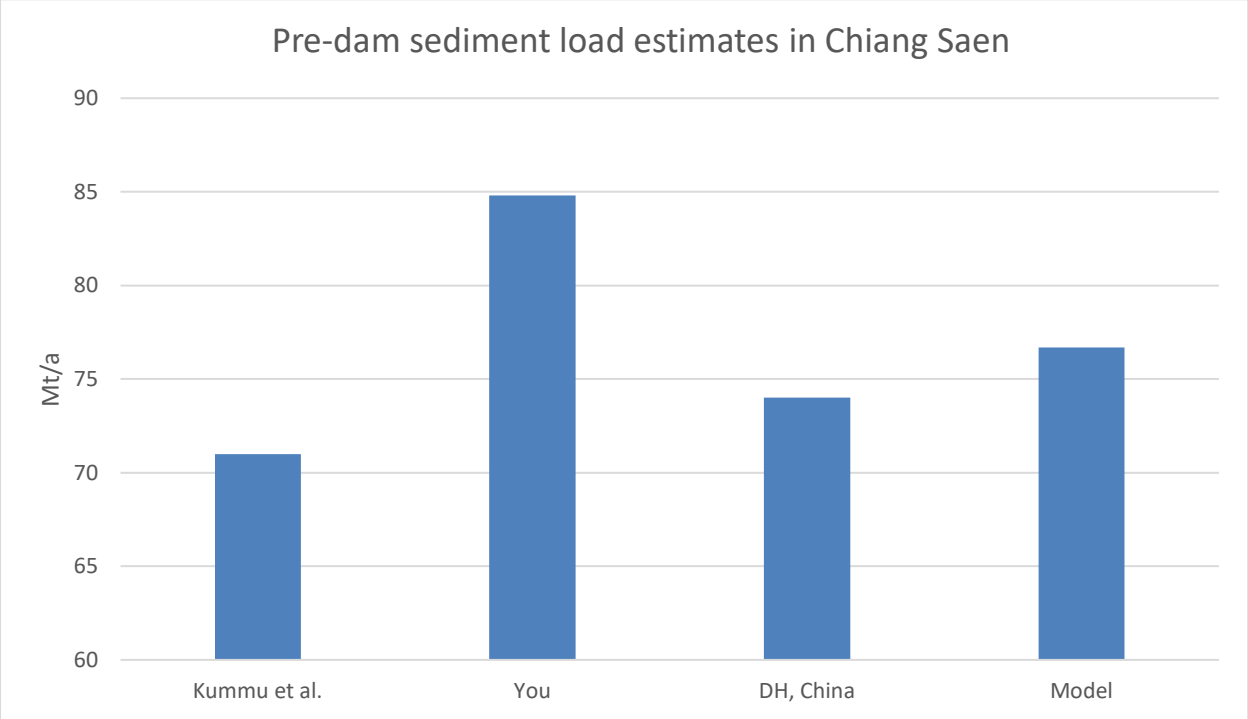

Figure 194.. Pre-dam Chiang Saen TSS load estimates from different sources compared to the average modelling value.

Model calibration gives for annual average sediment load in Pakse 139 Mt. This can be compared to Kummu et al. (2007) estimate 131 Mt based on MRC data. In Kratie model gives annual load 160 Mt which is in line with previous estimates (see Kummu 2007).

Fu et al. (2007) give annual sedimentation volume of 20.7 – 21.9 Mm^3 for Manwan. Calibrated model gives average sedimentation volume 21.2 Mm^3 for weakly consolidated sediment option. Strong consolidation in turn gives 22.5 Mm^3 annual loss of volume. Kummu et al. estimate that Manwan dam has resulted in 40 Mt annual sediment loss in Chiang Saen. Calibrated model gives significantly different numbers: for silt and clay 9.8 Mt/a reduction and for total sediment load including sand 27.8 Mt/a.

6.12.2. Near future sediment trapping

The near future scenario assumes that all dams are built at the same time. Of course this is unrealistic but gives indication of trapping time scales and magnitudes. In the future, given more time, the model should be run phased adding reservoirs during each phase.

The scenario used here is the BDP2 20 year dam scenario including the mainstream dams. The reason for using this scenario is that it has been set up earlier and was quick to implement for an initial analysis.

An important limitation of this analysis is that in reality dams would change their operations as they are filling up but here the monthly rule curves are maintained constant.

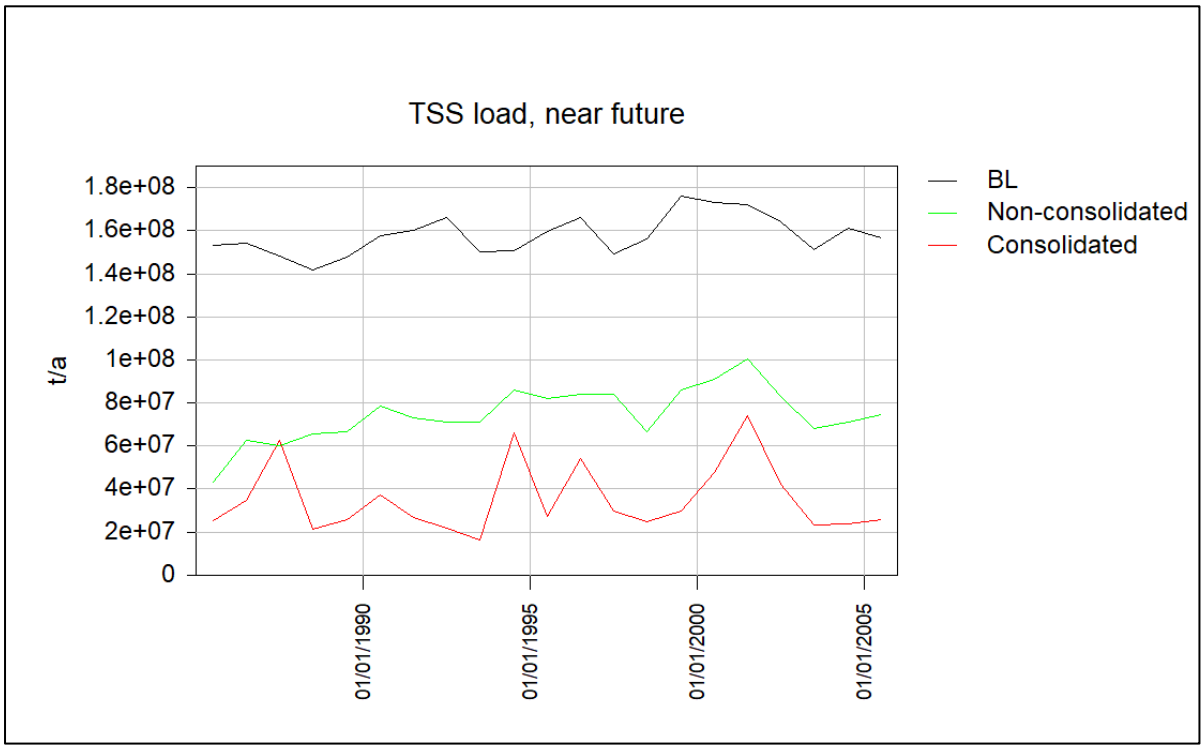

Figure 195. Impact of dams in the near future

As practically all sand is trapped by the dams only the finer fraction (clay and silt) loads are presented here and indicated as “TSS” in the graphs. Near future, 50 year and 100 year time windows are presented here. It can be seen from the figures that if the reservoir sedimentation is weakly consolidated (“non-consolidated”) the sediment trapping efficiency remains more or less constant over time. If sediments consolidate effectively the trapping efficiency first picks up (**Error! Reference source not found.** and **Error! Reference source not found.**) because reservoir depth decreases and sedimentation becomes more effective. After more than 100 years when the consolidating reservoirs start to fill up the trapping efficiency starts to decrease (**Error! Reference source not found.**) as resuspension starts to increase.

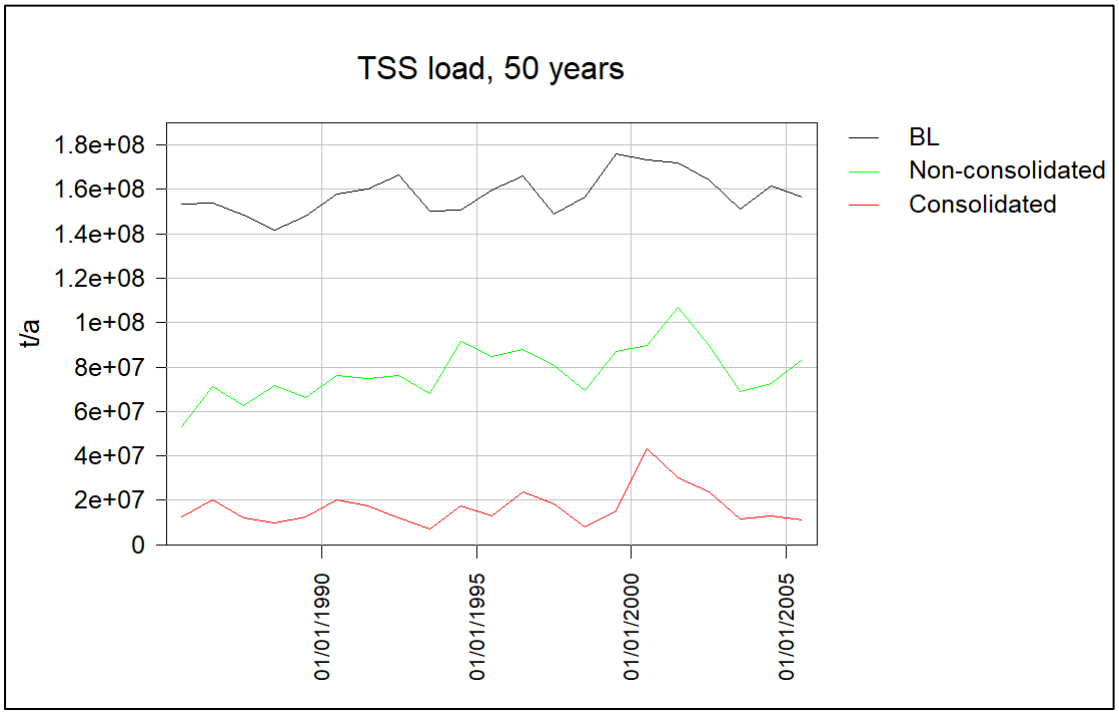

Figure 196. Impact of dams after 50 years.

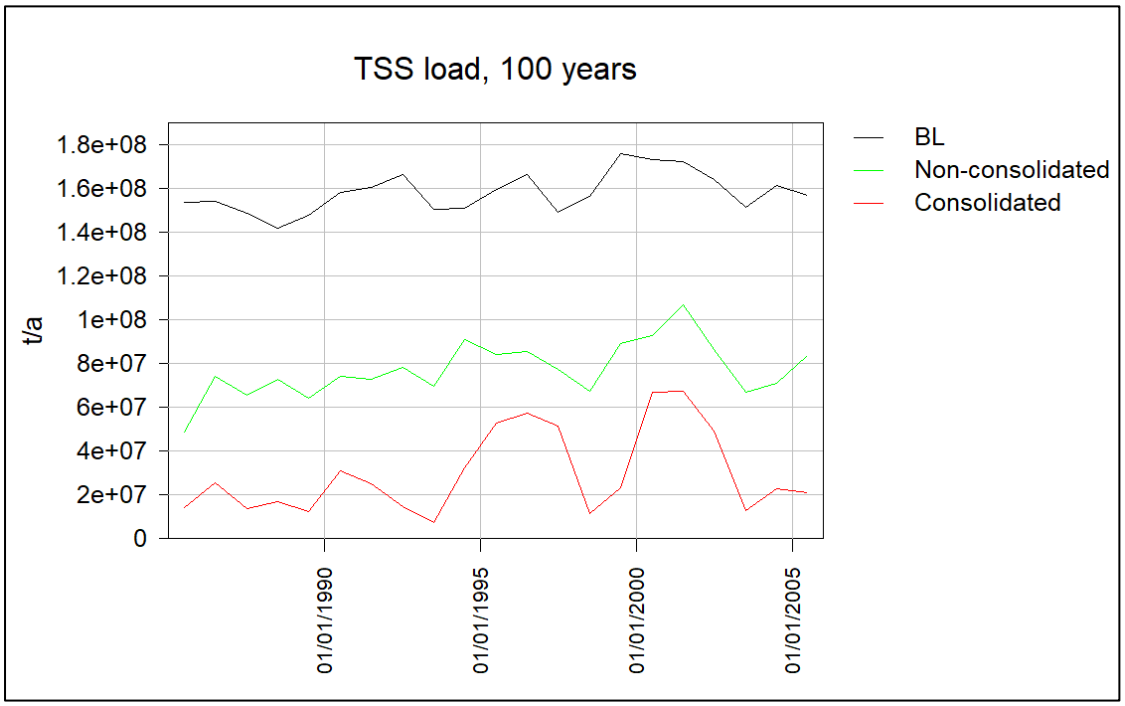

Figure 197. Impact of dams after 100 years.

6.12.3. Conclusions

Building of the Mekong dams affect downstream sediments long time. After more than 100 years there is indication that sediment loads start to increase when reservoirs are starting to fill.

Sediments are trapped practically fully by the dams but the finer fractions (clay and silt) are trapped from 50% to 88% depending on how effectively the dams consolidate finer sediments.

DSF results for 2020 give 65% dam trapping efficiency and 2040 and 2040CC scenarios give 97% efficiency. The BDP2 scenario used in this analysis is not directly comparable to the Council Study 2040 scenario but the study indicates that the 97% reduction in sediments may be too extreme. Even relatively small difference in the trapping efficiency has large impacts when the released sediment loads are small (see impact assessment report for productivity sensitivity for sediments) and this warrants further study on the sediment trapping efficiency.

When assessing the results, it should be noted that DSF sediment trapping is based on the empirical Brune data which doesn't directly take into account grain size, reservoir depth, resuspension shear stress etc. unlike the approach presented in this report. On the other hand, it must be also kept in mind that the physical model can't be considered superior or definitive before further model checking and data gap filling has been conducted.

6.13. Basic model setup data requirements

There are five key sets of data required for the basic model setup (**Figure 198**). These include:

DEM and river line (spatial): Digital Elevation Model (DEM) in BIL, GeoTIFF or ASC data format. The river line map is optional but recommended as it enables confirmation of the software generated river network.

Land use (spatial): Map of land use in BIL, GeoTIFF or ASC data format.

Soil classification (spatial): Map of soil types in BIL, GeoTIFF or ASC data format. Soil depths should be acquired if possible but are optional. If detailed soil information is not available, values can be based on land use types and typical soil parameters from literature.

Model control components locations (spatial), details and operation rules: The location of existing model control components such as reservoirs, weirs, groundwater extraction, irrigation areas, diversions and flood detention areas is required to represent the hydrological system of the basin of interest. In addition, information on the model control components and how they are operated is required. This may include reservoir volumes, weir heights, irrigation command areas, operation rules, pumping volumes or cropping regimes.

Hydro-meteorology station location (spatial) and time series (temporal): Temperature and precipitation are the key drivers of the model. Precipitation and maximum temperature daily time series are required for as many stations throughout the basin as possible, and for as long a time period as possible. For more detailed evapotranspiration simulation PAN evaporation, air humidity, wind speed, air pressure and cloudiness need to be obtained. The model interpolates the time series

so that each grid cell is assigned a precipitation and temperature for every time step. Hydrology time series are used to calibrate the model.

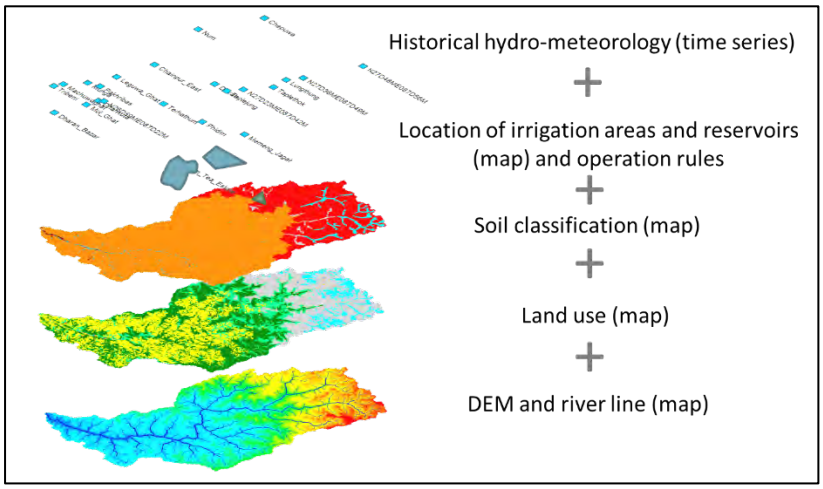

Figure 198. Basic model setup data requirements

6.14. VMOD calibration process

Model integrated help divides calibration into two phases. In the first phase consists of manually adjusting water quantities to the right level. Usually this would entail two parameters, one for orographic (height) correction for rainfall to better account for increased rainfall on mountain slopes and the other for evaporation adjustment when min/max daily temperature is used for potential evapotranspiration estimation. During the second phase autocalibration is utilised.

Usually the main parameters to calibrate are:

- vinfots (rainfall height/orographic correction)
- petcorr (potential evaporation correction, important especially when the Tmin/Tmax method is used)
- infkz, kz and kx (vertical and horizontal soil conductivities)
- dz2 (second soil layer depth)
- rfmult and rwmult (river conductivity and width multipliers).
- tanb_coeff (global coefficient of river and soil slopes, useful especially when grid cell size changes).

The need for soil parameter calibration arises from the fact that usually soil information is quite rudimentary.

Model calibration tools are presented in **Figure 199** - **Figure 201**.

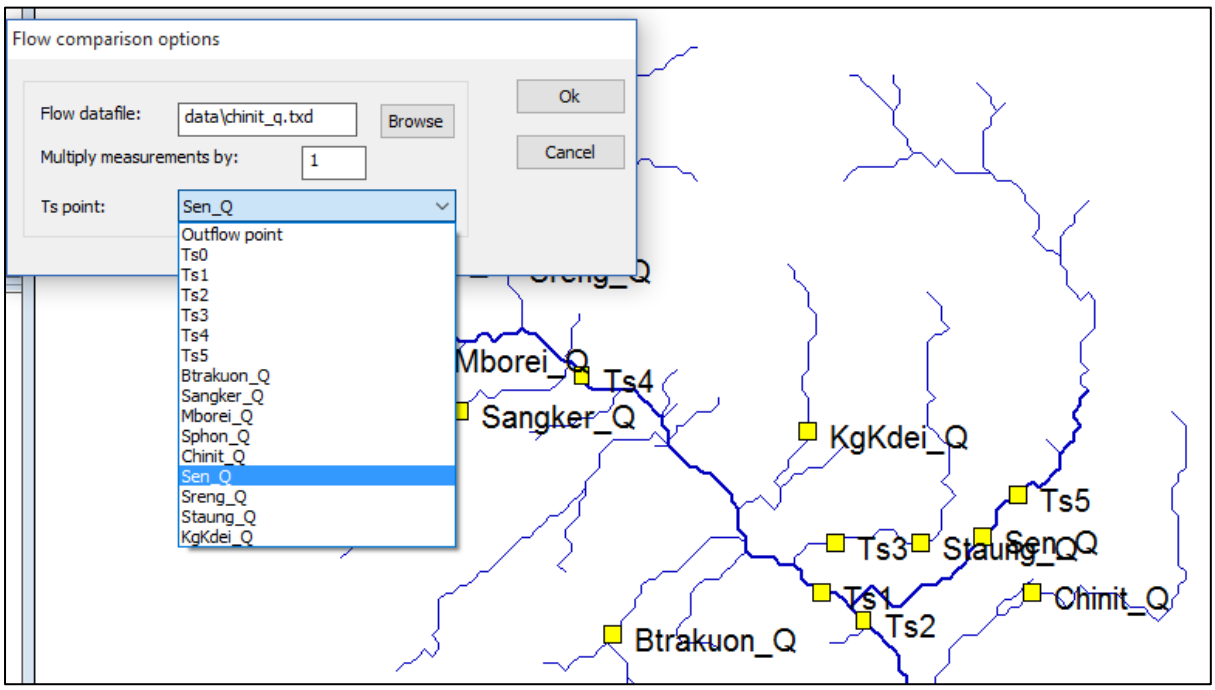

Figure 199. Station definition for autocalibration and R^2 and average flow comparison.

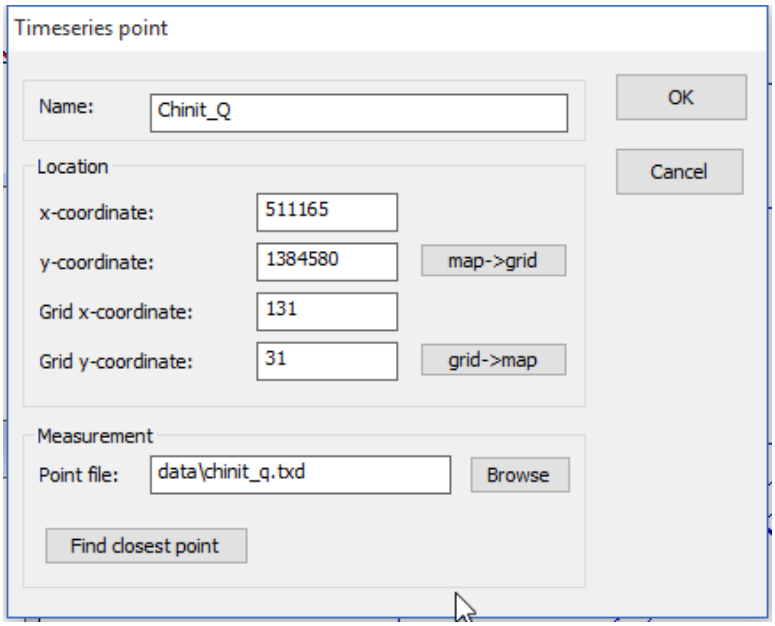

Figure 200. Monitoring data can be included in the model output time series for automatic comparison.

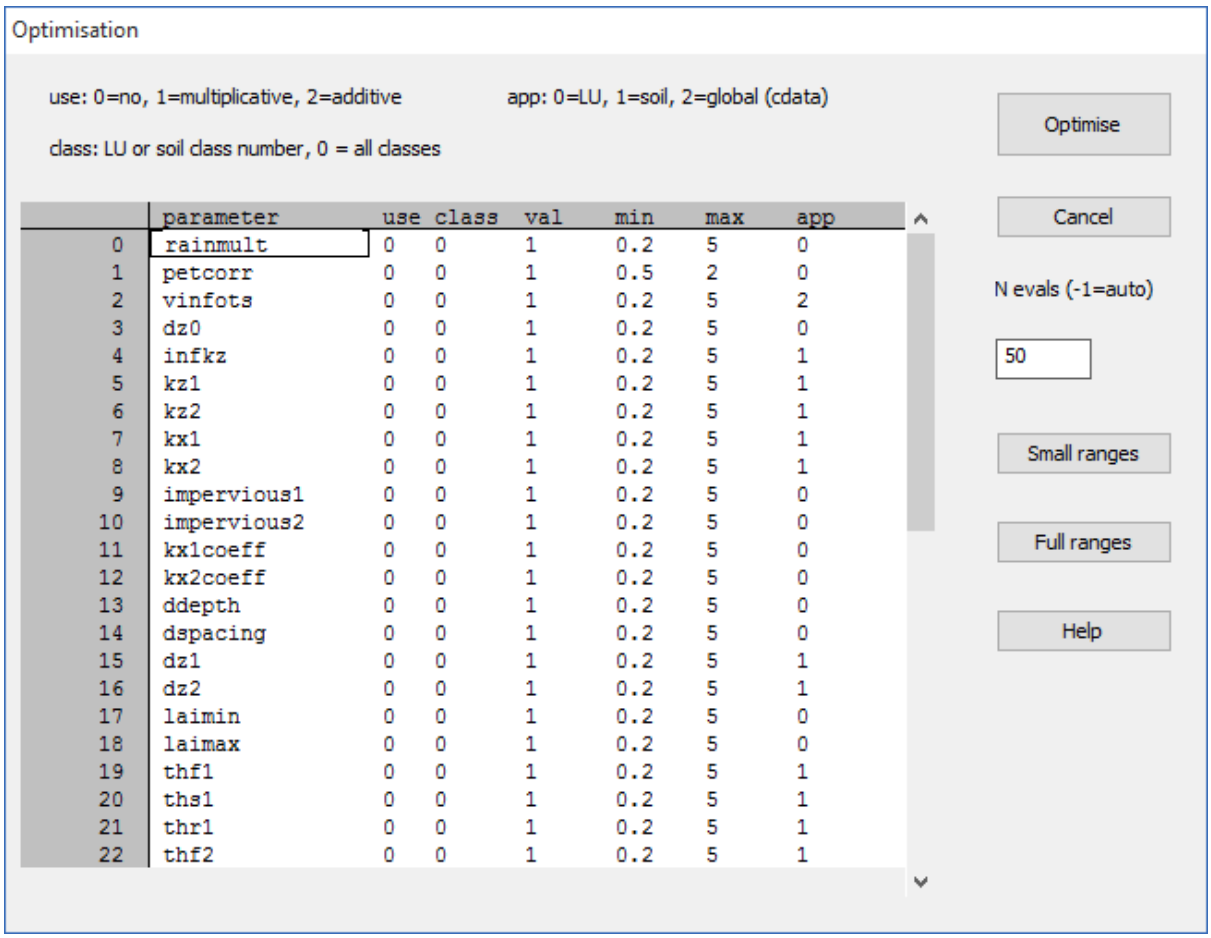

	parameter	use	class	val	min	max	app
0	rainmult	0	0	1	0.2	5	0
1	petcorr	0	0	1	0.5	2	0
2	vinfots	0	0	1	0.2	5	2
3	dz0	0	0	1	0.2	5	0
4	infkz	0	0	1	0.2	5	1
5	kz1	0	0	1	0.2	5	1
6	kz2	0	0	1	0.2	5	1
7	kx1	0	0	1	0.2	5	1
8	kx2	0	0	1	0.2	5	1
9	impervious1	0	0	1	0.2	5	0
10	impervious2	0	0	1	0.2	5	0
11	kx1coeff	0	0	1	0.2	5	0
12	kx2coeff	0	0	1	0.2	5	0
13	ddepth	0	0	1	0.2	5	0
14	dspacing	0	0	1	0.2	5	0
15	dz1	0	0	1	0.2	5	1
16	dz2	0	0	1	0.2	5	1
17	laimin	0	0	1	0.2	5	0
18	laimax	0	0	1	0.2	5	0
19	thf1	0	0	1	0.2	5	1
20	ths1	0	0	1	0.2	5	1
21	thr1	0	0	1	0.2	5	1
22	thf2	0	0	1	0.2	5	1

Figure 201. In the autocalibration parameters to be calibrated can be adjusted for all classes (class = 0) or selected land use or soil type.

6.15. VMOD model limitations

Like all models, the IWRM/VMOD modelling tool is a simplified representation of a complex system. It is therefore always recommended that the user gain an understanding of the system of interest, and the key drivers for hydrology, before attempting to undertake scenario analysis. Understanding of the system can be gained through field visits to the basin of interest, expert observations and review of available materials and reports. Also, comparing model results with monitoring data and running model with different parameters, environmental conditions and scenarios provides valuable insights into the watershed processes and functions.

7. Annex 7 - 3D-EIA Model Description and Validation

7.1. 3D hydrodynamic equations

The fundamental physical principles governing motions of water masses in a lake or sea are the laws of conservation of momentum, mass, and energy. These physical laws are expressed mathematically by the equations of motion, the continuity equation, and the thermodynamic energy equation. The continuity equation is:

$$\begin{aligned}
\frac{du}{dt} &\equiv \frac{\partial u}{\partial t} + u\frac{\partial u}{\partial x} + v\frac{\partial u}{\partial y} + w\frac{\partial u}{\partial z} = fv - \frac{1}{\rho}\frac{\partial p}{\partial x} \\
\frac{dv}{dt} &\equiv \frac{\partial v}{\partial t} + u\frac{\partial v}{\partial x} + v\frac{\partial v}{\partial y} + w\frac{\partial v}{\partial z} = -fu - \frac{1}{\rho}\frac{\partial p}{\partial y} \\
\frac{\partial w}{\partial t} &\equiv \frac{\partial w}{\partial t} + u\frac{\partial w}{\partial x} + v\frac{\partial w}{\partial y} + w\frac{\partial w}{\partial z} = -\frac{1}{\rho}\frac{\partial p}{\partial z} - g
\end{aligned} \qquad (1)$$

- t = time
- d/dt = the total derivative relative to the rotating system of orthogonal coordinates
- x, y, z = horizontal and vertical coordinates
- u, v, w = the components of the velocity along the three coordinate axes, respectively
- f = the Coriolis parameter,
- p = pressure,
- ρ = water density, and
- g = the gravitational acceleration of the earth.

Integration of the equation (1) into a discrete form leads to generation of turbulence terms. A standard approach for turbulence parameterization is the so-called eddy viscosity principle. It relates the turbulent fluxes to the gradient of the transported property by means of an eddy viscosity (for momentum) or eddy diffusivity (for sediment, water quality and tracers).For calculating eddy viscosity/diffusivity, turbulence models in the model are based on the Kolmogorov [1942] and Prandtl [1945] formulation, which relates these turbulent exchange coefficients to the product of a velocity scale and a length scale

$$\upsilon_t = c_\mu \sqrt{kL} \qquad (2)$$

where *k* is the turbulent kinetic energy (TKE) in m^2/s^2, *L* is the turbulent macro length scale in m and c_μ is the dimensionless stability function. One of the turbulence models used in the 3D-EIA is the $k-\varepsilon$. In it the length scale is substituted by the normalized dissipation rate which has the unit W/kg= m^2/s^3

$$\varepsilon = \left(c_\mu^0\right)^3 \frac{k^{3/2}}{L} \qquad (3)$$

with the constant $c_\mu^0 = 0.5562$.

7.2. 3D hydrodynamic modelling

The 3D model family structure is illustrated in **Figure 202**. Its elements are the flow model which is driven by the geographical, meteorological and hydrodynamic data, resolving 3 dimensional flow fields, and water quality model, driven by the flow fields as well as water quality and load data. The separation of flow and water quality calculation has proved to be essential for practical water quality calculations because of efficiency and separation of concerns. The model use is controlled by data management tools and graphical user interfaces.

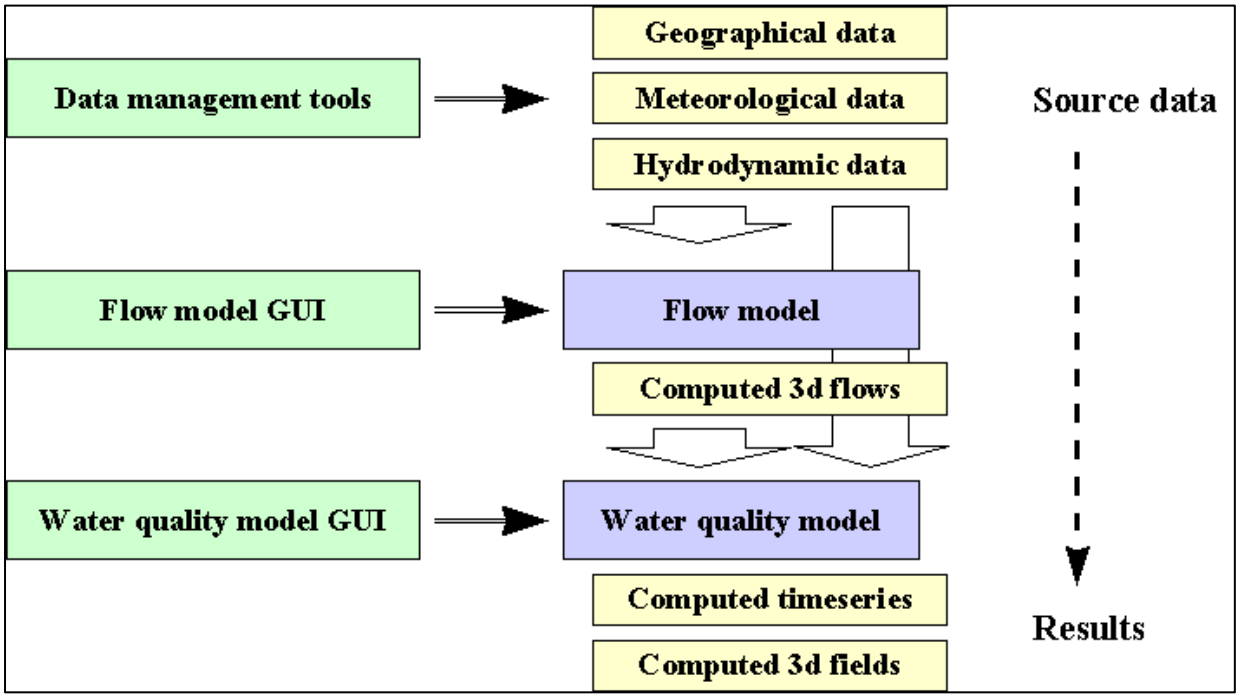

Figure 202. 3D-EIA modelling system structure. GUI = Graphical User Interface.

The available model components are as follows

- computation of basic hydrodynamics
- inclusion of stratification (temperature, salinity and impurities)
- optional turbulence schemes including k-L and k-ε
- computation of heat fluxes
- different sub-models for calculating the effects of wind fetch on currents
- different sub-models for waves
- different sub-models for sedimentation, sediment transport and resuspension
- inclusion of morphological changes due to erosion
- flooding of coastal areas, wetlands and floodplains
- oil transport and dispersion described as 3 dimensional process

- chemical processes (e.g. evaporation, dissolution, emulsification on surface, in the water column and on the bottom)
- several water quality and ecosystem models for dissolved oxygen, BOD, turbidity, nutrients, heavy metals, carbon, different phytoplankton groups, macrophytes, fish production, bacteria, benthic processes etc; some models are directly coupled with the basic 3D-EIA hydrodynamic model and some are separate utilising pre-computed flow fields

The hydrodynamic part of the model system carries of fundamental role as the basis for any transport and impact computation. That is why specific attention has been devoted to its development. Some of the hydrodynamic model characteristics are listed below:

- advanced numerical schemes have been adopted (e.g. TVD **Figure 203** and Lagrangian transport)
- fully coupled nesting for describing critical areas with high resolution and embedding them into coarser resolution grids taking into account large scale phenomena
- algorithmic and code optimization results in fast execution times
- parallelization for multi-processor computers
- transportable code from PC:s to mainframes
- code developed and tested over 20 years in over 200 practical applications

The model equations and solution principles are presented in Koponen et al. 2015.

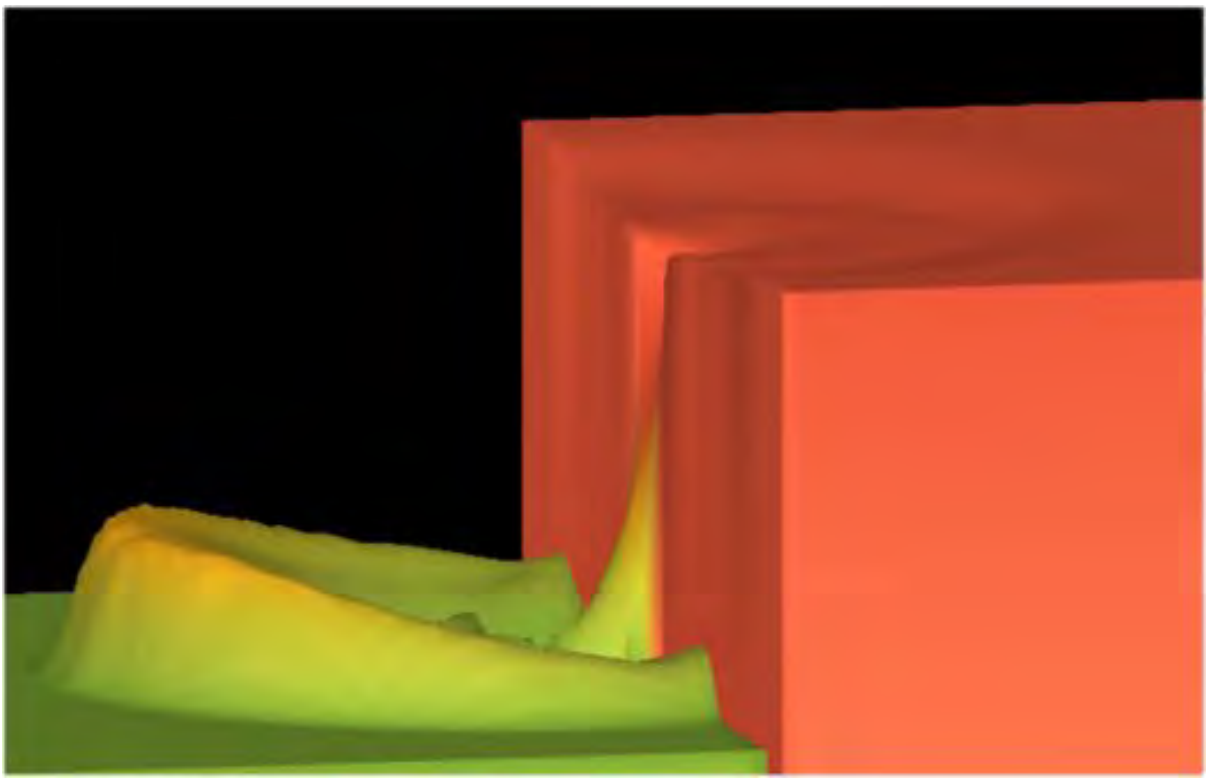

Figure 203. 3D-EIA model computed flood wave propagation from a dam break. Colours indicate water elevations. TVD shock capturing scheme.

Justifications for using the 3D-EIA council study include:

- no licence fees
- works with same data formats as the other selected IWRM tools
- works under same data processing and user interface software as the other selected IWRM tools
- can be coupled with the 1D RNet for channel network-floodplain system modellling
- has been extensively tested and adapted for Mekong conditions
- very fast to construct
- modest data requirements
- can be very easily converted to 2D model for instance for flood modelling only.

Although there exists other 3D models available such as DELFT 3D, MIKE3D and TELEMAC 3D, it would be impossible to adapt them in any reasonable time to the Mekong conditions and

7.3. Review of 2D flood models

As Tonle Sap modelling basis is flood modelling, a review of 2D models is presented here in order to understand nature of 2D hydrodynamic flood modelling, issues involved and the EIA-2D/3D performance compared to other models. It is based on the most comprehensive and in-depth comparison of different 2D flood models by the England Environment Agency Flood and Coastal Erosion Risk Management Research Development Programme (Benchmarking the latest generation of 2D hydraulic modelling packages, Report – SC120002, 2013). The comparison includes three groups of models:

1. Full Shallow Water Equations (depth-integrated Navier-Stokes momentum equations, also 2D St Venant equations) - ANUGA, Ceasg, Flowroute-iTM, InfoWorks ICM, ISIS 2D, ISIS 2D GPU, JFLOW+, MIKE FLOOD, SOBEK, TUFLOW, TUFLOW GPU, TUFLOW FV and XPSTORM
2. Non-convective momentum acceleration - UIM, RFSM EDA, LISFLOOD-FP (convective acceleration represents the change in momentum due to change in velocity)
3. Approximate methods - ISIS Fast Dynamic, RFSM Direct.

Other earlier desktop comparison includes additional models. The list of the models and their use is presented in ANNEX II. Other 2D flood models not covered by benchmark study include BreZo, DIVAST, DIVAST TVD, FloodFlow, Flowroute, Grid-2-Grid, HEMAT, Hydro ASZ2, 2D RS/CS, Mike-21, RIC-Nays, TELEMAC, TRENT, Multi-Hydro, RMA2, Kalypso, Guad2D, DHM21, TASE/SWAN, Flowrute, CE-QUAL-W2, ADCIRC, CH2D and CCHE2D.

The desktop study lists criteria for selecting 2D flood models:

- User manual and technical reference
- Technical support (including training)
- Data compatibility
- Flexibility of data input
- Model setup
- Adding structures

- Run time
- Stability
- Presentation of flood depth and velocity predictions
- Visualisation tools
- File management
- Sensitivity testing
- Uncertainty analysis.

A simpler list could be:

- Usability (user interface, user support, ease of data processing and setting up the model, visualisation, statistical analysis tools etc.)
- Accuracy (how well a model represents any given flood case)
- Applicability (can the model compute stably different types of flows in variable conditions)
- Scalability for different scales
- Efficiency (reasonable run times)

It should be noted that in most of the cases 2D flood modelling is applied with 5x5 to 20x20 m^2 grid sizes. This either limits the modelling area or requires application of parallel processing where large number parallel processors is utilised. For instance utilisation of massive parallelism of Graphical Processing Units has become popular for huge problems.

2D flood models can be divided into two categories depending on their numerical solution scheme: “An important consideration in numerical methods is the approach used to proceed through the calculation in time. The solution is normally obtained in time step increments. However, numerical schemes can be divided in two major categories depending on the approach used to discretise the shallow water equations through time. In implicit schemes, the discretisation approach applied to the space gradients involves values at both the previous time step (n) and the new time step (n+1). In explicit schemes, it involves values from the previous time step only. Implicit schemes are of greater theoretical accuracy. However the approach also implies that at each new step, the solution cannot proceed through the computational grid one node (or finite volume) at a time, and that a system of algebraic equations covering the entire computational domain must be solved. Explicit schemes (which represent the vast majority of newly developed schemes) are simpler to implement. However, they are subject to some form of time-step limitation (for stability) analogous to the CourantFriedrichs-Lewy condition ($u.\Delta t/\Delta x<1$). Implicit schemes are not subject to such stringent limitations, but time steps are nevertheless limited by considerations of accuracy.” “Although implicit schemes are more stable than explicit ones, it is virtually impossible to ensure the complete stability of any of them. Particular instability problems may arise in both schemes when the input data contains rapid changes and in the transition between pressurised and free-surface flow.”

It would seem that implicit methods are superior in terms of providing larger time steps and faster execution speeds. However, the speedup can’t be realised in most of practical cases:

- implicit methods typically require 5 – 10 times more work for each time step; consequently time step should be 5 – 10 times larger than for the explicit methods which may be difficult for accuracy reasons; however, when only stationary solution without time evolution such as flood extent during peak flow is required this can be obtained very efficiently with implicit methods

- programming of implicit methods is much more resource intensive than explicit methods; this time could be dedicated to developing model applicability, robustness etc. instead
- code is much less transparent than with explicit methods
- inclusion of specific boundary values, structures, conditions and processes becomes in many cases difficult
- code flexibility is decrease and additions to the model can become major tasks.

In some models like TELEMAC where resolution can be extremely high the implicit method becomes more justified and even necessary (**Figure 204**).

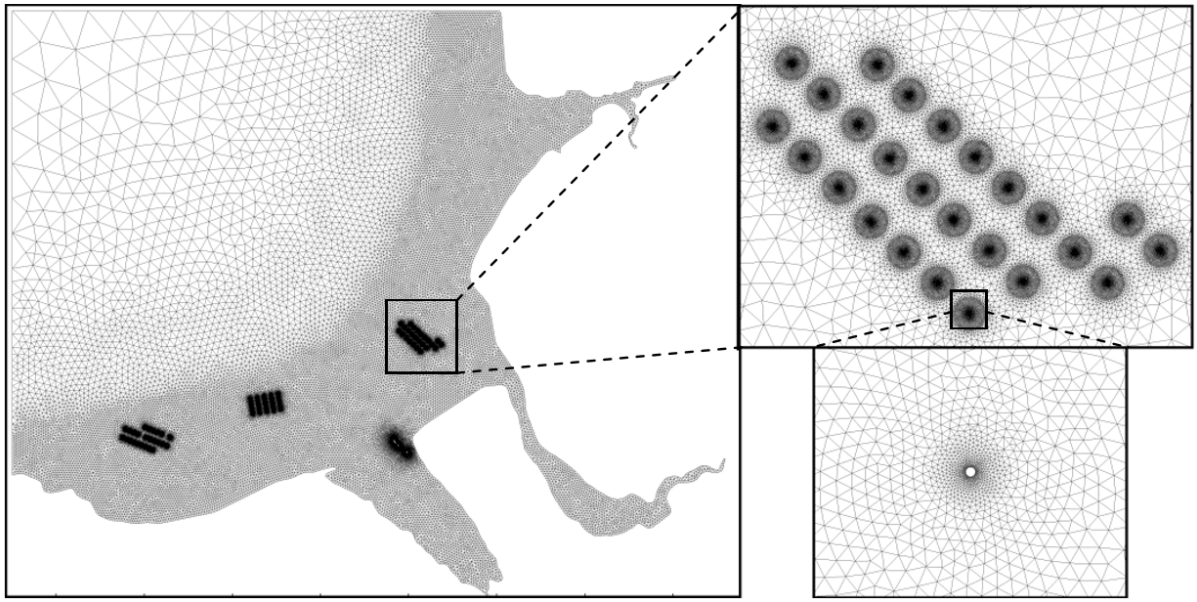

Figure 204. High resolution Liverpool Bay TELEMAC 2D mesh, with wind farm locations highlighted.

The above TELEMAC grid is an example of unstructured grid. Another computationally more effective approach is to use nested modelling to increase focus on area of interest (**Figure 205**).

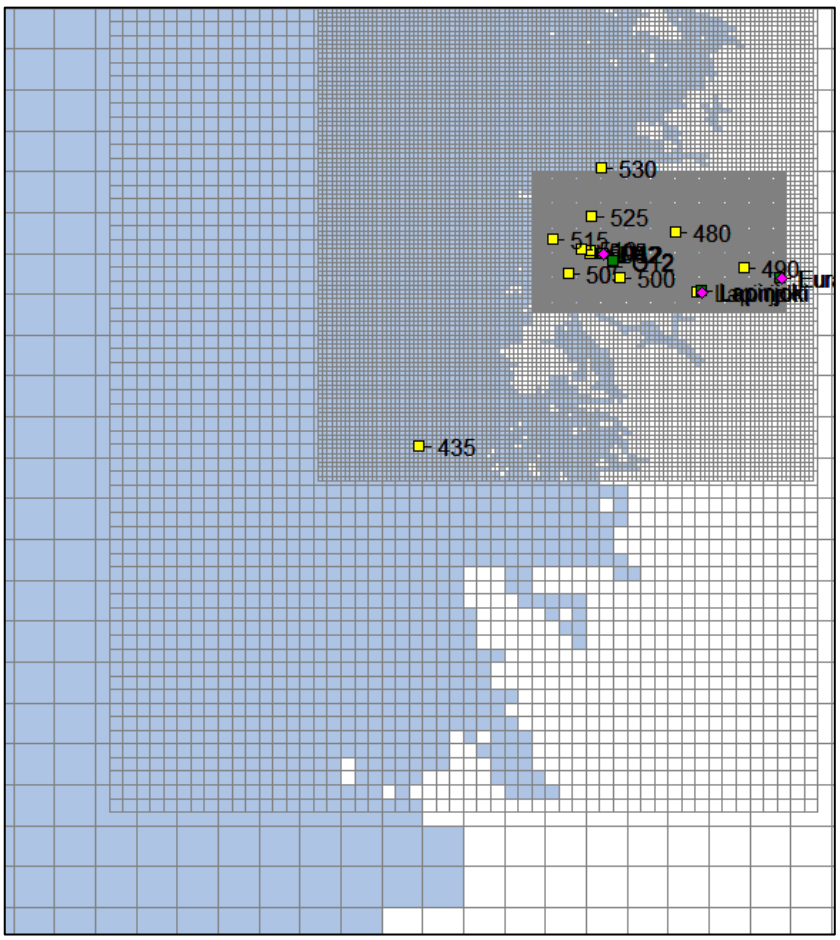

Figure 205. Grid nesting in the 3D-EIA model.

Test 4 of the benchmark study is presented below to compare EIA-2D/3D with other model. The test consists of a flat horizontal floodplain of dimensions 1000m x 2000m, with a single inflow boundary condition, simulating the failure of an embankment by breaching or overtopping, with a peak flow of 20m^3/s and 5h duration. The boundary condition is applied along a 20m line in the middle of the western side of the floodplain. The objective of the test is to assess the package's ability to simulate the celerity of propagation of a flood wave and predict transient velocities and depths. It is relevant in particular to the modelling of fluvial and coastal inundation resulting from breached embankments. (see **Figure 206**).

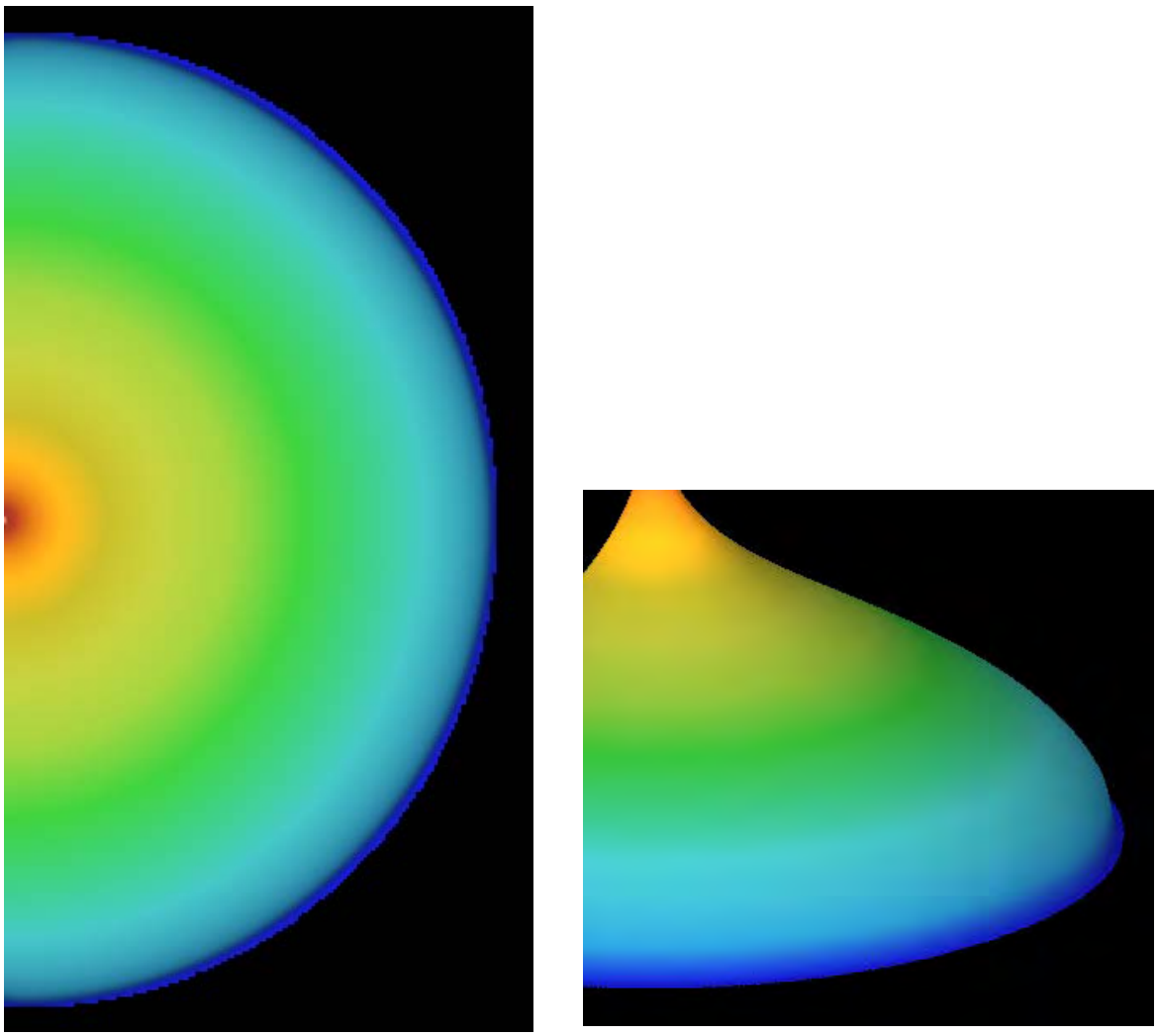

Figure 206. Benchmark case study no 4 of a dam overtopping/ break. Figure shows modelled water levels after the break. Left figure: 3D-EIA computed water levels from above, right: same as a side view.

The case study results are compared in **Figure 207** and **Figure 208**. In the first figure the contour lines after 1h and 3h are compared. In the second figure water depth time series is compared. It should be noted that 3D-EIA/1D compares well with the other model results. In the time series water arrives to the time series point at 50 minutes and the peak 0.18 m is at 250 minutes.

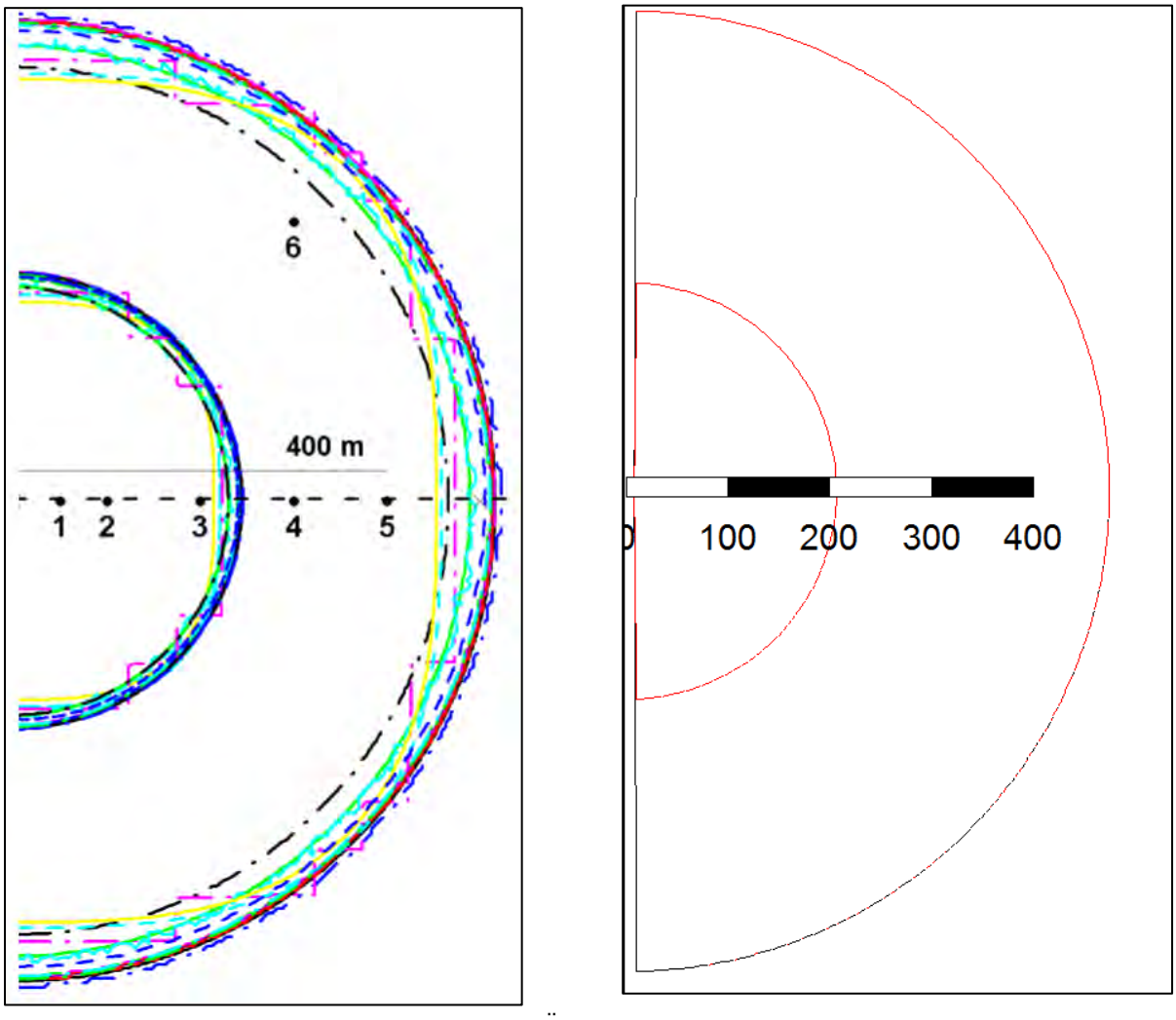

Figure 207. 0.15m depth contours at times 1h (smaller half circles) and 3h (larger half circles). Left the benchmark study models, right 3D-EIA/2D.

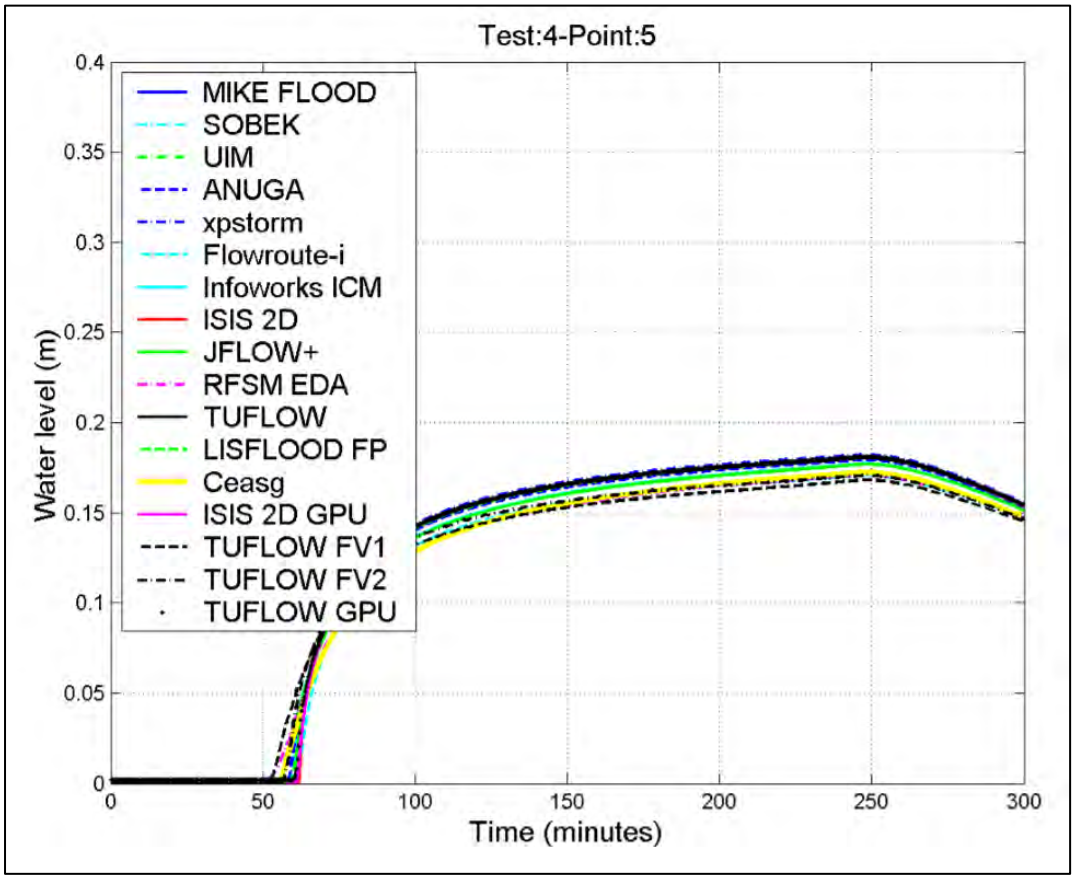

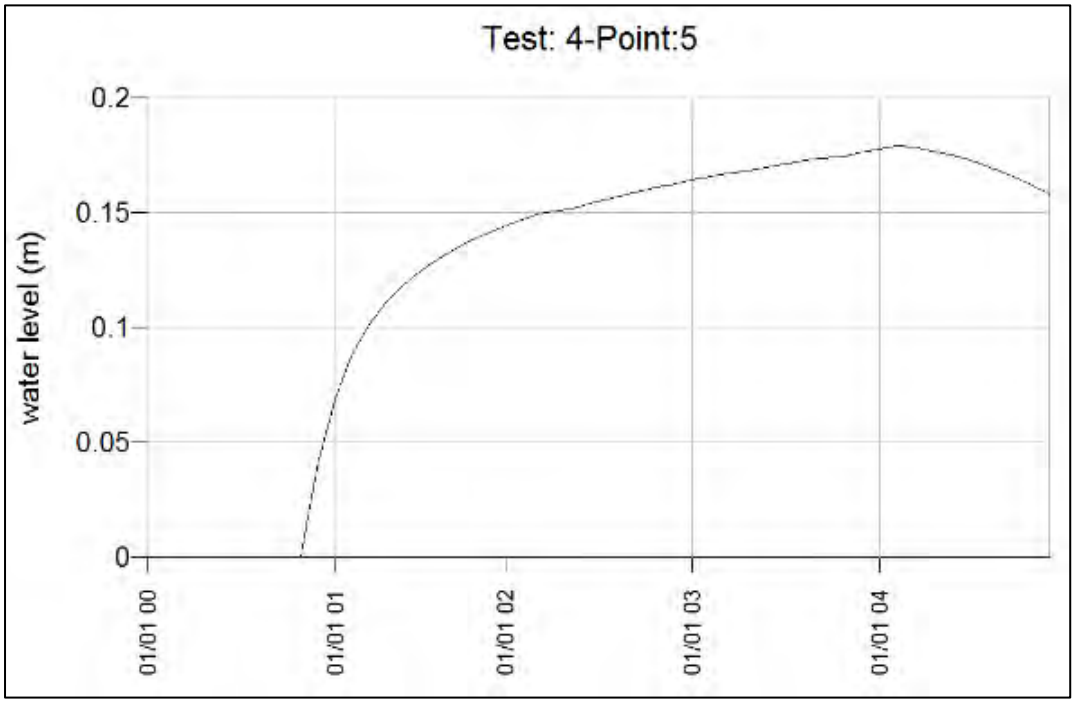

Figure 208. Computed water levels (depths) 400 m from the dam break site. Above benchmark study results, bottom 3D-EIA/2D.

Table 7. Benchmark study Case 4 computation times.

(1) Name	(2) Version	(3) Multi-processing	(4) Grid resolution (expected: 5m or 80,000 elements)	(5) Time-stepping	(6) Run time
ANUGA	1.1beta_7501	No	80,149 elements	Adaptive	3650s
Ceasg	1.12	Yes – GPU	5m	0.5s	72s
Flowroute-*i*™	3.2.0	Yes – 4 CPUs	5m	Adaptive	21s
InfoWorks ICM	2.5.2	Yes – GPU	79,857 triangles	20s	44s
ISIS 2D	3.6 (ADI)	Partial [1]	5m	5s	82s
ISIS 2D GPU	1.17	Yes	5m	Adaptive	25s
JFLOW+	2.0	Yes – GPU	5m	Adaptive Average 0.9s	17.6s
LISFLOOD-FP	5.5.2	Yes	5m	Adaptive	21s
MIKE FLOOD	2012	Yes – 8 CPUs	5m	10s	32.1s
RFSM- EDA	1.2	No	861 [1]	Adaptive, typically 12s	13s
SOBEK	2.13	No	5m	2s	1014s
TUFLOW	2012-05-AA Single precision	No	5m	Adaptive (1–30s)	47s
TUFLOW GPU	2012-05-AA	Yes – 448 GPU cores	5m	Adaptive (0.8–1.7s)	25s [2]
TUFLOW FV [3]	2012.000b First order (and second order)	Yes – 12 CPU cores	5m	Adaptive (~0.7s) (~0.4s)	142s (481s)
UIM	209.12	OMP	5m	0.1s	17,000s
XPSTORM	2011 2010-10-AB-iDP-w32	No	5m	5s	84s

Table 8. 3D-EIA/2D Case 4 computational times.

EIA-3D version	characteristics	Runtime 2820QM	Estimated runtime I7-4790K	parallel processing
2D no connective accelaration	time-steps 3 s, flooding 20 s	180 s	90 s	45 s
2D convective accelaration	time-steps 3 s, flooding 20 s	190 s	95 s	43 s
3D	external time step 3 s; k-ε turbulence model, internal field, bottom friction time	460 s	230 s	115 s

Table 7 and 8 compare computation times between the benchmark models and 3D-EIA/2D. Compared to the models that don't use multiprocessing EIA base model speeds 180 s – 190 s compare well considering the processor used (2820QM) is 5 years old. Modern desktop processors are about twice as fast and would require 90 – 90 s computation time. The non-multiprocessing models SOBEK requires 1014s, ANUGA 3650s, TUFLOW 47s and XPSTORM 84s. 3D-EIA/2D includes parallelisation (multiprocessing) but it has not yet been adopted to the flood modelling option as the parallelism is based on division of the active computation domain and it is changing constantly with flooding. It is to be expected that computation times are halved when parallelism is implemented resulting in 43s – 45s execution times. These compare favourably to the other model parallel execution times.

The 3D-EIA model run times can't compete against dedicated 2D flood modelling software for very large applications consisting of millions of grid cells. The dedicated modelling depends on specialized solution algorithms (e.g. implicity and multigrid) and/or massive parallelism requiring homogenised equations. At the same time applicability of the dedicated models is constrained. For instance most of the cases they have restrictions for 3D, water quality, boundary values, coupling with 1D river models, treatment of hydraulic structures, advanced friction and diffusion terms, momentum advection etc.

7.4. Justification for use of 3D approach

The two figures below illustrate rationale for **3D hydrodynamic** modelling in comparison to 2D one. The first one shows effect of vegetation on the flow and the second effect of stratification on flow.

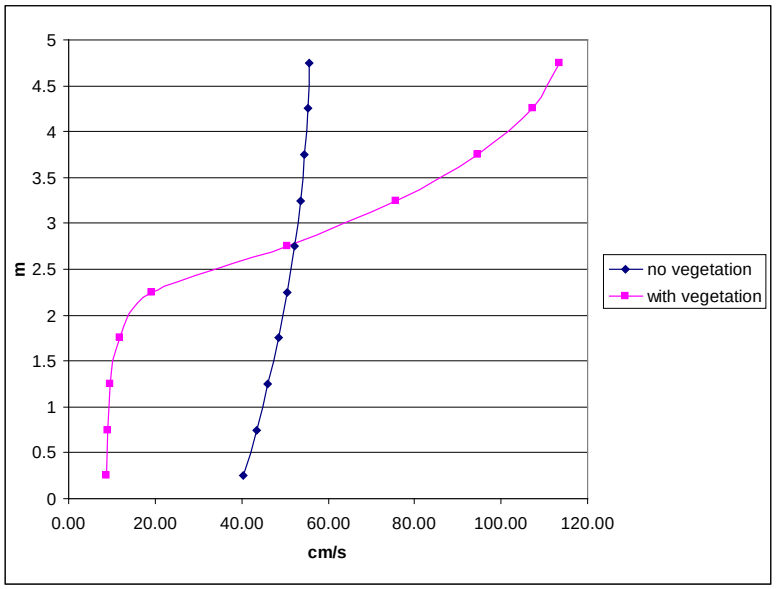

Figure 209. Impact of vegetation friction on simulated vertical flow profile (3D-EIA model). Vegetation height 2 m. Nonlinear bottom friction 0.005 and vegetation friction 0.1.

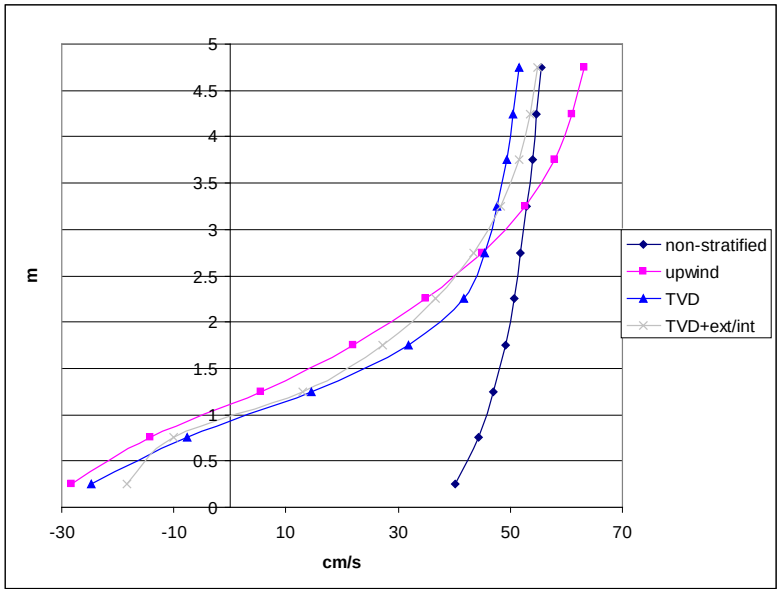

Figure 210. Vertical velocity distribution in strongly stratified situation. Observe that the stratified flow includes return flow. The stratified case has been computed with different transport methods.

The main benefit of 3D flood modelling comes for erosion, sedimentation, productivity and water quality description. These require 3D description as has been demonstrated in detail by the MRC WUP-FIN Tonle Sap modelling project 2001 – 2003 and continued until 2015 together with other MRC modelling activities.

7.5. Coupled 1D/2D/3D hydrodynamic modelling

Coupled 1D-3D modelling is required fully physical and accurate description of the Delta channel-floodplain-coastal system description. It has proposed to the countries that this approach would be implemented in possible next phase of the Council Study.

There exists large number of **1D hydrodynamic** models for river channel flow and water levels. Here 1D Rnet under the IWRM modelling framework has been selected for combining with the 3D model because:

- licence fee free
- works with same data formats as the other selected IWRM tools
- works under same data processing and user interface software as the other selected IWRM tools
- can be coupled with the 2D and 3D flood models under the IWRM framework
- is compatible with the MIKE21 and HEC-RAS schematization; in other words can import and export the schematization
- very fast model construction when data in suitable format is available
- modest data requirements.

However, the IWRM flood modelling system has been built in a way that the 1D Rnet can be replaced in principal with any other model such as the ISIS. This applies for coupling also when 1D model source code is available or common data exchange method can be defined.

The complex nature of the floodplain flow is exemplified in **Figure 211**. The MRCS Flood and Mitigation Programme report “Hydrological and Flood Hazards in the Focal Areas” (2010 Deltares, Royal Haskoning and UNESCO IHE) recommends for Xe Bang Fai: “Develop a new 1D/2 D hydraulic model of the lower Se Bangfai including the Mekong from Nakhon Phanom to Mukhdahan. With the availability of the DEM and land use data the development of such a model is much easier than of a 1D-model as the riverfloodplain interaction is objectively derived from the DEM.” Referring to other parts of the report this emphasises that generation of a combined 1D/2D model is much easier than trying to schematize floodplain flow with a 1D model. This is because a floodplain 1D model set-up would require not only experienced modeller but also subjective and difficult choices for the schematization.

Facilitation of flood modelling is not the only reason for applying 2D or 3D floodplain modelling. It is obvious that impact on any structures to floodplain flow and flooding are practically impossible to estimate reliably with a 1D model. Also morphological, water quality and ecological assessments require 2D or 3D approach.

SOBEK and MIKE family of models are examples of coupled 1D/2D models. As far as known there exists no other coupled 1D/2D/3D model than the 3D-EIA/RNet combination. Although 3D modelling is not normally required for basic flood modelling it becomes necessary when morphological, water quality or environmental considerations are added to flooding.

An alternative way of modelling river channel-floodplain systems is to use adaptive grid that can focus with high resolution to river channels. An example of this is for instance TELEMAC 2D and 3D. The approach is applicable only for limited areas as the applications are computationally intensive.

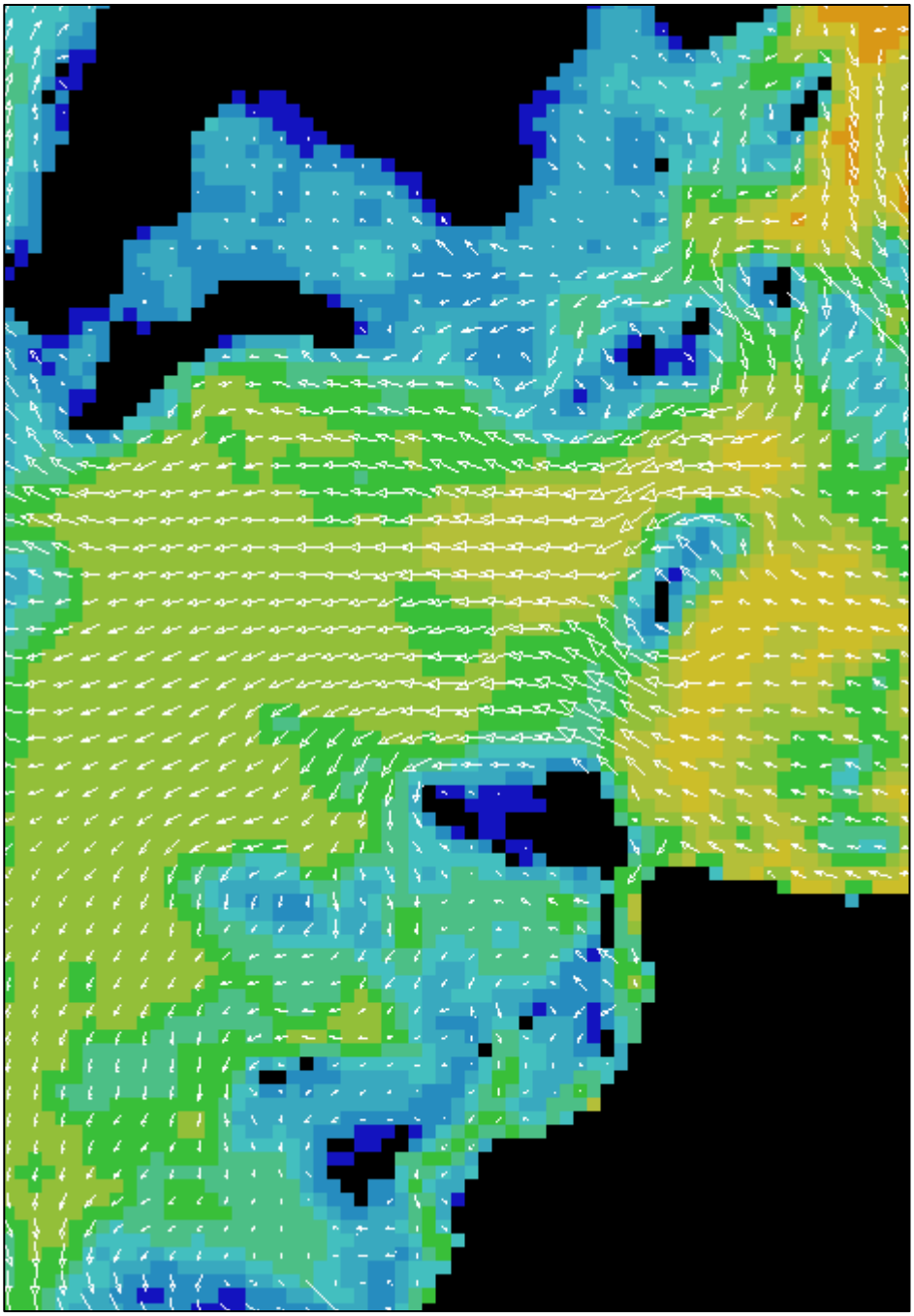

Figure 211. Modelled (3D-EIA) floodplain flow in the Xe Bang Fai. Colours show water depths.

A coupled 3D-EIA/1D RNet model is built with a few steps:

1. Develop and calibrate a 1D RNet model separately
2. Develop a 3D-EIA model separately
3. Place the applications into a same folder and run the 1D model for a short while to generate necessary model input files
4. From the RNet model menu export the 1D-3D grid connection file (Data/ Export grid connection file); software asks for the 3D model dimensions and lower left corner coordinates to generate the connection file; the 3D model information is available from menu Model/Grid parameters.
5. Run the I1d2d3d.exe model from the 3D-EIA user interface (Source data/Application setup/ Model executable); the executable automatically executes and synchronizes both the 3D and 1D models.
6. Compare modelled flooding to observations such as floodplain water depth monitoring or remote sensing images. Calibrate the floodplain friction affecting flood wave propagation based on this data.

The grid connection between the 1D and 3D models is crucial part of the combined model. **Figure 212** shows how the 1D and 3D models are connected through a broad crested weir formula for lower water levels. When bank or dyke is fully submerged weir formula is not used. The dyke or bank heights are prescribed in the 1D model as explained in the previous chapter. The weir formula and other aspects of model coupling are explained in detail in the RNet model help.

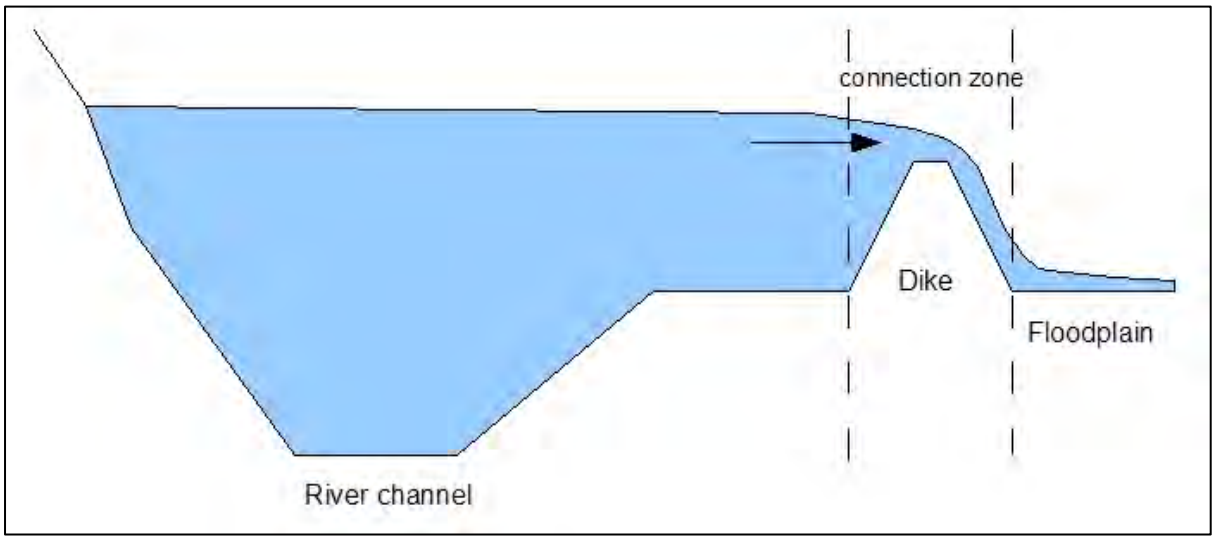

Figure 212. Coupled model 1D-3D connection.

During the Council Study the coupled 1D/3D model has been tested extensively and compared with other flood modelling software (see above) as well as further improved to maintain stability and accuracy in highly variable terrain and land use. Stability has been improved mainly through limiting of too small water depths in flooding and drying. Hundreds of model runs have been conducted to test model sensitivity for different parameters and finding of optimal combination of them. The work has resulted in a simple modelling implementation process where only friction parameters need to be calibrated. In addition to the basic linear and nonlinear flow friction coefficients there exists possibility

to set up land use dependent (vegetation) flow friction. The vegetation friction is not applied above prescribed vegetation height.

An example of coupled 1D/2D flood propagation modelling is shown in **Figure 213**. The snapshots are obtained from an animation that the 3D model during a computation.

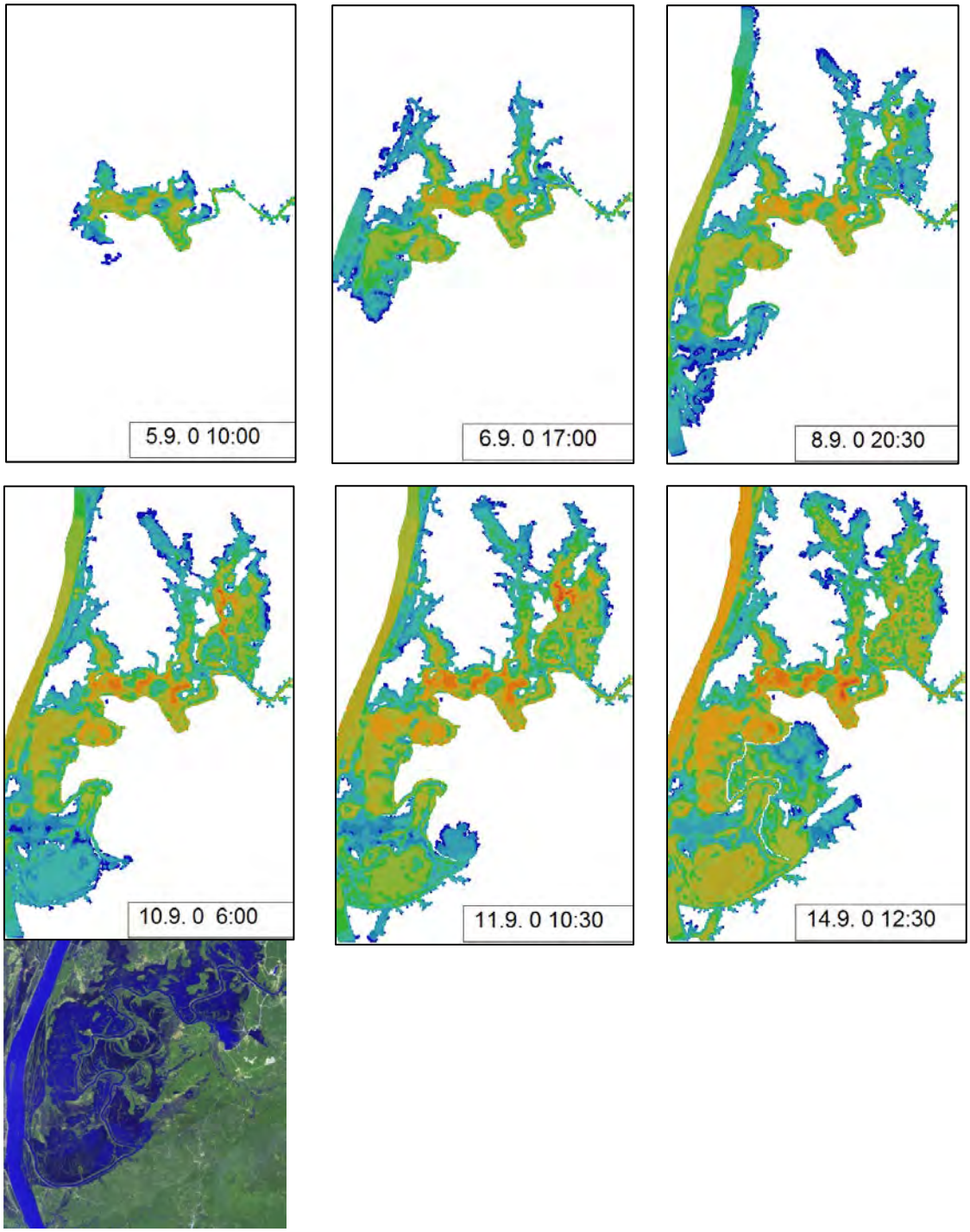

Figure 213. Snapshots from the modelled flood propagation animation. The last figure shows satellite picture of lower Xe Bang Fai flooding taken September 17th 2000 (source Hydrological and Flood Hazards in the Focal Areas, MRCS Report May 2010).

7.6. Floodplain sedimentation

Floodplain sedimentation has important implications for floodplain morphology and productivity. In the flood mapping annex a simple floodplain bulk sedimentation methodology is described. However, it is necessary a rough rapid assessment tool because it doesn't take into actual floodplain flow and sedimentation patterns that can be highly variable. Also the rough estimate doesn't describe spatial sedimentation distribution. For instance in the Tonle Sap floodplains sedimentation has formed natural levees along the lake edges. Below procedure and results for floodplain 1D/2D/3D sedimentation computation are described that are used for the Delta Impact Model calibration and validation.

To set up the 1D RNet model for sediment computation one needs to follow these steps:

1. Go to the Data/ Water quality variables and add a variable of name TSS, SSED, SS0 (clay), SS1 (silt) or SS2 (sand)
2. Add a load point to the upper part of the river with the "Add data item" button (**Figure 214**)
3. Give the name of the time series file of sediment loads obtained from modelling or rating curve (see previous chapters); here TSS load is given and it is multiplied by 0.6 to get silt portion; the computation variable name (step 1), load variable name and name in the txd-file should be the same
4. One can select in the "Model/ Computation parameters" menu either diffusive upwind or non-diffusive FC (Flux Corrected) method.

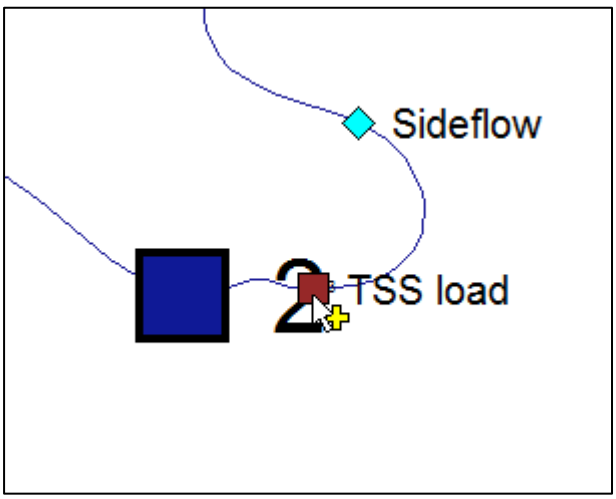

Figure 214. Addition of a sediment load file to the model.

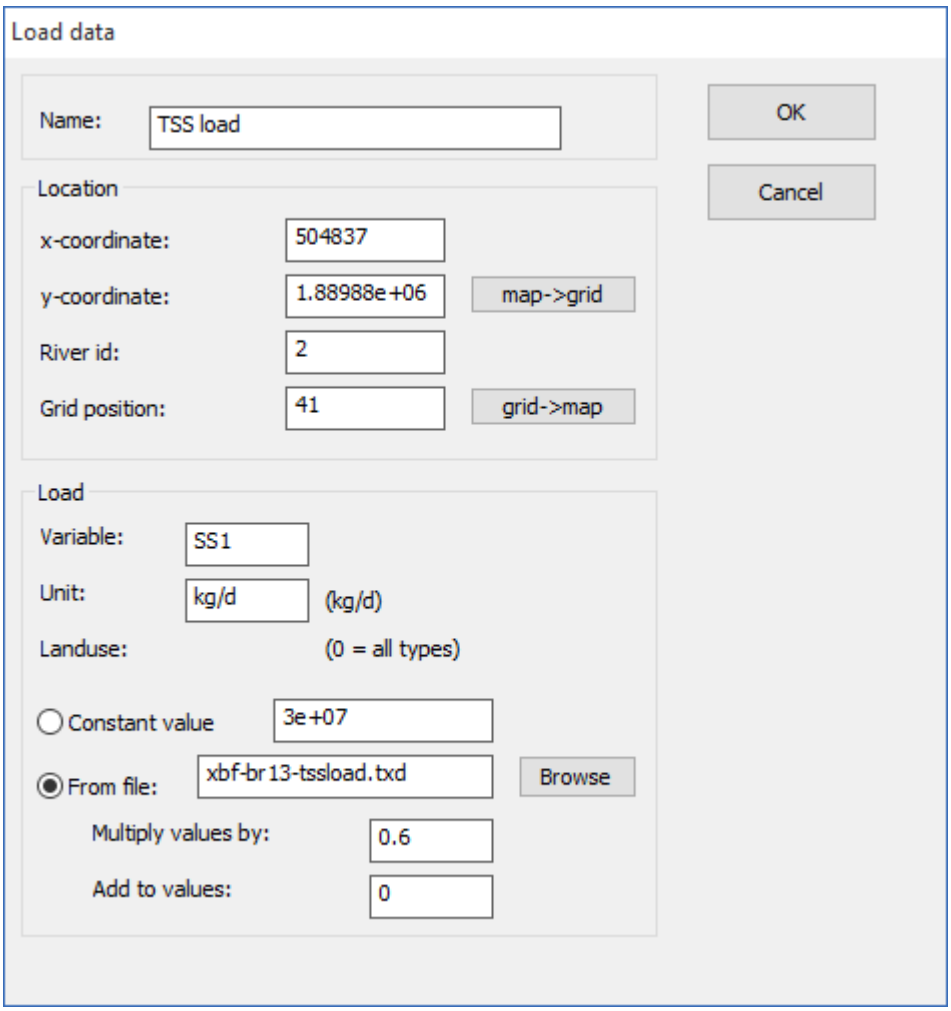

Figure 215. Sediment and water quality load dialogue window in the 1D RNet model user interface.

The concentration parameter names in the 1D and 3D model don't need to be the same as the model consideres only order in the coupling.

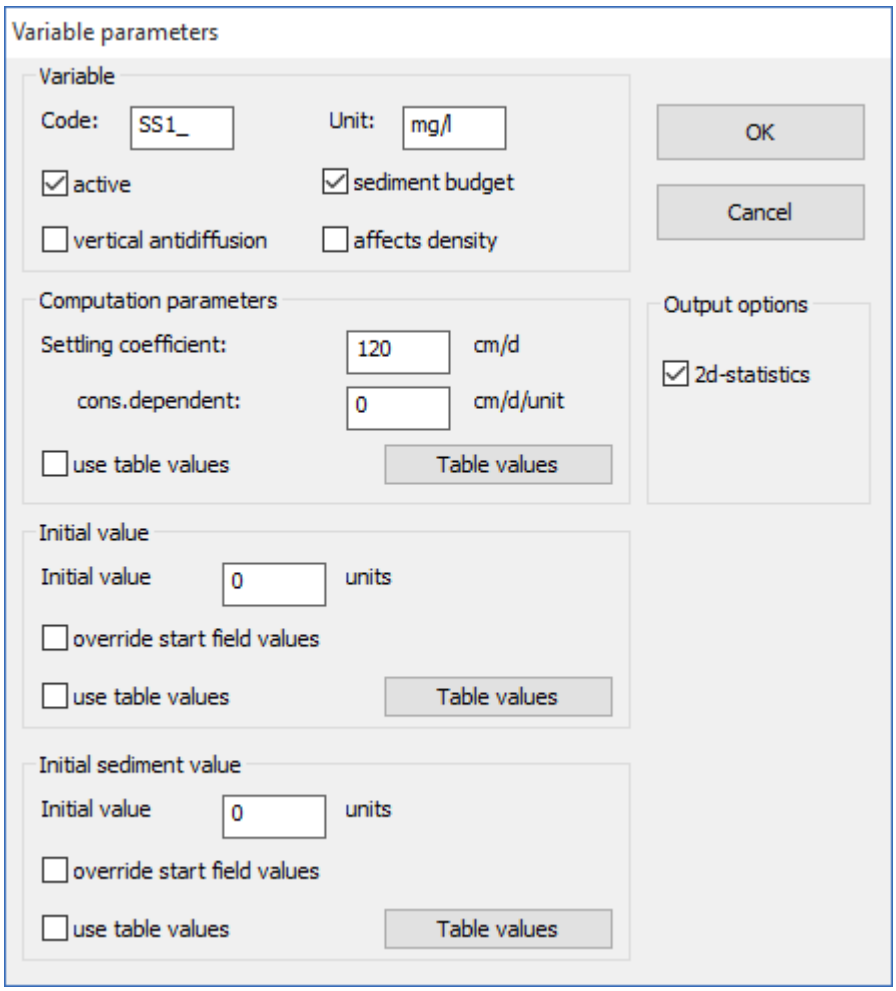

Figure 216. Sediment and water quality variable dialogue window in the 3D-EIA model user interface.

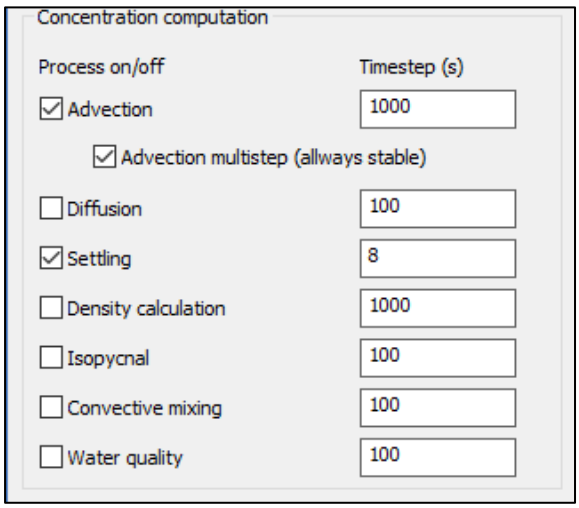

Figure 217. 3D-EIA model concentration computation time steps.

Figure 218 shows computed silt sedimentation for the period 1.9.2000 – 14.9.2000 and **Figure 219** corresponding average concentrations. One should observe that areas of high concentrations on the floodplain depend on water spilled from the river and the amount of spilled water diminishes as the water levels on the floodplain and the river level off. Thus the situation is highly dynamic as can be seen from the snapshot **Figure 220** on 13.9. In the figure Northern spillage has been diminished and the Southern major spillage is increasing.

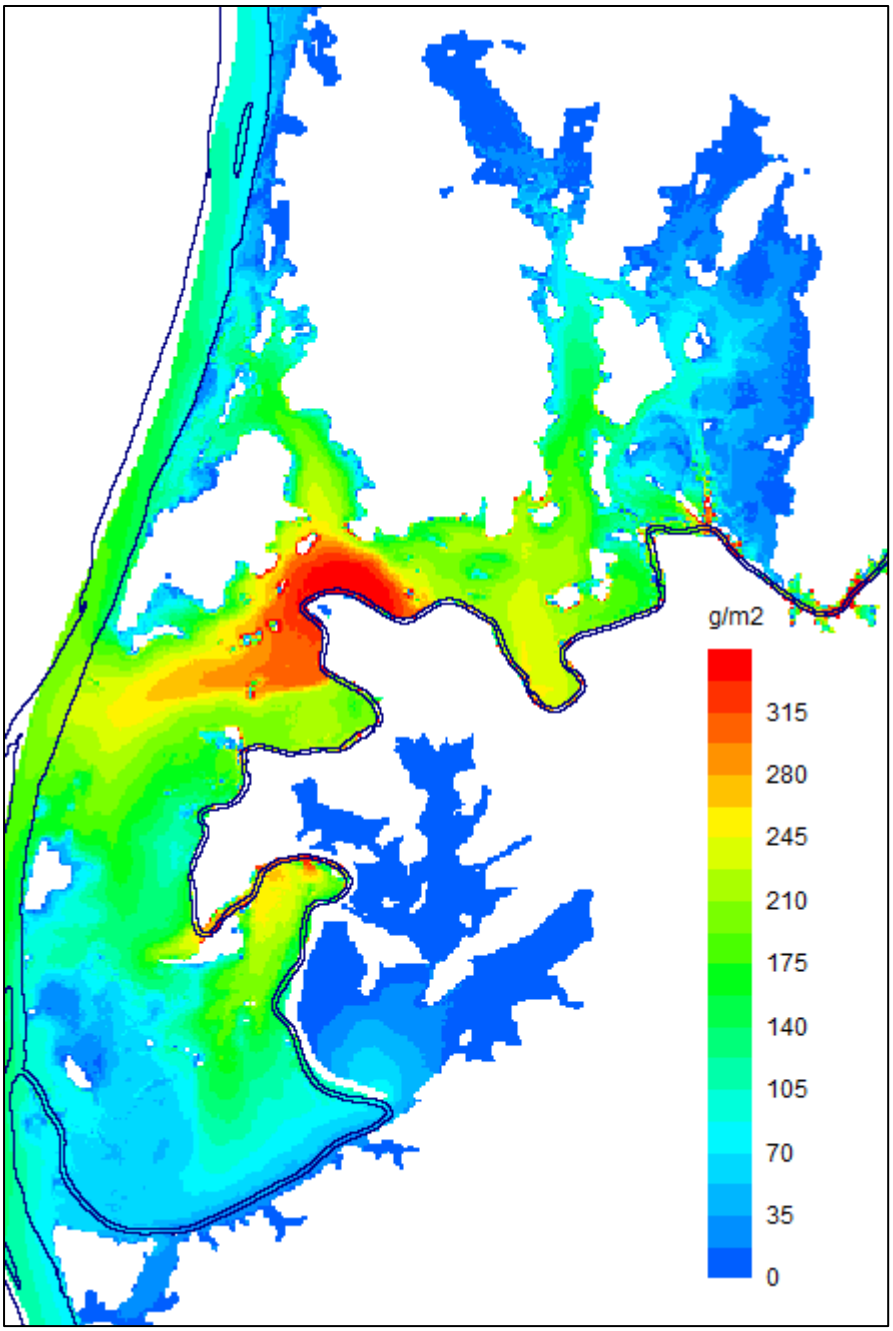

Figure 218. Simulated floodplain silt sedimentation during period 1.9.2000 – 14.9.2000.

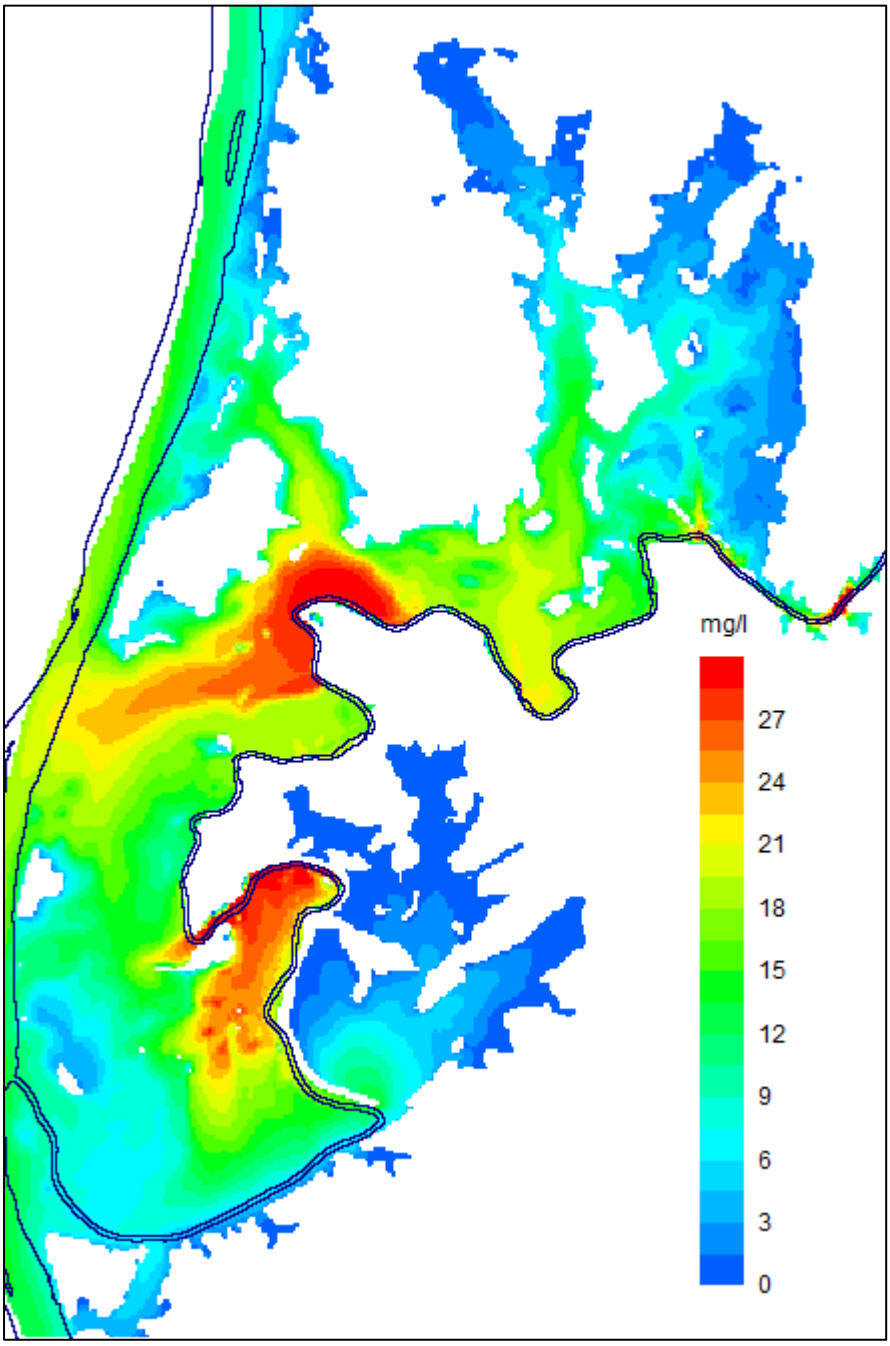

Figure 219. Simulated average silt concentration during period 1.9.2000 – 14.9.2000. River sediment load obtained from USGS LOADEST rating curve.

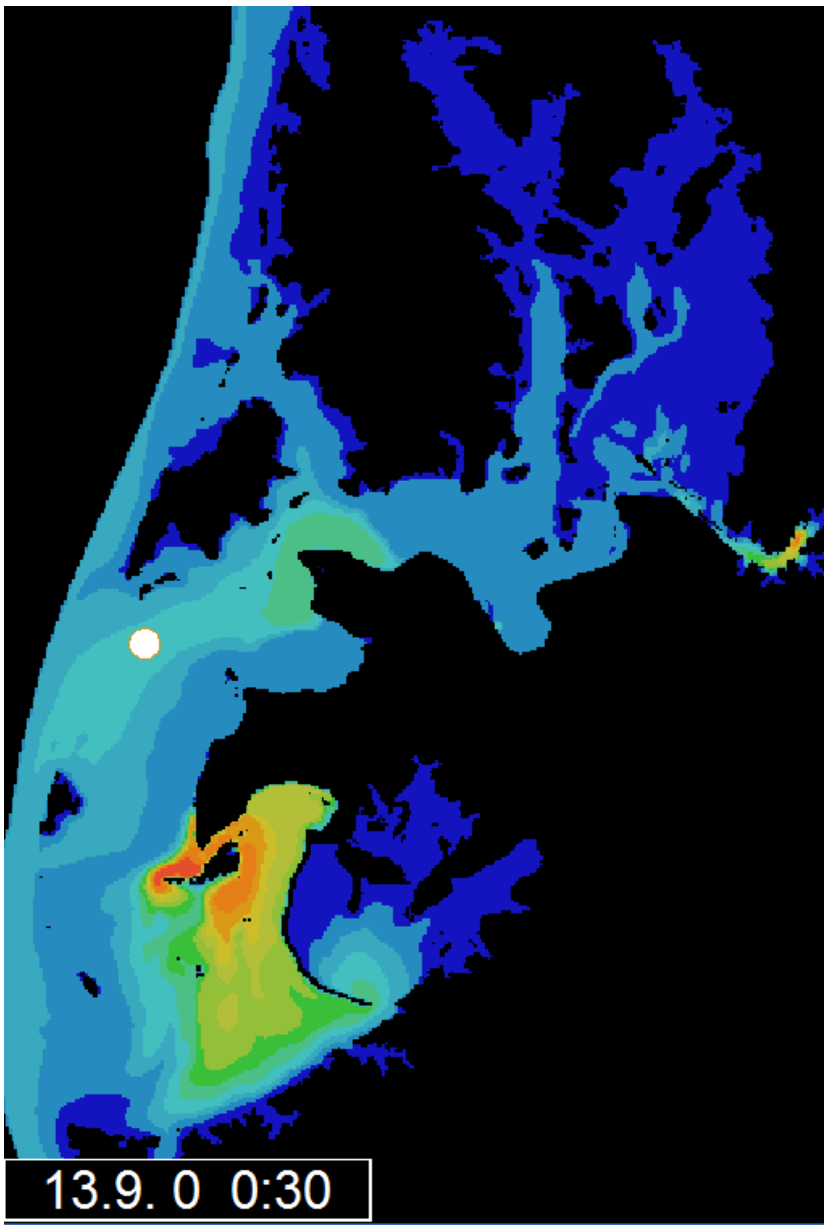

Figure 220. Simulated silt concentration on 13.9.2000. Compare to the previous figure.

8. Annex 8 - 3D Tonle Sap Productivity Model Description and Validation

8.1. Periphyton

The primary and fish production model is presented in detail in Koponen, Lamberts et al. 2010.

Several definitions are in use for the heterogeneous associations of organisms embedded in a mucous matrix of up to 5 mm thick found on most submerged substrates. Common in all definitions of periphyton is that there is a matrix of polysaccharides which may contain heterotrophic bacteria, cyanophyceae, algae, fungi and detritus, attached to a substratum. Periphyton of the Tonle Sap ecosystem is either epiphytic (using plants as substrate) or epipelic (growing on sediments). It is unclear how well periphyton can become established in the dynamic environment of the lake bottom with constantly re-suspended sediments. There is no literature on the periphyton of the Tonle Sap ecosystem. Its presence on submerged surfaces, however, is conspicuous (Figure 221). Colonisation of newly submerged surfaces and maturation of a periphyton community takes about two weeks (Van Dam et. al. 2002).

Figure 221. Left: periphyton on the bamboo bars of a fish cage in Tonle Sap lake. Right: phytoplankton blooms in the north-western part of the Tonle Sap lake during low water (depth approx. 60 cm) in late April 2005.

Periphyton production depends on the presence of a suitable substrate, nutrients, water quality, the exposure time to light and the time since colonisation. The general equation for annual periphyton production in the ecosystem is:

$$PP_{PF} = PPY_{PF} \cdot \sum_{i=1}^{n} \sum_{j=1}^{365} SA_i \cdot ZE_{i,j} \cdot AD_{i,j} \cdot ET_j \qquad \text{(Eq. 3)}$$

where PP_{PF} is the annual primary production by periphyton in the ecosystem (mg C), PPY_{PF} is primary productivity by periphyton (mg $C.m^{-2}.h^{-1}$), n is the number of grid cells, SA_i is the surface area (m^2) of grid cell *i*, $ZE_{i,j}$ is the euphotic depth (m) of cell *i* on day *j*, $AD_{i,j}$ is the area density (m^{-1}) of cell *i* on day *j* and ET_j is the exposure time (h) to light on day *j*. The impact of other factors such as nutrients, water quality and population composition are reflected in the productivity rates PPY_{PF}. The area density factor describes the substrate surface area per volume of space in the ecosystem. This area is provided mostly by rooted macrophytes and the bottom area.

8.2. Phytoplankton

Phytoplankton consists of photo-autotroph or mixotroph prokaryotic bacteria and eukaryotic protists (unicellular organisms) that form part of the seston. Phytoplankton production and biomass is influenced by six direct, primary factors: temperature, mixed water depth, hydraulic exchange, light penetration, nutrient concentrations and (zooplankton) feeding. The general equation for annual phytoplankton production in the ecosystem is

$$PP_{PP} = PPY_{PP} \cdot \sum_{i=1}^{n} \sum_{j=1}^{365} SA_i \cdot ZE_{i,j} \cdot ET_j \qquad \text{(Eq. 4)}$$

where PP_{PP} is the annual primary production by phytoplankton in the ecosystem (mg C), PPY_{PP} is primary productivity by phytoplankton (mg $C.m^{-3}.h^{-1}$), and the other factors are as described in the periphyton equation.

8.3. Rooted macrophytes

Rooted macrophytes have been grouped as primary producers because of their immobility and overall vertical growth. Floating vegetation, in contrast, is mobile and will expand horizontally rather than vertically, which has implications for the modelling of primary production.

Three main macrophyte vegetation types are distinguished: short-tree and shrubland vegetation with grasslands, forest, and aquatic herbaceous vegetation, together comprising at least 190 species. Based on primary production rates that are average for a year by rooted macrophytes and the area they occupy, it is possible to calculate primary production by rooted macrophytes for an ecosystem for a one year production time. The general equation for the model of primary production by rooted macrophytes in the ecosystem is:

$$PP_{RMP} = \sum_{i=1}^{n} PPY_{RMPi} \cdot SA_i \cdot t_i \qquad \text{(Eq. 5)}$$

where PP_{RMP} is primary production by rooted macrophytes (g C), PPY_{RMPi} is the average daily primary productivity by rooted macrophytes for grid cell *i* (g $C.m^{-2}.day^{-1}$), SA_i is surface area (m^2) of grid cell *i* and t_i the number of non-flooded days of cell *i* in that year, i.e. for which z = 0. The assumptions are that when flooded, primary production stops, and resumes when the flooding ends. Part of the macrophytes production is assumed to be available for fish production either directly or indirectly through invertebrate consumption after flooding. PPY_{RMPi} is assumed equal to zero in places that are permanently flooded:

$$e_i \le ALW : PPY_{RMPi} = 0 \qquad \text{(Eq. 6)}$$

with e_i the elevation above sea-level of cell *i*, and ALW the average low water level for the ecosystem.

8.4. Ecosystem productivity

Ecosystem production is based on and limited by the total endogenous production and import of organic matter. The primary products basis for the aquatic food webs of the Tonle Sap ecosystem is:

$$SPB = PP_{PF} + PP_{PP} + PP_{RMP} \cdot f_T + PP_{FMP} \cdot f'_T + OM_{EXO} \qquad \text{(Eq. 7)}$$

where SPB is the secondary production basis (g C), PP_{PF} is periphyton primary production, PP_{PP} is phytoplankton primary production, PP_{RMP} is rooted macrophytes primary production, f_T is the transferability factor for rooted macrophytes, PP_{FMP} is floating macrophytes primary production, f'_T is the transferability factor for floating macrophytes and OM_{EXO} is exogenous organic matter.

During the dry season before the flood waters enter the Tonle Sap, the lake is shallow, turbid and nitrogen limited. Cyanobacteria (blue-green algae) can thrive in these conditions. Some cyanobacteria species can move towards the surface by oscillating filaments or gas vesicles. In these conditions the effective light penetration should be increased or the cyanobacteria movement included in the model.

The productivity model described above was adapted to the 3D-EIA model framework, and specifically to the Tonle Sap application. Contribution by PP_{FMP} and OM_{EXO} are assumed to be minor compared to the other production components and there are not included in the 3D model.

8.5. Sediment concentration and light penetration

The 3D-EIA model has two options for calculating the productive layer. The first method is euphotic depth approach which doesn't distinguish light penetration or productivity differences within the productive layer. The depth of the euphotic layer can be assumed to be same as Secchi depth. The second method applied in the simulation model is to calculate light penetration distribution in the water column. The light penetration depends on the Secchi depth/ water clarity.

In both methods one has to estimate Secchi depth. It is assumed that the Secchi depth depends on water turbidity, and water turbidity in turn depends primarily on Total Suspended Solids (TSS) concentration. In reality other factors such as phytoplankton concentration affect turbidity, but they are ignored in the current formulation. WUP-FIN project has done simultaneous Secchi depth and TSS measurements in 2001 – 2002. Some of the measurements and exponential fit are shown in Figure 222. The form of the exponential fit is:

$$S_d = \alpha e^{-\beta c}$$

- S_d = Secchi depth
- α, β = estimated parameters
- c = TSS concentration

The values found for α and β in the Tonle Sap case are 250 cm and 0.054 $(mg/l)^{-1}$ respectively.

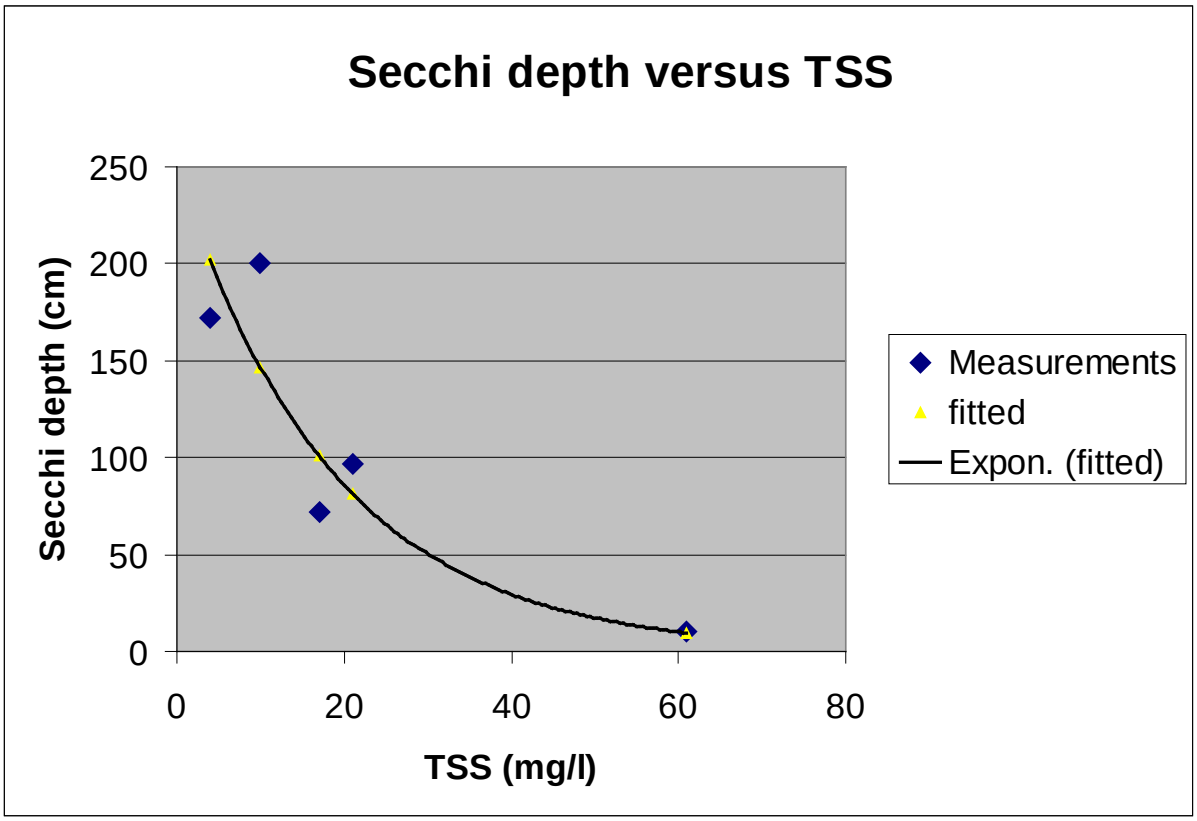

Figure 222. Secchi depth as a function of Total Suspended Solids (TSS) concentration. Exponential fit shown.

Light penetration/ attenuation is modelled after short wave radiation intensity in the water column:

$$I = I_0 e^{-\beta z}$$

- I = light intensity at depth z
- I_0 = light intensity on the surface of the water column
- $\beta = 1.65/S_d$

In the model average light intensity for each model layer is estimated from the above equation.

8.6. Land use class dependent parameterisation

The land use classes used in the Tonle Sap model are based on 2000 JICA data and classification as well as MRC 2010 land cover classification. Only the main classes are used and the original JICA classes are aggregated:

1. agricultural land (until JICA type 11)
2. grassland (until JICA type 17)
3. shrublands (until JICA type 21)
4. forest (until JICA type 32)
5. water (until JICA type 37)
6. soil and rocks (until JICA type 40)
7. urban areas (until JICA type 59).

Productivity model parameters can be given separately for each land use class. The most obvious examples are vegetation height and leaf area index (area of leaves and branches compared to the corresponding ground area). Both impact periphyton production by defining how much area is available for periphyton.

Figure 223 shows some of the land use dependent model parameter values. For the productivity model following parameters are important:

- h (vegetation height in m)
- Pe (periphyton productivity in mgC/m2/hr)
- LAI (Leaf Area Index)
- Py (phytoplankton productivity in mgC/m3/hr)
- Pt (terrestrial vegetation productivity in mgC/m2/hr).

In testing the model these parameter values except vegetation height have been kept constant for all land use classes.

Land use parameters

	until type	h m	cov (0-1)	drag	SOD mg/m2/d	aere (0-1)	Pe mgC/m2/h	LA
0	2	1	0.6	0.3	0.5	0.4	200	6
1	11	1	0.9	0.3	1.2	0.3	200	6
2	17	0.5	0.8	0.3	1	0.9	200	6
3	21	5	0.7	0.6	1.4	0.2	200	6
4	32	12	0.6	0.5	1.1	0.1	200	6
5	37	0	0	0	0	1	200	6
6	40	0.2	1	0.05	0.05	1	200	6
7	59	0	0	0	0	1	200	6

Ok
Cancel
Insert Line
Remove Line

Figure 223. Model land use classes (left column) and part of the corresponding parameter values.

8.7. Periphyton model formulation

The equation used for periphyton in the model is:

$$PP_{PF} = PPY_{PF} \cdot LAI \cdot e^{\beta(\frac{t_w - T}{T})} ET \cdot f_E$$

- PP_{PF} = periphyton primary production per unit area (mgC/m^2)
- PPY_{PF} = periphyton primary productivity (mgC/m^2/hr)
- LAI = Leaf Area Index
- β = growth exponent coefficient
- t_w = wetting time (d); if $t_w > T$, t_w is set to T in the equation
- T = growth time scale (d)
- ET = exposure time (hr)
- f_E = euphotic factor, ≤ 1.

The model values for β and T have been tentatively set to 3 and 14 (d) respectively (Figure 224). In the model ET is calculated from the sun's angle over the horizon. When sun is near or below horizon the exposure time is assumed to be zero. Otherwise the exposure time is added. The angle is calculated from latitude, longitude and time of the day.

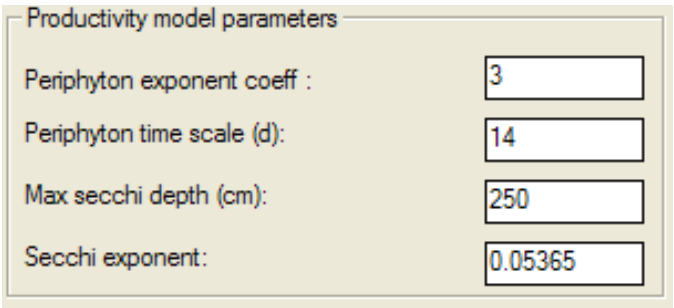

Figure 224. Model values for land use class independent parameters.

The euphotic factor can be estimated to be:

$$f_E = \frac{z_E}{z_{\max}}$$

- z_E = euphotic depth = Secchi depth (m)
- z_{max} = maximum water depth (m).

z_{max} is calculated in each grid cell separately by subtracting ground elevation from Tonle Sap maximal water level 10.5 m. Another possibility would be to use each year's maximal water depth, but this would enhance production in dry years compared to the wet ones.

Another option is to calculate the euphotic factor for each model layer based on light penetration and wetted vegetation height:

$$f_E = e^{-\beta z} D_w / H_v$$

- β = 1.65/S_d
- z = characteristic light penetration depth for the layer (m)
- D_w = wetted vegetation height in a layer (m).
- H_v = vegetation height (m)

The first factor takes into account attenuation of light, the second one calculates what proportion of *LAI* is available in any layer for periphyton.

It is assumed that there is no periphyton on the lake bottom. Otherwise it is assumed that ground is also available for periphyton production in addition to vegetation.

8.8. Phytoplankton and terrestrial vegetation model formulation

Phytoplankton model formulation is:

$$PP_{PP} = PPY_{PP} \cdot ET \cdot f_E$$

- PP_{PP} = periphyton primary production per unit area (mgC/m^2)
- PPY_{PF} = periphyton primary productivity (mgC/m^3/hr)
- ET = exposure time (hr)
- f_E = euphotic factor.

The euphotic factor for each model layer is based on light penetration and vegetation height:

$$f_E = e^{-\beta z} D$$

- β = 1.65/S_d
- z = characteristic light penetration depth for the layer (m)
- D = model layer thickness (m).

The formulation for the terrestrial vegetation production is:

$$PP_{RMP} = PPY_{RMP} \cdot ET$$

- PP_{RMP} = terrestrial vegetation primary production per unit area (mgC/m^2)
- PPY_{RMP} = terrestrial vegetation primary productivity (mgC/m^2/hr)
- ET = exposure time (hr).

It is assumed that there is no terrestrial vegetation production occurs when land is covered by water. Terrestrial vegetation is assumed to decay or mobilised to the water phase with the rate obtained from

Amazon measurements. The value used in Tonle Sap is 5% of the terrestrial growth mobilised each day.

Only part of terrestrial growth will end up as fish food. Part of the production remains in the very slowly decaying material like tree trunks, is washed out of the system, is collected by humans or is deposited permanently in the soils.

8.9. Productivity dynamics

In the current model formulation the main factors impacting productivity dynamics are time of the day (sun above or below horizon), water depth and suspended solids concentration (light penetration or euphotic depth + sediment nutrients). In addition there is time lag after substrate wetting before periphyton is fully grown. Figure 225 illustrates periphyton growth. Comparison can be made to phytoplankton in Figure 226.

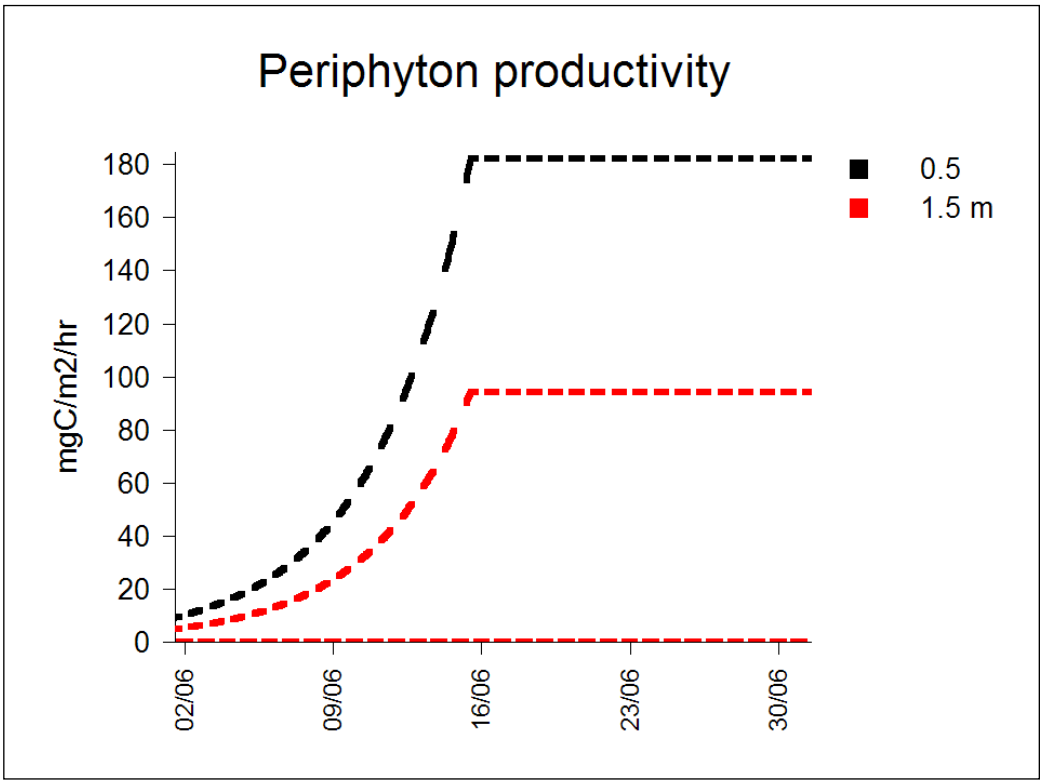

Figure 225. Periphyton growth in two depths.

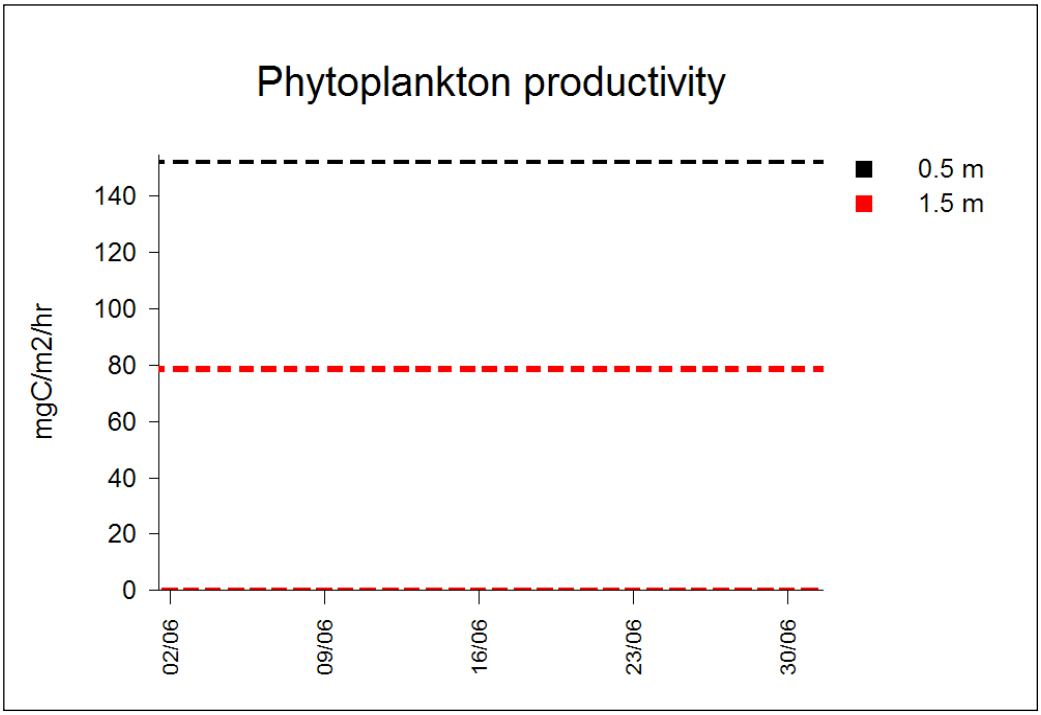

Figure 226. Phytoplankton productivity in two depths. Growth is not taken into account in the simulation.

8.10. Sediment nutrients

Sediments contain nutrients that maintain ecosystem productivity. The most important nutrients are nitrogen (N) and phosphorus (P). Here it is assumed that the system is not nitrogen limited as it is provided by nitrogen fixation and decaying plant material. Obviously there is need for more detailed nutrient cycle description. For instance the shallow and turbid dry season lake seems to be nitrogen limited and nutrient inputs from fertilisers should be included in the model.

Impact of the sediment nutrients on phytoplankton and periphyton is described with the equation:

$$c_P = P_{SDD} c + P_{SBD} \frac{c_B}{h_B}$$

$$A_P = 1 - P_{pr} + P_{pr} G_f \frac{c_P}{c_P + P_K}$$

- A_P = nutrient dependent growth coefficient
- c_P = bioavailable phosphorus
- c = suspended sediments concentration (g/m^3)
- c_B = bottom sediment amount (g/m^2)
- h_B = distance from bottom
- P_{SSD} = fraction of bioavailable phosphorus in suspended sediments
- P_{SBD} = fraction of bioavailable phosphorus in bottom sediments
- P_{pr} = fraction of production impacted by suspended sediments
- G_f = growth factor = $1+P_K/P_{AV}$
- P_K = half saturation concentration of bioavailable phosphorus
- P_{AV} = bioavailable phosphorus concentration corresponding to average production

Impact on terrestrial vegetation is described with similar equation except suspended solids are not considered and h_B is replaced with equivalence distance from bottom (terrestrial vegetation is assumed to grow only when land is dry). The distance formulation assumes that especially in the floodplains the impact of the sediment nutrients can be felt more strongly near the bottom.

The nutrient impact is taken into account in the primary production equations described before by multiplying them with the coefficients A_P and $A_{PT.}$

In addition to recent sedimentation one to two year old bottom sediments impact the growth in the model. This reflects the assumption that sediments release nutrients relatively fast in the Tonle Sap conditions and/or are consolidated after three years. Especially the prevailing floodplain anoxia is assumed to play an important role in effective nutrient release. If needed the time scales can be changed easily to describe more internally loaded conditions. The bottom sediment nutrients are reset in the model each year in July. Figure 227 shows how sediments are represented for the phytoplankton and periphyton. Two year or older sediments don't impact any more production.

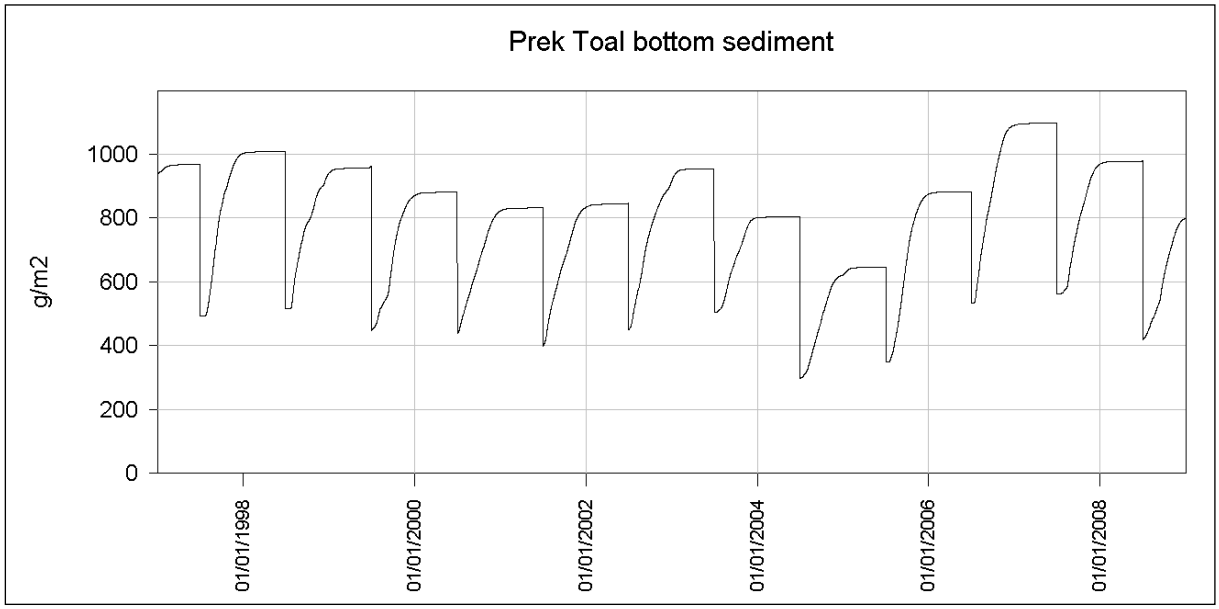

Figure 227. Bottom sediment representation for production. Previous year sediment impacts the growth. Sediment is reset each July. Time series from Prek Toal.

It is estimated that sediments contain approximately 130 mg phosphorus for each kg of sediment (Uusitalo 2009, personal communication). The value 130 mg P for each kg of sediment corresponds to 0.013% sediment phosphorus content. In the model it is assumed that 0.004% of the sediment phosphorus (the total bioavailable phosphorus) is available in suspended state to the organisms and 0.0002% in the bottom sediments at any given moment. The sensitivity of the production to the phosphorus is determined largely by the phosphorus half saturation constant (P_K). 2 µg/l is currently used in the model. The range of the half saturation constant in the literature is typically 1 – 50 µg/l and 1 µg/l is often used as a default value. All model sediment nutrient parameter values are presented in Figure 228.

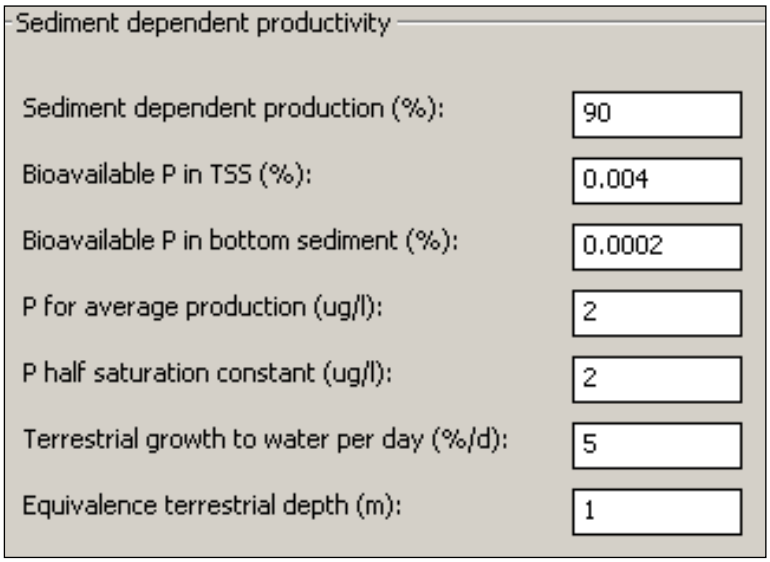

Figure 228. Nutrient parameters used in the Tonle Sap productivity model.

8.11. Fisheries production based on the primary production

Prof. Wolfgang Junk (Max-Planck-Institute for Limnology, Working Group of Tropical Ecology) has estimated Tonle Sap fisheries production based on the primary production and Amazon data. The following factors and coefficients are used in the Junk Tonle Sap fisheries production estimate:

- 1 kg of primary production in terms of carbon corresponds to about 2 kg of dry plant or animal matter
- 1 kg of fish dry weight corresponds to 3 kg of fresh weight
- Conversion Factor (CF) relates production of a higher trophic level to a lower one (food uptake in relation to growth rate)
- CF can be defined (i) from algae to fish, (ii) from algae to zooplankton and from zooplankton to fish, and (iii) from fish to predatory fish
- production depends mostly on young and small fish which transfer food uptake into growth very efficiently
- algae with high food value has CF 0.1 – 0.15 (fraction of carbon or dry matter fish production in terms of carbon or dry matter production in algae)
- blue-green algae is less valuable as food and has CF 0.001 via microbial loop
- valuable algae consist of 2/3 of the total algal biomass and 1/3 are blue-green algae
- predatory fish have CF 0.1 in relation to lower trophic level fish
- 50% of high food value algae is utilised directly by fish
- 50% of high food value algae is utilised by zooplankton and other invertebrates and has CF 0.001 in terms of fish
- 25% of the fish are eaten by predatory fish
- bulk (99%) of the terrestrial production has low food value and passes through microbial loop having CF 0.001
- 1% of the terrestrial production has high food value (young leaves, flowers, fruits) and has CF 0.1
- terrestrial production has CF 0.001 via microbial loop
- it is assumed that 100% of the terrestrial production ends up contributing to the fish production (this is not clear from Junk, but this assumption makes modelled and estimated terrestrial productions equal)
- each fish eating bird (cormoran, pelican, heron etc.) consumes 2 kg fish daily; there are total 50’000 fish eating birds which consume annually 36’500 tn fish
- only 50% of the floodplain algal production is utilised by the fish because of the low oxygen conditions not suitable for fish (this is inferred value, compare to the calibration chapter).

The last assumption is problematic because the primary production is very heterogeneous and concentrates near the lake and river edges where also oxygen conditions are the best. For an accurate estimate the primary production should be weighted with oxygen conditions through the model simulations. Before this the coefficient C_{OX} is used to take into account the habitat oxygen conditions.

Based on these values and assumptions the coefficients for transfer of primary production in carbon into fish biomass fresh weight are

1. Lake phytoplankton biomass production (phy_L) → lake fish dry biomass production without predatory fish: fb_{0L} = 2/3*2*phy_L*(0.5*CF + 0.5*CF*CF) + 1/3*2*phy_L*CF*CF
2. Floodplain algal biomass (phy_F + per_F) → floodplain fish dry biomass production without predatory fish: fb_{0F} = C_{OX}*[2/3*2*(phy_F + per_F)*(0.5*CF + 0.5*CF*CF) + 1/3*2*(phy_F + per_F)*CF*CF]
3. Terrestrial biomass production (ter) → fish dry biomass production without predatory fish: fb_{0T} = 2*ter*(0.01*CF + 0.99*CF*CF*CF)
4. Total fresh biomass production taking into account predatory fish: fb_1 = 3*(fb_{0L} + fb_{0F} + fb_{0T}) * (1 - 0.25 + 0.25*CF)
5. Annual total fresh fish biomass production taking into account predation by birds: fb_2 = (1-36'500 tn)*fb_1, where fb_1 is an annual value.

These equations can be used for obtaining annual fish production values from the productivity model. Assuming approximately linear fish growth they can be also used for daily fish biomass production for different parts and habitats in the Tonle Sap system.

The distribution of 2005 simulated fish production is shown in Figure 229. Naturally the fish are mobile and migrate long distances. The production distribution doesn't show the actual fish biomass in any given location but the potential for feeding and growth. The red areas correspond to common understanding of the most productive fisheries in the Tonle Sap, at least during the previous fishing lot system.

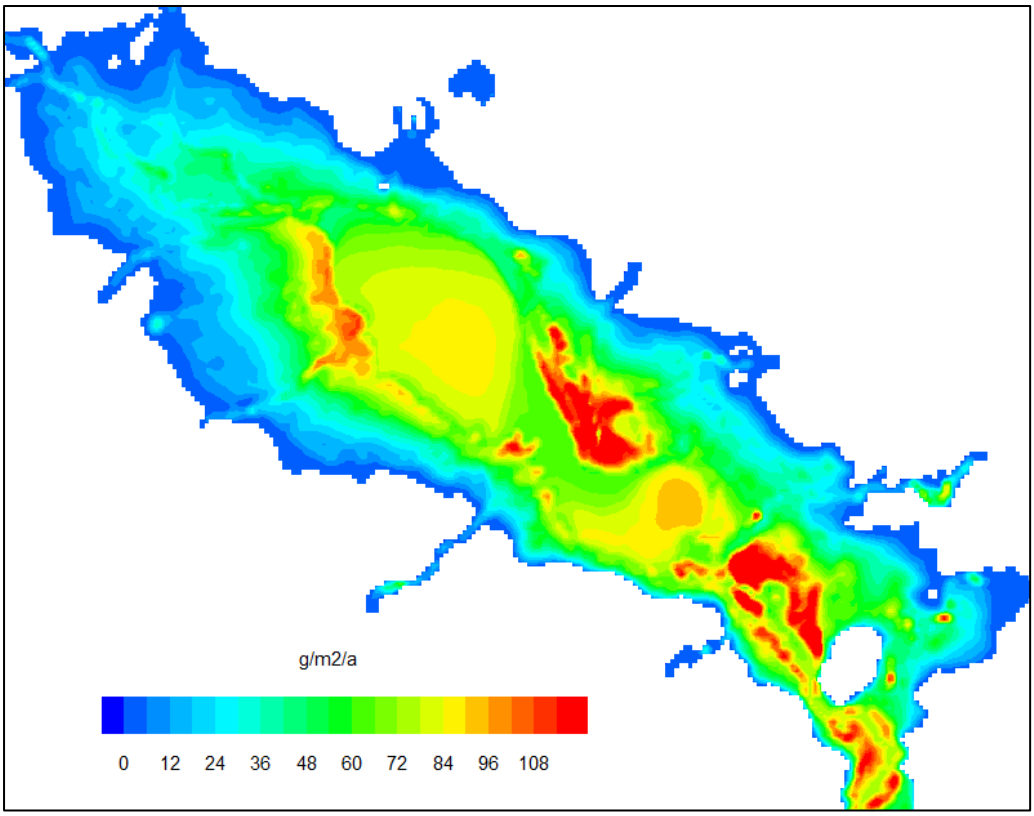

Figure 229. Distribution of 2005 fish production.

Some of the main limitations of the simple modelling approach is that it doesn't take into account migration, juvenile survival and other possible important factors that may have major impact on fisheries. Because of this an improved fisheries and fish population model should be developed in the future.

For C_{OX} = 0.5 and CF 0.1, 0.12 and 0.13 Junk obtains following table for the average annual fish production.

Table 9. Estimated (Junk) Tonle Sap annual fresh fish production.

Fish Production	CF = 0.1 *tn/y*	CF = 0.12 *tn/y*	CF = 0.15 *tn/y*
lake algae	129'039	158'418	204'945
floodplain algae	103'230	127'635	163'959
floodplain scrubs	22'209	22'353	22'545
total	254'478	308'406	391'449

The most striking feature of the table is the prominent role of the algal production compared to the terrestrial one. This is because of the high food value of the algae compared to the terrestrial production.

The table below summarises the available fish for spawning for different values of CF. Clearly, with the assumptions used, CF = 1 is not a sustainable value. Thus CF needs to be between 1.2 – 1.5. Another possibility is that C_{OX} is higher than assumed in the estimates. For instance C_{OX} = 0.8 would yield 60'000 tn more fish annually and the available fish for spawning would be 48'000 tn.

Table 10. Estimated (Junk) Tonle Sap annual total fresh fish production.

Fish Production	CF = 0.1 *tn/y*	CF = 0.12 *tn/y*	CF = 0.15 *tn/y*
total fish production	254'478	308'406	391'449
predation by birds	36'500	36'500	36'500
fisheries consumption	230'000	230'000	230'000
remains for spawning	-12'022	41'906	124'949

Junk observes that "The last, but most critical assumption is the annual recruitment, because food use efficiency depends on the number of young fishes. High numbers of young fishes increase food use efficiency. Many species spawn outside the lake upstream in the Mekong River and fry is swept in the lake with rising water level. Therefore, varying amounts of larvae reaching the lake and its floodplain in different years may explain large variations in fish yield despite similar figures in primary production. High recruitment rates lead to high numbers of fishes and high use of food resources and this is indicated by the CF. I have considered this aspect by varying CF. The model reacts very sensitive to this parameter." The importance of recruitment is also highlighted by the "outliers" of the statistical analysis.

Another important parameter is the C_{OX}. Changing it from 0.5 to 0.8 would increase the floodplain algae dependent fish production by 60'000 tn annually for CF = 1.

The lake production varies less than the floodplain production. The highest total production period is around September – November. The annual lake and floodplain algal productions are approximately equal. The total production varies between 250'000 and 350'000 tonnes of fish.

The results have been obtained using CF = 0.1 and C_{OX} = 0.5. The results are quite similar to the estimated ones except simulated floodplain algal production is 33 % higher than the estimated one (see table below).

Table 11. Estimated (Junk) and simulated average Tonle Sap annual fish production.

Fish Production	Estimated	Simulated	Difference
	tn/y	*tn/y*	*%*
lake	129000	127000	-2
floodplain algae	103000	137000	33
terrestrial	22000	23600	7

Figure 230 presents comparison between the modelled annual total fish production and Dai fishery catch. The correlation coefficient is 0.7. It should be noted that the real relation between the total Tonle Sap fish production and Dai fishery catch is unknown because the total production is not well known. The Dai fishery catch obviously reflects total production but additional factors such as hydrology may have strong impact on the fishing efficiency.

The figure eliminates two anomalous years, 2004 and 2005. These can't be explained by the lake conditions. The issue is discussed in more detail in the Halls et. al. annex. In these years Dai fishery catch exceeds the modelled total production: 2004 386'000 tn / 258'000 tn and 2005 529'000 tn / 282'000 tn. The natural conditions were quite similar in these years to the other average years. The only difference that has been indicated by the available data is the higher juvenile density in the Mekong water flow into the lake.

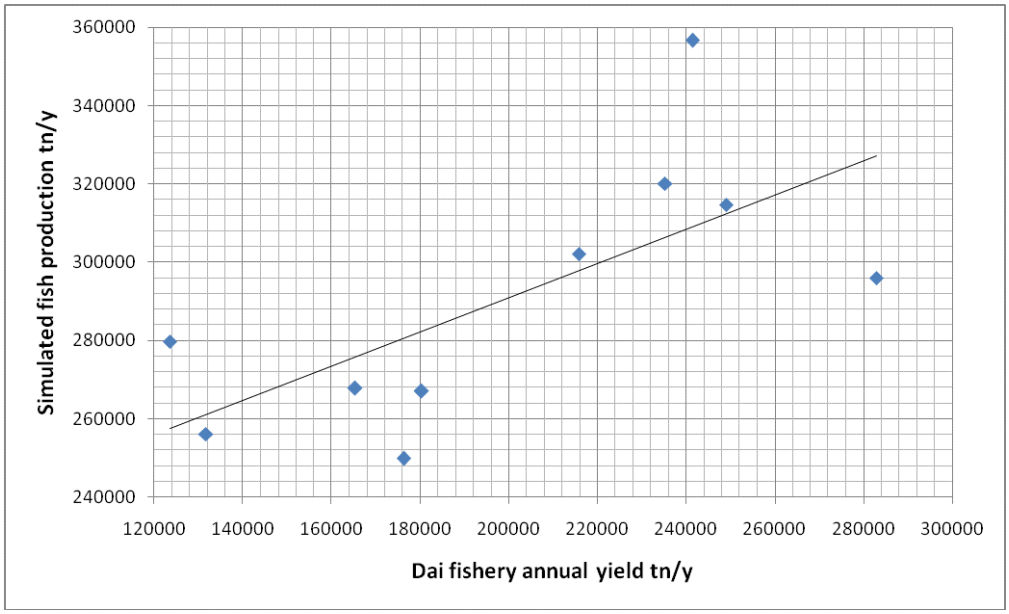

Figure 230. Comparison between the Dai fishery catch and modelled primary procudction. Correlation coefficient = 0.7.

The Dai fishery production correlation to the primary production can be compared to the modelled floodplain sedimentation and flood index (flood area x duration) in Figure 231. Large number of other

factors were also studied and the modelled floodplain sedimentation explains by far best the observed Dai fishery catch (R^2 = 0.95**).**

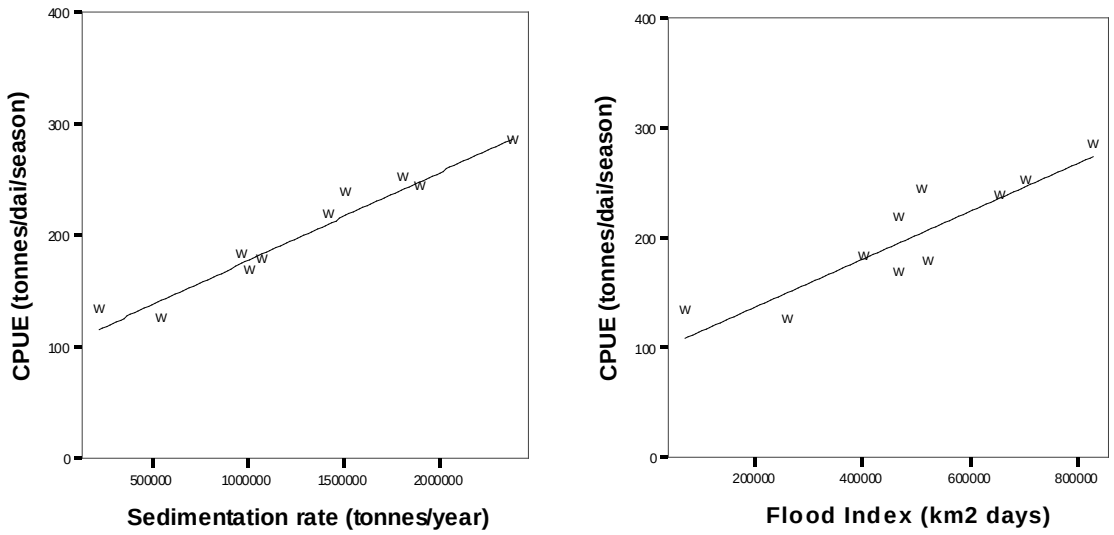

Figure 231. Fish biomass index plotted as a linear function of (left) rate of sedimentation and (right) the flood index (right) with fitted regression models. CPUE = 98.65 + 7.929E-05 x Sediment rate (d.f =10; R^2 = 0.95; $p < 0.001$) and CPUE = - 59431 + 2.742 x FI (d.f =10; R^2 = 0.80; $p < 0.001$), respectively.

9. Annex 9 - Tonle Sap 3D-EIA WQ (Water Quality) Model Description and Validation

9.1. Modelling water quality

Water quality is usually understood as the content of different soluble and non-soluble substances in water that define the suitability of the water to some specific need. Such substances or water quality variables are, for example, nutrients and algae. Summary variables, such as turbidity, can also be used.

Water quality modelling is the method, in which the concentrations of given water quality variables area computed in a river, lake or sea area, based on different internal and external factors that affect the variables concentrations. External factors include, for example, river and point loads to the area, and internal factors, for example, water flow, temperature stratification and salinity gradients. The aim of the modelling process is to simulate the real situation in the modeled water area as well as possible, and find out the effect of different factors to the water quality in the area.

One of the most important capabilities of a simulation model is the ability to simulate effects of changes to the existing situation. First the model is calibrated to the current situation as well as possible, after which the initial data is set to correspond the planned change. Results can then be compared to existing situation simulation or other simulation scenarios.

9.2. Transport of substances

Dispersion is modelled using advection-diffusion equation, that states that a concentration advects (moves with) a given flow, and diffuses (spreads) with given diffusion speed. For one variable in three spatial dimensions the equation can be written as follows:

$$\frac{\partial c}{\partial t} + u\frac{\partial c}{\partial x} + v\frac{\partial c}{\partial y} + w\frac{\partial c}{\partial z} = D_h\frac{\partial^2 c}{\partial x^2} + D_h\frac{\partial^2 c}{\partial y^2} + D_v\frac{\partial^2 c}{\partial z^2} + L$$

- c = concentration of a substance, units/m3
- t = time, s
- u,v,w = known water flow velocity components, m/s
- D_h = horizontal concentration diffusivity, m^2/s
- D_v = vertical concentration diffusivity, m^2/s
- L = other processes, such as sedimentation and decay.

The first term on the left size is the variation of concentration with time. The three next terms on the left size describe the advection of the substance with the flow field. The first three terms on the right side describe the diffusion of the substance in horizontal (2 first terms) and vertical (3rd term) directions. Last term on the right side depends on what processes and reactions are selected for the modelled variable.

To compute the water quality first the water flows must be computed using a flow model. Flows can be computed and used in two ways:

1. The flows are assumed to be linearly dependent on the boundary and wind forcing and linearly combinable, so that a number of precomputed static flow fields can be combined to create a flow field for given boundary flows and wind direction.
2. The flow is computed dynamically using the flow model and stored periodically - the water quality model then uses these stored flow fields.

The first approach requires some work to compute the static flow fields, the second one requires relatively more computation power and storage space to compute and store the flow data. The first approach is suitable for longer time periods (>few months) whereas the second one suits for shorter time periods where good accuracy is required. **For the Tonle Sap (and in the future for reservoirs) the selected approach is the first one**. This is because the model has been designed to work either with small changes in water depths and dynamic flow fields or large (or small) water depth changes and the static flow fields. Also, the static approach provides possibility to use higher model resolution.

To model a water body the target area must be described to the computational model as a model grid, which is a set of connected rectangular grid boxes of suitable size, that describe the bathymetry of the target area to the model as well as possible. Typical grid box size in horizontal direction at the target area of a model application is some hundred meters, while at the border of the model area the grid box size might typically be few kilometers. Vertical depth of a grid box close to surface is about one meter increasing to few tens of meters deeper down. The total amount of grid boxed in one model application may be up to tens of thousands of grid boxes.

A computer model is then formulated so that when a situation in a model grid is known at time t, the computer model can be used to compute the situation in the grid after a given time step Δt. The result is a new known state at time $t+\Delta t$. Computation of water quality consists of moving substances from one grid box to another using the known flows, and computing reactions, such as sedimentation, within each grid box for the time step.

The grid is usually three dimensional, that is, there are several grid boxes in both horizontal directions and several layers of boxes in vertical direction. The grid can be nested, so that there is a grid of smaller boxes inside a grid of larger boxes. This enables more accurate modelling of specific areas with connections to larger systems. There is no need for this type of approach in the Tonle Sap or reservoirs and nesting has not been tested for them.

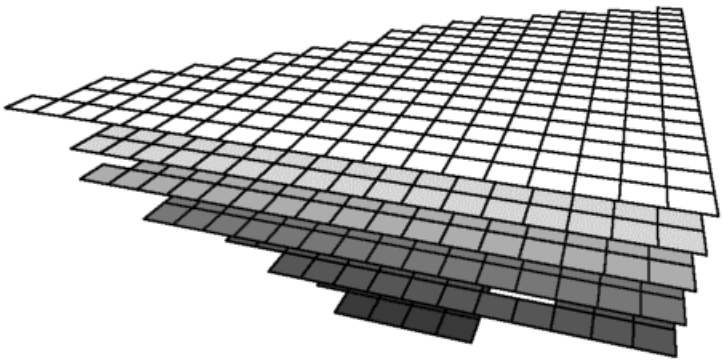

Figure 232. A side view of a simple 3d model grid - deeper vertical layers are shown in darker shades of grey.

9.3. The 3D-EIA WQ Model

As explained in the previous chapter water quality computation with the 3D-EIA WQ model is based on using the computed flow data to solve transport of substances. This way the factors affecting water quality, such as water exchange, advection of substances with water, and different physical processes affecting the water quality can be described approximating existing real situation in nature. When existing boundary values and current generating forces are well known, it is possible reach good agreement with model results and existing reality as represented by monitoring data.

The ecosystem model is built in co-operation with the Finnish Environment Institute. The computational ecosystem model is an integral part of the EIA water quality model. The transport and spreading of biological variables is similar to any water quality variable in the model, so transport of algae and nutrients is also defined by computed currents. The growth of algae and other biological processes happen in each model grid box as the local conditions and nutrient levels in that grid box define.

The water quality model computes concentrations for each defined water quality variable in each grid box for the whole computation period. The computed concentrations can be saved as time series from pre-selected points, as instantaneous concentration fields, or as an average concentration field for the whole computational period. Results can be analyzed statistically and compared, for example, to measurements and remote sensing data.

Typical variables computed using the water quality model are the ecosystem model related variables: dissolved nitrogen and phosphorus (DIN, DIP), and different variables describing the amount of algae in the water. Often also oxygen, biological and chemical oxygen consumption (OXYG, BOD7, COD7) and total nutrients (NTOT, PTOT) are computed.

To compute any variable concentration, flow defining boundary conditions, initial situation, loading data and calibrated model parameters are needed. To calibrate and verify model results it is also recommended to have measurement data from the simulated time period.

The modelling process has following steps (**Figure 233**):

1. The flow data needed by the water quality model is computed using the flow model. Static or dynamic flow fields can be used. If static flow fields are used, a set of pre-computed flow fields are combined using existing boundary condition data, resulting an estimated flow situation at the given time. Dynamic field is simply a flow computation result that is saved by given time intervals by the flow model and used directly in the water quality model.

2. To compute loadings to the water, incoming river flows and corresponding nutrient concentration in the rivers, point load data and concentration boundary conditions are needed. These values are typically time-varying, so the data is in the form of time series. Often all required data is not known as well one would wish, in these cases the best available values for the missing data must be used.

3. The concentrations can be computed as the currents and loading are given. In computation of the transport of substances with water, as well as vertical and horizontal mixing are taken into account for all modelled variables. Additional factors that can be included in the computation are, for example, settling and sedimentation.

4. It is necessary to calibrate the model for each application using measured values.The sedimentation speed and other computation parameters may vary from one application to another, and cannot usually be directly measured. For example, in lakes and coastal areas the ecosystem parameters are quite different.

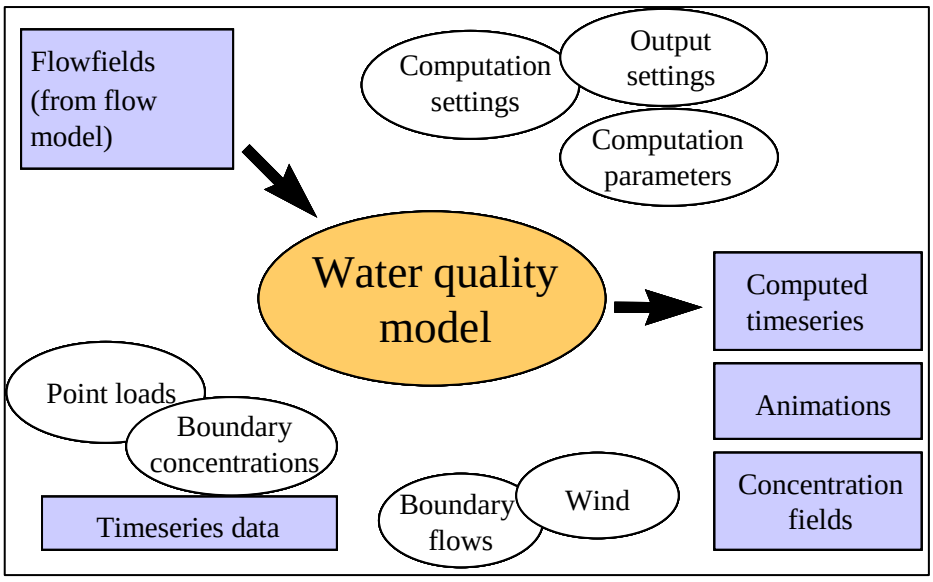

Figure 233. Work flow for water quality modelling.

Summary of required input data:

- flow fields (static or dynamic)
- wind and boundary flows, if static flow fields are used
- point loads
- boundary concentrations
- initial situation concentration
- water quality measurements for calibration and verification

Summary of produced output data:

- computed 3d-time depended concentration fields
- computed time series from selected points
- 2d-animations
- computation period average concentration field

9.4. Basic 3D-EIA WQ model construction for the Tonle Sap

The technique described here is based on computing each individual contribution to flow from wind and different in- and outflows and combining these for total flow field for each specific wind and flow condition. As explained above another technique is computation of dynamic flow fields that include all wind and in- and outflows but this has not been applied to flooding yet and is not applicable for Tonle Sap.

For the DEM and land use file preparation it is easiest to use the WUP-FIN RLGis software. The computation technique uses water depths rather than elevations for the topography/ bathymetry. Negative elevations are not allowed and that's why for instance 100 m needs to be added to the original elevations that are in the MSL (Mean Sea Level) reference system. (Elevations go negative in the Tonle Sap River.)

In order to obtain water depths for water level 11 m that is here considered maximum water elevation, one needs to utilise "GeogrComp/ Grid/ transform values" in the RLGis software and use -1 for **Multiply** and 111 for **Add** (**Figure 234**). RLGis "Modify layer data" button tool to clear areas that are not connected to the main lake (**Figure 234**). After eliminating negative depths from the bathymetry the grid values can be exported to the 3D flow model by reading the data into Excel and copying it to the flow model in "File/ New/ Create model/ Create empty grid". Necessary grid coordinates can be obtained from the RLGis layer that is to be imported into the flow model (**Figure 235**).

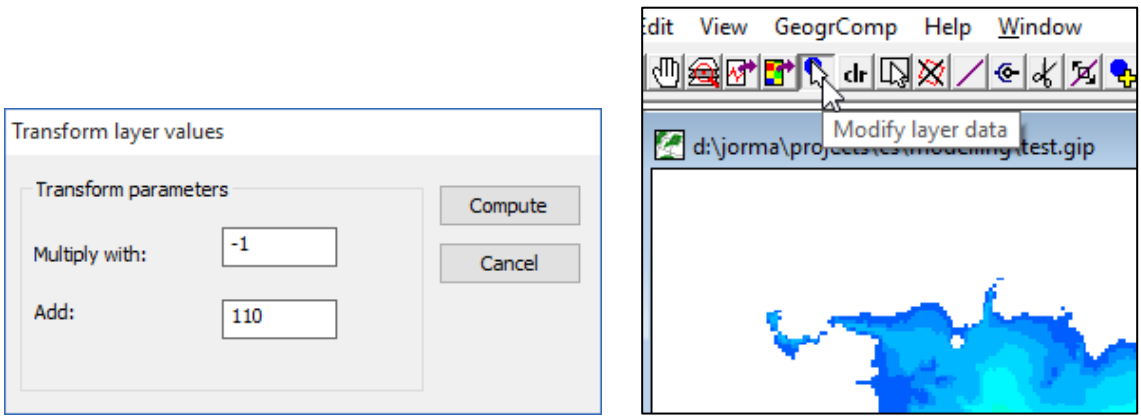

Figure 234. RLGis DEM editing for the flow 3D-EIA model.

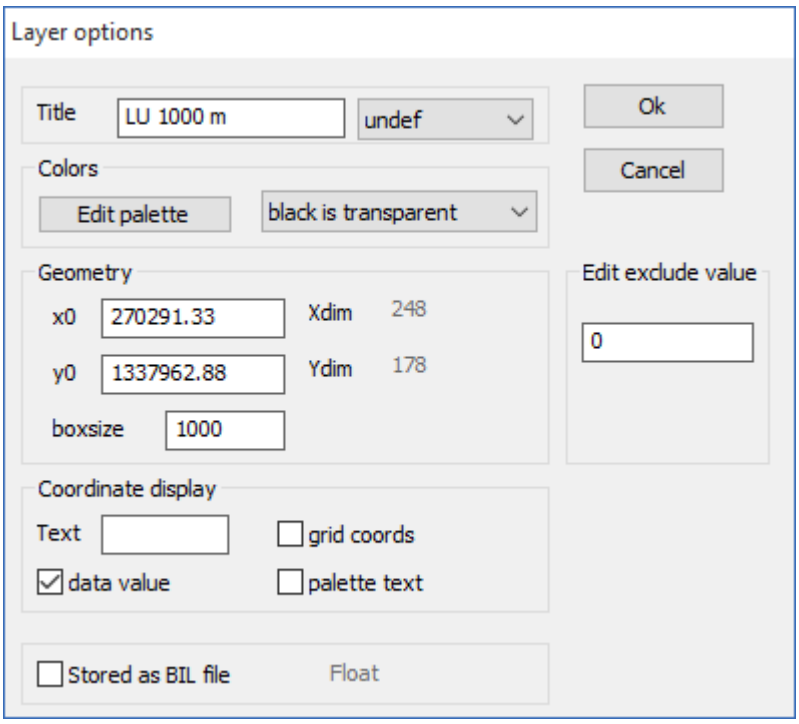

Figure 235. Layer coordinates in RLGis for flow model set up.

Land use data can be export to the flow model similarly to the bathymetry. Because no productivity is computed in this case the land use parameters that need to be defined for each land use class are:

- Vegetation height (m)
- Vegetation coverage (0 – 1)
- Additional vegetation drag.

For the selected technique the flow fields need to be computed for discrete water levels and the water quality model interpolates between these for each specific lake water level. It is enough to produce only one bathymetric map file for the maximum water level: the flow model decreases the depths for different water levels automatically through a dialogue window where reference water level is given as well as lower water levels through adding for instance -1, -2, -3 etc. ().

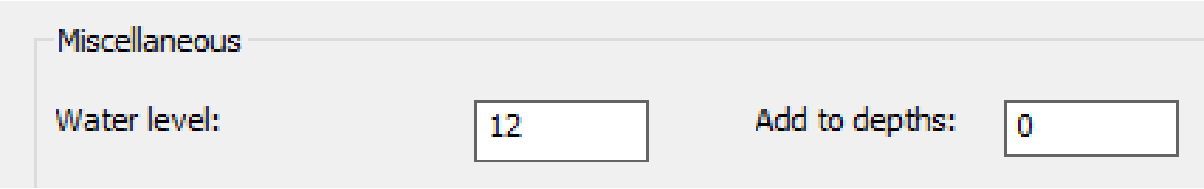

Figure 236. Specification of water levels in the 3D flow model.

At least two wind directions and 9 inflows need to be computed when the western inflows have been combined (**Figure 237**). Each factor including inflows is computed separately without considering mass balance (that is outflow). In that way in- and out-flows are not coupled and allow volume changes in the Lake.

Special technique has been developed for the Tonle Sap that takes into account changing water-land boundary. In the original model formulation incoming rivers needed to be carved in the DEM to maintain river channel for all water levels including the lowest one. This resulted in very deep channels in the highest water levels. The new solution method takes into account changing water-land boundary and provides inflows and water quality loads on this boundary eliminating need for fixed river inflow points and deep channels.

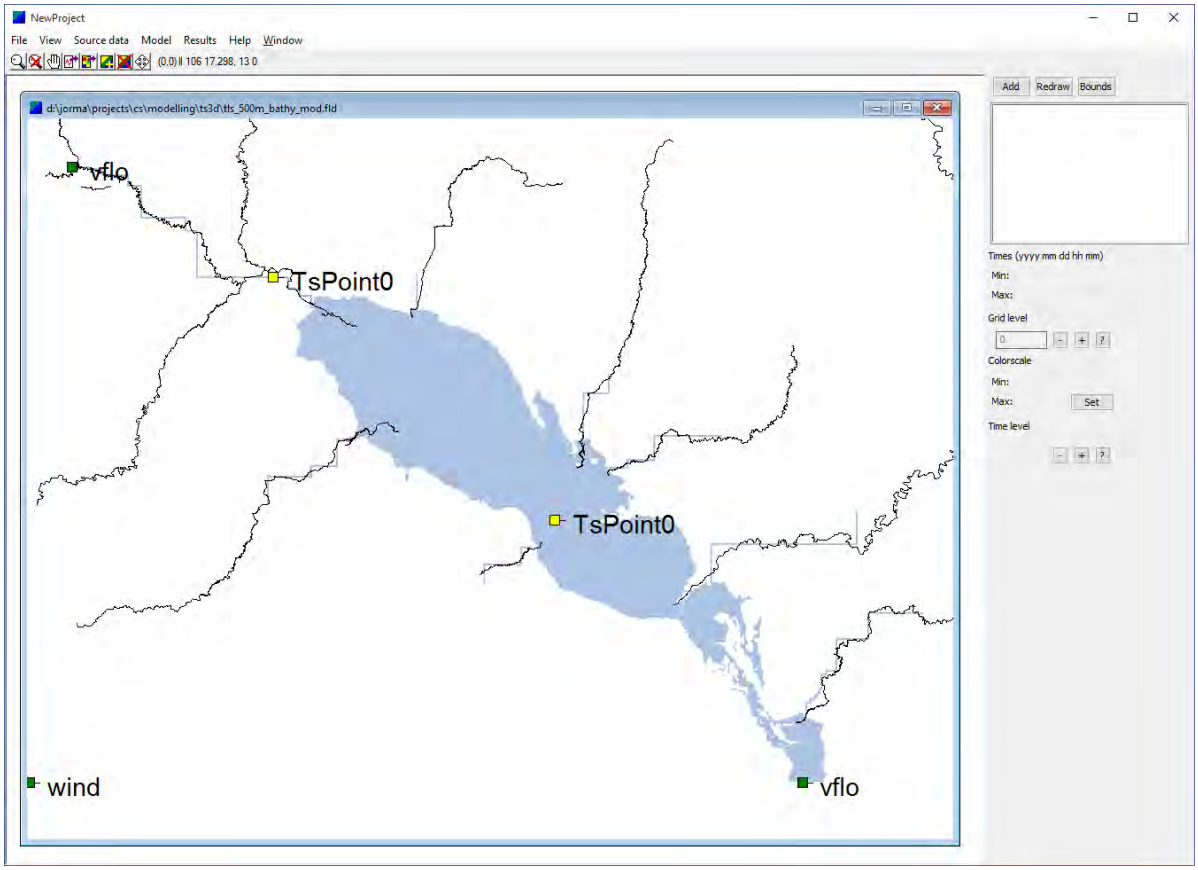

Figure 237. User interface view on the 3D-EIA Tonle Sap model showing main tributaries.

The 3D-EIA WQ model construction is easy as it is based on computed flow fields. After the basic model construction each set of flow fields for all discrete water levels is provided through an example flow field (**Figure 238**). Model interpolates flows and volumes in between the discrete water levels. The different flow fields for different water levels are identified with indexing starting from 0. The sets are provided for each wind speed, wind direction and in- or outflow. Changing in- or out-flows are given as time series (**Figure 238**).

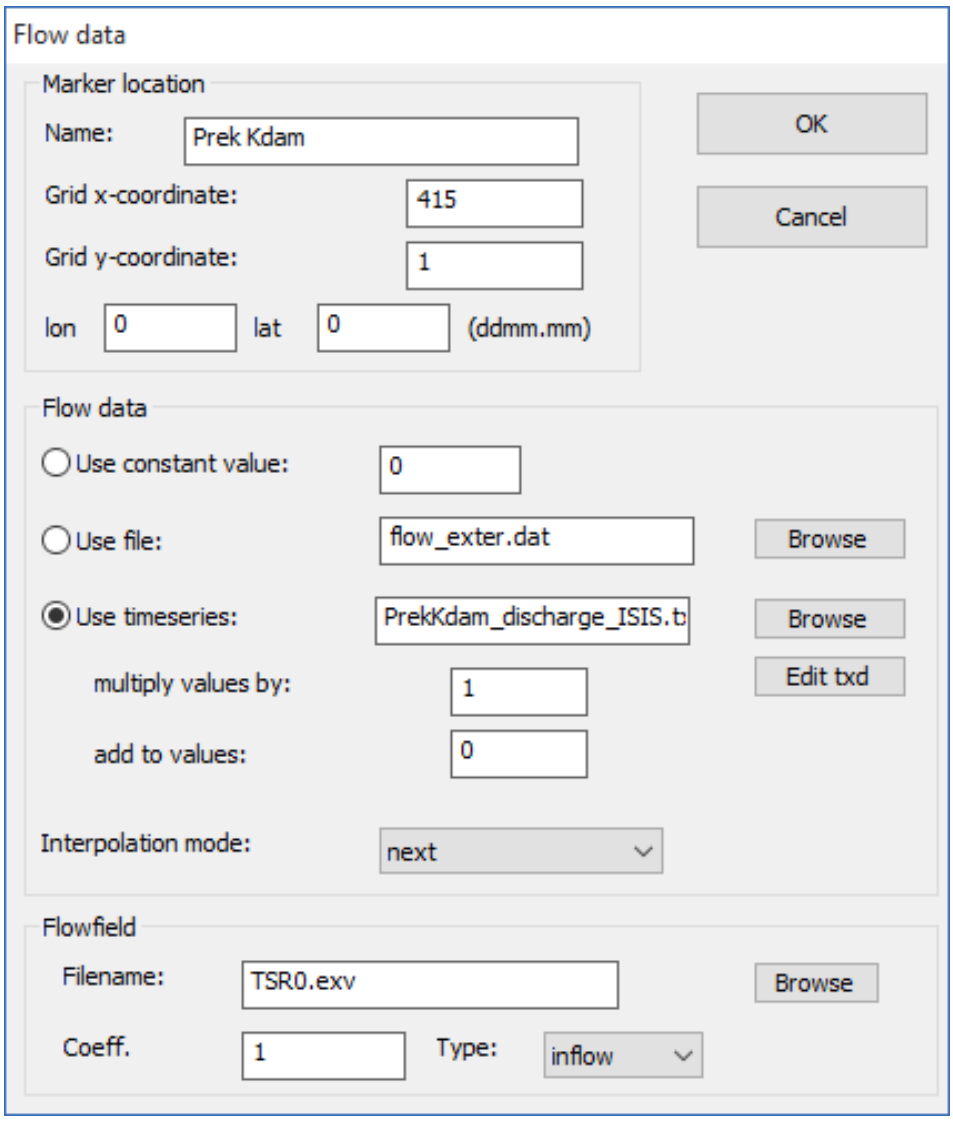

Figure 238. 3D-EIA WQ model definitions for Tonle Sap Prek Kdam in- and out-flow. In this case positive values are considered inflow and negative ones outflow.

Reservoir or lake water levels can be prescribed as time series or computed from in- and out-flows. The former definition is shown in **Figure 239** as a flow point definition and the latter in **Figure 240**.

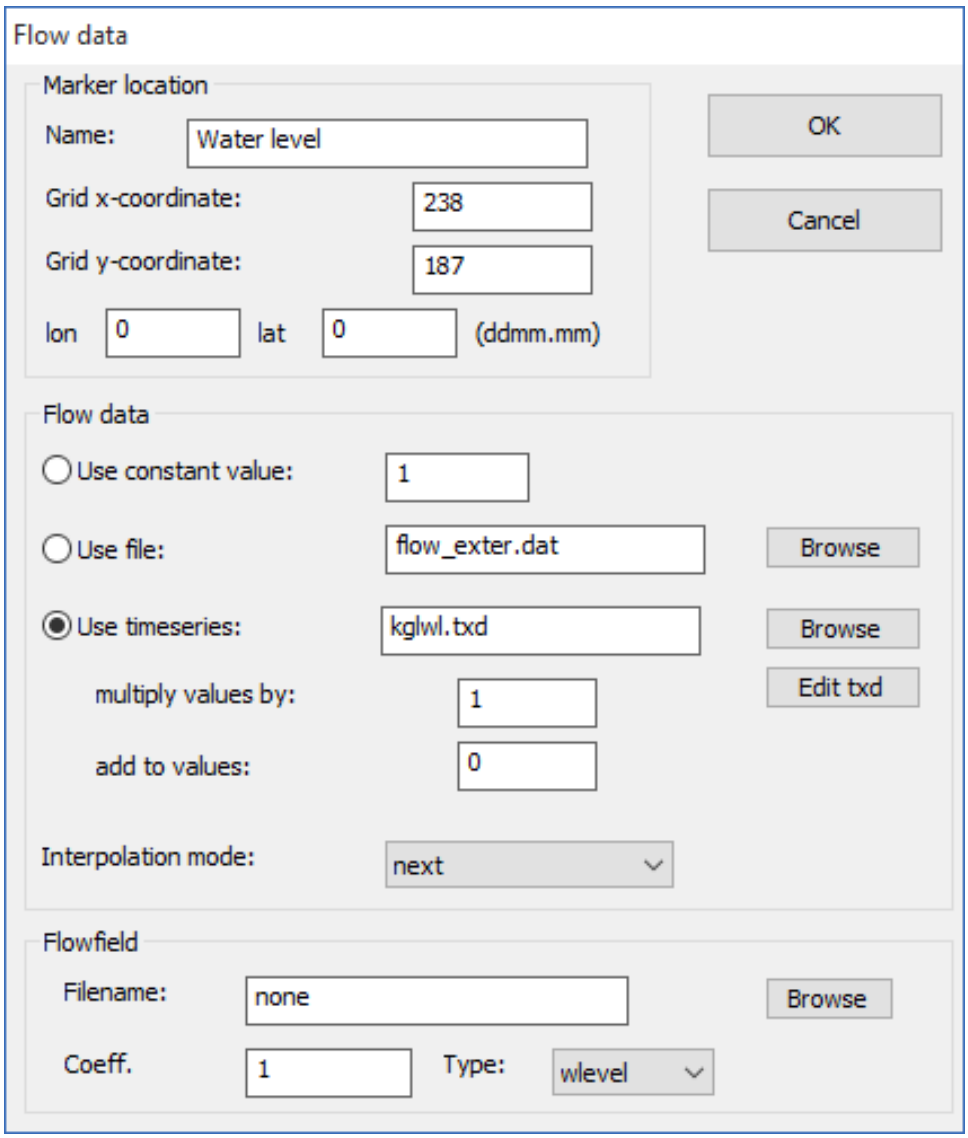

Figure 239. Specification of the Tonle Sap model water levels and volumes through measured Kompong Loung water levels.

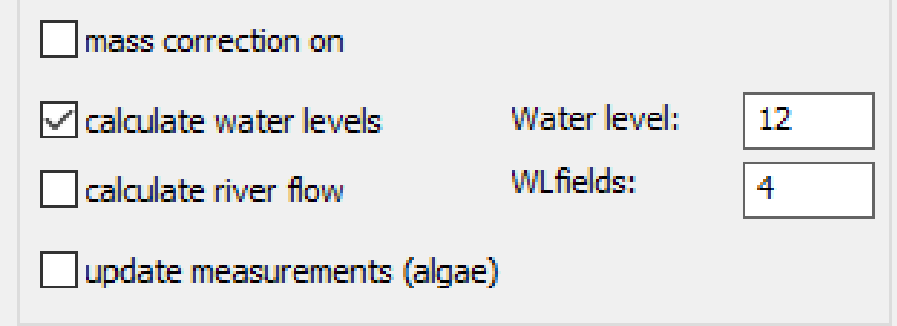

Figure 240. Specification of model water levels and volumes through mass balance computation.

9.5. Computation of oxygen

Lack of oxygen is a typical problem in nutrient and organic material rich lakes, reservoirs and floodplains. Oxygen computation requires two variables, oxygen (OXYG) and biological oxygen consumption (BOD7). These are present in the model as default.

Water oxygen content is increased by wind aeration and incoming oxygen rich waters. Oxygen is depleted from the water by BOD7 decay and also by bottom sediment oxygen consumption. Parameters affecting these processes are wind aeration and sediment oxygen consumption coefficients in Model/Computation parameters, and BOD7 settling and decay coefficients in BOD7 variable

To compute the oxygen

- check that OXYG and BOD7 variables exist and are active
- add a BOD7 load to the model area using Add-tool or Source data/Loads/Add button
- check that parameters listed above have reasonable values, (e.g. 9e-5 for oxygen wind aeration, 0 – 1.5 for sediment oxygen consumption, 2 cm/d for BOD7 settling and -0.1 for BOD7 decay).

9.6. Nutrient and algal loads

Loads are used to define point load sources such as waste water outlets to the model. A point load is differs from a constant concentration so that the flow associated with the load is not taken into account. The load unit is kg/d or tn/d. Available load types are:

- Normal point load – normal load, divided equally to the load area
- Bottom – all load is divided to grid boxes at bottom.
- Atmospheric fallout – all load is put to the grid boxes at surface.
- Discharge from shore – the load is divided to grid boxes next to shoreline; this type is used also for river loads in the Tonle Sap with changing boundary between water and the floodplain.

The ecosystem model uses two variables to describe bioavailable nutrients, the bioavailable nitrogen DINN, and the bioavailable phosphorus DIPP. These variables are seldom measured directly, so the loads of these variables are typically estimated from total nutrient loads by using coefficients of bioavailability. During the WUP-FIN project bioavailable particulate phosphorus was measured directly (Uusitalo et al. 2003).

If riverine algae amounts are known there can also be loads for the biomass variables ALG1 and ALG2.

Phosphorus (DIPP)

The coefficients of bioavailability represented below are based on measurements made from water bodies and waste water sources. The bioavailable phosphorus amounts for different locations and sources are estimated as follows (for direct bioavailability measurements see Uusitalo et al. 2003):

1. At open sea where the suspended solid concentration is typically less than 1 mg/l, the best estimate for bioavailable phosphorus is PO_4 analyzed from Nucleopore-filtered (0,45 μm) sample. For non-filtered samples, as least part of the suspended solid associated phosphorus dissolves and raises the PO_4 –concentration. The PO_4 concentration analyzed from a non-filtered sample might be even two times the concentration analyzed from a of a filtered sample

2. For river waters the bioavailability coefficient is based on total nutrient measurements and measured algae concentrations (Ekholm 1998, Ekholm & Krogerus 2003). The coefficient value is typically 20%.

3. For point loads the bioavailability coefficient vary depending on the waste water source. For example, the following coefficients can be used (Ekholm 1998, Ekholm & Krogerus 2003):

- Community waste waters, chemical phosphorus precipitation 40%
- Community waste waters, no chemical phosphorus precipitation 80%
- Industry waste waters, average 30%
- Fish farming 30%

The DIPP load unit in the model is kg/d. The concentration unit is μg/l.

Nitrogen (DINN)

The bioavailable nitrogen fraction is typically a sum of inorganic nitrogen compounds (NO_2+NO_3+NH_4). Point load sources often contain organic material containing nitrogen that may also be bioavailable, therefore the amount bioavailable nitrogen is estimated using bioavailability coefficient in the same way as for phosphorus. The following coefficients can be used:

- Atmospheric fallout 100%
- Community waste waters 90%
- Industry waste waters, average 70%
- Fish farming 30%

The DINN load unit in the model is kg/d. The concentration unit is μg/l.

Phytoplankton (ALG1, ALG2)

In model computed timeseries pictures the algae biomass are given in area units, e.g. g/m^2. The model is calibrated using measured chlorophyll concentrations modified by the following formula:

$$\text{biomass } [g/m^2] = 0{,}15 * \text{a-chlorophyll } [\mu g/l]^{1,2} * \text{productive layer depth } [m] \quad (1)$$

The regression between biomass and a-chlorophyll is based on parallel measurements made in Finnish sea areas (n=148, R^2=84%).

If the depth of productive layer is 10 m, conversion between chlorophyll and biomass is done using the following formula:

$$\text{biomass } [g/m^2] = 1{,}5 * \text{a-chlorophyll } [\mu g/l]^{1,2} \quad (2)$$

The model biomass concentration unit is mg/l. This unit is used in animations and end and average fields. There are also some algae loads from rivers, the load unit for these loads is tons/d.

9.7. Other model source data

The wind data dialog defines the wind data used by the model. This data is usually set during the model construction, and need no modification later. If dynamic flows (averaged flow fields over prescribed time intervals in contrast to superponated static flow fields) are used wind data does not need to be defined. The wind can be given to the model in three ways, as a constant value, useful mostly in testing, as a wind timeseries read from a time series file, or as a wind file that is in format understood by the computational model.

Water temperatures affect the ecosystem model process speeds. The temperature can be given as a constant value, as timeseries file, or in a specific format text file (Temp file). If timeseries file is used the file must contain time, temperature value and depth value on each line. If this option is used, the temperature is interpolated in vertical direction from the available data points, in horizontal direction the temperature is same for the whole area. If different values in horizontal direction are required, the Temp file option must be used.

Radiation data is used in the ecosystem model as one of the factors affecting the growth of algae. Radiation unit is MJ $m^{-2}d^{-1}$. Radiation can be also estimated by the model based on latitude and weather information.

Ice data is used in the ecosystem model to modify light conditions. Ice data is written to files in model construction time. The files can be taken into use by defining the file name in *Ice data* dialog. Ice data is horizontally varying. Naturally ice data is not normally required for the Mekong except in modeling lakes and reservoirs in the Tibetan Plateau.

9.8. Generic ecosystem model

Water ecosystem modeling includes in addition to the computation transport of nutrients used by the algae by using the water quality model, also the computation of biomass, nutrient intake, and growth of algae, and also nutrient release from dead algae, and nutrient sedimentation. Ecosystem model enables computation of algae biomass at different loading and weather conditions.

The ecosystem model is constructed on top of the water quality model, so that the water quality model variables represent the different algae groups and biologically available nutrients. The interactions between different algae groups and nutrient variables are complex, and these are described and computed in a separate ecosystem model module. **Figure 241** shows the main variables and interactions of a generic ecosystem model.

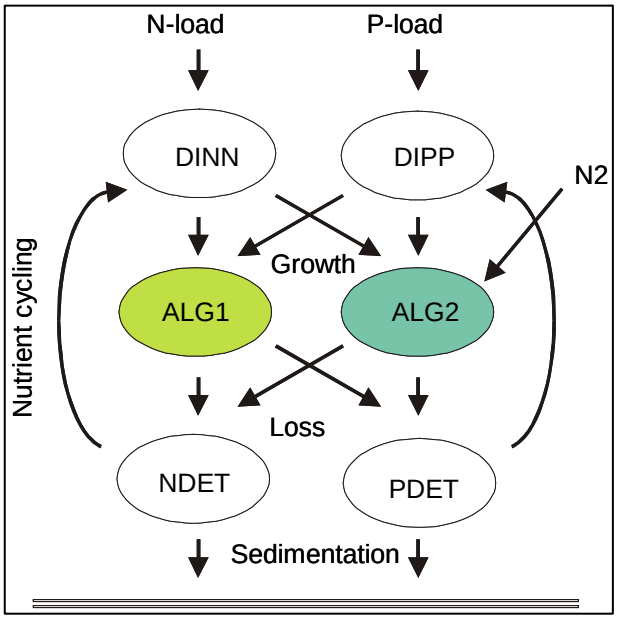

Figure 241. Ecosystem model main variables and interactions.

The main variables of the ecosystem model are:

1. DIPP – biologically available phosphorus (PO_4 or 20-80% from total phosphorus). Phosphorus is in most cases the most important growth limiting nutrient. DIPP concentration can be estimated from the measured filtered PO_4 concentration. For point loads often a total phosphorus value multiplied by a coefficient of availability is used.

2. DINN – biologically available nitrogen. The importance of nitrogen as a growth limiting nutrient is typically much smaller than that of phosphorus. Nitrogen-limited situations can exist, for example, at certain times in the mouth if large rivers. DINN is typically a sum of inorganic soluble nitrogen components (NO_2+NO_3+NH_4), but point load sources also often include organic compounds containing nitrogen, that may be in a form that algae can use. For point loads the DINN is typically estimated using total nitrogen load multiplied by a coefficient of availability.

3. ALG1 – phytoplankton without nitrogen-fixing blue-green algae. Most of the basic production in water areas is produced by the algae represented by ALG1 - variable. The growth of phytoplankton is limited in the model by nutrient availability, light availability and temperature, even though the importance on temperature as a limiting factor of ALG1 is rather small. As the algae dies the nutrients it contained are moved to detritus nutrient variables (PDET, NDET), that settle towards bottom at constant rate.

4. ALG2 – blue-green algae that is capable of fixing nitrogen from atmosphere, *Nodularia*, *Aphanizomenon* and *Anabaena.* The behavior of blue-green algae differs from other algae in two principal ways. Firstly, the growth of blue-green algae is strongly temperature limited - in practice there is no growth below +15°C. The other difference is that the growth of blue-green algae is never limited by the availability of nitrogen.

In addition to above variables, the model computes detritus (dead algae biomass) nutrients, which are needed to simulate the ecosystem internal nutrient recycling and nutrient sedimentation. The variables used for the detritus nutrients are

- NDET – nitrogen in detritus
- PDET – phosphorus in detritus.

9.9. Algae models

There model includes three basic algae model variations:

-
- Algae model (Algae 2p)
- Foodweb model (Foodweb 2p+3z) and
- Filamentous algae model (Algae 2p+f).

In the Tonle Sap case these basic models, especially 2p, are developed to better account for sediment caused light limitation and zooplankton and fish grazing.

9.9.1. **Algae model (1p)**

This is the simplest of the available algae models including only one algae group, phosphorus and nitrogen:

$$
\begin{aligned}
P_{use} &= K_{Pa} + K_{Pb}C_P - K_{Psto}(C_{mor} + C_A) \\
N_{use} &= K_{Na} + K_{Nb}C_N - K_{Nsto}(C_{mor} + C_A) \\
R_{gr} &= K_{Agr1}\left(\frac{P_{use}}{P_{hsat} + P_{use}}\right)\left(\frac{N_{use}}{N_{hsat} + N_{use}}\right)\left(\frac{L}{L_{hsat} + L}\right)C_A \\
R_{resp} &= (K_{res1} + K_{res2}C_A)\,C_A \\
SED_x &= \frac{\partial\left((K_{sed1_x} + K_{sed2_x}C_x)\,C_x\right)}{\partial z} \\
\frac{\partial C_{mor}}{\partial t} &= -SED_{mor} + R_{resp} \\
\frac{\partial C_P}{\partial t} &= -SED_P - SED_{mor}K_{Psto} \\
\frac{\partial C_N}{\partial t} &= -SED_N - SED_{mor}K_{Nsto} \\
\frac{\partial C_A}{\partial t} &= -SED_A + R_{gr} - R_{resp}
\end{aligned}
$$

C_{mor}	is the dead algae concentration (mg l^{-1})
C_P	is the phosphorus concentration (μg l^{-1})
C_N	is the nitrogen concentration (μg l^{-1})
C_A	is the live algae concentration (mg l^{-1})
R_{gr}	is the algal growth rate (mg l^{-1} d^{-1})
R_{resp}	is the algal respiration (mortality) rate (mg l^{-1} d^{-1})
P_{use}	is the phosphorus fraction that can be utilised by the algae (μg l^{-1})
N_{use}	is the nitrogen fraction that can be utilised by the algae (μg l^{-1})
K_{Psto}	is the phosphorus stochiometric coefficient (μg P/ mg A)
K_{Pa}	is the phosphorus utilisation constant (μg l^{-1})
K_{Pb}	is the phosphorus utilisation coefficient
K_{Agr1}	is the maximal algal growth rate (d^{-1})
P_{hsat}	is the phosphorus half saturation constant (μg l^{-1})
L	is the incoming short-wave radiation (W m^{-2} d^{-1})
K_{res1}	is the linear respiration (mortality) coefficient (d^{-1})
K_{res2}	is the quadratic respiration (mortality) coefficient ($d^{-1}mg^{-1}$)
SED_x	is the sedimentation rate for component x (μg or mg d^{-1})
K_{sed1_x}	is the linear sedimentation coefficient (cm d^{-1})
K_{sed2_x}	is the quadratic sedimentation coefficient (cm d^{-1} / μg or mg l^{-1})

The growth, respiration and sedimentation rates depend on temperature and temperature correction is applied to them in the model.

9.9.2. **Algae model (2p)**

The algae model simulates nitrogen in four forms: ammonium, nitrate, the intracellular nitrogen of phytoplankton and nitrogen in detritus. Phosphorus was modeled in three forms: phosphate, the intracellular phosphorus of phytoplankton and phosphorus in detritus. There can be two algae groups, of which the other one can be nitrogen-fixing cyanobacteria.

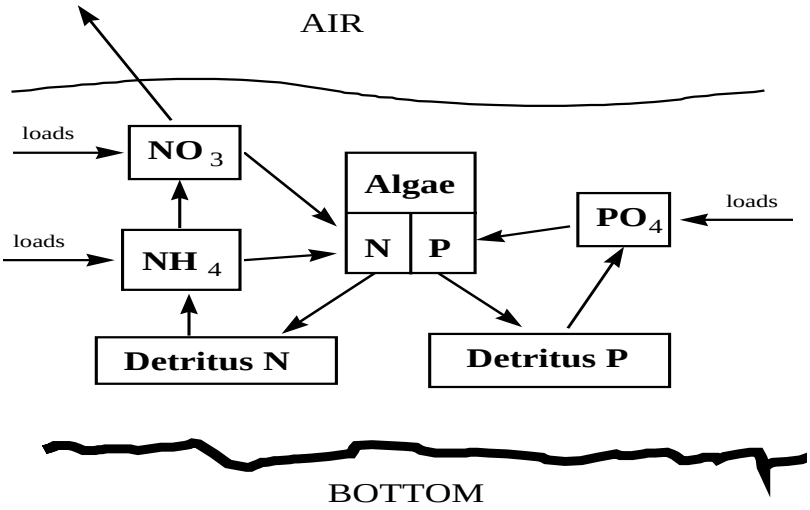

Figure 242. Flow diagram of the algae model 2p.

The essential calculation variables for algae model are NDET (detritus nitrogen), NO3T (nitrate), NH4T (ammonium), PDET (detritus phosphorus), PO4T (phosphate), ALGB (phytoplankton group) and PALB, NALB (this groups intracellular nutrients). There can be other plankton group, which can also be cyanobacteria ALGS. If this group is simulated, the intracellular nutrients PALS, NALS have to simulate too.

Detritus nitrogen (equation A1 below) is formed from phytoplankton intracellular nitrogen (c_{NA}), when phytoplankton dies, settles onto the bottom or is predated by zooplankton. Intracellular nitrogen is released immediately after the decay of algae (M_A). Respiration (R_A) do not effect on intracellular nutrients. The detritus nitrogen changes to ammonium (β_0) while the detritus sinks (ν_{Ndet}).

Ammonium (equation A2) comes from atmospheric and riverine load and via the decay of detritus nitrogen. The release from the sediment is included to the load term. Ammonium is nitrified at first to nitrite and then to nitrate by bacteria. The nitrification rate (β_1) is assumed to be constant. Different phytoplankton species prefer either ammonium or nitrate as their nutrient (equations A16,A17). In the model this is taken into account by the preference coefficient (a_P), which determines the uptake rate of nitrate and ammonium for different species (Scavia *et al.* 1976). The sedimentation rate of ammonium is initially zero.

Nitrite is assumed to decay so rapidly to nitrate that it is not simulated in the model. The nitrate load comes from rivers and atmosphere. Denitrification takes place in the whole water column or near the

bottom sediment. The nitrate uptake of phytoplankton is simulated similarly as ammonium (equations A3, A17, A18).

The cycle of bioavailable phosphorus (equations A4, A5, A7) is described in a similar way as bioavailable nitrogen. If dissolved nitrogen (nitrate and ammonium) is considered as one simulation variable, we get the phosphorus equations by replacing nitrogen (N) in the nitrogen equations (equations A1, A2, A3, A6) with phosphorus (P). Of course the parameter values can be different.

The growth of phytoplankton (equation A9) depends on temperature (equations A21,A22) (Frisk and Nyholm 1980) and intracellular nutrient concentration (equation A20) (Jörgensen 1988). Nutrient uptake depends on concentration in water, intracellular concentrations and also temperature (equations A18, A19, A20, A21). The dependence on intracellular concentration is linear and that on the concentration in water follows the Michaelis-Menten formula. The effect of light attenuation on growth is taken into account in two ways by different growth rates in the different layers and by three light limiting factors. (eqs. 24-26)

The decay (respiration, mortality, grazing, sedimentation) rates of phytoplankton depends on temperature (equations A21,A22). The phytoplankton concentrations (ALGB) decrease very fast after the spring bloom, when the nutrients run out. In the model, fast sedimentation (S_{fl}) depends on the intracellular nutrients of phytoplankton. It begins when the concentration of the intracellular nutrients (characteristic quantity equation A20) decreases below the critical value (fl). A vertical mean value is used because now the sedimentation happens at the same time at all depths.

The other algae group (ALGS) is able to fix N_2 nitrogen (eqs.) and its' decaying rate do not increase after critical value (fl), but the other functions and rates are similar as for the other group.

Algae model variables

	symbol	definition	unit
-	*c*Ndet	nitrogen in detritus	mg/m^3
-	*c*NH	ammonium concentration	mg/m^3
-	*c*NO	nitrate concentration	mg/m^3
-	*c*NA	nitrogen in algae 1 cells	mg/m^3
-	*c*NC	nitrogen in algae 2 cells	mg/m^3
-	*c*Pdet	phosphorus in detritus	mg/m^3
-	*c*PO	phosphate concentration	mg/m^3
-	*c*PA	phosphorus in algae 1 cells	mg/m^3
-	*c*PC	phosphorus in algae 2 cells	mg/m^3
-	*c*A	algae 1 biomass	mg/m^3
-	*c*C	algae 2 biomass	mg/m^3
-	*L*Ndet	detritus nitrogen load	kg/d
-	*L*NH	ammonium load	kg/d
-	*L*NO	nitrate load	kg/d

-	*L*Pdet	detritus phosphorus load	kg/d
-	*L*PO	phosphate load	kg/d

-	*t*	time	d
-	*h*	depth of cell	m
-	*I*	total irradiance	MJ/m^2/d
-	*T*	temperature of layer	^{o} C
-	*T*c	reference temperature	^{o} C

Algae model parameters

	symbol	definition	value	unit
-	*0*	detritus nitrogen mineralization rate	0.005-0.05	1/d
-	*MNpros*	mineralization portion	0.8-1	-
-	*nNdet*	settling of detritus nitrogen	0-200	cm/d
-	*SNdet*	sedimentation of detritus nitrogen	0-30	cm/d
-	*1*	nitrification rate	0.-0.2	1/d
-	*DNO*	denitrification rate near sediment	0-20	cm/d
-	*DNOw*	denitrification rate in water	0-0.1	1/d
-	*ap*	preference coefficient	0.5-3	-
-	*g0*	detritusphosporus mineralization rate	0.005-0.05	1/d
-	*MPpros*	mineralization portion	0.8-1	-
-	*nPdet*	settling of detritus phosphorus	0-200	cm/d
-	*SPdet*	sedimentation of detritus phosphorus	0-30	cm/d
-	*mAmax*	maximal growth rate of algae 1	0.1-5 /d	
-	*mCmax*	maximal growth rate of algae 2	0.1-5 /d	
-	*KP*	half-saturation coefficient of phosphorus uptake of algae	1-25	mg/l
-	*KN*	half-saturation coefficient of nitrogen uptake of algae	4-90	mg/l
-	$\left(\frac{c_{PA}}{c_A}\right)_{\min}$	minimum phosphorous ratio	0.003-0.012	gP/gC
-	$\left(\frac{c_{PA}}{c_A}\right)_{\max}$	maximum phosphorous ratio	0.014-0.044	gP/gC
-	$\left(\frac{c_{NA}}{c_A}\right)_{\min}$	minimum nitrogen ratio	0.05-0.096	gN/gC
-	$\left(\frac{c_{NA}}{c_A}\right)_{\max}$	maximum nitrogen ratio	0.097-0.335	gN/gC
-	*uPmax*	maximal uptake rate of P	0.003-0.01	gP/gC/d

-	*uNmax*	maximal uptake rate of N	0.03-0.1	gN/gC/d
-	*MAmax*	maximal mortality rate of algae 1	0.01-0.2	1/d
-	*MCmax*	maximal mortality rate of algae 2	0.01-0.2	1/d
-	*RAmax*	maximal respiration rate of algae 1	0.-0.1	1/d
-	*RCmax*	maximal respiration rate of algae 2	0.-0.1	1/d
-	*Topt*	optimal temperature	6-27	^{o} C
-	*aT*	coefficient for temperature limiting factor	1.-1.7	-
-	fl	limit value for fast sedimentation	0.-0.08	-
-	*Sfl*	fast sedimentation acceleration	0.-4.	-
-	*fixNmax*	nitrogen fixation rate	0.-0.1	gN/gC/d
-	*fixNP*	maximal N:P rate for fixation	0.-7.	-
-	*fixDIN*	maximal DIN concentration for fixation	0.-20.	Mg/m^3
-	*Iopt*	optimal radiation	6-20	MJ/m^2/d
-	K*I*	half saturation coefficient for radiation	6-20	MJ/m^2/d
-	PBS	coefficient for light limiting function	1-3(8)	-
-	*α*	coefficient for light limiting function	0.-0.5(2.5)	MJ^{-1} m2 d
-	*β*	coefficient for light limiting function	0.-0.5(1)	MJ^{-1} m2 d

Algae model equations, rates and limiting factors

Equations

$$\frac{\partial c_{N\,\mathrm{det}}}{\partial t} = N_A\ M_A - \beta_0 c_{N\,\mathrm{det}} - \nu_{Ndet} c_{N\,\mathrm{det}}\ h^{-1} + L_{N\,\mathrm{det}} \quad \text{(A1)}$$

$$\frac{\partial c_{NH}}{\partial t} = -\beta_1 c_{NH} - u_N\ \ frNH + \beta_0 c_{N\,\mathrm{det}} M_{Npros} + L_{NH} \quad \text{(A2)}$$

$$\frac{\partial c_{NO}}{\partial t} = \beta_1 c_{NH} - u_N\ \ frNO - c_{NO}\ \mathrm{D}_{\mathrm{NO}} h^{-1} - c_{NO}\ \mathrm{D}_{\mathrm{NOw}} + L_{NO} \quad \text{(A3)}$$

$$\frac{\partial c_{P\,\mathrm{det}}}{\partial t} = P_A\ M_A - \gamma_0 c_{P\,\mathrm{det}} - \nu_{Pdet} c_{P\,\mathrm{det}}\ h^{-1} + L_{P\,\mathrm{det}} \quad \text{(A4)}$$

$$\frac{\partial c_{PO}}{\partial t} = -u_P + \gamma_0 c_{P\,\mathrm{det}} M_{Ppros} + L_{PO} \quad \text{(A5)}$$

$$\frac{\partial c_{NA}}{\partial t} = u_N - c_{NA}\ M_A \quad \text{(A6)}$$

$$\frac{\partial c_{PA}}{\partial t} = u_P - c_{PA} M_A \quad \text{(A7)}$$

$$\frac{\partial c_A}{\partial t} = (\mu_{\mathrm{A}} - M_A - R_A) c_A \quad \text{(A8)}$$

$$\frac{\partial c_{NC}}{\partial t} = u_{NC} + (fix_N - M_C)c_{NC} \quad \text{(A9)}$$

$$fix_N = fix_{N\max}, when \frac{c_{NO} + c_{NH}}{c_{PO}} < fix_{NP} \; and \; c_{NO} + c_{NH} < fix_{din}$$

$$\frac{\partial c_{PC}}{\partial t} = u_{PC} - c_{PC} M_C \quad \text{(A10)}$$

$$\frac{\partial c_C}{\partial t} = (\mu_X - M_C - R_C)c_C \quad \text{(A11)}$$

Rates

$$\mu_A = \mu_{max} f(S)\, f(I)\, f(T) \quad \text{(A12)}$$

$$M_A = \mathrm{M}_{\mathrm{Amax}}\, f(T)(1 + \mathrm{S}_{\mathrm{fl}} n\lim) \quad \text{(A13)}$$

nlim = 0, when *f(S)* fl (A14)

nlim = 1, when *f(S)* fl (A15)

$$frNH = \frac{NH\,a_p}{NH\,a_p + NO} \quad \text{(A16)}$$

$$frNO = \frac{NO}{NH\,a_p + NO} \quad \text{(A17)}$$

$$u_N = \frac{\left(\frac{\mathrm{c_{NA}}}{\mathrm{c_A}}\right)_{\max} - \left(\frac{\mathrm{c_{NA}}}{\mathrm{c_A}}\right)}{\left(\frac{\mathrm{c_{NA}}}{\mathrm{c_A}}\right)_{\max} - \left(\frac{\mathrm{c_{NA}}}{\mathrm{c_{NA}}}\right)_{\min}} \cdot \frac{\mathrm{u_{Nmax}}(N\mathrm{c_{NH}} + \mathrm{c_{NO}})}{\mathrm{K_N} + \mathrm{c_{NH}} + \mathrm{c_{NO}}} \mathrm{c_A} \quad \text{(A18)}$$

$$u_P = \frac{\left(\frac{c_{PA}}{c_A}\right)_{\max} - \left(\frac{c_{PA}}{c_A}\right)}{\left(\frac{c_{PA}}{c_A}\right)_{\max} - \left(\frac{c_{PA}}{c_A}\right)_{\min}} \cdot \frac{u_{P\max} PO}{K_P + PO} c_A \quad \text{(A19)}$$

Limiting factors

$$f(S) = \frac{\left(\frac{P_A}{A}\right) - \left(\frac{P_A}{A}\right)_{min}}{\left(\frac{P_A}{A}\right)_{max} - \left(\frac{P_A}{A}\right)_{min}} \cdot \frac{\left(\frac{N_A}{A}\right) - \left(\frac{N_A}{A}\right)_{min}}{\left(\frac{N_A}{A}\right)_{max} - \left(\frac{N_A}{A}\right)_{min}} \quad \text{(A20)}$$

$$f(T) = f(T_s) \exp\left[\int_{T_s}^{T} \ln \theta dT\right] \quad \text{(A21)}$$

$$\theta = a_T + (1 - a_T) T / T_{opt} \quad \text{(A22)}$$

$f(I) = 1$,when $I \geq Iopt$ (A23)

$f(I) = I/Iopt$,when $I < Iopt$ (A24)

$$f(I) = \frac{I}{I + K_I} \quad \text{(A25)}$$

$$f(I) = PBS(1 - e^{\frac{-\alpha I}{PBS}})e^{\frac{-\beta I}{PBS}} \quad \text{(A26)}$$

Also half saturation and linear limitation optimal are available for the light limitation formulation.

9.9.3. Foodweb model (2p+3z)

The flowdiagram of the initial foodweb is presented in fig . There are dissolved organic carbon (DOCT), bacteria (BACT), two algae groups (ALGB, ALGS) and three size depended zooplankton groups NANO, MIRC and MESO. The zooplanktons graze algae and bacteria and also smaller zooplankton groups.

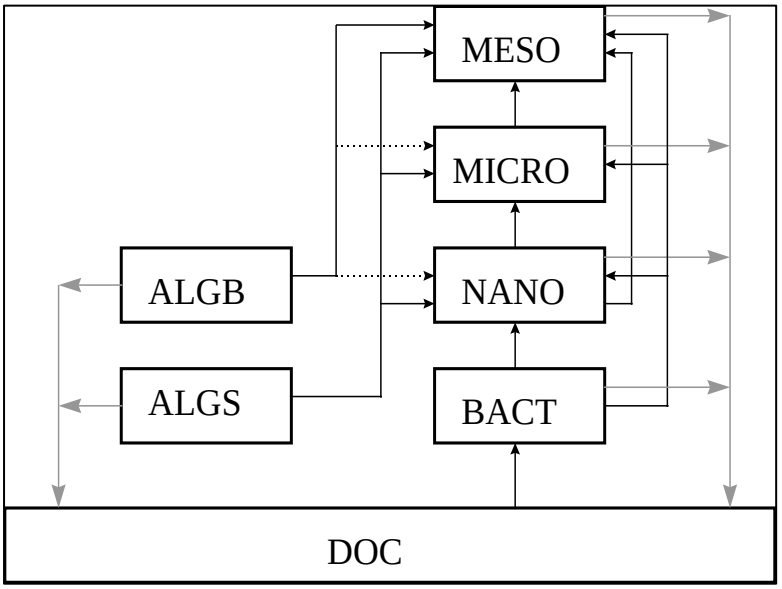

Figure 243. Flowdiagram of the carbon cycle in the foodweb model.

Dissolved organic carbon is eaten by bacteria. The maximal bacteria biomass is calculated from the amount of DOC. This carrying capacity and temperature are limiting the growth of bacteria. The algae variables are simulated as described in algae model with the predation pressure. The zooplankton grows by grazing other species. The assimilation efficiency tells which part of the prey become the biomass of predator. Respiration and non-assimilated carbon are summed to DOC, which make cycle complete. Parameters, which value is cal. are calculated by model and reg. values are got from regression equations.

The calculation variables for ALGS, ALGB (algae groups), DOCT (dissolved organic carbon) and BACT (bacteria) are reserved, but the structure of 'zooplankton' groups NANO, MICR, MESO can be modified. These variables can be also ZOOP (zooplankton), FISH (small fish) and FISP (predator fish). The foodweb is simplest, when there is one algae group (ALGB) and one zooplankton group (MESO). When the foodweb model is used also algae model variables (NDET, NO3T, NH4T, PDET, PO4T, ALGB, NALB, PALB and possibly ALGS, NALS and PALS) have to be calculated.

9.9.4. Filamentous Algae model with two phytoplankton groups (2p+f)

This chapter describes the structure of the 2p+f algae model, which can simulate two groups phytoplankton and two groups of filamentous algae biomass.

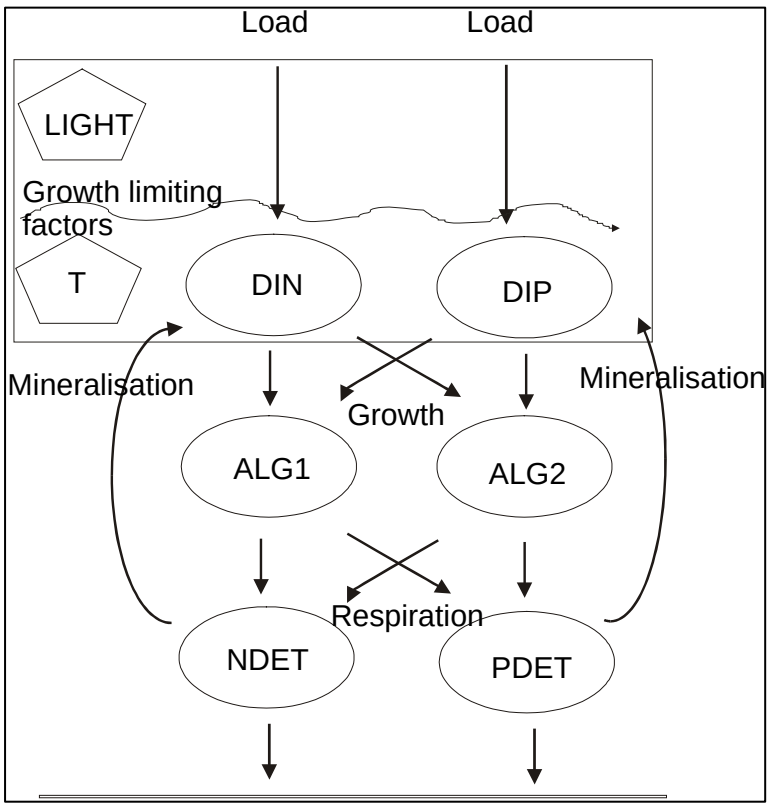

Figure 244. The 2p+f model structure. Filamentous algae are not shown but they are similar to the phytoplankton groups.

The model needs loads of inorganic nutrients, wind data, water temperature and radiation data as model input. Concentrations of inorganic nutrients and phytoplankton are needed for initial values and model validation.

The model simulates concentrations of phytoplankton biomass, dissolved inorganic phosphorus and nitrogen, and phosphorus and nitrogen in detritus. Phytoplankton biomass (wet-weight) can be calculated in two competing groups, of which one group, cyanobacteria (group2), is able to fix nitrogen. The calculation variables are named in the model user interface as following:

ALG1 *phytoplankton biomass, group 1 (mg/l)*

ALG2 *phytoplankton biomass, group 2 (mg/l)*

DIPP *concentration of dissolved inorganic phosphorus (µg/l)*

DINN *concentration of dissolved inorganic nitrogen (µg/l)*

PDET *detritus nitrogen concentration (mg/l)*

NDET *detritus nitrogen concentration (mg/l)*

The growth of phytoplankton is limited by dissolved phosphorus and nitrogen concentrations and light intensity. The nutrient and light limitation of growth rate is calculated according to the Michaelis-Menten kinetics. The half-saturation coefficients of phosphorus, nitrogen and light are the

concentrations (or light intensity) which would cause half of the maximal phytoplankton growth rate, if no other factor is limiting the growth. However, in the equation of growth rate, the limitations of each nutrient and light are multiplied instead of the usual way to take the minimum of the three limiting factors. So, the growth rate depends on availability of both nutrients and light at the same time, not just on the minimum factor. Algae growth is temperature limited. Temperature limitation of phytoplankton growth, as well as other temperature dependent processes is defined by two parameters: optimal temperature for the process and strictness of the temperature dependence. Light availability can be limited by the presence of ice cover. The growth is further limited by shelf-shading when the actual biomass is reaching the maximum biomass describing the carrying capacity of the area. When the actual biomass reaches the minimum biomass, which mimics the over wintering stages of the phytoplankton species, the loss rate becomes zero and the algae cannot get extinct during the unfavourable season.

All losses of biomass are described by one loss rate that is temperature dependent. The maximum loss rate is lower for the nitrogen-fixers (group 2, ALG2) because they are anticipated by grazers due to their toxins. When the algal cells die, algal biomass changes into detritus nitrogen (NDET) and detritus phosphorus (PDET) and these detritus nutrients start to settle at a constant speed and release DIN and DIP back to the water column at temperature dependent rates. The rate of phosphorus regeneration is often set roughly twice as fast as nitrogen regeneration. When detritus reach the lowest grid cell of the 3D model, the detritus N and P start to sediment at constant rates, permanently out the nutrient cycle. Denitrification is not described as a separate process but included to the sedimentation term of detritus nitrogen.

The transport of all variables is calculated 3-dimensionally, except the biotic interactions between dissolved nutrients and algal biomass in the mixed surface layer. The mixing depth is given as a model parameter. There is no algal growth and no interactions between dissolved nutrients and algal biomass below the mixed layer.

2p+f model variables.

symbol	definition	Unit
c_C	Biomass of cyanobacteria (wet weight)	g m-2
c_A	Biomass of the other algae (wet weight)	g m-2
c_{DIN}	DIN concentration	mg m-3
c_{DIP}	DIP concentration	mg m-3
c_{Ndet}	Detritus nitrogen	mg m-3
c_{Pdet}	Detritus phosphorus	mg m-3
L_{DIN}	DIN load	mg m-3 d-1
L_{DIP}	DIP load	mg m-3 d-1
I	Total radiation	MJ m-2d-1
T	Temperature	o C
Ice	Ice-cover (0,1)	-
t	Time	d

h	Depth of grid cell	m

2p+f model parameters

Symbol	definition	Value (Baltic Sea)	unit
N_{inC}	Nitrogen in cyanobacteria		
P_{inC}	Phosphorus in cyanobacteria	0.00268	-
N_{inA}	Nitrogen in the other algae	0.0193	-
P_{inA}	Phosphorus in the other algae	0.00268	-
$\mu_{C\max}$	Maximal growth rate of cyanobacteria	0.5	d-1
$\mu_{A\max}$	Maximal growth rate of the other algae	0.7	d-1
R_{Cmax}	Maximum loss rate of cyanobacteria	0.1	d-1
R_{Amax}	Maximum loss rate of the other algae	0.15	d-1
K_{NC}	Half-saturation coefficient of DIN for cyanobacteria	0	mg m-3
K_{PC}	Half-saturation coefficient of DIP for cyanobacteria	2	mg m-3
K_{NA}	Half-saturation coefficient of DIN for the other algae	7	mg m-3
K_{PA}	Half-saturation coefficient of DIP for the other algae	1	mg m-3
K_{IC}	Half saturation coefficient of radiation for cyanobacteria	20	MJ m-2 d-1
K_{IA}	Half saturation coefficient of radiation for the other algae	15	MJ m-2 d-1
$C_{\min}$	Minimum biomass of cyanobacteria	0.5	g m-2
$A_{\min}$	Minimum biomass of the other algae	0.01	g m-2
$A_{\max}$	Maximum total biomass of algae	300	g m-2
β_0	Maximal detritus nitrogen mineralisation rate	0.018	d-1
γ_0	Maximal detritus phosphorus mineralisation rate	0.043	d-1
$v_{N\det}$	Settling rate of detritus nitrogen	1	m d-1
$v_{P\det}$	Settling rate of detritus phosphorus	1	m d-1
S_{Ndet}	Sedimentation rate of detritus nitrogen	0.16	m d-1
S_{Pdet}	Sedimentation rate of detritus phosphorus	0.01	m d-1
T_{opt}	Optimal temperature		
	for the growth of cyanobacteria	25	o C
	for the growth of the other algae	15	o C
	for losses	25	o C
	for detritus nitrogen mineralisation	18	o C
	for detritus phosphorus mineralisation	18	o C
a_T	Coefficient for temperature limiting factor		

	for the growth of cyanobacteria	1.14	-
	for the growth of the other algae	1.001	-
	for losses	1.05	-
	for detritus nitrogen mineralisation	1.31	-
	for detritus phosphorus mineralisation	1.60	-
I_{red}	Radiation attenuation by ice	0.5	-
h_{mix}	Depth of mixing layer	20	m

2p+f model equations, rates and limiting factors.

Equations

$$\frac{\partial c_C}{\partial t} = (\mu_C - R_C)c_C$$

$$\frac{\partial c_A}{\partial t} = (\mu_A - R_A)c_A$$

$$\frac{\partial c_{DIN}}{\partial t} = \beta\ c_{NDet} - \mu_A N_{inA} c_A h_{mix}^{-1} - \mu_C N_{inC} c_C h_{mix}^{-1} + L_{DIN}$$

$$\frac{\partial c_{DIP}}{\partial t} = \gamma\ c_{P\,\mathrm{det}} - \mu_A P_{inA} c_A h_{mix}^{-1} - \mu_C P_{inC} c_C h_{mix}^{-1} + L_{DIP}$$

$$\frac{\partial c_{N\,\mathrm{det}}}{\partial t} = N_{inA}\ R_A c_A h_{mix}^{-1} + N_{inC}\ R_C c_C h_{mix}^{-1} - \beta c_{N\,\mathrm{det}} - \nu_{\mathrm{Ndet}} c_{N\,\mathrm{det}} h^{-1} - S_{\mathrm{Ndet}} c_{N\,\mathrm{det}} h^{-1}$$

$$\frac{\partial c_{P\,\mathrm{det}}}{\partial t} = P_{inA}\ R_A c_A h_{mix}^{-1} + P_{inC}\ R_C c_C h_{mix}^{-1} - \gamma c_{P\,\mathrm{det}} - \nu_{\mathrm{Pdet}} c_{P\,\mathrm{det}} h^{-1} - S_{\mathrm{Pdet}} c_{P\,\mathrm{det}} h^{-1}$$

Rates

$$\mu_C = \mu_{\mathrm{Cmax}} f_{CN}(c_{DIN}, c_{DIP})\ \ f_{CI}(I)\ \ f(T) f_{AC}(c_A, c_C)$$

$$\mu_A = \mu_{\mathrm{Amax}} f_{AN}(c_{DIN}, c_{DIP})\ \ f_{AI}(I)\ \ f(T) f_{AC}(c_A, c_C)$$

$$R_C = R_{\mathrm{Cmax}} f(T)(c_C - C_{\min})/c_C$$

$$R_A = R_{\mathrm{Amax}} f(T)(c_A - A_{\min})/c_A$$

$$\beta = \beta_0 f(T)$$

$$\gamma = \gamma_0 f(T)$$

Limiting factors

$$f_{CN}(c_{DIN}, c_{DIP}) = \frac{c_{DIN}}{c_{DIN} + K_{NC}} \frac{c_{DIP}}{c_{DIP} + K_{PC}}$$

$$f_{AN}(c_{DIN}, c_{DIP}) = \frac{c_{DIN}}{c_{DIN} + K_{NA}} \frac{c_{DIP}}{c_{DIP} + K_{PA}}$$

$$f\ (T) = \exp\left[\int_{T_{opt}}^{T} \ln\theta dT\right], \text{ where } \theta = a_T + (1 - a_T)\,T/T_{opt}$$

$$f_{CI}(I) = \frac{I(1 - IceI_{red})}{I(1 - IceI_{red}) + K_{IC}}$$

$$f_{AI}(I) = \frac{I(1 - IceI_{red})}{I(1 - IceI_{red}) + K_{IA}}$$

$$f_{AC}(c_A, c_C) = 1 - \frac{c_A + c_C}{A_{\max}}$$